A TWO-DIMENSIONAL MATHEMATICAL MODEL INVESTIGATION OF THE HYDRODYNAMICS AND SEDIMENT TRANSPORT OF SALDANHA BAY AND LANGEBAAN LAGOON

By

Michael-John Barnardo Wiese

Thesis presented in partial fulfilment of the requirements for the degree of Masters of the Science of Civil Engineering at Stellenbosch University.

Study leader: Prof GR Basson

March 2013

DECLARATION

I, the undersigned, hereby declare that the work contained in this thesis is my own original work and that I have not previously in its entirety or in part submitted it at any university for a degree.

…….. ……

MB Wiese **Date**

OPSOMMING

Sedert die konstruksie van die breekwater en die kaai gedurende die vroeg 1970's in Saldanhbaai, is verskeie veranderings aan die kuslyn in die gebied van die Langebaan strandmeer mond waargeneem. Hierdie veranderinge sluit in die erodering van Langebaan Strand, geleë naby die dorp van Langebaan. 'n Ondersoek is onderneem om die moontlike impak van die bogenoemde strukture op die hidrodinamika en sedimentvervoer van die Saldanhabaai en die Langebaan strandmeer stelsels, veral die strandmeer se kanale, met die fokus op die ingang na die Langebaan strandmeer te ondersoek. 'n Twee-dimensionele numeriese model is gebruik vir hierdie ondersoek.

Die verouderde inligting van die seebodem wat beskikbaar was vir die opwekking van die numeriese model het die kalibrasieproses bemoeilik. Alhoewel hierdie proses bemoeilik is kon 'n aanvaarbare kalibrasie bereik word. Aangesien die gemodelleerde area en die werklike area nie ooreengestem het nie is resultate van die numeriese model omsigtig benader en die resultate geskik gevind om die kennis oor die moontlike impak wat die breekwater en die kaai op die hidrodinamika en sedimentvervoer van Saldanhabaai en die Langebaan strandmeer het, te verbreed. Resultate uit die sedimentvervoer model verskaf slegs 'n aanduiding van die sedimentvervoer wat deur gety veranderings en wind gegenereer word. Werklike sediment vervoer sal die effect van golfaksie ook in ag moet neem, wat in hierdie studie uitgesluit is. Golfaksie is van kardinale belang by sediment vervoer langs 'n kuslyn.

Resultate van die numeriese model, gebaseer op gety en wind alleen, het aangedui dat geen groot impak op die hidrodinamika en sedimentvervoer as gevolg van die konstruksie van die breekwater en die kaai in Saldanhabaai ervaar word nie. Gedurende die ondersoek van die impak van verskeie ekstreme watervlak en uiterste windtoestande, is dit opgemerk dat 'n 1 in 100 jaar windsnelheid oor die langste stryklengte na Langebaan Strand gelei het tot die grootste vloei snelhede in die hoofkanale voor die konstruksie van die breekwater en die kaai. Na die konstruksie van die breekwater en die kaai is gevind dat gety storms die grootste snelhede en dus ook die meeste sedimentvervoer gegenereer het by Langebaan Strand.

Uit hierdie ondersoek is dit aanbeveel dat toekomstige studies opgedateerde opmetings van die gebied moet uitvoer wat akkurate modellering, gebaseer op die toestande soos in die veld, sal verseker. Verdere aanbevelings oor die ondersoek van sediment vervoer is die modellering van .golfaksie wat van kardinale belang is in sediment vervoer langs ‘n kuslyn en dus meer realistiese resultate sal lewer.

SYNOPSIS

Since the construction of the causeway and the jetty during the early 1970's in Saldanha Bay, various alterations to the coastline in the area of the Langebaan Lagoon mouth were observed. These alterations include the erosion of Langebaan Beach located near the town of Langebaan. An investigation was undertaken to identify the possible impact these structures had on the hydrodynamics and sediment transport of the Saldanha Bay and Langebaan Lagoon systems, focusing on the entrance to the Langebaan Lagoon. A two-dimensional numerical model was implemented for this investigation.

The outdated information available for the generation of a bathymetry, which indicated the conditions prior to the erosion of Langebaan Beach, complicated the calibration process. However, calibration of the numerical model was acceptable. Due to the bathymetry not providing an indication on the current situation at the Langebaan Lagoon mouth, the results from the numerical model were approached with caution, providing an overview of the hydrodynamics present in Saldanha Bay and Langebaan Lagoon and would be able to broaden the understanding of the impact the causeway and jetty had on the hydrodynamics and sediment transport of Saldanha Bay and Langebaan Lagoon. Results provided by the sediment transport model only provide an indication on the effect tidal variations and wind forcing have on the bay and lagoon and not realistic total sediment transport rates due to the omission of wave action during the modelling process.

Results from the numerical model, based on tidal oscillations and wind forcing only, have indicated that no major impact on the hydrodynamics and sediment transport were experienced due to the construction of the causeway and the jetty. During the investigation of the impact of various extreme water level and extreme wind conditions, it has been observed that a 1 in 100 year wind velocity across the longest fetch towards Langebaan Beach resulted in the greatest velocities prior to the construction of the causeway and the jetty, and after the construction of the causeway and the jetty tidal storms, or storm surge, generated the greatest velocities and thus the most sediment transport in the main channels of the mouth of the Langebaan Lagoon.

From this investigation it was recommended that future studies would require an updated survey of the area, to ensure accurate modelling of the conditions as experienced during field surveys. Further recommendations on the investigation of sediment transport were the inclusion of wave action to provide realistic results. Wave action is a fundamental part of sediment transport along the coastline.

ACKNOWLEDGEMENTS

CSIR, Stellenbosch for their assistance in setting up the bathymetry and the provision of maps of the Saldanha Bay and Langebaan Lagoon systems.

SANParks for the permits and permission to enter the West Coast National Park during the surveys at the Langebaan Lagoon mouth and the additional information concerning the Langebaan Lagoon.

The Hydrographer of the South African Navy for the provision of records on the tidal water levels in Saldanha Bay.

WeatherSA for the provision of wind records at their stations surrounding the area investigated.

DWA for providing the boat and field equipment used during surveys.

"When you put your hand in a flowing stream, you touch the last that has gone before and the first of what is still to come"

- Leonardo Da Vinci

TABLE OF CONTENTS

Declaration i

Opsomming ii

Synopsis iv

Acknowledgements vi

LIST OF FIGURES xi

LIST OF TABLES xvi

VOLUME 1

1 Introduction 1

1.1 Background 1

1.2 Purpose of the study 4

1.3 Structure of this report 5

2 Background 6

2.1 Langebaan Lagoon 6

2.2 Saldanha Bay 10

3 Literature review 15

3.1 Currents and circulation 15

3.2 Hydrodynamic circulation parameters 19

3.2.1 Tides 19

3.2.2 Climate change 24

3.2.3 Storm surge 27

3.2.4 Wind 29

3.3 Sediment composition 32

3.4 Coastal rehabilitation 35

4 Methodology 45

5 Numerical modelling 48

5.1 Introduction 48

5.2 Choice of software 49

5.3 Hydrodynamic model 51

5.3.1 Capabilities of the software 51

5.3.2 Hydrodynamic calculation 52

5.3.3 Input parameters 55

5.3.4 Bathymetry 57

5.3.5 Time step size 66

5.3.6 Wind observations 68

5.3.7 Wind modelling 74

5.3.8 Tidal levels 79

5.3.9 Simulation period 83

5.3.10 Reporting of results 84

5.4 Sediment transport model 85

5.4.1 Capabilities of the software 85

5.4.2 Input parameters 86

5.4.3 Sediment transport calculations 90

5.4.4 Reporting of results 91

6 Field survey 92

6.1 Introduction 92

6.2 Planning 93

6.2.1 Time of observation 93

6.2.2 Locations and sampling points 97

6.3 Instruments 101

6.3.1 Pressure test for water levels 101

6.3.2 Transport and approvals 103

6.3.3 Acoustic Doppler Current Profiler (ADCP), Rivercat 15 104

6.3.4 Garmin Colorado 300 GPS 107

6.3.5 Bed-load Sediment Sampler (BSS) 108
6.3.6 Suspended Sediment Sampler (SSS) 111
6.4 Practical complications during survey 114
6.5 Data analysis 116
6.5.1 Overview 116
6.5.2 Hydrodynamic analysis 117
6.5.3 Sediment transport analysis 118
6.6 Survey results 120
6.6.1 Water levels 120
6.6.2 Velocity 122
6.6.3 Lagoon bed grading 125
6.6.4 Sediment transport 128
7 Calibration 133
7.1 Introduction 133
7.2 Tidal level 135
7.3 Bathymetry 137
7.4 Velocity 139
7.5 Sediment transport 141
7.6 Conclusion 143
8 Investigation scenarios 145
8.1 Introduction 145
8.2 Tidal fluctuations excluding wind forcing 150
8.3 Tidal fluctuations including a 1 in 50 year wind from the north 159
8.4 Tidal fluctuations including a 1 in 50 year wind from the south 166
8.5 Tidal fluctuations including a 1 in 50 year wind across the longest fetch 172
8.6 Tidal fluctuations including a 1 in 100 year wind along the longest fetch 178
8.7 1 in 50 year tidal storm event excluding wind forcing 183

8.8 Sea level rise excluding wind forcing 189
8.9 Long term simulation excluding wind forcing 194
8.10 Conclusions from investigated scenarios 197
9 Limitations and qualifications 205
10 Conclusions 207
11 Recommendations 210
12 References 211

_____ *(Bound separately)*

Appendix A Sediment composition according to 1977 report
Appendix B Langebaan aerial photographs
Appendix C Wind analysis
Appendix D Tidal analysis for field survey
Appendix E Grading of sediment samples
Appendix F Calibration
Appendix G Measured sediment transport parameters
Appendix H Investigated scenario results
Appendix I Sediment transport formulae

LIST OF FIGURES

FIGURE 1-1: STUDY AREA 2
FIGURE 2-1: LANGEBAAN LAGOON 7
FIGURE 2-2: SALDANHA BAY 11
FIGURE 2-3: SMALL BAY 12
FIGURE 3-1: EXAMPLE OF SEMIDIURNAL TIDE DURING A 24-HOUR LUNAR DAY 20
FIGURE 3-2: EXAMPLE OF ONE MONTH WATER LEVEL INDICATING EXTREME HIGH AND LOW TIDES TWICE A MONTH 21
FIGURE 3-3: EXAMPLE OF ONE YEAR ASTRONOMICAL TIDAL VARIATION INDICATING EXTREME HIGH AND LOW TIDES TWICE A YEAR 21
FIGURE 3-4: EXPECTED SEA-LEVEL RISE FOR 2090, BASED ON SEA-LEVELS FOR 1990 (CHURCH ET. AL., 2011). 25
FIGURE 3-5: UPWELLING 28
FIGURE 3-6: EKMAN TRANSPORT 29
FIGURE 3-7: WAVE ENERGY IN SALDANHA BAY PRIOR TO THE CONSTRUCTION OF THE CAUSEWAY AND JETTY (FLEMMING, 1977) 33
FIGURE 3-8: 1960 AERIAL PHOTOGRAPH OF THE LANGEBAAN LAGOON MOUTH 36
FIGURE 3-9: 1988 AERIAL PHOTOGRAPH OF THE LANGEBAAN LAGOON MOUTH 37
FIGURE 3-10: 2000 AERIAL PHOTOGRAPH OF THE LANGEBAAN LAGOON MOUTH 38
FIGURE 3-11: GROYNES CONSTRUCTED AT LANGEBAAN LAGOON AS ON 13 APRIL 2009 40
FIGURE 3-12: SATELLITE IMAGE OF LANGEBAAN BEACH ON 18 FEBRUARY 2004 41
FIGURE 3-13: SATELLITE IMAGE OF LANGEBAAN BEACH ON 7 AUGUST 2005 41
FIGURE 3-14: SATELLITE IMAGE OF LANGEBAAN BEACH ON 13 APRIL 2009 42
FIGURE 3-15: AERIAL PHOTOGRAPHS OF 1960, 1988 AND 2000 AT THE LOCATION OF CLUB MYKONOS INDICATING BEACH ENCROACHMENT 43
FIGURE 5-1: GIS DATA PROVIDED BY THE SA NAVY 58
FIGURE 5-2: MAPS FOR THE GENERATING OF THE BATHYMETRY COMPARED TO RECENT AERIAL PHOTOGRAPH 59
FIGURE 5-3: COASTLINE FROM GIS DATA COMPARED TO RECENT AERIAL PHOTOGRAPH 59

FIGURE 5-4: MIKEZERO BATHYMETRY EDITOR WITH MAPS IMPORTED IN THE BACKGROUND 60
FIGURE 5-5: MIKEZERO BATHYMETRY EDITOR WITH INFORMATION DIGITALIZED FROM MAPS 61
FIGURE 5-6: INTERPOLATION RESULTS FROM SURFER8 SOFTWARE 62
FIGURE 5-7: FINAL BATHYMETRY AFTER CONSTRUCTION OF THE HARBOUR 64
FIGURE 5-8: FINAL BATHYMETRY PRIOR TO CONSTRUCTION OF THE HARBOUR 65
FIGURE 5-9: LOCATIONS OF WEATHER STATIONS 69
FIGURE 5-10: PERCENTAGE OCCURRENCE IN WIND DIRECTION AT LANGEBAAN AND GEELBEK WEATHER STATION 70
FIGURE 5-11: SEASONAL VARIATION IN WIND DIRECTION 71
FIGURE 5-12: SEASONAL VARIATION IN WIND VELOCITY 71
FIGURE 5-13: LONGEST FETCH TOWARDS LANGEBAAN BEACH 74
FIGURE 5-14: 1 IN 50 YEAR HOURLY WIND SPEED IN M/S (BOSMAN ET. AL., 2011) 76
FIGURE 5-15: 1 IN 100 YEAR HOURLY WIND SPEED MEASURED IN M/S (BOSMAN ET. AL., 2011) 77
FIGURE 5-16: CORRECTION FACTOR FOR WIND SPEED RETURN PERIODS BASED ON THE 1 IN 50 YEAR EVENT (MILFORD, 1987) 77
FIGURE 5-17: WXTIDE STATION LOCATOR WINDOW 80
FIGURE 6-1: TIME OF MAXIMUM SEDIMENT TRANSPORT DURING A TIDAL CYCLE 94
FIGURE 6-2: IDEAL TIME FOR SURVEY DURING TIDAL VARIATIONS 95
FIGURE 6-3: IDENTIFICATION OF SURVEY LOCATIONS 98
FIGURE 6-4: LOCATIONS OF POINTS FOR SURVEY 98
FIGURE 6-5: LOCATION OF WATER LEVEL SURVEY 101
FIGURE 6-6: BOAT PROVIDED BY THE DEPARTMENT OF WATER AFFAIRS 103
FIGURE 6-7: ACOUSTIC DOPPLER CURRENT PROFILER (ADCP) RIVERCAT 15 104
FIGURE 6-8: ADCP SENSORS 105
FIGURE 6-9: GARMIN COLORADO 300 GPS 107
FIGURE 6-10: BED-LOAD SEDIMENT SAMPLER 108
FIGURE 6-11: EXAMPLE OF BED-LOAD SEDIMENT SAMPLE 110
FIGURE 6-12: SUSPENDED SEDIMENT SAMPLER 111
FIGURE 6-13: EXAMPLE OF SUSPENDED SEDIMENT SAMPLE 113
FIGURE 6-14: SURVEYED WATER LEVELS COMPARED TO WXTIDE PREDICTED WATER LEVELS 120

FIGURE 6-15: ADJUSTED, RECORDED WATER LEVEL DATA COMPARED TO WXTIDE WATER LEVEL DATA FOR THE 18TH OF MARCH 2011 121
FIGURE 6-16 : DEPTH AND VELOCITY SURVEY RESULTS FOR EACH LOCATIONS SURVEYED 124
FIGURE 6-17: GRADATION OF MEASURED SEDIMENT SAMPLES 125
FIGURE 7-1: WATER LEVEL CALIBRATION 136
FIGURE 8-1: SECTIONS ANALYZED FOR INVESTIGATION IN SALDANHA BAY 148
FIGURE 8-2: SECTIONS ANALYZED FOR INVESTIGATION IN LANGEBAAN LAGOON 149
FIGURE 8-3: THE EFFECT OF TIDAL FLUCTUATIONS EXCLUDING WIND CONDITIONS IN SALDANHA BAY DURING EBB TIDE 151
FIGURE 8-4: THE EFFECT OF TIDAL FLUCTUATIONS EXCLUDING WIND CONDITIONS IN SALDANHA BAY DURING FLOOD TIDE 152
FIGURE 8-5: THE EFFECT OF TIDAL FLUCTUATIONS EXCLUDING WIND CONDITIONS ON THE LANGEBAAN LAGOON DURING EBB TIDE 153
FIGURE 8-6: THE EFFECT OF TIDAL FLUCTUATIONS EXCLUDING WIND CONDITIONS ON THE LANGEBAAN LAGOON DURING FLOOD TIDE 154
FIGURE 8-7: THE EFFECT OF TIDAL FLUCTUATIONS INCLUDING A 1 IN 50 YEAR WIND FROM THE NORTH IN SALDANHA BAY DURING EBB TIDE 160
FIGURE 8-8: THE EFFECT OF TIDAL FLUCTUATIONS INCLUDING A 1 IN 50 YEAR WIND FROM THE NORTH IN SALDANHA BAY DURING FLOOD TIDE 161
FIGURE 8-9: THE EFFECT OF TIDAL FLUCTUATIONS INCLUDING A 1 IN 50 YEAR WIND FROM THE NORTH IN THE LANGEBAAN LAGOON DURING EBB TIDE 162
FIGURE 8-10: THE EFFECT OF TIDAL FLUCTUATIONS INCLUDING A 1 IN 50 YEAR WIND FROM THE NORTH IN THE LANGEBAAN LAGOON DURING FLOOD TIDE 163
FIGURE 8-11: THE EFFECT OF TIDAL FLUCTUATIONS INCLUDING A 1 IN 50 YEAR WIND FROM THE SOUTH IN THE SALDANHA BAY DURING EBB TIDE 167
FIGURE 8-12: THE EFFECT OF TIDAL FLUCTUATIONS INCLUDING A 1 IN 50 YEAR WIND FROM THE SOUTH IN THE SALDANHA BAY DURING FLOOD TIDE 168
FIGURE 8-13: THE EFFECT OF TIDAL FLUCTUATIONS INCLUDING A 1 IN 50 YEAR WIND FROM THE SOUTH IN THE LANGEBAAN LAGOON DURING EBB TIDE 169
FIGURE 8-14: THE EFFECT OF TIDAL FLUCTUATIONS INCLUDING A 1 IN 50 YEAR WIND FROM THE SOUTH IN THE LANGEBAAN LAGOON DURING FLOOD TIDE 170
FIGURE 8-15: THE EFFECT OF TIDAL FLUCTUATIONS INCLUDING A 1 IN 50 YEAR WIND FROM THE NORTH-NORTHWEST IN SALDANHA BAY DURING EBB TIDE 173

FIGURE 8-16: THE EFFECT OF TIDAL FLUCTUATIONS INCLUDING A 1 IN 50 YEAR WIND FROM THE NORTH-NORTHWEST IN SALDANHA BAY DURING FLOOD TIDE 174
FIGURE 8-17: THE EFFECT OF TIDAL FLUCTUATIONS INCLUDING A 1 IN 50 YEAR WIND FROM THE NORTH-NORTHWEST IN THE LANGEBAAN LAGOON DURING EBB TIDE 175
FIGURE 8-18: THE EFFECT OF TIDAL FLUCTUATIONS INCLUDING A 1 IN 50 YEAR WIND FROM THE NORTH-NORTHWEST IN THE LANGEBAAN LAGOON DURING FLOOD TIDE 176
FIGURE 8-19: THE EFFECT OF TIDAL FLUCTUATIONS INCLUDING A 1 IN 100 YEAR WIND FROM THE NORTH-NORTHWEST IN SALDANHA BAY DURING EBB TIDE 179
FIGURE 8-20: THE EFFECT OF TIDAL FLUCTUATIONS INCLUDING A 1 IN 100 YEAR WIND FROM THE NORTH-NORTHWEST IN SALDANHA BAY DURING FLOOD TIDE 180
FIGURE 8-21: THE EFFECT OF TIDAL FLUCTUATIONS INCLUDING A 1 IN 100 YEAR WIND FROM THE NORTH-NORTHWEST IN LANGEBAAN LAGOON DURING EBB TIDE 181
FIGURE 8-22: THE EFFECT OF TIDAL FLUCTUATIONS INCLUDING A 1 IN 100 YEAR WIND FROM THE NORTH-NORTHWEST IN LANGEBAAN LAGOON DURING FLOOD TIDE 182
FIGURE 8-23: THE EFFECT OF TIDAL FLUCTUATIONS INCLUDING A 1 IN 50 YEAR STORM EVENT IN SALDANHA BAY DURING EBB TIDE 184
FIGURE 8-24: THE EFFECT OF TIDAL FLUCTUATIONS INCLUDING A 1 IN 50 YEAR STORM EVENT IN SALDANHA BAY DURING FLOOD TIDE 185
FIGURE 8-25: THE EFFECT OF TIDAL FLUCTUATIONS INCLUDING A 1 IN 50 YEAR STORM EVENT IN LANGEBAAN LAGOON DURING EBB TIDE 186
FIGURE 8-26: THE EFFECT OF TIDAL FLUCTUATIONS INCLUDING A 1 IN 50 YEAR STORM EVENT IN LANGEBAAN LAGOON DURING FLOOD TIDE 187
FIGURE 8-27: THE EFFECT A GLOBAL SEA LEVEL RISE IN SALDANHA BAY DURING EBB TIDE 190
FIGURE 8-28: THE EFFECT A GLOBAL SEA LEVEL RISE IN SALDANHA BAY DURING FLOOD TIDE 191
FIGURE 8-29: THE EFFECT A GLOBAL SEA LEVEL RISE IN LANGEBAAN LAGOON DURING EBB TIDE 192
FIGURE 8-30: THE EFFECT A GLOBAL SEA LEVEL RISE IN LANGEBAAN LAGOON DURING FLOOD TIDE 193

FIGURE 8-31: BATHYMETRY AT ENTRANCE TO LANGEBAAN LAGOON AT INITIATION OF LONG TERM SCENARIO 195
FIGURE 8-32: BATHYMETRY AT ENTRANCE TO LANGEBAAN LAGOON AT END OF LONG TERM SCENARIO 195
FIGURE 8-33: MORPHOLOGICAL CHANGE IN BATHYMETRY EXPERIENCED OVER FIVE YEARS 196
FIGURE 8-34: COMPARISON ON HYDRODYNAMIC VELOCITIES AT SECTION L2, NEAR LANGEBAAN BEACH, DURING A FLOOD TIDE PRIOR TO THE CONSTRUCTION OF THE CAUSEWAY AND THE JETTY 200
FIGURE 8-35: COMPARISON ON HYDRODYNAMIC VELOCITIES AT SECTION L2, NEAR LANGEBAAN BEACH, DURING A FLOOD TIDE AFTER THE CONSTRUCTION OF THE CAUSEWAY AND THE JETTY 200
FIGURE 8-36: COMPARISON ON HYDRODYNAMIC VELOCITIES AT SECTION L2, NEAR LANGEBAAN BEACH, DURING AN EBB TIDE PRIOR TO THE CONSTRUCTION OF THE CAUSEWAY AND THE JETTY 201
FIGURE 8-37: COMPARISON ON HYDRODYNAMIC VELOCITIES AT SECTION L2, NEAR LANGEBAAN BEACH, DURING AN EBB TIDE AFTER THE CONSTRUCTION OF THE CAUSEWAY AND THE JETTY 201
FIGURE 8-38: COMPARISON ON SEDIMENT TRANSPORT AT SECTION L2, NEAR LANGEBAAN BEACH, DURING A FLOOD TIDE PRIOR TO THE CONSTRUCTION OF THE CAUSEWAY AND THE JETTY 202
FIGURE 8-39: COMPARISON ON SEDIMENT TRANSPORT AT SECTION L2, NEAR LANGEBAAN BEACH, DURING A FLOOD TIDE AFTER THE CONSTRUCTION OF THE CAUSEWAY AND THE JETTY 202
FIGURE 8-40: COMPARISON ON SEDIMENT TRANSPORT AT SECTION L2, NEAR LANGEBAAN BEACH, DURING AN EBB TIDE PRIOR TO THE CONSTRUCTION OF THE CAUSEWAY AND THE JETTY 203
FIGURE 8-41: COMPARISON ON SEDIMENT TRANSPORT AT SECTION L2, NEAR LANGEBAAN BEACH, DURING AN EBB TIDE AFTER THE CONSTRUCTION OF THE CAUSEWAY AND THE JETTY 203

LIST OF TABLES

TABLE 2-1: TIDAL CHARACTERISTICS OF SALDANHA BAY AND LANGEBAAN LAGOON 8
TABLE 2-2: DEVELOPMENT IN AND AROUND SALDANHA BAY AND LANGEBAAN LAGOON (CLARK ET. AL., 2009) 11
TABLE 3-1: CHARACTERISTICS OF THE PRINCIPAL TIDE-PRODUCING FORCE CONSTITUENTS (VAN DER MERWE, 1994) 22
TABLE 3-2: CLIMATE CHANGE IMPACTS ON SEA LEVEL IN SOUTH AFRICA (MATHER, 2008) 24
TABLE 3-3: NET FLOW DIRECTION IN THE WATER COLUMN AT VARIOUS DEPTHS DUE TO WIND, AS EXPERIENCED IN THE SOUTHERN HEMISPHERE (PICKARD & EMERY, 1990) 31
TABLE 5-1: WEATHER STATION DATA 68
TABLE 5-2: ANNUAL DISTRIBUTION OF OCCURRENCE IN SPECIFIED WIND DIRECTION 72
TABLE 5-3: STATISTICAL ANALYSIS ON WIND SPEED FOR 1 IN 50 AND 1 IN 100 YEAR RETURN PERIODS 75
TABLE 5-4: EXTREME WIND VELOCITIES 78
TABLE 5-5: ANNUAL EXTREME WATER LEVELS ABOVE MEAN SEA LEVEL 81
TABLE 5-6: STORM EVENT WATER LEVELS ABOVE MEAN SEA LEVEL 82
TABLE 6-1: FIELD SURVEYS REQUIRED FOR CALIBRATION 92
TABLE 6-2: SURVEY TIMES 96
TABLE 6-3: PLANNED SURVEY TIMES AND LOCATIONS 99
TABLE 6-4: LABORATORY ANALYSIS REQUIRED FOR SEDIMENT SAMPLES 119
TABLE 6-5: VELOCITY RESULTS PROVIDED BY THE ADCP 122
TABLE 6-6: PERCENTAGE DISTRIBUTION AS STATED BY PREVIOUS STUDIES 126
TABLE 6-7: SEDIMENT COMPOSITION COMPARISON 126
TABLE 6-8: SEDIMENT TRANSPORT ANALYSIS 130
TABLE 6-9: SURVEYED VELOCITY AND SEDIMENT TRANSPORT COMPARISON 131
TABLE 7-1 : PERCENTAGE OF VELOCITY SURVEYS WITHIN DISCREPANCY RATIOS 139
TABLE 7-2 : PERCENTAGE OF SEDIMENT TRANSPORT SURVEYS WITHIN DISCREPANCY RATIOS 142
TABLE 7-3: SEDIMENT CALIBRATION PARAMETERS USED IN NUMERICAL MODEL 144

TABLE 8-1: PARAMETERS USED FOR INVESTIGATED SCENARIOS..... 146

LIST OF SYMBOLS

MSL	Mean Sea Level
Ω	A function of the angular speed of rotation of the Earth around its axis
Φ	Geographical latitude
u_E	Ekman velocity in the x-direction
v_E	Ekman velocity in the y-direction
τ_y	Wind stress on the sea surface in the y-direction
D_E	The Ekman depth or the depth where friction influence which varies with latitude due to the effects of Coriolis force:
A_z	The coefficient for the eddy viscosity, for vertical mixing, as a property of the flow and not the fluid
$\|f\|$	Friction coefficient
x, y, z	Cartesian coordinates
u, v, w	Flow velocity components for the x-, y- and z-components respectively
S	Magnitude of point source discharge
t	Time step in seconds
g	Gravitational acceleration of 9.81m^3/s
F_u, F_v	Horizontal diffusion terms
T	Temperature
s	Salinity
T_s	Temperature of source
s_s	Salinity of source
D_v	Vertical turbulent (eddy) diffusion coefficient
$\hat{H}$	Source term due to heat exchange with atmosphere
F_T, F_s, F_c	Horizontal diffusion terms
D_h	Horizontal diffusion coefficient
h	Depth
C_n	Courant number
x	Cell spacing defined by the bathymetry in metres
c	Celerity of the water in m/s
h	Water depth at cell in metres
σ_g	Geometric standard deviation, also known as gradation

d_{84}	Particle diameter where 84 % of sediments are finer
d_{16}	Particle diameter where 16 % of sediments are finer
s	Relative density of sediment
ρ_s	Density of the sediment in kg/m^3
ρ	Density of the liquid in kg/m^3
U_f	Friction velocity
C	Chezy roughness coefficient
V	Water velocity in m/s
M	Manning's M roughness in m$^{1/3}$/s
φ_t	Dimensionless rate of total-load sediment transport
ϴ	Dimensionless bed shear stress
d	Median particle size d_{50}
q_t	Total-load sediment transport
q_b	Bed-load sediment transport
q_s	Suspended sediment transport
p	Probability of all the particles in a single layer in being motion
θ'	Dimensionless shear stress related to skin friction
θ_c	Shear stress required for the initiation of motion of particles on the bed
c_b	Bed concentration of suspended sediment
a	Reference level for the concentration of suspended sediment of $2d_{50}$
k_N	Nikuradse's equivalent roughness coefficient of $2.5d_{50}$
I_1, I_2	Einstein's integrals
z	Shear velocity related to the skin friction
w_s	Settling velocity of the sediment
κ	the Von Karman constant of 0.4
D_{gr}	Dimensionless particle size
G_{gr}	Dimensionless total load sediment transport rate
C, m, A	Parameters depending on the dimensionless particle size, D_{gr}
F_{gr}	Sediment mobility number
g	Gravitational acceleration of 9.81
ν	Kinematic viscosity of water
U_f^n	total shear velocity

n	A constant depending on D_{gr} ranging from 0 for coarse materials to 1 for fine materials
φ_b	Bed-load sediment transport
θ'	Dimensionless bed shear stress

1 INTRODUCTION

1.1 Background

In the past few decades, man has become increasingly aware of the effect of his actions on the natural environment, especially in terms of developments. It is important to find a balance between development enhancing economic growth and environmental sustainability to ensure a brighter future.

Saldanha Bay and Langebaan Lagoon, near the towns of Saldanha and Langebaan 100 km north of Cape Town, South Africa, is a great example of the balance which has to be maintained between industrial development at the harbour and the ecological environment. If human development is done without proper regard of the natural environment, undesirable consequences to the environment will result.

Saldanha Bay, well known for being the only natural harbour located along the west coast of South Africa, was identified as an ideal location for an international port. Construction of harbour structures initiated during the early 1970's and included the construction of a causeway, stretching from the mainland to Marcus Island at the entrance of Saldanha Bay, and an iron-ore jetty, splitting the bay into two sections as indicated in **Figure 1-1**. The section of Saldanha Bay north of the jetty was identified as Small Bay and Big Bay to the south of the jetty. Each of these two bays consists of unique, independent hydrodynamic conditions.

To the south of Big Bay a unique system rich in flora and fauna is located, known as the Langebaan Lagoon. The lagoon has no river connected to it, therefore only consisting of a single connection to Big Bay where water can enter and exit the system. Due to the semi-enclosed nature of the lagoon, a change in the hydrodynamics of Big Bay could influence the hydrodynamic and sediment transport conditions in the lagoon system.

Figure 1-1: Study Area

Since the development of the harbour structures during the 1970's, various changes along the coastline have occurred in the Saldanha Bay and Langebaan Lagoon areas, including the erosion of Langebaan Beach located at the mouth of the lagoon. These changes could have been a possible result of alterations in the hydrodynamic conditions.

Previous studies on the hydrodynamic and sediment transport conditions of the Saldanha Bay and Langebaan Lagoon systems prior to the construction of the causeway and jetty were very limited. This complicated the identification of the impacts and alterations caused by these structures. Studies conducted after these developments were also limited due to the confidential nature of these reports. However, the utilization of two-dimensional computer modelling provided a better understanding of the influence harbour structures had on the surrounding area.

The application of a two-dimensional model provided an indication of the alterations in the hydrodynamics and sediment transport patterns in Saldanha Bay and Langebaan Lagoon systems due to the harbour development in Saldanha Bay. This model was also used to identify the impact various extreme conditions in the hydrodynamic driving forces had on these two systems prior to and after the construction the causeway and the jetty, the impact on the sediment transport patterns and the possibility of an alteration in the hydrodynamic driving forces as a cause for the erosion of the beach at the entrance to the lagoon, excluding the effects of wave action.

This investigation is aimed to establish the effects of tidal and wind driven currents, before and after the construction of the Saldanha Bay harbour, on the seabed at the lagoon and main channels of the Langebaan Lagoon at the mouth of the lagoon. Therefore, the effects of littoral drift as a result of wave action on the coastline were excluded from this investigation. For a realistic analysis on the sediment transport and erosion of beaches along the coastline, wave action has to be included in the numerical model.

1.2 Purpose of the study

Previous work on the hydrodynamics and sediment transport conditions in the Saldanha Bay and Langebaan Lagoon systems were very limited. These limitations complicated the understanding of the impact development in Saldanha Bay had on the hydrodynamic and sediment transport conditions in both the bay and the lagoon.

However, two-dimensional computer modelling can provide a solution to the investigation of past or future conditions. These models can also be utilized to investigate the impact of various alterations in wind and water level conditions.

The purpose of this investigation is to utilize two-dimensional computer modelling on the Saldanha Bay and Langebaan Lagoon systems and provide a better understanding on the hydrodynamic and sediment transport conditions before and after the harbour developments in Saldanha Bay. The area of interest was identified at the Langebaan Lagoon mouth, where erosion of Langebaan Beach occurred.

Scenarios also investigated with the two-dimensional model include extreme conditions in the hydrodynamic driving forces providing great velocities ideal for sediment transport and the influence developments in Saldanha Bay had during these extreme conditions. These conditions, ideal for large velocities, were based on the conclusions from a literature review.

Sediment transport at the mouth of the lagoon was investigated based hydrodynamic currents generated by tidal variation and wind forcing and the effects of these currents on the lagoon bed and the main channels of the lagoon. It should be noted that during this report wave action were excluded from the numerical model and therefore excluded the effects of these two driving forces on the erosion of Langebaan Beach. However, the erosion of Langebaan Beach is mentioned in the report..

Note that for a realistic analysis of the sediment transport along the coastline, wave action would have to be included in the two-dimensional model to include factors such as littoral drift, cross-shore erosion and sediment budget.

1.3 Structure of this report

This document has been divided into 11 sections, providing information on the investigation of the hydrodynamic and sediment transport conditions in the Saldanha Bay and Langebaan Lagoon systems. A basic understanding of this document is provided in **Section 1**.

- **Section 2** provides background on Saldanha Bay and Langebaan Lagoon and a basic understanding of the area investigated.
- In **Section 3** a literature review is provided, consisting of conclusions from previous studies and a theoretical approach to the parameters dominating the hydrodynamic and sediment transport conditions in the Saldanha Bay and Langebaan Lagoon systems.
- The methodology for this investigation is discussed in **Section** 4.
- **Section 5** provides an explanation to the software used for the two-dimensional modelling, the dynamics behind the software and the approach used to model the area investigated.
- In **Section 6** the field survey, instruments used, measuring techniques and results are explained, which were used for the calibration of the two-dimensional numerical model.
- In **Section 7** the calibration of the model are discussed and the accuracy of the model is determined.
- **Section 8** discusses the scenarios modelled based on the extreme hydrodynamic forcing conditions and the results observed during each of these scenarios.
- **Section 9** states the limitations and qualifications experienced during this investigation.
- Conclusions for this investigation are provided in **Section 10**.
- **Section 11** provides recommendations for further investigations.

2 BACKGROUND

2.1 Langebaan Lagoon

The Langebaan Lagoon, proclaimed as a RAMSAR site in April 1988, has drawn international interest to its unique ecological environment, rich in bird life, rocky intertidal invertebrates, fish species and benthic macro-fauna. This unique environment is surrounded and protected by the West Coast National Park, which covers 27 000 hectares, including the lagoon, inshore islands located in Saldanha Bay and the beach stretched along the Atlantic Ocean.

The lagoon consists of a long and shallow marine area with a length of 16 kilometres and a width of two to three kilometres. Depths in the range of two to six metres have been measured, with a greatest depth of 16 metres recorded between the town of Langebaan and Schaapen Island, also known as Skaapen Island. Three utilization zones can be identified in the Langebaan Lagoon. These zones limit accessibility to the public and the activities allowed in the lagoon. The wilderness zone includes the southern end of the lagoon, including the wetlands at the southern edge of the lagoon, and the inshore islands. Permission needs to be granted for access to this zone. The middle reaches of the lagoon is a limited recreation zone, allowing activities such as sailing and canoeing, but motorboat activities are not allowed. The third zone is located near the town of Langebaan at the entrance to the lagoon. Multi-purpose recreational activities are allowed in this section of the lagoon, including power boats, water skiing and fishing.

At the entrance to the lagoon, the beach on the east bank has experienced extensive erosion which resulted in the complete erosion of this beach. Deeper sections of the lagoon create a channel which guides the flow of the lagoon and connects to Saldanha Bay by flowing around Schaapen Island near the location of one of the previously mentioned beach, as indicated in **Figure 2-1**.

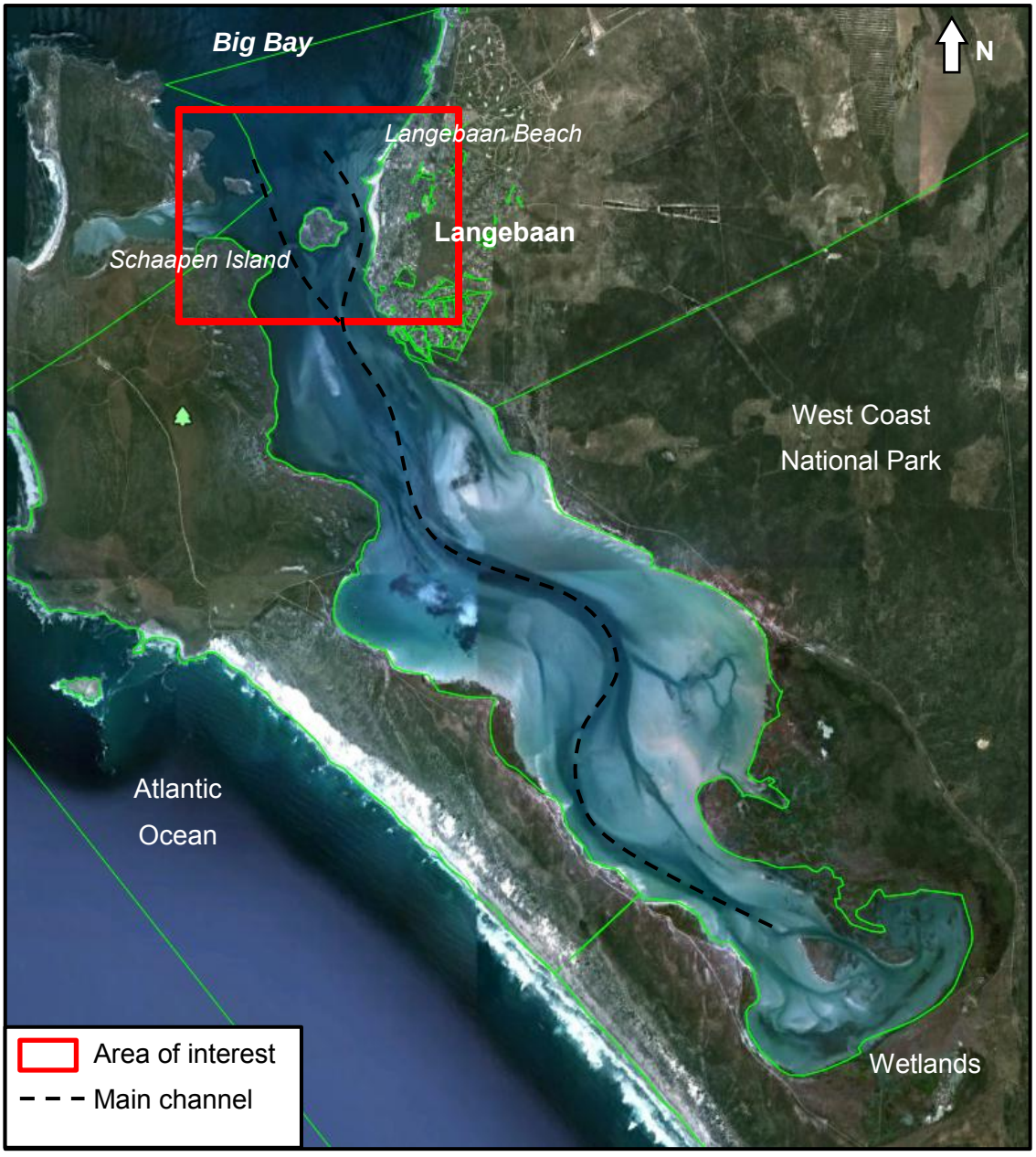

Figure 2-1: Langebaan Lagoon

Even though the lagoon consists of a main channel directing the flow, no river is connected to the lagoon which results in the lagoon only experiencing in- and outflows at a single point. Therefore, water level fluctuations caused by tides generates an inflow of water during flood tides and extracting water during ebb tides, similar to the breathing action of a lung. Due to the negligible inflow of fresh water into the lagoon and tidal variations forcing saltwater into the lagoon, the entire lagoon consists of salt water and no fresh water is present which limited development in the past. The tidal forced

breathing of the lagoon results in little to no seasonal variation in water depths, but rather water depths imitating tidal fluctuations. Tidal characteristics for Saldanha Bay are provided in **Table 2-1** (Van Ballegooyen et al., 2008). These average extreme water levels indicate a variation of 0.5 metres between spring and neap tides and 0.5 metres to 1.5 metre water level differences between the high and low tidal peaks for the neap and spring tide conditions respectively. During a spring tide, 12% of the volume of the lagoon system is exchanged (eWISA, 2012).

Table 2-1: Tidal characteristics of Saldanha Bay and Langebaan Lagoon (SANHO 2012)

Extreme water level mark	Metres above Chart Datum
Highest Astronomical Tide (HAT)	2.03
Mean High Water Spring (MHWS)	1.76
Mean High Water Neap (MHWN)	1.26
Mean Level (ML)	0.99
Mean Low Water Neap (MLWN)	0.76
Mean Low Water Spring (MLWS)	0.26
Lowest Astronomical Tide (LAT)	0

These water level fluctuations generate very small velocities in the lagoon, with greater velocities located at the entrance to the lagoon. Flow velocities of about 0.2 m/s have been recorded in the middle reaches of the lagoon where depths are in the range of 2 m to 6 m and 1 m/s have been recorded at the deepest section between Langebaan and Schaapen Island at the entrance to the lagoon (eWISA, 2012).

Alterations in the tidal conditions and water level fluctuations in Big Bay can result in alterations in the velocities expected in the lagoon. These alterations in the velocity expected in the lagoon can have major implications on the sediments distribution, sediment transport and composition of sediments in the lagoon.

Sediment entering the lagoon from the southern edge is minimal and trapped by the wetlands located in this area. Thus the source for sediments available is the fine, unconsolidated quartzitic sand particles located in Saldanha Bay, the Langebaan Lagoon and along the beaches. Beaches located in the Langebaan Lagoon have been stabilized by the vegetation, however, at the entrance to the lagoon major development

activities have resulted in the removal of vegetation near the coastline, which increase the risk of erosion of these beaches.

Thus, when investigating the hydrodynamic and sediment transport conditions in the Langebaan Lagoon, especially at the entrance to the lagoon, an understanding of the dynamics of Saldanha Bay is required. Alterations in the hydrodynamic conditions in Saldanha Bay, including variations in the tidal levels and wave properties, could have major impacts on the Langebaan Lagoon. During this investigation hydrodynamics were focused on wind and tides and the effect these two parameters has on the sediment transport at the Langebaan Lagoon mouth and the morphological impacts on the main channels of the lagoon, thus excluding the effect of waves.

For an accurate investigation the alterations to the coastline and realistic sediment transport rates, wave action needs to be included. Wave action is a fundamental part of sediment transport along the coastline, which includes cross-shore drift and sediment budget.

2.2 Saldanha Bay

Saldanha was founded due to the bay being mistaken for Table Bay in Cape Town in 1601 (Burman & Levin, 1974). The rich population of fish, seals and birds in Saldanha Bay provided food for travellers and being the only natural harbour on the west coast of South Africa, served as a perfect shelter for ships during storms. A fishing community developed in the north of Saldanha Bay, the most sheltered area, and an ideal docking location for fishing vessels. Developments were however limited due to the lack of fresh water.

Development along the northern shore of Saldanha Bay during the early 1900's were focused on factories for the fishing community, providing onshore packing and freezing facilities for deep sea trawlers. An increase in the demand for fish resulted in more work opportunities at the factories which lead to an increase in the population of the surrounding community and therefore stimulated the development of the town of Saldanha.

During the 1970's the construction of an international port in Saldanha Bay was initiated. Major developments impacting the hydrodynamics of the bay started in 1973 with the construction of a causeway, stretching from the mainland to Marcus Island, as illustrated in **Figure 2-2**. Development continued as listed in **Table 2-2** (Clark et. al., 2009).

Table 2-2: Development in and around Saldanha Bay and Langebaan Lagoon (Clark et. al., 2009)

Year	Development
1973	Causeway to Marcus Island
1973-1974	General Maintenance Quay and Rock Quay
1974-1976	Iron-Ore Jetty and 24 m deep access canal
1980	Multi-purpose terminal added to iron-ore jetty
1984	Small crafts harbour
1998	Multi-purpose jetty extended
2005	Construction of 250 metre groyne at Langebaan
2007	Construction of 360 metre groyne at Langebaan

Figure 2-2: Saldanha Bay

Figure 2-3: Small Bay

One of the most important developments during the construction of the harbour was the construction of the causeway between the mainland and Marcus Island in 1973. Not only did this decrease the entrance to Saldanha Bay, but it also had environmental impacts on the island. The main purpose for the construction of the causeway is the provision of shelter from the wave action to ore-carriers docking at the jetty.

Another major development is the iron-ore jetty, perpendicular to the coastline, dividing the bay into two sections. Small Bay located north of the iron-ore jetty and protected by the causeway and Big Bay to the south which connects to the lagoon at the southern boundary and the ocean to the west. Each of these two bays now had their own properties in terms of hydrodynamics. From **Figure 2-3** is can be noted that the majority of the jetty is a solid structure and the end seems to be a floating structure. Previous investigations, as discussed in **Section 3.1**, identified wind as the dominant driving force

in Saldanha Bay. A floating structure would influence the fetch of wind driven currents and including this structure in the bathymetry were therefore very important during the hydrodynamic modelling.

The hydrodynamics of the Saldanha Bay system are more complicated than the flooding and ebbing flow present in the Langebaan Lagoon. During summer months, surface water is heated while water at greater depths remains at a cooler temperature. This difference in temperature at various depths results in different flow directions with a change in depth. The surface water is dominated by the wind conditions while the deeper, cooler water is primarily tidal driven in a clockwise rotation towards the Langebaan Lagoon. During winter months the change in temperature is much lower, resulting in a more uniform flow in the water column (Monteiro & Brundrit, 1990). To accurately simulate the three-dimensional upwelling experienced in Saldanha Bay and especially at the entrance to Small Bay, three-dimensional modelling would be required. However, for an investigation on the hydrodynamic conditions at the Langebaan Lagoon mouth, two-dimensional modelling would be adequate and would provide a depth averaged flow from the bay to the lagoon.

The construction of the causeway and the jetty split Saldanha Bay into two sections with their own hydrodynamic conditions. Small Bay, illustrated in **Figure 2-3**, is protected from wave action with maximum velocities of about 0.02 m/s, while Big Bay is more exposed to wave energy with maximum velocities of about 0.2 m/s (Luger, 1999).

Not only did these developments and the upgrade to an international port influence the hydrodynamics of Saldanha Bay, but also increased work opportunities, new developments and a new attraction force for economic growth. However, an increase in the population results in expansion of urban areas, pressuring the environment and also possibly affecting dune migration and beach erosion processes due to the removal of vegetation, e.g. along the coastline near Club Mykonos and discussed in **Section 3.4** as a result of the expansion of urban developments.

The erosion of the Langebaan Beach at the mouth of the Langebaan Lagoon is an example of the changes that have occurred on the coastline due to erosion. Attempts to

rehabilitate this beach include the construction of two groynes in 2005 and 2007, as mentioned in **Table 2-2**.

3 LITERATURE REVIEW

3.1 Currents and circulation

The investigation on the hydrodynamics and sediment transport on the Langebaan Lagoon mouth would require a comprehensive understanding of the dynamics of Saldanha Bay and Langebaan Lagoon prior to and after the construction of the causeway and the jetty. However, literature on the hydrodynamic and sediment transport conditions prior to the construction of the causeway and the jetty is very limited and studies after the construction were not accessible due to the restrictions in terms of confidentiality preventing public perusal.

The literature available would be able to provide enough information for the compilation of a two-dimensional numerical model. From this information the primary hydrodynamic driving forces could be identified on which the hydrodynamic and sediment transport models could be based.

In 1975, an investigation was conducted on the hydrodynamics prior to the construction of the causeway and the jetty in Saldanha Bay by Shannon and Stander. With very limited data, it was concluded that the top five metres of the Saldanha Bay depended on the direction and speed of the wind which resulted in flows in the range of 0.1 m/s to 0.2 m/s. These values were between 2% and 3% of the velocity of the wind. Velocities at the mouth of Saldanha Bay were noted as “small” and at the mouth of the lagoon, the greatest velocities recorded were about 1 m/s, which were tidal driven instead of the wind forced hydrodynamics experienced in Saldanha Bay (Shannon & Stander, 1977).

An attempt was made at two-dimensional modelling of the bay and the lagoon in 1982 by the CSIR. This model proved realistic for the tidal driven lagoon, but recommendations were made to use a three-dimensional model for the modelling of Saldanha Bay due to a variation in flow directions at different depths as a result of a thermo cline present in Saldanha Bay during the summer months. This model was based on tidal fluctuations which resulted in 0.02 m/s and 0.2 m/s for Small Bay and Big Bay respectively (Luger, 1999).

Further investigations undertaken by the CSIR included the effect of the causeway on the northern shore of Small Bay. Currents were measured by means of drogues, which concluded that the top two metres of water were mainly wind driven while waters from two to six metres were well mixed and contained a more significant tidal driving force in a mainly clockwise rotation.

In 1990, a study undertaken by Monteiro and Brundrit were based on a time-series dataset. A stratified thermo cline was noticed at the depths of three to six metres during summer, with surface water temperatures rising to 18 ºC and 20 ºC and lower temperatures of 11 ºC to 13 ºC at greater depths. This thermo cline could result in different flow directions of warmer water located above the thermo cline and colder water located below, which explains the flow variations experienced by the CSIR and Shannon and Stander in previous reports. During winter seasons, a more isothermal water column was present, with temperatures at 13 ºC and 14 ºC. From the results of the study it was concluded that an absence of the thermo cline provided a more uniform flow in the water column (Monteiro & Brundrit, 1990).

The abovementioned thermo cline is a result of upwelling due to southern winds during the summer months. Southern winds force the colder water from the Atlantic Ocean into Saldanha Bay, and warmer water in Saldanha Bay is forced to the surface and maintained by means of atmospheric heat fluxes. During winter months, atmospheric temperatures decrease and a dominant north-north-westerly wind is present, therefore less upwelling generated due to a southern wind (Monteiro & Largier, 1999).

Monteiro and Brundrit also concluded that the construction of the jetty and the causeway had a great influence on the hydrodynamics of Small Bay, in terms of tidal forcing on the water circulation being reduced, the degree of stratification and the increase in residence time of water in Small Bay.

An investigation based on historical drogue data was done during 1991 on the relative importance of the two forcing mechanisms, winds and tides, compared to the studies done by Shannon and Stander in 1977, prior to the construction of the jetty and causeway.

Results were very biased on low wind speeds as a result of the lack of greater wind speed conditions. Certain areas had little to no data available. This investigation confirmed the conclusions found by Monteiro and Brundrit, stating that wind is the dominant driving factor for the hydrodynamics in Small Bay, as well as Big Bay for surface waters above the thermo cline during the summer months. A more homogeneous distribution is observed during the winter months due to the lower temperatures as a result of the water being exposed to sunlight for shorter periods of time (Weeks et. al., 1991a).

Further investigation by Weeks was done on the effect of passage of a cold front of advection of water across the mouth of Small Bay. It has been concluded that surface water was flowing out of Small Bay while bottom water flowed in during wind velocities larger than 15 m/s in a north-north-easterly direction (Weeks et. al., 1991b)

More recent information confirmed the results from previous observations, with little correlation between the wind conditions and currents at great depths in Saldanha Bay. Significant tidal influence was observed at the entrance of the lagoon with velocities up to 1 m/s and the tides forcing the breathing action of the lagoon, referred to in **Section 2.1**.

An Environmental Impact Assessment by Van Ballegooyen et al, 2008, stated that southern winds generates an anti-clockwise rotation in Big Bay and a clockwise rotation in Small Bay, while north-north-western winds generates a clockwise rotation in both Small and Big Bay. Furthermore, it has been stated that there is very little change in salinity in the Saldanha Bay system, therefore, excluding a change in salinity during this investigation (Van Ballegooyen et al., 2008).

From these studies mentioned above, it can be concluded that the circulation of Big Bay and Small Bay, even though separated by the jetty, is dominated by wind forcing, especially on the surface during the summer months due to the thermo cline. However, the thermo cline is absent during the winter months with a more unified flow direction in the water column, similar to the approach of a two-dimensional model where a depth-averaged distribution is assumed in a water column.

It can further be concluded that the hydrodynamics of the Langebaan Lagoon is forced by a change in water level with minimal impacts from wind. This water level forced breathing action results in well-mixed water mass and thus no flow in multiple directions in the water column due to the presence of a thermo cline.

Due to this investigation focusing on tidal and wind forcing, and the area of interest located at the mouth of the Langebaan Lagoon where a well-mixed water column results in the absence of the thermo cline, a two-dimensional model was applied instead of the recommended three-dimensional model. The previously recommended three-dimensional modelling of Saldanha Bay would take into consideration the influence of the thermo cline and the possible influence of a halocline for a water column experiencing major changes with a change in depth.

The two-dimensional model provided sufficient information on the hydrodynamics of Saldanha Bay to generate the appropriate conditions at the Langebaan Lagoon mouth. Therefore, three-dimensional modelling was not implemented to generate the hydrodynamic conditions in Saldanha Bay. The mouth of the Langebaan Lagoon is primarily tidal driven and it is therefore assumed that the water column is more homogeneous, ideal for two-dimensional modelling. During this investigation, the literature review was extended to provide a better understanding of the dynamics of tidal fluctuations which result in a change in the water level, the effect of a higher mean sea-level due to sea level rise and wind observations at the area of interest and the effect of wind on water.

3.2 Hydrodynamic circulation parameters

3.2.1 Tides

A basic understanding of tidal recurrences and effects of various tides are important to understand the driving force behind the hydrodynamic currents generated in the lagoon as identified in **Section 3.1**. By understanding tidal dynamics, predictions for periods of high velocities in the mouth of the lagoon can be identified and therefore periods of high sediment transport can be identified.

Tidal oscillations vary with time due to the various factors influencing the water levels. The primary factors resulting in tidal oscillations are the gravitational forces from the sun and the moon on the ocean. These gravitational forces result in high and low water levels across the ocean, which varies with time and location depending on the position of the moon and the sun relative to the earth.

Tides can be divided into three main constituents:

- Semidiurnal
- Diurnal
- Long period constituents

Semidiurnal constituents are the high and low tides experienced twice (lunar day consisting of 24.8 hours), as indicated in **Figure 3-1** (water levels are in metres above MSL). These tides are most common in South Africa and have a period of about 12.42 hours. Single high and low tides occurring in each lunar day, with a period of about 23.93 hours, are less common and known as diurnal constituents.

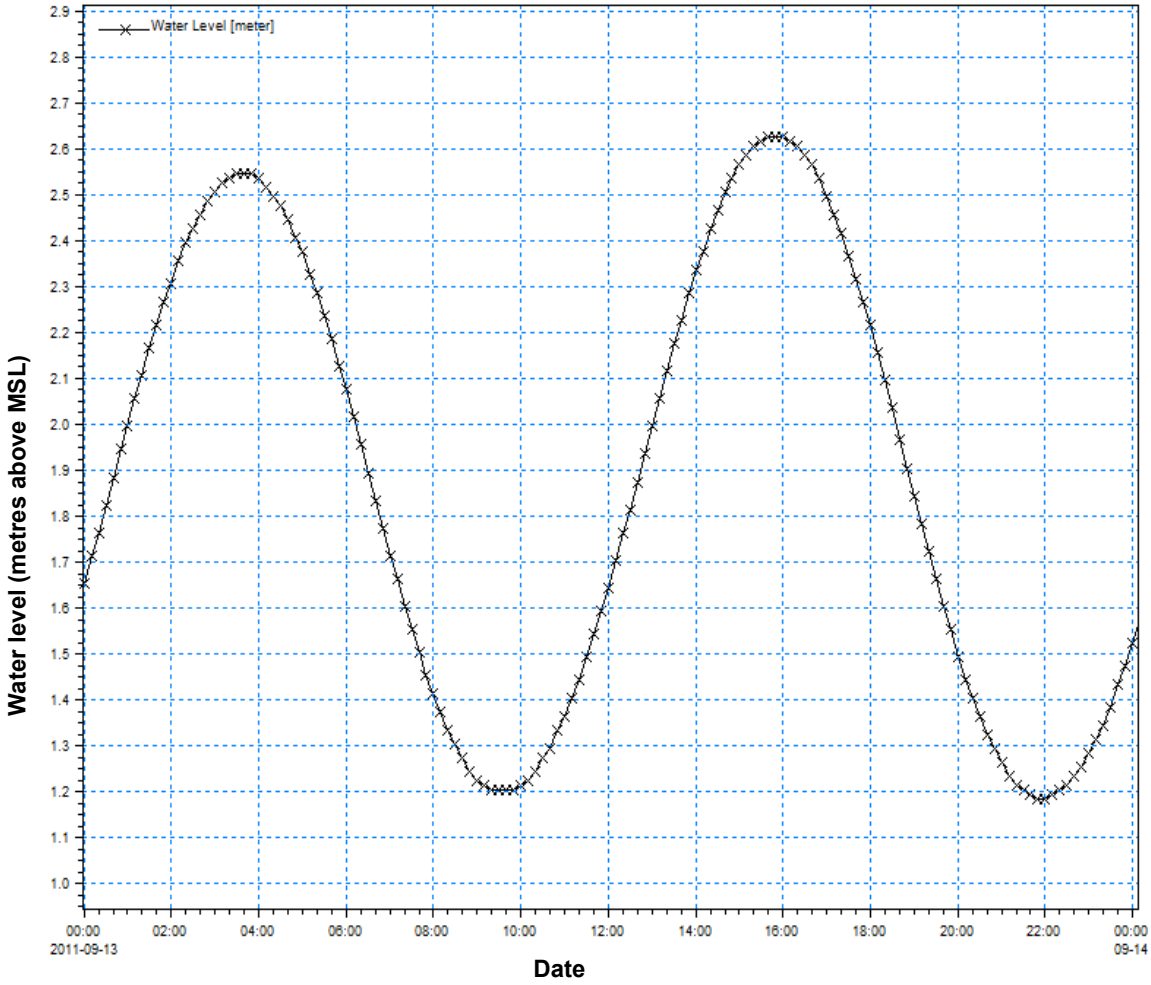

Figure 3-1: Example of semidiurnal tide during a 24-hour lunar day

Long period constituents provide the extreme high and low condition in a two-week period, thus twice a month as indicated in **Figure 3-2**. These extreme high and low conditions are identified during full moon and new moon, and are also known as spring tides.

Two extreme peaks during a period of one year can be identified during March and September. These peaks are known as astronomical tides.

Figure 3-3 illustrates the tidal fluctuations experienced during a one-year period.

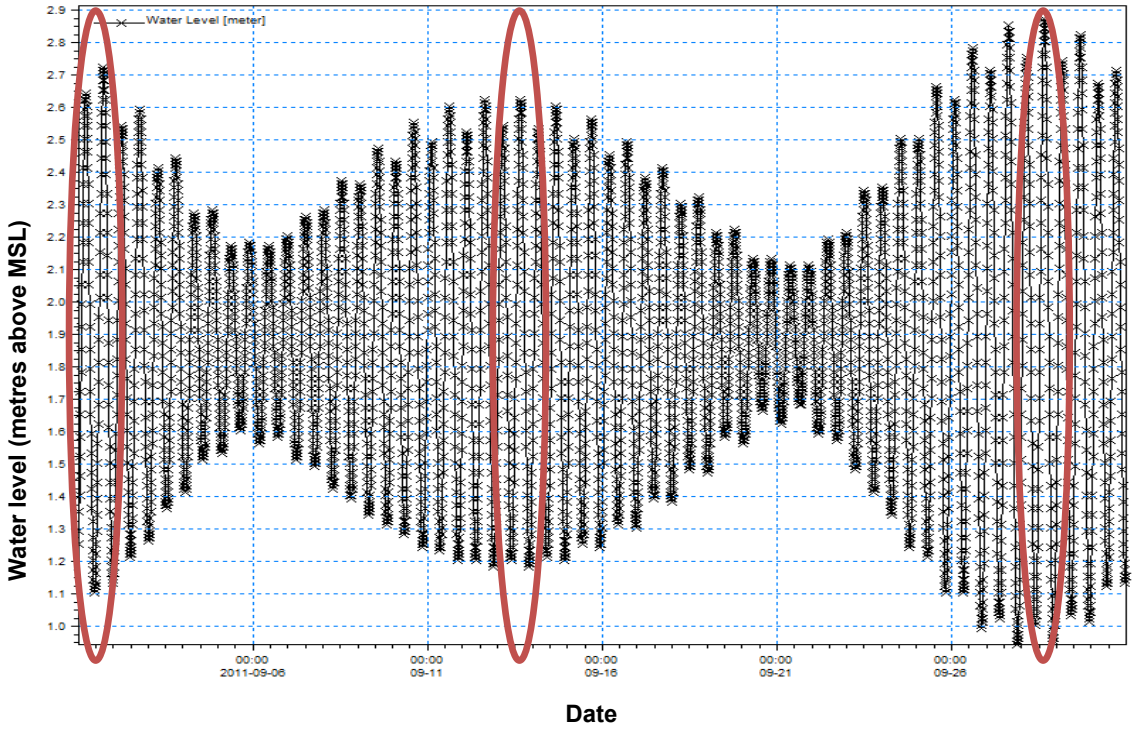

Figure 3-2: **Example of one month water level indicating extreme high and low tides twice a month**

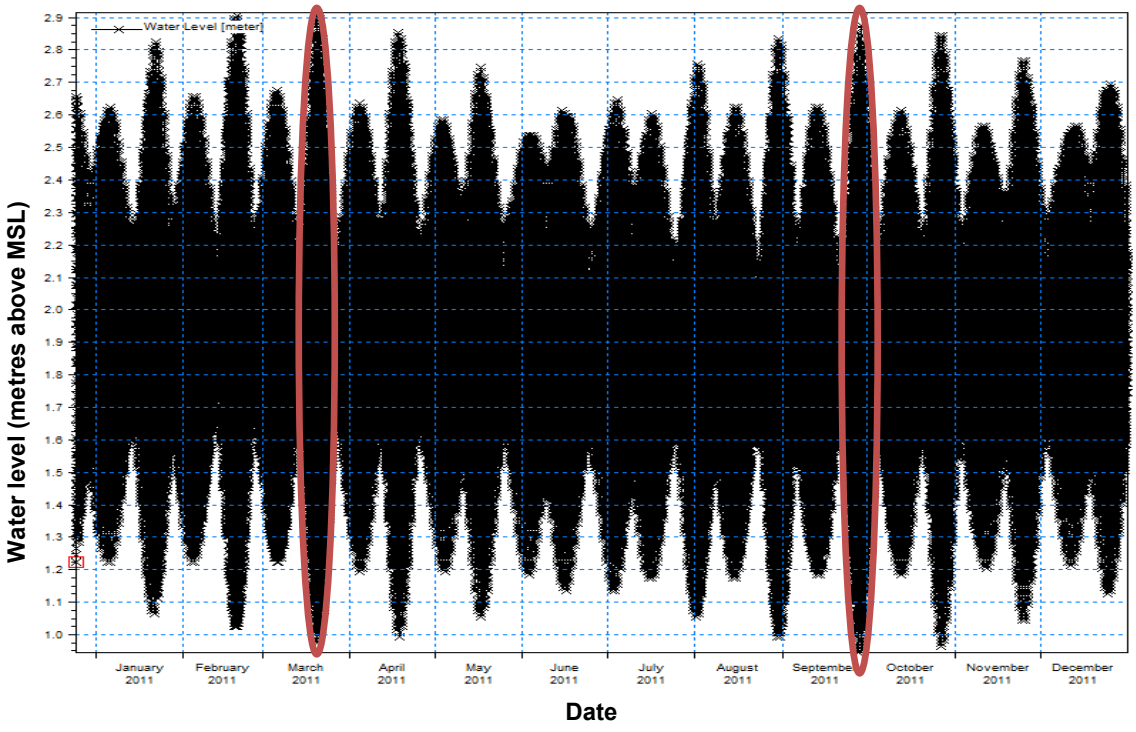

Figure 3-3: **Example of one year astronomical tidal variation indicating extreme high and low tides twice a year**

Table 3-1 (Van der Merwe, 1994) provides the periods for the abovementioned extreme tidal conditions and the relative fluctuation of the water level as a percentage.

Table 3-1: Characteristics of the principal tide-producing force constituents (Van der Merwe, 1994)

Name	Period (in solar hours)	Relative size of contribution (%)
Semidiurnal		
• Principal lunar	12.42	100
• Principal solar	12.00	47
• Large lunar elliptic	12.66	19
• Lunar-solar semi-diurnal	11.97	13
Diurnal		
• Lunar-solar diurnal	23.93	58
• Principal lunar diurnal	25.82	42
• Principal solar diurnal	24.07	19
• Large lunar elliptic	26.87	8
Long Period		
• Lunar fortnightly	327.9	17
• Lunar monthly	661.3	9
• Solar semi-annual	4383	8

Due to the closed nature of the Lagoon, water level variations caused by the tides will result in pressure differences. Water then flows from higher pressures at high water levels to lower pressures at low water levels to create an equal pressure distribution in the water mass. Greater pressure differences will result in larger in- and outflow volumes for a constant time-period of more or less 12.42 hours, as mentioned in **Table 3-1** for principal lunar semidiurnal tides. These in- and outflows are similar to the breathing action of a lung, as referred to in **Section 2.1**.

If it is assumed that the cross-section of the boundary where water enters and exits the lagoon remains constant and thus the area of the cross-section being constant, it can be concluded that greater pressure differences due to tidal variation, resulting in greater in- and outflows, will result in greater velocities at the mouth of the Langebaan Lagoon.

These high velocity conditions have more energy and will thus result in greater sediment transport.

3.2.2 Climate change

Tidal variation in Big Bay would determine the velocities and sediment transport in the Langebaan Lagoon. For this study, water level fluctuation was limited to long period oscillation, thus excluding wave action. In **Section 3.2.1**, water level fluctuations due to tidal dynamics are explained; however, a global rise in sea level might influence the hydrodynamics and sediment transport in the lagoon. This variation is identified as a gradual change which occurs with more frequent dramatic events (Bindschadler, 2006).

There are only three datasets in South Africa with records of sufficient length that can be used to determine the historical effects of sea level variations. These datasets are located at Port Nolloth, the South African Navy's Hydrological Office at Simon's Town (Cape Town) and Durban. From these datasets it has been identified that an average change of the sea-level is as indicated in **Table 3-2** (Cartwright, 2011).

Table 3-2: Climate change impacts on sea level in South Africa (Mather, 2008)

Station	Change in Sea Level (in mm per year)	Change measured between
Western Cape	1,2 (± 0,4)	1962 to 1987
Durban	2,7 (± 0,05)	1970 to 2003

Major changes in the sea level rise along the west coast of South Africa can be described as consistent when compared to other changes globally. This is due to the increase in frequent, intense south-west storms experienced along the west coast of South Africa during spring and autumn, when the tidal difference is at its highest as a result of the two astronomical tides in March and September. This increase in intensity of the storms results in an increase in wave heights and which increases coastal erosion during these storm events (Mather, 2008).

Changes occurring along the coastline can be directly associated with the human settlement along the coast, leading to removal of coastal dunes, stabilization of sand which used to feed and replenish beaches and sand mining to restore damaged coastlines. All these factors contribute to the vulnerability to sea level rise at the

coastline. More frequent, intense storms on a more vulnerable coastline would result in an increase in coastal erosion during storms.

For the area situated between Melkbos Strand, 35 kilometres north of Cape Town, and Swakopmund, Namibia, the impacts of sea-level rise has been considered as negligible, but can have a negative impact on Saldanha Bay settlements, the sea wall and possibly alter the estuary and Lagoon habitats (Cartwright, 2011). The expected sea-level rise for 2090 at this location is 0.4 metres, as illustrated in **Figure 3-4** (Church et. al., 2011).

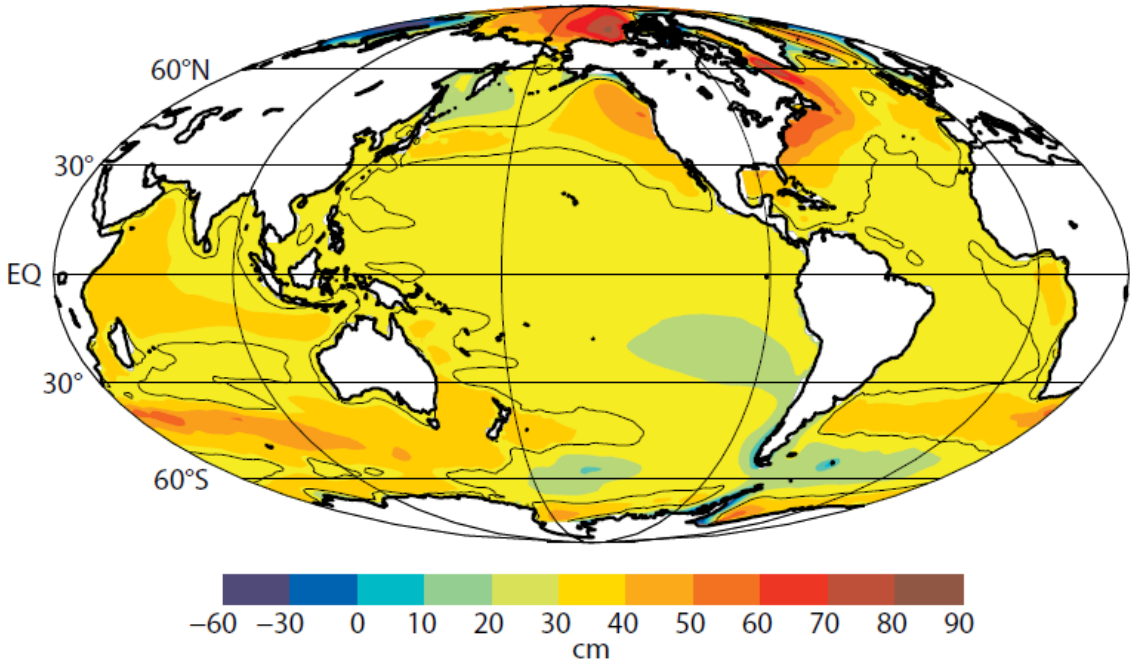

Figure 3-4: Expected sea-level rise for 2090, based on sea-levels for 1990 (Church et. al., 2011).

As mentioned previously, a global rise in sea level is not known to be a gradual, peaceful change over a period of time, but rather a change going hand in hand with dramatic events, e.g. storms. Therefore, a third fluctuation in water level was identified for the numerical model, due to the impact of storm surge.

During this investigation, storm events were modelled as a single scenario, and the water levels, as expected in 2090, were modelled as a separate scenario. Due to the time required for two-dimensional modelling, a single model running for such a long period of time, integrating storm surge events with a sea level rise could not be

modelled. It would be recommended that further investigations based on sea level rise would integrate storm events with a global rise in sea level, because of the morphological effects storm surge events could have on the bathymetry.

3.2.3 Storm surge

During the discussion on climate change in **Section 3.2.2**, it was mentioned that a change a sea level would not be a gradual change, over time, but rather a change associated with dramatic events, e.g. storms. Therefore, storm surge were included in this investigation.

The following processes have been identified as a source for these storm events included in this investigation. They have been identified as (Harris, 1963):

- Pressure effect
- The effect of waves
- Direct wind effect

During this investigation, the sources were limited to storm surge as a result of a pressure effect and a direct wind effect.

The pressure effect, also known as pressure set-up, is the water level change due to a change in the atmospheric pressure. In the open ocean, water levels will rise at low pressures and fall in regions where high pressures occur. The rising water level counteracts the lower atmospheric pressure and vice versa during high atmospheric pressures. This pressure effect results in a 10 millimetre increase in water level for every millibar decrease in atmospheric pressure (Harris, 1963).

The second source for storm surge identified during this investigation is surface winds. The effect of wind on surface water generates a hydrodynamic current perpendicular to the direction of the wind, known as *Ekman Transport*. When a wind is directed parallel to the coastline, water is either pushed towards of pulled away from the coastline. This phenomenon is known as upwelling, illustrated in **Figure 3-5**.

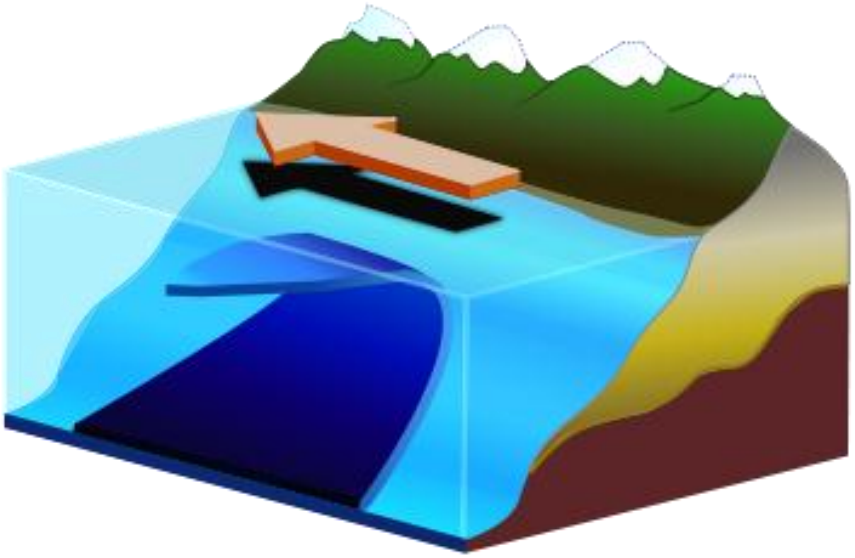

Figure 3-5: Upwelling

During this investigation, recorded water levels were analysed to identify the greatest water levels for each year. From this information, extreme tidal water levels were identified and implemented at a tidal peak in the numerical model to simulate storm surge or storm tide levels.

3.2.4 Wind

A basic understanding of the effect of wind on a water surface would provide a better understanding to the hydrodynamic driving force in Saldanha Bay. The Ekman transport theory introduces the effects of wind on a water surface and flow patterns in shallow water. A balance between Coriolis forces and the momentum transfer between the wind and the water surface cause a flow in a 45 degree angle to the downwind direction. This deviation differs to the right for the Northern Hemisphere, and left for the Southern Hemisphere. However, the magnitude of the flow decrease and the deviation in direction increase with an increase in depth, resulting in a spiral known as the Ekman spiral. The layer between the surface and the lowest point of the spiral, where the influence of the wind dissipates or a section thereof, is known as the Ekman layer.

As illustrated in **Figure 3-6 c**., the resultant of the spiral will be perpendicular to the left of the wind direction for the Southern Hemisphere and to the right for the Northern Hemisphere.

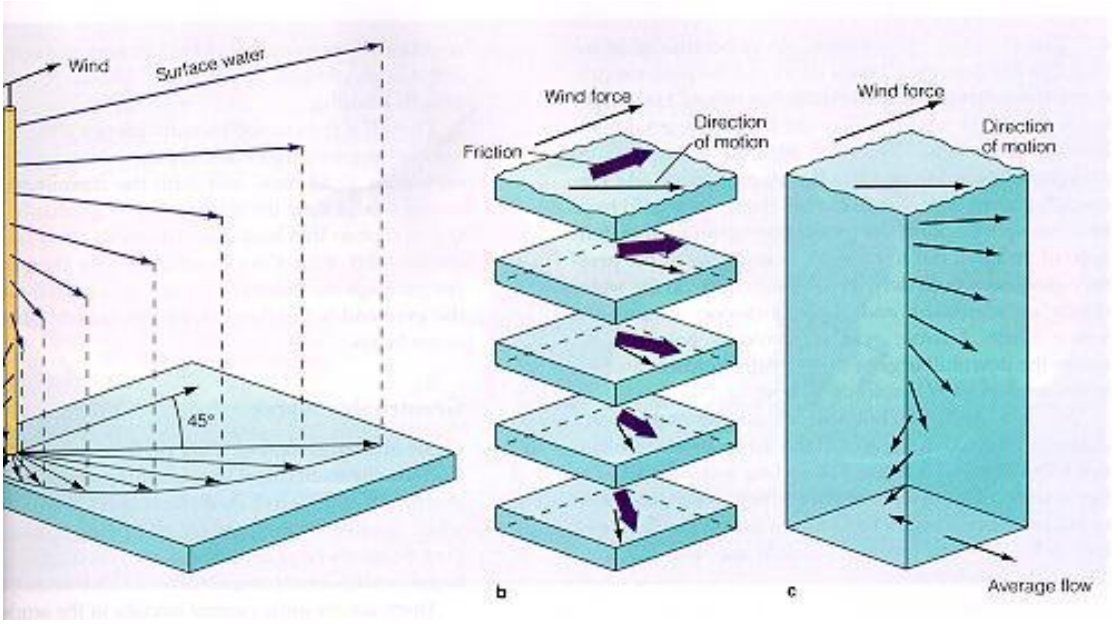

Figure 3-6: Ekman transport

Well defined spirals are very rarely observed due to assumptions on which the theory is based. These include the following (Pond & Pickard, 1983):

- No boundaries
- Infinitely deep water to avoid bottom friction
- The eddy viscosity in a water column is constant with depth
- A steady wind blowing for a long time
- Homogeneous water and a level sea surface
- A constant Coriolis parameter (= 2Ωsinφ)

where

Ω	A function of the angular speed of rotation of the Earth around its axis
Φ	Geographical latitude

Ekman velocities can be described by the following equations (Beer, 1983):

$$u_E = \pm v_0 cos\left({\pi}/{4} + {\pi z}/{D_E}\right) exp\left({\pi z}/{D_E}\right) \quad \textbf{(3-1)}$$

and

$$v_E = v_0 sin\left({\pi}/{4} + {\pi z}/{D_E}\right) exp\left({\pi z}/{D_E}\right) \quad \textbf{(3-2)}$$

where

$$v_0 = {\left(\sqrt{2\pi\tau_y}\right)}/{(D_E \rho |f|)} \quad \textbf{(3-3)}$$

u_E	Ekman velocity in the x-direction
v_E	Ekman velocity in the y-direction
τ_y	Wind stress on the sea surface in the y-direction
D_E	The Ekman depth or the depth where friction influence which varies with latitude due to the effects of Coriolis force:

$$D_E = \pi\left(2A_z/|f|\right)^{1/2} \quad \textbf{(3-4)}$$

A_z The coefficient for the eddy viscosity, for vertical mixing, as a property of the flow and not the fluid

$|f|$ Friction coefficient

In water depths where the Ekman depth is deeper than the actual water depth, the effect of frictional stress from the seabed is included to the effects of pressure forces and Coriolis forces. These frictional forces will impact the effects of the Coriolis force and therefore result in an Ekman current spiral forming at the bottom Ekman layer (Pickard & Emery, 1990). The Ekman layer at the top and the Ekman layer at the bottom overlap in shallow water and tend to cancel out. Therefore only the pressure force remains, resulting in currents in the direction of the wind instead of currents perpendicular to the wind direction (Pond & Pickard, 1983). **Table 3-3** indicates the relationship between the surface flow direction and the net flow direction in the water column, in comparison with the wind direction for a specified relationship between the water depth, H, and the Ekman depth (Pickard & Emery, 1990).

Table 3-3: Net flow direction in the water column at various depths due to wind, as experienced in the Southern Hemisphere (Pickard & Emery, 1990)

H/D_E	Surface flow direction	Net flow direction
1 or more	45°	90° left of wind
0.5	45°	60° left of wind
0.25	22°	25° left of wind
0.1	3°	6° left of wind

3.3 Sediment composition

The construction of the causeway and the jetty resulted in alterations of the circulation and wave energy in Saldanha Bay and Langebaan Lagoon. Even though wave energy were excluded from this investigation due to the hydrodynamic nature of the Langebaan Lagoon, the impact of a change in littoral drift due to the change in wave energy on the coastline of Saldanha Bay were included in the literature study to provide an understanding of the sediment transport dynamics in Saldanha Bay and the alterations to the sediment transport dynamics due to the construction of the causeway and the jetty.

Changes in wave energy can be illustrated in **Figure 3-7** (Flemming, 1977), indicating the distribution of wave energy across the Bay prior to harbour construction. The area indicated as "semi-exposed" to the north of the Bay have been sheltered after the construction of the causeway, resulting in less wave energy on the coastline in this area. After the construction of the causeway, wave peak periods of 10 s to 12 s were recorded with a wave height of 1.1 m at the entrance to Saldanha Bay and 2.3 m outside Saldanha Bay. This change in energy distribution would affect the sediment transport, sediment particle size distribution and possibly the sediment composition in Saldanha Bay as well as the lagoon.

The sediment particle size distribution, as in the 1977 report by Flemming prior to the construction of the causeway and the jetty, are available in **Appendix A**. These figures indicate that the majority of the sediment particles in Saldanha Bay are very fine (0.063 mm to 0.125 mm) in diameter, at the mouth and the west of the lagoon medium sand particles (0.25 mm to 0.5 mm) are dominant while fine sand (0.125 mm to 0.25 mm) can be located in the east of the lagoon. The area at the deepest location of the lagoon and the location where the largest velocities have been recorded in the past between Schaapen Island and the town of Langebaan contain some coarse material (0.5 mm to 1 mm) (Flemming, 1977).

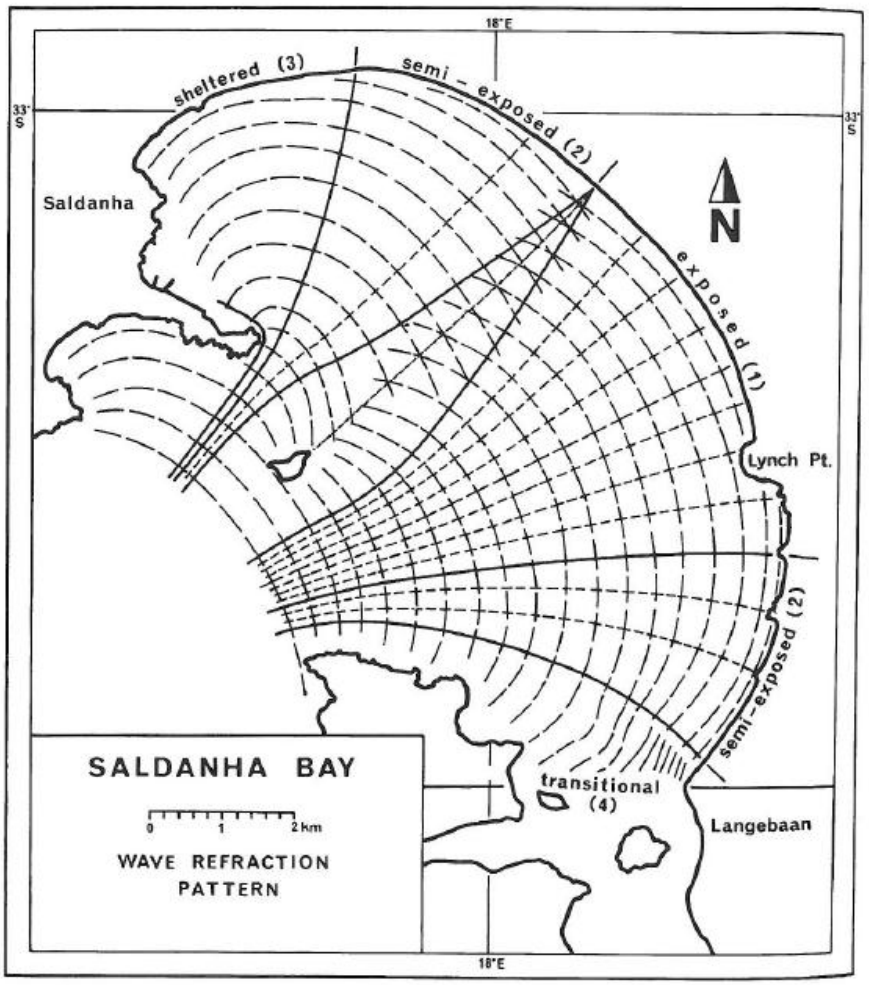

Figure 3-7: Wave energy in Saldanha Bay prior to the construction of the causeway and jetty (Flemming, 1977)

In 1989 investigations on the sediment properties were done. These investigations consisted of surveys, primarily focusing on the traces of mud in the sediment, which indicated the influence of dredging activities during the construction of the causeway and the jetty during the early 1970's on the sediment dynamics of Saldanha Bay.

Additional sediment investigations were done during 1999 after maintenance dredging occurred in Small Bay adjacent to the jetty. An increase in mud has been observed in the areas of the multi-purpose quay, the main channel's end, around the ore jetty, the Yacht Club basin and the mussel farm located in Big Bay adjacent to the jetty. Big Bay remained largely unaffected by these events in Small Bay due to the current velocities flushing Big Bay from these small particles. The effects of the 1999 dredging seemed to

have been recovered by 2000 and 2001. Results from the 2000 survey were unrealistic to the observed trend and were therefore considered to have possible processing errors (Clark et. al., 2009).

In 2004 a near full recovery could be observed at five to six of the sites in Small Bay. The Multi-purpose quay, adjacent to the main channel, which is the deepest section of Small Bay, had a substantial amount of mud (smaller than 0.063 mm) in the sediment (Clark et. al., 2009).

Maintenance dredging in the period of 2007 and 2008 again increased the mud contents in the sediments samples, similar to the effect from earlier samples, especially in the areas off the Yacht Club and the Multi-purpose quay. Sheltered sites indicated deposition of fine-grained materials over a long period of time. From 2000 to 2008 the deposition of mud and other fine particles in Big Bay, including the end of the jetty, were minimal due to the higher velocities and stronger wave action than experienced in Small Bay.

Even though there has been a minor increase in mud traces from 2004 to 2008, the effects from the construction in Saldanha Bay and maintenance dredging during this period could not be recognized. However, investigations have concluded that metal traces from the activities in the harbour have been identified in the lagoon.

Settling of mud particles were also inhibited at exposed areas along the coastline during dredging activities, due to the effect of wave action. Wave action resulted in particles spread into the lagoon or even out to sea. However, it has been stated that the maximum deposition thickness in the Langebaan Lagoon is insignificant (Luger et al., 1998). However, activities in Saldanha Bay can possibly influence the hydrodynamics, sediments composition and sediment transport in the Langebaan Lagoon.

3.4 Coastal rehabilitation

Various changes in the coastline have occurred along the coastline of Saldanha Bay and at the mouth of the Langebaan Lagoon. These changes include the erosion of Langebaan Beach. Luger et al. stated that the environmental conditions influencing the beach erosion included deep-water swell, locally generated sea, wind driven currents and tidal currents (Luger et al., 2006)/

Of the above mentioned factors, this investigation was aimed to determine the impacts of wind driven currents and tidal currents. Note that during a morphological investigation on the erosion of Langebaan Beach, all of the abovementioned should be investigated to accurately investigate the erosion events.

An investigation based on three aerial photographs prior to coastal rehabilitation attempts illustrates the changes which occurred at the Langebaan Lagoon mouth.

The first photograph in **Figure 3-8**, dating back to 1960, illustrates the conditions prior to the construction of the causeway and the jetty. Minor development is visible near the town of Langebaan and sandy beaches are located between Schaapen Island and Langebaan and north of Langebaan.

Figure 3-8: 1960 aerial photograph of the Langebaan Lagoon mouth

Conditions, more or less a decade after the construction of the causeway and the jetty in Saldanha Bay, are illustrated in the 1988 aerial photograph provided in **Figure 3-9**. The town of Langebaan has expanded since the 1960 conditions, possibly as a result of an increase in work opportunities due to the upgrading of the harbour. Beachfront properties resulting in the removal of vegetation along the northern beach are visible. This encroachment of housing, due to an increase in tourism and recreational attractions, and additional access roads to the beach possibly resulted in instability of the shoreline and were potentially a cause for the major shoreline problems. This encroachment interrupts the land-shore sediment interchange, which results in less material available for cross-shore sediment transport due to wave action and thus the erosion of the beaches which also results in steeper slopes in the beach areas. The erosion of Langebaan Beach from the north can be identified. The shape of Langebaan

Beach has transformed from a trapezoidal shape to a more triangular shape with major alteration on the northern side of the beach. A sandy beach located to the southern end of Langebaan can be identified in the 1988 photograph, but is absent in the 1960 photograph. The poor visibility of the main channel between Schaapen Island and Langebaan in the 1960 aerial photograph limits the analysis on the changes in the main tidal channel from 1960 to 1988.

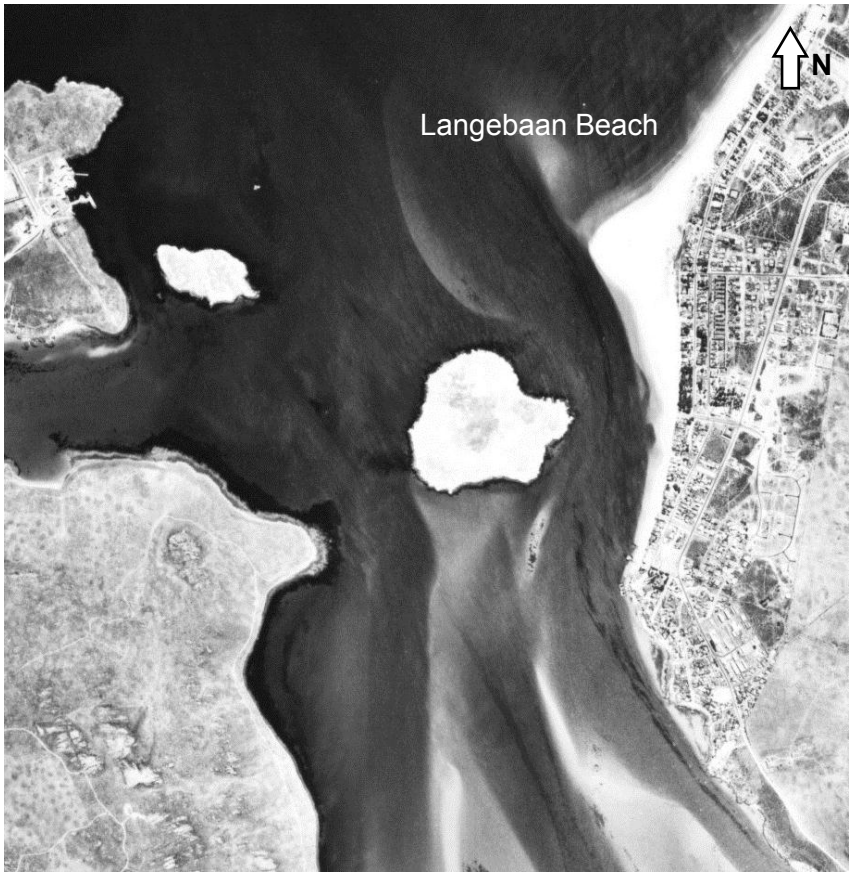

Figure 3-9: 1988 aerial photograph of the Langebaan Lagoon mouth

The 2000 aerial photograph, provided in **Figure 3-10**, illustrates the possible long-term implications of the alterations to the hydrodynamics and sediment transport as a result of the causeway and jetty constructed in Saldanha Bay. Complete erosion of the beach to the north of Langebaan can be identified with temporary protection along the beachfront properties in the form of large boulders to dissipate the hydraulic energy and prevent further erosion. Erosion on Langebaan Beach is much more extensive than previously, with the triangular shaped beach shifting south to form an acute triangular shape. This is due to the erosion from the north, forcing the erosion of the northern section of the

beach. The main channel of the lagoon has moved westward and a sandbank seems to appear next to the location of Langebaan Beach (Luger et al., 2006).

Figure 3-10: 2000 aerial photograph of the Langebaan Lagoon mouth

From these three aerial photographs, the major cause of the erosion seems to originate from Saldanha Bay and not the lagoon, in the form of long shore currents, generated by means of waves. However, even though waves were identified as the cause for the erosion of Langebaan Beach, this investigation was focused on the effect tidal and wind forcing had on the hydrodynamics and sediment transport patterns at the mouth of the Langebaan Lagoon, prior to and after the harbour developments. The main tidal channel of the lagoon, passing between Langebaan and Schaapen Island have moved in a westward direction, away from the location of Langebaan Beach, and therefore does not

seem to erode Langebaan Beach from the south. A change in depth could not be confirmed due to the lack of historic information on the Langebaan Lagoon mouth.

The change in shape of the beaches could be a result of various tidal levels when the photographs were taken. However, from the last photograph erosion protection structures are visible toward the north-eastern beach, indicating alterations along the coastline.

A first solution to counter the erosion of the beaches was the construction of a rock revetment structure over a 1.4 km stretch of the eroding Langebaan Beach. This only proved to be a short term solution and erosion continued to cut back on sand beaches adjacent to the rock revetments. Energy were no longer dissipated due to sediment transport, but rather transferred and focused on the areas where sand is available for transport.

Alternative methods were investigated to prevent the on-going erosion and the rehabilitation of the beaches that experienced erosion. The most appropriate methods had to include a natural restoration of the beaches by altering local hydrodynamics to prevent further erosion.

In 2003 two structures were designed to alter the local hydrodynamics in an attempt to rehabilitate Langebaan Beach, as indicated in **Figure 3-11**. These structures, known as groynes consisted of Geotextile Sand Containers (GCS's) and are similar to erosion protection structures often used in river systems to counter scouring at locations where high velocities are expected. The local hydrodynamics along the coastline, due to wave action, are altered in an attempt to dissipate energy by decreasing flow velocities and result in the deposition of sediments which were transported by means of littoral drift. This deposition would, in the long term, result in the rehabilitation of the beach.

Figure 3-11: Groynes constructed at Langebaan Lagoon as on 13 April 2009

The first groyne was constructed in 2005 at the mouth of the Langebaan Lagoon. This 250 metres long, curved shaped structure serves as a collection bay were the sediment would be trapped, settle and rehabilitate the beach.

Groyne 2, constructed in 2007, is located to the north of the first groyne and is a straight structure stretching for 360 metres perpendicular to the coastline. The effects of these structures can be seen on the satellite imagery in **Figure 3-12**, **Figure 3-13** and **Figure 3-14**. In each of these figures Schaapen Island is visible in the bottom left corner.

Figure 3-12: Satellite image of Langebaan Beach on 18 February 2004

Figure 3-13: Satellite image of Langebaan Beach on 7 August 2005

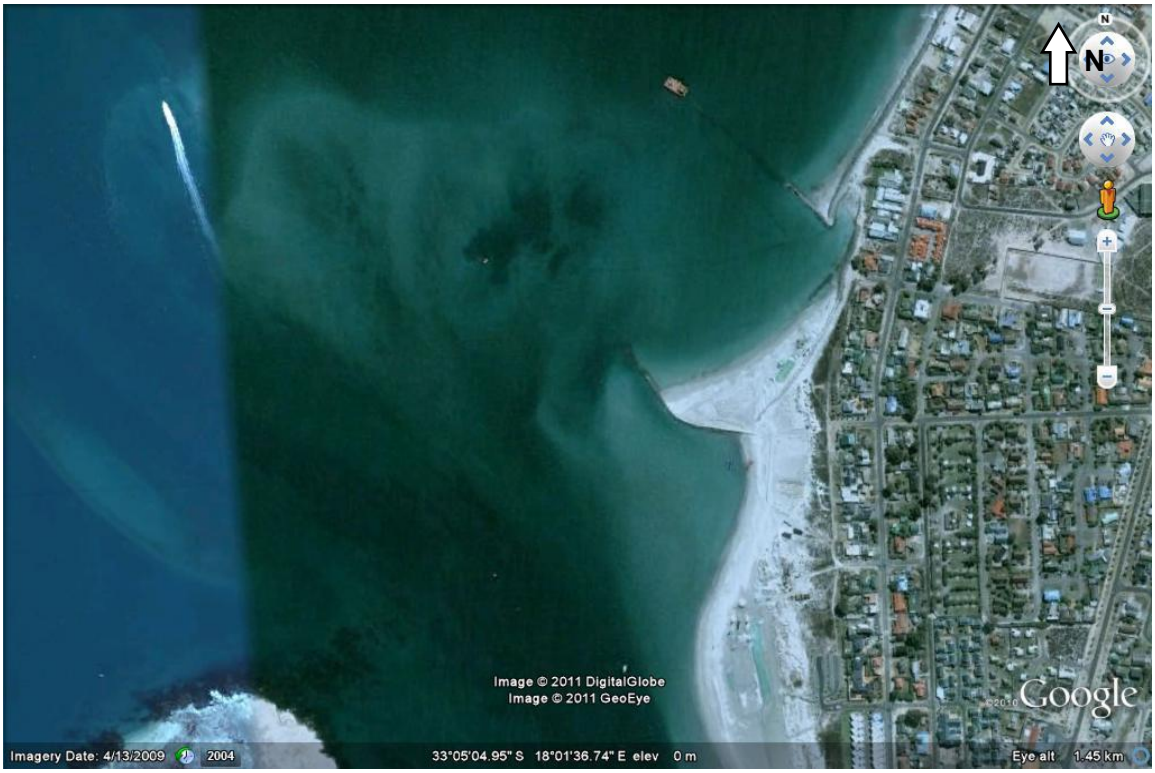

Figure 3-14: Satellite image of Langebaan Beach on 13 April 2009

Other areas which experienced erosion of the beaches causing harm to properties and possible hazards to the environment are located at Club Mykonos Holiday Resort at Langebaan, which is also an example of beach encroachment, as illustrated in **Figure 3-15**. The encroachment of developments on the coastline resulted in the removal of vegetation and dune destruction, which increased the vulnerability of the beaches. In 2008 beach front houses became exposed to the erosion and environmental hazards such as sewage tanks located three to four metres from the dune edge were exposed.

Figure 3-15: Aerial photographs of 1960, 1988 and 2000 at the location of Club Mykonos indicating beach encroachment

Previous studies on the area identified the following possible reasons for the erosion at these locations (Clark et. al, 2009):

- Change in the hydrodynamic patterns, including the change in wave condition, in Saldanha Bay due to the construction of the causeway and the jetty in the bay, as well as other large developments
- Cut off of the natural sand supply due to the dense development in the area
- Destruction of vegetation on dunes, enhancing erosion
- Discharge of storm water in frontal dunes area
- Steep slopes caused by housing developments cutting back into the dunes
- High wave actions and tidal conditions associated with effects of global warming

As mentioned previously, a possible reason for the erosion of the coastline includes the alteration in hydrodynamic patterns in Saldanha Bay. These include the alterations to wave action on the coastline in Saldanha Bay, due to the construction of the causeway, as mentioned in **Section 3.3**.

Even though this investigation focused on the morphological effects of the causeway and the jetty, rehabilitation structures could not be included in the numerical model due to their size relative to the area modelled and the grid used during the numerical model. However, locations of rehabilitation structures provided an indication of areas where extensive erosion has occurred and where high sediment transport rates could be expected in the numerical model.

4 METHODOLOGY

The literature review provided in **Section** 3 provides an understanding of the hydrodynamic conditions and sediment characteristics as concluded from previous studies. These conclusions include the identification of the hydrodynamics in Langebaan Lagoon dominated by the tidal oscillations and hydrodynamics in Saldanha Bay primarily dominated by wind. The sediment properties for the Saldanha Bay and Langebaan Lagoon systems are medium to fine particles, with small areas indicating coarser materials consisting of larger sand particles. Sand particles are mostly non-cohesive materials, but traces of mud have been identified in Small Bay.

Even though sediment transport along the coastline are dominated by littoral drift as a result of wave action, the sediment transport investigated during this study was focused on the primary circulation forcing factors present in Saldanha Bay and Langebaan Lagoon, identified as tidal variations and wind forcing. The omission of waves during the numerical model would not provide realistic sediment transport rates, but would provide an indication on the contribution tidal and wind forcing and a change in the hydrodynamic circulation made to the sediment transport rates at the Langebaan Lagoon mouth.

As a result to these conclusions mentioned above, a two-dimensional numerical model was selected, based on water level fluctuations generated by the tidal oscillations and wind events, excluding littoral drift as a result of wave action. Two-dimensional modelling would be adequate to investigate the conditions in the main channels of the Langebaan Lagoon, where a more uniform water column is expected.

A third condition had to be defined, known as the bathymetry. The bathymetry of the numerical model is a representation of the bed topography at the area of interest, consisting of a grid of cells. Each of these cells contained information for the specific area, e.g. the depth. This bathymetry was generated from hardcopy maps and GIS data provided by the CSIR and SA Navy. However, the data from these two sources were outdated, thus limiting the accuracy of the numerical model.

Sediment transport models were used and were coupled to the results from the hydrodynamic model on a calculation time step basis. These sediment transport models provided an indication of the rate of sediment transport across the bathymetry and morphology of the bathymetry during various extreme conditions in the tidal water levels and the wind.

However, these numerical models had to be calibrated to recorded data before various scenarios could be implemented and the impact of the causeway and jetty on the hydrodynamics in the lagoon mouth were determined. For this calibration process, a field survey was required.

Even though the numerical model had to be calibrated before the investigation on various scenarios, it could be utilized to identify the locations where high velocities can be expected. Based on the results from the uncalibrated numerical model, 31 locations were identified for the recording of water depth, water velocity, flow direction, suspended sediment transport and bed-load sediment transport data. Each of these locations was targeted to be surveyed twice, once during flood tide and once during an ebb tide. However, due to time constraints, only 34 surveys were done in total.

Surveys based on the water depth, flow direction and average velocity of the water column were done by a single instrument, an Acoustic Doppler Current Profiler (ADCP) Rivercat 15. The two sediment transport surveys were done with a suspended sediment sampler for suspended sediments and bed-load sediment samples for sediment particles transported along the lagoon bed.

Water levels were also surveyed to determine the accuracy of the lag due to the water level change implemented at the entrance to Saldanha Bay. These surveys were done at a fixed point.

Finally, results from the field survey were analysed and calibration of the numerical model could be done. For the calibration of the hydrodynamic model, the roughness of the bathymetry was used and the sediment transport model was calibrated by means of the sediment particle parameters. These sediment parameters were compared to the results from the survey.

Once an acceptable calibration was achieved, the various scenarios could be implemented. For these scenarios, extreme water levels and extreme wind events had to be identified. Extreme wind conditions were also implemented in the two dominant wind directions and a third wind direction, indicating the longest fetch towards the location of Langebaan Beach.

Extreme water level conditions were based on storm tides, providing an extremely high tidal peak and also the effect of a global sea level rise, based on the results from the literature review in **Section 3.2.2**.

The abovementioned scenarios were based on the analysis of recorded tidal and recorded wind data.

5 NUMERICAL MODELLING

5.1 Introduction

When facing complex situations with multiple variables possibly having an influence on the flow, scaled laboratory models can be constructed for the investigation of pre-defined problems or to determine the weight of each of these variables. This solution also provides a more practical approach to modelling. However, small alterations in the model can result in great cost implications. A more cost effective method would include the utilization of mathematical models. These calculations can either be done in one-, two- or three-dimensions, depending on the complexity of the situation at hand.

When calculations are done in two and three-dimensions, the entire area of interest is divided into cells. Differential equations are solved for a central point in each of these cells with results from one cell determining the conditions for the next. Therefore, calculations for a large area can become time consuming, even for a steady state situation. If a time variable is added to the calculations, for example a change in wind or water levels, the calculations become more complex and time consuming.

Computers, being able to process information and execute calculations at high speeds, enable the two and three-dimensional investigation of complex systems in a more practical period of time. Not only are simulations run in a much shorter period of time, but the results can be better visualized in a user-friendly environment, assisting in the understanding of the results.

However, this virtual demonstration of the reality needs to be compared with actual data to ensure accuracy of the simulations. If this is not done, the results could provide unrealistic results which have no value to the problem at hand. Various software approaches the accuracy determination and calibration aspect of numerical modelling differently.

A large variety of software packages are available for two-dimensional simulations. The parameters available and deliverables required from the package should be identified as to ensure that the right choice in software is made.

5.2 Choice of software

A large variety of two-dimensional modelling software was available for the calculations of complex flow. The model chosen should be able to simulate large, complex areas of a coastal nature. The criteria used for the choice of software include:

- Hydrodynamic modelling with wind and water level variations as input parameters
- Sediment transport of non-cohesive sand particles
- Morphological calculation
- Availability of software

Software meeting all of the abovementioned criteria is available as either freeware, with no cost implications for the use of the software, or as licensed software, which limits the capabilities of the software to the available licensed packages. One of the major differences between the above-mentioned is the technical support structure.

For more complex flow models, the use of licensed software with a good technical support structure is advised. This support structure would be of assistance in the identification of error messages, the analysis thereof and the cause of unrealistic results and the understanding behind the dynamics of the software.

MIKE21, developed by DHI Water and Environment, is a professional engineering package able to model free-surface flows in two dimensions. The application of this software includes the modelling of:

- Lakes
- Estuaries
- Bays
- Coastal areas

This software package allows two-dimensional hydrodynamic modelling by means of calculations done on a single grid, multiple grid or flexible mesh across the area of interest with wind and water level fluctuation as driving forces. An additional “non-

cohesive sediment transport" model was used for the sediment transport calculations. Even though a flexible mesh would be ideal to exclude cells with no influence on the model, typically on land, the software choice was limited to the single grid due to availability.

Another software package also considered was the MIKE21C modelling software, specializing in river morphology. This package is, however, limited to the application of hydrodynamics and sediment transport, where the MIKE21 package can include waves and ecological investigation at a later stage if required.

5.3 Hydrodynamic model

5.3.1 Capabilities of the software

The selected modelling software, MIKE21 by DHI Water and Environment, has the ability to simulate unsteady flow by means of mathematical calculations, taking into account density variations, bathymetric parameters and external forcing factors. This software is useful for the modelling of shallow water which is well mixed due to tidal and wind currents, providing homogeneous salinity and temperatures in the water columns.

Other applications of the software include:

- The assessment of hydrographical conditions for design, construction and operation of structures and plants in stratified and non-stratified waters
- Environmental impact assessment studies
- Coastal and oceanographic circulation studies
- Optimization of port and coastal protection infrastructures
- Lake and reservoir hydrodynamics
- Cooling water, recirculation and desalination
- Coastal flooding and storm surge
- Inland flooding and overland flow modelling
- And forecast and warning systems

The focus during this study would be the utilization of the software for the purposes of coastal circulation and sediment transport forced by water level fluctuations and wind forcing on the water surface.

5.3.2 Hydrodynamic calculation

MIKE21's hydrodynamic mathematical solutions are based on two-dimensional Reynolds averaged Navier-Stokes equations. These are subject to the assumptions of Boussinesq and hydrostatic pressure. Therefore, the model consists of solutions involving the following equations, and closed by means of a turbulent closure scheme (DHI Water and Environment, 2006):

- Continuity
- Momentum
- Temperature
- Salinity
- Density

The abovementioned equations can be expressed as follow (DHI Water and Environment):

Local continuity equation:

$$\partial u/\partial x + \partial v/\partial y + \partial w/\partial z = S \quad \textbf{(5-1)}$$

where

x, y, z	Cartesian coordinates
u, v, w	Flow velocity components for the x-, y- and z-components respectively
S	Magnitude of point source discharge

The x- and y-components of the momentum equation, respectively:

$$\partial u/\partial t + \partial u^2/\partial x + \partial vu/\partial y + \partial wu/\partial z = fv - g\,\partial \eta/\partial x - \partial p_\alpha/p_0\partial x - g/p_0 \int_z^\eta \partial \rho/\partial x\,\partial z + F_u + \partial/\partial z\left(v_t\,\partial u/\partial z\right) + u_s S \quad \textbf{(5-2)}$$

$$\partial v/\partial t + \partial v^2/\partial y + \partial uv/\partial x + \partial wv/\partial z = -fu - g\,\partial \eta/\partial y - \partial p_\alpha/p_0\partial y - g/p_0 \int_z^\eta \partial \rho/\partial y\,\partial z + F_v + \partial/\partial z\left(v_t\,\partial v/\partial z\right) + v_s S \quad \textbf{(5-3)}$$

where

x, y, z	Cartesian coordinates
u, v, w	Flow velocity components for the x-, y- and z-components respectively
t	Time
g	Gravitational acceleration of 9.81m^3/s
F_u, F_v	Horizontal diffusion terms

General transport-diffusion equations for the transports of temperature and salinity:

$$\partial T/\partial t + \partial uT/\partial x + \partial vT/\partial y + \partial wT/\partial z = F_T + \partial/\partial z\left(D_v\,\partial T/\partial z\right) + \hat{H} + T_s S \quad \textbf{(5-4)}$$

$$\partial s/\partial t + \partial us/\partial x + \partial vs/\partial y + \partial ws/\partial z = F_s + \partial/\partial z\left(D_v\,\partial s/\partial z\right) + s_s S \quad \textbf{(5-5)}$$

where

T	Temperature
s	Salinity
T_s	Temperature of source
s_s	Salinity of source
t	Time
D_v	Vertical turbulent (eddy) diffusion coefficient
$\hat{H}$	Source term due to heat exchange with atmosphere

Horizontal diffusion terms are defined by:

$$(F_T, F_s) = \left[\partial/_{\partial x}\left(D_h\, \partial/_{\partial x}\right) + \partial/_{\partial y}\left(D_h\, \partial/_{\partial y}\right)\right](T, s) \qquad \textbf{(5-6)}$$

where

F_T, F_s, F_c	Horizontal diffusion terms
D_h	Horizontal diffusion coefficient
h	Depth

The abovementioned equations consist of an integration factor including a variation in depth, ideal for three-dimensional modelling. This factor will become a constant for two-dimensional calculations, due to a constant distribution of parameters assumed in the water column. Therefore, no variations in depth are taken into account for two-dimensional calculations (DHI Water and Environment, 2006).

The spatial analysis for these primitive equations is performed by means of a cell-centred finite element method. These two-dimensional elements were rectangles for the chosen MIKE21 model, but can also be triangle or quadrilateral elements for flexible mesh models. The shape of these cells is defined during the construction of the modelling area, also known as the bathymetry.

5.3.3 Input parameters

The input parameters of MIKE21 hydrodynamic models can be sub-divided into the following categories:

- Domain and time parameters
- Initial conditions
- Boundary conditions
- Driving forces
- Calibration parameters

The first mentioned, domain and time parameters contain the overall information on the model and specific simulation. This information includes a connection of a bathymetry, the overall period simulated by the model and the time steps used for the hydrodynamic calculations.

The bathymetry of a model is a representation of the area of interest, an “image” consisting of cells containing the depth at a specific point. Other data also included in the bathymetry is the geographical location of the site.

Water level information and the velocity components at the initiation of the simulation are of great importance. These values can either result in a smooth start to the model, or a sudden wave moving through the bathymetry. This wave action can also have negative implications on the sediment transport model and possibly result in a change of the bathymetry.

The initial water levels were derived from the water level time series, utilized in the model to simulate the tidal fluctuations, for the date requested at the first time step. This water level was applied to the entire bathymetry and water level fluctuations or flows were then generated from the boundary. The boundary of the model is the location where water can enter or exit the model and can either be user-specified or program detected. A third option for the boundary conditions of the model is a closed model, where no water enters or exits the model.

Additional driving forces, e.g. sources and sinks, wind and wave radiation stresses can also be incorporated into the model. Wind conditions require the wind direction and velocity when implemented as a driving force of currents. For this investigation only extreme water level fluctuations due to tides and the effect of wind were simulated, as defined in **Section 3.1**.

To enable the effect of wind on water, a friction coefficient is required. This can either be entered as a constant value or a value determined by the wind velocity. The wind friction coefficient can also be used as calibration parameter, along with bed resistance parameters, defined by a Chezy or Manning M value, and momentum dispersion coefficients. During this investigation, a program default wind friction coefficient was implemented.

5.3.4 Bathymetry

DHI Water and Environment created an engine on which pre- and post-processing of input parameters can be done before used in a computational model. This engine also lays the foundation, linking all the data to the necessary models and even models to one another if it is required. One of the functions included in this engine, also known as MIKEZERO, is a Bathymetry Editor.

The Bathymetry Editor establishes a working environment for the creating and editing of digital bathymetries, where various external sources can be imported or manually created to design the desired bathymetry. This program also has the ability of various interpolation methods before exporting the bathymetry to a format desired by MIKE21.

During this investigation, the influence of the hydrodynamic and sediment transport conditions prior to and after the construction of the causeway and the jetty were investigated. To investigate this influence, two bathymetries had to be created, one excluding the causeway and the jetty, and a second including these two structures in Saldanha Bay. The first mentioned were more complicated to generate due to no data available indicating the conditions prior to the construction of the causeway and the jetty.

Hardcopies of maps on the bathymetry of the Langebaan Lagoon and Saldanha Bay were provided by the CSIR. These maps date back to 1995, before the construction of rehabilitation structures and removal of the beach at Langebaan, but after the construction of the causeway and the jetty in Saldanha Bay. These maps also excluded the erosion of Langebaan Beach, thus providing outdated information in the bathymetry of the area of interest.

The South African Navy also provided GIS shape files on the bathymetric data of the Langebaan Lagoon in the form of contour lines and points indicating depths, as indicated in **Figure 5-1**. This data were similar to the data on the maps, not indicating the erosion experienced at Langebaan Beach. **Figure 5-2** and **Figure 5-3** illustrate the difference between the situation displayed by the GIS data, hardcopy maps provided and the current situation on the aerial photograph. No bathymetric data could be found after the erosion of Langebaan Beach occurred, therefore qualifying the bathymetry as outdated.

The GIS data provided accurate depth contours of the lagoon prior to the erosion of the beach, but excluded data on Saldanha Bay, which had to be extracted from the maps.

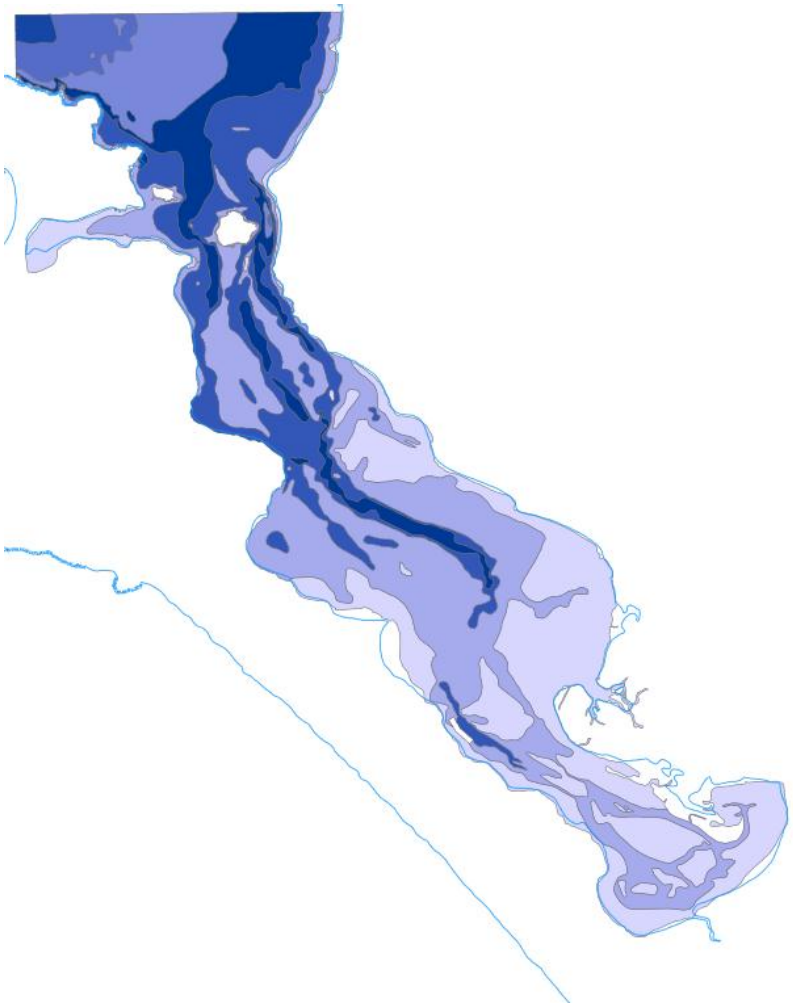

Figure 5-1: GIS data provided by the SA Navy

Figure 5-2: Maps for the generating of the bathymetry compared to recent aerial photograph

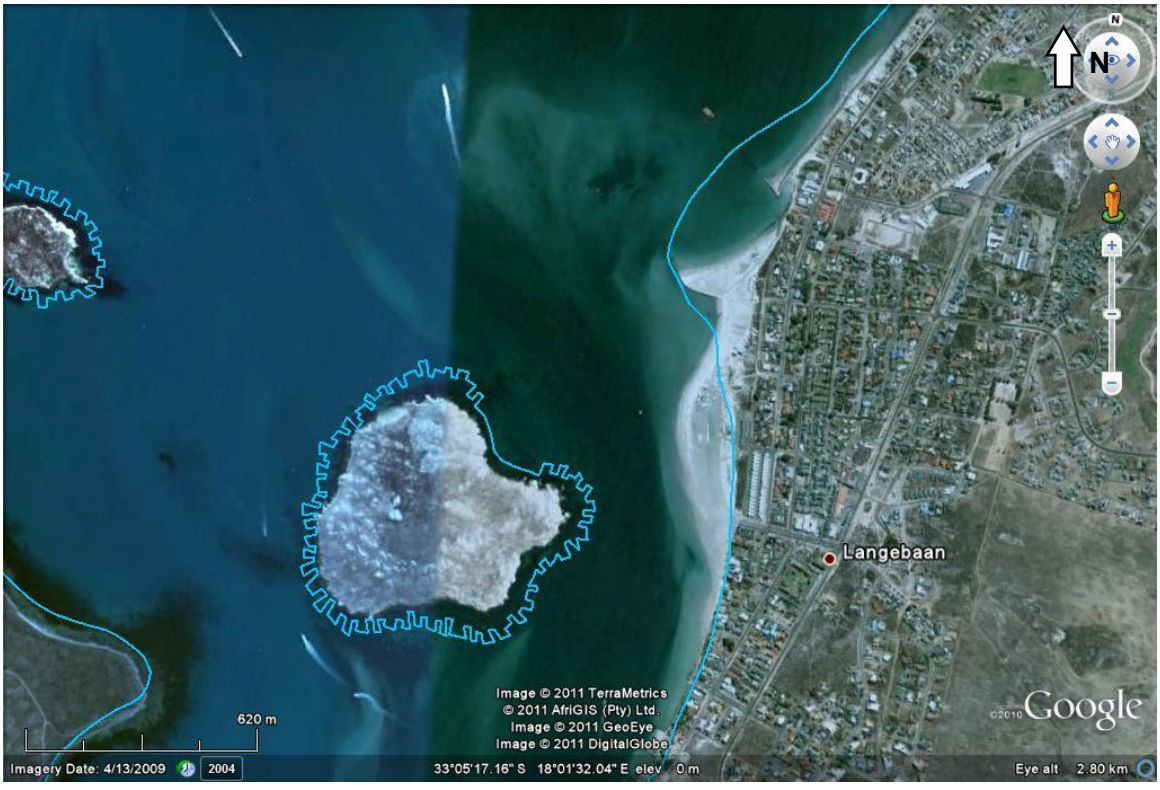

Figure 5-3: Coastline from GIS data compared to recent aerial photograph

The bathymetry were generated in depths from MSL, therefore all the other model parameters were also generated relative to the MSL datum.

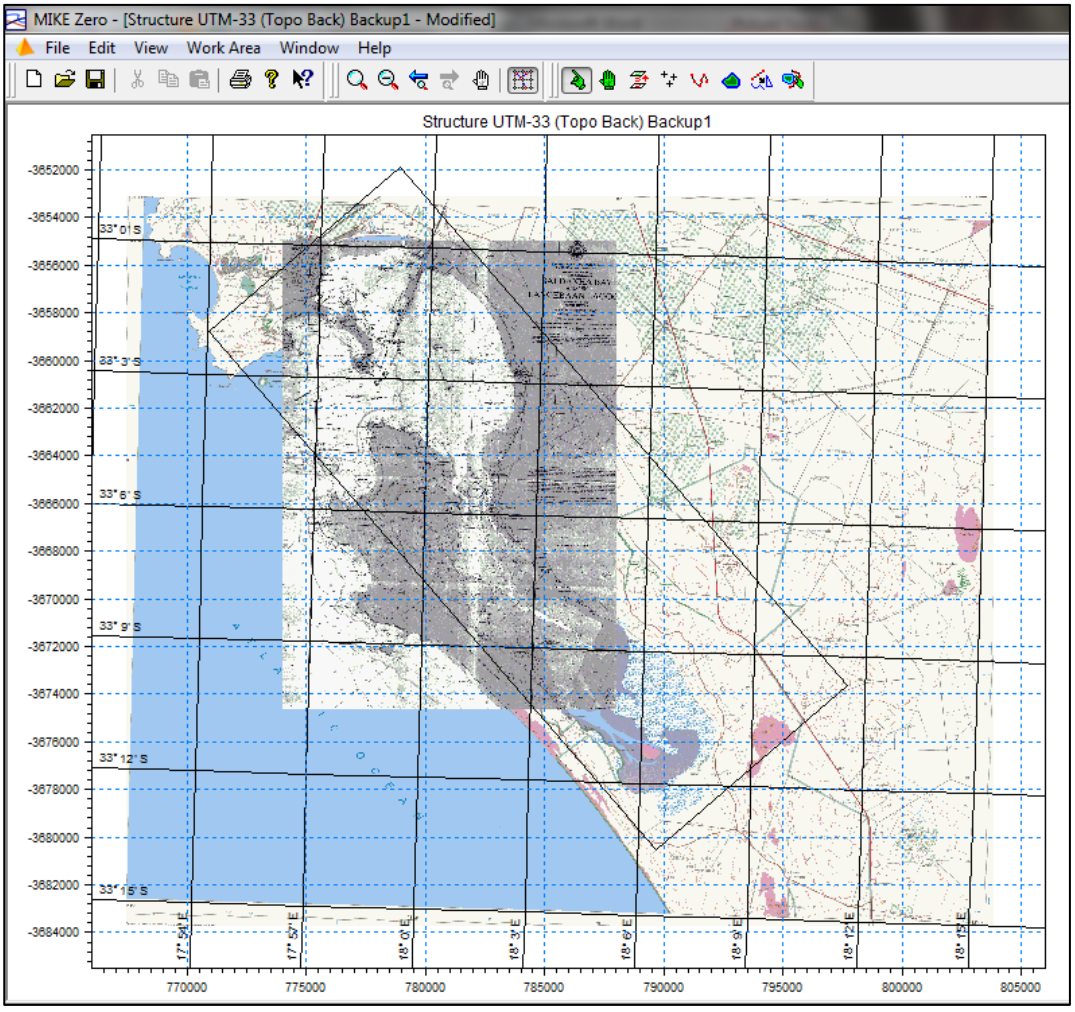

Figure 5-4: MIKEZERO Bathymetry Editor with maps imported in the background

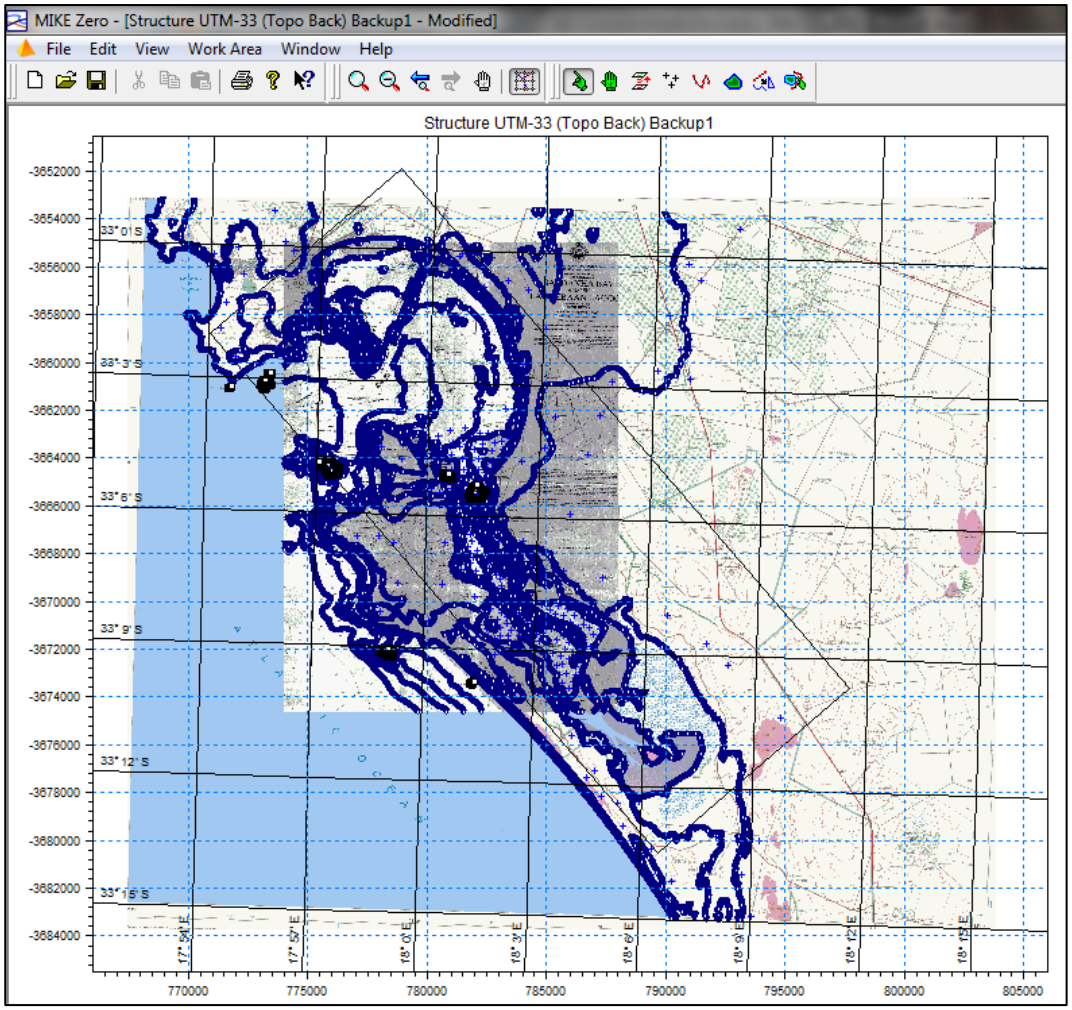

Figure 5-5: MIKEZERO Bathymetry Editor with information digitalized from maps

After the data from the GIS and maps were imported into the Bathymetry Editor, as indicated in **Figure 5-4** and **Figure 5-5**, an area was identified which included the entire Saldanha Bay and Langebaan Lagoon, for the exporting of the bathymetry which would be utilized in the numerical model. When exported to the desired format, the area would be subdivided into a grid consisting of equal sized cells. Each of these cells contained an average ground level of the area represented. Note that not all cells were covered by the contours and points; therefore interpolation would have to be done.

MIKEZERO's Bathymetry Creator includes a function for interpolation between these defined contours and points to create a bathymetry which could be used within the MIKE21 Flow Model. The interpolation done by the Bathymetry Creator has however been found to be inaccurate for this exercise. Interpolation done by alternative software,

Surfer8, has proven more appropriate and realistic to the recorded data as illustrated in **Figure 5-6**.

Note that the grid set up by Mike21 arrange the rows in a descending order, where Surfer arrange the rows in ascending order, thus the mirrored illustration in **Figure 5-6**. These interpolated values were reviewed and modified by hand to provide a similar bathymetry as provided in the data received. These modifications included the jetty, causeway and the surrounding islands.

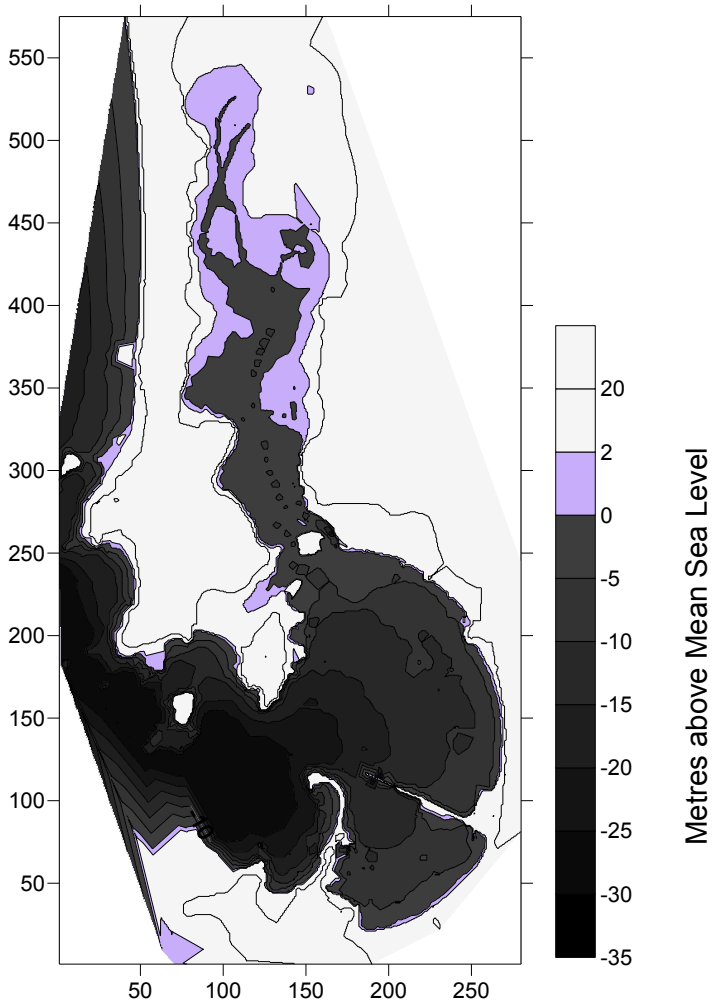

Figure 5-6: Interpolation results from Surfer8 software

After the completion of the interpolation, data were exported according to a specified grid size. The grid size for this study was determined by the distance between Schaapen Island in the lagoon mouth and the mainland at Langebaan. A minimum of eight cells

were desired over the distance of 450 metres, as measured on the GIS data. Therefore, a grid of 50 metres by 50 metres would adhere to the requirements.

Elevations in the bathymetry were limited to 20 metres above MSL, which is unlikely to be submerged by the tidal levels, and depths of 30 metres below MSL were proven to be more or less the maximum depth located at the mouth of Saldanha Bay.

Further modifications to the bathymetry included a 500 metre open channel extending from the mouth of the Saldanha Bay for currents and water levels entering the boundary of the bathymetry to stabilize before entering Big Bay. If this was excluded, unrealistic results could have been expected in Big Bay which would provide unrealistic results for the hydrodynamics and sediment transport in Saldanha Bay and Langebaan Lagoon.

Note that the additional extension to the bathymetry adds a large number of cells to the simulation and will therefore result in more time required for the simulations.

The final bathymetry based on the conditions after the construction of the causeway and the jetty is provided in **Figure 5-7**. This model was used in the MIKE21 Flow model to identify the impacts on conditions after the construction of the causeway and the jetty.

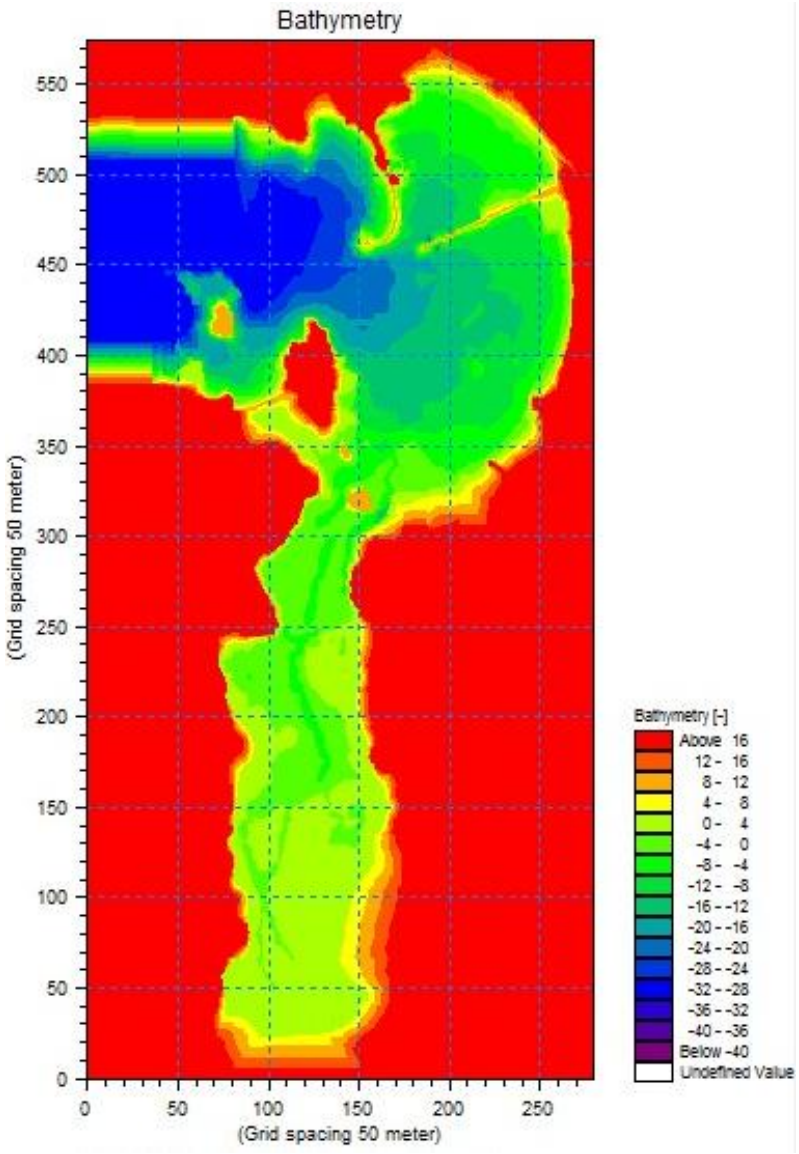

Figure 5-7: Final bathymetry after construction of the harbour

Data received could be used for creating a bathymetry after the construction of the causeway and the jetty; however, a bathymetry would have to be created prior to construction. For this procedure, similar steps were followed as mentioned above, excluding the contours indicating the causeway and the jetty. **Figure 5-8** illustrates the result for the bathymetry based on the conditions prior to construction of the jetty and the causeway, as utilized in the MIKE21 Flow model.

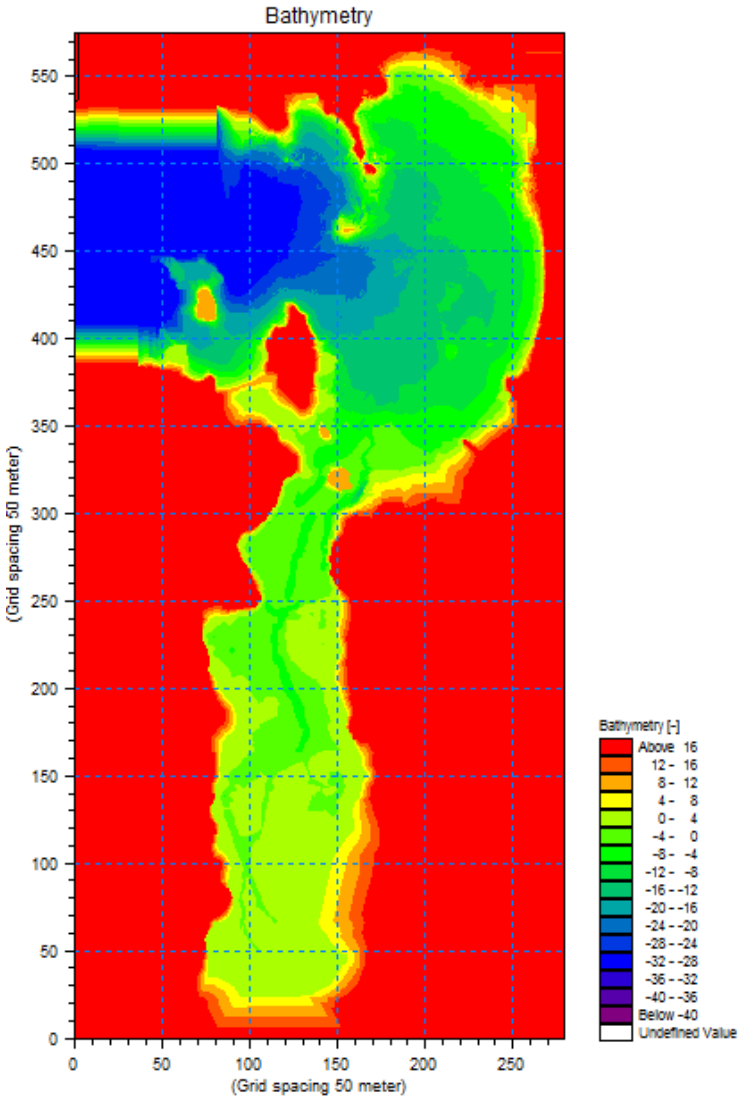

Figure 5-8: Final bathymetry prior to construction of the harbour

For the investigation based on various scenarios, both these bathymetries were utilised in the models, which enabled a comparison in the conditions prior and after the construction of the harbour expansion.

5.3.5 Time step size

The maximum time step allowed for acceptable results is based on the Courant number. This number is calculated by the software for each of the cells, but will eventually be determined for the model by the most extreme value calculated for a single cell. The following equation demonstrates the relationship between the Courant number, the cell size, the time step size and the celerity of the water:

$$C_n = c\frac{\Delta t}{\Delta x} \quad \textbf{(5-7)}$$

where

C_n	Courant number
x	cell spacing defined by the bathymetry in metres
t	time step size in seconds
c	Celerity of the water in m/s

with

$$c = \sqrt{gh} \quad \textbf{(5-8)}$$

where

g	Gravitational acceleration of 9.81 m^3/s
h	Water depth at cell in metres

When a very large Courant number is calculated, it can be concluded that the water velocity is greater than the calculation speed. This can be identified by a hacksaw shape on a time series graph of the results at a specific location, illustrating a number of small peaks over a short period of time or even when water levels rise to unrealistic depths. The time step should then be decreased to a more appropriate size, resulting in a smaller Courant number. The Courant number can be greater than one in this case, because an implicit scheme is used.

MIKE21 Flow Model suggests a maximum Courant number of up to five, but this is dependent on the bathymetry. For a complex model such as Saldanha Bay and Langebaan Lagoon, a maximum Courant number of two were used.

With the specified maximum Courant number of two and grid size of 50 metres by 50 metres, a maximum time step of five seconds has been approved. If a smaller grid displaying more detail is required, a smaller time step would have to be used to maintain a Courant number of two. This would result in more time required for simulations.

5.3.6 Wind observations

Wind has been identified as the primary driving force for Saldanha Bay, as mentioned in **Section 3.1**. Wind records based on surrounding weather stations were analysed and compared to the results from previous studies in order to identify the dominant wind direction at the area of interest. From the analysis of these records, appropriate wind directions were identified which were used in the numerical model.

Previous investigations on the wind observations at Saldanha and Langebaan were based on a two-year record during the late 1940's from a weather station located at the Langebaan airfield. Analysis of this data indicated that the dominant winds during the summer months are south-westerly winds, generated by the high pressure anticyclone located to the west of South Africa. These winds result in erosion of the sandy dune areas along the west coast. During winter months the high pressure system migrates to central parts of South Africa, resulting in north-eastern winds dominating at Saldanha (Coetzee, 1949).

More recent data consisting of longer record lengths were also analysed. This analysis determined the dominant wind direction and the possibility of a change in wind direction from the results in previous studies. WeatherSA provided data consisting of hourly records for four weather stations near Saldanha Bay and Langebaan Lagoon. The locations of these weather stations are illustrated in **Figure 5-9** and further data on the record lengths and coordinates of these weather stations are provided in **Table 5-1**. One of the stations, Langebaan, has been relocated to the southern end of the Langebaan Lagoon in 1997 and renamed to Geelbek.

Table 5-1: Weather station data

Map ID	Station Name	Record length	Latitude	Longitude
1	Cape Columbine	1936 – 2009	32°49'37.20"S	17°51'18.00"E
2	Geelbek	1997 – 2009	33°11'45.60"S	18° 7'26.40"E
3	Langebaan	1994 – 1997	33° 4'48.00"S	18° 1'12.00"E
4	Langebaan AWS	1973 – 2009	32°58'19.20"S	18° 9'25.20"E

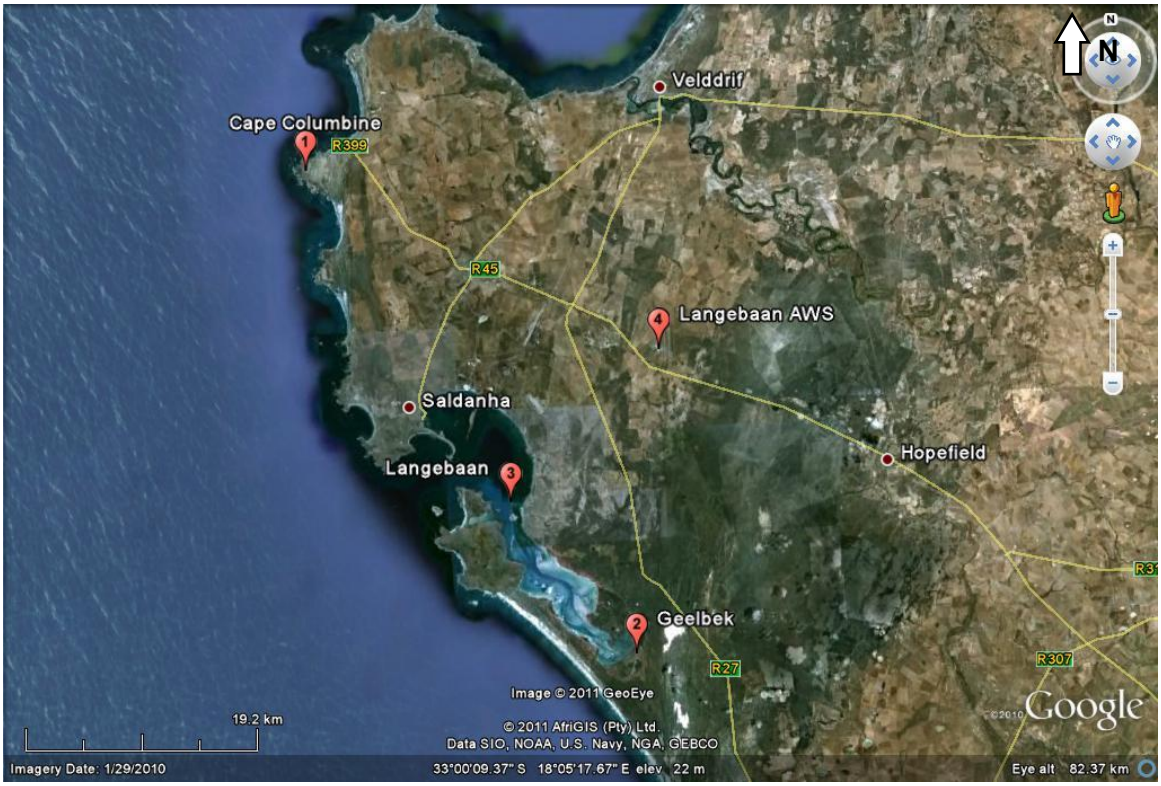

Figure 5-9: Locations of weather stations

The stations situated at Langebaan and Geelbek provided the best indication for the winds dominating in the area of interest, located at the northern and southern edges of the lagoon. Weather stations located at Cape Columbine and Langebaan AWS were 21 kilometres and 12 kilometres from Saldanha Bay, respectively. The stations at the southern and northern edges of the lagoon were analysed to identify the wind conditions and the dominant wind direction at the Saldanha Bay and Langebaan Lagoon.

The analysis on the four-year and 13 year wind records from the Langebaan and Geelbek weather stations respectively, provided the wind directions displayed in **Figure 5-10** as a percentage of occurrences in 16 wind directions.

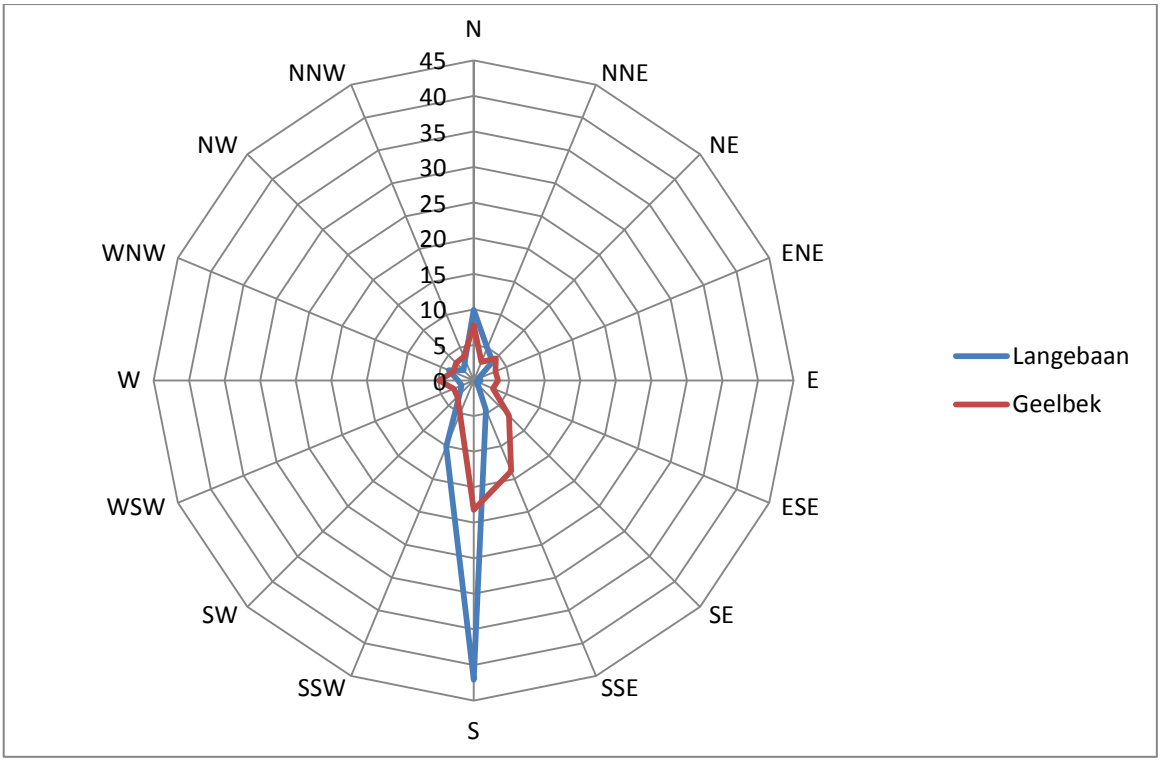

Figure 5-10: Percentage occurrence in wind direction at Langebaan and Geelbek weather station

Figure 5-10 indicates that the shapes of the curves generated from the percentage of occurrence for both these stations are long and narrow along the north–south axis, indicating a dominant northern-southern wind direction. Other regular winds indicated by the records for the Geelbek station are in a south south-eastern direction. However, this south south-easterly wind is not experienced at the Langebaan station. The direction of this south south-easterly wind is similar to the orientation of the lagoon. Records for these two stations were combined to determine average wind conditions experienced in the two systems.

A combination of the Langebaan and Geelbek records was used for the analysis to determine the seasonal variation in wind direction and velocity. The seasonal variations were also compared to an analysis of the entire dataset to determine the deviation from the average measurements.

Results on the analysis based on the seasonal variation are provided in **Figure 5-11** and **Figure 5-12**. A monthly distribution of the wind directions in the 16 wind directions are provided in **Table 5-2** as a percentage of occurrences.

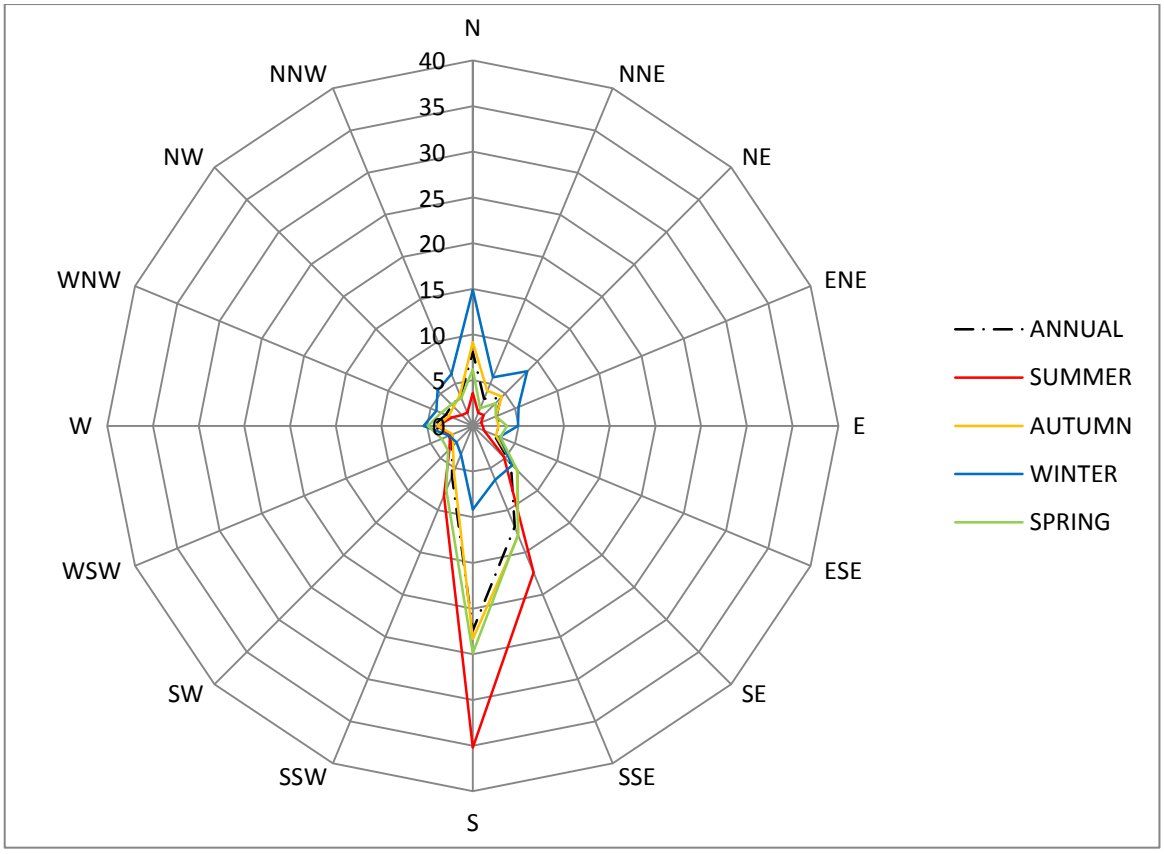

Figure 5-11: Seasonal variation in wind direction

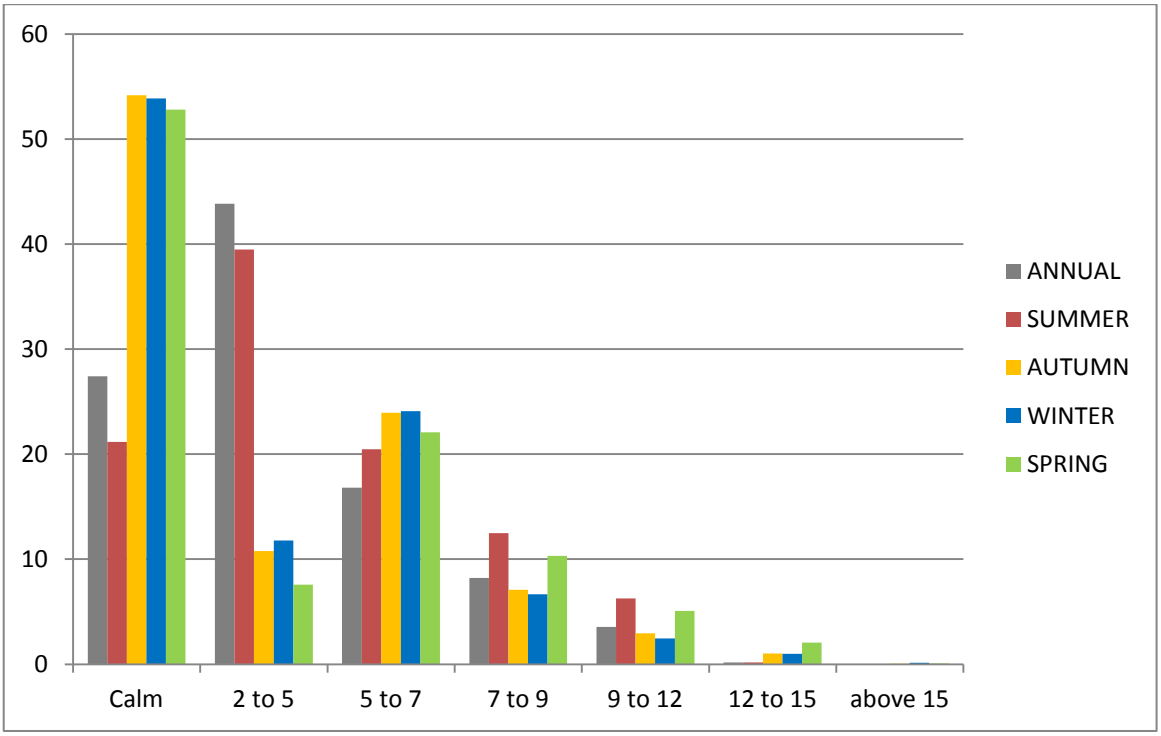

Figure 5-12: Seasonal variation in wind velocity

Table 5-2: Annual distribution of occurrence in specified wind direction

	Wind Directions																
	N	**NNE**	**NE**	**ENE**	**E**	**ESE**	**SE**	**SSE**	**S**	**SSW**	**SW**	**WSW**	**W**	**WNW**	**NW**	**NNW**	**Calm (< 2 m/s)**
Jan	2.3	0.8	0.7	0.2	0.3	0.4	3.1	16.6	34.2	7.6	2.7	2.5	3.5	2.5	1.4	1.2	19.9
Feb	2.8	1.0	0.8	0.5	0.6	0.5	3.5	17.0	32.8	6.9	3.1	2.0	3.0	1.5	1.1	1.1	21.6
Mar	2.5	1.1	0.9	0.6	0.6	0.8	4.5	15.5	27.6	6.9	2.9	2.1	2.6	1.5	0.9	1.0	28.0
Apr	6.0	2.0	2.2	1.1	1.5	1.3	4.8	10.5	18.0	4.4	2.3	2.1	3.3	2.0	2.2	2.1	34.1
May	11.9	3.5	3.7	1.4	1.3	1.4	4.2	5.3	11.9	2.6	1.9	1.8	3.0	2.6	3.5	5.1	34.8
Jun	13.7	4.0	4.5	2.2	2.6	1.7	4.0	3.8	6.2	2.4	1.4	1.3	3.6	3.1	3.9	4.9	36.7
Jul	11.4	3.7	5.2	3.7	2.4	1.4	4.3	4.3	7.5	2.5	2.0	2.3	4.2	3.1	4.0	4.4	33.6
Aug	10.8	2.7	4.2	1.8	2.4	1.6	4.5	6.1	8.9	3.5	2.8	3.1	5.0	4.2	5.2	5.6	27.5
Sep	6.8	1.2	2.9	2.5	3.0	1.9	5.6	9.0	14.6	4.5	3.1	3.6	4.5	4.2	4.2	4.0	24.3
Oct	4.4	1.3	1.4	1.1	2.2	2.0	5.5	12.1	24.5	7.4	3.4	3.0	4.0	2.9	2.3	2.4	20.1
Nov	3.6	0.8	1.2	0.8	1.6	1.7	4.0	12.5	28.4	8.6	3.5	3.4	4.7	2.7	2.1	1.8	18.5
Dec	2.9	1.0	0.8	0.4	0.7	0.4	2.8	13.7	33.4	8.4	3.7	3.1	4.0	2.4	1.5	1.4	19.6

From **Table 5-2** and **Figure 5-11**, indicating the seasonal wind direction distribution based on the percentage of occurrence, it can be concluded that the dominant wind direction varies for summer and winter months. During summer months the dominant wind direction are from the south and during winter months a dominant wind from the north can be expected at the mouth of the lagoon. The southern edge of the lagoon, at the Geelbek station, might experience a south to south-south-eastern wind during summer and northern winds, similar to the northern boundary, during winter.

According to **Figure 5-12**, the wind velocities during the summer months are in the range of 2 m/s to 5 m/s and lower velocities can be expected during winter, with the dominant average wind velocity below 2 m/s. The seasonal variation in direction and velocity can be viewed in **Appendix C**. Also attached in this appendix is the monthly direction distribution of the wind according to the records at Langebaan and Geelbek.

Results from this analysis are similar to the results in previous studies based on earlier records. Therefore, no major changes in the wind directions are expected over a long period of time.

The analysis on the wind records in the area of Saldanha Bay and Langebaan Lagoon has indicated two dominant wind directions. The dominant wind direction during summer months has been identified as a southern wind and a northern wind dominated during winter months at the mouth of the lagoon.

5.3.7 Wind modelling

Even though the effect of wind is considered as minimal on the circulation of the hydrodynamics in the Langebaan Lagoon, as identified in **Section 3.1**, it has been identified as one of the main hydrodynamic forcing factors influencing the circulation in Saldanha Bay, as stated in **Section 3.1**. For the implementation of wind into the numerical model, two factors had to be identified. These are the velocity and the direction.

During the investigation of the dominant winds at Langebaan in **Section 5.3.6**, it has been identified that dominant winds are in the north-south direction. A third wind direction was added to the investigation. This third wind direction can be identified by the longest fetch to Langebaan Beach at the town of Langebaan, which was subject to extensive erosion.

As illustrated in **Figure 5-13**, the longest fetch stretches from the town of Saldanha, through the mouth of Small Bay towards the Langebaan Beach. This wind direction can be identified as a north-eastern direction, with winds moving across the water surface for about 12 kilometres before reaching the beach.

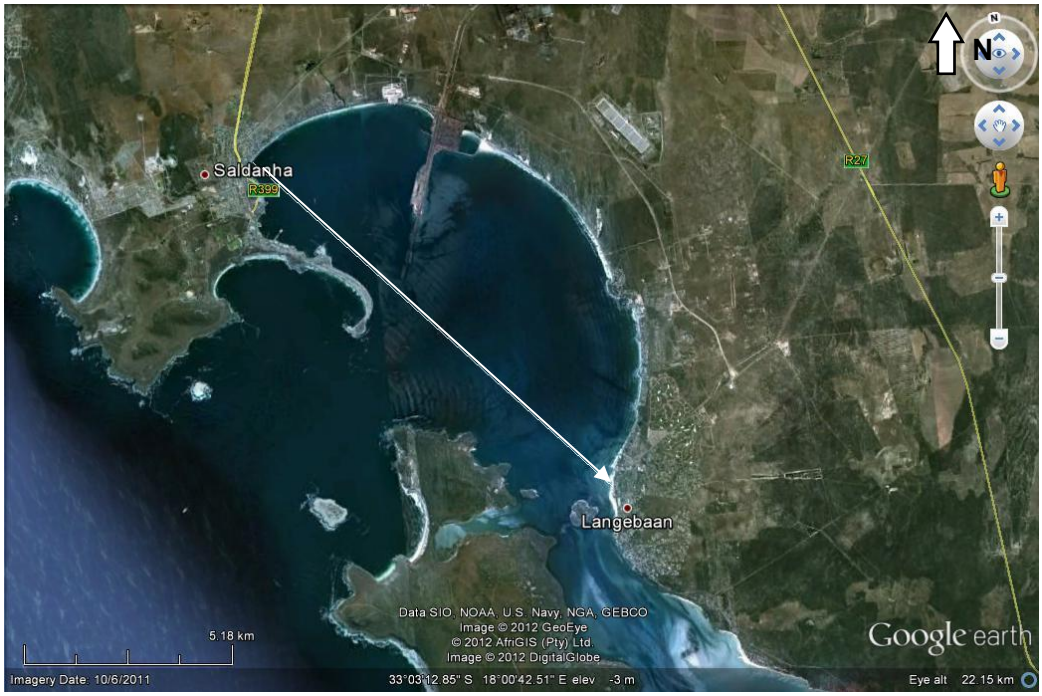

Figure 5-13: Longest fetch towards Langebaan Beach

These three wind directions were combined with specified return period wind speeds to investigate the impact of wind on the circulation and sediment transport of the Saldanha Bay and Langebaan Lagoon systems. These velocities were based on the hourly wind speeds, and not the wind gusts. Wind gusts are short in duration, about three seconds, with extremely high velocities.

Similar to the data analysis in **Section 5.3.6**, a statistical analysis was done on the two data records for the stations located at Geelbek and Langebaan to determine the 1 in 50 year and 1 in 100 year return period wind speeds. A total record length of 16 years was available for the analysis on the hourly wind velocities. The maximum value for each year from 1994 to 2009 was identified and applied to various statistical methods. The results were as listed in **Table 5-3**.

Table 5-3: Statistical analysis on wind speed for 1 in 50 and 1 in 100 year return periods

Median		10.1		
Mean		10.4		
Standard deviation		1.8		
Skewness coefficient		0.493		
Return Period (years)	**Log-Normal**	**Log-Pearson Type III**	**General Extreme Value**	**Extreme Value Type I**
50	14.7	14.7	14.6	15.1
100	15.4	15.5	15.3	16.1

Another method of identifying the wind velocities for the above mentioned return periods is described in the 2011 SANCOLD Guidelines for freeboards on Dams. Isopleths for the 1 in 50 and 1 in 100 year hourly wind speeds are provided in **Figure 5-14** (Bosman, Basson, Tente, & Basson, 2011) and **Figure 5-15** (Bosman, Basson, Tente, & Basson, 2011) as extracted from the 2011 SANCOLD Guidelines. A correction factor should be applied to the 1 in 50 year winds to identify wind events for other return periods as suggested by Milford (Milford, 1987). This proposed correction factor is illustrated in **Figure 5-16** (Milford, 1987). When this adjusted factor is applied to the 1 in 50 year

hourly wind speed in **Figure 5-14** (Bosman et. al., 2011), similar answers to **Figure 5-15** (Bosman et. al., 2011) were obtained.

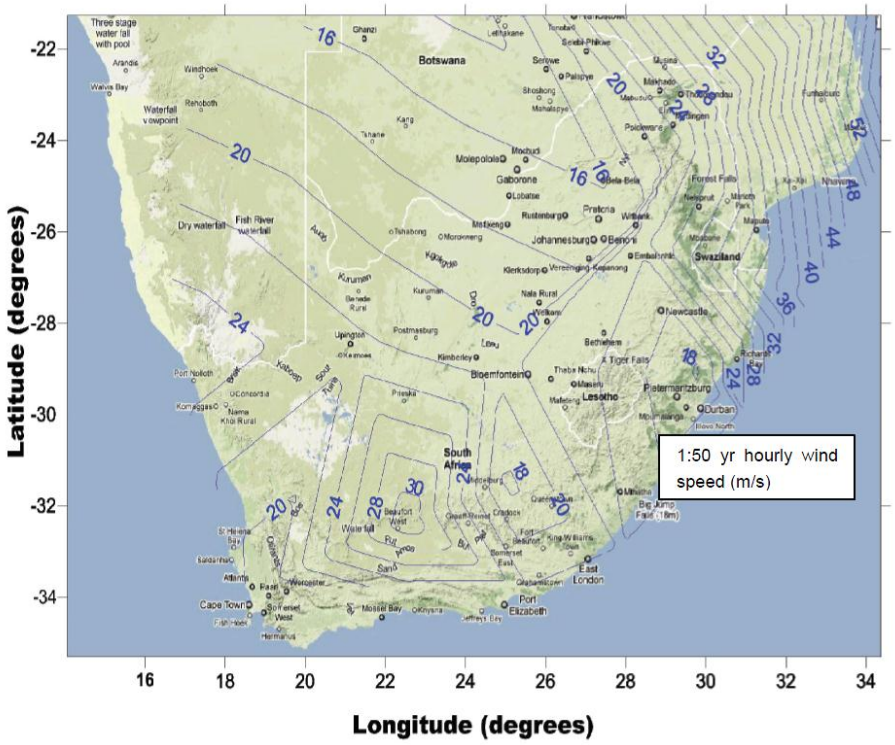

Figure 5-14: 1 in 50 year hourly wind speed in m/s (Bosman et. al., 2011)

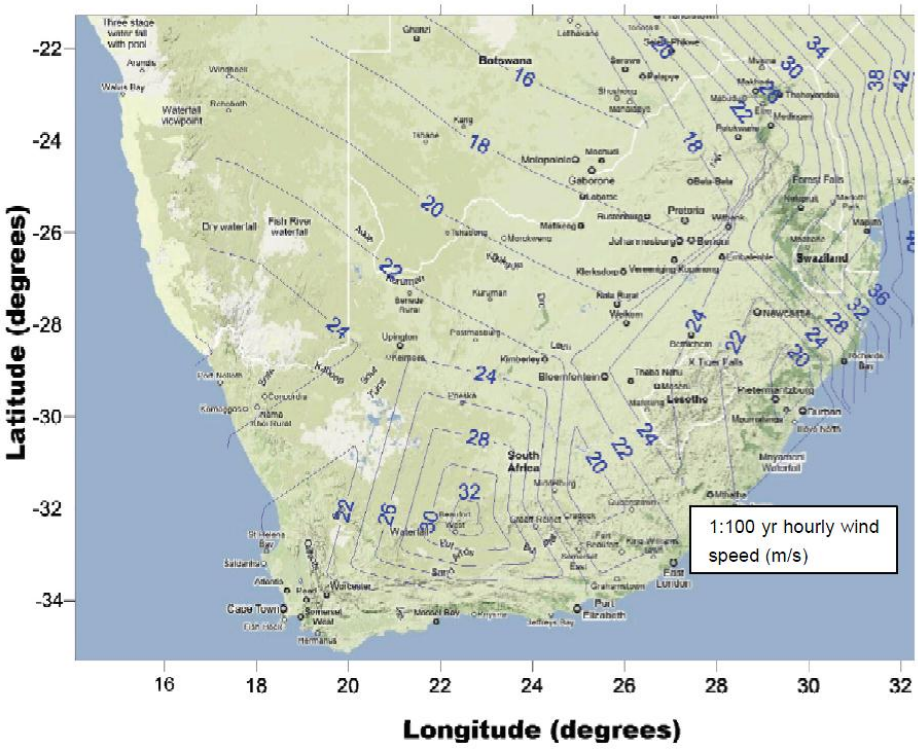

Figure 5-15: 1 in 100 year hourly wind speed measured in m/s (Bosman et. al., 2011)

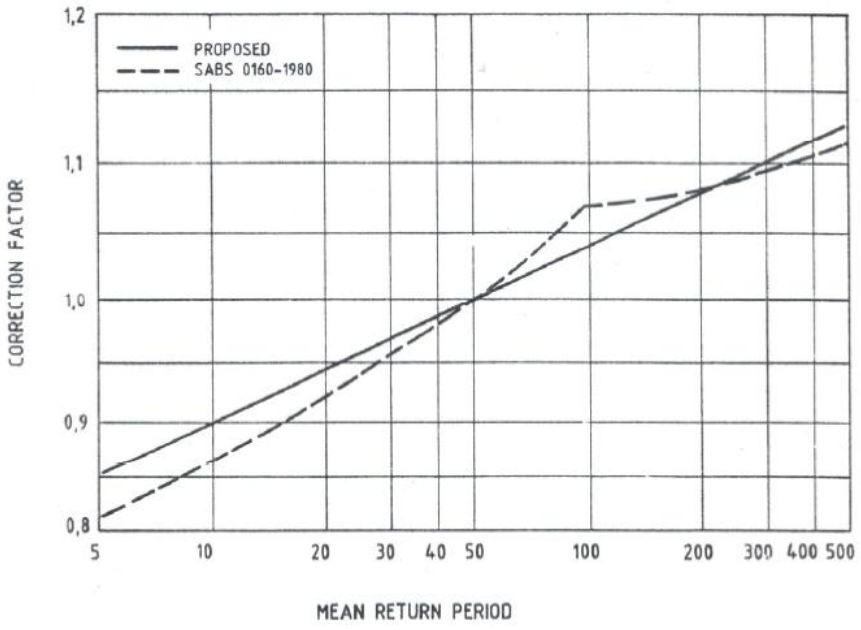

Figure 5-16: Correction factor for wind speed return periods based on the 1 in 50 year event (Milford, 1987)

The values derived from the 2011 SANCOLD Guidelines are much higher than the results from the statistical analysis. A more conservative approach were followed by applying the greater values resulting from the 2011 SANCOLD Guidelines for the investigation on the effect of extreme wind events on the hydrodynamics and sediment transport, as displayed in **Table 5-4.**

Table 5-4: Extreme wind velocities

Return Period	Velocity (m/s)
50 year	19
100 year	20.5

During the investigation of various extreme wind condition scenarios, a constant wind and direction were applied to identify the most extreme conditions when combining this wind with a flood or ebb tide. However, during the calibration of the hydrodynamic model, wind was applied as a time series, simulating realistic wind conditions as experienced during the field survey.

However, these wind conditions implemented in the numerical model would have no effect unless a wind friction coefficient is implemented. An option is provided by the MIKE21 hydrodynamic software to apply a varying wind friction coefficient depending on the velocity of the wind. The default values applied during this investigation provides a coefficient of 0.016 for velocities smaller than 14 m/s and 0.024 for velocities greater than 25 m/s. Linear interpolation was implemented for velocities between these two values.

5.3.8 Water levels

The tidal fluctuations generating the hydrodynamic conditions for the Langebaan Lagoon, as identified in **Section 3.1**, were based on a time series indicating the water level variations. This time series does not include minor variations in the water level due to waves, but rather the tidal variation identified over a longer period of time.

Two datasets provided information on the tidal water level fluctuations for the Saldanha Bay and Langebaan Lagoon systems. The first consisted of recorded data, provided by the SA Navy. Hourly measurements were recorded, but contained multiple omissions in the dataset. Record lengths were also limited due to complications during the analysis of the data provided by the measuring instruments.

The second dataset consisted of water levels based on predictions by computer software, known as WXTide. The nearest location to the point of interest was at the Saldanha harbour, as indicated in **Figure 5-17**, and data were provided in ten minute increments, ensuring accuracy at the peak of the tidal change.

This ten minute increment was much larger than the estimated five second time step size used in the numerical model and water levels for each of the time steps had to be calculated. MIKEZERO automatically interpolated between the two neighbouring values to estimate the water level for each of the time steps during calculations. This interpolation is a common procedure due to time steps for calculations regularly being so much smaller than the time steps used for water level variations and other time series datasets.

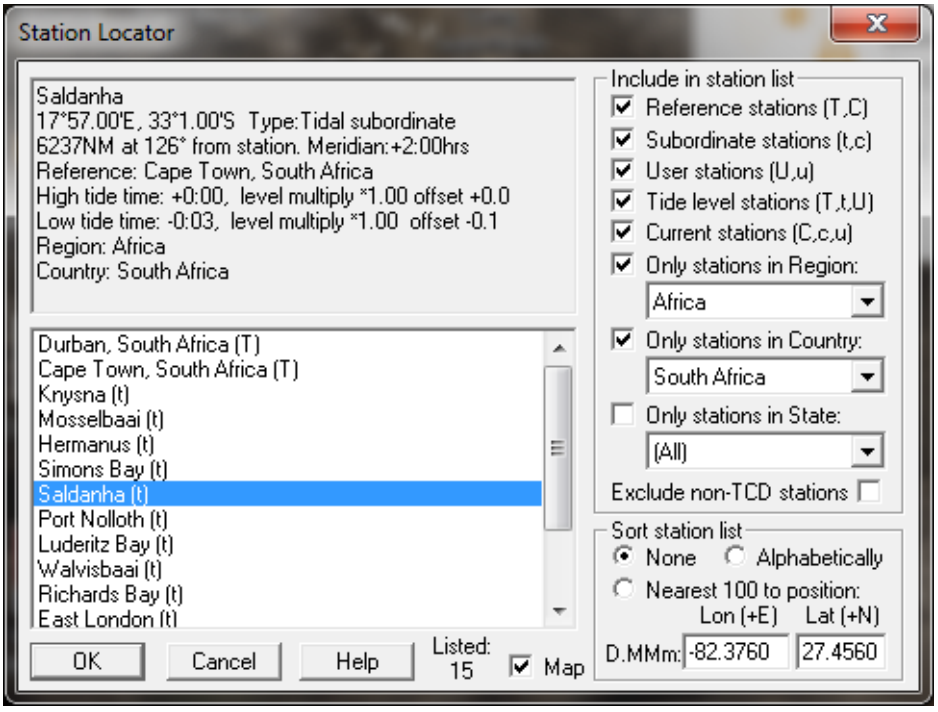

Figure 5-17: WXTide Station Locator window

Even though the interpolation provided values for the time steps required by the model, it is of great importance to have accurate water levels at the change of the tide and times where the tidal change provides a maximum gradient to simulate the maximum velocities in the lagoon. The time estimated between the flood and ebb peaks remains constant, therefore a larger difference in height would result in more water exiting at the lagoon mouth and thus greater flows. Greater flows through the lagoon mouth would have more energy and therefore more sediment transport is expected during this time.

WXTide, containing a complete and more continuous dataset than the recorded data, were utilized for the generation of a time series providing information on the water levels for the numerical model. The time steps used in the dataset were identical to the ten minute time steps provided by the WXTide software and for a similar period of time.

It should be noted that the zero water level provided by the software is based on the MSL datum as mentioned in **Section 5.3.4**.

The water level variations implemented in the numerical model were entered at the western boundary of the bathymetry where Saldanha Bay connects to the ocean. These

water level fluctuations generated the tidal oscillations running across the bathymetry to generate the required circulation in the Langebaan Lagoon.

For the identification of the simulation time modelled during the various scenarios, a worst case in tidal peaks was identified. As mentioned in **Section 3.2.1**, extreme tidal condition occurs during the months of March and September. An analysis on these annual extreme water levels for a five-year period is displayed in **Table 5-5** providing data on the highest water level and the consecutive low tide water level. These extreme fluctuations in the water level provided greater velocities in the lagoon and therefore resulted in more sediment transport.

Table 5-5: Annual extreme water levels above Mean Sea Level

	March			September		
	Max	Min	Difference	Max	Min	Difference
2007	2.915	0.985	1.93	2.865	1.055	1.81
2008	2.845	1.055	1.79	2.765	1.045	1.72
2009	2.825	1.075	1.75	2.815	1.015	1.8
2010	2.905	1.005	1.9	2.875	0.965	1.91
2011	2.915	0.975	1.94	2.875	0.955	1.92

The greatest change in water levels were observed during March 2011, but due to the restrictions on two-dimensional modelling caused by the thermo cline during the summer months, as referred to in **Section 3.1**, the greatest variation in water level during September was used to determine the simulation period for the numerical model. Therefore simulation scenarios were modelled for the period of September 2011.

Additional to the investigations on water level fluctuations combined with various extreme wind events, extreme tidal conditions were also investigated. These extreme tidal conditions included the effect of a global sea level rise and the effect of storm tides.

For the investigation of sea-level rise, an additional 0.4 metres, as qualified in **Section 3.2.2**, were added to the water levels provided by WXTide. As mentioned previously, the effects of sea level rise will not be a gradual change, but rather changes that can be identified with extreme storm events. These storm events generate extreme water levels which alter the coastline and allow the devastating results of the expected

global sea level rise. During this investigation the effect of short period water level fluctuations were excluded, therefore the storm events implemented were based on storm tides.

For the investigation of the impact storm tide events had on the circulation and sediment transport, two return periods have been identified. These are the 1 in 50 and 1 in 100 year storm events, similar to the return periods identified for extreme wind conditions.

Water levels for the above mentioned storm events were identified by means of a statistical analysis on the tidal high water levels. The annual greatest water levels from the recorded data provided by the SA Navy were identified, ranked accordingly and examined. The results are as listed in **Table 5-6**.

Table 5-6: Storm event water levels above Mean Sea Level

Return Period (years)	Water level (m)
1 in 50	3.306
1 in 100	3.334

These extreme water levels were implemented at a tidal peak of a shorter period water level database. Due to the nature of these storm events, no specific time and date could be allocated to the water levels, however, the hydrodynamic and sediment transport results could be compared with other scenario results.

For the implementation of the water level fluctuations in the investigation, three water level datasets were generated. The first provided tidal oscillations as predicted for the month of September 2011, a second provided water levels as expected during the month of September 2011 including an additional 0.4 metres for the influence of sea level rise and a third provided storm tide water levels expected during a storm event.

5.3.9 Simulation period

A simulation period is required by the numerical model, to identify the water levels and wind conditions during this time. This simulation period required a starting date and the number of time steps used during calculations. From these two parameters, along with the time step size as discussed in **Section 5.3.5**, an end time and date can be calculated and therefore the simulation period of the model.

In **Section 3.1**, a thermo cline was mentioned, resulting in complex flows not suitable for two-dimensional modelling. However, this phenomenon is only present during summer months and absent during winter months. Thus the ideal conditions for the simulations would be during winter months for the simulation of various scenarios.

Greatest tidal levels were predicted for Saldanha Bay and Langebaan Lagoon during the change from winter to spring. This is the result of semi-solar tides, as mentioned in **Section 3.2.1**, and would generate the largest velocities, thus the highest expected sediment transport. An analysis in **Section 5.3.8** indicates that the greatest difference between high and low tides during this time of the year in the past five years were predicted for September 2011.

Therefore the aim of the simulation of the various scenarios was focused on the transition time from winter to spring, during September 2011. The entire month were simulated as to ensure all extreme conditions were investigated. Simulations used for the calibration of the model were set to the dates when field surveys were done.

5.3.10 Reporting of results

The reporting of simulation results can be saved as fractions of the simulation. These fractions include parts of the bathymetry when focus is required for a specific area and parts of the simulation time and time step sizes. Even though all the required computations are done and simulation times are not affected by these reporting fractions, the result file size can be decreased and thus create easier manageable result files for post-processing analysis.

Information provided in the results can also be defined by the user, depending on the requirements from the model and information required in models based on the hydrodynamic results, for example sediment transport modelling. These results include:

- Water depths and surface elevations
- Flux densities and velocities in the main directions
- Densities
- Salinities and temperatures
- Current speed and direction
- Wind velocities
- Air pressure
- Drag coefficients
- Precipitation
- Evaporation
- Courant number
- Eddy viscosity

During this study results were focused on the flux and water depth for the purpose of the sediment transport model. Also included in the results from the hydrodynamic model were the velocities for a better understand of the hydrodynamic conditions.

5.4 Sediment transport model

5.4.1 Capabilities of the software

The MIKE21 Non-Cohesive Sediment Transport model has the ability to calculate the sediment transport for non-cohesive materials. This model is based on the results from the MIKE21 Hydrodynamic model provided in **Section 5.3**. The sediment transport module is therefore uncoupled from the hydrodynamic model. These hydrodynamic results should provide information on the flux in the x- and y-directions and the water depth, which is utilized in the sediment transport model.

Application areas for the software include:

- Shoreline management
- Optimization of port layouts
- Shore protection works
- Stability of tidal inlets
- Sedimentation in dredging channels or port entrances
- Erosion over buried pipelines
- River morphology

During this investigation the model were implemented to determine the sediment transport rates in Saldanha Bay and Langebaan Lagoon, focusing on the mouth to the lagoon where a beach has experienced extensive erosion, and the morphological effects of the sediment transport.

5.4.2 Input parameters

To determine the sediment transport conditions in the Saldanha Bay and Langebaan Lagoon systems, a sediment transport model had to be created. This sediment transport model determined the sediment transport rates and the final morphology experienced on the bathymetry. The input parameters for this sediment transport model can be divided into the hydrodynamic parameters, providing the hydrodynamic conditions for the area of interest, and the sediment parameters.

Hydrodynamic conditions for the sediment transport model were based on the results from the hydrodynamic model, discussed in **Section 5.3**. This limited the bathymetry and simulation period of the sediment transport model to the bathymetry and simulations period provided by the results from the hydrodynamic model.

Even though the bathymetry and simulation time is determined by the results from the hydrodynamic model, further filtering of these parameters can be done for the sediment transport calculations. However, this filtering can only be done on fragments of the existing hydrodynamic data consisting of the same cell size and factors of the time step size. Calculations cannot be executed on a finer domain and time steps than provided by the hydrodynamic model.

For the specified domain and simulation time, water level and flow data in both the x- and y-directions should be provided by the hydrodynamic model. These results are then utilized by the sediment transport model in the sediment transport calculations to determine the sediment transport rates and the resulting morphological changes.

Finally, sediment properties need to be defined. These consist of:

- Particle Size
- Gradation
- Relative density
- Porosity

The particle size represents the median of the particle distribution, also identified by the symbol d_{50}. This parameter can vary across the bathymetry, but no provision can be made for various layers of bed material at specified depths. Thus variations in the particle size can only be done in two dimensions, and not the third dimension of depth.

However, the sediment model assumes that the particle size has a log-normal distribution based on two parameters, being the particle size median and the geometric standard deviation, also known as the gradation. The gradation of the sediment indicates the variation in particle size and provides the S-shape to the sediment grading curve, as displayed in **Appendix E**. This parameter is defined as a function where 16 % and 84 % of sediment weights are finer. This can be calculated by means of the following equation:

$$\sigma_g = \sqrt{\frac{d_{84}}{d_{16}}} \qquad \textbf{(5-9)}$$

where

σ_g	Geometric standard deviation, also known as gradation
d_{84}	Particle diameter where 84 % of sediments are finer
d_{16}	Particle diameter where 16 % of sediments are finer

The gradation of the sediment can be determined for each cell individual, or for an entire grid, however, no variation in sediment properties with a change in depth were allowed by MIKE21.

Once the particle size and gradation are identified, a mass has to be allocated to sediments. This is done by means of a relative density.

The relative density is a representative factor of the density of the sediment relative to the density of the liquid it is being transported in, in this case the saltwater. Due to the Lagoon entirely consisting of saltwater, a density of 1025 kg/m^3 was used for the liquid. The density of the sediment was determined by means of field surveys. Note that the

wet density should be used in the model. The relationship for the relative density discussed is as follow (DHI Water and Environment, 1995):

$$s = {\rho_s}/{\rho} \quad \textbf{(5-10)}$$

where

s	Relative density
ρ_s	Density of the sediment in kg/m^3
ρ	Density of the liquid in kg/m^3

It should be noted that MIKE21's Non-Cohesive Sediment Transport model has been developed for sands with a relative density ranging from 2.5 to 2.7. However, values between 1.65 and 3.65 are allowed for this model (DHI Water and Environment, 1995). For values outside the developed range of 2.5 to 2.7, caution should be taken.

During sediment transport calculations, the weight of the water filling the voids between sediment particles would not contribute to the sediment weight. MIKE21 provides a parameter indicating the factor of sediment consisting of water. This factor is the porosity of the sediment. A default value of 0.4 was used, which is realistic for sand particles.

Sediment transport is not only determined by the particle properties, but also the effects of the roughness of the bathymetry. This roughness can be identified as a Manning M or Chezy value and applied to the following equation to determine the friction velocity:

$$U_f = \frac{\sqrt{g}}{C} V \quad \textbf{(5-11)}$$

where

U_f	Friction velocity
C	Chezy roughness coefficient

V	Water velocity in m/s

If a Manning M value has been defined instead of the Chezy coefficient as implemented in the equation above, a conversion is automatically done by the software based on the following relationship:

$$C = Mh^{1/6} \quad \textbf{(5-12)}$$

where

C	Chezy's roughness coefficient
M	Manning's M roughness in $m^{1/3}/s$
h	Water depth in metres

Note that a similar roughness coefficient has been applied in the sediment transport model as identified during the calibration of the hydrodynamic model.

Sediment transport will only commence once the hydrodynamic velocity exceeds a friction barrier. This barrier is determined by a "critical shield parameter". Once the dimensionless shear stress exceeds this parameter, sediment particles are moved from rest. Note that the critical shield parameter does not apply to all sediment transport formulae.

Other parameters include the water temperature which influence the settling velocity and would therefore influence the calculations in the equations where suspended loads are determined. The default value of 10°C indicated similarities to the water temperature conditions experienced during winter months in Saldanha Bay.

Calibration of the model was based on alterations in the particle size, gradation and relative density of the sediment material. The influence of these parameters on the sediment transport was determined by the calculation method used.

5.4.3 Sediment transport calculations

The sediment transport model provided five options for the calculations of sediment movement, due to tidal and wind driven currents only (wave driven currents were excluded). During the modelling of sediment transport, one of these approaches identified and utilized accordingly. Sensitivity of parameters for each of the calculations differs; therefore all the calculation methods were investigated during the calibration of the model. The five formulae are as follow, and further explained in **Appendix I**:

- *Engelund and Hansen*:
- Engelund and Fredsøe:
- *Zyserman and Fredsøe*:
- *Ackers and White*:
- *Meyer-Peter and Műller*:

Parameters for the formulation of sediment transport were used along with the field survey parameters to identify the appropriate method. Limitations of each method mentioned above were included in the choice of formulation for the sediment transport calculations. For the sediment survey during the field investigation, a suspended sediment sample and base-load sediment sample were extracted, providing similar parameters as the *Engelund and Fredsøe* and *Zyserman and Fredsøe* methods. However, the final results of the simulations only provide the total sediment transport for the model, and not for each of the suspended and bed-load sediment transport rates.

Therefore, the choice of formulation depended on the most appropriate sediment transport calibration results compared to the results from the field surveys.

5.4.4 Reporting of results

All calculations for the sediment transport model are saved in a results file, thus the domain and period of time for the results depends on the predefined simulation parameters. Note that due to the hydrodynamic model used as a base for the sediment transport model, all results and calculations are limited to that of the hydrodynamic model and factors thereof.

These results provided the following information:

- Sediment transport in the x- and y-direction in $m^3/s/m$ for each of the user-defined time steps
- The average sediment transport in the x- and y-directions in $m^3/yr/m$ for the entire simulation
- The initial rates of bed level change in m/day
- The new bathymetry after the effect of sediment transport

6 FIELD SURVEY

6.1 Introduction

For the calculations of the hydrodynamic conditions and the sediment transport in the Saldanha Bay and Langebaan Lagoon systems prior to and after the construction of the causeway and the jetty, a two-dimensional numerical model was used. However, to ensure that accurate and realistic results were provided by these models, a comparison to field recorded data were required.

A numerical model is of no use if the results from the model are not compared with actual data in the field. This data is required to determine the accuracy and the calibration of the model, as to ensure that the scenarios being investigated provide accurate and realistic results. The surveys required for the calibration of the hydrodynamic and sediment transport models are listed in **Table 6-1**.

Table 6-1: Field surveys required for calibration

Survey required	Calibration in 2D model
Depth	Determine accuracy of the bathymetry and provide calibration weights to other surveys
Water level	Provide information on the lag from the boundary of the model to the point of interest
Water velocity	Calibration of the hydrodynamic model
Flow direction	
Sediment transport	Calibration of the sediment transport model

Instruments required were identified and careful planning was done on the time and locations of surveys. The time and location of surveys were determined by the most favourable sediment transport conditions. Depth and velocity data would be available during all surveys, but sediment transport is not guaranteed for all velocity samples.

6.2 Planning

6.2.1 Time of observation

Field surveys were required to determine the accuracy of the hydrodynamic and sediment transport models. However, time periods had to be identified when surveys would provide information on all the required data mentioned in **Table 6-1**.

The first step to identify the ideal time periods for the surveys was the identification of time periods when the greatest velocities were expected during the tidal fluctuations, to ensure measurements of the sediment transport conditions. A graph indicating the change in tides can be illustrated by means of a sinus function, creating highs and lows repeating over a time period, as illustrated in **Figure 6-1**. At the peaks of the graph, the change in tide is indicated, changing the tidal forcing in the Langebaan Lagoon from a flooding to an ebb tide or vice versa. The gradient of this graph indicates the distance over a time period, thus velocity. At the amplitude of the sinusoidal graph in this illustration the gradient is zero, thus no velocity should theoretically be measured. From here the gradient increases to either a positive or negative value, thus a velocity will be measured in either a flooding or ebbing tide depending on the orientation of the gradient. A maximum velocity was identified at a point where the gradient is at its greatest, thus at a point halfway between the two peaks.

Maximum gradients, thus the highest velocities, were obtained during a point in time when the difference in the peak values was at a maximum. Due to the constant time available between the two peaks, the difference in amplitudes determined the gradient, and thus the velocity. These extreme differences in high and low water levels occurred during full moon, also known as spring tides.

During these periods of high velocities, greater hydraulic energy was identified and thus a more ideal situation for sediment transport was identified. During these periods of time, all surveys were theoretically available, thus providing ideal conditions for the field investigation.

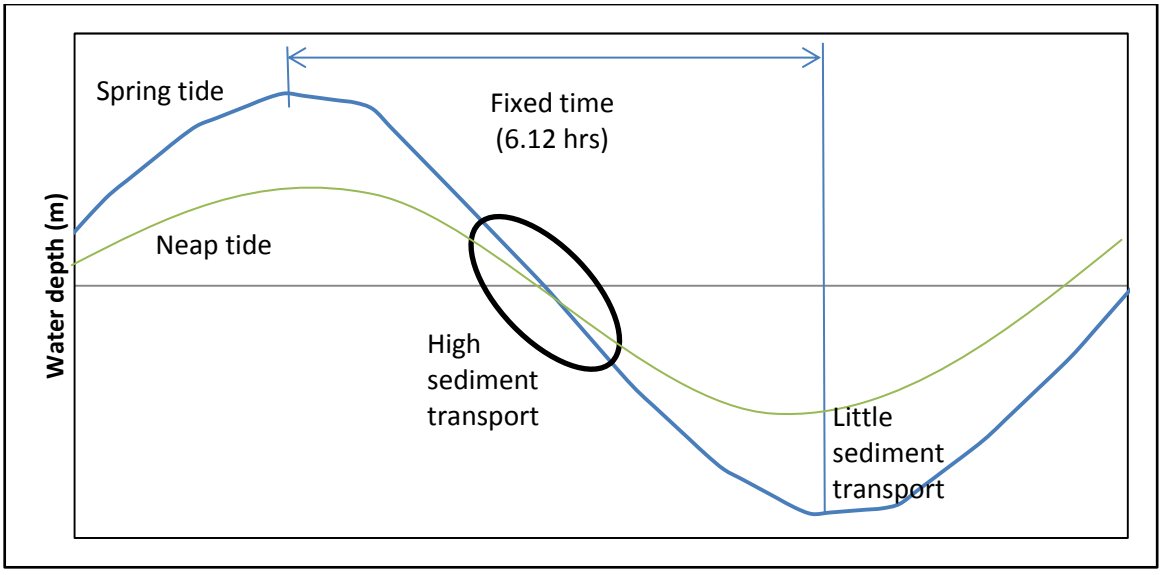

Figure 6-1: Time of maximum sediment transport during a tidal cycle

Dates for extreme tidal conditions ideal for sediment transport were identified as the spring tide during March 2011. The tidal condition identified not only provided extreme high tides due to spring tide, but also annual extreme conditions identified in **Section 3.2.1**. **Appendix D** provides data on the scheduled high and low tides during this period.

Once the dates for the extreme tidal conditions were identified, the ideal time of day to conduct these surveys was established. These times were however limited to sunrise and sunset due to visibility limitations during surveys. The time of day available for surveys was determined by the time of high and low tides and therefore the times when greatest velocities can be expected during the day.

Available in **Appendix D** is the change between high tide and low tide water levels, from which the slope of the tidal cycle can be calculated. A maximum value in the slope thus indicated the time of maximum velocity and therefore the appropriate time for surveying. The days identified for the survey were limited to the days providing large enough gradients or high velocities, thus resulting in ideal conditions for sediment transport.

Appropriate velocities are expected to reign during the middle half between the high and low tidal peaks as indicated in **Figure 6-2**. Thus a 25% delay in time from the peak before the ideal conditions for sediment transport was reached.

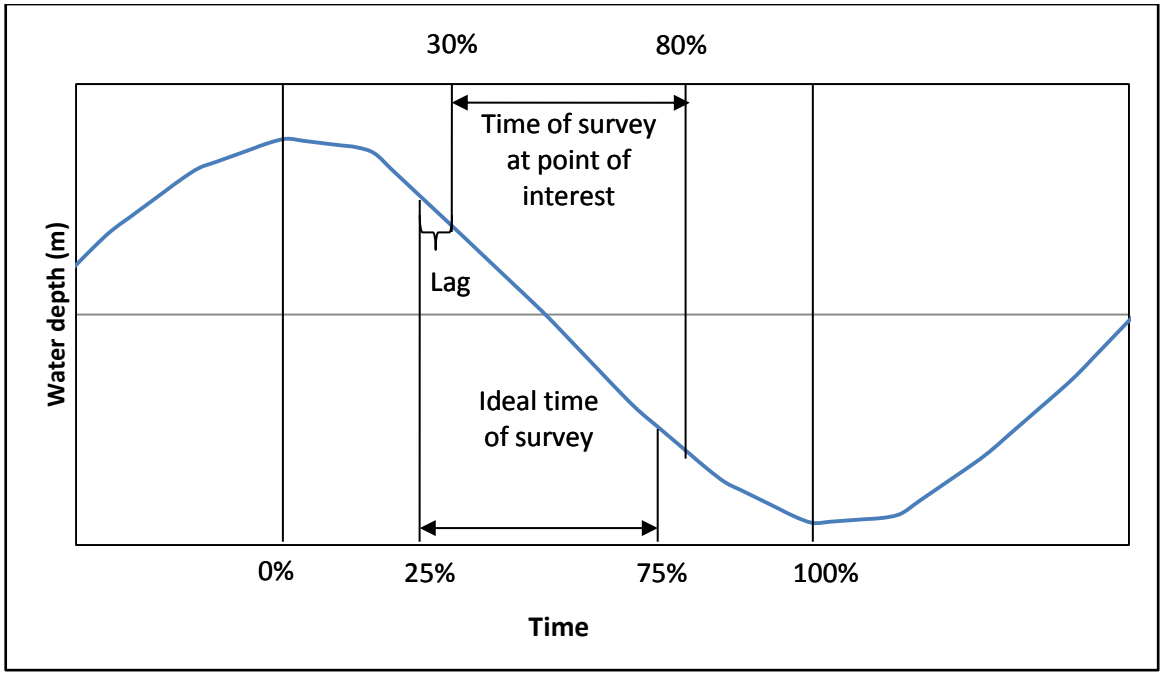

Figure 6-2: Ideal time for survey during tidal variations

A lag in water level variations across the Saldanha Bay and Langebaan Lagoon systems was expected due to the distance from the point where the water levels were predicted by the WXTide software, mentioned in **Section 5.3.8**, to the area being surveyed. Due to the area surveyed being located at the mouth of the lagoon, a minimum lag of 5% in time based on the period between the two tidal peaks were implemented, as displayed in **Figure 6-2**. Therefore, surveys starting at a time 30% after the peak of the tidal change and ended 80% after the same tidal change. This resulted in survey times as displayed in **Table 6-2**.

Table 6-2: Survey times

Run	Day	Time			Number of surveys
		Start	End	Available minutes	
17/03/2011	Thursday	09:28	12:31	183	12
		15:35	18:38	183	11
18/03/2011	Friday	10:11	13:14	183	12
		16:17	19:00	163	12
19/03/2011	Saturday	06:30	07:45	75	4
		10:52	13:56	184	11

These recommended times provided three opportunities for surveys during ebb tides and three opportunities for surveys during flood tides. The ideal was to survey each of the locations during both flood and ebb tides, thus allowing a comparison between the flooding and draining currents dominating in the Langebaan Lagoon.

A more detailed table on the survey time and locations are available in **Appendix D**.

6.2.2 Locations and sampling points

The times available for observations, calculated in **Section 6.2.1** and provided in **Appendix D**, determined the number of points available for surveying. An estimated time of 10 to 15 minutes were provided for the planning of the surveys. These points would also have to be a minimum of 50 metres apart, the width and length of a single cell in the numerical model as estimated in **Section 5.3.4**, as to ensure the calibration of the numerical model would be done across multiple cells on the bathymetry.

The hydrodynamic model for the period of time identified in **Section 6.2.1**, excluding wind conditions, was applied to identify locations where relatively high velocities ideal for sediment transport could be observed. Greatest velocities were expected to be located in the main channel of the Langebaan Lagoon entrance, where survey locations would also be required. Three velocity categories were identified as listed below.

- Velocities larger than 0.8 m/s
- Velocities between 0.75 m/s and 0.8 m/s
- Velocities between 0.7 m/s and 0.75 m/s

The last two mentioned could possibly result in sediment transport, due to an increase in hydrodynamic velocities during favourable wind conditions. However, velocities above 0.8 m/s were used for the identification of locations where sediment transport was expected.

The location of these velocities larger than 0.8 m/s were identified for time steps in the hydrodynamic model results based on the ideal time for surveys identified in **Section 6.2.1**. An example of the locations is available in **Figure 6-3**.

Five sections across the Lagoon were identified for the surveys. Two of these were located across the entire width of the Langebaan Lagoon, with one to the north and one to the south of Schaapen Island (sections A and E). Two more sections were identified between the town of Langebaan and Schaapen Island (sections B and C), and one to the east of the island (section D). These sections are displayed in **Figure 6-4**.

Figure 6-3: Identification of survey locations

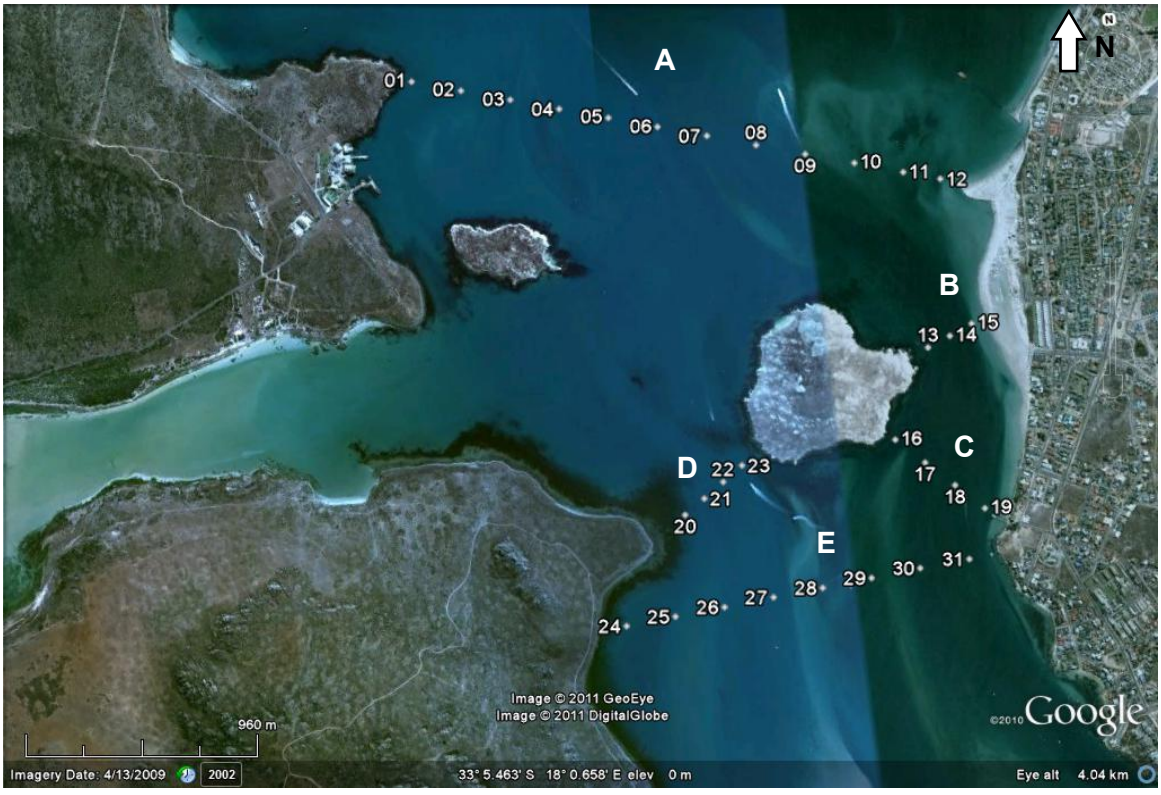

Figure 6-4: Locations of points for survey

Greatest velocities, as mentioned previously, were identified at the locations to the west of the island, between the town of Langebaan and the island. Other velocities of interest have been identified on the same side of the island, but more to the south. Even though these sections are expected to provide the most data on the sediment transport, changes in the area due to erosion and the application of an outdated bathymetry could have resulted in unrealistic and outdated hydrodynamic results in this area.

Each of the previously mentioned sections, indicating the locations where surveys were done, had to be allocated to a time slot provided in **Table 6-2**. A time limit of 15 minutes was used for each survey, including the transportation from one point to the next. From these assumptions, 12 points have been identified for section A, three for section B, four for sections C and D, and eight for section E illustrated in **Figure 6-4**. The times allocated to each of these locations are provided in **Table 6-3**.

Table 6-3: Planned survey times and locations

Run	Day	Time			Section	Number of surveys required	Surveys available at 15 minutes per location
		Start	End	Available minutes			
1	Thursday	09:28	12:31	183	A	12	12.2
2		15:35	18:38	183	B, C, D	11	12.2
3	Friday	10:11	13:14	183	D, E	12	12.2
4		16:17	19:00	163	A	12	10.9
5	Saturday	06:30	07:45	75	C	4	5.0
6		10:52	13:56	184	B, C, D	11	12.3

This concludes to a total number of 31 locations surveyed for each of the tides, thus a total of 62 surveys during the field investigation. The distribution of surveyed locations was also done to assure a minimum distance of 50 metres between the points, which is the width and length of a single cell in the numerical model. Distances between the points in the figure above were more or less in the order of 150 to 250 metres.

Each of the points was loaded onto a Geographical Positioning System (GPS), to ensure that the surveys were done more or less at the planned locations. Waypoints were also recorded for the locations where the surveys were executed.

6.3 Instruments

6.3.1 Pressure test for water levels

Water levels were identified at a specified location in the modelling area, which would be used to determine the water level accuracy of the model and the accuracy of the lag due to the distance from the water level variations at the boundary of the model and the area of interest.

Measurements from the instrument used were based on the pressure difference due to a change in water levels. This change in pressure would be identified by the instrument and a depth could be determined. The depth measurements were however set to a user-defined datum, which could either be the height of a fixed structure above the numerical model's datum or a conservative datum resulting in higher than realistic water levels and modified to the required datum during data processing. Last mentioned approach was used due to the lack of information on the fixed structures in the Langebaan Lagoon.

The Langebaan Yacht Club's jetty, as illustrated in **Figure 6-5** is located at the southern edge of Langebaan, south of Schaapen Island and at the southern edge of the area of interest. Thus, the maximum lag expected in the area of interest was identified at this location.

Figure 6-5: Location of water level survey

The instrument was attached to a solid, fixed structure, thus not changing in depth due to tidal variations, ensuring accurate measurements of the water depth, about five to six metres above the numerical model's datum.

Due to the yacht club experiencing minor water level fluctuations caused by boating activities, recording time steps of 12 minutes were applied. This ensured that tidal changes were recorded and relatively small variations due to the boating activities at the yacht club do not influence the sinusoidal shape of the expected graph.

6.3.2 Transport and approvals

With the exception of the water level measurements at a fixed location, surveys were required at locations in the waters of the Langebaan Lagoon. These surveys would require a vessel of some sort, to transport the instruments to the estimated locations and to execute the surveys from. The boat had to be equipped with engines strong enough to operate in at least one metre per second currents and be large enough to host four crew members, including a skipper, and the equipment.

A skipper would also be required, with the necessary documents, in order to navigate the vessel on the lagoon waters. The Department of Water Affairs (DWA) provided the boat, skipper and an additional crew member to assist with the surveys.

Figure 6-6: Boat provided by the Department of Water Affairs

Due to the Langebaan Lagoon being located within the West Coast National Park borders and the majority of the surveys being within their borders, special consent were required from South African National Parks (SANParks) for the surveys to commence.

6.3.3 Acoustic Doppler Current Profiler (ADCP), Rivercat 15

Surveys executed from the vessel included the depth, water speeds, flow direction, suspended sediment transport and bed-load sediment transport at each of the locations identified in **Section 6.2.2**.

A single instrument was used for the surveying of the hydraulic and physical parameters of the area. The ADCP, provided by DWA, were able to provide an average water velocity for a water column, the direction of flow and the average depth. These measurements could either be done while in motion or when stationary. Due to the stationary conditions required for the sediment transport survey, the surveys by the ADCP were also done while stationary.

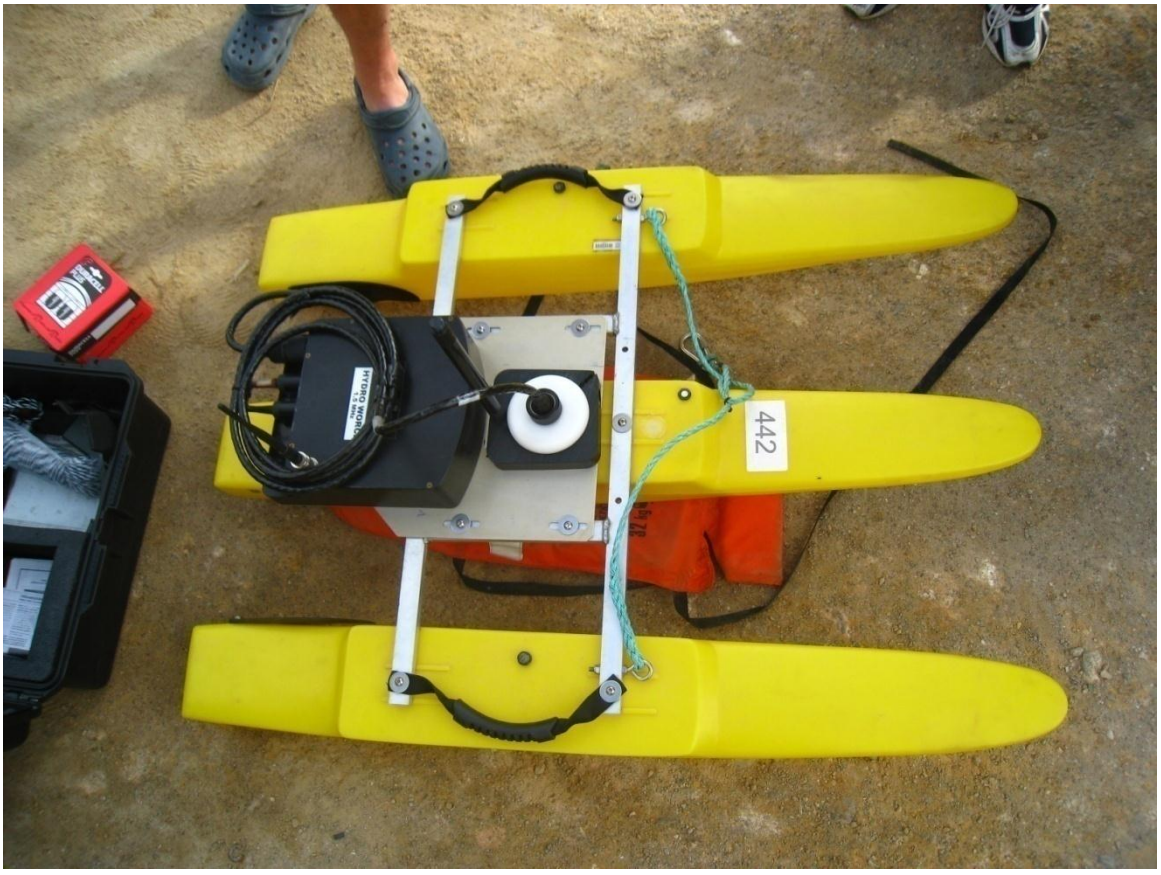

Figure 6-7: Acoustic Doppler Current Profiler (ADCP) Rivercat 15

Survey data recordings could be transmitted from the ADCP in one of two ways. The first by means of a Wi-Fi connection, sending data from the ADCP while in the water to a laptop on board the vessel. The Wi-Fi connection allows a distance between the instrument and the boat. During this method of data transfer the instrument would not be influenced by alterations in the surface flow conditions in the proximity of the boat.

The other is by means of a cable connecting the ADCP to a laptop, limiting the distance between the boat and the ADCP. Due to the limitation of the ADCP's distance from the boat, the flow records and readings could be influenced by the flow alterations experienced near the boat.

Other influences on the accuracy of these tests were the number of sensors on the instrument used to record the data from which signals are sent and received. More sensors would result in more data to use for calculation of the parameters mentioned above. The ADCP used for the field investigation had three sensors as indicated in **Figure 6-8**.

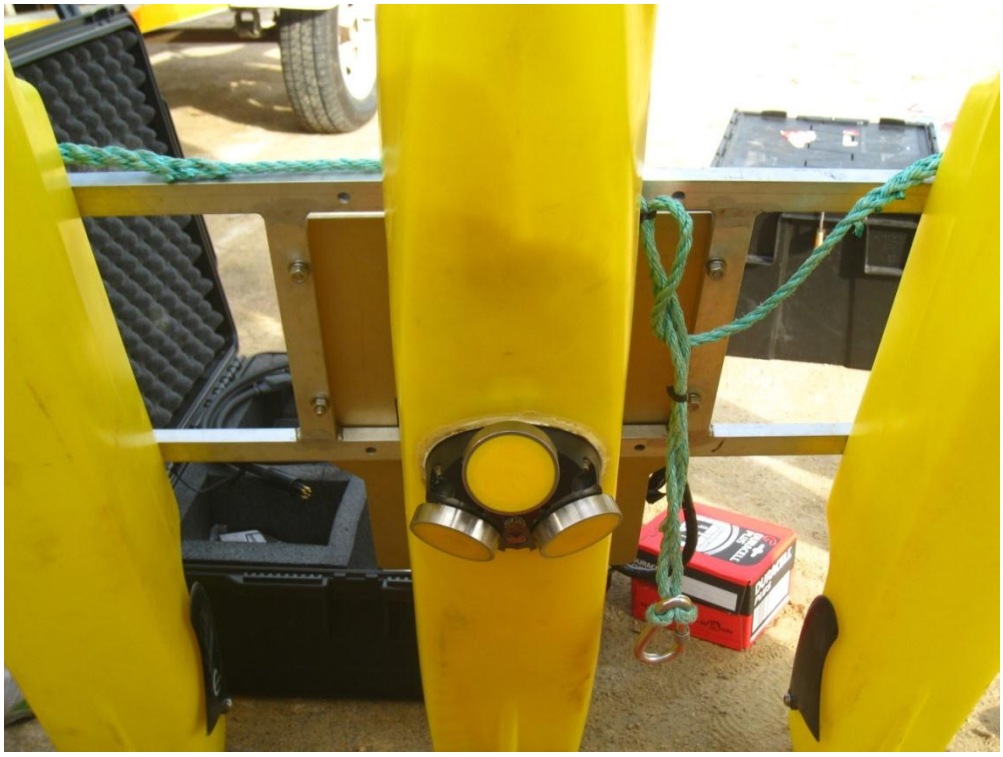

Figure 6-8: ADCP sensors

Another function of the ADCP, but not used for this exercise, is the recording of GPS coordinates where surveys were done and paths followed to get to these locations. During this investigation, recording of locations were done by means of a handheld GPS device provided by the University of Stellenbosch which also contained information on the planned locations as identified in **Section 6.2.2**.

6.3.4 Garmin Colorado 300 GPS

The locations identified for the field surveys, as mentioned in **Section 6.2.2**, had to be identified while in the field. A GPS would be the ideal instrument, with preloaded waypoints to the locations being surveyed. The University of Stellenbosch provided a Garmin Colorado 300 GPS for the identification of the required locations where surveys were done.

Locations where the actual surveys were done would also have to be identified during the post processing of the recorded data, due to the possibility of the boat drifting during the surveys. These waypoints were stored onto the GPS and extracted at a later stage. The identification of these points would also ensure that calibration of the correct cells in the numerical model was done.

Figure 6-9: Garmin Colorado 300 GPS

Due to the cells sizes of 50 metres by 50 metres in the numerical model, the accuracy of the GPS may not exceed 25 metres. The accuracy of the GPS has been proven to be within this limit.

6.3.5 Bed-load Sediment Sampler (BSS)

Two sediment surveys were required during the measurement of sediment transport. These are defined by the method of transport. The Bed-load Sediment Sampler (BSS) is a device used to measure the amount of particles moving along the ocean floor. Particles enter the square nose of the device and are then captured in a permeable bag. These particles can then be dried, weighed and a weight per time unit of sediment movement can be calculated.

Figure 6-10: Bed-load sediment sampler

The bag, which must be able to let the water through and fine enough to capture small particles, are located behind the 100 millimetre wide mouth of the device. This bag should be stretched and tied to the back of the device to ensure that the particles entering the bag with ease, are forced to the back of the bag and do not exit the instrument while the survey is conducted. Measurements can become unrealistic if particles cannot move freely into the bag.

The device was lowered to the ocean floor by means of a rope tied to the weighed centre of the device. A slight tilt forward due to the rope not tied to the weighted centre could result in the instrument tumbling and releasing all the captured particles. The stem at the top of the instrument indicates the location of the weighted centre of the device.

Fins located at the back of the instrument allow the currents carrying the particles to steer the nose of the device in an upstream direction, thus capturing the particles forced by the current.

The BSS should be lowered to the ocean floor with care and not dropped at a high velocity on the ocean floor. If the instrument is lowered at a high velocity onto the ocean floor, particles are lifted into suspension and forced through the nose of the device and into the bag, thus resulting in an unrealistic measurement of the bed-load sediment transport.

Once the instrument is on the ocean bed, it should remain there for a specified time. The duration of the instrument on the ocean floor should be recorded as to determine the time in which a recorded weight entered the device. The bag however should not be filled completely, as this would result in particles not entering the device and therefore not providing realistic results.

Samples were emptied into a plastic bag and then labelled accordingly to provide enough data for identification during post processing. This information includes data on whether the sample was during ebb or flood tide and the location of the sample. The surveyed waypoint and planned waypoint according to the GPS were also provided on the label, as indicated in **Figure 6-11**.

Figure 6-11: Example of bed-load sediment sample

The information provided by the GPS would identify the specific location of the survey and the time and data when the survey was done. When correlating this with the planned times in **Section 6.2.1**, the tide could be identified.

6.3.6 Suspended Sediment Sampler (SSS)

Not all sediments are transported on the ocean bed. A very small percentage is in suspension in the water column. These particles were retrieved by means of a suspended sediment sampler, illustrated in **Figure 6-12**. The aim of this survey was to retrieve a water sample of a water column which contains very fine sediment particles in that particular column. These particles are much finer than the particles rolling on the ocean bed surveyed by means of a BSS. Therefore, the experiments done on these surveys were much more complicated and require more time for processing.

Figure 6-12: Suspended sediment sampler

Particles in suspension enter the instrument through a nozzle and are captured in a sealed bottle. The only variation on the instrument during various surveys was the nozzle size, to control the inflow of water entering the bottle. The variation in the nozzle

size was determined by the depth of the water column surveyed. Depths at the points of interest were determined in the following ways:

- Results from the numerical model, which provided an average depth over a 50 square metre area. These depths provided very little information on the specific location surveyed and could result in surveys repeated to obtain the correct sample size.
- Knots every half metre on the BSS rope were used, providing a more or less indication of the depth. The half metre knots were not very accurate, but provided an indication of the accuracy of the ADCP.
- Depths were also provided by the ADCP and were used to support the depths found in the previous methods.

The last two of the abovementioned methods provided more reliable data on the depth. From this depth analysis, the appropriate nozzle was installed and the time required for the sampler in the water could be estimated, resulting in less repetition of the survey and thus saving time.

Ideal sample sizes were achieved when the bottle was filled to the tapered area as indicated in **Figure 6-12**. If the bottle was filled to the top, the last section of the water column might not be surveyed and a half-full bottle provided samples too small for analysis.

Similar to the BSS, if the SSS were lowered onto the ocean floor at a high velocity, bed-load sediments were lifted into suspension and possibly entered the bottle. This would provide unrealistic data for the survey.

After the survey was done, the bottle in the SSS was emptied into a sample bottle, closed and labelled accordingly, as illustrated in **Figure 6-11**. Labels on these bottles provided information on the location as planned in **Section 6.2.2**, the waypoint provided by the GPS and the date of the survey, similar to the labelling of the BSS samples.

Figure 6-13: Example of suspended sediment sample

6.4 Practical complications during survey

During the field investigation, some unexpected, practical complications occurred. These complications were noted for the purpose of future investigations and are summarized below:

Movement of the boat during surveys:

- The effects of the wind could complicate the survey, especially when the tide and wind forces on the vessel were in opposite directions. This caused movement of the vessel during survey and the possibility of the survey for the BSS and SSS not observed at similar locations as recorded by the GPS. Another possible effect on the survey was the dragging of the BSS on the ocean bed, causing more sediment to enter the sampler than realistically experienced.
- Due to the effects of the wind on the vessel mentioned above, the locations as planned could not be clearly identified in the field and more time was required to find the planned GPS waypoint.
- Movement of the ADCP during stationary surveys could result in a relative velocity measured between the movement of the boat and the velocity of the current. This would result in smaller velocities than actually experienced.
- The movement of the vessel could also occur if the wrong anchor was used, for example a rock anchor on a sandy terrain. Using the engines of the vessel to stabilize the boat at the location surveyed could have an influence on the ADCP results, especially velocity measurements.

Time constraints

- As mentioned previously, more time was required to find the planned locations due to the effects of the wind and currents on the vessel, especially when these were in opposite directions.
- Configuration of the ADCP before each of the surveys required more time than expected.

- Due to very small samples provided by the BSS, time periods for the survey were increased. The initial time of three minutes was not sufficient, resulting in time periods of up to ten minutes. This resulted in a delay on the surveys and thus not enough time to survey all the locations as planned.

Restricted areas

- Survey points one, two and three on section A were located in the military base and thus in a restricted area. Therefore no surveys were obtained in this area.

Instruments

- The BSS is an ideal instrument for rivers and streams with little flora on the river bed. For this specific study, it has been found that biological material entered the bag and formed part of the sample. Biological material itself was not a problem, but the vegetation located at the ocean floor could have blocked the entrance to the BSS, thus limiting the sample size and providing incorrect data. This could also occur in rivers where long grass is located on the bed and covers the entrance to the device. From the Langebaan Lagoon it was expected that kelp and sea grass could cover the nose of the instrument.
- Small sample sizes would result in combinations of the samples to provide enough data for laboratory test of the various sections surveyed. These combinations were subdivided into a northern, middle (east and west of Schaapen Island), and a southern section. The ideal was grading samples for each of the points surveyed; however, this was not possible.
- Mechanical failures on the ADCP resulted in data transfers by means of a cable instead of the Wi-Fi connection. This limited the distance between the vessel and the ADCP, which could result in inaccurate measurements of the velocities due to the influence of the vessel on the hydrodynamic samples.

6.5 Data analysis

6.5.1 Overview

A total of 34 of the 62 planned survey locations were sampled and would be used for the calibration of the numerical model. The following analyses were done to determine the calibration parameters:

- Velocity of the water columns
- Depth of the water column sampled
- Average sediment in suspension
- Dry mass of the bed-load sediment
- Grading of the bed-load sediment

A grading sample at the southern end of Schaapen Island consisting of the bed material was also provided for a clear indication on the grading of the material composition of the mouth of the Langebaan Lagoon. This was compared to the data from previous studies, as mentioned in **Section 3.3**, and samples, which could indicate a change in the material due to sediment transport.

6.5.2 Hydrodynamic analysis

Water velocities, flow direction and depth for a specified water column and similar units in the numerical model had to be identified to ensure that similar results were compared.

Records from the survey provided the time and date of each of the surveys. This information was used to set up a database for the hydrodynamic survey results. Each of the surveys provided a water velocity and flow direction, which would be compared to the results of a similar location in the numerical model after data processing was done.

Directions of the current were provided by the survey in degrees from north rotating clockwise, similar to the directional orientation applied by the MIKE21 software. North was the 0 or 360 degree angle.

It should be noted that depths were measured from the water level and not MSL as mentioned in **Section 5.3.8**. Thus depths were relative to the tidal water levels. The water levels at that specific time were therefore subtracted from the depths to obtain the actual depth at the specified point based on MSL.

6.5.3 Sediment transport analysis

Samples providing data on both the bed-load and suspended sediment transport were identified and used for laboratory analyses. Other samples which provided too little data for analysis were removed from the survey. Only 17 of the 34 sediment transport samples were of adequate size for analysis.

Due to the size of the sediment samples being too small for individual laboratory analysis, a combination of samples were used to create a large enough sample for analysis. This would result in average sediment grading for the combined location samples. Therefore, samples from Saldanha Bay's side of the Langebaan Lagoon north of Schaapen Island were combined (section A), the surveys located around the island (Sections B, C and D) were combined and the samples south of Schaapen Island (section E) were combined. The fourth sample consisted of sediment mass extracted from the bed. This sample contained material not necessarily in motion, but could indicate the difference between the parameters of material in motion and material on the ocean bed.

The following details, as listed in **Table 6-4**, were requested for analysis on the sediment samples. These tests included a sediment concentration test on the suspended sediment, dry mass on the bed-load sediment samples and the grading of the combined samples. The last mentioned were executed by means of two methods, a sieve analysis and a hydrometer analysis.

Table 6-4: Laboratory analysis required for sediment samples

Sample Name	Sediment Samples				Combined sediment sample name
	Suspended (sediment concentration)	Bed Load (dry mass)	Grading		
			Sieve Analysis	Hydro meter	
	mg/l	kg			
A04.17/3.002	x	x	x	x	Front
A12.17/3.007	x	x			
A11.17/3.008	x	x			
A10.17/3.009	x	x			
A08.17/3.011	x	x			
A04.17/3.015	x	x			
D23.18/3.021	x	x	x	x	Middle
B14.18/3.023	x	x			
B15.18/3.024	x	x			
C17.18/3.027	x	x			
C18.18/3.028	x	x			
C17.19/3.032	x	x			
E27.19/3.029	x	x	x	x	Back
E29.19/3.030	x	x			
E31.19/3.031	x	x			
E27.19/3.034	x	x			
E31.19/3.036	x	x			
SAMPLE .037			x	x	Bed Sample

6.6 Survey results

6.6.1 Tidal levels

A water level survey was done to identify the accuracy of the lag provided by the two-dimensional model due to the distance from the location where a change in water level is implemented in the numerical model to the point of interest located at the mouth of the Langebaan Lagoon.

The survey of the water level measurements started on the 16th of March 2011 at 15:12 and ended on the 19th of March 2011 at 12:48 with 12 minute intervals between measurements. **Figure 6-14** indicates the WXTide information compared to the measured data and the adjustments to the measured data due to a change in the datum as discussed in **Section 6.3.1**.

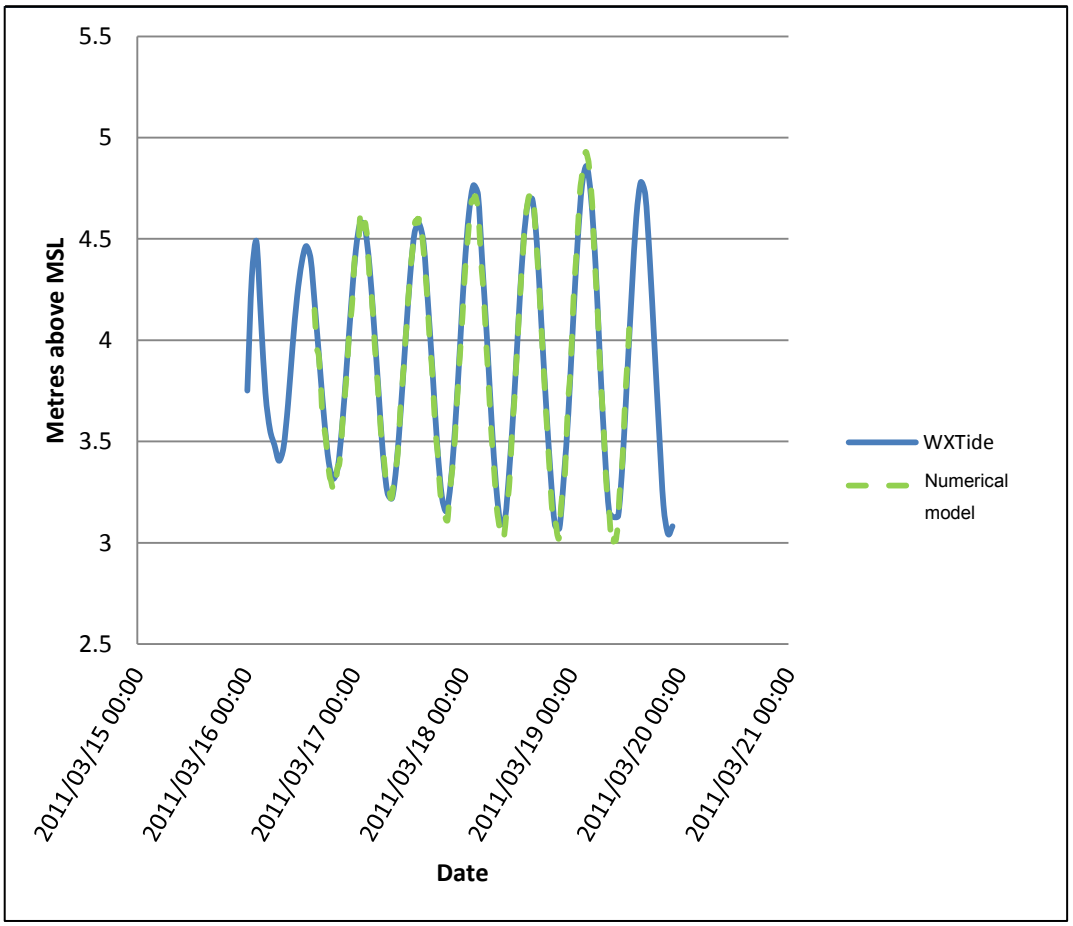

Figure 6-14: Surveyed water levels compared to WXTide predicted water levels

When focusing in on the correlation between the adjusted, recorded data and WXTide predicted data set, the following can be identified:

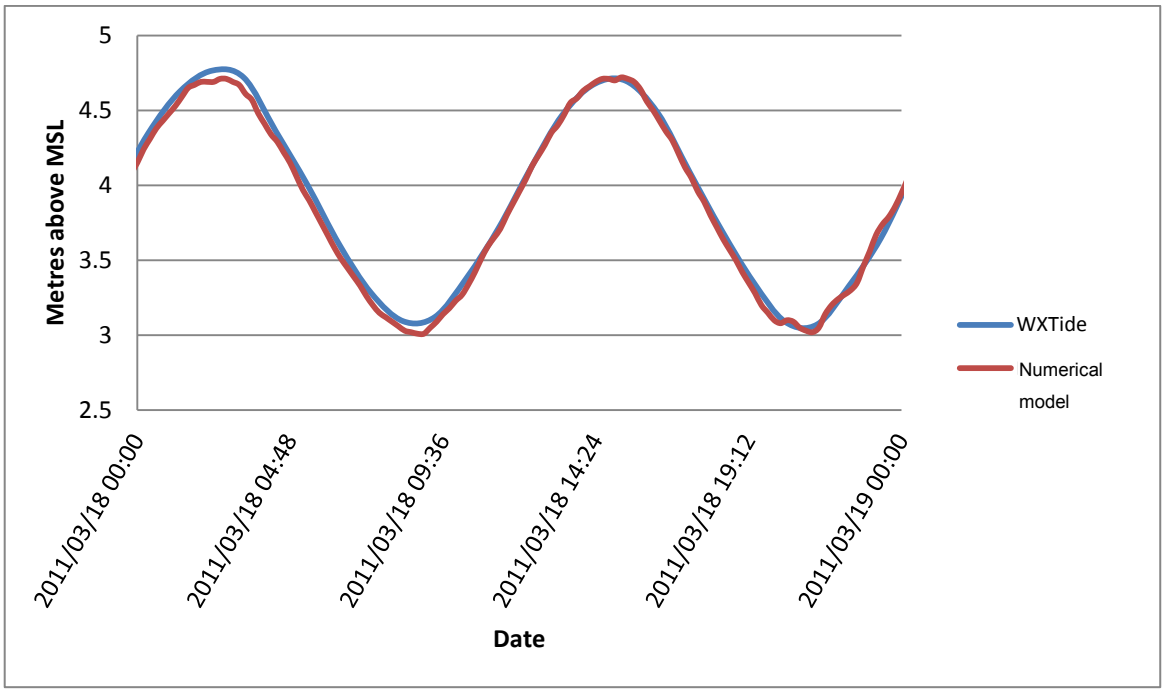

Figure 6-15: Adjusted, recorded water level data compared to WXTide water level data for the 18th of March 2011

Figure 6-15 indicates the differences when focusing in detail at the differences between the WXTide data and the adjusted measured data. A good correlation between the two datasets were observed, however, a time offset between the two datasets was expected due to the lag in water level between the location according of the WXTide water level predictions and the measuring station at the Langebaan yacht club. This lag is not visible on the figures above due to the time intervals for the recording of the data (12 minutes) and the intervals used for the prediction of the water levels (10 minutes). If the lag is smaller than the 10 minute interval used for the prediction of water levels, it would not be observed. Note that a smaller time step for the water level data measurements could result in a more accurate lag in the water level, but also the recording of wave action at the location of the measuring station.

The measured water level data were compared with the water level data at a similar point for the calibration of the numerical model and not the predicted water levels provided by WXTide as illustrated above.

6.6.2 Velocity

Velocity, consisting of both a magnitude and direction, were provided in metres per second and degrees from the north bearing rotating clockwise. Both these parameters are provided by the ADCP and are therefore depth averaged as mentioned in **Section 6.3.3**. The results are provided in **Table 6-5**.

Table 6-5: Velocity results provided by the ADCP

Date & Time	GPS Waypoint	Section	Point Number	Survey	
				Velocity	Direction
17/03/2011 10:37	002	A	4	0.34	160
17/03/2011 11:11	003	A	5	0.24	164
17/03/2011 11:37	004	A	6	0.21	160
17/03/2011 12:03	005	A	7	0.25	155
17/03/2011 16:11	007	A	12	0.48	339
17/03/2011 16:47	008	A	11	0.50	325
17/03/2011 17:13	009	A	10	0.62	348
17/03/2011 17:28	010	A	9	0.36	319
17/03/2011 17:44	011	A	8	0.32	326
17/03/2011 17:56	012	A	7	0.35	350
17/03/2011 18:08	013	A	6	0.25	274
17/03/2011 18:20	014	A	5	0.22	290
17/03/2011 18:33	015	A	4	0.11	39
18/03/2011 10:53	016	B	13	0.09	259
18/03/2011 11:14	017	B	14	0.71	166
18/03/2011 11:47	018	B	15	0.52	160
18/03/2011 12:13	019	D	21	0.53	152
18/03/2011 12:32	020	D	22	0.16	149
18/03/2011 12:47	021	D	23	0.67	172
18/03/2011 15:58	022	B	13	0.54	26
18/03/2011 16:29	023	B	14	0.65	343
18/03/2011 16:50	024	B	15	0.55	349
18/03/2011 17:25	025	D	21	0.04	327
18/03/2011 17:50	026	D	22	0.04	328
18/03/2011 18:17	027	C	17	0.00	25

Date & Time	GPS Waypoint	Section	Point Number	Survey	
				Velocity	Direction
18/03/2011 18:38	028	C	18	0.05	14
19/03/2011 06:45	029	E	27	0.35	356
19/03/2011 07:15	030	E	29	0.36	345
19/03/2011 07:33	031	E	31	0.85	359
19/03/2011 10:52	032	C	17	0.36	215
19/03/2011 11:07	033	C	18	0.44	208
19/03/2011 11:27	034	E	27	0.52	178
19/03/2011 11:42	035	E	29	0.31	180
19/03/2011 11:56	036	E	31	0.59	181

Figure 6-16 provides an comparison between the velocity and depth results for each of the locations surveyed. A number of locations were surveyed twice, once during flood tide and the other during ebb tide, resulting in two results for a single location. The difference experienced in depth at a single location can be explained by the change in water level due to tidal fluctuations and the difference in velocity measurements due to surveys during different times in the tidal change, different hydrodynamics experienced during flood and ebb tides, or a faulty reading as explained in **Section 6.4**, for example at location 17 where a zero velocity were recorded.

The velocities measured were compared with the numerical model velocities at similar locations to determine and enhance the accuracy of the model. These values were also used in comparison with the sediment transport results to identify the critical velocity which generated sediment transport.

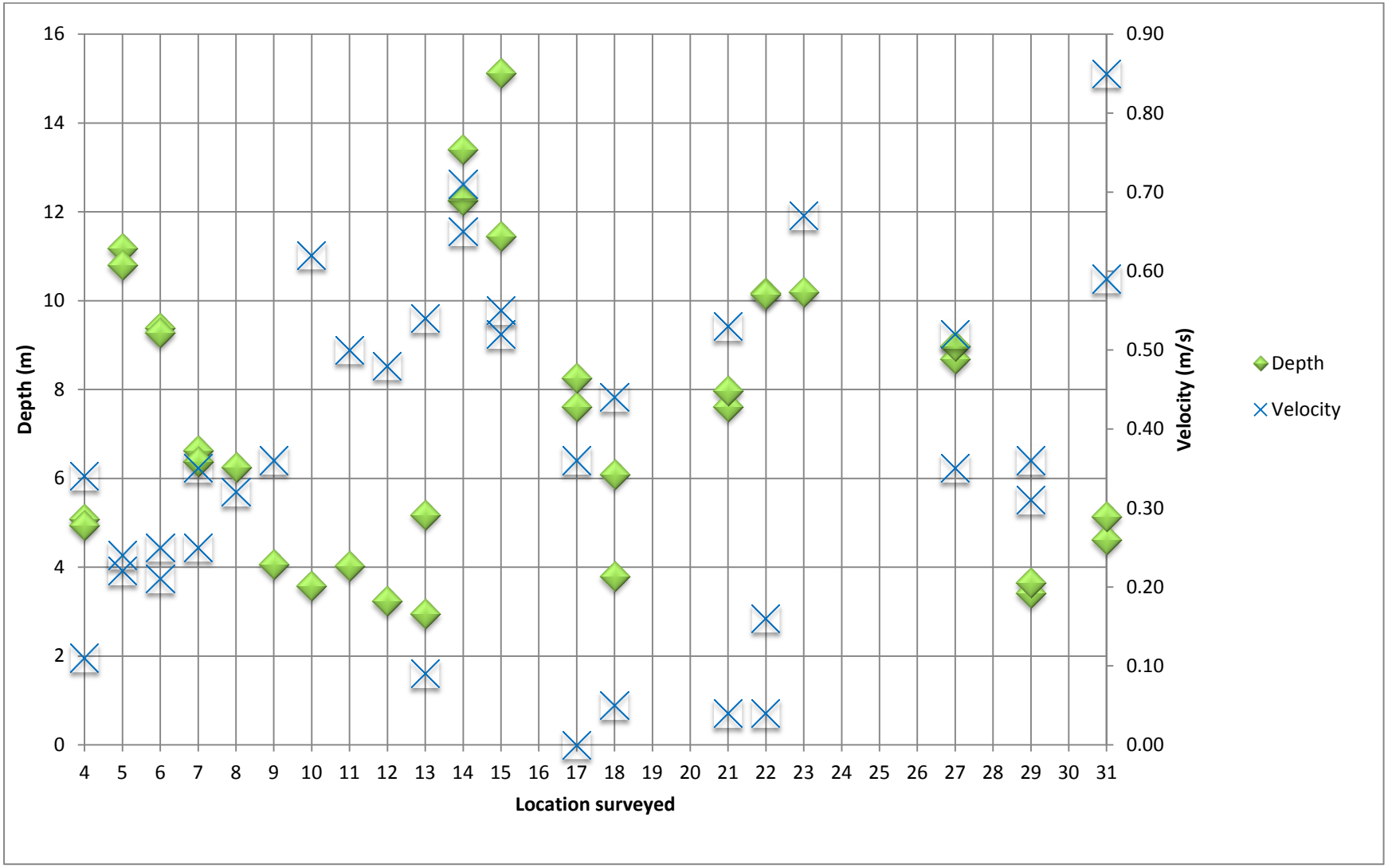

Figure 6-16 : Depth and velocity survey results for each locations surveyed

6.6.3 Lagoon bed grading

The combination of the samples as discussed in **Section 6.5.3**, were analysed in a laboratory to identify the grading of the Langebaan Lagoon sediments. These analyses included sieve and hydrometer tests to determine the grading of the sediments. The results are displayed in **Figure 6-17** and more detailed results are provided in **Appendix E**.

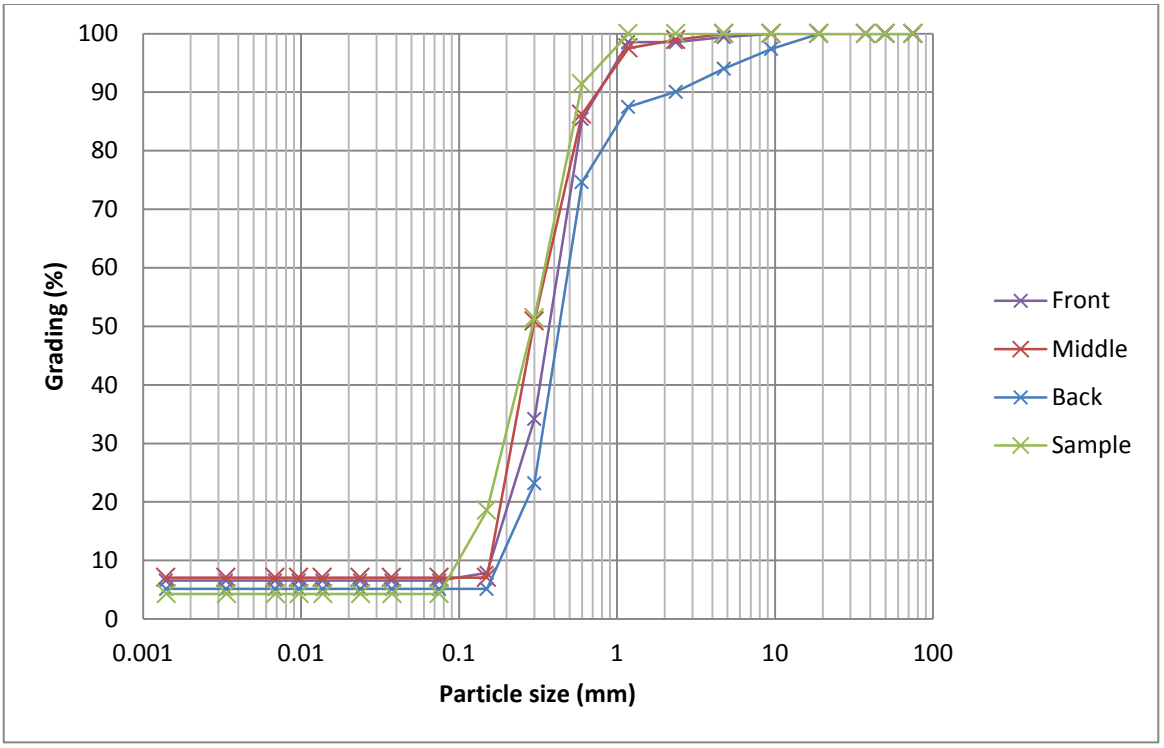

Figure 6-17: Gradation of measured sediment samples

Table 6-6 was derived from the sediment composition distribution figures provided by previous investigations, as mentioned in **Section 3.3** and attached in **Appendix A**. The back (southern) and front (northern) areas of the lagoon mouth consisted of medium to fine particles, and the areas around the island consisted of more medium to coarse particles, especially towards the mainland.

Table 6-6: Percentage distribution as stated by previous studies

Particle size		Percentage distribution					
		Back		Middle		Front	
Diameter (mm)	Description	From	To	From	To	From	To
0.063-0.125	Very Fine	5	10	0	5	0	5
0.125-0.25	Fine	25	50	10	25	50	50
0.25-0.5	Medium	50	50	25	50	25	25
0.5-1	Coarse	10	25	25	50	10	25
1-2	Very Coarse	5	10	10	25	5	10

Survey data, as illustrated in **Figure 6-17**, indicates that the northern section, southern section and areas around the island consisted of dominant medium to fine particles. The additional sample at a location near the southern edge of the island has proven to consist of a better distribution towards fines particles, yet also a dominant medium to fine sediment composition.

The combination of the sediment samples created difficult circumstances for the comparison between previous results and more recent surveys. The previous data indicated larger particle sizes in the main channels, as expected due to larger velocities. However, this cannot be confirmed by recent surveys.

A general distribution of the sediment particles across the lagoon bed were analysed and provided results as indicated in **Table 6-7**. These results indicate similar distributions with the d_{50} grain size defined as a medium to fine particle.

Table 6-7: Sediment composition comparison

	Front		Middle		Back	
	Previous investigations	Sample	Previous investigations	Sample	Previous investigations	Sample
d_{50}	0.125 – 0.25	0.35	0.25 – 1	0.3	0.25 – 0.5	0.42
d_{25}	0.25 – 0.5	0.22	0.125 - 1	0.2	0.125 – 0.25	0.3
d_{10}	0.063 – 0.25	0.15	0.063 – 0.25	0.15	0.063 – 0.125	0.17

Sediment samples consisting of transported sediments, not seabed material, and combined sediment samples used for laboratory analysis where compared with the results from previous investigations and indicated very little change in sediment

composition. However, a more detailed investigation consisting of bed samples would be required to estimate whether major changes in the sediment composition have occurred.

6.6.4 Sediment transport

The sediment transport data has been divided into two datasets. These were the suspended sediment transport and the bed-load sediment transport. Each of these results were analysed differently, but used as a combined value for calibration, due to the single value results provided by the numerical model.

As requested in the laboratory analysis in **Section 6.5.3**, results for the bed-load sediment samples were provided in kilograms for each of the samples. This mass was then converted to a transport value by means of the following equation:

$$Bed - load\ sediment\ transport = {Sample\ mass}/{Sample\ Time \times Mouth\ opening} \quad \textbf{(6-1)}$$

As stated previously, the mouth opening of the instrument was 100 millimetres wide and the additional required data was provided during the survey. This additional data for the bed-load sediment transport are provided in **Table 6-8**.

The suspended sediment sample data were in milligrams per litre. This also needed to be converted to the similar units as the bed-load sediment transport before the total sediment transport could be calculated. For the specific water column, the following equation was applied:

$$Suspended\ sediment\ transport = {sample}/{1000} \times velocity \times depth \quad \textbf{(6-2)}$$

Both the velocity and the depth were measured by means of the ADCP for the specific water column. These calculations would provide a sediment transport in similar units as the bed-load sediment transport.

Suspended sediment samples were recorded for the entire water column, as explained in **Section 6.3.6**, therefore a single sample consisted of the suspended sediment for an entire water column. No distinction could be made for various depths of the suspended

sediment samples, which resulted in the overestimated calibration of the numerical model and therefore more conservative results for sediment transport.

The suspended sediment transport and the bed-load sediment transport were added together to obtain a total sediment transport, which provided results in a similar nature as found in the numerical model. Results for the sediment transport are available in **Table 6-8**.

Table 6-8: Sediment transport analysis

Date & Time	GPS Waypoint	Section	Point Number	Suspended sediment		Bed-load sediment			Total ST (kg/m/s)
				Sample (mg/l)	Transport (kg/m/s)	Sample (kg)	Time (min)	Transport (kg/m/s)	
2011/03/17 10:37	002	A	4	0.460	8.0E-04	189	3	1.1E-05	8.1E-04
2011/03/17 16:11	007	A	12	0.345	5.3E-04	6	3	3.3E-07	5.4E-04
2011/03/17 16:47	008	A	11	0.722	1.5E-03	7	3	3.9E-07	1.5E-03
2011/03/17 17:13	009	A	10	0.586	1.3E-03	31	3	1.7E-06	1.3E-03
2011/03/17 17:28	010	A	9	0.470	9.4E-04	93	3	8.9E-07	9.4E-04
2011/03/17 17:44	011	A	8	0.427	2.9E-03	16	3	1.0E-07	2.9E-03
2011/03/18 12:47	021	D	23	0.376	3.0E-03	3	5	6.9E-07	3.0E-03
2011/03/18 16:29	023	B	14	0.416	2.6E-03	37	9	8.3E-08	2.6E-03
2011/03/18 16:50	024	B	15	0.549	0.0E+00	5	10	5.8E-06	5.8E-06
2011/03/18 18:17	027	C	17	0.614	1.2E-04	175	5	5.7E-07	1.2E-04
2011/03/18 18:38	028	C	18	0.718	2.2E-03	17	5	1.6E-06	2.2E-03
2011/03/19 06:45	029	E	27	0.540	6.6E-04	47	5	3.0E-06	6.7E-04
2011/03/19 07:15	030	E	29	0.592	2.3E-03	36	2	3.8E-06	2.3E-03
2011/03/19 07:33	031	E	31	0.585	1.7E-03	46	2	1.7E-06	1.7E-03
2011/03/19 10:52	032	C	17	0.449	2.1E-03	51	5	1.3E-06	2.1E-03
2011/03/19 11:27	034	E	27	0.576	1.7E-03	38	5	1.2E-05	1.8E-03
2011/03/19 11:56	036	E	31	0.460	8.0E-04	360	5	1.1E-05	8.1E-04

Table 6-9: Surveyed velocity and sediment transport comparison

Date & Time	GPS Waypoint	Velocity	Sediment transport	Comment
2011/03/17 10:37	002	0.34	8.1E-04	
2011/03/17 16:11	007	0.48	5.4E-04	
2011/03/17 16:47	008	0.5	1.5E-03	
2011/03/17 17:13	009	0.62	1.3E-03	
2011/03/17 17:28	010	0.36	9.4E-04	
2011/03/17 17:44	011	0.32	2.9E-03	Very high sediment transport
2011/03/18 12:47	021	0.67	3.0E-03	
2011/03/18 16:29	023	0.65	2.6E-03	
2011/03/18 16:50	024	0.55	5.8E-06	Very high sediment transport
2011/03/18 18:17	027	0	1.2E-04	Zero velocity
2011/03/18 18:38	028	0.05	2.2E-03	Very low velocity
2011/03/19 06:45	029	0.35	6.7E-04	
2011/03/19 07:15	030	0.36	2.3E-03	Very high sediment transport
2011/03/19 07:33	031	0.85	1.7E-03	Very high sediment transport
2011/03/19 10:52	032	0.36	2.1E-03	Very high sediment transport
2011/03/19 11:27	034	0.52	1.8E-03	
2011/03/19 11:56	036	0.59	8.1E-04	Very low sediment transport

Table 6-9 provides information on the relationship between the velocities recorded and the sediment transport associated with these velocities. Very low velocities provided sediment transport, indicating that the expected 0.8 metres per second critical velocity for the initiation of sediment transport overestimated. However, unrealistic velocities provided impossible sediment transport results, for example a zero velocity resulting in sediment transport. This concludes that the field surveys have experienced difficulties as mentioned in **Section 6.4** which resulted in inaccurate survey results.

Results with a realistic comparison between the hydrodynamic velocities and sediment transport rates, as indicated in **Table 6.9**, were used during the calibration process. Unrealistic results identified in this table were also analysed during the calibration process, but not necessarily applied for the purpose of calibration. If the hydrodynamic velocities at the abovementioned locations were identified as realistic and sediment

transport rates not, sediment transport rates were removed from the calibration process, and vice versa.

7 CALIBRATION

7.1 Introduction

To determine the impact of extreme wind and tidal conditions in the Saldanha Bay and Langebaan Lagoon systems prior to and after the construction of the causeway and jetty in Saldanha Bay, a numerical hydrodynamic model was used. This numerical model had to be compared to recorded data to ensure accurate and realistic results.

In **Section 5.3.4**, it has been identified that the bathymetry generated for the numerical model was outdated in comparison with aerial photographs. Parameters in the numerical model were used to calibrate the model in order to provide better results on the models used to investigate various extreme wind and tidal conditions.

A combination of four parameters was used to determine the accuracy of the model. These included the water levels, depths at specified points, water flow velocities and sediment transport rates. The model depths provided an indication of the accuracy of the water flow velocity and the sediment transport as calibration factors and the degree of change in the bathymetry that has occurred due to erosion at that specific location.

Water velocity calibration factors had a direct impact on both the water level calibration, due to its impact on the lag, and the sediment transport calibration. Modifications to the roughness values for the calibration of the water levels influenced the velocity of the currents, and the velocity determines the energy available for the sediment transport. Therefore, the roughness sufficient for the velocities and the water levels were used for calibration and sediment particle parameters and formulae were used for the calibration of the sediment transport model.

Calibration values related to the bathymetry depths, velocity and sediment transport rates were analysed based on a discrepancy ratio (r). The following three categories were used:

- $0.75 < r < 1.5$
- $0.5 < r < 2$
- $0.33 < r < 3$

Calibration results are attached in **Appendix F**.

The numerical model used for calibration included wind conditions.

7.2 Tidal level

The calibration of the water levels provided by the model was aimed at 0.1 m accuracy. This provided an indication if the roughness and bathymetry depth values provided a realistic lag on the tidal variation at the Langebaan Lagoon mouth. It was important that the water levels were not adjusted in time, but only in height due to the change in datum, as mentioned in **Section 6.3.1**, and the roughness of the bathymetry used to create the desired lag.

It should be noted that the roughness also had an impact on the velocities determined by the hydrodynamic model. Therefore the calibration of the water levels was done in parallel with the velocity calibration and not as a separate calibration calculation. A roughness for Manning's M value of 29 $m^{1/3}/s$ has proven to cohere best to both of these calibrations.

Figure 7-1 illustrates the correlation between the depths for the specified point where the water levels are measured and the depth provided by the MIKE21 model. The average accuracy for the water level calibration had a maximum deviation from the survey of 5.2%. This is an average deviation of 0.04 m, and a total of seven of the 349 time steps surveyed exceeding the accuracy limit of 0.1 m.

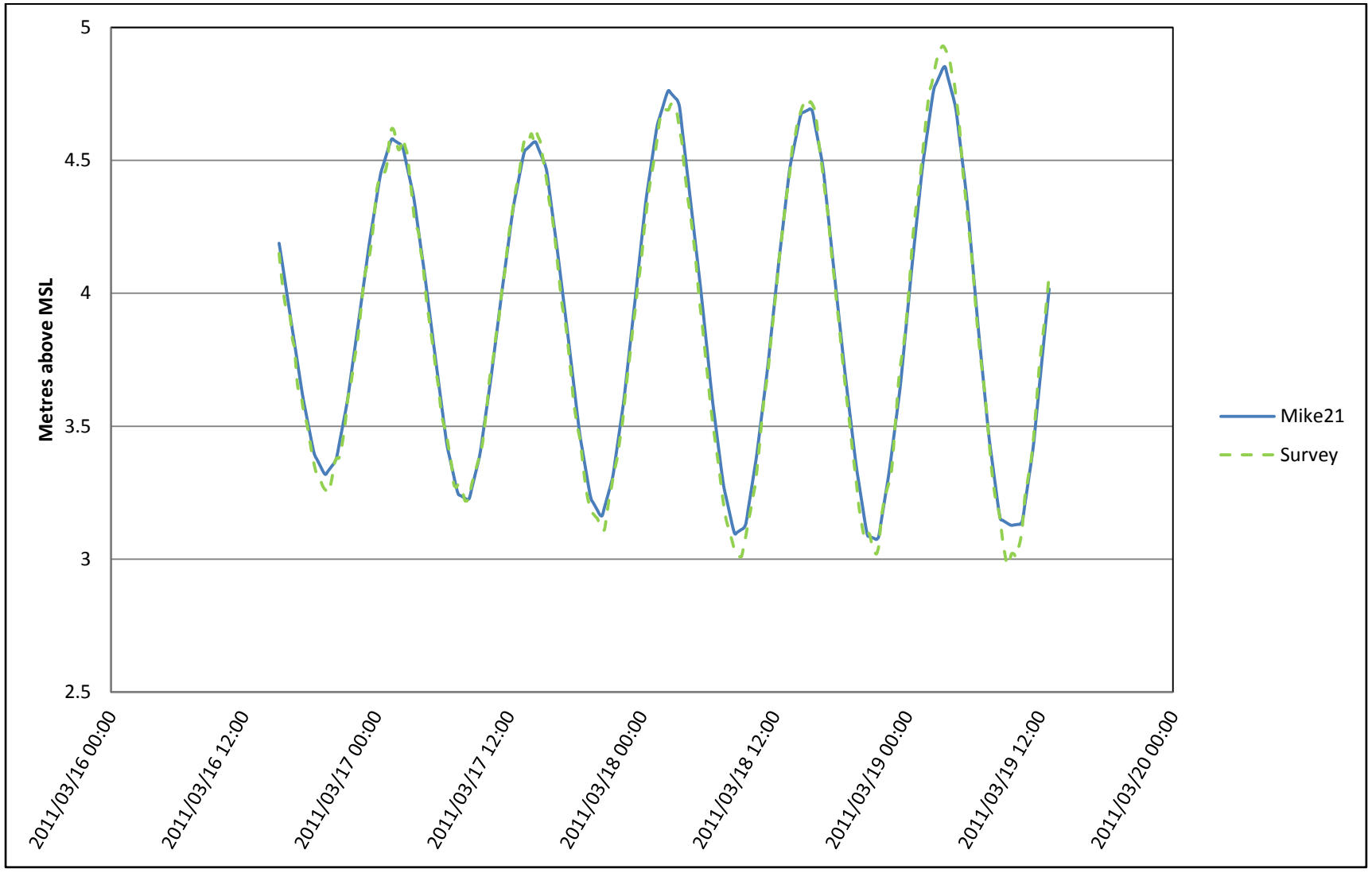

Figure 7-1: Water level calibration

7.3 Bathymetry

In order to identify whether there has been alterations to the seabed (e.g. the scouring of Langebaan Beach) since the conditions used for the generation of the bathymetry, a depth analysis were conducted. Actual depths were compared to the depths identified in the numerical model. If the change in the bathymetry were too large, different velocities and sediment transport could be expected for the two scenarios. Therefore, the depth calibration determined whether the velocity and sediment transport calibration would be acceptable.

Of the 34 points surveyed, with an overall accuracy of 47% for these 34 points. Five points were within 10% with an average accuracy of 5.2%, as provided in **Appendix F** (Note that the percentage used is only an indication of the accuracy).

The surveys executed at locations which provided a more accurate depth analysis and therefore indicating little difference between the model and reality carried a greater weight to the overall calibration. The less accurate points were located near the main channels to the west of Schaapen Island, near the Langebaan beach which experienced heavy cutback, and to the east of Schaapen Island,

The points located at the survey locations 14, 18, 22, 29 and 31, as illustrated in **Figure 6-4**, were calibrated during one of the tides, but not the opposite tide. The depth difference experienced for points 22, 29 and 31 were all within 0.55 metres, which could possibly be an influence due to wave actions on the lagoon or even boating activities near the point being surveyed, which has not been accounted for in the numerical model. Points 14 and 18 were both located in the main current to the east of Schaapen Island. The bathymetry is expected to change rapidly over short distances which were difficult to identified and model with the selected bathymetry cell size of 50 metres by 50 metres. Therefore, surveys at similar locations, but not at the exact same location, could lead to different depths for a single cell in the model.

It should be noted that the bathymetry may not be altered to fit better depth calibrations. The bathymetry was generated from existing records dating back to 1995. Alterations to the bathymetry could result in the modelling of an area which never existed. The depth is only an indication to the reliability of the survey data at the specified location.

7.4 Velocity

There were two factors investigated during the calibration of the velocity of the model. These were the magnitude and the direction of the velocity. The magnitude calibration was aimed at a range of discrepancy ratios in a direction within 45 degrees. Results for the magnitude of the velocities are provided in **Table 7-1**. Similar margins for calibration were applied during the sediment transport calibration process.

Table 7-1: Percentage of velocity surveys within discrepancy ratios

Data source	Current study	
	Average of all recorded data (31 locations)	Average of realistic recorded data (25 locations)
0,75 < r < 1.5	45	45
0,5 < r < 2	61	60
0,33 < r < 3	75	76

As stated in **Section 6.4**, some complications occurred with the equipment from the middle of the first day. This resulted in surveys done near the boat where the engine of the boat could have an influence on the velocities recorded. Wind velocities also increased, resulting in the boat moving during the execution of surveys and resulted in the use of the boat's engines to stabilize the boat.

The direction of the currents indicates that 26 of the points surveyed are within 45 degrees, of which 21 are within 22.5 degree. The 22.5 degrees to each side of the current provides the total angle of 45 degrees mentioned above as the ideal calibration conditions for the flow direction, as provided in **Table F-1** in **Appendix F**.

Two of the points not cohering to the velocity direction requirements were located near the convergence of the two main channels and the water mass located in Saldanha Bay, north-east of Meeuw Island.

One of the points surveyed had a deviation of more than 90 degrees, resulting in a measurement in the opposite direction than provided by the model. The depth calibration indicates that the bathymetry at that point changed by more than seven metres. This point is located within the main channel near the beach at Langebaan which has experienced extreme erosion. At this location, the channel deviates from a north-western to a north-eastern direction during ebb tides. This almost 60 degree bend in the main channel could result in extreme directional variations between reality and the model if the location surveyed are on the edge of the cell used for calibration.

7.5 Sediment transport

There are five formulae available for the calculation of sediment transport as mentioned in **Section 5.4.3**. Each of these five approaches was analysed to find the formulae providing the most accurate results. The parameters required by each of the approaches were identified and were considered along with the reliability of the data used for these parameters.

The primary variable during the sediment transport calibration was the relative density. Surveys done on the grading of the material in different locations in the mouth of the Langebaan Lagoon have been applied to construct a two-dimensional distribution of the sediment particle size across Saldanha Bay and Langebaan Lagoon. Particle sizes were based on the d_{50} and sediment grading were based on the d_{84} and d_{16} values derived from the data in **Appendix E**.

For the sediment transport calibration, results from the numerical model were compared to the observed results. The ratio between the predicted and observed rates provided a discrepancy ratio (r). This discrepancy ratio was compared to accuracy ranges commonly used during sediment transport calculations in reservoir sedimentation, as stated in WRC Report No. TT 91/97 (Basson & Rooseboom, 1997).

The most acceptable calibration was found for the *Engelund and Hansen* sediment transport theory, with a relative wet density of 2.57. 17 locations were surveyed during the field investigations, of which three points cohered to the depth calibration and ten locations did provided an acceptable correlation with the hydrodynamic velocities measured during the field survey (see **Table 6-9**). Thus, due to poor survey measurement and complications with the measurements, ten surveys were applied for the sediment transport calibration.

Table 7-2 : Percentage of sediment transport surveys within discrepancy ratios

Data source	WRC Report No. TT 91/97	Current study	
	Average of field data	Average of all recorded data (17 locations)	Average of realistic recorded data (10 locations)
0,75 < r < 1.5	32	27	50
0,5 < r < 2	64	40	75
0,33 < r < 3	88	47	89

Table 7-2 indicates that a good calibration was achieved when considering data where a realistic relationship were identified between hydrodynamic and sediment transport surveys.

7.6 Conclusion

Even though the outdated bathymetry created challenging circumstances for calibration of the numerical model, parameters used for calibration were generally within acceptable values.

The application of WXTide software for water level predictions has proven to be very accurate, especially for the required lag. Calibration expectations for the lag and the velocity based on a Manning's M roughness value of 29 $m^{1/3}/s$ was realistic for a medium grained non-cohesive sandy material.

Sediment transport calibration was limited due to survey data available and the correlation to depth calibrations. The relative density of 2.57 with the default porosity of 40 % provided by MIKE21 is realistic for wet sand material and well within the default values suggested by the MIKE21 software for non-cohesive sediment. This value also correlates well to the dry density of 1.67 as measured during the field investigation.

Even though good calibrations were obtained with realistic calibration values, only half of the points could be calibrated to the desired specifications. However, results should be analysed with caution.

Even though the calibration of the sediment transport model were considered good, the model would only provide an indication of the sediment transport due to the omission of wave action on the coastline. For a thorough investigation on the beach erosion experienced at Langebaan, wave action has to be included. Therefore, the models used to determine the impact of extreme wind and tidal driven currents in the Saldanha Bay and Langebaan Lagoon systems would not be able to accurately determine the erosion experienced at Langebaan Beach, but only an indication on the changes experienced on the seabed and in the main channels of the lagoon.

Table 7-3: Sediment calibration parameters used in numerical model

Calibration Parameter	Value
Bed resistance as a Manning M roughness ($m^{1/3}/s$)	0.29
Relative density	2.57
Porosity	0.4
Particle size	4 particle size ranges across bathymetry
Gradation	4 gradation ranges across bathymetry
Sediment transport theory	*Engelund & Hansen*

8 INVESTIGATION SCENARIOS

8.1 Introduction

During the analysis of previous studies on the hydrodynamics of the Saldanha Bay and Langebaan Lagoon systems, two current driving forces have been identified for water circulation. It has been concluded that wind dominated the hydrodynamics in Saldanha Bay and water level variations due to tidal oscillations determined the hydrodynamic conditions in the Langebaan Lagoon (Shannon & Stander, 1977).

Based on these two hydrodynamic driving forces, a variety of scenarios were identified to determine the possible impact of the causeway and jetty in Saldanha Bay on extreme tidal and wind driven currents. For this investigation the two dominant wind directions, identified as a northern and southern wind in **Section 5.3.7** and **Section 5.3.8**, and a third wind direction along the longest fetch were investigated, as well as extreme water level fluctuations. Scenarios identified are listed in **Table 8-1**.

Table 8-1: Parameters used for investigated scenarios

Scenario	Model parameter used
Tidal fluctuations excluding wind forcing	Predicted tidal levels for September 2011 with no wind
Tidal fluctuations including a 1 in 50 year wind from the north	Predicted tidal levels for September 2011 with a wind velocity of 19 m/s from a 0 ° angle
Tidal fluctuations including a 1 in 50 year wind from the south	Predicted tidal levels for September 2011 wind a velocity of 19 m/s from a 180 ° angle
Tidal fluctuations including a 1 in 50 year wind along the longest fetch	Predicted tidal levels for September 2011 with a wind velocity of 19 m/s from a 337.5 ° angle
Tidal fluctuations including a 1 in 100 year wind across the longest fetch	Predicted tidal levels for September 2011 with a wind velocity of 20.5 m/s from a 337.5 ° angle
Tidal fluctuations with a 1 in 50 year storm surge event added, excluding wind forcing	Predicted tidal levels over 3 days with a maximum tidal high water level of 3.306 metres (1 metre surge added to the highest astronomical tide of 2.03 metres) above MSL
Sea level rise excluding wind forcing	Predicted tidal levels for September 2011 increased by 0.4 metres

The first mentioned scenario based on tidal fluctuations excluding the effects of wind forcing was used as a base model to compare the other scenarios with. This scenario consisted of a hydrodynamic driving parameter, present in all other models, and would therefore be able to indicate the changes that occur due to additional wind forcing or extreme changes in the water level.

An additional model was added to the above scenarios to determine the impact of long-term tidal fluctuations on the Saldanha Bay and Langebaan Lagoon systems and the morphology of these two systems due to sediment transport.

For each of the scenarios mentioned, including the long term model, the conditions prior to the construction of the harbour structures and the conditions after the construction of the causeway and the jetty were modelled. Changes to parameters, excluding the bathymetry modifications to simulate effect prior to and after the construction of the causeway and the jetty, were implemented as mentioned previously in **Table 8-1**.

Sediment transport was also modelled for each of the scenarios. During the scenarios mentioned previously, sediment transport as a result of the tidal and wind driven currents in Saldanha Bay and Langebaan Lagoon were investigated, excluding the effects of wave action on the coastline and thus excluding littoral drift.

Results for each of the models were extracted from selected cross-section in Saldanha Bay and Langebaan Lagoon. These cross-sections are provided in **Figure 8-1** and **Figure 8-2**, respectively.

Six cross-sections were identified in Saldanha Bay, providing data on the hydrodynamic and sediment transport conditions at the entrance of Saldanha Bay, entrance to the harbour, conditions in Small Bay and conditions in Big Bay.

For Langebaan Lagoon, ten cross-sections have been identified. Similar to the locations where surveys were done for the field investigation, cross-sections were identified at the entrance to the lagoon, in each of the main channels and to the south of Schaapen Island. In the main channel on the east of Schaapen Island, five cross-sections were investigated to determine the influence of the tidal forcing on the sediment transport at the coastline and the possibility of the erosion of the beach.

Results extracted from the cross-sections for each of the scenarios are available in **Appendix H**. These results include the hydrodynamic and sediment transport conditions for both the flooding and ebbing tides.

Note that the labelling mentioned post and prior, referring to the conditions after the construction of the causeway and the jetty and conditions prior to this structure, respectively.

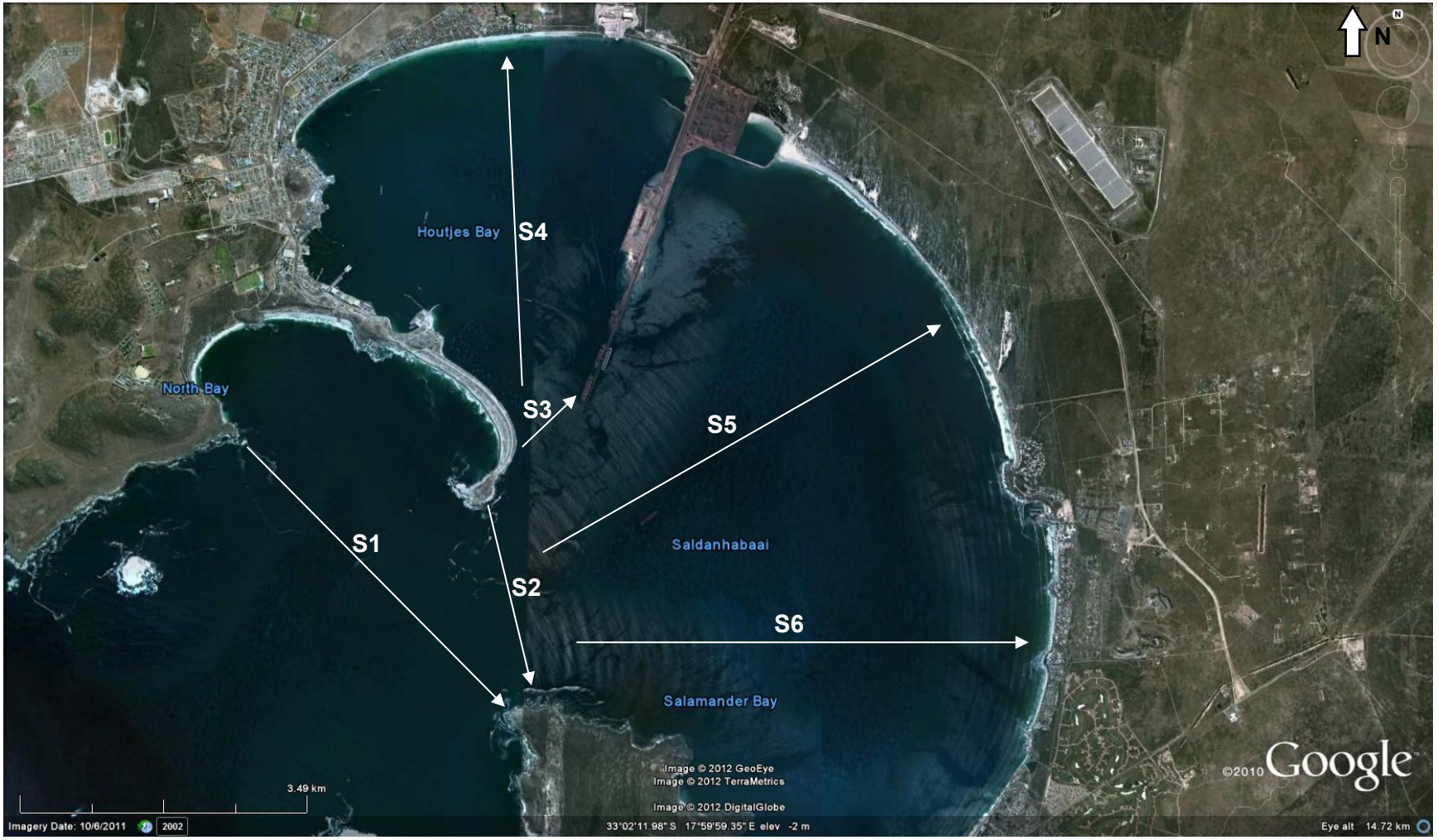

Figure 8-1: Sections analysed for investigation in Saldanha Bay

Figure 8-2: Sections analysed for investigation in Langebaan Lagoon

8.2 Tidal fluctuations excluding wind forcing

A first investigation was based on a common factor present in all other scenarios, the tidal fluctuations. The scenario based on this common factor was used to indicate the impact of various changes in the wind and tidal conditions on the hydrodynamics and sediment transport in Saldanha Bay and Langebaan Lagoon. Basic alteration in the hydrodynamics and sediment transport due to tidal action prior to and after the construction of the causeway and jetty were also derived from this scenario.

The annual extreme tidal conditions during September 2011, as identified in **Section 5.3.8**, were utilized during these simulations for both conditions prior to and after the construction of the causeway and the jetty.

Figure 8-3 and **Figure 8-4** illustrates the hydrodynamic conditions in plan expected during the flood and ebb tides for both the conditions prior to and after the construction of the causeway and the jetty in Saldanha Bay. During both ebb and flood tides, the velocities at the entrance to Saldanha Bay after construction were greater than velocities prior to construction. Flood tides indicated a 25 % increase in velocity from 0.24 m/s to 0.30 m/s during flood tides and a 12 % increase from 0.23 m/s to 0.26 m/s during ebb tides for conditions prior to and after the construction of the causeway and the jetty respectively. At the location of the causeway prior to construction, large velocities were indicated during both flood and ebb tides, which were absent after the construction of the causeway.

A general clockwise rotation towards the Langebaan Lagoon was observed during flood tides at the location of Big Bay for conditions prior to and after the construction of the causeway and the jetty, and anti-clockwise for the location of Small Bay. During ebb tides, flow in the opposite direction was observed, with a variation in flow direction at the entrance to the Langebaan Lagoon.

	Prior to construction	**After construction**
Ebb Tide	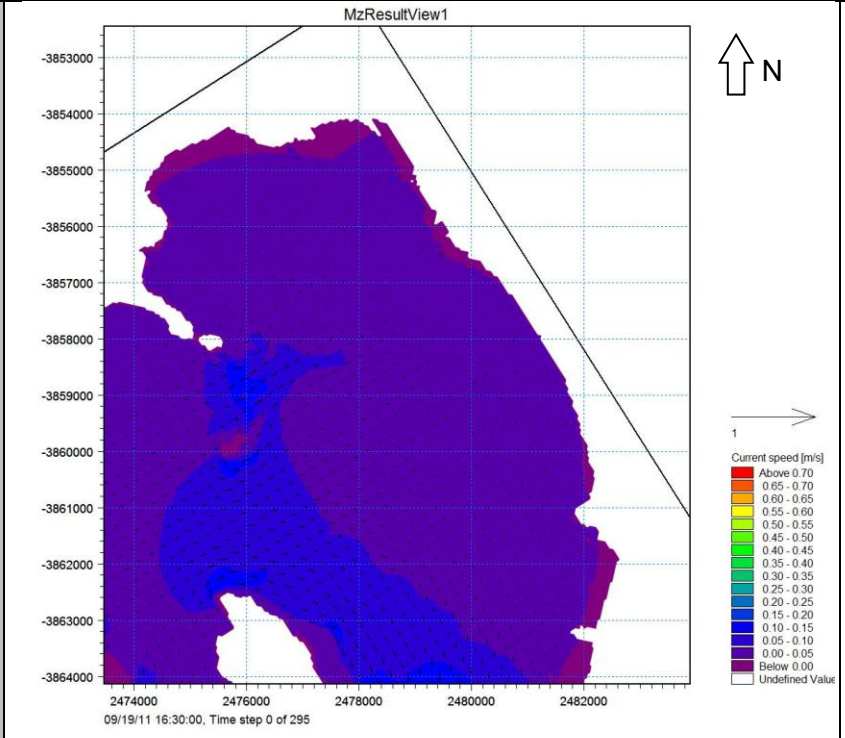	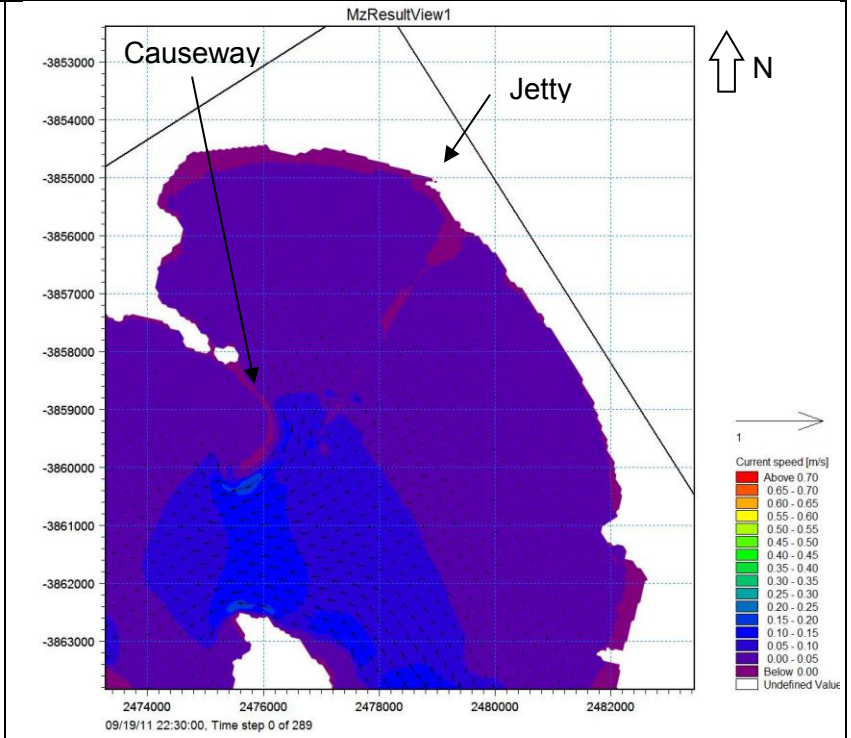

Figure 8-3: The effect of tidal fluctuations excluding wind conditions in Saldanha Bay during ebb tide

	Prior to construction	**After construction**
Flood Tide	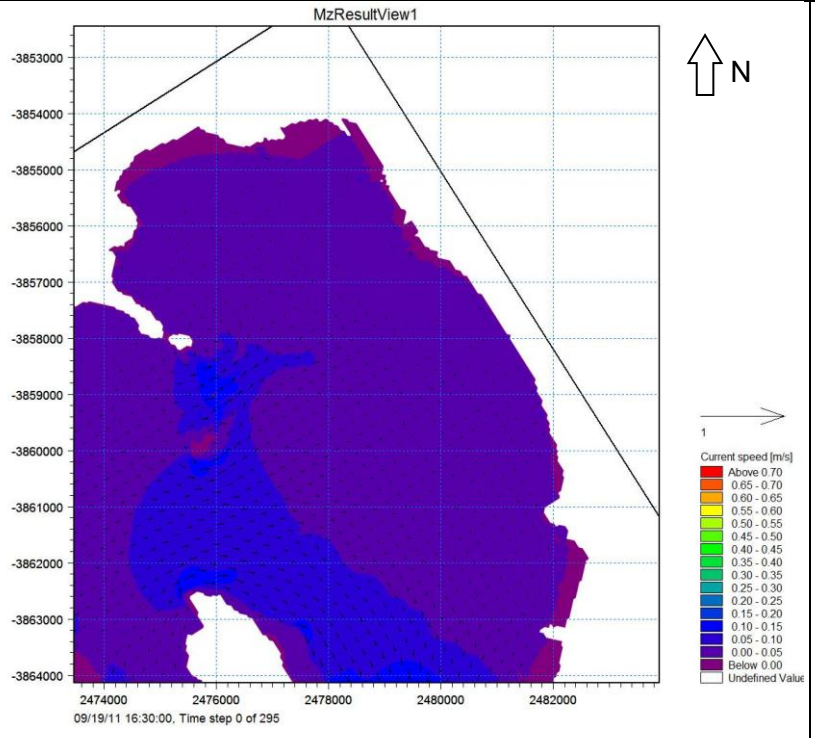	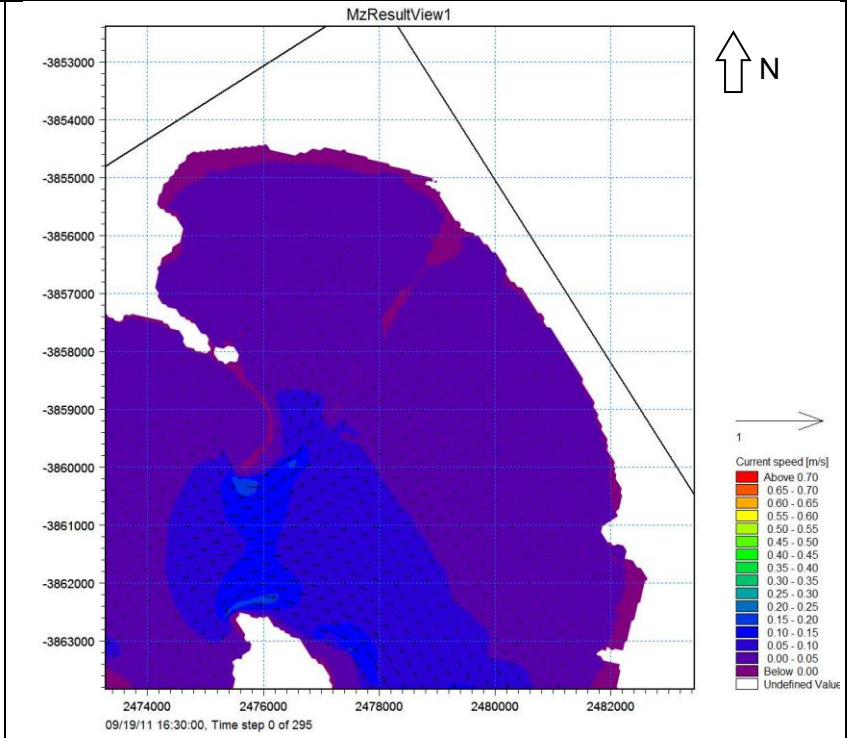

Figure 8-4: The effect of tidal fluctuations excluding wind conditions in Saldanha Bay during flood tide

	Prior to construction	**After construction**
Ebb Tide	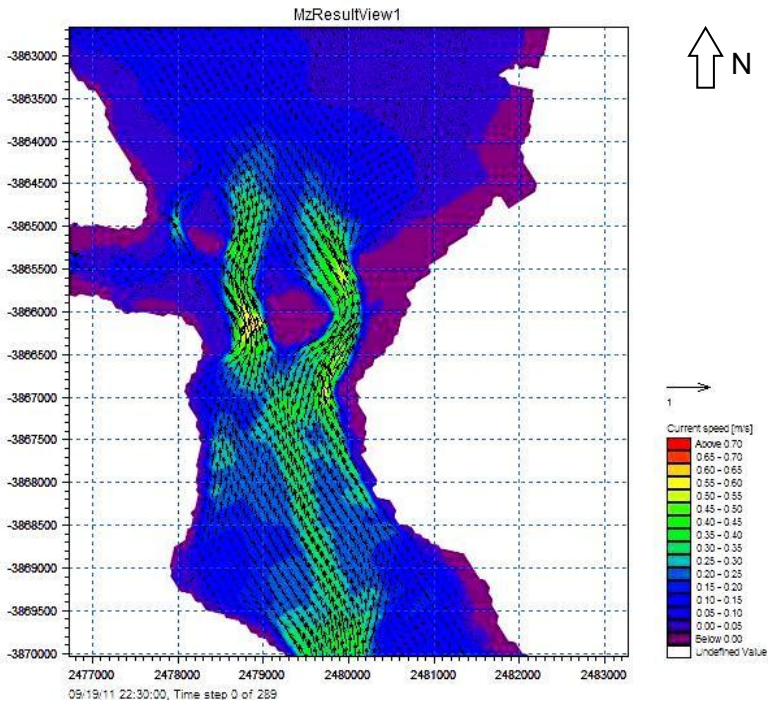	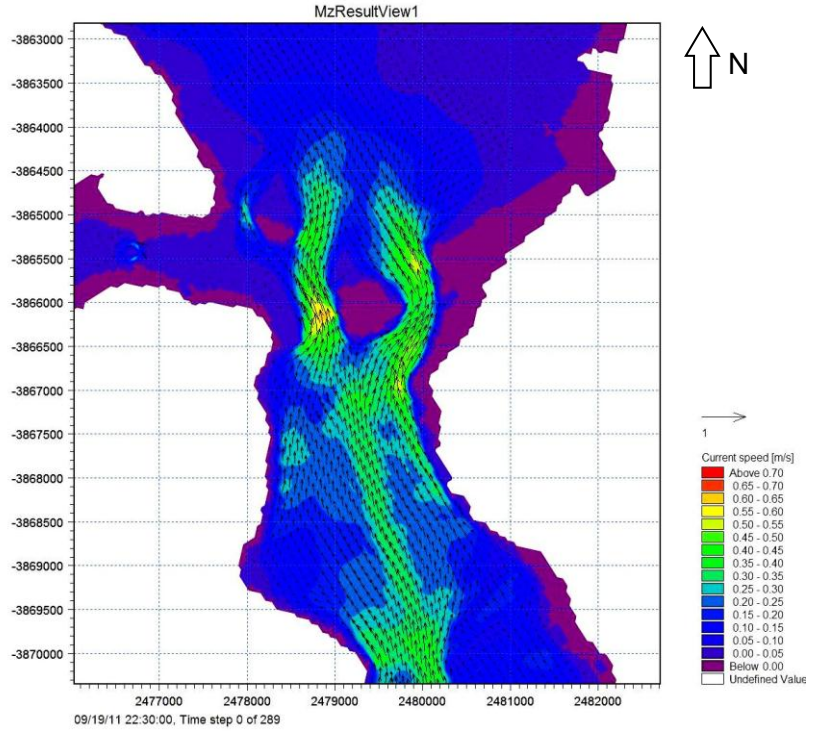

Figure 8-5: The effect of tidal fluctuations excluding wind conditions on the Langebaan Lagoon during ebb tide

	Prior to construction	**After construction**
Flood Tide	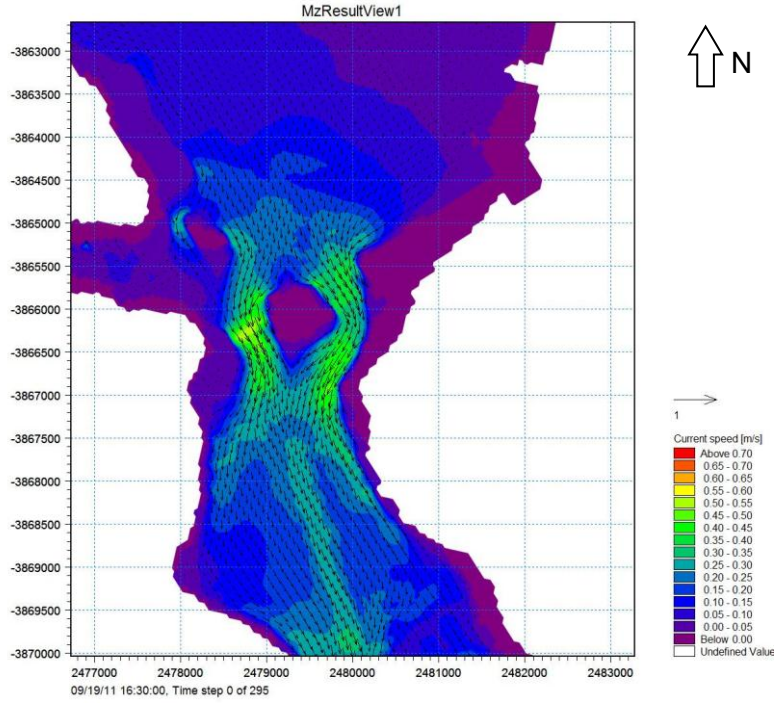	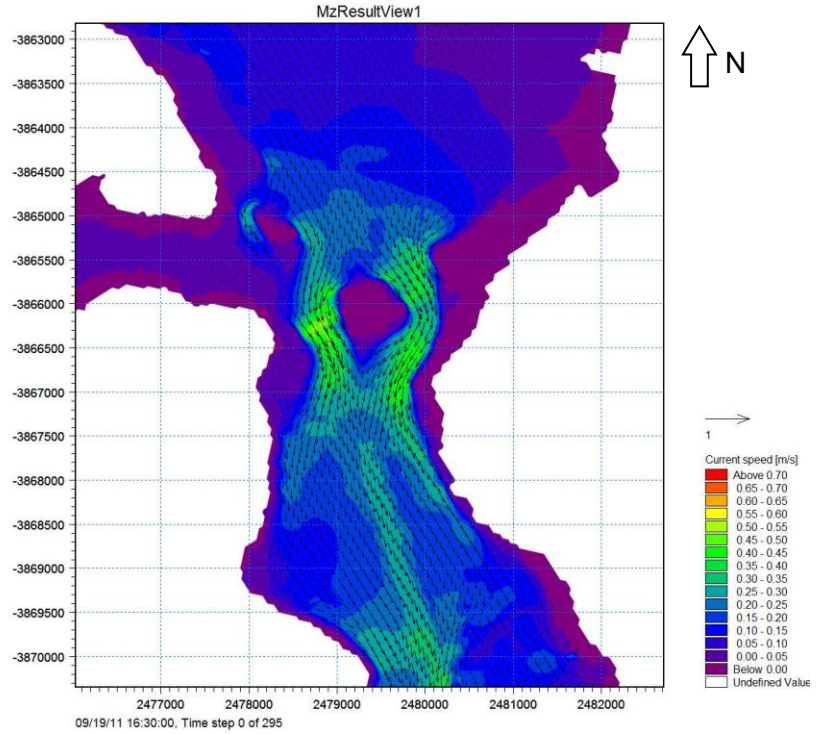

Figure 8-6: The effect of tidal fluctuations excluding wind conditions on the Langebaan Lagoon during flood tide

Conditions for the lagoon during both flood and ebb tides prior to and after construction are illustrated in **Figure 8-5** and **Figure 8-6**. The hydrodynamic conditions prior to and after the construction of the causeway indicate no changes in flow direction. However, changes in the hydrodynamics were observed during flood and ebb tides. During flood tides, the clockwise rotation of the hydrodynamics in Saldanha Bay resulted in water entering the lagoon from a north-eastern direction, flowing in a south-western direction. Ebb tides extracted water from the lagoon which flows directly towards the boundary between Saldanha Bay and the Atlantic Ocean. During these flow conditions, water flowed from the south towards a north-eastern direction. Therefore, the direction of flow during flood and ebb tides at the lagoon differs in direction.

The results on the cross-sections, illustrated in **Figure 8-1** and **Figure 8-2** and results provided in **Appendix H.1**, indicates large alterations due to the harbour development in the hydrodynamic velocities at the location of the causeway and the jetty. As indicated for sections S1 and S2, flow velocities have increased due to the construction of the causeway. During conditions prior to the harbour development, larger velocities were located at the south of the entrance to Saldanha Bay. Sediment transport results are possibly inaccurate due to a lack of sediment particle data at this location. However, larger velocities located to the south of the entrance to Saldanha Bay would result in sediment transport. For both these sections, similar patterns for the flooding and ebbing tides were observed before and after the construction of the causeway and jetty.

Section S3, located at the entrance of Small Bay, indicates a major increase in velocity of 39 % during flood tides and 24 % during ebb tides. These greater velocities resulted in sediment transport and possible erosion located at the structures. Major alterations in the flooding and ebbing tides were also observed. Previous studies have proposed three-dimensional modelling at this location due to the complex flow patterns (Luger, 1999).

Sections S4, S5 and S6 indicate alterations in the water velocities at the entrance to Saldanha Bay, with very little variation in hydrodynamics toward the coastline. Near the coastline, flooding and ebbing tides provided similar velocities for both conditions before and after the construction of harbour structures, thus indicating very little influence from the harbour structures on the velocities based on tidal forcing.

Velocities in Saldanha Bay, based on tidal forcing, were in the order of 0.3 m/s, similar to velocities in Saldanha Bay during previous investigations (Luger, 1999). The lack of sediment particle information can however influence the results on sediment transport in Saldanha Bay.

Section L1 is located at the entrance to the lagoon, where the two main channels around Schaapen Island connects to Big Bay. Hydrodynamic conditions at this section indicate large velocities during ebb tides in the main channels and a more equal velocity distribution across the cross-section during flood tides. This difference between flooding and ebbing tides was caused by the flow contractions around the island, splitting the water entering or exiting the lagoon, depending on the tide. During a flood tide, sections downstream of the island provided hydrodynamic conditions indicating two main channels while the currents upstream of the island have not been split into two main channels and were therefore more equally distributed. Sediment transport at section L1 were expected towards the sides of the cross-section during ebb tides at the locations of the two main channels. The smaller velocities during flood tide could result in very little to no sediment transport.

Sections L2, L3, L4, L5 and L6 were located in the eastern main channel between the town of Langebaan and Schaapen Island. This channel was located at Langebaan Beach which experienced extensive erosion in the past. In general, velocities generated by ebb tides provide greater maximum velocities than flood tide conditions. Sections L2, L4, L5 and L6 indicated a greater velocity near the coastline at Langebaan and section L3 a more equally distributed flow velocity across the cross-section for ebb tides. This was a result of the change in flow direction around the island. Flood tides indicated a similar situation for sections L5 and L6, however, sections L2 and L3 indicated larger velocities near the island. The equal distribution of velocity experienced in section L4 indicated a change in the flow direction experienced in the main channel.

Greater velocities of about 0.8 m/s to 0.95 m/s were observed near the coastline at Langebaan in these cross-sections, which would indicate more sediment transport. This location where greater sediment transport is expected is also located near the beach which experienced extensive erosion.

The velocities of 0.9 m/s to 1 m/s, located in the eastern channel, were much greater than the velocities located in Saldanha Bay, of about 0.25 m/s, and were therefore more influenced by water level alterations than Saldanha Bay. These greater velocities are also an indication of more regular sediment transport activities.

Section L7 and L8 were located in the main channels to the west of Schaapen Island. Maximum velocities were similar to the velocities in the eastern main channel and thus suitable for sediment transport.

Section L7 indicated a large variation in the flow distribution across the cross-section for flood and ebb tides. Ebb tides indicated a clear location of the main channel near the island and very little flow near the coastline, while flood tides indicated an increase in velocity when moving from the coastline to the main channel. Similar to the situation for sections upstream and downstream of Schaapen Island, flow contractions resulted in a change in velocities during flood and ebb tides.

Section L8 indicated similar flow velocities for both flood and ebb tides. However, during flood tides, greater velocities near the coastline were observed, but not large enough to result in sediment transport.

Sections L9 and L10 are located at the south of Schaapen Island, where two main channels around the island joined into a single main channel. Section L9 clearly indicated the two main channels during flood tide, providing larger velocities towards the sides of the cross-section. During ebb tides, the two main channels were also identified with a smaller difference between the main channels and the area located between these two main channels. Larger velocities were observed near the town of Langebaan, towards the eastern channel.

Velocities during the flood and ebb tides at section L10 were evenly distributed across the lagoon, with greater velocities located in the main channel of the lagoon during ebb tides. These greater velocities were absent during flood tides, rather generating larger velocities towards the eastern side of the lagoon. Maximum velocities were also decreasing at this location, indicating less sediment transport.

The effect of the construction of the causeway and jetty in Saldanha Bay had minor influences on the tidal generated currents in the lagoon, and thus minor influences on the sediment transport patterns in the Langebaan Lagoon. The tidal water level fluctuations were not influenced by the structures in Saldanha Bay and therefore should not influence the tidal driven velocities in the Langebaan Lagoon.

Sediment transport was generated by the model at velocities in the order of 0.3 m/s to 0.4 m/s in the lagoon. These velocities were similar to the recorded data during the field investigation, where sediment transport was generated by velocities in a similar range. Most of the sediment transport activities were generated around the island.

8.3 Tidal fluctuations including a 1 in 50 year wind from the north

To determine the effect of wind on the hydrodynamics and sediment transport of the Saldanha Bay and Langebaan Lagoon systems, a significant wind speed had to be identified and the direction of the wind, as required by MIKE21. During this scenario, a 1 in 50 year wind velocity, as identified in **Section 5.3.6**, were implemented from the north. Northern winds have been identified as one of the dominant wind directions during winter months. Results from this scenario were compared to the results in **Section 8.2**.

Figure 8-7 and **Figure 8-8** illustrates the effect of a 1 in 50 year northern wind on the hydrodynamics of Saldanha Bay. A clockwise rotation was observed at the location of Big Bay during all conditions, both prior to and after the construction of the causeway and the jetty during both flood and ebb tides. The location of Small Bay indicated an anti-clockwise rotation for all conditions, during flood and ebb tides for both conditions prior to and after construction. These circulation patterns confirm the conclusions during previous investigations (Luger et al., 1999), stating that a dominant clockwise rotation was observed in Big Bay and an opposite rotation dominating in Small Bay. A major difference in the hydrodynamics was observed near the causeway prior to construction during flood tides, where high velocities were observed entering Saldanha Bay.

In **Figure 8-7**, **Figure 8-8**, **Figure 8-9** and **Figure 8-10** a main current was identified for each of the tidal conditions at the entrance to the Langebaan Lagoon. During ebb tides, water extracted from the lagoon due to a decrease in water level was flushed along the west of the lagoon entrance. These currents, consisting of large velocities, flowed towards the entrance of Saldanha Bay and into the Atlantic Ocean. The main current observed during flood tides indicated that water flowing along the clockwise rotation of Big Bay, enters the lagoon to the east of the entrance of the lagoon, at the location of Langebaan Beach. These variations in hydrodynamic conditions during flood and ebb tides were similar for both conditions prior to and after the construction of the causeway and the jetty. Therefore, no influence on the hydrodynamics due to the development in Saldanha Bay was observed.

	Prior to construction	**After construction**
Ebb Tide	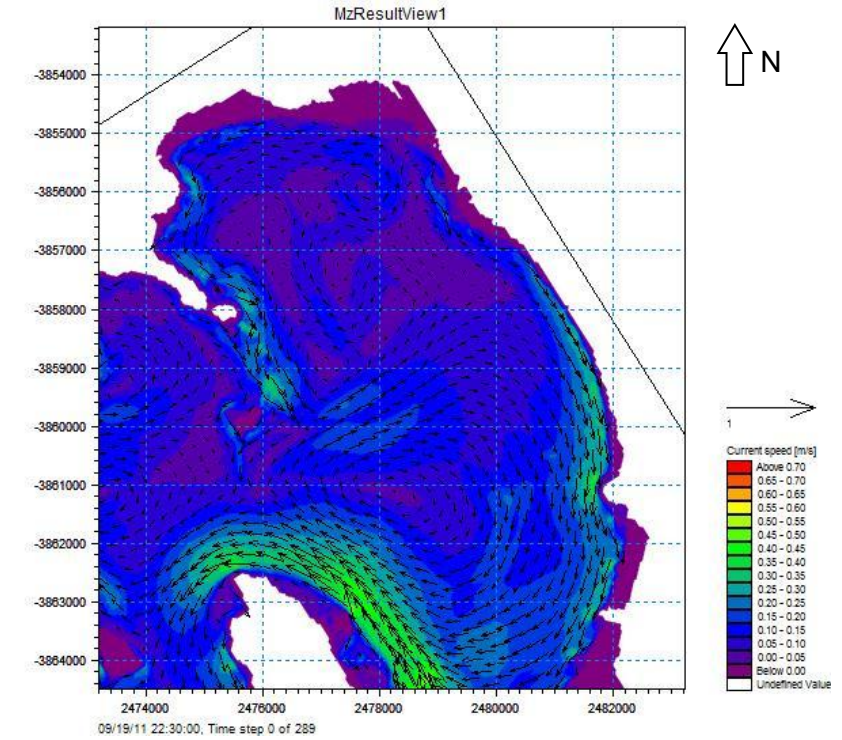	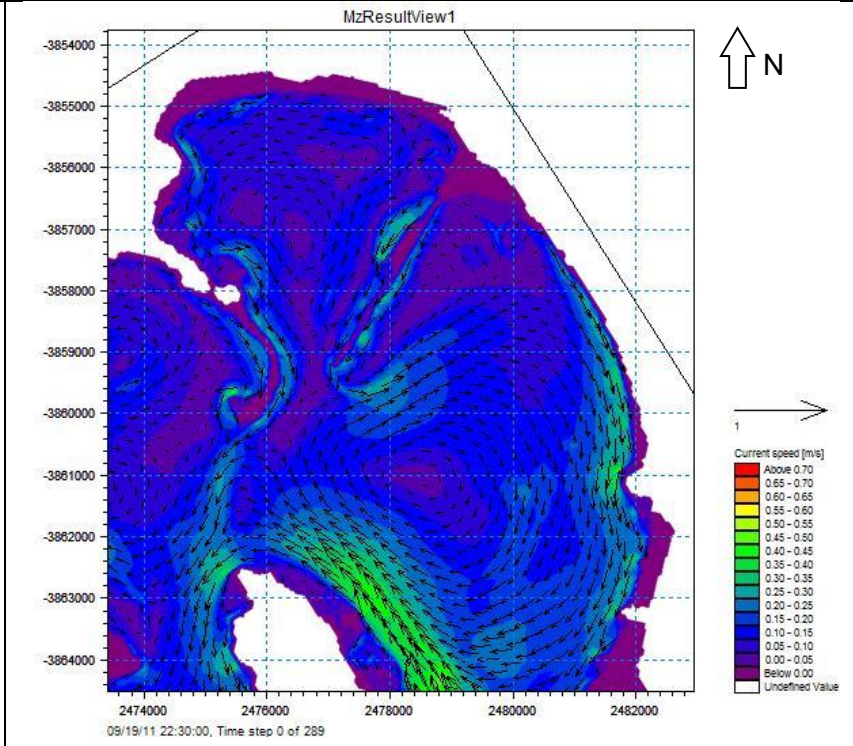

Figure 8-7: The effect of tidal fluctuations including a 1 in 50 year wind from the north in Saldanha Bay during ebb tide

	Prior to construction	**After construction**
Flood Tide	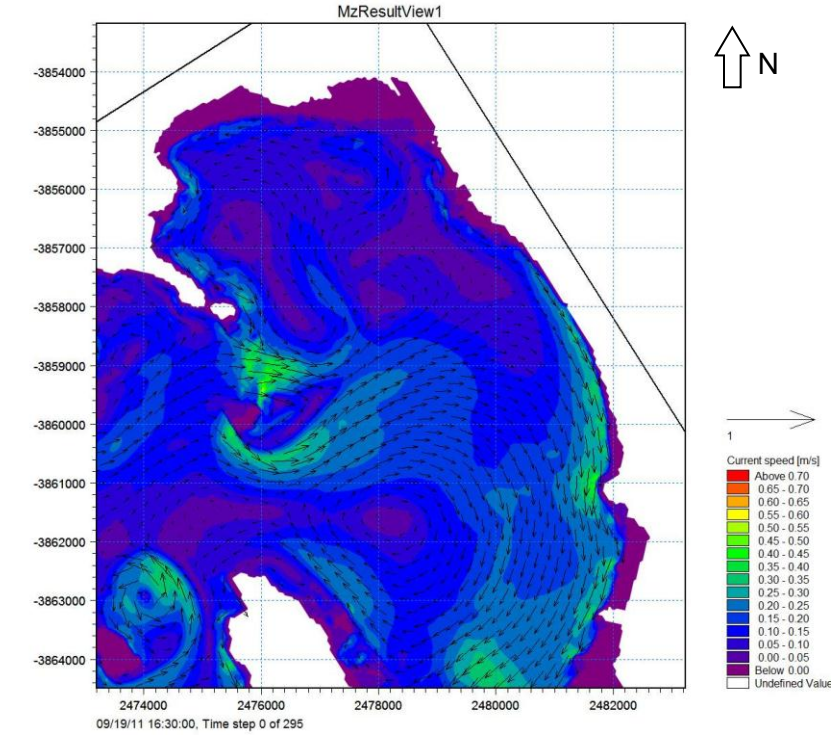	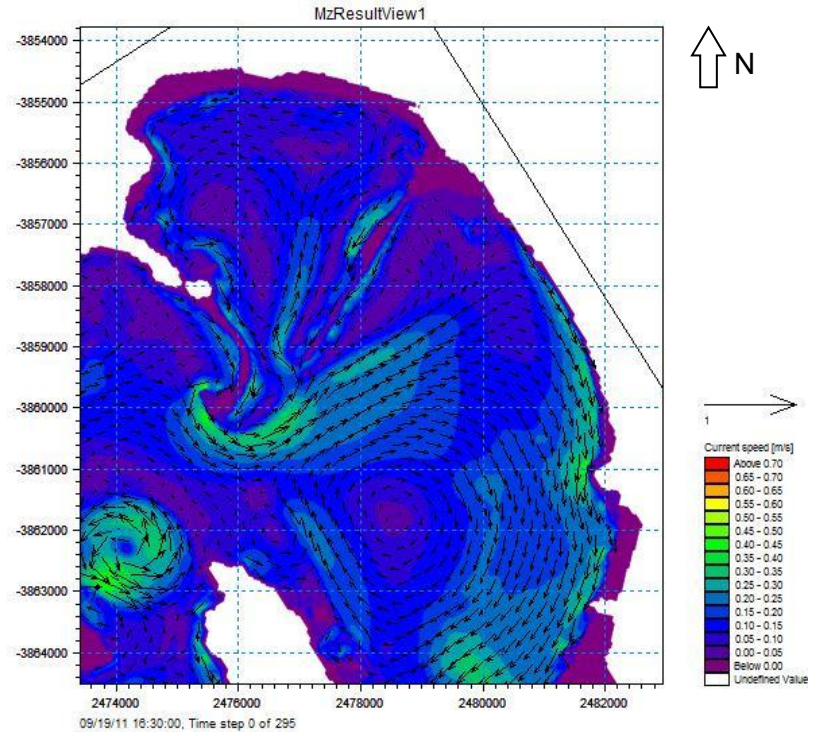

Figure 8-8: The effect of tidal fluctuations including a 1 in 50 year wind from the north in Saldanha Bay during flood tide

	Prior to construction	**After construction**
Ebb Tide	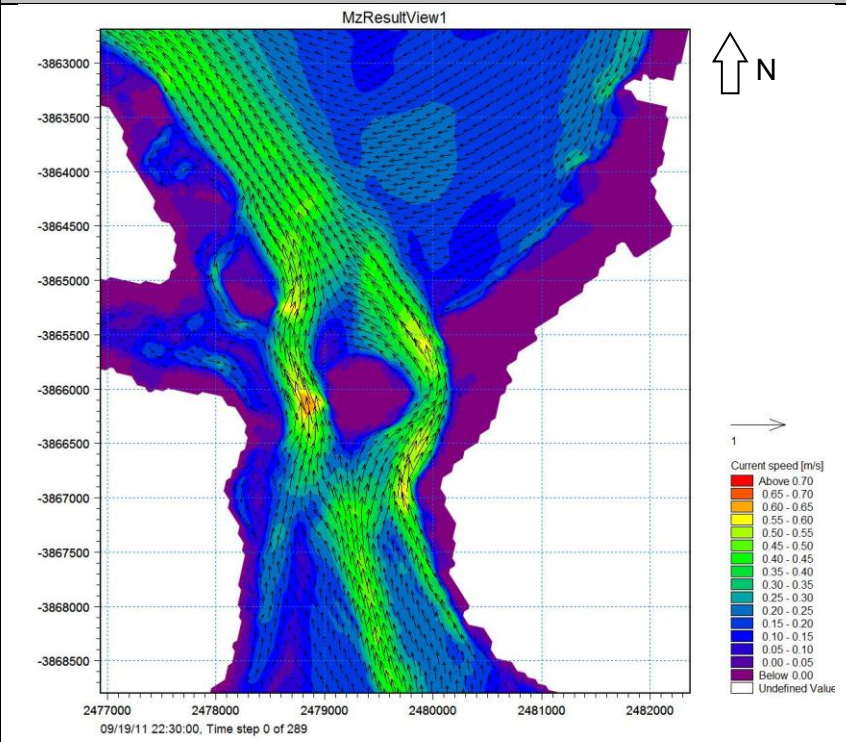	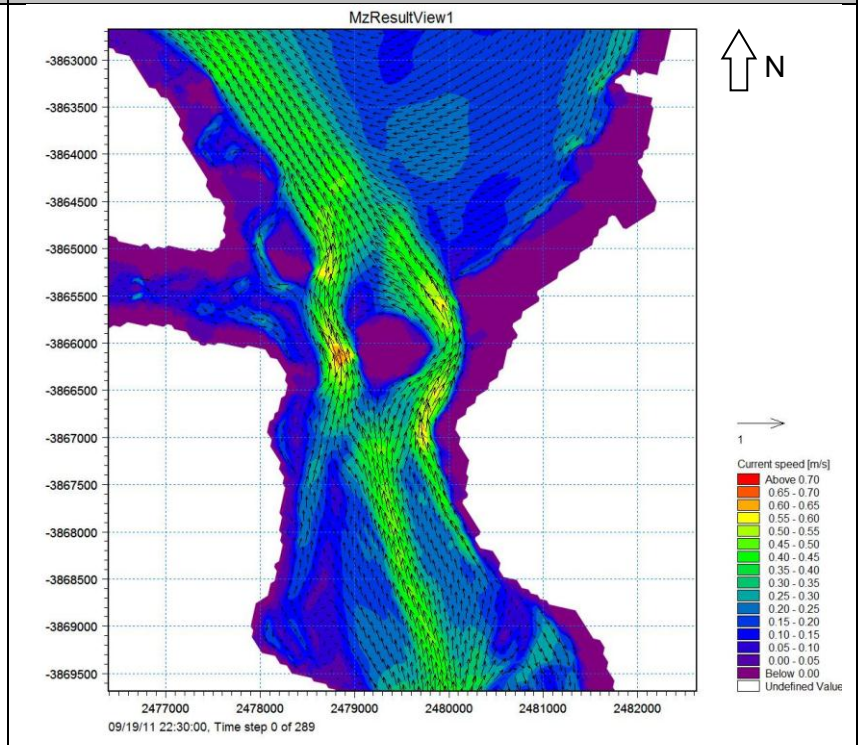

Figure 8-9: The effect of tidal fluctuations including a 1 in 50 year wind from the north in the Langebaan Lagoon during ebb tide

	Prior to construction	**After construction**
Flood Tide	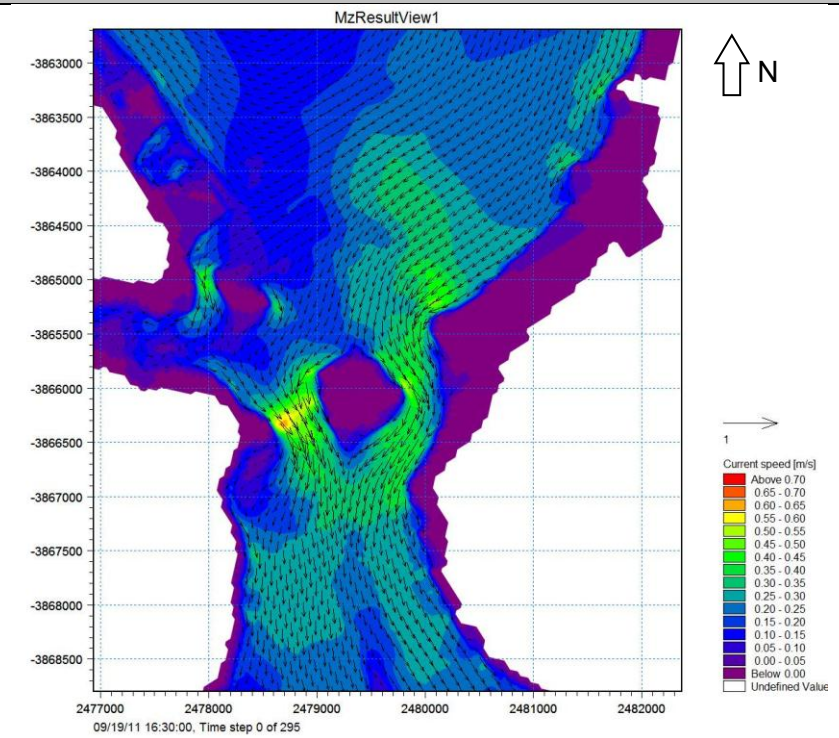	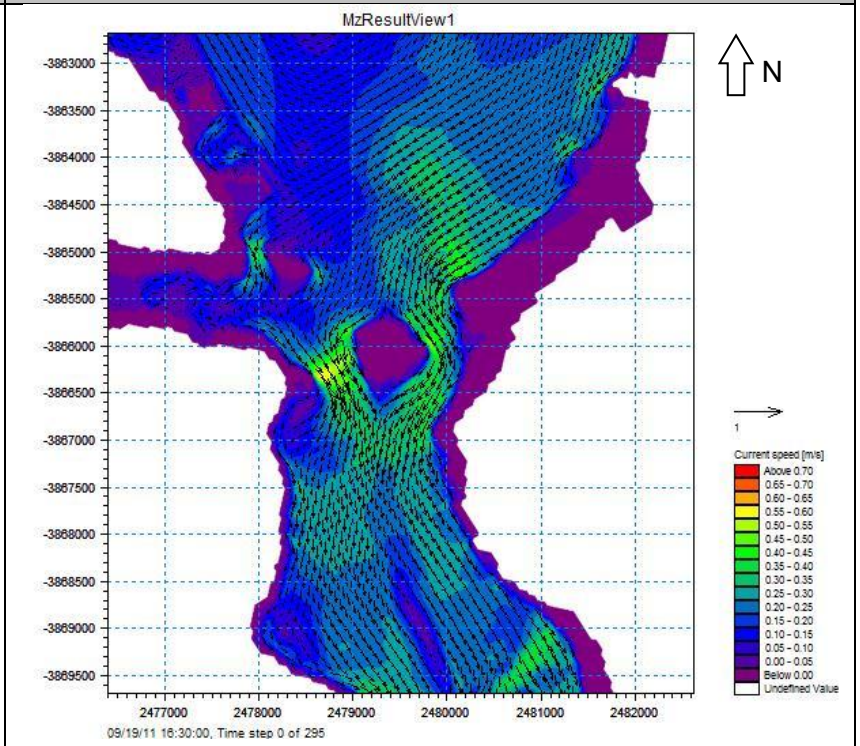

Figure 8-10: The effect of tidal fluctuations including a 1 in 50 year wind from the north in the Langebaan Lagoon during flood tide

Figure 8-9 and **Figure 8-10** provided no indication of a change in hydrodynamics prior to and after the construction of the causeway and the jetty, with similar result to conditions excluding the effect of wind in **Section 8.2**.

Results based on the cross-sections are provided in **Appendix H.2**, indicating the influence of a 1 in 50 year northern wind on the hydrodynamics and sediment transport of Saldanha Bay and Langebaan Lagoon. Each of these cross-sections provided data on the flooding and ebbing hydrodynamic and sediment transport conditions, and was compared to the results from the scenario based on tidal fluctuation excluding wind forcing discussed in **Section 8.2**. Cross-sections were extracted for the conditions prior to the construction of the causeway and the jetty and conditions after these constructions.

At the entrance to Saldanha Bay, the flood tides generated greater velocities near the coastline towards the sides of the cross-section and ebb tide generated greater velocities towards the middle of the cross-section. Velocities along the eastern coastline of Saldanha Bay indicated an increase in velocity for both flood and ebb tides compared to the conditions excluding wind forcing. However, sections S4 and S6 experience a decrease in velocity of 10% to 15 % during flood tides for both conditions prior to and after the construction of the causeway and the jetty, while an increase of 10 % to 20 % was experienced during ebb tides. Similar to the previous mentioned sections, section S5 experienced an increase of 2 % in velocity during a flood tide and decrease of 2 % during an ebb tide.

Cross-sections in the lagoon experienced a decrease of 1 % in velocity due to the influence of a northern wind for both flood and ebb tides. The cross-section at the entrance to the lagoon indicated a minor increase in velocity for flood tides at the western channel, but a decrease for ebb tides across the entire cross-section.

Velocities in the eastern main channel also indicated a decrease in flow velocities with little to no variation in conditions prior to and after the construction of the jetty and the causeway. Section L7 indicated very little variation in velocity due to the wind during flood tides, but section L8 to the south of section L7 indicates a decrease in velocity for both tidal conditions. The area south of Schaapen Island in section L9 provides little

variation for ebb tides during the wind event, but a decrease in velocity was observed to the south at Section L10.

Previous investigations mentioned that wind could have a minor influence on the velocities in the lagoon, but major effects on the hydrodynamics of Saldanha Bay (Shannon & Stander, 1977). This has been confirmed by the results from the model.

The overall decrease in velocity experienced in the lagoon for both flood and ebb tides were in the order of 1 %, however, resulted in a decrease in sediment transport in the lagoon. Minor variations in the velocity resulted in major differences in the sediment transport patterns.

The sediment transport pattern observed was similar to the hydrodynamic observations. At the entrance to Saldanha Bay, much greater sediment transport rates were observed to the south of the mouth due to the wind from the north. Sediment transport rates at the coastline to the east of Saldanha Bay experienced very little to no sediment transport.

At the Langebaan Lagoon mouth, sediment transport velocities decreased up to 56 % due to the wind from the north. There has however been a minor increase of 1 % in sediment transport after the construction of the causeway and the jetty.

8.4 Tidal fluctuations including a 1 in 50 year wind from the south

A second wind scenario was based on the dominant wind conditions during summer months, identified as a southern wind in **Section 5.3.6**. A similar wind speed as utilized in the previous scenario was implemented based on the 1 in 50 year event. Results from this investigation were compared to the results of the scenario excluding wind forcing, discussed in **Section 8.2**.

Results of this scenario, provided in **Figure 8-11** and **Figure 8-12**, indicates an opposite flow direction in the hydrodynamics as observed for a northern wind. At the location of Small Bay a clockwise rotation was observed, instead of the anti-clockwise rotation during a wind event from the north, and at the location of Big Bay an anti-clockwise rotation was present. These conditions were present for both flood and ebb tides, prior to and after the construction of the causeway and the jetty.

Figure 8-13 and **Figure 8-14** also indicated opposite conditions than previously observed. Ebb tides exit the lagoon to the east along the mainland to follow the anti-clockwise rotation observed in Big Bay. During flood tides, water entering Saldanha Bay followed the anti-clockwise rotation of Big Bay, but deviates into the lagoon along the western bank. No hydrodynamic differences could be identified around Schaapen Island or towards the south for conditions prior to and after the construction of the causeway and the jetty.

	Prior to construction	**After construction**
Ebb Tide	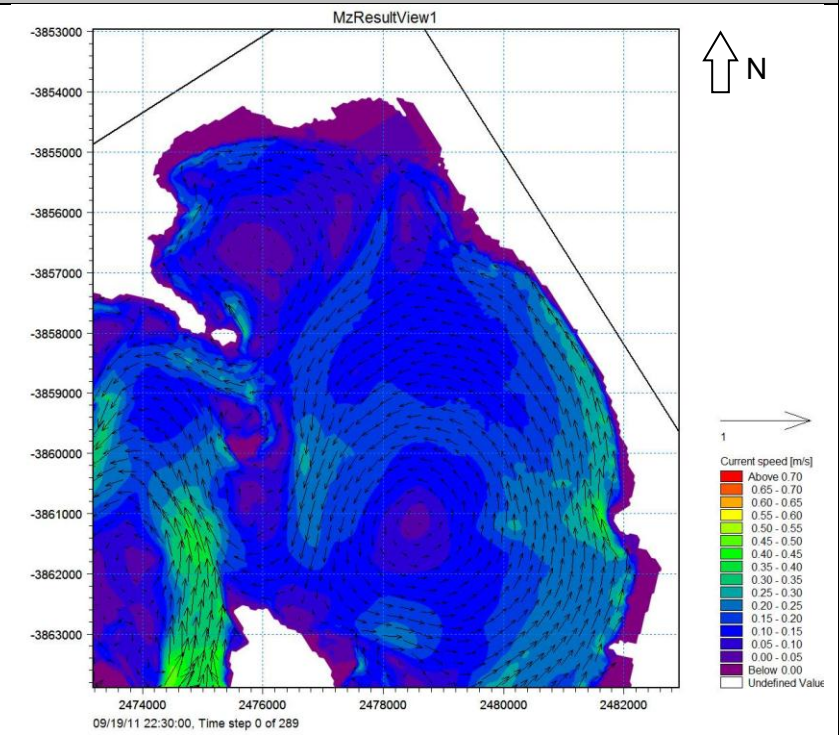	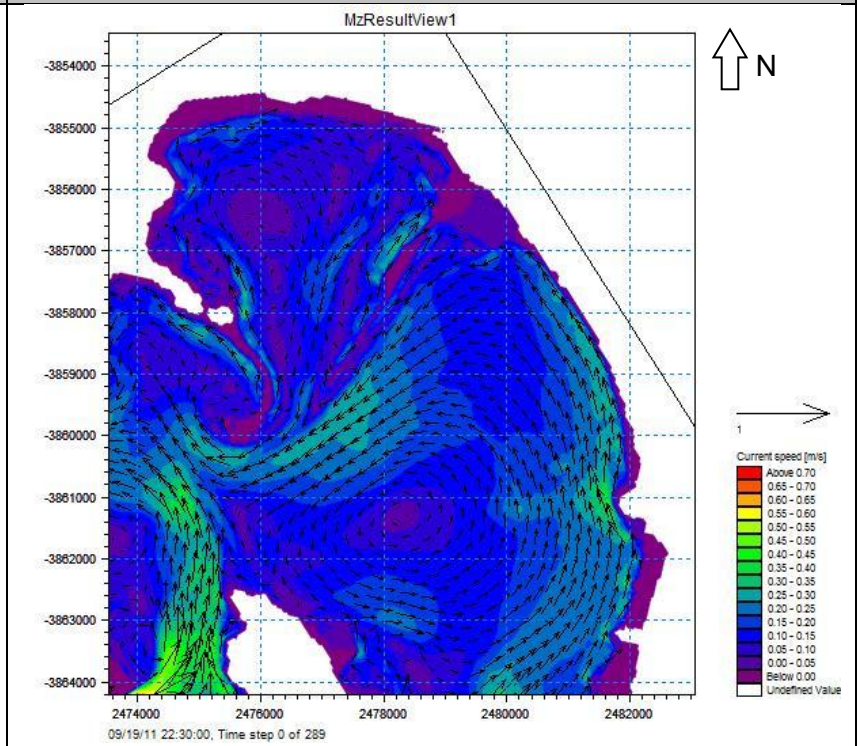

Figure 8-11: The effect of tidal fluctuations including a 1 in 50 year wind from the south in the Saldanha Bay during ebb tide

	Prior to construction	**After construction**
Flood Tide	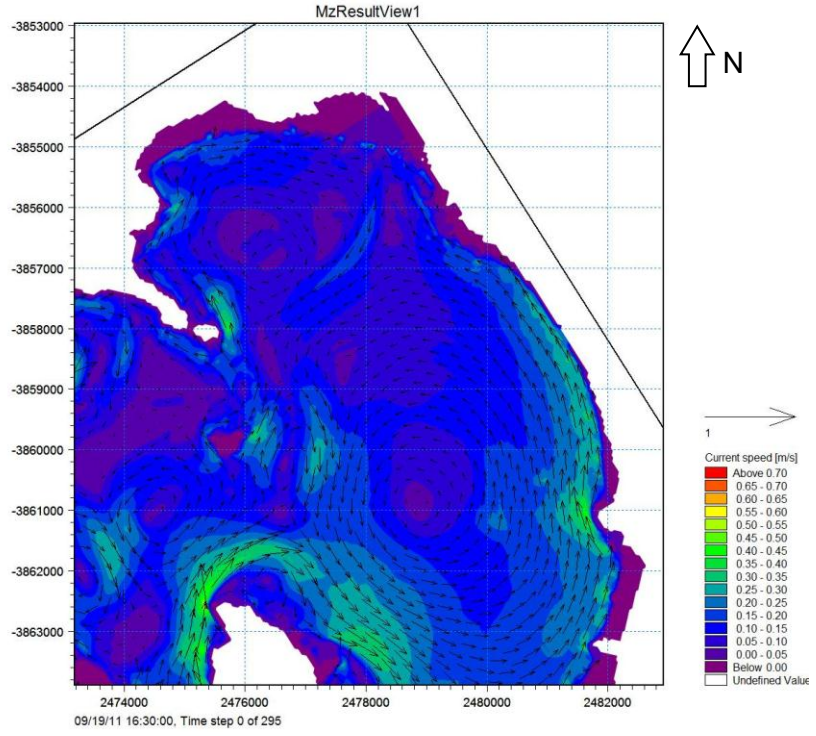	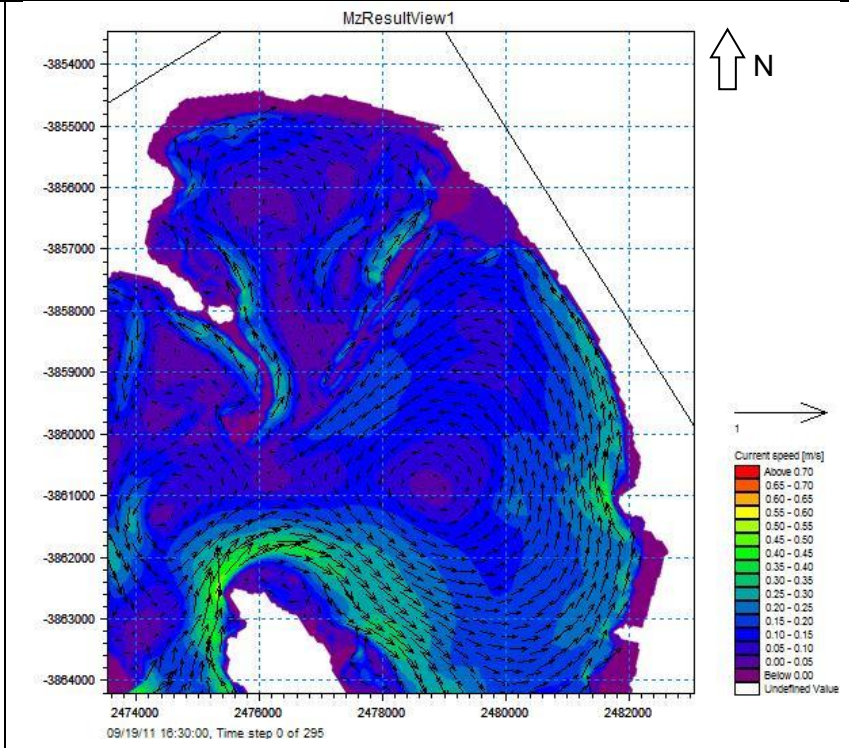

Figure 8-12: The effect of tidal fluctuations including a 1 in 50 year wind from the south in the Saldanha Bay during flood tide

	Prior to construction	**After construction**
Ebb Tide	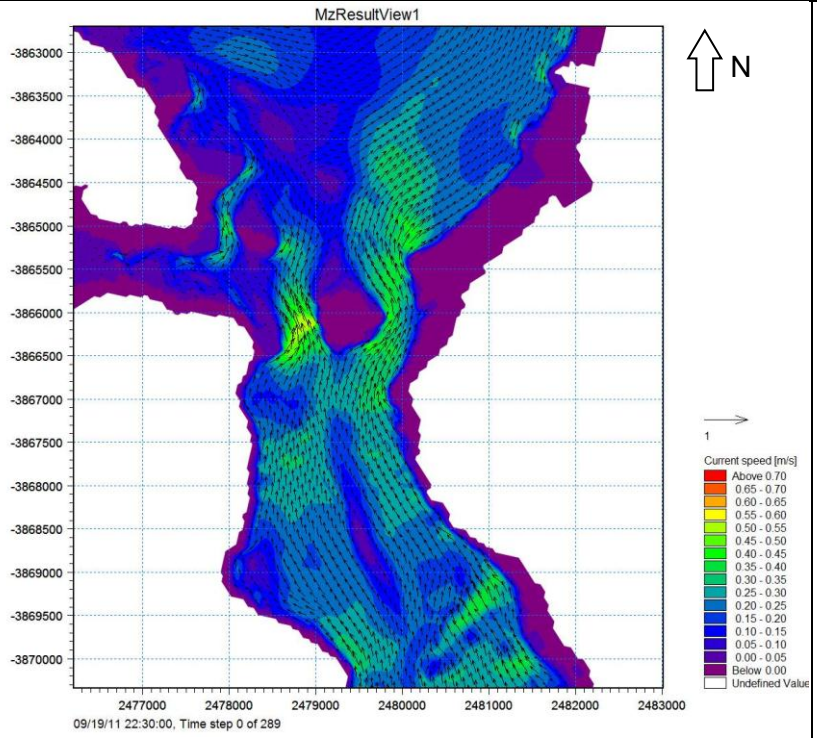	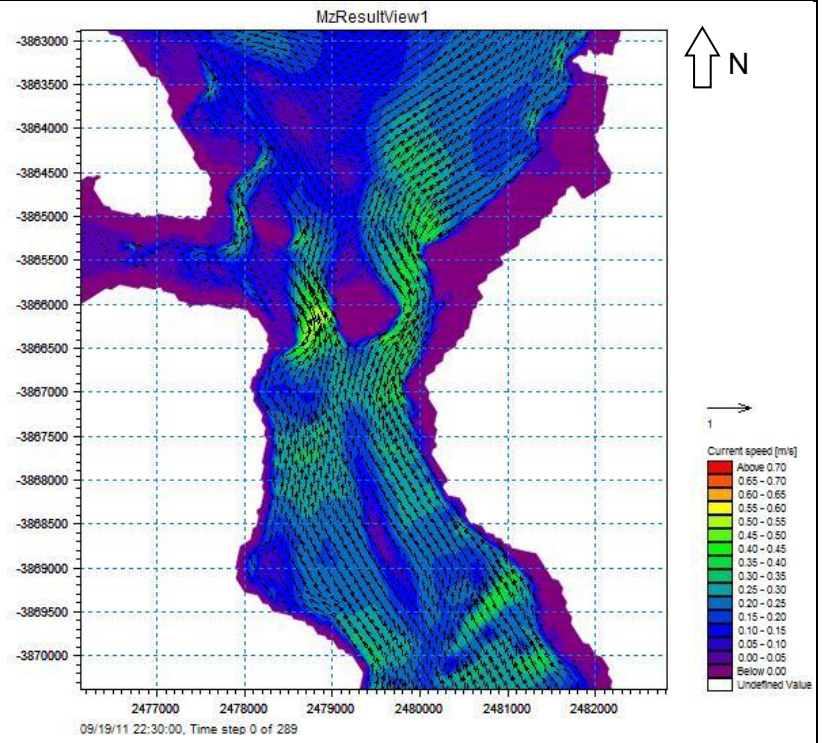

Figure 8-13: The effect of tidal fluctuations including a 1 in 50 year wind from the south in the Langebaan Lagoon during ebb tide

	Prior to construction	**After construction**
Flood Tide	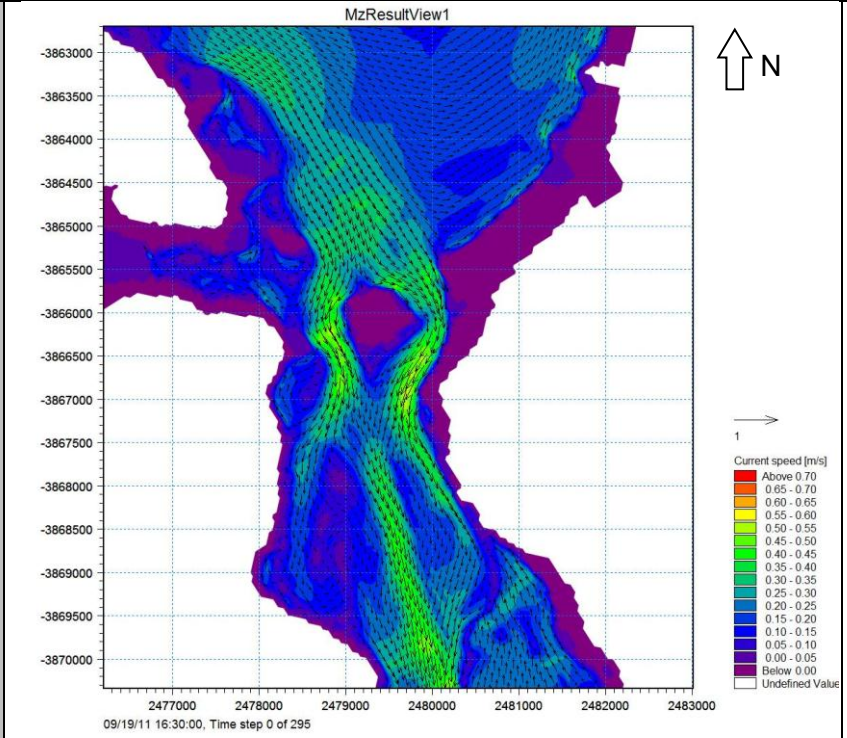	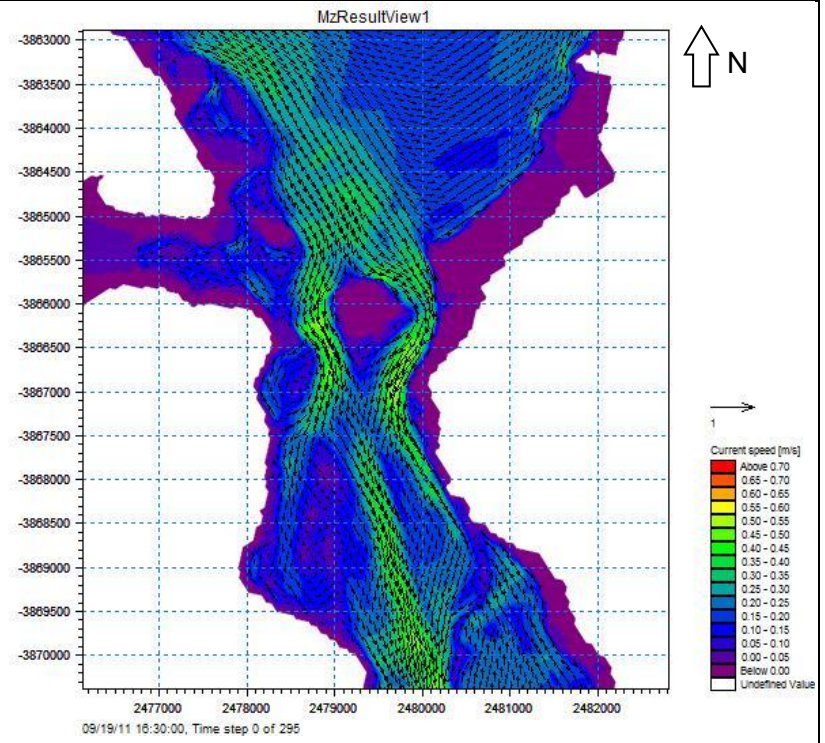

Figure 8-14: The effect of tidal fluctuations including a 1 in 50 year wind from the south in the Langebaan Lagoon during flood tide

Appendix H.3 provides the hydrodynamic and sediment transport conditions at various cross-sections compared to the conditions excluding wind forcing. Results from these extracts indicated greater velocities at the south of the entrance channel entering Saldanha Bay and smaller velocities to the north during flood tides. During ebb tides, greater velocities were provided at the northern section of the entrance channel to Saldanha Bay and smaller velocities to the south, exactly opposite to the velocities experienced during flood tides. Near the coastline of both Small Bay and Big Bay, larger velocities were observed than experienced during no wind conditions for both flood and ebb tides. The above mentioned conditions are similar for both conditions prior to and after the construction of the causeway and the jetty.

Even though these conditions were similar for both conditions prior to and after the construction of the causeway and the jetty, greater differences in the hydrodynamics and sediment transport were observed at the locations where the causeway and the jetty were constructed.

Hydrodynamic conditions in the Langebaan Lagoon indicated smaller velocities due to the effect of the wind, which also resulted in smaller sediment transport during a southern wind. Differences prior to and after the construction of the causeway and the jetty were minor, therefore indicating little to no influence on the hydrodynamics and sediment transport of the Langebaan Lagoon during a dominating southern wind.

8.5 Tidal fluctuations including a 1 in 50 year wind across the longest fetch

A third wind direction was investigated to determine the impact of a wind directed towards Langebaan Beach, at the town of Langebaan, and the impact of this wind on the possible erosion of the beach. The longest fetch direction, as identified in **Section 5.3.6** as a north-north-western wind direction, were implemented with a similar wind velocity as utilized in previous scenarios.

Figure 8-15, **Figure 8-16**, **Figure 8-17** and **Figure 8-18** indicates similar hydrodynamic conditions to the conditions present during a northern wind with a clockwise rotation at the location of Big Bay for conditions prior to and after the construction of the causeway and the jetty, but a variation in the hydrodynamic circulation in Small Bay. Conditions after the construction of the causeway and jetty indicate water entering along the centre of Small Bay and rotate in a clockwise and anti-clockwise rotation from the middle of the bay. The clockwise rotation towards the jetty was blocked by the jetty and forced towards the entrance of Small Bay. Conditions prior to the construction of the jetty indicated that water continued towards the location of Big Bay and join the clockwise rotation dominating in Big Bay. The above mentioned hydrodynamic circulation was similar during flood and ebb tides.

Hydrodynamic circulation at the entrance to the lagoon indicated similar flow pattern as observed during a wind from the north. Ebb tides continued along the clockwise rotation of Big Bay and towards the entrance of Saldanha Bay and flood tides enter from the east, deviating from the clockwise rotation in Big Bay to enter the lagoon. No major variation in the hydrodynamics was observed in **Figure 8-17** and **Figure 8-18** for conditions prior to and after the construction of the causeway and jetty in Saldanha Bay.

	Prior to construction	**After construction**
Ebb Tide	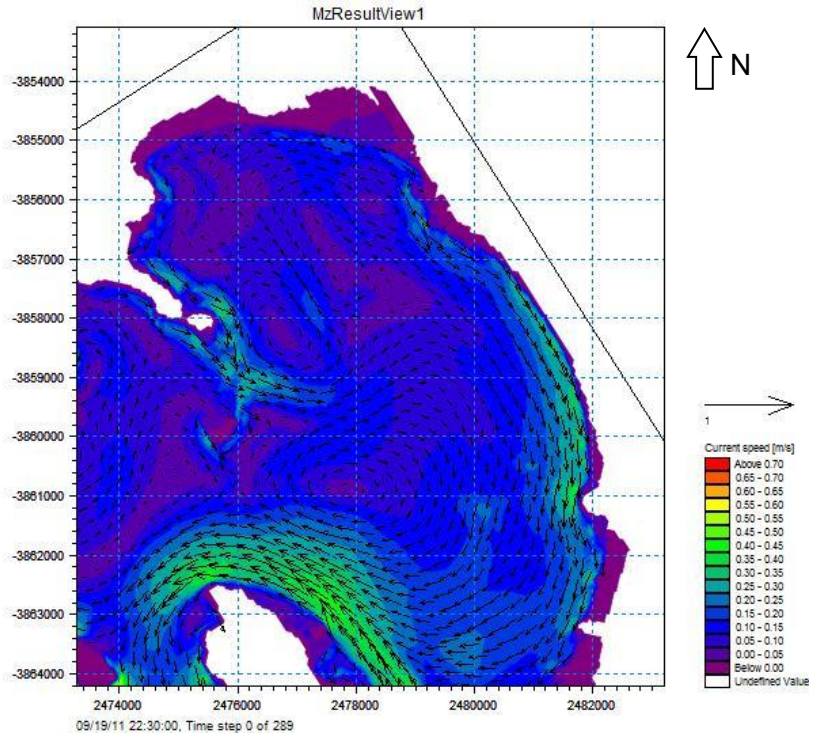	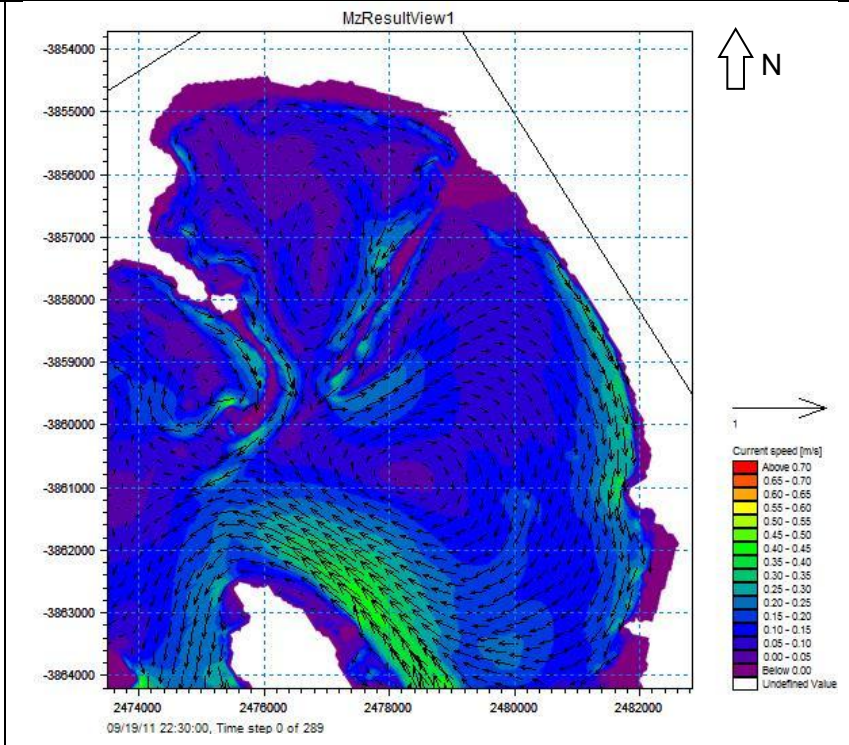

Figure 8-15: The effect of tidal fluctuations including a 1 in 50 year wind from the north-northwest in Saldanha Bay during ebb tide

	Prior to construction	After construction
Flood Tide	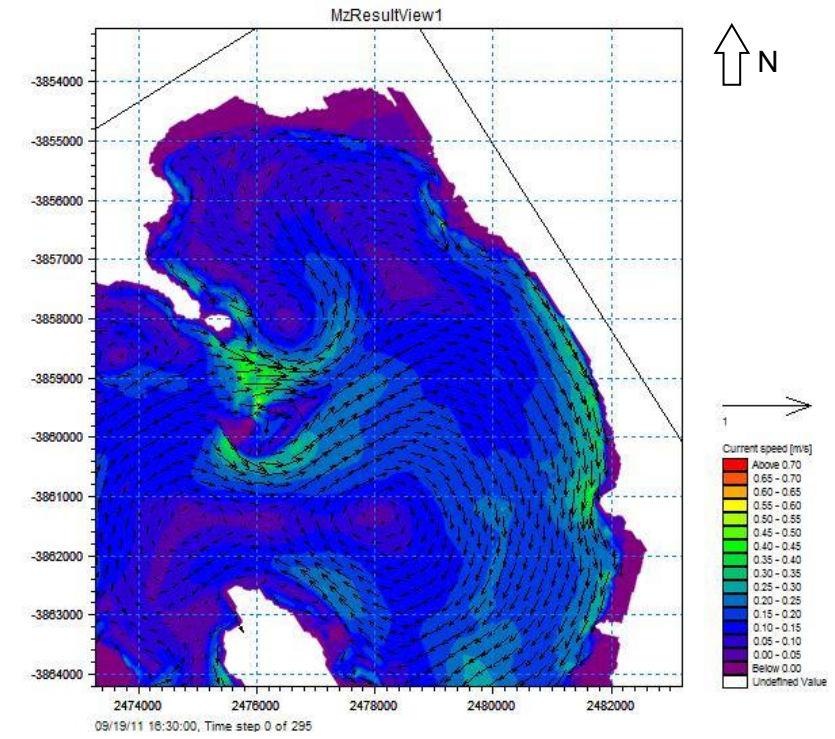	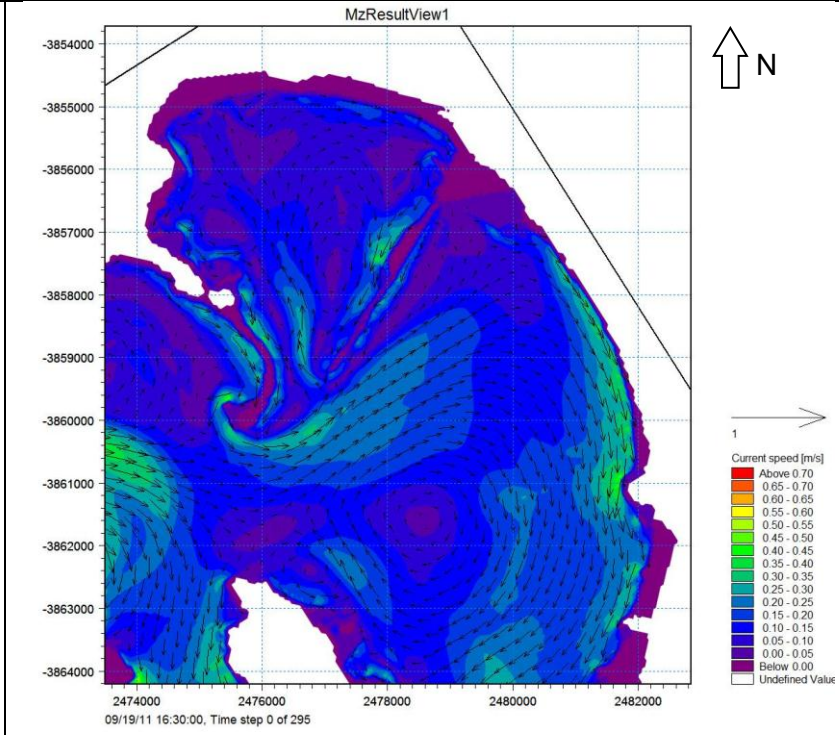

Figure 8-16: The effect of tidal fluctuations including a 1 in 50 year wind from the north-northwest in Saldanha Bay during flood tide

	Prior to construction	**After construction**
Ebb Tide	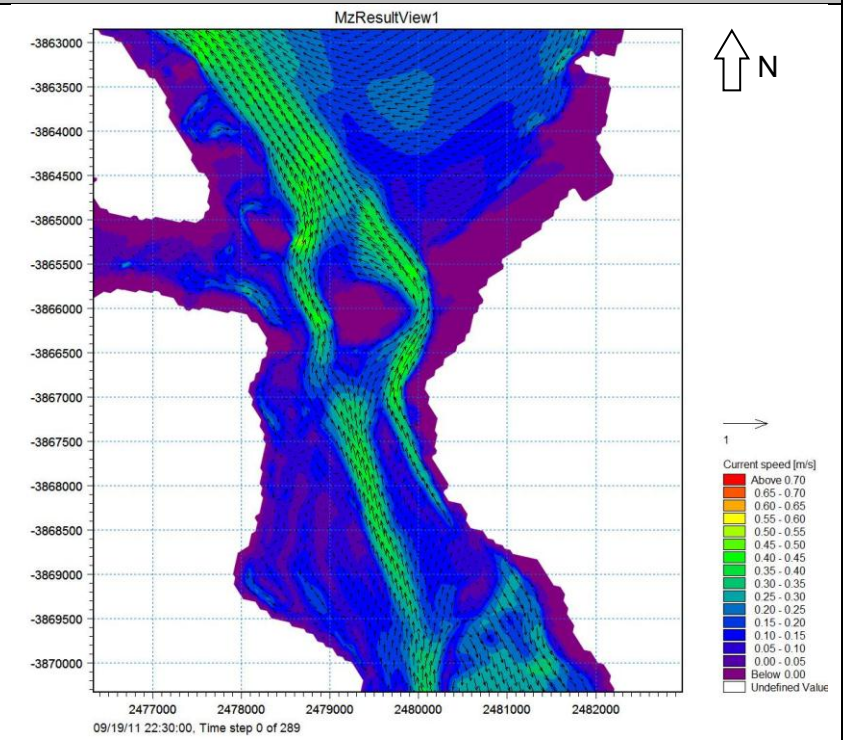	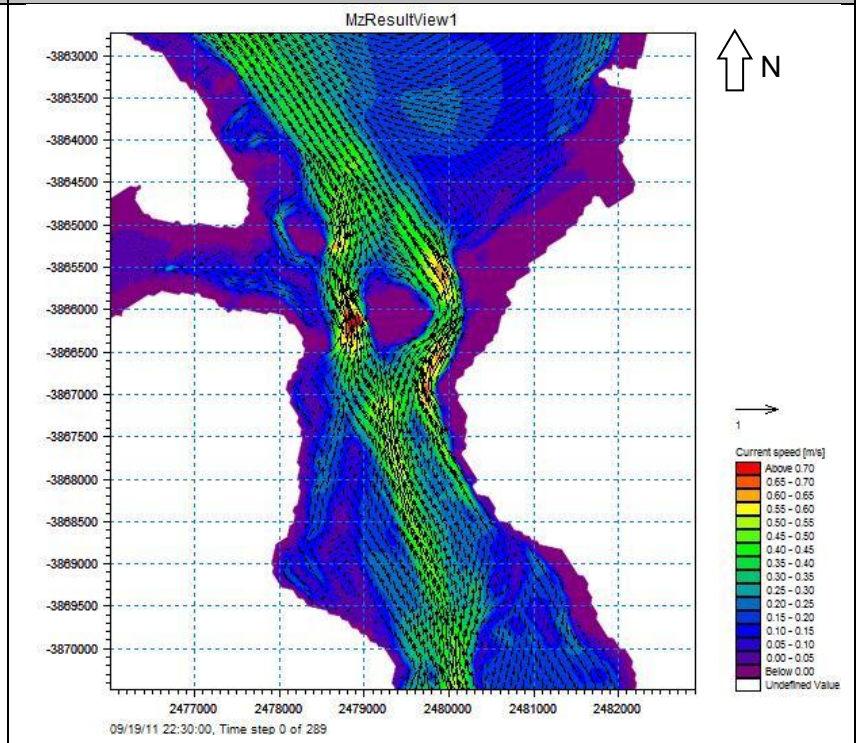

Figure 8-17: The effect of tidal fluctuations including a 1 in 50 year wind from the north-northwest in the Langebaan Lagoon during ebb tide

	Prior to construction	**After construction**
Flood Tide	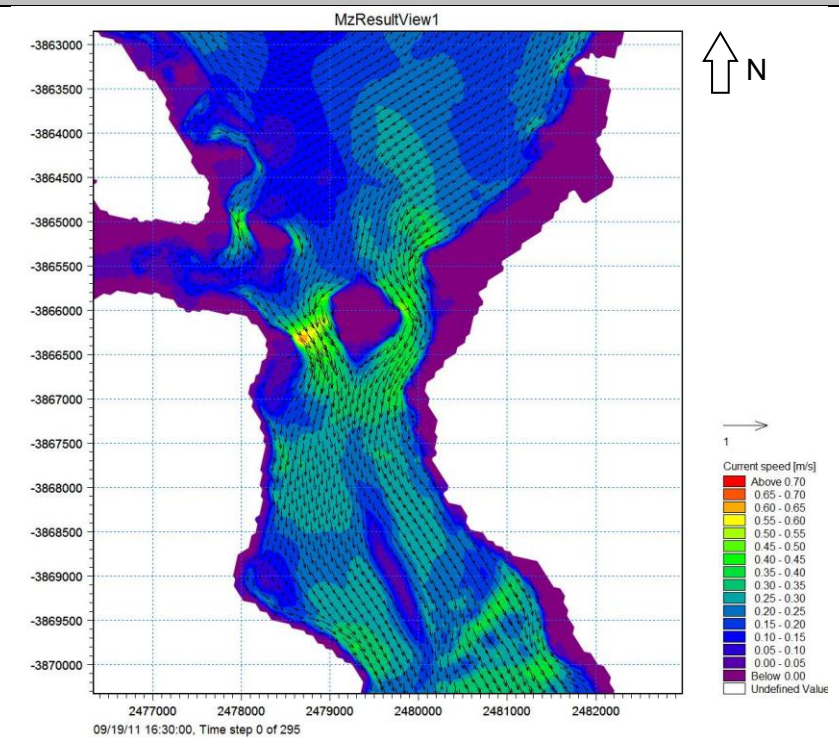	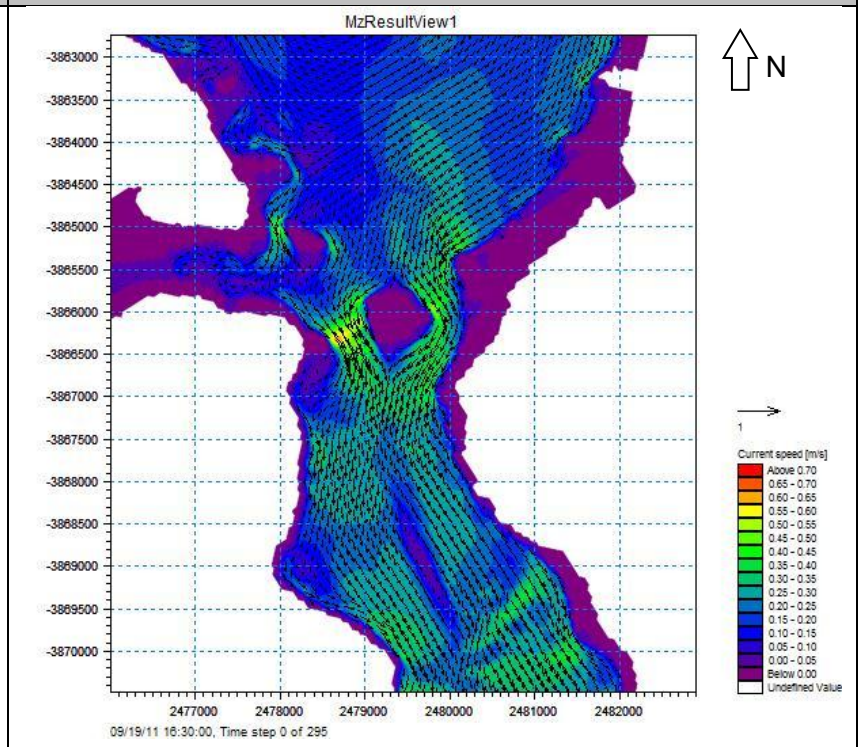

Figure 8-18: The effect of tidal fluctuations including a 1 in 50 year wind from the north-northwest in the Langebaan Lagoon during flood tide

The results based on the cross-sections, attached in **Appendix H.4**, indicate a large difference in hydrodynamic conditions prior to and after the construction of the causeway and the jetty in Saldanha Bay. These differences are much larger than the hydrodynamic differences observed during the winds from the north and the south.

Velocities in the lagoon are similar to the velocities during the scenario where wind forcing was excluded. However, greater velocities were observed at sections L3, L4, L5, L7 and L8 towards the west of the cross-sections for flood tides. These sections are all located in the two main channels around Schaapen Island.

8.6 Tidal fluctuations including a 1 in 100 year wind along the longest fetch

A variation in the wind velocity was investigated for the wind direction along the longest fetch towards the location of Langebaan Beach. The previously implemented 1 in 50 year velocity was replaced with a 1 in 100 year velocity as identified in **Section 5.3.6**. These conditions were compared to the results observed in **Section 8.2**, indicating the conditions excluding wind forcing.

Figure 8-19, **Figure 8-20**, **Figure 8-21** and **Figure 8-22** illustrated the hydrodynamic circulation in Saldanha Bay and Langebaan Lagoon. These figures provided similar results to the circulation observed during the 1 in 50 year wind velocity in the same direction. The major difference was expected during an investigation on the velocities at the various cross-sections.

Appendix H.5 provides the results on the cross-sections extracted from the numerical model.

Results based on the information extracted from the cross-sections in **Figure 8-1** and **Figure 8-2** indicate greater velocities in Saldanha Bay for both the flood and ebb tide prior to the construction of the causeway and the jetty. However, after the construction of the causeway and the jetty, these velocities decreased during winds along the longest fetch, resulting in a decrease in hydraulic energy. This decrease in hydraulic energy would result in less sediment transport than during calm wind conditions.

Velocities in the lagoon indicated similar results to the hydrodynamics in Saldanha Bay. Velocities prior to the construction of the causeway and the jetty were much greater than during calm conditions, but after the construction of these two structures, a major decrease in velocity was observed.

	Prior to construction	**After construction**
Ebb Tide	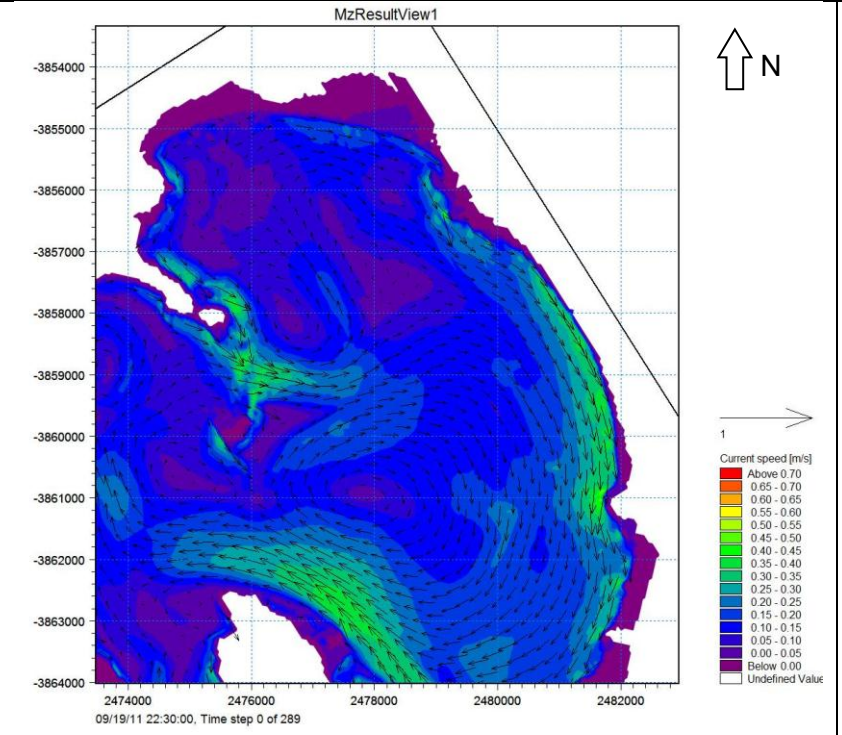	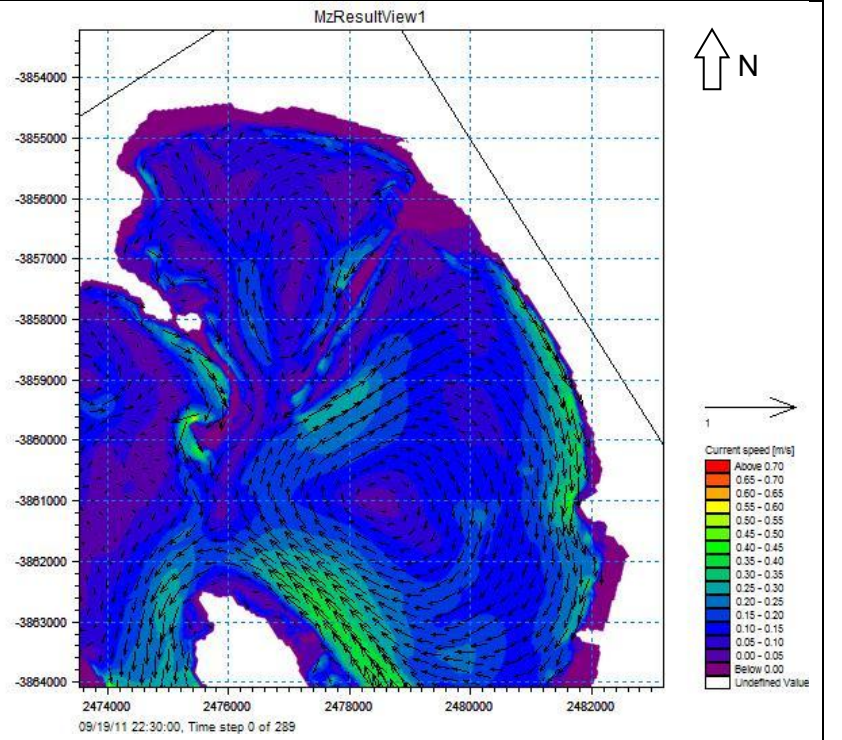

Figure 8-19: The effect of tidal fluctuations including a 1 in 100 year wind from the north-northwest in Saldanha Bay during ebb tide

	Prior to construction	**After construction**
Flood Tide	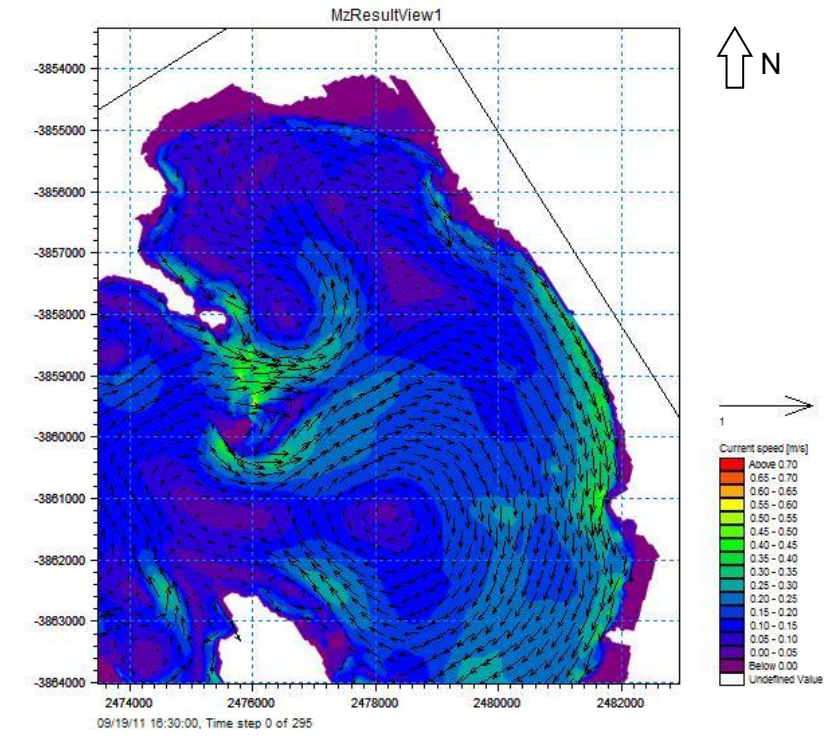	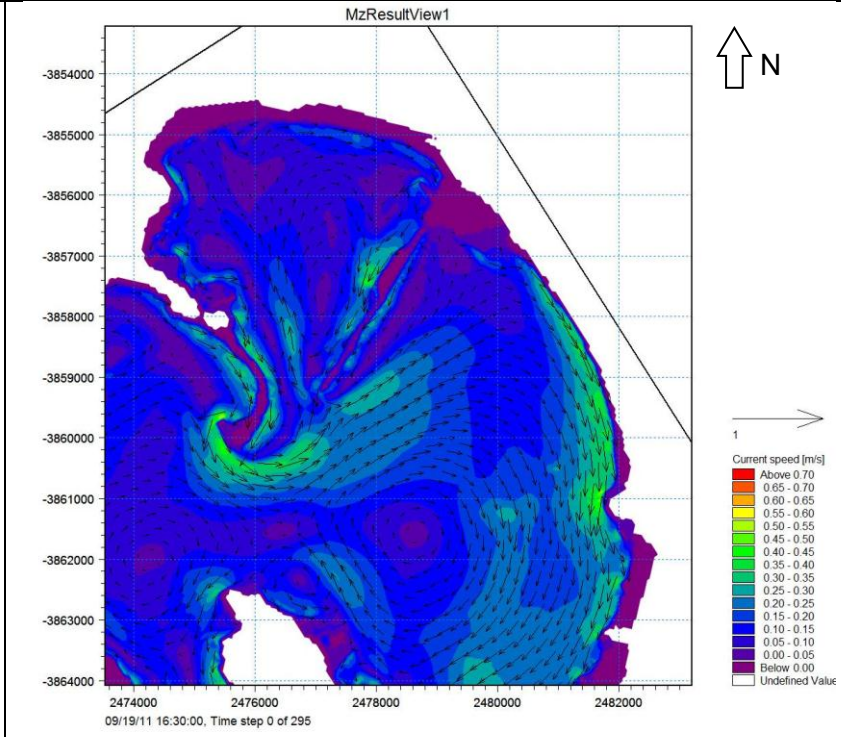

Figure 8-20: The effect of tidal fluctuations including a 1 in 100 year wind from the north-northwest in Saldanha Bay during flood tide

	Prior to construction	**After construction**
Ebb Tide	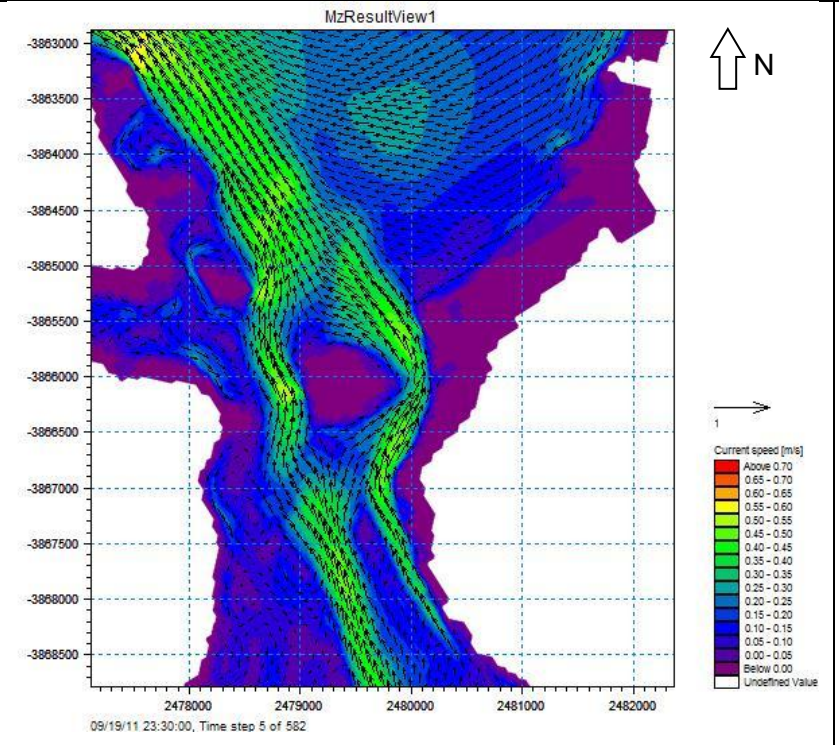	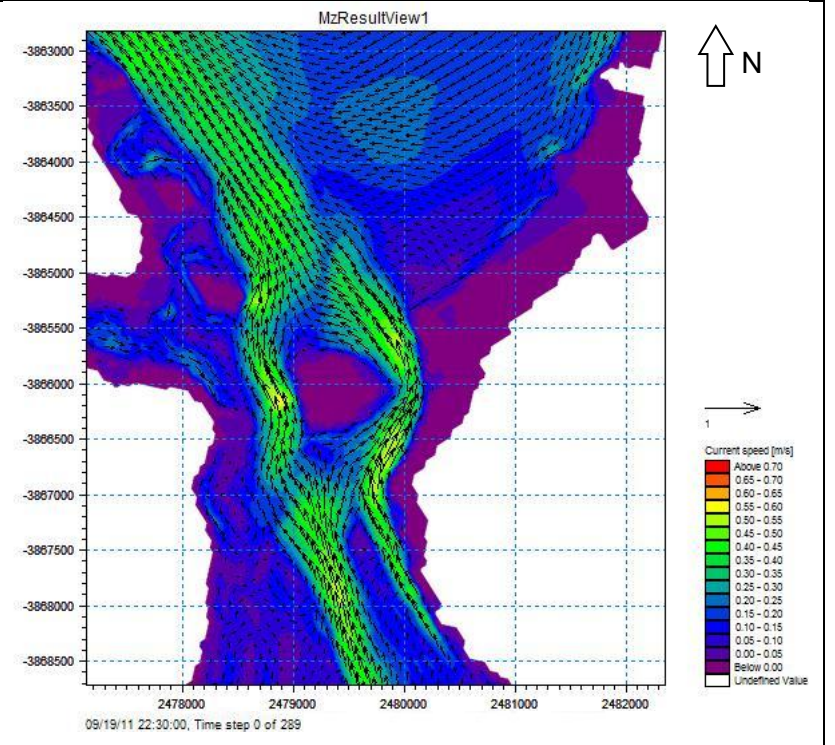

Figure 8-21: The effect of tidal fluctuations including a 1 in 100 year wind from the north-northwest in Langebaan Lagoon during ebb tide

	Prior to construction	**After construction**
Flood Tide	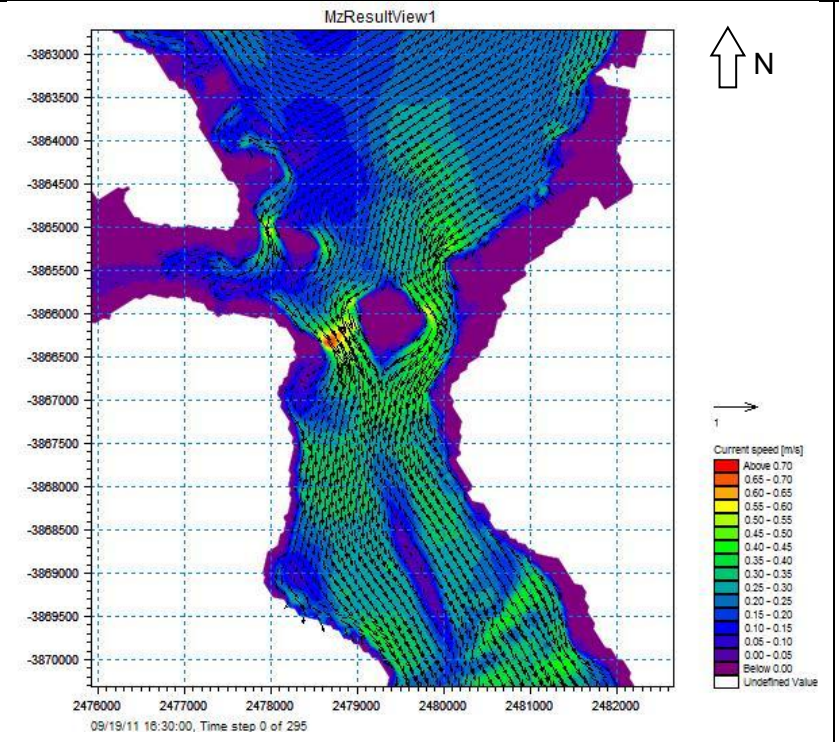	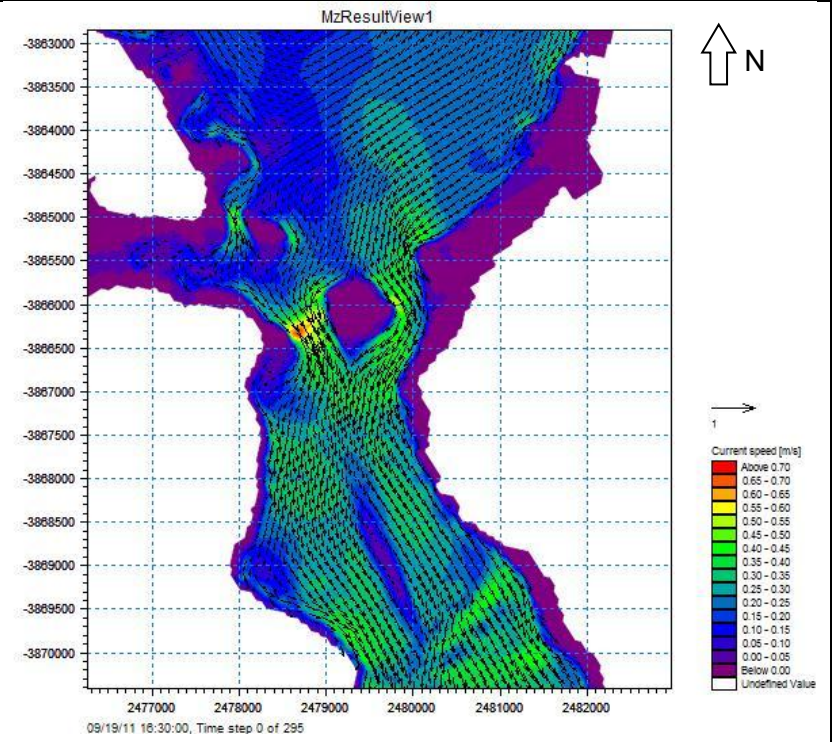

Figure 8-22: The effect of tidal fluctuations including a 1 in 100 year wind from the north-northwest in Langebaan Lagoon during flood tide

8.7 1 in 50 year tidal storm event excluding wind forcing

According to the literature review, changes in wind conditions would have major impacts on the hydrodynamics and sediment transport of Saldanha Bay and minor influences on the Langebaan Lagoon. However, alterations to the water levels in Big Bay would provide much greater changes in the hydrodynamics and sediment transport of the lagoon.

One of these water level alterations is a result of tidal storm events, resulting in a sudden extreme increase in the water level. These storm events were also accompanied by major wind events. However, during this scenario based on a change in water level, no wind forcing was included.

The scenario in the water level changes due to a storm event was based on the 1 in 50 year tidal storm and associated water level fluctuation. The sudden peak in the tidal fluctuations were implemented into the tidal water level fluctuations and analysed. Results on the cross-section information for the hydrodynamics and sediment transport are available in **Appendix H.6**.

The hydrodynamic patterns in Saldanha Bay were similar to the scenario excluding the effects of wind, but greater velocities were observed for flooding conditions. However, ebbing conditions provided smaller velocities than observed during the first mentioned scenario, thus resulting in sediment transport into Saldanha Bay, but not extracted sediment particles.

Water level fluctuations were expected to have greater effects on the hydrodynamics in the lagoon than in Saldanha Bay. This is confirmed in all the cross-sections, where flooding and ebbing velocities are greater than the conditions during normal tidal action, with the flooding velocities indicating a much greater increase in velocity than the ebbing velocities.

	Prior to construction	**After construction**
Ebb Tide	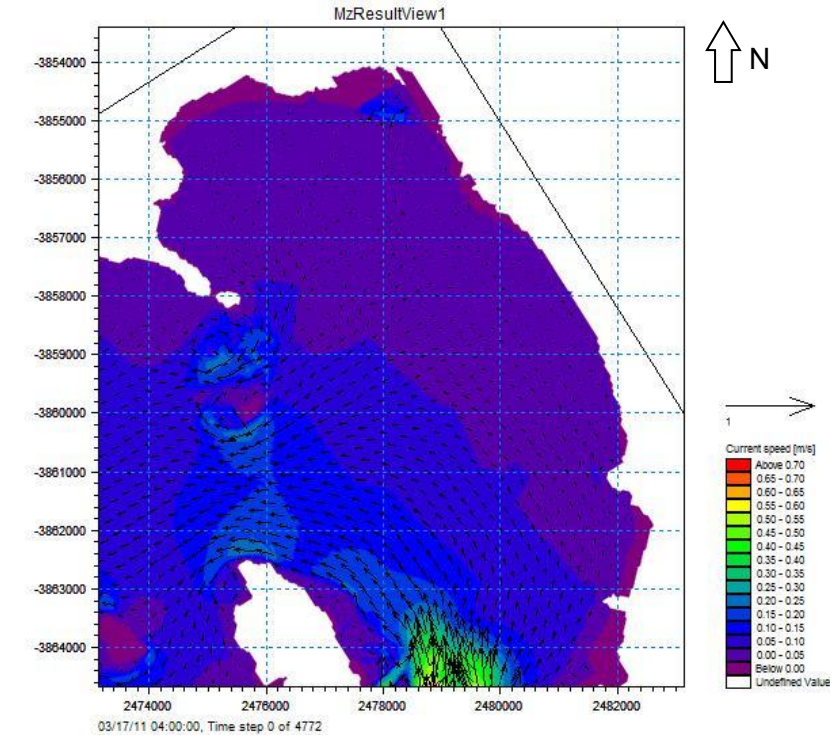	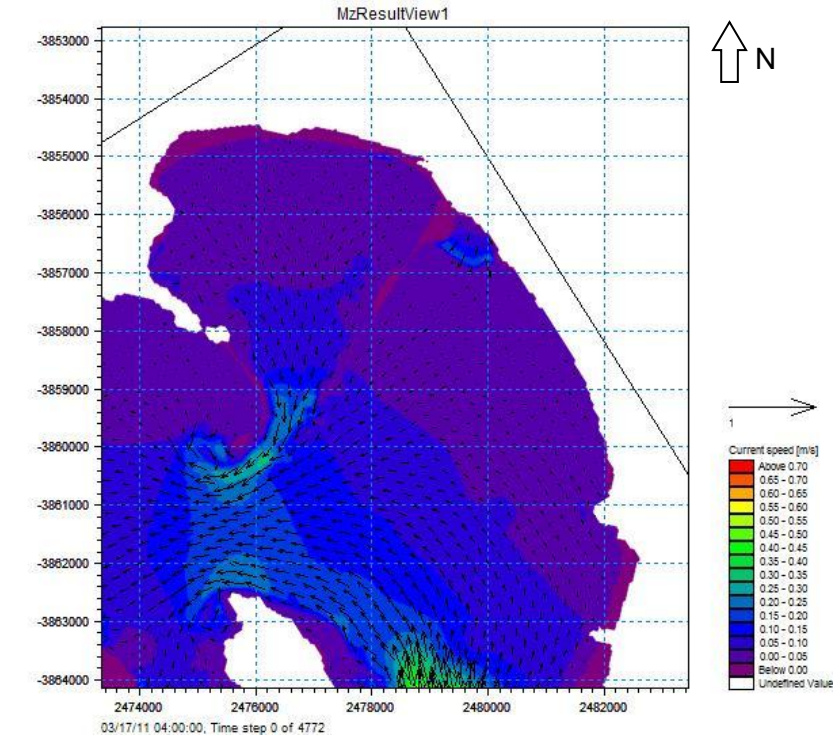

Figure 8-23: The effect of tidal fluctuations including a 1 in 50 year storm event in Saldanha Bay during ebb tide

	Prior to construction	**After construction**
Flood Tide	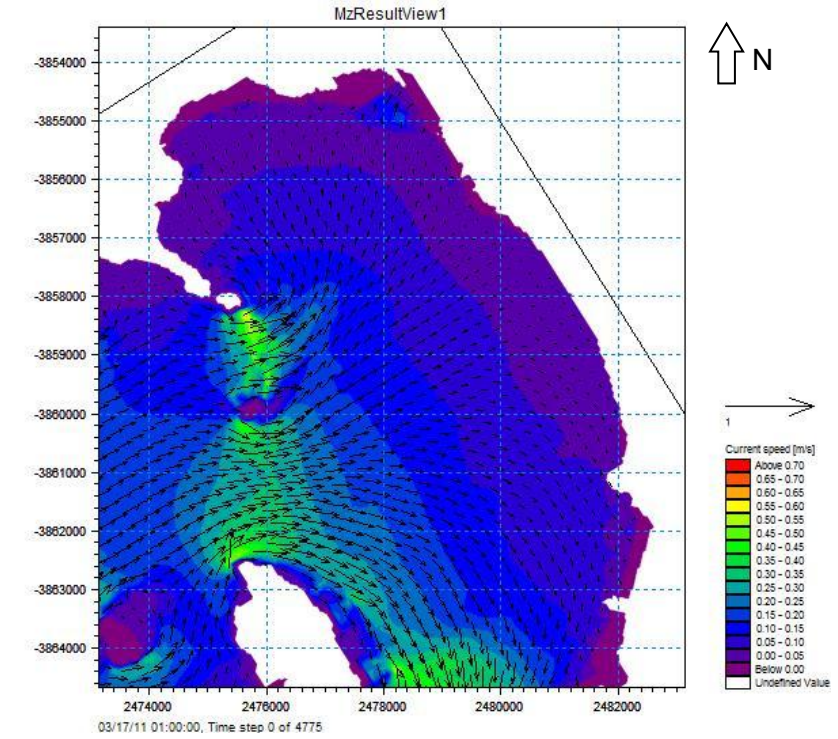	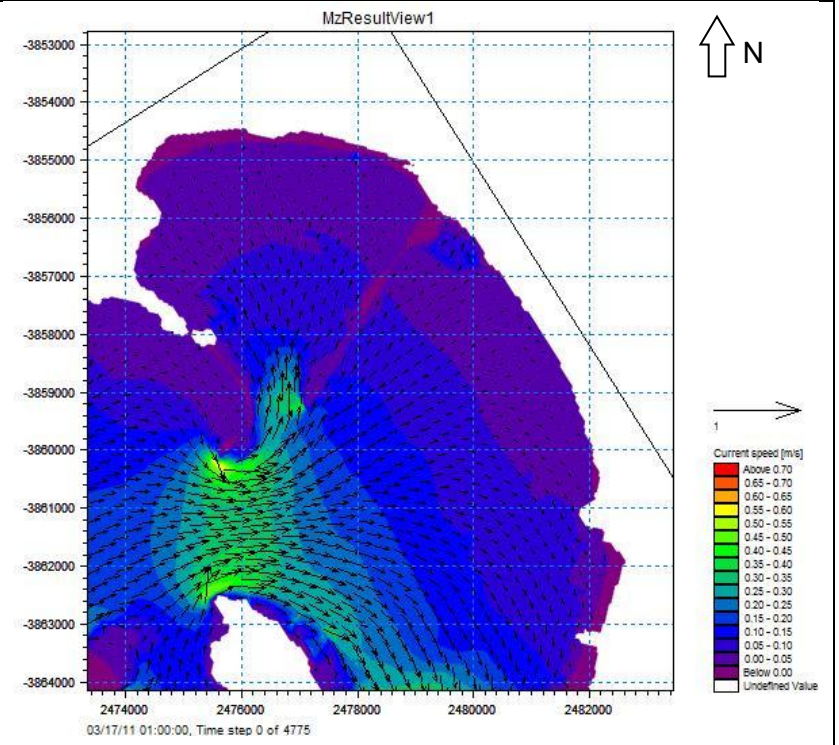

Figure 8-24: The effect of tidal fluctuations including a 1 in 50 year storm event in Saldanha Bay during flood tide

	Prior to construction	After construction
Ebb Tide	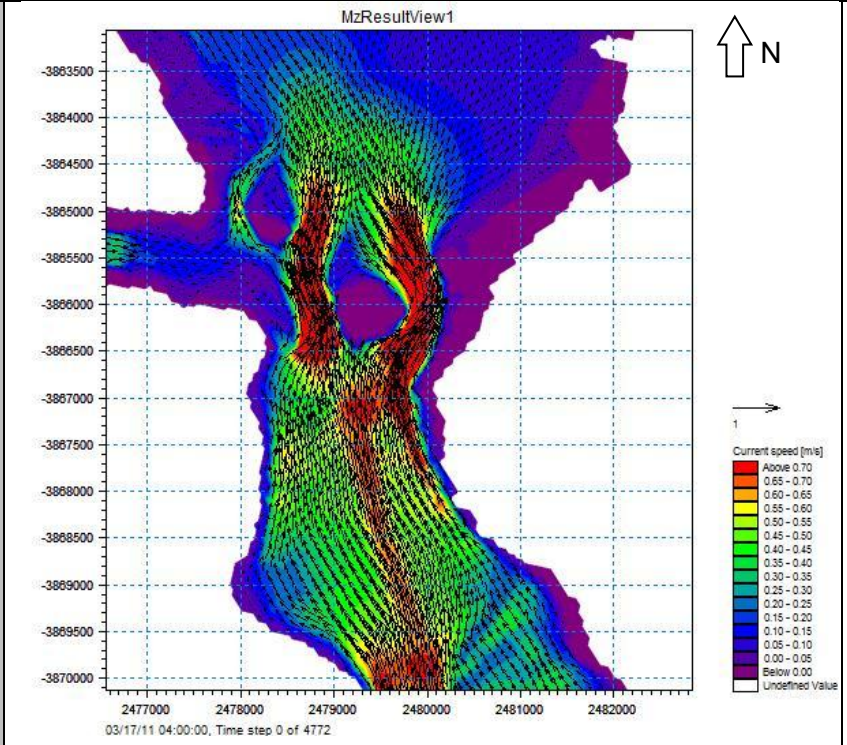	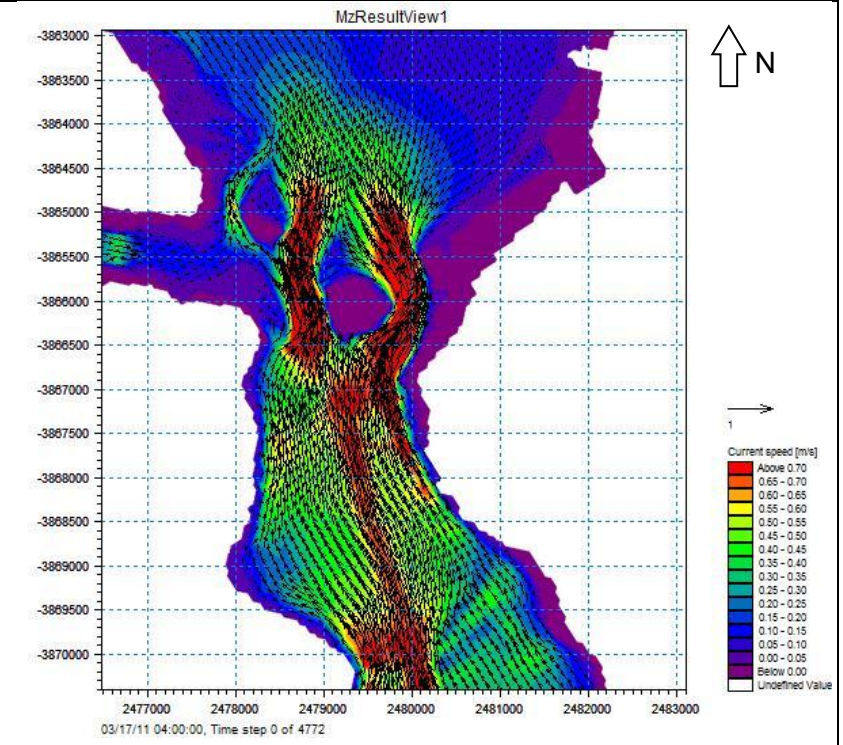

Figure 8-25: The effect of tidal fluctuations including a 1 in 50 year storm event in Langebaan Lagoon during ebb tide

	Prior to construction	**After construction**
Flood Tide	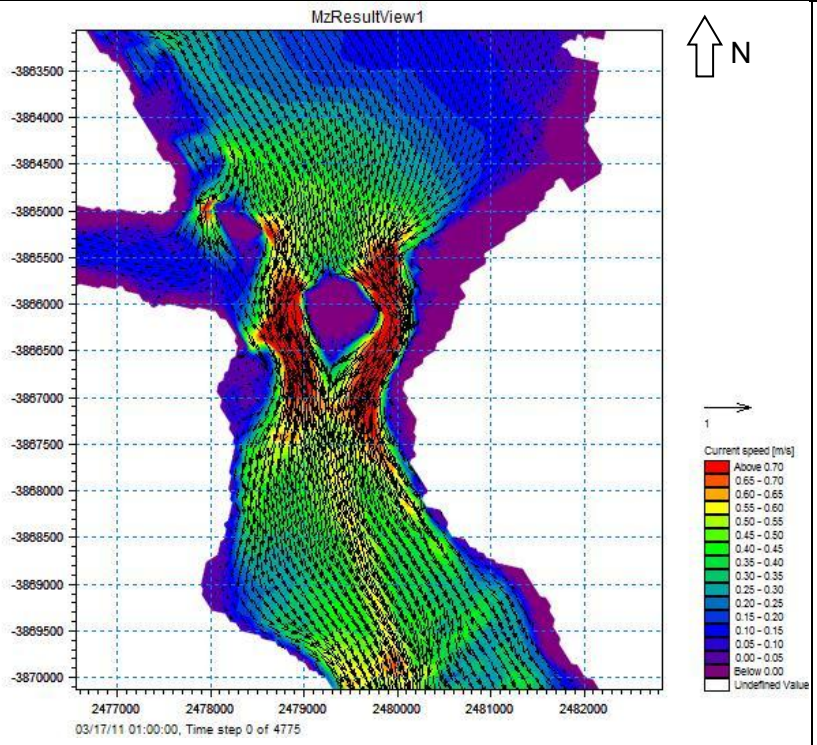	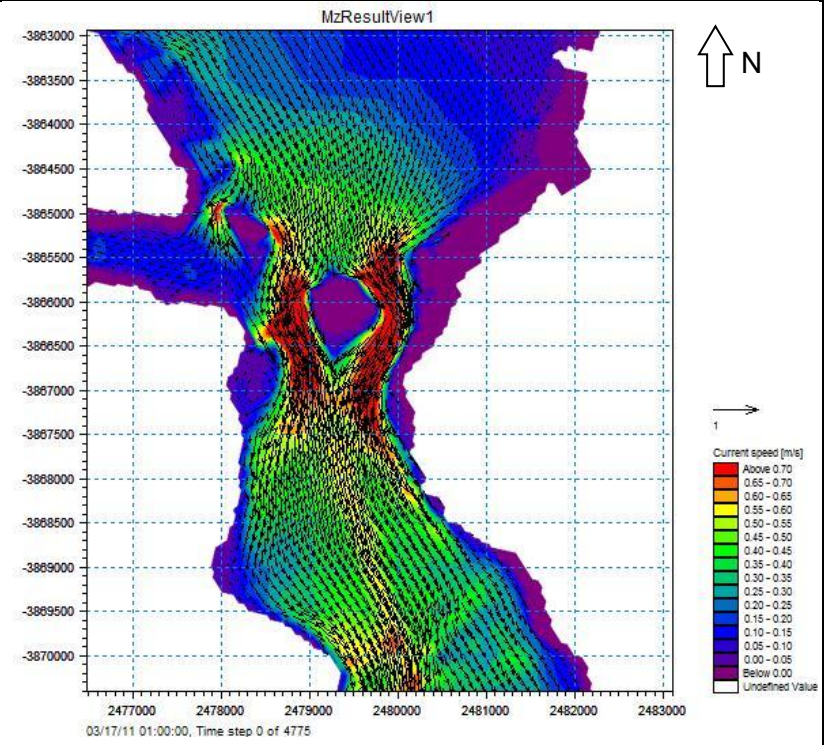

Figure 8-26: The effect of tidal fluctuations including a 1 in 50 year storm event in Langebaan Lagoon during flood tide

Along with these great increases in velocities is an increase in sediment transport. The greater flooding velocity would result in more sediments transported into the lagoon and less extracted during the withdrawal of water from the lagoon.

These flood events resulting in major water level fluctuations could have great implications on the sediment transport and added to the scouring near the Langebaan Beach. However, from **Appendix H.6**, very little sediment transport was observed near the location of Langebaan Beach. Note that scouring of the Langebaan Beach would require the modelling of wave action.

Figure 8-23 and **Figure 8-24** illustrates the circulation in Saldanha Bay during a 1 in 50 year tidal storm event excluding the influence of wind. Similar circulation patterns were observed during the scenario based on the tidal fluctuations excluding wind in **Section 8.2**, with no significant changes.

Even though no significant changes in the circulation of Saldanha Bay were observed, a variation in the velocities in the lagoon was expected due to the tidal driven nature of this system. **Figure 8-25** and **Figure 8-26** indicates the circulation and flow patterns for the lagoon. Larger velocities can be observed at the entrance to the lagoon, but no significant changes in the flow patterns entering and exiting were observed.

Therefore, a change in water level as a result of storm events has minor influence on the circulation in Saldanha Bay and Langebaan Lagoon. However, the influence of the extreme water levels resulted in an increase in velocities in the lagoon, therefore an increase in sediment transport.

8.8 Sea level rise excluding wind forcing

As observed in the previous scenarios, an increase in tidal levels resulted in an increase in velocities in the Langebaan Lagoon. During this scenario, the influence of global sea level rise as a result of climate change was investigated. As identified in **Section 3.2.2**, a rise in sea level of 0.4 m was implemented on the tidal input utilized in previous scenarios.

Figure 8-27, **Figure 8-28**, **Figure 8-29** and **Figure 8-30** illustrates very little to no variation in the circulation when compared with the scenario based on tidal conditions excluding wind.

The sea level rise scenario was based in the first scenario, only investigating the impact of tidal oscillations, with an increase in the water level of 0.4 m. Results in the cross-sections, as provided in **Appendix H.7**, indicate very little to no difference between the velocities and sediment transport of the tidal scenario excluding the effects of wind. Minor increase in the flooding velocities was observed for sections located in the lagoon.

Thus, the greater sea levels would have no major impacts on the hydrodynamics and sediment transport of Saldanha Bay and Langebaan Lagoon, but as mentioned in **Section 3.2.2**, a global sea level rise would not be a gradual process, but rather a change that occurs via dramatic events, such as storms which, as resulted from the previous scenario, have a great impact on the hydrodynamics and sediment transport of Saldanha Bay and the Langebaan Lagoon.

	Prior to construction	**After construction**
Ebb Tide	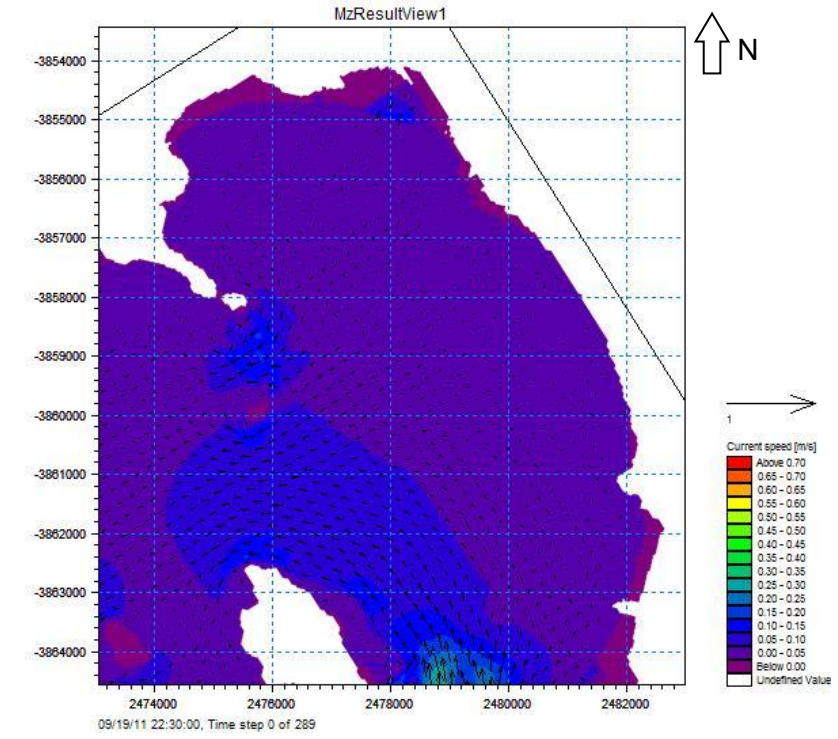	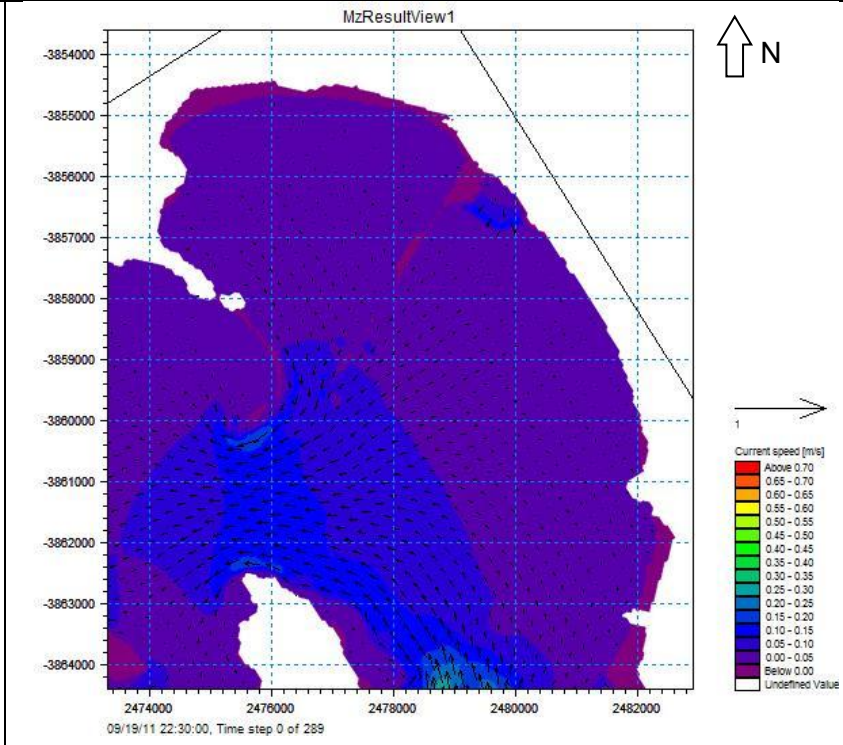

Figure 8-27: The effect a global sea level rise in Saldanha Bay during ebb tide

	Prior to construction	**After construction**
Flood Tide	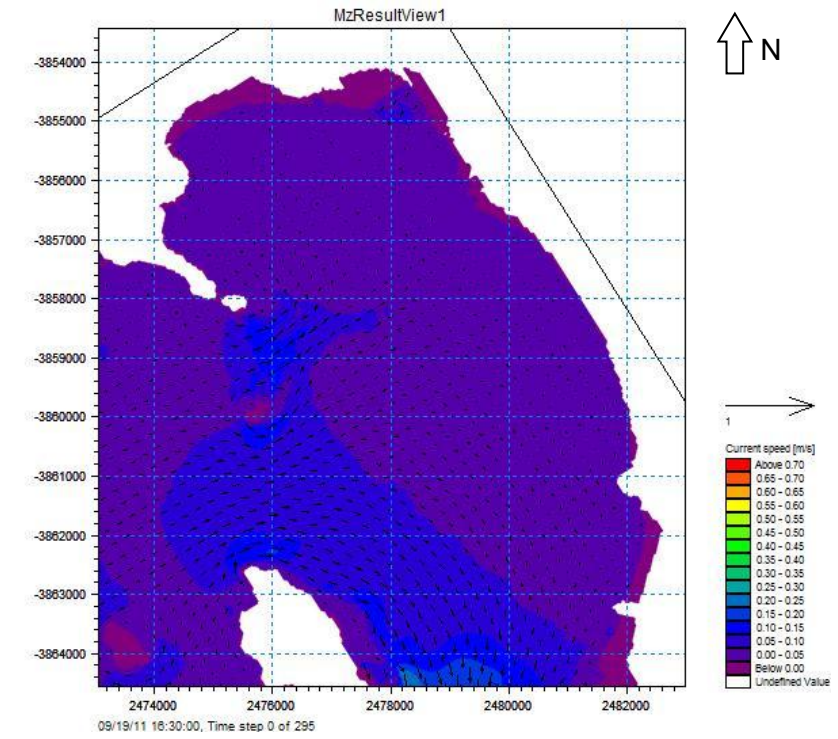	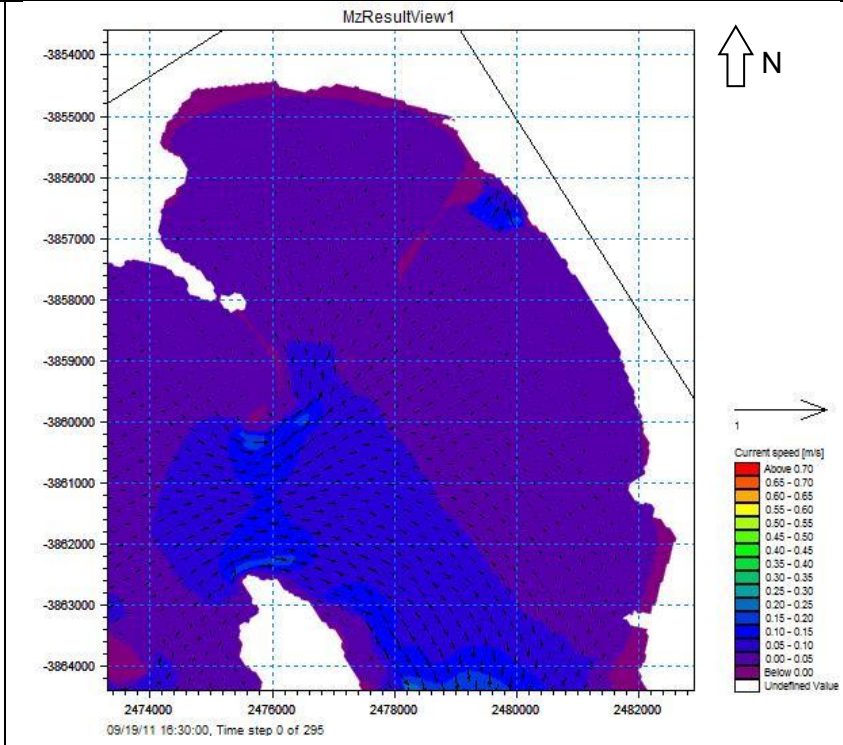

Figure 8-28: The effect a global sea level rise in Saldanha Bay during flood tide

	Prior to construction	**After construction**
Ebb Tide	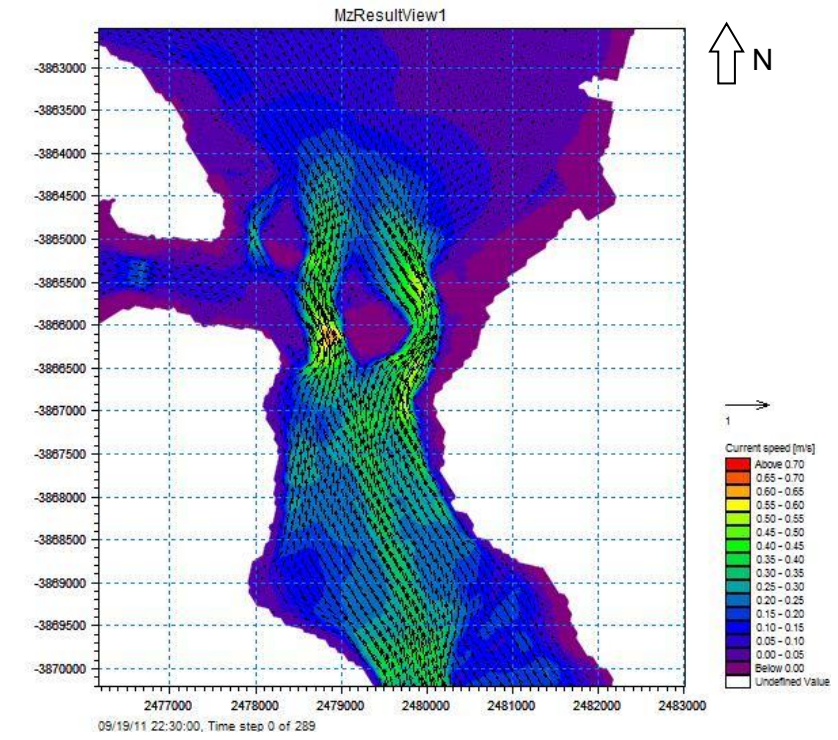	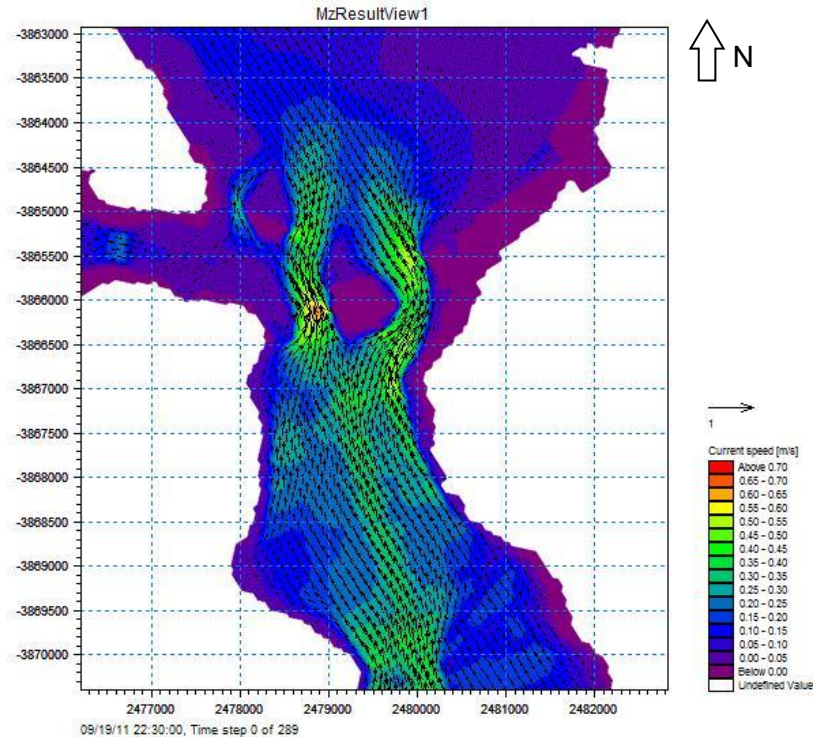

Figure 8-29: The effect a global sea level rise in Langebaan Lagoon during ebb tide

	Prior to construction	**After construction**
Flood Tide	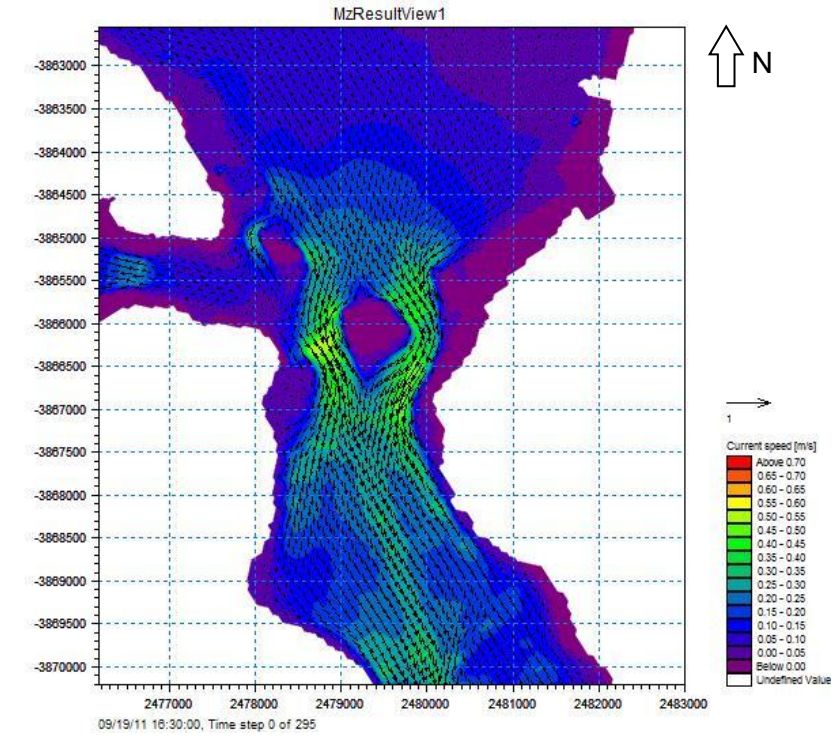	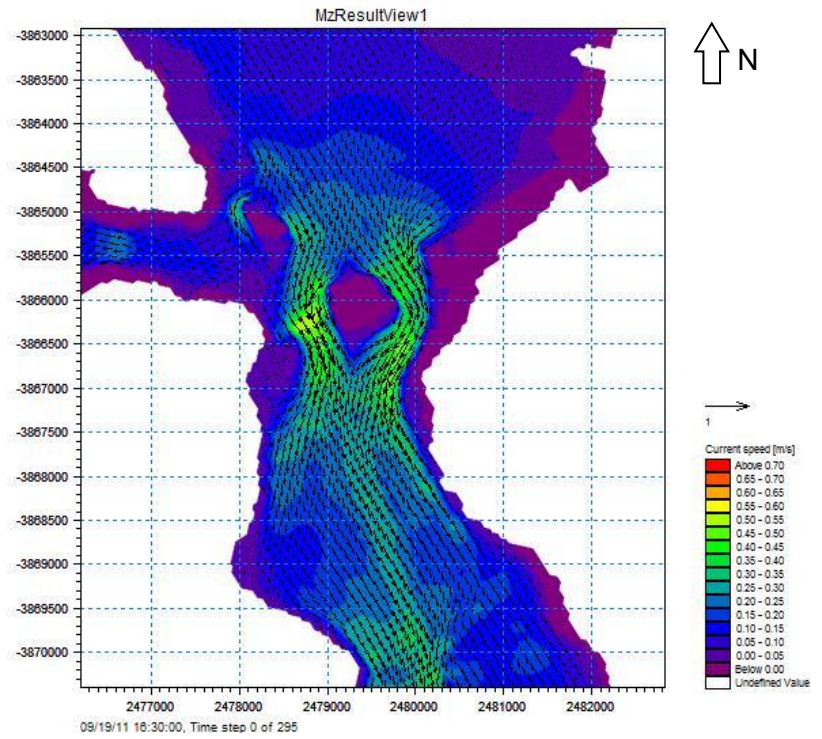

Figure 8-30: The effect a global sea level rise in Langebaan Lagoon during flood tide

8.9 Long term simulation excluding wind forcing

An additional scenario was investigated, aimed to identify the long term impact of tidal forcing on the sediment transport and morphology of the bathymetry, excluding the effects of wind forcing on the Saldanha Bay and Langebaan Lagoon systems. If wind were included in this scenario, variations in direction and speed would be required to simulate realistic conditions over a long period of time. Due to the omissions in the wind data provided, winds were investigated in a single direction and a constant velocity when included in the numerical models. Therefore, wind was excluded during this scenario, resulting in this model being based on similar forcing parameters as provided in the first scenario discussed in **Section 8.2**, consisting of the tidal oscillations predicted by the WXTide software.

These tidal oscillations were extracted at 10 minute intervals, similar to the water levels extracted in **Section 5.3.8**. However, water levels for a total period of five years were identified and implemented to determine the long term effects of the sediment transport patterns on the bathymetry for both conditions prior to the construction of the causeway and the jetty, and after the construction of these structures in Saldanha Bay.

The model simulated six months at a time. After six months, the updated bathymetry due to sediment transport morphology were saved and implemented in the numerical model. This ensured that the hydrodynamic and sediment transport conditions were up to date with the changes experienced by the bathymetry due to the sediment transport.

However, results indicated that little to no changes occurred in the bathymetry after a period of five years due to sediment transport. There were also no major changes between the conditions prior to and after the construction of the causeway and the jetty. **Figure 8-31** and **Figure 8-32** illustrates the initial and final bathymetries respectively at the entrance to the Langebaan Lagoon after the construction of the causeway and the jetty. When the change in the bathymetry was investigated, no major alterations could be observed, as indicated in **Figure 8-33**. The greatest alterations in the bathymetry were observed in the western main channel adjacent to Schaapen Island, with a total decrease in depth of 8 mm after five years.

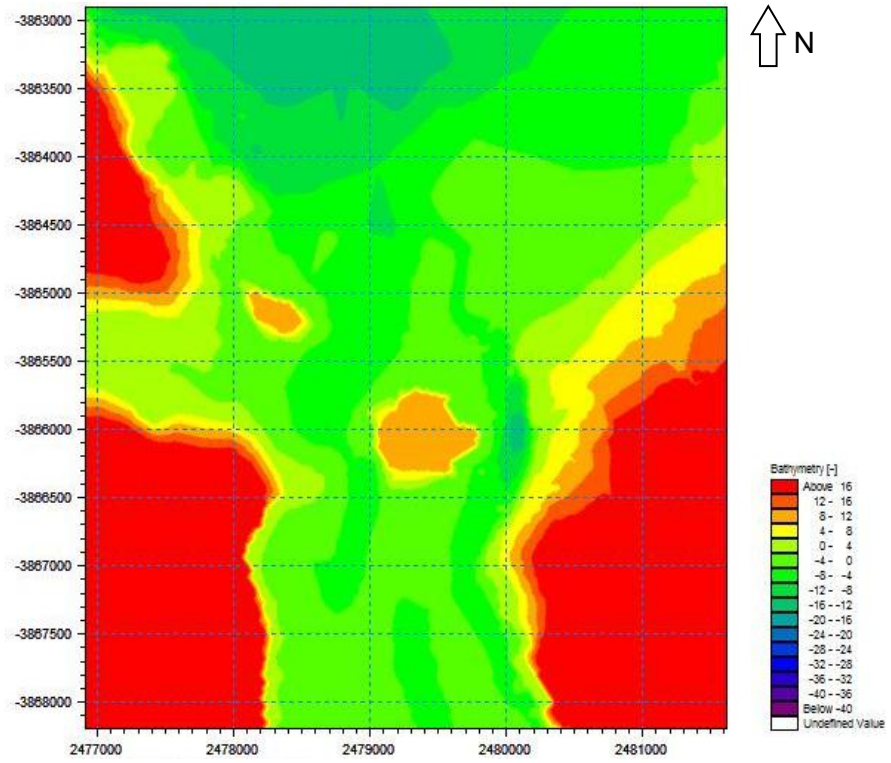

Figure 8-31: Bathymetry at entrance to Langebaan Lagoon at initiation of long term scenario

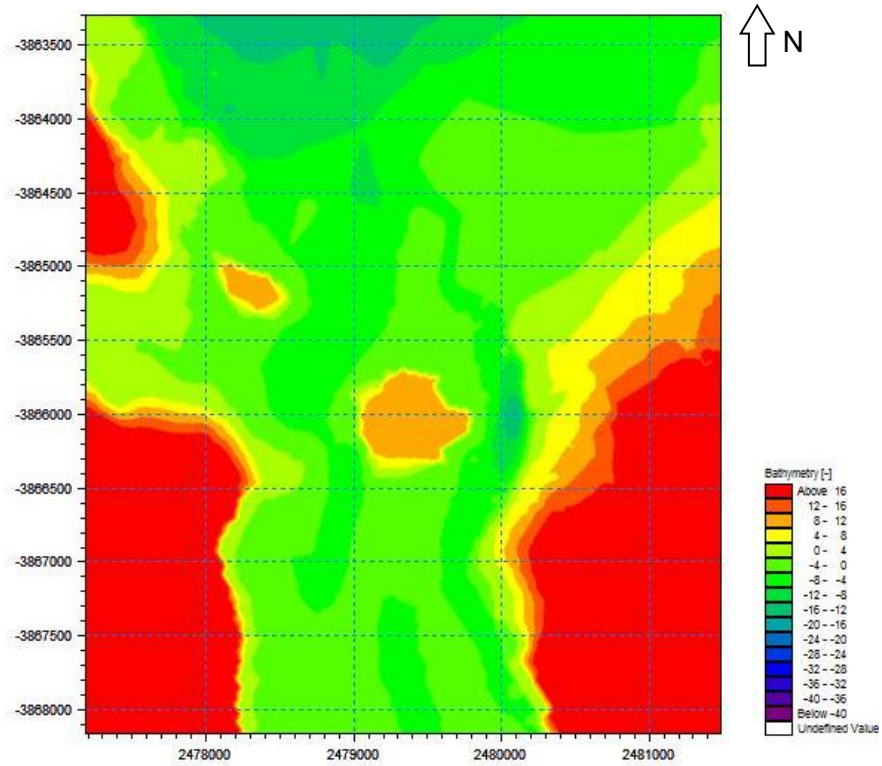

Figure 8-32: Bathymetry at entrance to Langebaan Lagoon at end of long term scenario

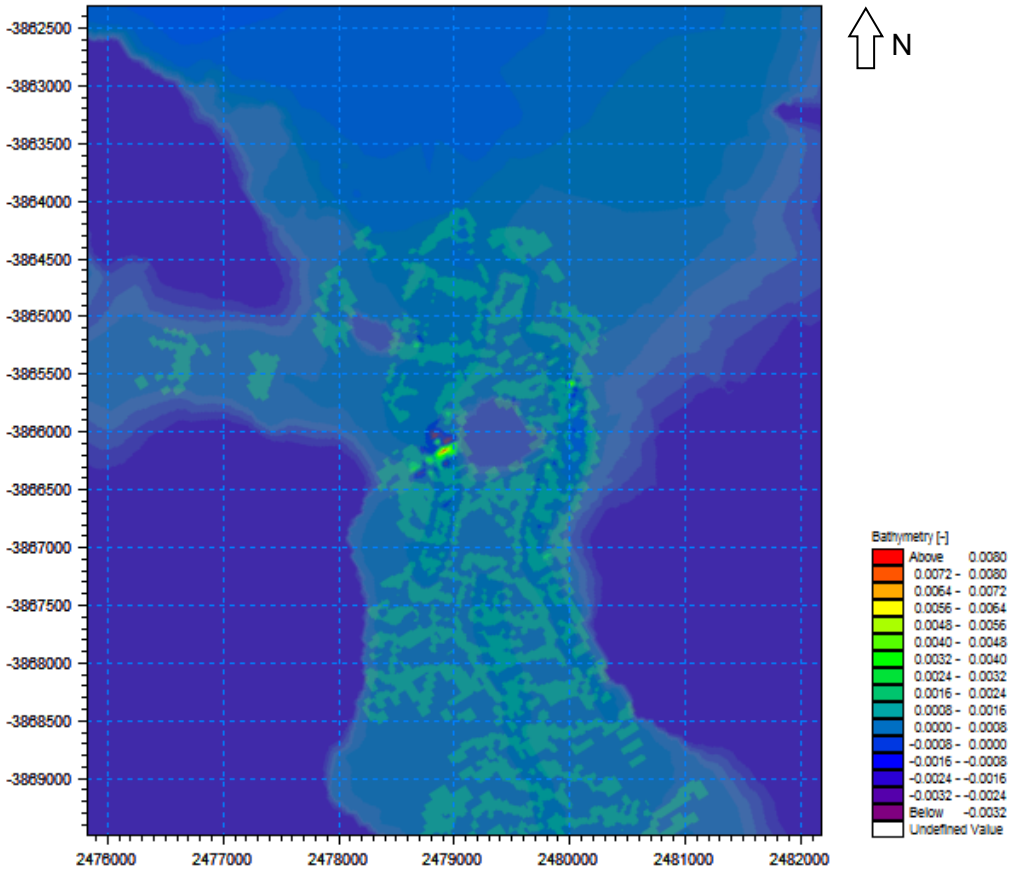

Figure 8-33: Morphological change in bathymetry experienced over five years

The hydrodynamic and sediment transport conditions for the long term scenario were similar to the conditions identified in **Section 8.2** which experienced relatively large maximum sediment transport rates, however, very little change were observed in the bathymetry. This is possibly due to the to and fro movement of sediment particles during flood and ebb tide generated by the tidal variation. During one tide, e.g. flood, a sediment particle can be removed from its initial position and during the next tide, e.g. ebb; particles are transported back to its initial position. Note that the position mentioned above refers to the 50 metre by 50 metre cell used in the numerical model, which is much larger than the area covered by a single sediment particle.

Therefore, it can be concluded that the changes in the tidal forced hydrodynamics due to the construction of the causeway and the jetty in Saldanha Bay were not the primary cause of the erosion experienced at Langebaan Beach. These conditions do generate great sediment transport rates, but were not identified as the primary cause of beach scouring near the town of Langebaan.

8.10 Conclusions from investigated scenarios

After the construction of the causeway and the jetty at Saldanha Bay, various changes were observed in the coastline in the area of the Langebaan Lagoon mouth. These changes included the erosion of Langebaan Beach.

During this investigations, the effect of these structures in Saldanha Bay were simulated by means of a two-dimensional numerical model. This model provided the opportunity to investigate the impact these structures had on the hydrodynamic and sediment transport conditions in Saldanha Bay and Langebaan Lagoon during various extreme conditions.

These extreme conditions were identified, based on the hydrodynamic driving forces dominating in Saldanha Bay and Langebaan Lagoon. The hydrodynamic driving forces were identified as wind and tidal variations along, as discussed **Section 3.1**, excluding wave driven currents in the littoral zone.

Results from these scenarios confirmed the conclusions in previous reports on water circulation stating that Small Bay and Big Bay were dominated by wind forcing, and that tidal variation in Big Bay dominated the hydrodynamic conditions in the Langebaan Lagoon (Shannon & Stander, 1977). The simulations on extreme wind conditions also indicated that the water circulation in Saldanha Bay was influenced by the direction of the wind. A clockwise rotation was observed during winds originating from the north in Big Bay and an anti-clockwise rotation was observed in Small Bay. During winds from an opposite direction, opposite rotations were observed for each of these bays.

The circulation in Big Bay provided an indication of the direction of flow when water enters or exits the lagoon during flood or ebb tides. It was observed that a clockwise rotation resulted in water entering the lagoon from a north eastern direction and exited towards a north western direction, while an anti-clockwise rotation resulted in water entering from a north western direction and exited towards a north eastern direction to continue in the circulation of Big Bay.

Further observations during this investigation indicated that major changes in the hydrodynamics have occurred at the locations of the causeway and the jetty during both

extreme wind and extreme tidal conditions. Greater velocities, resulting in more sediment transport, have also been observed for all extreme wind conditions along the coastline of Small Bay and Big Bay and very little change in flow velocities during extreme tidal conditions at these locations.

However, in the Langebaan Lagoon, extreme wind conditions had very little impact on the hydrodynamics and thus very little impact on the sediment transport conditions at the entrance to the Langebaan Lagoon, which confirmed previous findings that the hydrodynamics of the Langebaan Lagoon mouth is primarily tidal driven. Results from the hydrodynamic model also indicated that the construction of the causeway and the jetty in Saldanha Bay had very little to no impact on the hydrodynamic and sediment transport patterns at the Langebaan Lagoon mouth.

Overall, velocities in the Langebaan Lagoon were much greater than the velocities observed in Saldanha Bay, resulting in more sediment transport activities at the entrance to the lagoon than in Saldanha Bay.

Sediment transport calculations were based on the *Engelund and Hansen* sediment transport theory. This theory is primarily based on the d_{50} particle size, and gradation is excluded from sediment transport calculations. Different particle sizes were used across the bathymetry, based on the results from the field investigation.

One of the cross-sections investigated during various scenarios were located at Langebaan Beach, where extensive scouring have been observed. Section L2 stretched from Schaapen Island, located at the entrance to the lagoon, to the location where Langebaan Beach once were. **Figure 8-34**, **Figure 8-36**, **Figure 8-35** and **Figure 8-37** provide the hydrodynamic velocities experienced during flood tide prior to the construction of the causeway and the jetty, ebb tide prior to these developments, flood tide after these developments and ebb tide after the construction of the causeway and the jetty, respectively.

From the figures mentioned above, it has been identified that the scenario providing the greatest velocities at Langebaan Beach prior to the construction of the causeway and the jetty, were a 1 in 100 year wind along the longest fetch during both flood and ebb

tides. Maximum velocities across the cross-section for all the scenarios were greater during ebb tides than experienced during flood tides. A decrease of 1.5 m/s in the wind velocity for a wind from the same direction, resulting in a 1 in 50 year wind velocity, provided much weaker hydrodynamic velocities. These weaker velocities were a reasonable average when compared to the velocities observed during the other scenarios. The same return period for a storm surge event generated greater velocities than a wind along the greatest fetch.

After the construction of the causeway and the jetty, hydrodynamic velocities generated by means of the wind along the longest fetch decreased and the greatest hydrodynamic conditions were generated by means of tidal storm event (or tidal surge) for both flood and ebb tides. Velocities observed prior to the construction of the causeway and the jetty for this scenario increased and were found to generate a maximum velocity greater than the maximum velocity generated during the scenario of wind along the longest fetch prior to the harbour developments.

This severe change in velocity observed during the scenario where the wind direction is along the greatest fetch indicates that the fetch direction was disrupted by the construction of the jetty. **Figure 5-13** illustrates that the fetch direction should not be influenced by the location of the jetty, however, the cell size of the numerical model possibly affected the effect of a wind from this direction.

The smallest velocities during flood tide were observed for conditions when the wind forcing and tidal forcing provided opposing hydrodynamic currents, resulting in smaller hydrodynamic velocities for both conditions prior to and after the construction of the causeway and the jetty. Similar conditions were possibly the result for the smallest velocity after the construction of the causeway and jetty during ebb tides, observed during a 1 in 50 year wind along the longest fetch.

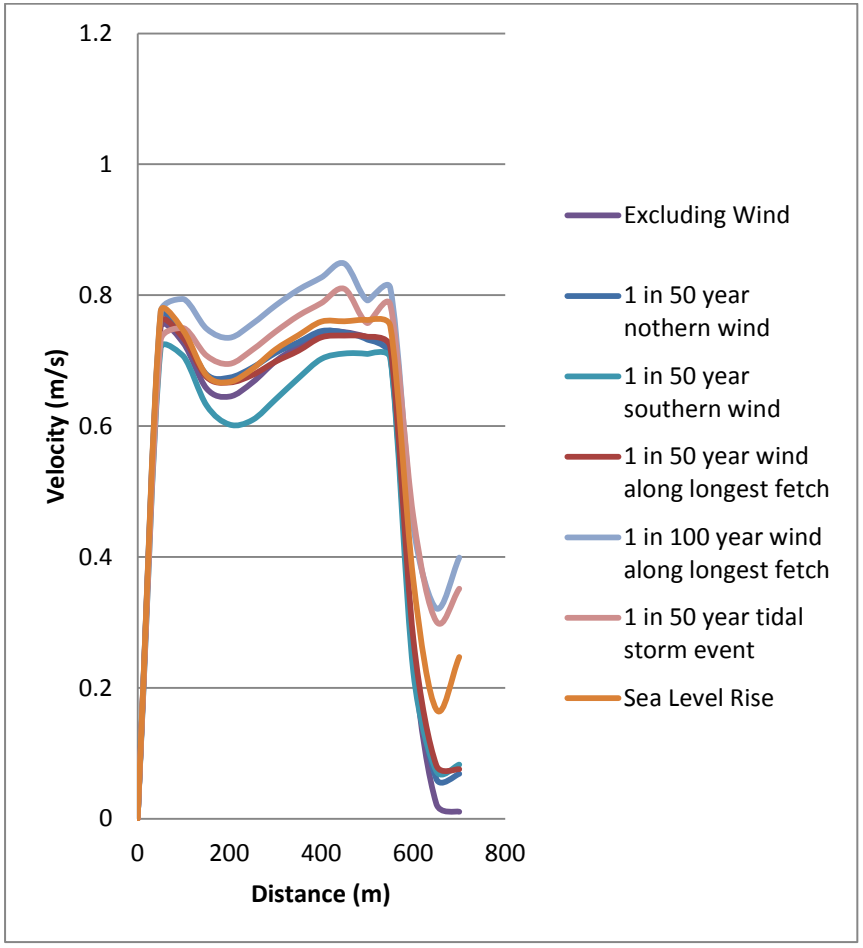

Figure 8-34: **Comparison on hydrodynamic velocities at section L2, near Langebaan Beach, during a flood tide prior to the construction of the causeway and the jetty**

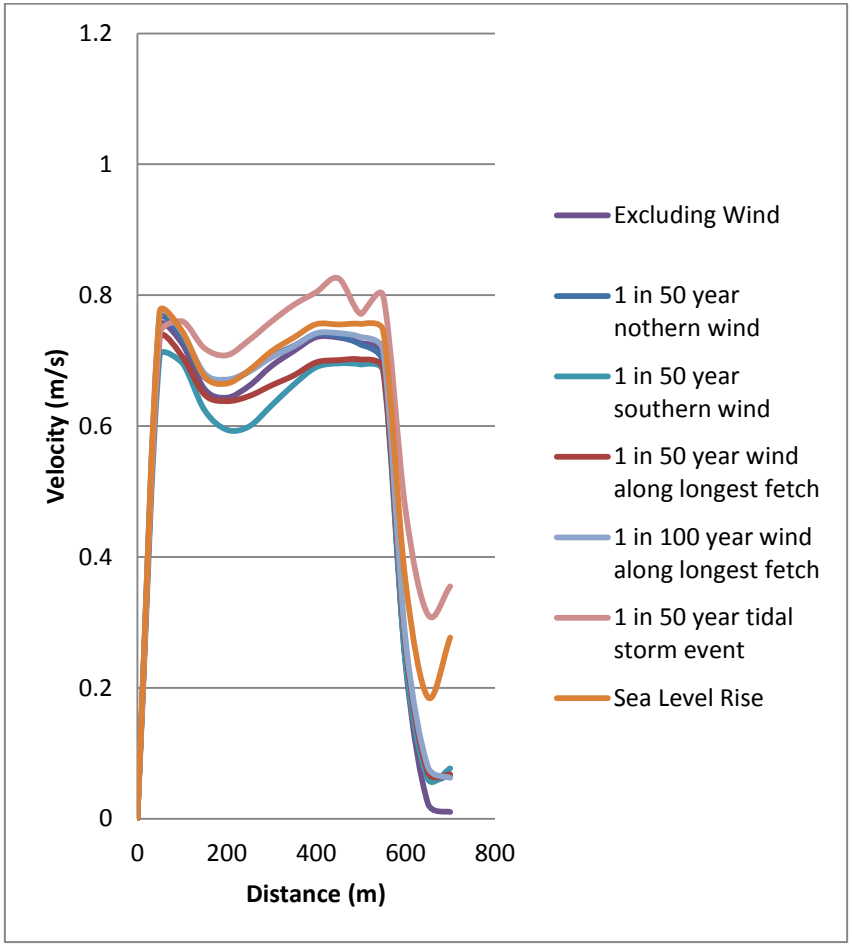

Figure 8-35: **Comparison on hydrodynamic velocities at section L2, near Langebaan Beach, during a flood tide after the construction of the causeway and the jetty**

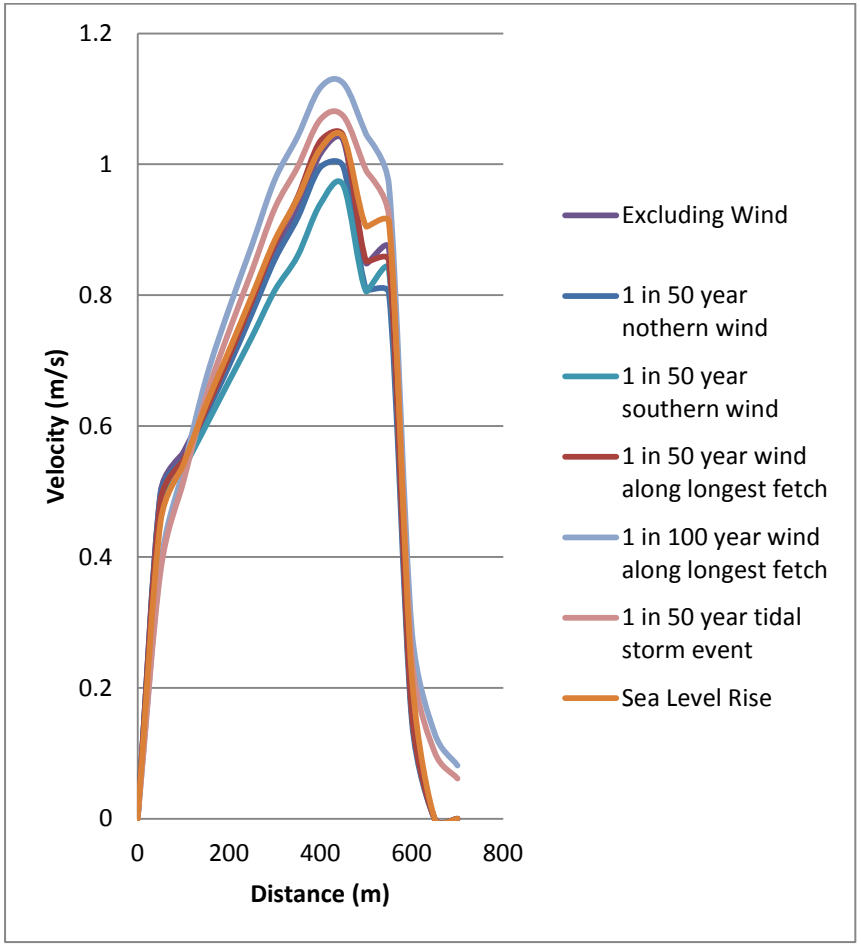

Figure 8-36: **Comparison on hydrodynamic velocities at section L2, near Langebaan Beach, during an ebb tide prior to the construction of the causeway and the jetty**

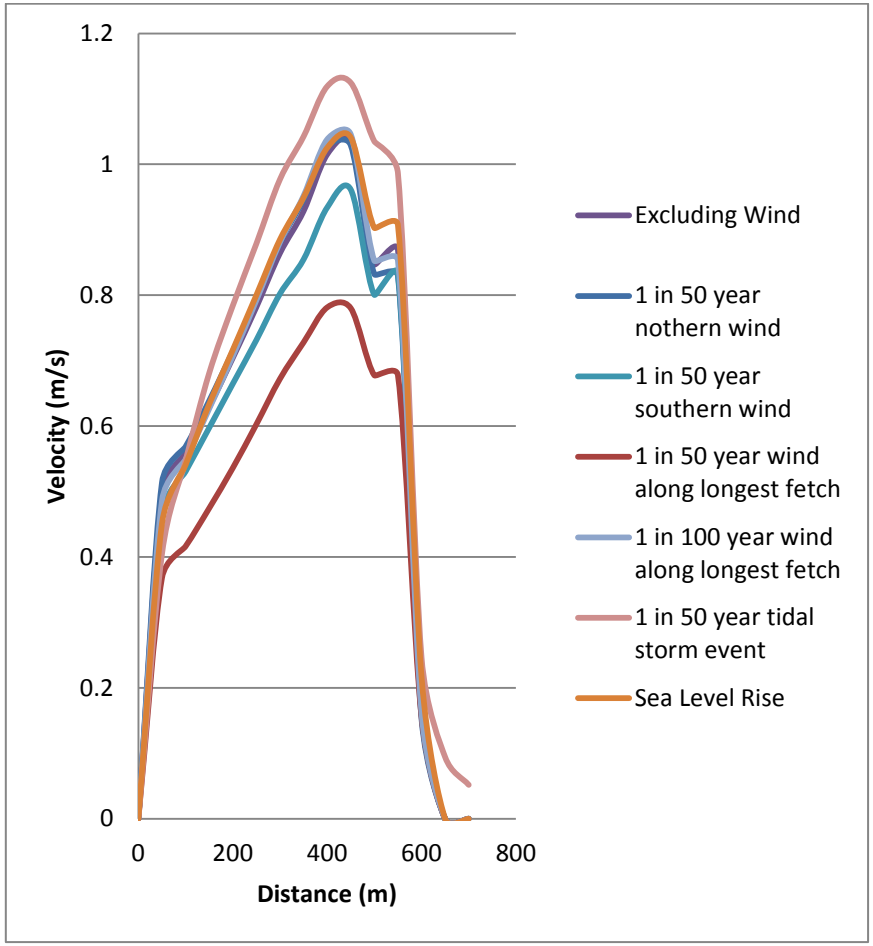

Figure 8-37: **Comparison on hydrodynamic velocities at section L2, near Langebaan Beach, during an ebb tide after the construction of the causeway and the jetty**

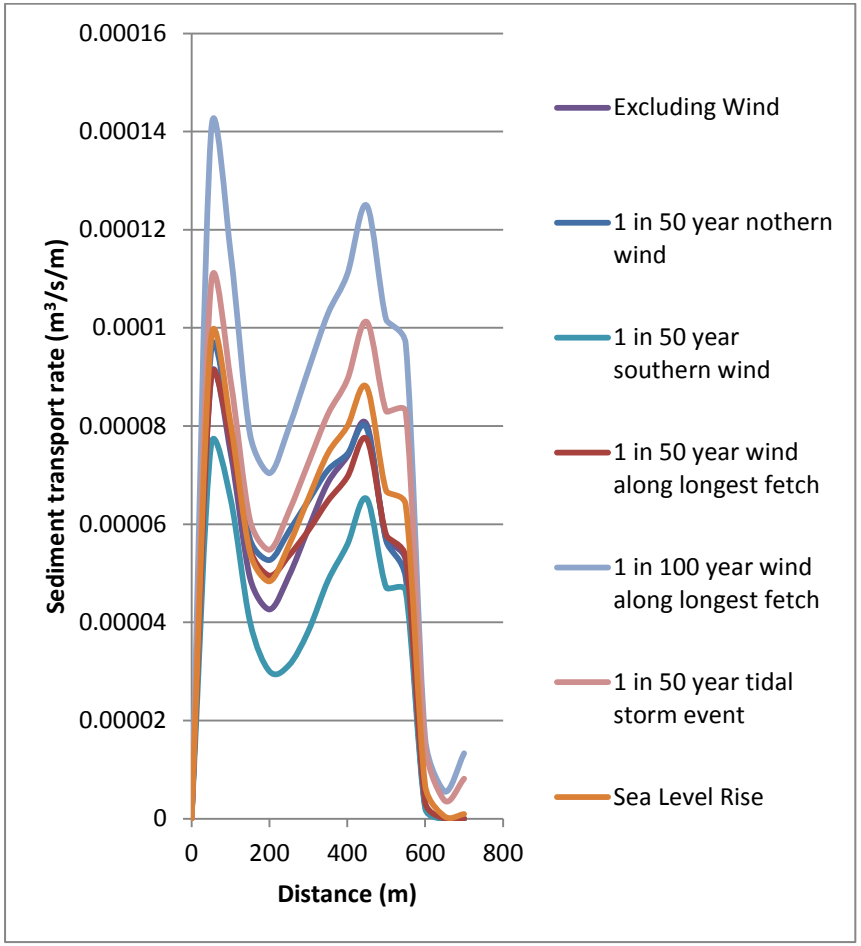

Figure 8-38: **Comparison on sediment transport at section L2, near Langebaan Beach, during a flood tide prior to the construction of the causeway and the jetty**

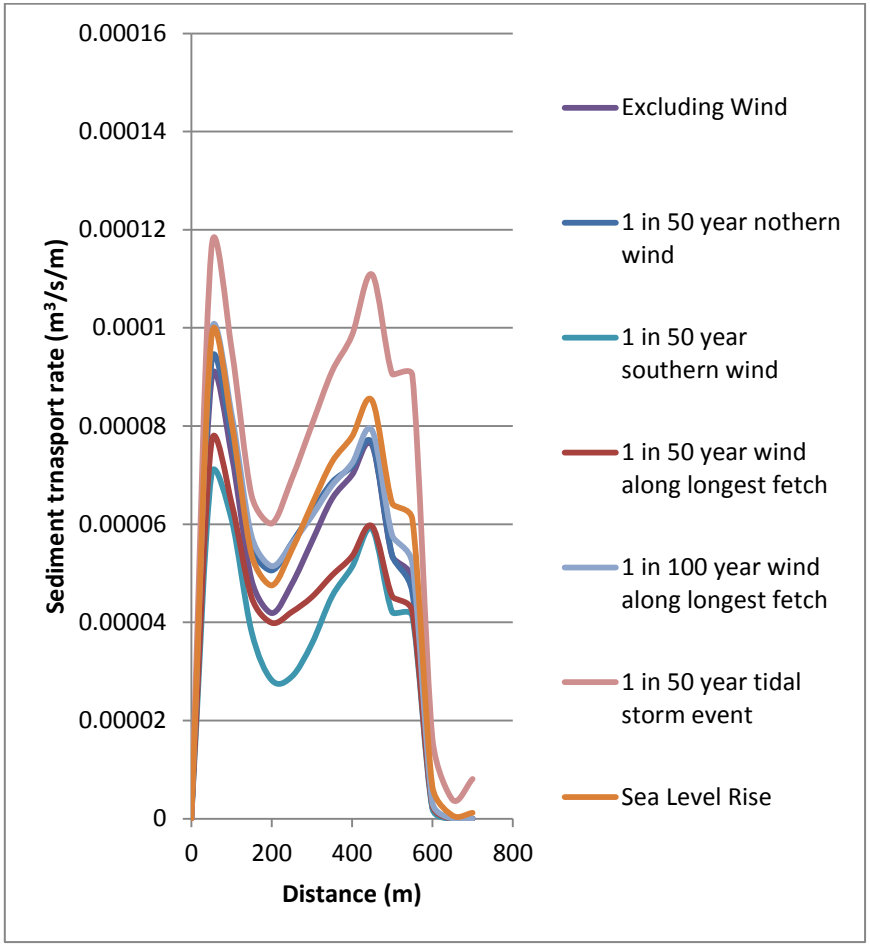

Figure 8-39: **Comparison on sediment transport at section L2, near Langebaan Beach, during a flood tide after the construction of the causeway and the jetty**

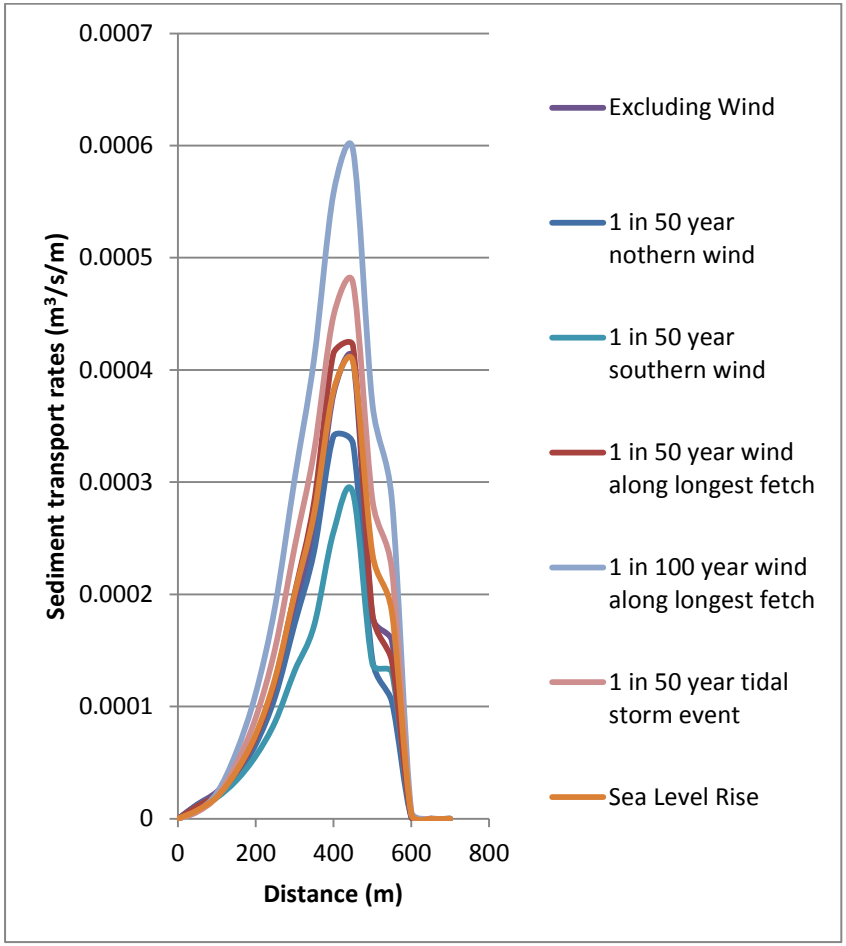

Figure 8-40: **Comparison on sediment transport at section L2, near Langebaan Beach, during an ebb tide prior to the construction of the causeway and the jetty**

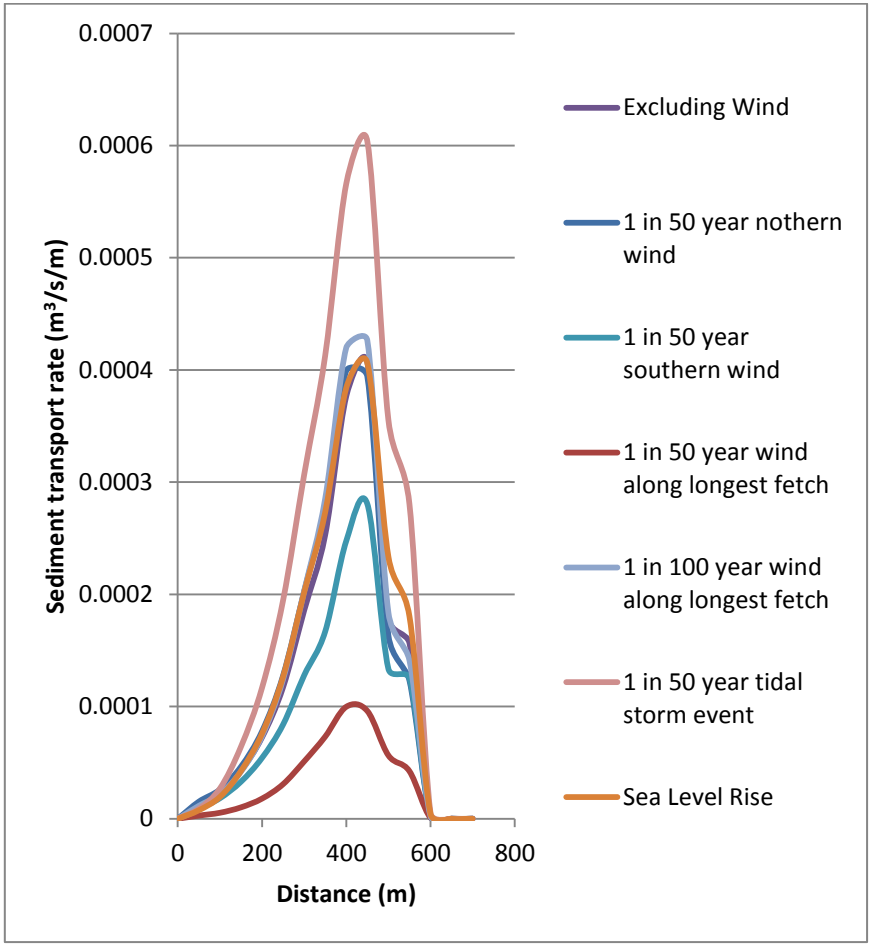

Figure 8-41: **Comparison on sediment transport at section L2, near Langebaan Beach, during an ebb tide after the construction of the causeway and the jetty**

From **Figure 8-34**, **Figure 8-36**, **Figure 8-35** and **Figure 8-37** it has been concluded that the scenario which impacted Langebaan Beach the most after the construction of the causeway and the jetty were the tidal storm events, also known as the storm surge. However, conditions prior to the construction of the causeway and the jetty indicates that a 1 in 100 year wind velocity along the longest fetch provided the greatest velocities at the location of Langebaan Beach, thus generating the most sediment transport during these events and the storm surge providing the second greatest velocities. The storm surge was based on a 1 in 50 year event and the wind on a 1 in 100 year event. The 1 in 50 year event for the same wind direction provided velocities smaller than the storm surge scenario. Therefore the storm surge event and tidal driven events generated greater velocities.

Observations from the sediment transport model indicated similar results for the various scenarios to the hydrodynamic results, as illustrated in **Figure 8-38**, **Figure 8-40**, **Figure 8-39** and **Figure 8-41**. However, sediment transport rates should be used with caution due to the omission of wave action on the coastline.

The to and fro tidal action was investigated by means of a five year period model based on the tidal predicted water levels provided by WXTide. This model indicated that no major changes in the bathymetry were observed and the influence of the construction of the causeway and the jetty had little to no impact on the sediment transport and erosion of Langebaan Beach, based on the tidal and wind forced hydrodynamics.

However, the effect of littoral drift due to wave action, which has been excluded from this investigation, could provide different results to the results mentioned above.

9 LIMITATIONS AND QUALIFICATIONS

The modelling of waves was excluded from this investigation due to the purpose of the study focusing on the effects of tidal and wind driven hydrodynamics, provided unrealistic morphological results. However, during morphological investigations the effects of littoral drift due to wave action should be included, which would contribute to the sediment transport rates.

Two-dimensional modelling provided accurate results for the Langebaan Lagoon system, however, a hydrodynamic analysis of Saldanha Bay, and especially Small Bay, would require a three-dimensional investigation as mentioned by CSIR in **Section 3.1**.

During this investigation, it has been identified that not all the studies done on Saldanha Bay and Langebaan Lagoon were available for public perusal. Literature reviews were limited due to confidentiality restrictions and previous reports dated back to the late 1970's.

Along with the very limited reports available for literature review, work done prior to the construction of the causeway and the jetty was also minimal. Very basic conditions on the hydrodynamics and sediment composition prior to the construction were documented.

Furthermore, outdated documents include the GIS information and maps used for the generation of a bathymetry for the numerical model. This complicated the calibrations process due to an outdated bathymetry and could result in inaccuracies near the entrance to the Langebaan Lagoon where Langebaan Beach has experienced extensive erosion. Further surveys of the area were not possible due to financial complications; therefore the outdated bathymetry had to be calibrated as best possible with the recorded data provided during a field investigation during this study.

Recorded data were also limited due to financial complications and had to be kept at a minimum. Instruments used during the field survey were ideal for the conditions, but possibly had some practical complications which possibly provided inaccurate survey results.

Other practical implications were run-time restrictions of the numerical model. A large area had to be modelled, which increase the time required to run each of the scenarios. Therefore detail had to be decreased to provide more suitable simulation times.

However, even though accuracy had to be decreased and the model was based on and calibrated to an outdated bathymetry, this model was proven acceptable for a high-level investigation, requiring less detail, of the hydrodynamics and sediment transport of the Saldanha Bay and Langebaan Lagoon.

If a more detailed analysis on the area is required, a survey would have to be done on the bathymetry to decrease the limitations of this model. More hydrodynamic and sediment transport surveys would also be required, as to ensure that an accurate representation of the area would be modelled.

10 CONCLUSIONS

Since the construction of the causeway and the jetty in Saldanha Bay, various changes along the coastline have been observed, especially at the mouth of the Langebaan Lagoon, where Langebaan Beach have experienced extensive erosion. During this investigation, a two-dimensional hydrodynamic mathematical model was used to determine the effects of these structures on the hydrodynamics and sediment transport of Saldanha Bay and Langebaan Lagoon, focussing on the main channels at the Langebaan Lagoon mouth, based on tides and wind as the hydrodynamic driving forces and excluding wave action.

From previous investigations, it has been identified that the hydrodynamics in Saldanha Bay is primarily driven by the wind conditions dominating in the area and the hydrodynamics in the Langebaan Lagoon is driven by tidal variations experienced in Big Bay, forcing and extracting the water during tidal oscillations, similar to the breathing action of a lung. The numerical model was based on these two parameters to identify the impact of the causeway and the jetty on the hydrodynamics and sediment transport in Saldanha Bay and Langebaan Lagoon during various extreme events in these two driving forces.

During the construction of the numerical model, it has been identified that the information available to generate the bathymetry was outdated. However, acceptable calibration was obtained for the numerical model. Due to the condition during field survey not being similar to the conditions provided by the numerical model, the results from the numerical model should be approached with caution.

Scenarios based on the extreme conditions of tidal and wind events confirmed the conclusions from previous investigations, stating that Saldanha Bay is dominated by wind events and Langebaan Lagoon dominated by the tidal variations experienced in Big Bay.

From the numerical model it was also concluded that the wind, dominating the circulation in Saldanha Bay, would determine the direction of flow entering or exiting the lagoon. A clockwise rotation generated by a northern wind direction in Big Bay resulted in water

entering from the north-east and exiting towards a north-western direction and an anti-clockwise rotation generated by southern winds in Big Bay resulted in opposite conditions, with water entering from the north-west and exiting in a north-eastern direction.

Further observations along the coastline of Small Bay and Big Bay indicated greater velocities during extreme wind conditions and very little variation in velocity during extreme tidal conditions, which confirmed the findings from previous investigations, stating that the hydrodynamics in Saldanha is primarily wind driven.

The hydrodynamics in the Langebaan Lagoon were most affected by extreme tidal variations in Big Bay. Wind events had very little impact on the hydrodynamics at the mouth of the lagoon and the conditions prior to and after the construction of the causeway and the jetty had very little to no influence on the hydrodynamics based on wind and tidal conditions in the Langebaan Lagoon.

An investigation on the hydrodynamic conditions and sediment transport at the location of Langebaan Beach, based on tidal variations and wind forcing, indicated that the greatest hydrodynamic velocities and sediment transport rates were observed during 1 in 100 year extreme wind conditions across the longest fetch identified by a north-north-western wind prior to the construction of the causeway and the jetty and 1 in 50 year extreme tidal storms, or storm surge conditions, after the construction of the harbour developments. However, the 1 in 50 year extreme wind condition provided smaller velocities than a similar return period storm surge event, which concludes that the hydrodynamics in the main channel of the lagoon near the location of Langebaan Beach at the Langebaan Lagoon mouth are primarily tidal driven.

Sediment transport rates only provided an indication of the effect wind and tidal driven hydrodynamics had on the sediment transport. Actual sediment transport rates are expected to be much greater due to the effect of wave action, which has been excluded from this investigation.

During a long-term simulation consisting of a five-year period to determine the effect of tidal forcing, excluding wind, on the sediment transport of the Saldanha Bay and Langebaan Lagoon systems, no major morphological impacts were observed in the bathymetry. One of the primary reasons for the lack of morphological observations on the coastline is due to the omission of wave action during this investigation. Further investigations on the morphology of Langebaan Beach should include wave modelling.

Therefore, it is concluded that tidal variations and storm surge events would generate the greatest hydrodynamic velocities at the Langebaan Lagoon mouth; however, these velocities had a minor morphological impact on the main channels of the Langebaan Lagoon at its mouth. Furthermore, the impact of the construction of the causeway and the jetty had a minor influence on the hydrodynamic velocities generated by means of tidal variations and wind forcing at the Langebaan Lagoon mouth.

11 RECOMMENDATIONS

As stated previously, various limitations were identified during this investigation. For further investigation of the hydrodynamics and sediment transport of the Langebaan Lagoon and Saldanha Bay, a detailed survey of the area would be required.

Along with the survey, the utilization of flexible mesh software packages should be investigated to assist in the modelling of the entire area and thus provide the opportunity for more detailed modelling without the complications of time constraints.

A three-dimensional model should be used for the modelling of Saldanha Bay as recommended in previous studies. Not only does the thermo cline during summer complicate the modelling of the bay, but complex flow patterns were expected at the entrance to Small Bay, also stated in a previous report.

After the construction of the causeway, there have been major alterations in the wave climates, resulting in a change in the effect of wave action on the coastline. Therefore, further investigations on the erosion of beaches and the morphology of the coastline should include wave action, and be investigated in much more detail.

12 REFERENCES

Anthoni, D. J. (2000). *Oceanography : Tides.* Retrieved 09 09, 2012, from Sea Friends: http://www.seafriends.org.nz/oceano/tides.htm

Beer, T. (1983). *Environmental Oceanography : An introduction to the Behaviour of Coastal Water.* New York: Pergamon PRess.

Bindschadler, R. (2006). Hitting the ice sheets where it hurts. *Science 311* , 1720 – 1721.

Bosman, D. E., Basson, J., Tente, T., & Basson, G. R. (2011). *Guideline on freeboard for dams.* Pretoria: Water Research Commission.

Brinkmann, B. (2010). Coastal Engineering Block Course. *Coastal Engineering Course* . University of Stellenbosch.

Burman, J., & Levin, S. (1974). *The Saldanha Bay Story.* Human and Rossouw.

Cartwright, A. (2011). *Coastal vulnerability in the context of climate change: A South African perspective.* Econologic.

Church, A., Gregory, J., White, N., Platten, S., & Mitrovica, J. (2011). *Understanding and Projection of Sea Level Change.*

Clark, B. M., Tunley, K., Angel, A., Hutchings, K., Steffani, N., & Turplie, J. (2011). *State of the Bay 2010 : Saldanha Bay and Langebaan Lagoon.* Cape Town: Anchor Environment.

Clark, B., Orr, K., Hutchings, K., Angel, A., & Turpie, J. (2009). *State of the Bay 2008 : Saldanha Bay and Langebaan Lagoon.* Cape Town: Anchor Environmental.

Coetzee, P. P. (1949). *Saldanhabaai: 'n Geografiese Studie.* Stellenbosch: Stellenbosch.

Dasgupta, S., Laplante, B., Murray, S., & Wheeler, D. (2009). *Cliomate Change and the Future Impacts of Storm-Surge Disasters in Developing Countries.* Washington, DC: Center for Global Development.

DHI Water and Environment. (2006). *MIKE21 : Non-Cohesive Sediment Transport : A Short Description.* Hørsholm, Denmark: DHI Water and Environment.

DHI Water and Environment. *MIKE21 and MIKE3 Flow Model FM : Hydrodynamic Model : Short Description.*

DHI Water and Environment. (1995). Mike21: Coastal Hydraulics and Oceanography:. *Hydrodynamic Module: Release 2.7* . DHI Water and Environment.

Engelund, F., & Fredsoe, J. *A Sediment Transport Model for Straight Alluvial Channels.*

eWISA. (2012). *Wetland - Langebaan.* Retrieved 09 09, 2012, from eWISA: http://www.ewisa.co.za/misc/wetlands/defaultwetWCLangebaan.htm

Flemming, B. (1977). *Distribution of recent sediments in Saldanha Bay and Langebaan Lagoon.* Transactions of the Royal Society of South Africa.

Hanekom, D. N., & de Graaf, D. G. (1995, 08 20). *Langebaan*. Retrieved 09 28, 2009, from Department of Environmental Affairs: http://www.environment.gov.za/Branches/BioConservation/17Ramsar/langebaan/langebaan_ris.htm

Harris, D. L. (1963). *Characteristics of the hurricane storm surge.* Washington, D.C: Deprtment of Commerce.

Kruger, A. C., Goliger, A. M., Retief, J. V., & Seleke, S. S. *Estimation of Extreme Wind Speeds in the Mixed Strong Wind Climate of South Africa.* Pretoria: South African Weather Service.

Ltd, G. (n.d.). *Geomatix*. Retrieved June 13, 2009, from Geomatix: http://www.geomatix.net

Luger, S. (1999). *A modeling driven environmental baseline assessment for the proposed New Hood Point outfall in East London.* Stellenbosch: CSIR.

Luger, S. A., Schoonees, J. S., Mocke, G. P., & Smit, F. (1998). Predicting and evaluating turbidity caused by dredging in the environmentally sensitive Saldanha Bay. *Preceedings of 26th Conference on Coastal Engineering* .

Luger, S., Prestedge, G., McClarity, A., Soltau, C., Schoonees, K., & Fleming, C. (2006). Morphological modelling for design of a beach restoration project. *International Conference on Coastal Engineering* .

Mather, A. (2008). Coastal erosion and sea-level rise : Are municipalities ready for this? Internal Document. eThekwini Municipality, KZN, South Africa.

Meillon, L. D. (1993). *Surface waves and sediment interaction in the nearshore region.* Port Elizabeth: University of Port Elizabeth.

Milford, R. V. (1987). *Annual Maximum Wind Speeds For South Africa.* Stellenbosch: University of Stellenbosch.

Mitchum, G. T., & Clarke, A. J. (1986). The frictional neashore response to frocing by synoptic scale winds. *Journal of Physical Oceanography* , 934 - 946
.

Monteiro, P. M., & Brundrit, G. B. (1990). Interannual chlorophyll variability in South Africa's Saldanha Bay system, 1974-1979. *South African Journal of Marine Science , 9*, 281-287.

Monteiro, P., & Largier, L. (1999). Thermal stratification in Saldanha Bay (South Africa) and subtidal, density driven exchange with coastal waters of the Benguela Upwelling System. *Estuarine, Coastal and Shelf Science, 49* , 877-890.

Physical and chemical characteristics of water in Saldanha Bay and Langebaan Lagoon1977*Transactions of the Royal Society of South Africa 42*3+4441-459

Pickard, G. L., & Emery, W. J. (1990). *Descriptive Physical Oceanography: An introduction.* Oxford: Pergamon Press.

Pond, S., & Pickard, G. L. (1983). *Introductory dynamical oceanography.* Oxford: Pergamon Press.

RAMSAR. (n.d.). *RAMSAR Convention.* Retrieved 09 09, 2012, from RAMSAR: http://www.ramsar.org

SANCOLD. (1990). *Guidelines on Freeboard for Dam.* Pretoria: The South African National Committee on Large Dams.

SANHO. (2012). South African Tide Tables 2012. *South African Navy Hydrographic Office* .

Schoonees, J. S., Huizinga, P., & Taljaard, S. (September 1995). *Saldanha Bay: Turbidity Caused by Dredging, Shipping and Storms.* Stellenbosch: CSIR Environmental Services.

Seminara, G., & Blondeaux, P. (2001). *River, Coastal and Estuarine Morphodynamics.* Genova: Springer.

Shannon, L.V. & Stander, G.H. (1977). Physical and chemical characteristics of water in Saldanha Bay and Langebaan Lagoon. *Transactions of the Royal Society of South Africa*, 42(3+4), 441-459.

Stellenbosch, U. o. (2009). *Revision of the SANCOLD Interim 1990 Guidelines on Freeboard for Dams.* Pretoria: Water Research Commission.

Van Balleggoyen, N., Steffani, N., & Pulfrich, A. (2008). *Environmental impact assessment: Proposed reverse osmosis plant, Iron-ore handeling facility, Port of Saldanha - Marine impact assessment specialist study.* Joint CSIR/Pisces Report.

Van der Merwe, E. (1994). *Dynamics of two haroursL PortElizabeth and Saldanha Bay.* Port Elizabeth: University of Port Elizabeth.

Verhagen, H. J. (2010). Coastal Structures. *Coastal Engineering Course* . Stellenbosch: University of Stellenbosch.

Weeks, S. J., Boyd, A. J., Monteiro, P. M., & Brundrit, G. B. (1991a). The currents and circulation in Saldanha Bay After 1975 deduced from historical measurements of drogues. *South African Journal of Marine Science , 11* (1), 525-535.

Weeks, S. J., Monteiro, P. M., Nelson, G., & Cooper, R. M. (1991b). A note on wind-driven replacement flow of the bottom layer in Saldanha Bay. *South African Journal of Marine Science* , 579-583.

Appendix A SEDIMENT COMPOSITION ACCORDING TO 1977 REPORT

LIST OF FIGURES

Figure A-1: Distribution of very coarse sand (1-2mm) in Saldanha Bay prior to construction (Flemming, 1977)

Figure A-2: Distribution of coarse sand (0.5-1mm) in Saldanha Bay prior to construction (Flemming, 1977)

Figure A-3: Distribution of medium sand (0.25-0.5mm) in Saldanha Bay prior to construction (Flemming, 1977)

Figure A-4: Distribution of fine sand (0.125-0.25mm) in Saldanha Bay prior to construction (Flemming, 1977)

Figure A-5: Distribution of very fine sand (0.063-0.125mm) in Saldanha Bay prior to construction (Flemming, 1977)

Figure A-6: Distribution of very coarse sand (1-2mm) in Langebaan Lagoon (Flemming, 1977)

Figure A-7: Distribution of coarse sand (0.5-1mm) in Langebaan Lagoon (Flemming, 1977)

Figure A-8: Distribution of medium sand (0.25-0.5mm) in Langebaan Lagoon (Flemming, 1977)

Figure A-9: Distribution of fine sand (0.125-0.25mm) in Langebaan Lagoon (Flemming, 1977)

Figure A-10: Distribution of very fine sand (0.063-0.125mm) in Langebaan Lagoon (Flemming, 1977)

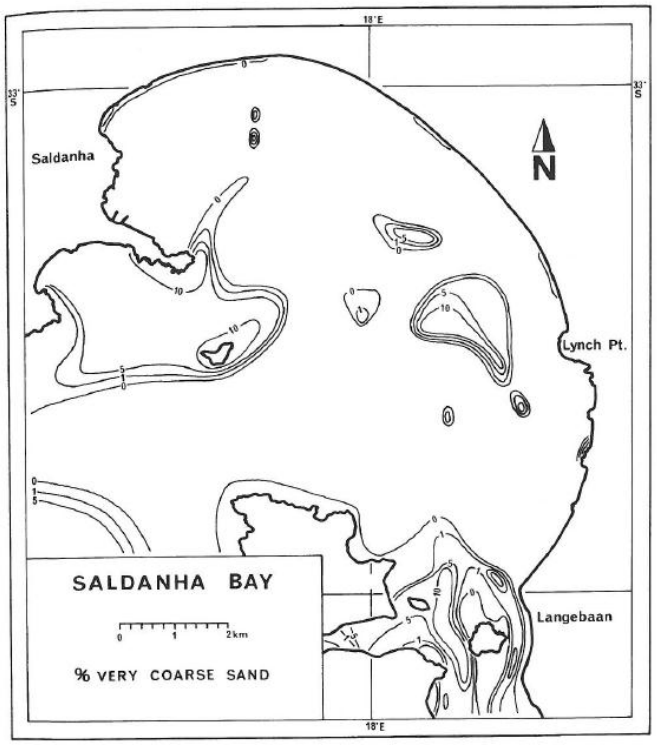

Figure A-1: Distribution of very coarse sand (1-2mm) in Saldanha Bay prior to construction (Flemming, 1977)

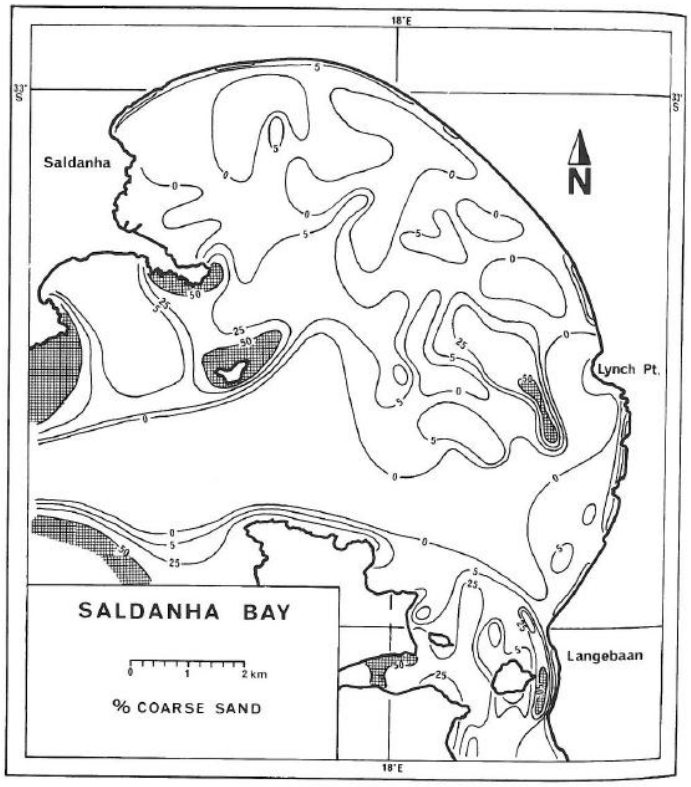

Figure A-2: Distribution of coarse sand (0.5-1mm) in Saldanha Bay prior to construction (Flemming, 1977)

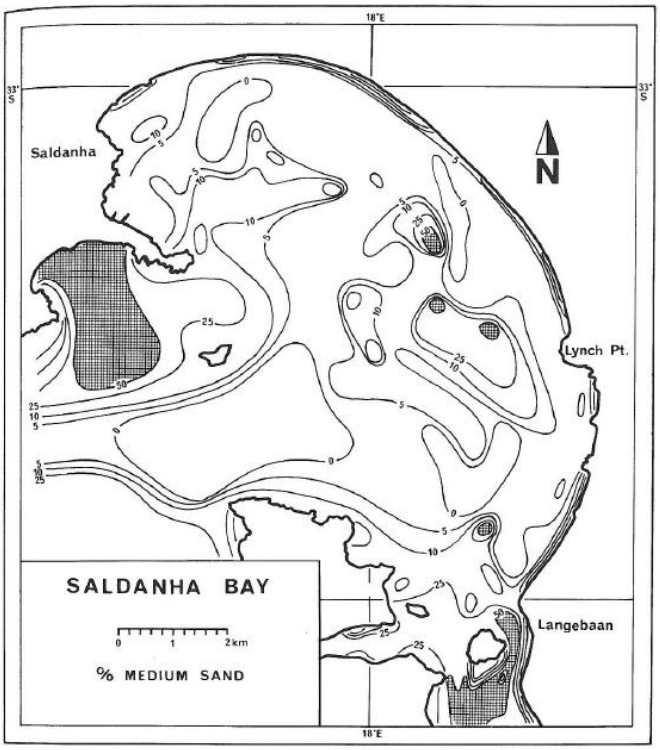

Figure A-3: Distribution of medium sand (0.25-0.5mm) in Saldanha Bay prior to construction (Flemming, 1977)

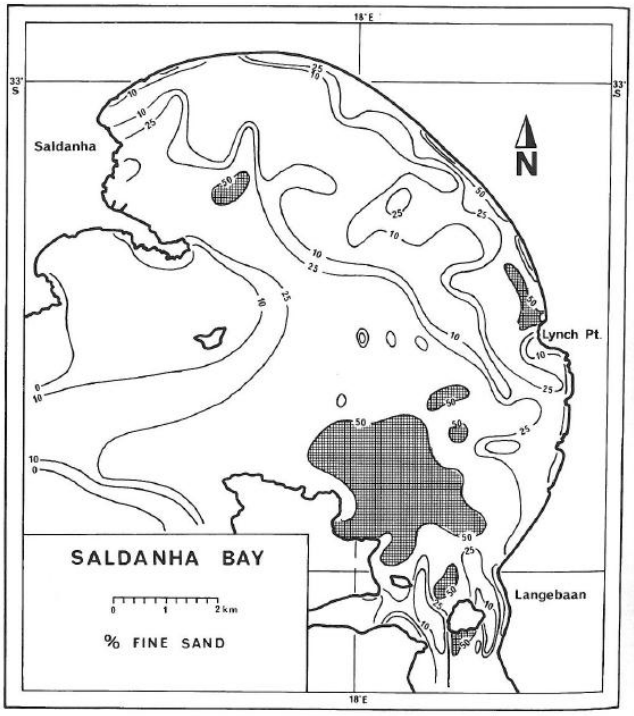

Figure A-4: Distribution of fine sand (0.125-0.25mm) in Saldanha Bay prior to construction (Flemming, 1977)

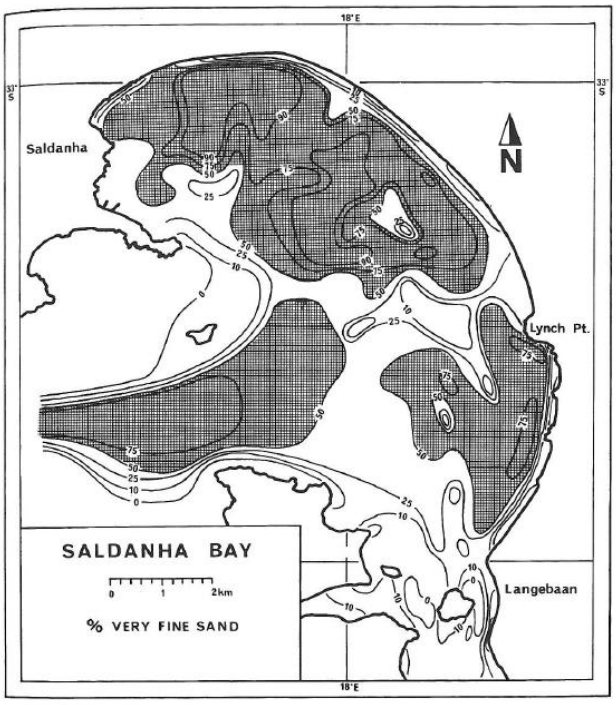

Figure A-5: Distribution of very fine sand (0.063-0.125mm) in Saldanha Bay prior to construction (Flemming, 1977)

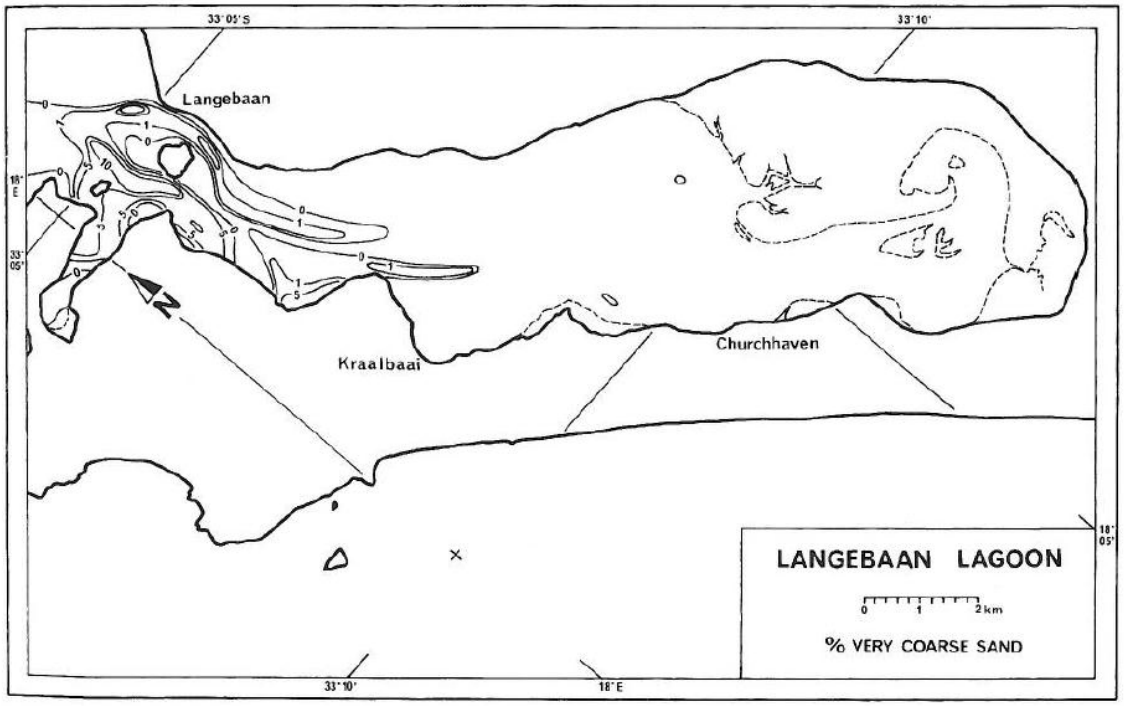

Figure A-6: Distribution of very coarse sand (1-2mm) in Langebaan Lagoon (Flemming, 1977)

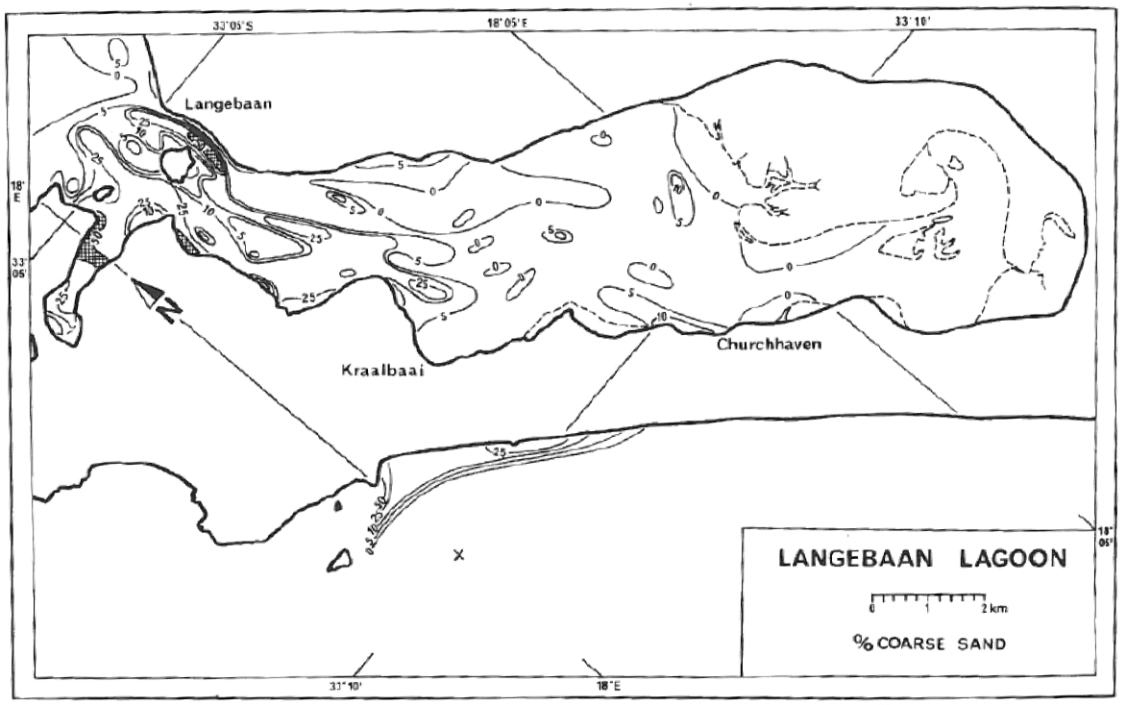

Figure A-7: Distribution of coarse sand (0.5-1mm) in Langebaan Lagoon (Flemming, 1977)

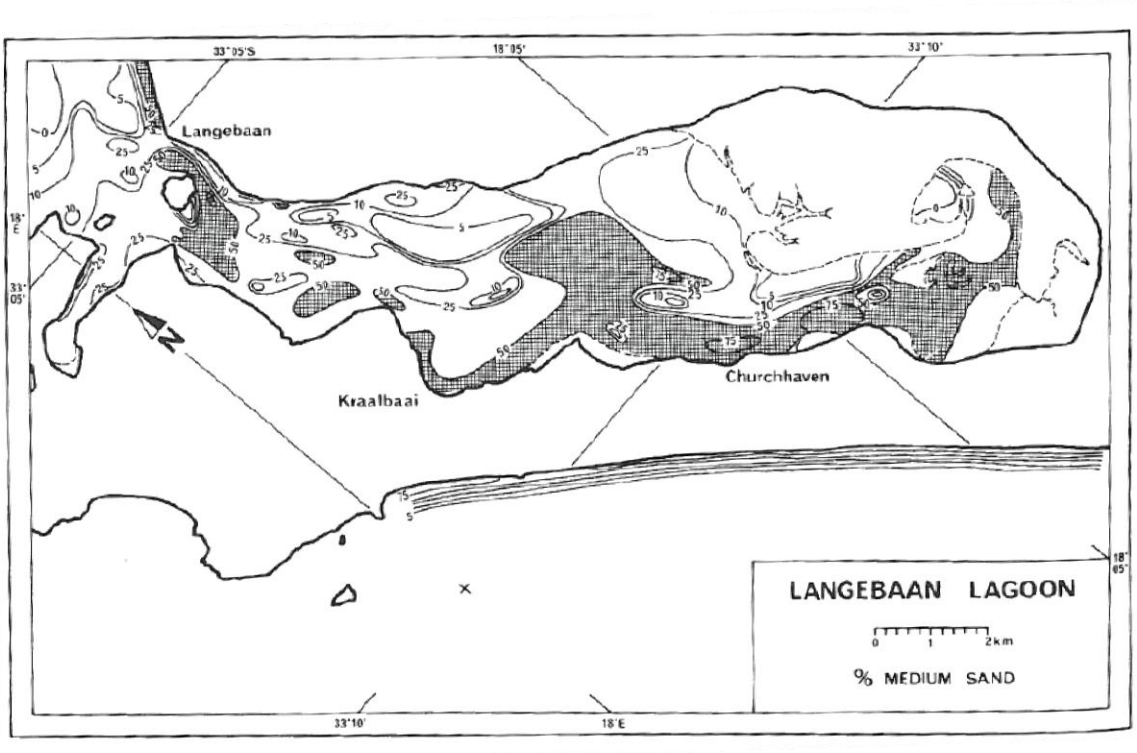

Figure A-8: Distribution of medium sand (0.25-0.5mm) in Langebaan Lagoon (Flemming, 1977)

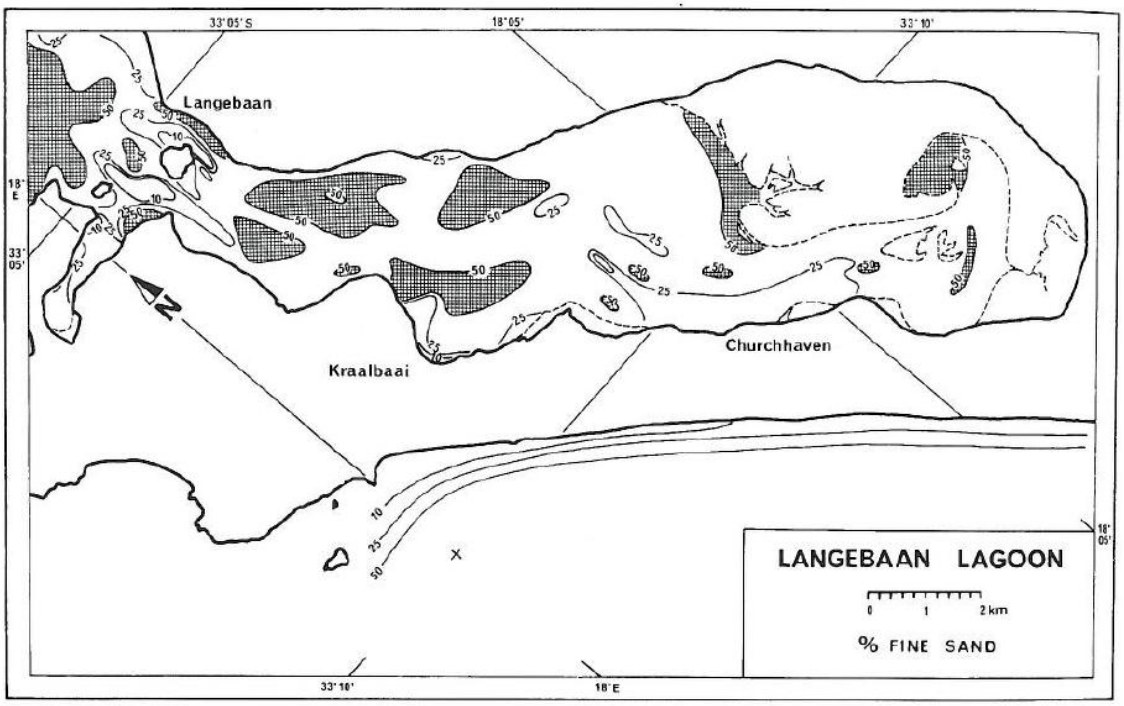

Figure A-9: Distribution of fine sand (0.125-0.25mm) in Langebaan Lagoon (Flemming, 1977)

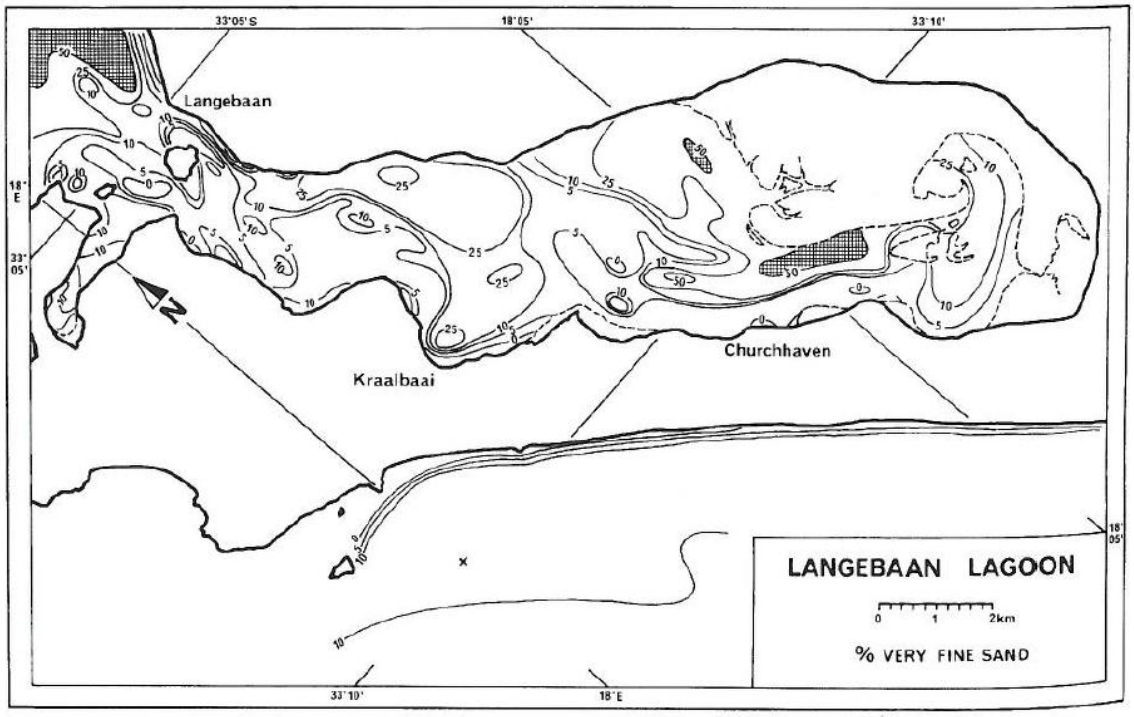

Figure A-10: Distribution of very fine sand (0.063-0.125mm) in Langebaan Lagoon (Flemming, 1977)

Appendix B LANGEBAAN AERIAL PHOTOGRAPHS

LIST OF FIGURES

Figure B-1: Aerial photograph of Langebaan beach in 1938
Figure B-2: Aerial photograph of Langebaan beach in 1960
Figure B-3: Aerial photograph of Langebaan beach in 1977
Figure B-4: Aerial photograph of Langebaan beach in 1988
Figure B-5: Aerial photograph of Langebaan beach in 2000
Figure B-6: Aerial photograph of Langebaan beach in 2004
Figure B-7: Aerial photograph of Langebaan beach in 2006
Figure B-8: Aerial photograph of Langebaan beach in 2011

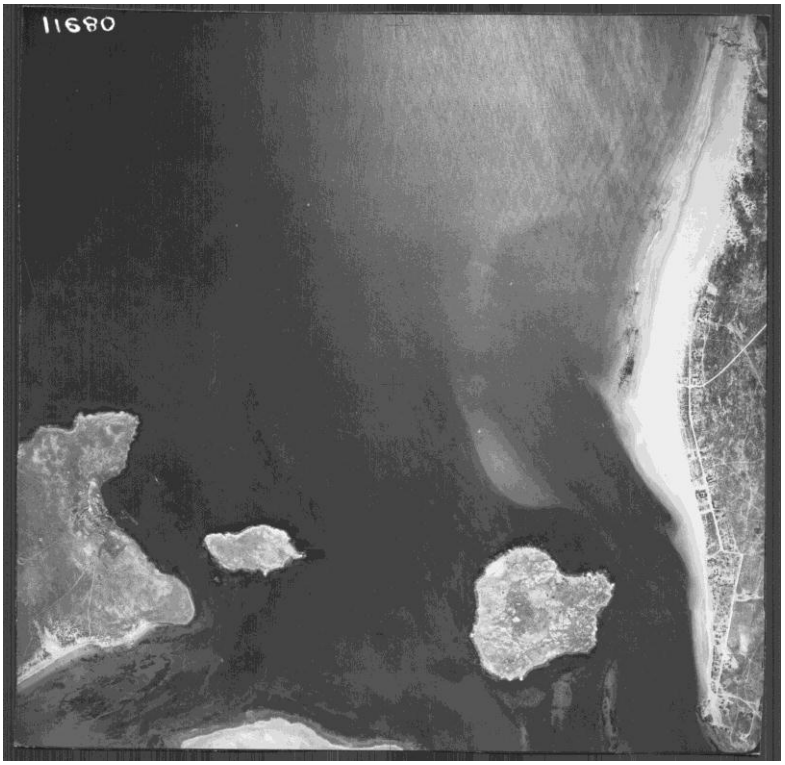

Figure B-1: Aerial photograph of Langebaan beach in 1938

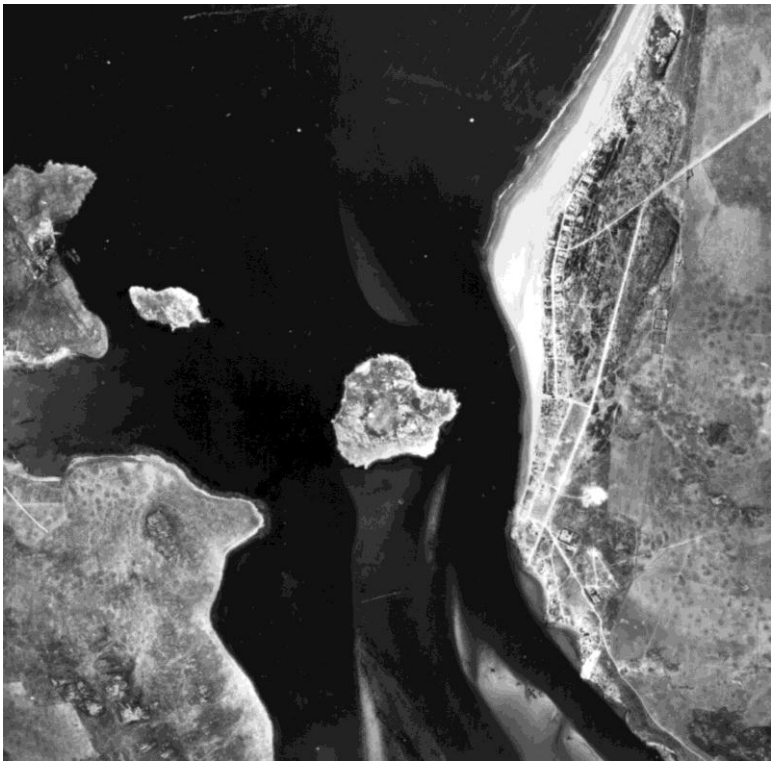

Figure B-2: Aerial photograph of Langebaan beach in 1960

Figure B-3: Aerial photograph of Langebaan beach in 1977

Figure B-4: Aerial photograph of Langebaan beach in 1988

Figure B-5: Aerial photograph of Langebaan beach in 2000

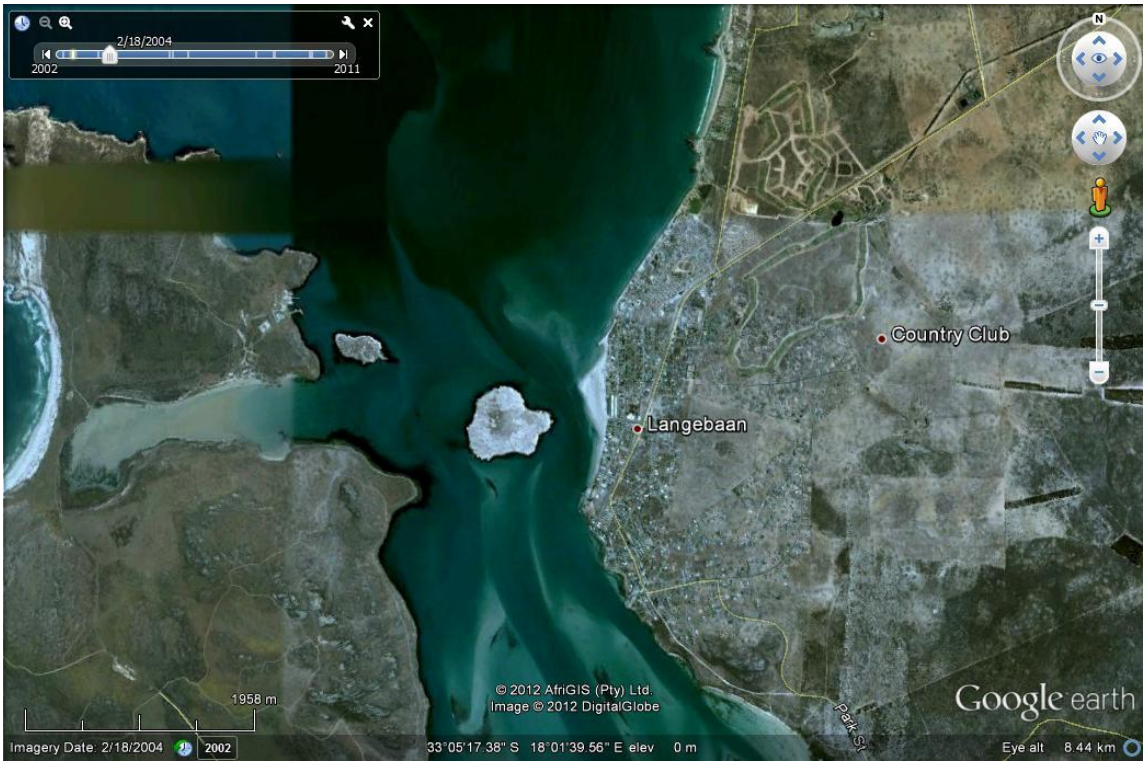

Figure B-6: Aerial photograph of Langebaan beach in 2004

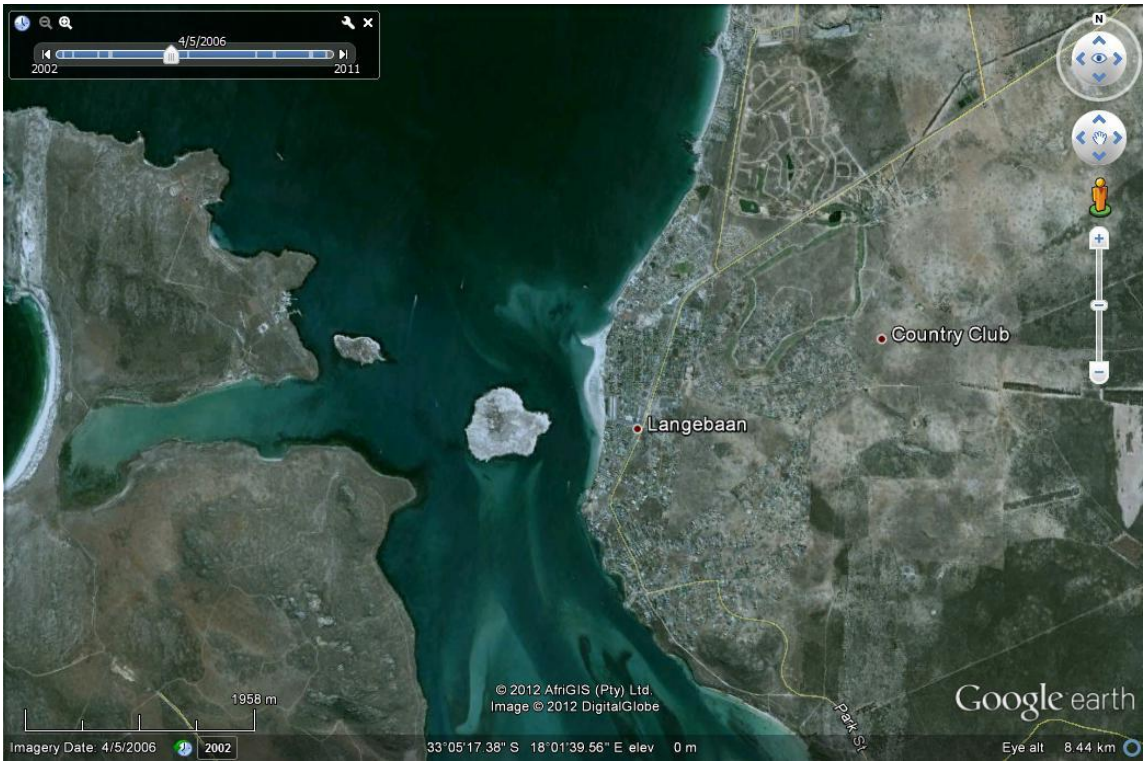

Figure B-7: Aerial photograph of Langebaan beach in 2006

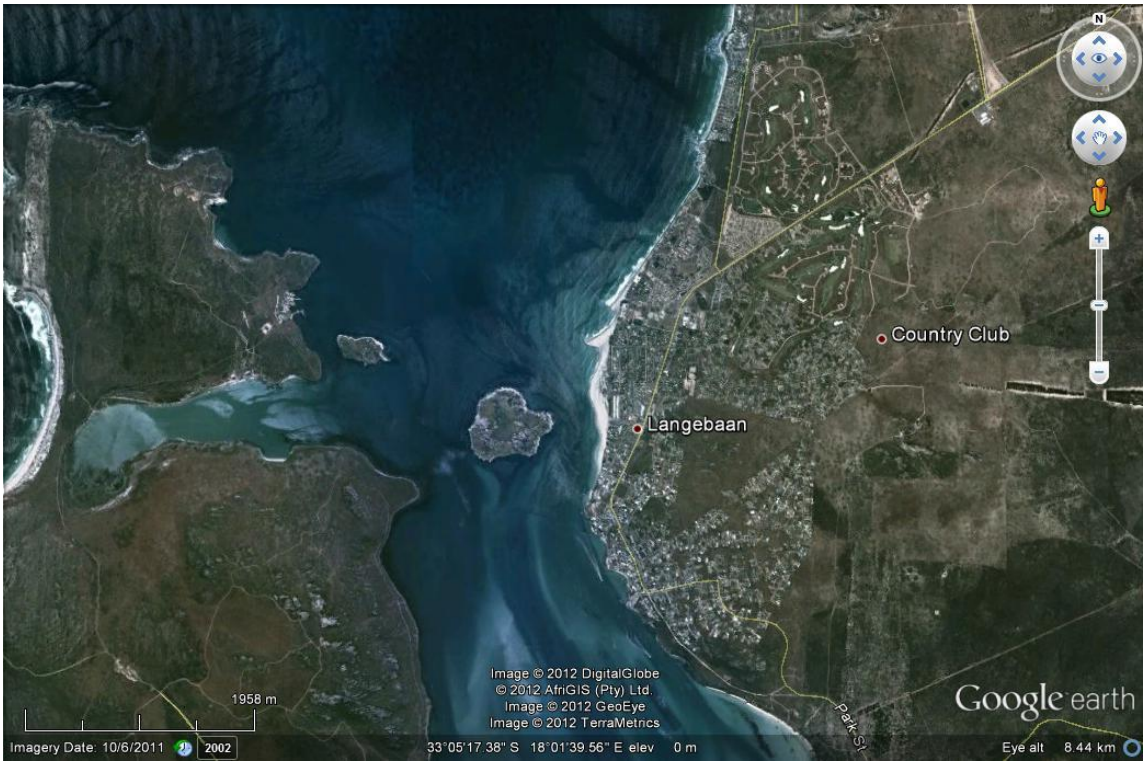

Figure B-8: Aerial photograph of Langebaan beach in 2011

Appendix C WIND ANALYSIS

LIST OF TABLES

Table C-1: Annual hourly wind conditions

Table C-2: Wind conditions during summer months

Table C-3: Wind conditions during autumn months

Table C-4: Wind conditions during winter months

Table C-5: Wind conditions during spring months

Table C-1: Annual hourly wind conditions

ANNUAL

Record size 36 579 hours

Observation percentage

	Velocity in m/s									
	Calm	0 to 2	2 to 5	5 to 7	7 to 9	9 to 12	12 to 15	above 15	Percentage in direction	Percentage in direction exceeding 5 m/s
N		1.52	4.13	1.44	0.62	0.31	0.05	0.01	8.07	2.42
NNE		1.37	1.57	0.19	0.06	0.02	0.00	0.00	3.21	0.27
NE		2.09	2.05	0.14	0.02	0.00	0.00	0.00	4.31	0.16
ENE		1.52	0.80	0.37	0.12	0.02	0.00	0.00	2.83	0.51
E		1.47	0.93	0.32	0.25	0.08	0.01	0.00	3.05	0.66
ESE		1.31	0.85	0.19	0.12	0.06	0.00	0.00	2.52	0.37
SE		1.77	3.37	0.53	0.18	0.06	0.00	0.00	5.91	0.77
SSE		1.63	5.46	2.30	1.61	0.91	0.06	0.00	11.97	4.88
S	9.58	1.77	10.13	5.36	3.49	1.61	0.03	0.00	22.39	10.49
SSW		0.53	3.04	1.75	0.52	0.11	0.01	0.00	5.97	2.39
SW		0.39	1.98	0.64	0.10	0.04	0.00	0.00	3.15	0.78
WSW		0.30	1.68	0.62	0.14	0.05	0.00	0.00	2.79	0.82
W		0.56	2.63	0.91	0.19	0.05	0.00	0.00	4.34	1.15
WNW		0.48	1.69	0.71	0.23	0.08	0.00	0.00	3.19	1.02
NW		0.49	1.68	0.69	0.27	0.07	0.01	0.00	3.21	1.04
NNW		0.63	1.86	0.65	0.28	0.09	0.00	0.00	3.51	1.02
		17.83	43.84	16.82	8.21	3.54	0.18	0.01	90.42	28.75

Table C-2: Wind conditions during summer months

SUMMER

Record size 31 174

Observation percentage

	Velocity in m/s									
	Calm	**0 to 2**	**2 to 5**	**5 to 7**	**7 to 9**	**9 to 12**	**12 to 15**	**above 15**	**Percentage in direction**	**Percentage in direction exceeding 5 m/s**
N		0.98	2.08	0.40	0.11	0.04	0.00	0.00	3.61	0.55
NNE		0.65	0.75	0.11	0.02	0.00	0.00	0.00	1.53	0.13
NE		0.99	0.65	0.02	0.00	0.00	0.00	0.00	1.67	0.03
ENE		0.64	0.18	0.09	0.09	0.01	0.00	0.00	1.00	0.19
E		0.62	0.18	0.12	0.13	0.07	0.00	0.00	1.11	0.31
ESE		0.93	0.32	0.05	0.03	0.01	0.00	0.00	1.34	0.09
SE		1.75	2.41	0.40	0.16	0.07	0.01	0.00	4.79	0.64
SSE		1.83	7.00	3.68	2.88	1.93	0.08	0.00	17.39	8.57
S	8.19	1.85	13.49	8.76	7.22	3.82	0.08	0.00	35.22	19.88
SSW		0.68	3.47	2.82	1.09	0.20	0.01	0.00	8.26	4.12
SW		0.44	2.17	0.93	0.07	0.00	0.00	0.00	3.61	1.00
WSW		0.22	1.69	0.76	0.04	0.00	0.00	0.00	2.70	0.80
W		0.37	2.24	1.14	0.13	0.00	0.00	0.00	3.88	1.27
WNW		0.34	1.16	0.64	0.25	0.04	0.00	0.00	2.43	0.92
NW		0.34	0.73	0.37	0.18	0.06	0.00	0.00	1.68	0.61
NNW		0.35	0.96	0.18	0.08	0.00	0.00	0.00	1.58	0.27
		12.98	39.47	20.46	12.47	6.26	0.18	0.00	91.81	39.37

Table C-3: Wind conditions during autumn months

AUTUMN

Record size 60576

Observation percentage

	Velocity in m/s									
	Calm	**0 to 2**	**2 to 5**	**5 to 7**	**7 to 9**	**9 to 12**	**12 to 15**	**above 15**	**Percentage in direction**	**Percentage in direction exceeding 5 m/s**
N		4.67	0.92	2.41	0.78	0.25	0.12	0.01	9.16	3.57
NNE		2.12	0.92	0.98	0.10	0.02	0.01	0.00	4.14	1.10
NE		2.34	1.16	0.96	0.07	0.00	0.00	0.00	4.54	1.04
ENE		1.39	0.81	0.25	0.17	0.08	0.01	0.00	2.72	0.52
E		1.44	0.81	0.29	0.11	0.14	0.04	0.01	2.84	0.59
ESE		1.40	0.77	0.46	0.08	0.03	0.01	0.00	2.74	0.58
SE		3.50	1.06	1.84	0.31	0.11	0.03	0.00	6.85	2.29
SSE		6.66	1.01	2.98	1.19	0.80	0.35	0.02	13.02	5.34
S	6.46	11.89	1.21	6.43	2.43	1.07	0.32	0.01	23.36	10.26
SSW		2.77	0.31	1.63	0.57	0.11	0.03	0.00	5.42	2.34
SW		1.55	0.25	1.05	0.17	0.01	0.01	0.00	3.04	1.24
WSW		1.22	0.18	0.84	0.13	0.02	0.00	0.00	2.40	1.00
W		1.97	0.38	1.29	0.19	0.03	0.01	0.00	3.87	1.52
WNW		1.44	0.30	0.85	0.19	0.04	0.00	0.00	2.83	1.09
NW		1.51	0.28	0.80	0.28	0.08	0.01	0.00	2.97	1.18
NNW		1.86	0.40	0.88	0.31	0.14	0.06	0.00	3.65	1.39
		47.71	10.78	23.95	7.10	2.93	1.03	0.04	93.54	35.06

Table C-4: Wind conditions during winter months

WINTER

Record size 61416

Observation percentage

	Velocity in m/s								Percentage in direction	Percentage in direction exceeding 5 m/s
	Calm	0 to 2	2 to 5	5 to 7	7 to 9	9 to 12	12 to 15	above 15		
N		7.61	1.15	3.42	1.48	0.72	0.41	0.08	14.88	6.11
NNE		2.94	1.09	1.46	0.19	0.05	0.01	0.00	5.75	1.72
NE		4.32	1.78	2.19	0.13	0.02	0.00	0.00	8.44	2.34
ENE		2.78	1.37	0.88	0.34	0.04	0.01	0.00	5.43	1.27
E		2.52	1.17	0.91	0.18	0.11	0.05	0.01	4.95	1.27
ESE		1.62	0.77	0.64	0.10	0.04	0.01	0.00	3.17	0.79
SE		3.11	0.80	1.90	0.20	0.06	0.02	0.00	6.09	2.18
SSE		3.26	0.72	1.78	0.36	0.20	0.07	0.01	6.40	2.42
S	5.71	4.68	0.77	2.68	0.78	0.22	0.03	0.01	9.16	3.71
SSW		1.72	0.23	1.10	0.23	0.06	0.03	0.01	3.38	1.43
SW		1.29	0.16	0.72	0.23	0.09	0.04	0.01	2.54	1.08
WSW		1.44	0.20	0.73	0.29	0.11	0.05	0.01	2.82	1.19
W		2.76	0.42	1.51	0.52	0.15	0.04	0.00	5.40	2.23
WNW		2.20	0.31	1.14	0.45	0.14	0.06	0.00	4.31	1.80
NW		2.77	0.36	1.46	0.55	0.20	0.07	0.01	5.43	2.30
NNW		3.13	0.49	1.55	0.62	0.27	0.08	0.00	6.14	2.52
		48.16	11.79	24.08	6.67	2.46	0.98	0.15	94.29	34.34

Table C-5: Wind conditions during spring months

SPRING

Record size 64204

Observation percentage

	Velocity in m/s									
	Calm	**0 to 2**	**2 to 5**	**5 to 7**	**7 to 9**	**9 to 12**	**12 to 15**	**above 15**	**Percentage in direction**	**Percentage in direction exceeding 5 m/s**
N		3.15	0.57	1.62	0.50	0.24	0.09	0.01	6.18	2.46
NNE		1.07	0.49	0.41	0.06	0.04	0.02	0.00	2.09	0.53
NE		1.82	0.87	0.75	0.08	0.02	0.00	0.00	3.53	0.84
ENE		1.39	0.62	0.42	0.20	0.08	0.01	0.00	2.72	0.71
E		1.90	0.72	0.61	0.30	0.19	0.04	0.00	3.76	1.14
ESE		1.67	0.68	0.48	0.18	0.16	0.09	0.00	3.26	0.90
SE		3.55	0.89	1.96	0.36	0.13	0.04	0.00	6.93	2.50
SSE		6.63	0.70	2.90	1.30	0.86	0.46	0.05	12.90	5.57
S	3.46	12.72	0.73	4.90	3.33	2.19	1.00	0.01	24.88	11.43
SSW		3.85	0.20	1.74	1.35	0.35	0.06	0.00	7.56	3.51
SW		1.94	0.17	1.19	0.43	0.06	0.03	0.00	3.82	1.71
WSW		1.88	0.12	1.02	0.47	0.14	0.04	0.00	3.67	1.67
W		2.50	0.18	1.45	0.58	0.14	0.05	0.00	4.89	2.22
WNW		1.92	0.21	0.88	0.48	0.17	0.08	0.00	3.74	1.61
NW		1.68	0.19	0.82	0.40	0.18	0.04	0.00	3.31	1.44
NNW		1.68	0.25	0.91	0.30	0.13	0.04	0.00	3.31	1.38
		49.34	7.58	22.07	10.31	5.09	2.07	0.09	96.54	39.62

Appendix D TIDAL ANALYSIS FOR FIELD SURVEY

LIST OF TABLES

Table D-1: Survey tide analysis

Table D-1: Survey tide analysis

Date	SUNRISE	SUNSET	TIDE			START TIME	END TIME	TIME AVAILABLE		CHANGE IN WATER LEVEL (m)	SLOPE OF TIDAL CHANGE
			LOW	HIGH	Flood / Ebb			Between Peaks hh:mm	Per Day hh:mm		
	06:47	19:08	05:51	11:59	Flood	07:41	10:45	03:04		0.7	2.74
2011/03/15	06:47	19:08	18:18	11:59	Ebb	13:52	17:02	03:09	06:13	0.9	3.42
	06:47	19:07	18:18	00:33	Flood	TOO EARLY	TOO LATE				
	06:47	19:07	06:51	00:33	Ebb	TOO EARLY	TOO LATE				
	06:47	19:07	06:51	12:57	Flood	08:40	11:43	03:03		1.1	4.33
2011/03/16	06:47	19:07	19:09	12:57	Ebb	14:48	17:54	03:06	06:09	1.2	4.65
	06:48	19:05	19:09	01:21	Flood	TOO EARLY	TOO LATE				
	06:48	19:05	07:38	01:21	Ebb	TOO EARLY	TOO LATE				
	06:48	19:05	07:38	13:45	Flood	09:28	12:31	03:03		1.4	5.49
2011/03/17	06:48	19:05	19:52	13:45	Ebb	15:35	18:38	03:03	06:07	1.4	5.49
	06:49	19:04	19:52	02:04	Flood	TOO EARLY	TOO LATE				
	06:49	19:04	08:21	02:04	Ebb	07:00	07:05	00:05		1.6	**6.11**
	06:49	19:04	08:21	14:28	Flood	10:11	13:14	03:03		1.6	**6.28**
2011/03/18	06:49	19:04	20:32	14:28	Ebb	16:17	19:00	02:42	05:51	1.6	**6.33**
	06:49	19:03	20:32	02:45	Flood	TOO EARLY	TOO LATE				
2011/03/19	06:49	19:03	09:02	02:45	Ebb	07:00	07:46	00:46	05:51	1.8	**6.88**

Date	SUNRISE	SUNSET	TIDE			START TIME	END TIME	TIME AVAILABLE		CHANGE IN WATER LEVEL (m)	SLOPE OF TIDAL CHANGE
			LOW	HIGH	Flood / Ebb			Between Peaks hh:mm	Per Day hh:mm		
2011/03/19	06:49	19:03	09:02	15:10	Flood	10:52	13:56	03:04	05:51	1.8	**7.04**
	06:49	19:03	21:13	15:10	Ebb	16:58	19:00	02:01		1.8	**7.14**
	06:50	19:01	21:13	03:25	Flood	TOO EARLY	TOO LATE			1.9	
	06:50	19:01	09:44	03:25	Ebb	07:00	08:28	01:28		1.9	**7.22**
	06:50	19:01	09:44	15:52	Flood	11:34	14:38	03:04		1.8	**7.04**
2011/03/20	06:50	19:01	21:53	15:52	Ebb	17:40	19:00	01:19	05:51	1.8	**7.18**
	06:51	18:59	21:53	04:06	Flood	TOO EARLY	TOO LATE				
	06:51	18:59	10:25	04:06	Ebb	07:00	09:09	02:09		1.9	**7.22**
	06:51	18:59	10:25	16:33	Flood	12:15	15:19	03:04		1.7	**6.65**
2011/03/21	06:51	18:59	22:35	16:33	Ebb	18:21	19:00	00:38	05:51	1.6	**6.36**
	06:52	18:58	22:35	04:47	Flood	TOO EARLY	TOO LATE				
	06:52	18:58	11:07	04:47	Ebb	07:00	09:51	02:51		1.7	**6.44**
	06:52	18:58	11:07	17:15	Flood	12:57	16:01	03:04		1.5	5.87
2011/03/22	06:52	18:58	23:18	17:15	Ebb	TOO EARLY	TOO LATE		05:55		
	06:52	18:57	23:18	05:30	Flood	TOO EARLY	TOO LATE				
	06:52	18:57	11:50	05:30	Ebb	07:24	10:34	03:10		1.5	5.68
2011/03/23	06:52	18:57	11:50	17:59	Flood	13:40	16:45	03:04	06:14	1.3	5.07

Appendix E GRADING OF SEDIMENT SAMPLES

LIST OF FIGURES

Figure E-1: Sediment grading north of Schaapen Island
Figure E-2: Sediment grading around Schaapen Island
Figure E-3: Sediment grading south of Schaapen Island
Figure E-4: Sediment grading of bed sample

LIST OF TABLES

Table E-1: Sediment grading analysis

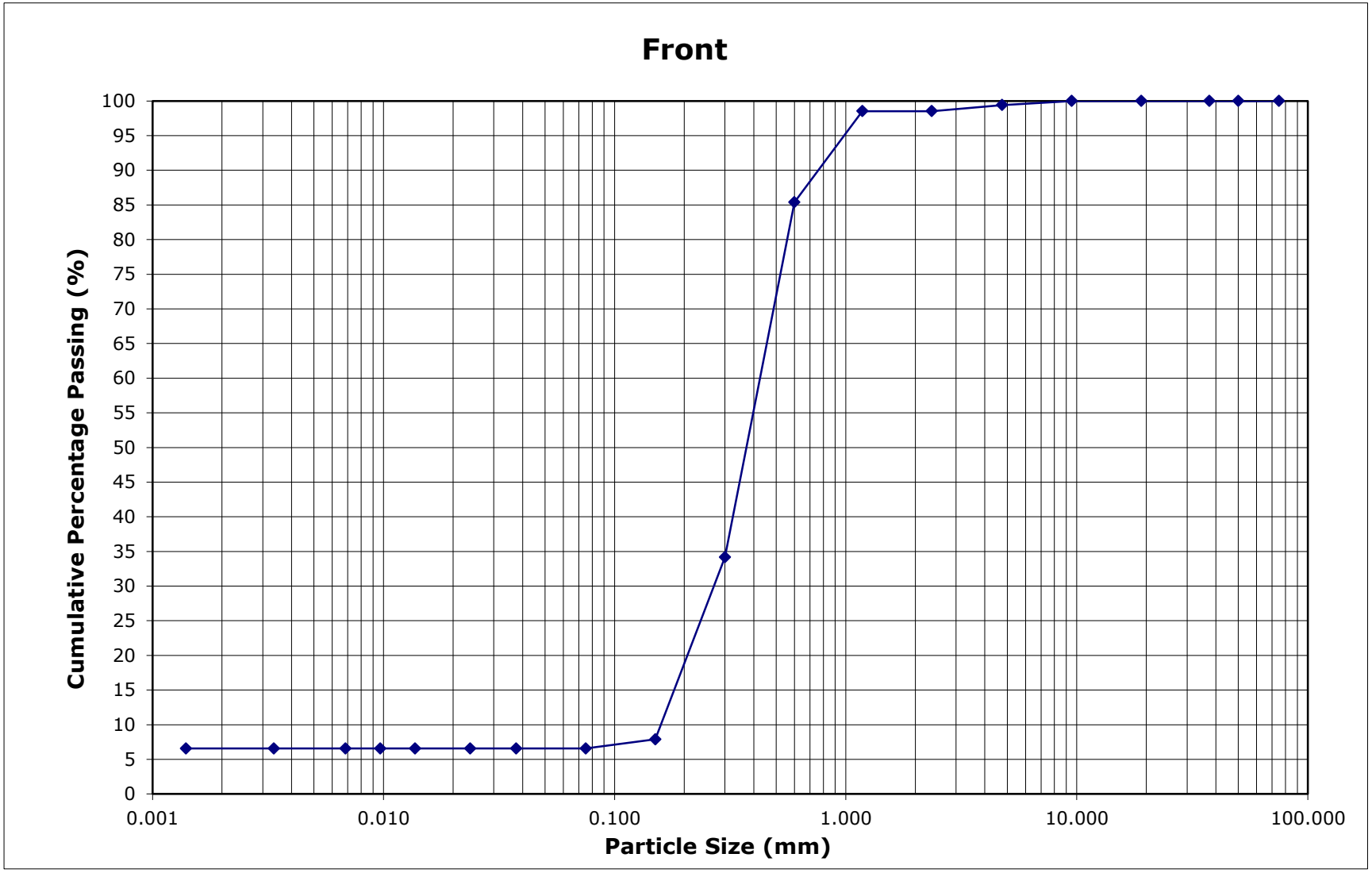

Figure E-1: Sediment grading north of Schaapen Island

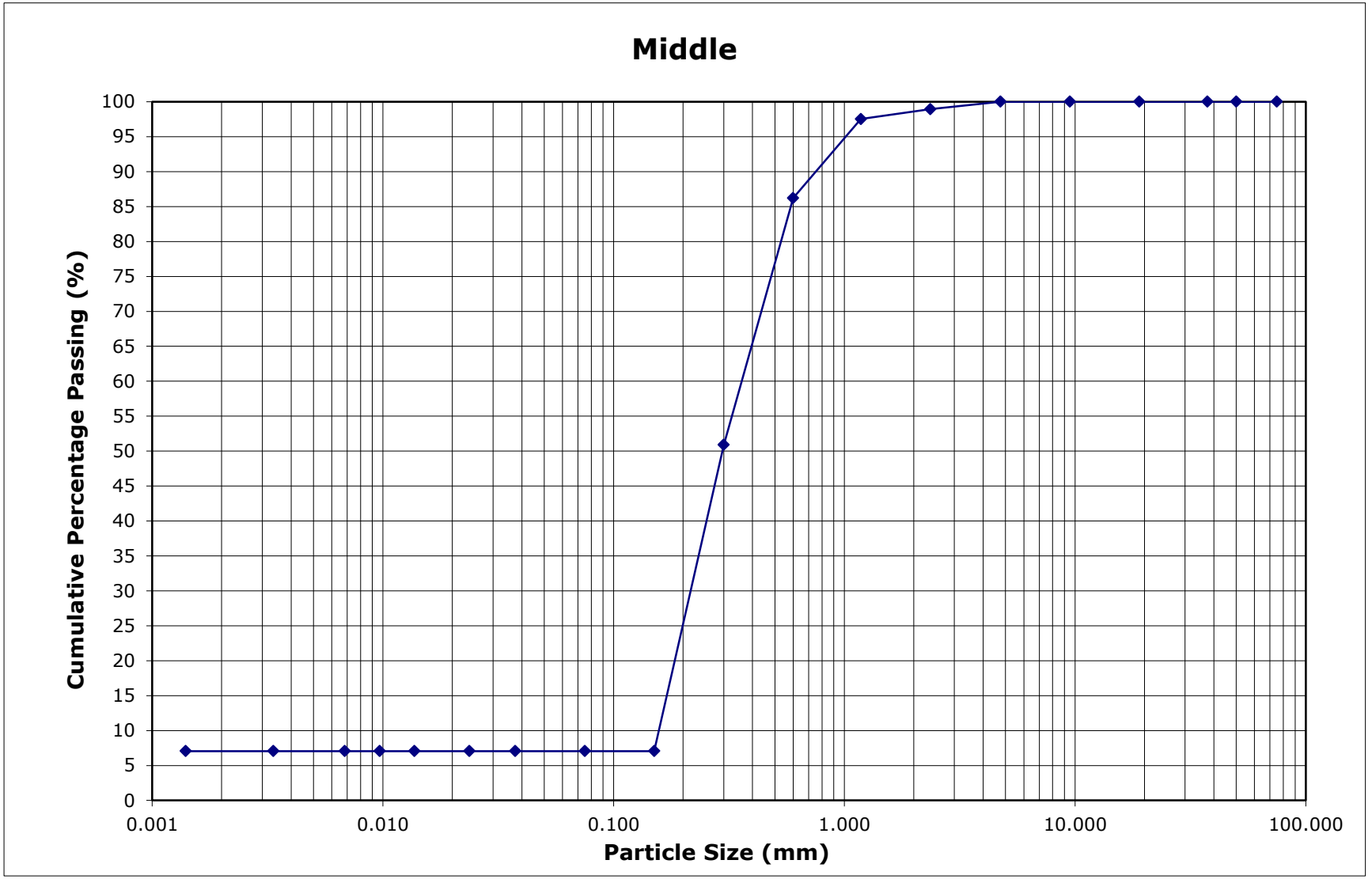

Figure E-2: Sediment grading around Schaapen Island

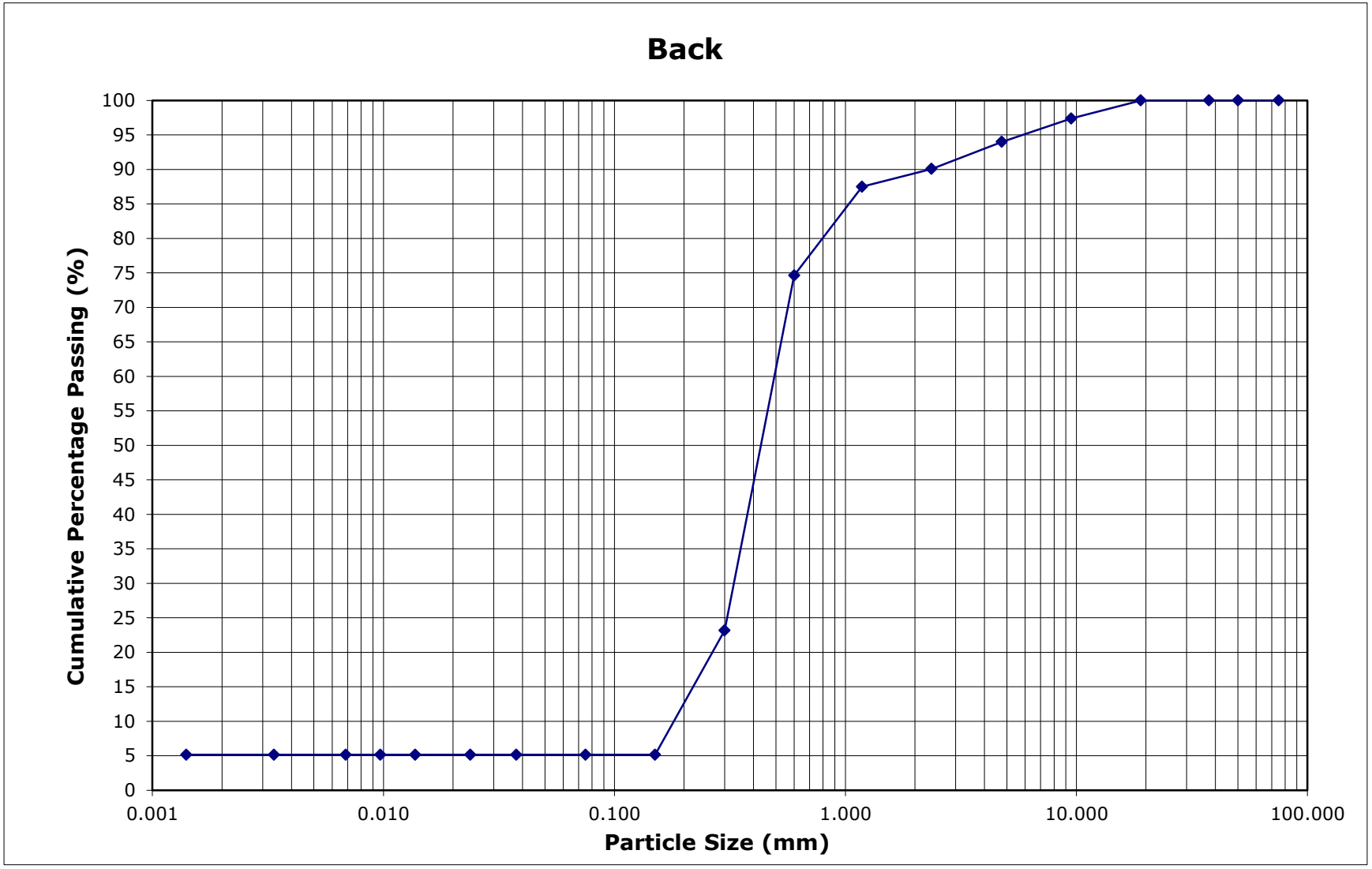

Figure E-3: Sediment grading south of Schaapen Island

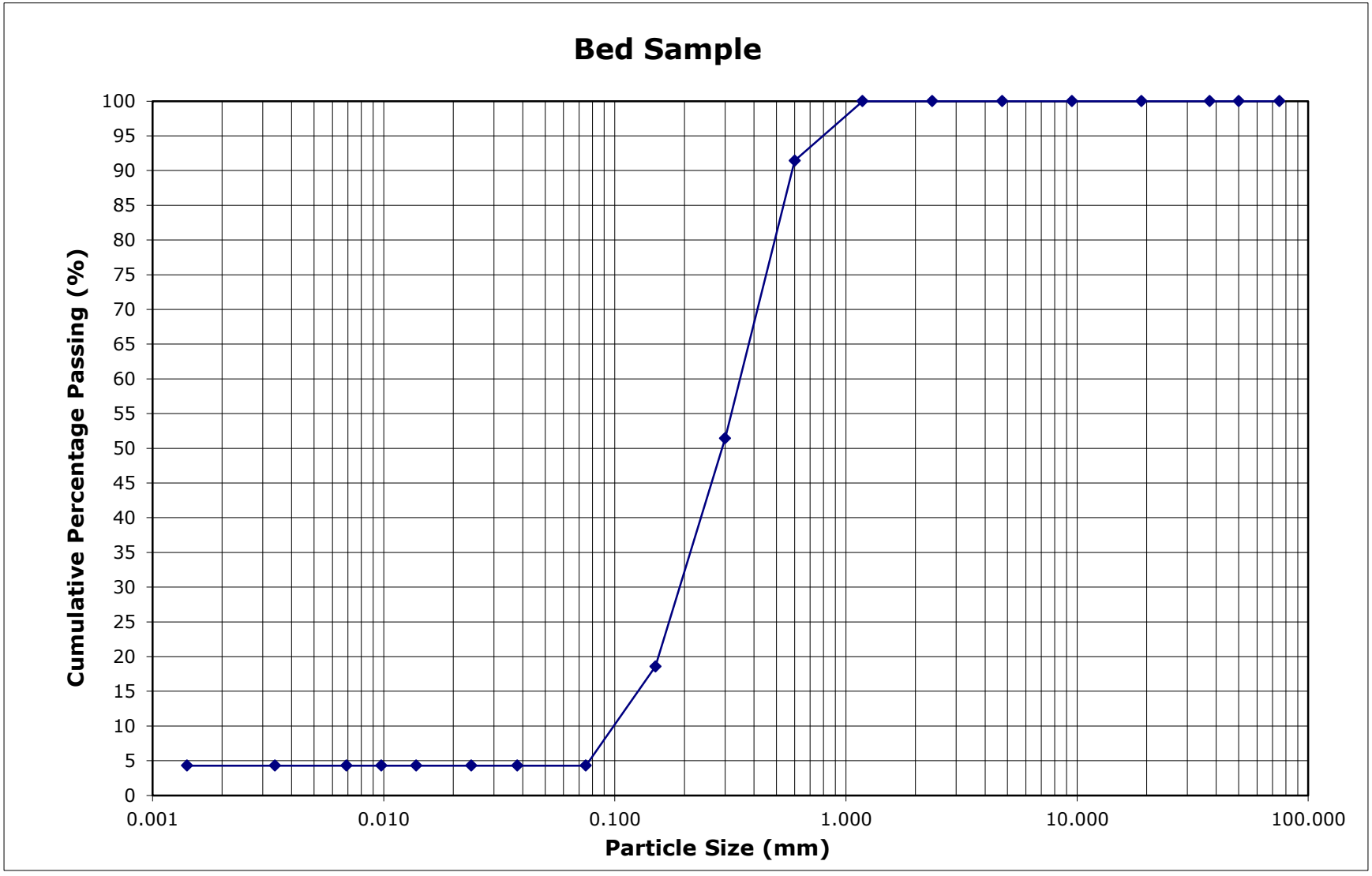

Figure E-4: Sediment grading of bed sample

Table E-1: Sediment grading analysis

	Geotek1	Geotek2	Geotek3	Geotek4
	Back	Middle	Sample	Front
Diameter (mm)	Concentration %	Concentration %	Concentration %	Concentration %
75	100.00	100.00	100.00	100.00
50	100.00	100.00	100.00	100.00
37.5	100.00	100.00	100.00	100.00
19	100.00	100.00	100.00	100.00
9.5	97.38	100.00	100.00	100.00
4.75	94.01	100.00	100.00	99.41
2.36	90.07	98.94	100.00	98.53
1.18	87.50	97.53	100.00	98.53
0.6	74.63	86.22	91.43	85.40
0.3	23.16	50.89	51.43	34.16
0.15	5.15	7.07	18.57	7.88
0.075	5.15	7.07	4.29	6.57
0.0376	5.15	7.07	4.29	6.57
0.0238	5.15	7.07	4.29	6.57
0.0137	5.15	7.07	4.29	6.57
0.0097	5.15	7.07	4.29	6.57
0.0069	5.15	7.07	4.29	6.57
0.0034	5.15	7.07	4.29	6.57
0.0014	5.15	7.07	4.29	6.57

Appendix F CALIBRATION

LIST OF TABLES

Table F-1: Hydrodynamic calibration

Table F-2: Sediment transport calibration

Table F-1: Hydrodynamic calibration

		Bathymetry				Hydrodynamics					
		Depth				Survey		Model		Devaition	
Date	Survey Point	Survey	Model	Difference (m)	Deviation (%)	Velocity	Direction	Velocity	Direction	Velocity (%)	Direction (deg)
2011/03/17 10:37:18 AM	4	5.09	5.44	0.35	7	0.34	160	0.25	148	28	12
2011/03/17 11:11:33 AM	5	11.17	7.04	4.13	37	0.24	164	0.28	157	17	7
2011/03/17 11:37:10 AM	6	9.38	7.38	2.00	21	0.21	160	0.31	160	48	0
2011/03/17 12:03:14 PM	7	6.63	7.51	0.88	13	0.25	155	0.33	165	32	10
2011/03/17 04:11:14 PM	12	3.23	7.27	4.04	125	0.48	-22	0.23	3	52	25
2011/03/17 04:47:49 PM	11	4.03	6.28	2.25	56	0.50	325	0.59	332	19	7
2011/03/17 05:13:32 PM	10	3.58	6.42	2.84	79	0.62	348	0.48	324	22	25
2011/03/17 05:28:05 PM	9	4.06	5.40	1.34	33	0.36	319	0.43	322	19	3
2011/03/17 05:44:12 PM	8	6.24	3.06	3.18	51	0.32	326	0.31	318	4	8
2011/03/17 05:56:50 PM	7	6.37	6.91	0.54	8	0.35	350	0.31	345	12	5
2011/03/17 06:08:49 PM	6	9.27	6.81	2.46	27	0.25	274	0.39	350	57	75
2011/03/17 06:20:23 PM	5	10.8	6.59	4.21	39	0.22	290	0.46	344	107	55
2011/03/17 06:33:55 PM	4	4.94	5.13	0.19	4	0.11	399	0.39	332	257	67
2011/03/18 10:53:59 AM	13	2.94	8.09	5.15	175	0.09	259	0.45	189	396	70
2011/03/18 11:14:16 AM	14	13.41	8.93	4.48	33	0.71	166	0.39	180	44	14
2011/03/18 11:47:42 AM	15	15.12	3.86	11.26	74	0.52	160	0.10	195	81	35
2011/03/18 12:13:21 PM	21	7.62	6.07	1.55	20	0.53	152	0.75	148	41	4
2011/03/18 12:32:18 PM	22	10.17	7.16	3.01	30	0.16	149	0.81	151	409	3
2011/03/18 12:47:56 PM	23	10.19	4.27	5.92	58	0.67	172	0.42	150	38	22
2011/03/18 03:58:52 PM	13	5.18	8.96	3.78	73	0.54	26	0.25	85	53	59
2011/03/18 04:29:28 PM	14	12.25	9.65	2.60	21	0.65	343	0.27	11	58	28
2011/03/18 04:50:02 PM	15	11.44	4.16	7.28	64	0.55	349	0.17	195	70	155
2011/03/18 05:25:04 PM	21	7.97	6.09	1.88	24	0.04	327	0.77	350	1829	23
2011/03/18 05:50:09 PM	22	10.14	6.84	3.30	33	0.04	328	0.74	343	1741	15
2011/03/18 06:17:12 PM	17	7.62	3.68	3.94	52	0.00	25	0.63	44	#DIV/0!	19
2011/03/18 06:38:52 PM	18	3.79	6.61	2.82	74	0.05	14	0.71	16	1324	2
2011/03/19 06:45:30 AM	27	8.68	6.64	2.04	24	0.35	356	0.52	501	49	144
2011/03/19 07:15:37 AM	29	3.42	4.97	1.55	45	0.36	345	0.58	357	60	12
2011/03/19 07:33:32 AM	31	4.62	6.51	1.89	41	0.85	359	0.72	287	15	73
2011/03/19 10:52:56 AM	17	8.26	3.44	4.82	58	0.36	215	0.31	205	13	10
2011/03/19 11:07:02 AM	18	6.09	6.49	0.40	7	0.44	208	0.44	196	1	12
2011/03/19 11:27:30 AM	27	8.98	6.58	2.40	27	0.52	178	0.52	181	0	3
2011/03/19 11:42:08 AM	29	3.65	3.65	0.00	0	0.31	180	0.36	179	16	1
2011/03/19 11:56:31 AM	31	5.14	6.72	1.58	31	0.59	181	0.61	179	4	2

Table F-2: Sediment transport calibration

		Bathymetry	Hydrodynamics		Sediment Transport											
			Devaition			Relative Density 2.5		Relative Density 2.55		Relative Density 2.57		Relative Density 2.6		Relative Density 2.65	
						Engelund and Hansen		Engelund and Hansen		Engelund and Hansen		Engelund and Hansen		Engelund and Hansen	
Date	Survey Point	Deviation (%)	Velocity (%)	Direction (deg)	Survey	Value	Devition (%)	Value	Devition (%)	Value	Devition (%)	Value	Devition (%)	Value	Devition (%)
2011/03/17 10:37:18 AM	4	7	28	12	4.8E-07	4.5E-07	6	4.2E-07	13	4.1E-07	15	4.0E-07	17	0.0E+00	100
2011/03/17 11:11:33 AM	5	37	17	7											
2011/03/17 11:37:10 AM	6	21	48	0											
2011/03/17 12:03:14 PM	7	13	32	10											
2011/03/17 04:11:14 PM	12	125	52	25	3.2E-07	3.4E-07	7	7.4E-07	31	7.2E-07	27	6.9E-07	23	2.7E-07	17
2011/03/17 04:47:49 PM	11	56	19	7	8.7E-07	5.6E-05	6283	2.1E-05	2559	8.0E-06	922	7.7E-06	884	2.1E-06	140
2011/03/17 05:13:32 PM	10	79	22	25	7.8E-07	4.8E-06	521	5.2E-05	5878	5.1E-05	5727	4.9E-05	5510	1.8E-05	2246
2011/03/17 05:28:05 PM	9	33	19	3											
2011/03/17 05:44:12 PM	8	51	4	8	5.6E-07	7.8E-07	40	3.2E-07	1	3.1E-07	2	3.0E-07	6	2.2E-09	100
2011/03/17 05:56:50 PM	7	8	12	5											
2011/03/17 06:08:49 PM	6	27	57	75											
2011/03/17 06:20:23 PM	5	39	107	55											
2011/03/17 06:33:55 PM	4	4	257	67											
2011/03/18 10:53:59 AM	13	175	396	70											
2011/03/18 11:14:16 AM	14	33	44	14											
2011/03/18 11:47:42 AM	15	74	81	35											
2011/03/18 12:13:21 PM	21	20	41	4											
2011/03/18 12:32:18 PM	22	30	409	3											
2011/03/18 12:47:56 PM	23	58	38	22	1.7E-06	1.9E-06	7	1.9E-06	4	1.8E-06	2	1.8E-06	2	1.1E-06	36
2011/03/18 03:58:52 PM	13	73	53	59											
2011/03/18 04:29:28 PM	14	21	58	332	1.8E-06	2.0E-06	11	1.2E-06	21	1.2E-06	23	1.2E-06	26	5.5E-08	97
2011/03/18 04:50:02 PM	15	64	70	155	1.6E-06	1.3E-06	16	5.3E-05	1509313	5.1E-05	1471102	4.9E-05	1416449	6.2E-10	100
2011/03/18 05:25:04 PM	21	24	1829	23											
2011/03/18 05:50:09 PM	22	33	1741	15											
2011/03/18 06:17:12 PM	17	52	#DIV/0!	19	3.5E-09	5.6E-05	1611618	2.2E-06	115	2.2E-06	110	2.1E-06	102	7.6E-06	216958
2011/03/18 06:38:52 PM	18	74	1324	2	7.0E-08	7.8E-05	110795	7.3E-05	103756	7.1E-05	101126	6.8E-05	97366	1.4E-05	19722
2011/03/19 06:45:30 AM	27	24	49	144	1.3E-06	2.7E-05	1963	1.5E-06	12	1.5E-06	14	1.4E-06	17	1.3E-06	3
2011/03/19 07:15:37 AM	29	45	60	12	4.0E-07	1.3E-05	3166	2.5E-05	1832	2.5E-05	1783	2.4E-05	1713	4.0E-06	913
2011/03/19 07:33:32 AM	31	41	15	73	1.4E-06	1.3E-06	6	1.4E-05	989	1.3E-05	962	1.3E-05	922	1.0E-06	27
2011/03/19 10:52:56 AM	17	58	13	10	1.0E-06	4.0E-06	284	1.2E-05	2959	1.2E-05	2881	1.1E-05	2771	3.0E-07	71
2011/03/19 11:07:02 AM	18	7	1	12											
2011/03/19 11:27:30 AM	27	27	0	3	1.3E-06	1.5E-05	1063	1.2E-06	12	1.2E-06	15	3.5E-06	151	1.3E-06	7
2011/03/19 11:42:08 AM	29	0	16	1											
2011/03/19 11:56:31 AM	31	31	4	2											

Appendix G MEASURED SEDIMENT TRANSPORT PARAMETERS

Table G-2: Sediment laboratory analysis results

Sample area	d50	d16	d84	σ	Wet density				Relative Wet Density	Dry density				Relative Dry Density	Porosity	Monster mass
					Proctor	Deurlatenheid1	Deurlatenheid2	Average		Proctor	Deurlatenheid1	Deurlatenheid2	Average			
Back	0.456	0.240	1.022	2.062	2025	1937	2010	1991	1.942	1754	1660	1725	1713	1.671	2.05E-09	534
Middle	0.297	0.181	0.581	1.794	2025	1937	2010	1991	1.942	1754	1660	1725	1713	1.671	2.05E-09	284
Bed Sample	0.293	0.137	0.544	1.997	2025	1937	2010	1991	1.942	1754	1660	1725	1713	1.671	2.05E-09	816
***Front*[1]**	0.393	0.196	0.592	1.736	2025	1754	2010	1929	1.882	1660	1660	1725	1681	1.640	2.05E-09	341
Front	0.393	0.196	0.592	1.736	2025	1937	2010	1991	1.942	1754	1660	1725	1713	1.671	2.05E-09	341
	0.355	**0.181**	**0.687**	**1.940**	2025	1937	2357	**2106**	1.942	1754	1660	1725	**1713**	1.671	**2.05E-09**	**1975**
					2106				**2.055**	**1713**				**1.671**		

[1] An additional laboratory result for the northern (front) section were provided, indicating a deviation from the expected values and the survey for an identical sample. It is assumed that there has been an error during the analysis and were therefore excluded from the investigation.

Appendix H INVESTIGATED SCENARIO RESULTS

APPENDIX H.1 TIDAL FORCING EXCLUDING WIND CONDITIONS

LIST OF FIGURERS

Figure H.1-1: Section S1 during tidal forcing excluding wind
Figure H.1-2: Section S2 during tidal forcing excluding wind
Figure H.1-3: Section S3 during tidal forcing excluding wind
Figure H.1-4: Section S4 during tidal forcing excluding wind
Figure H.1-5: Section S5 during tidal forcing excluding wind
Figure H.1-6: Section S6 during tidal forcing excluding wind
Figure H.1-7: Section L1 during tidal forcing excluding wind
Figure H.1-8: Section L2 during tidal forcing excluding wind
Figure H.1-9: Section L3 during tidal forcing excluding wind
Figure H.1-10: Section L4 during tidal forcing excluding wind
Figure H.1-11: Section L5 during tidal forcing excluding wind
Figure H.1-12: Section L6 during tidal forcing excluding wind
Figure H.1-13: Section L7 during tidal forcing excluding wind
Figure H.1-14: Section L8 during tidal forcing excluding wind
Figure H.1-15: Section L9 during tidal forcing excluding wind
Figure H.1-16: Section L10 during tidal forcing excluding wind

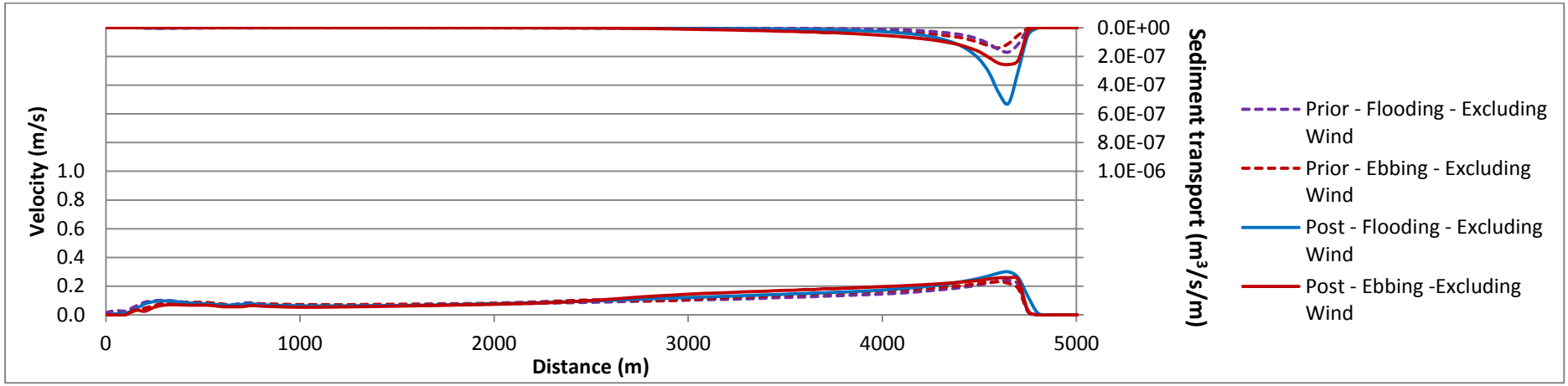

Figure H.1-1: Section S1 during tidal forcing excluding wind

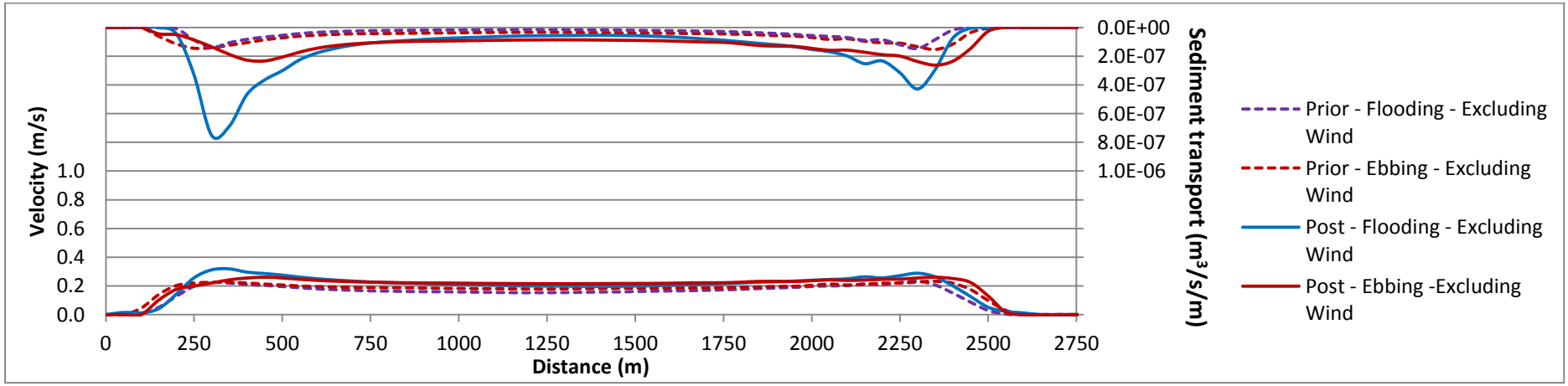

Figure H.1-2: Section S2 during tidal forcing excluding wind

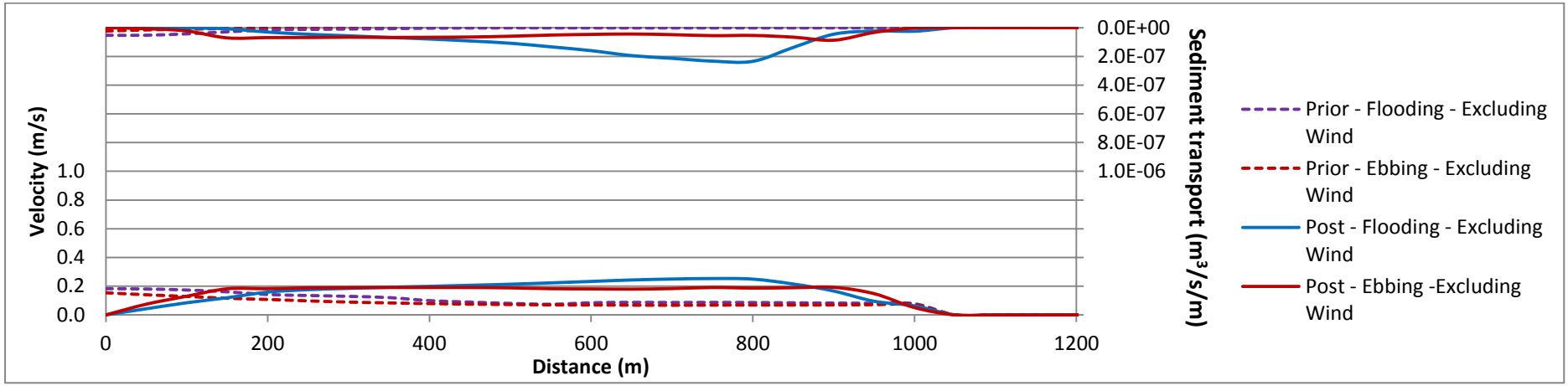

Figure H.1-3: Section S3 during tidal forcing excluding wind

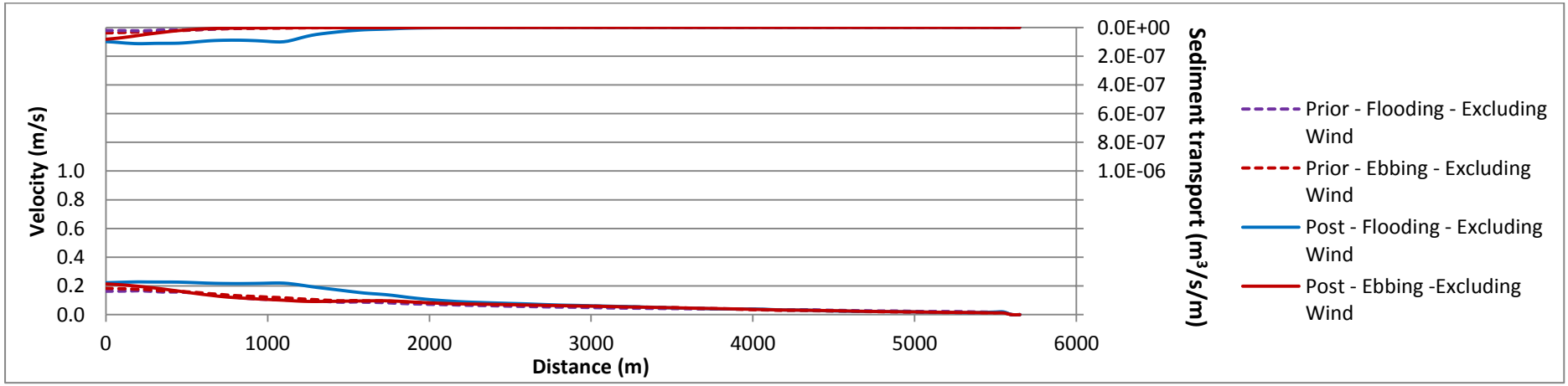

Figure H.1-4: Section S4 during tidal forcing excluding wind

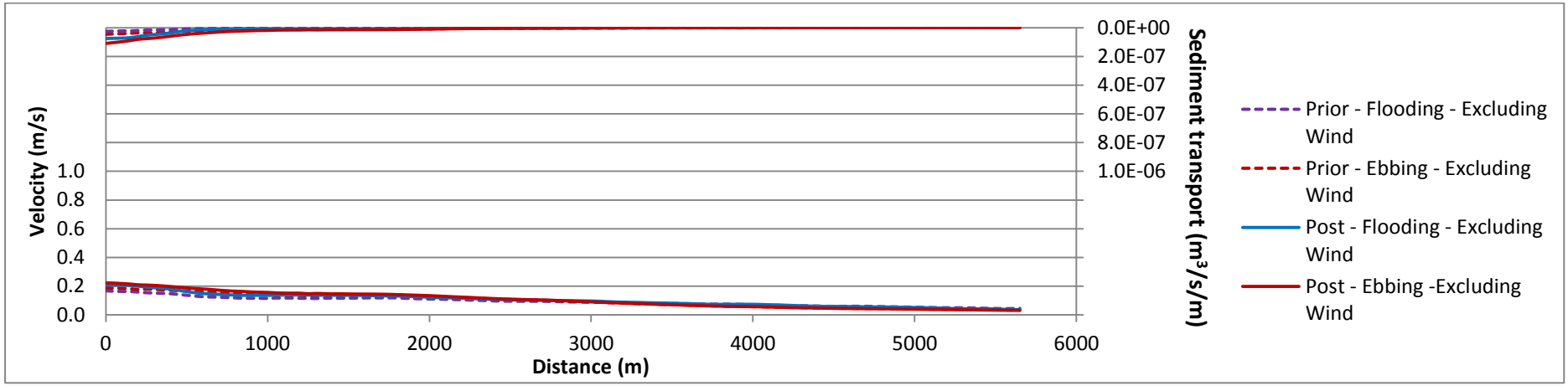

Figure H.1-5: Section S5 during tidal forcing excluding wind

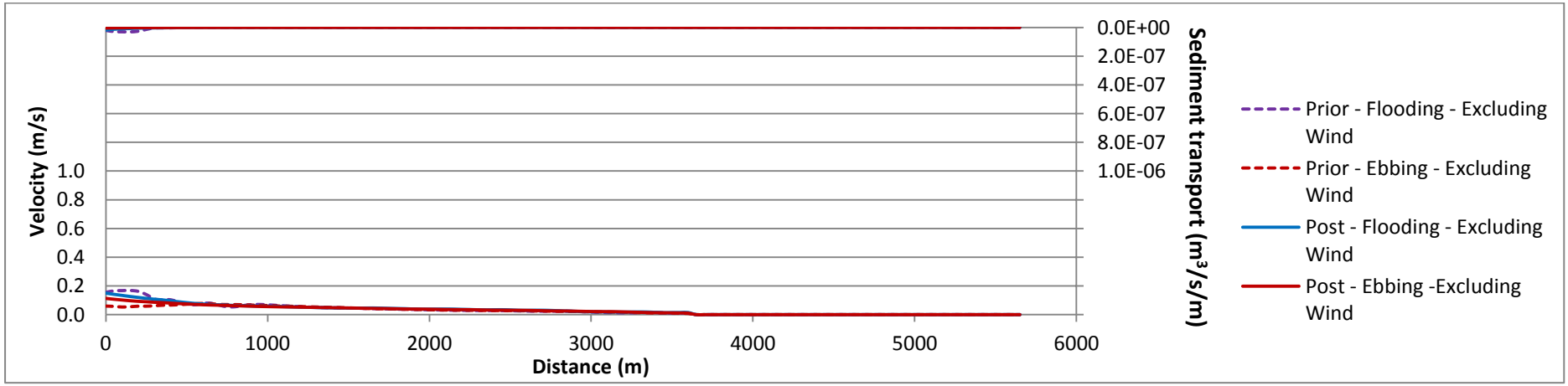

Figure H.1-6: Section S6 during tidal forcing excluding wind

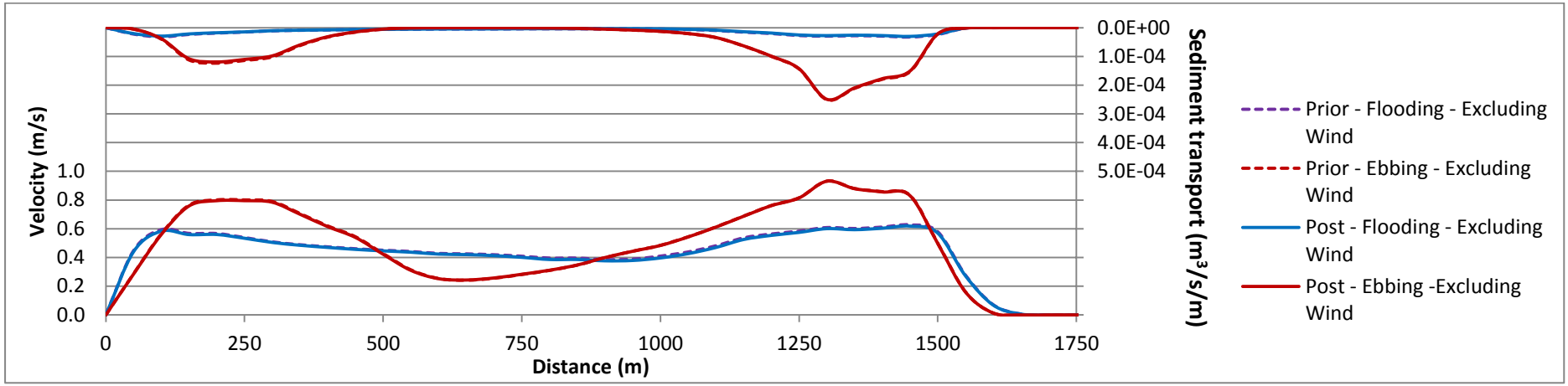

Figure H.1-7: Section L1 during tidal forcing excluding wind

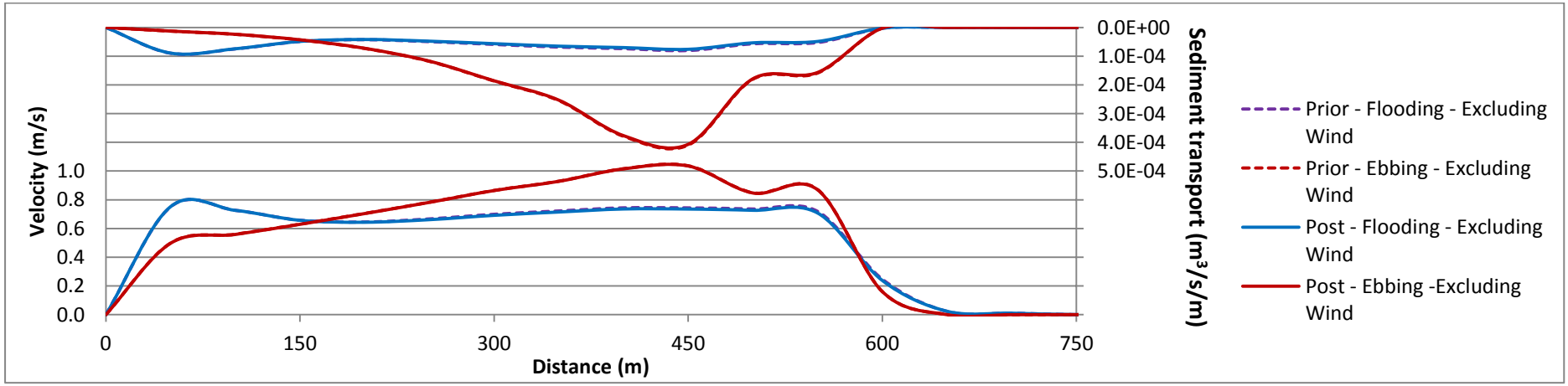

Figure H.1-8: Section L2 during tidal forcing excluding wind

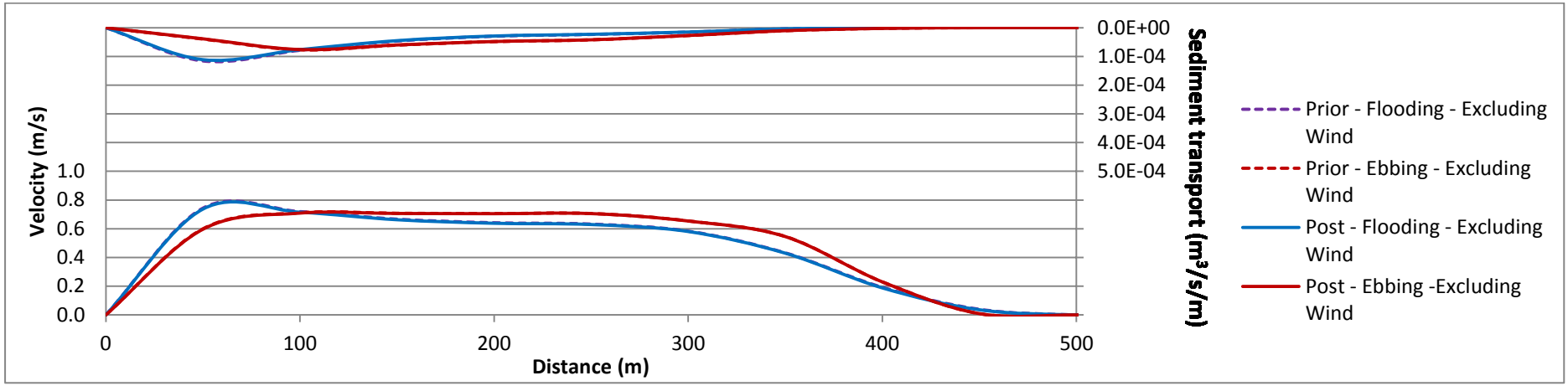

Figure H.1-9: Section L3 during tidal forcing excluding wind

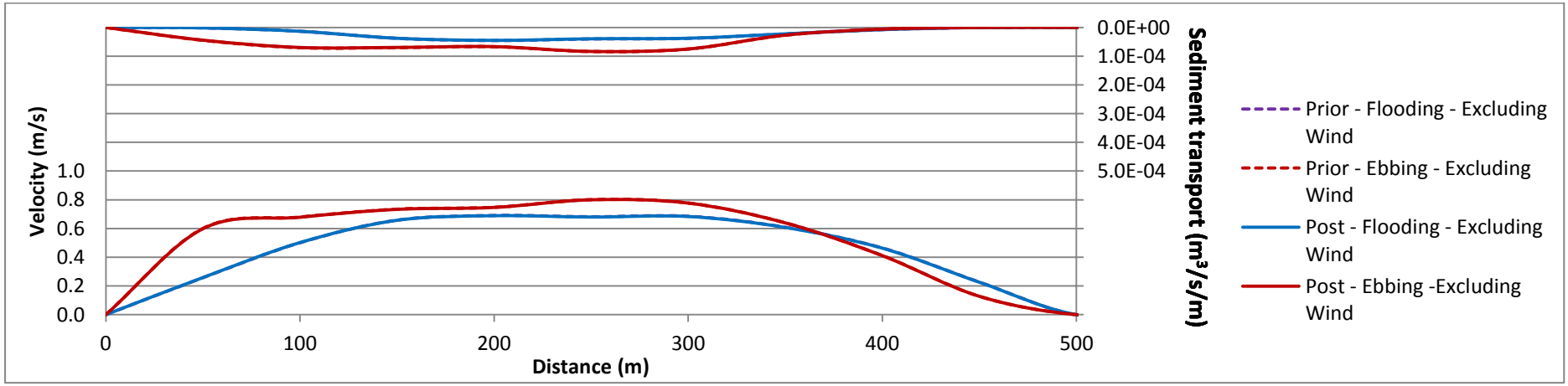

Figure H.1-10: Section L4 during tidal forcing excluding wind

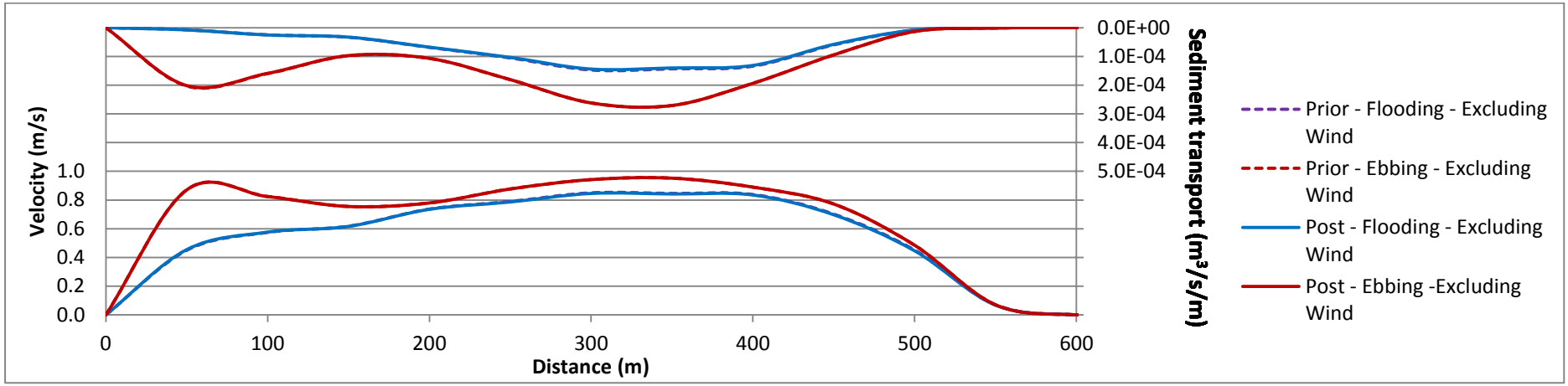

Figure H.1-11: Section L5 during tidal forcing excluding wind

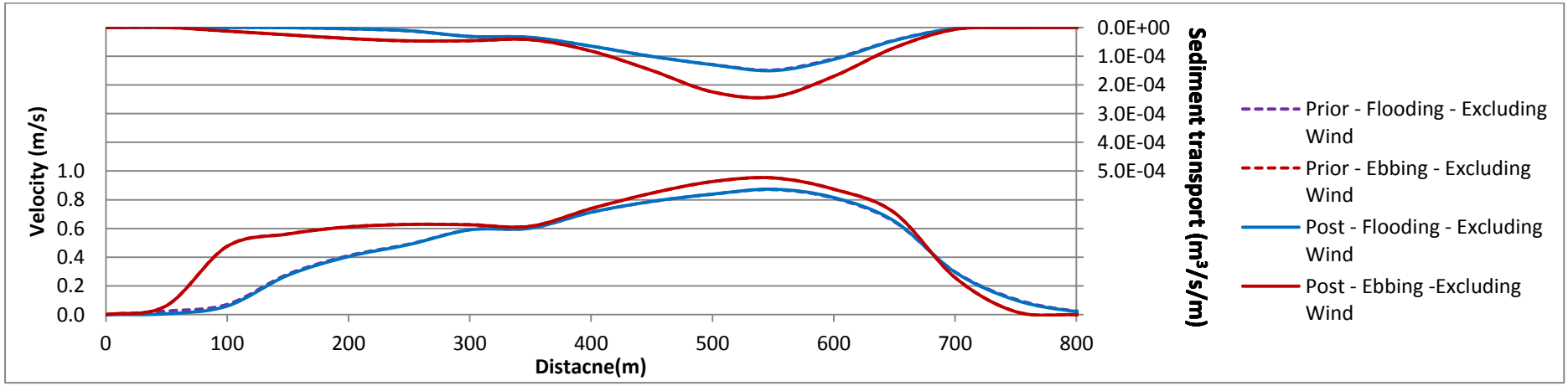

Figure H.1-12: Section L6 during tidal forcing excluding wind

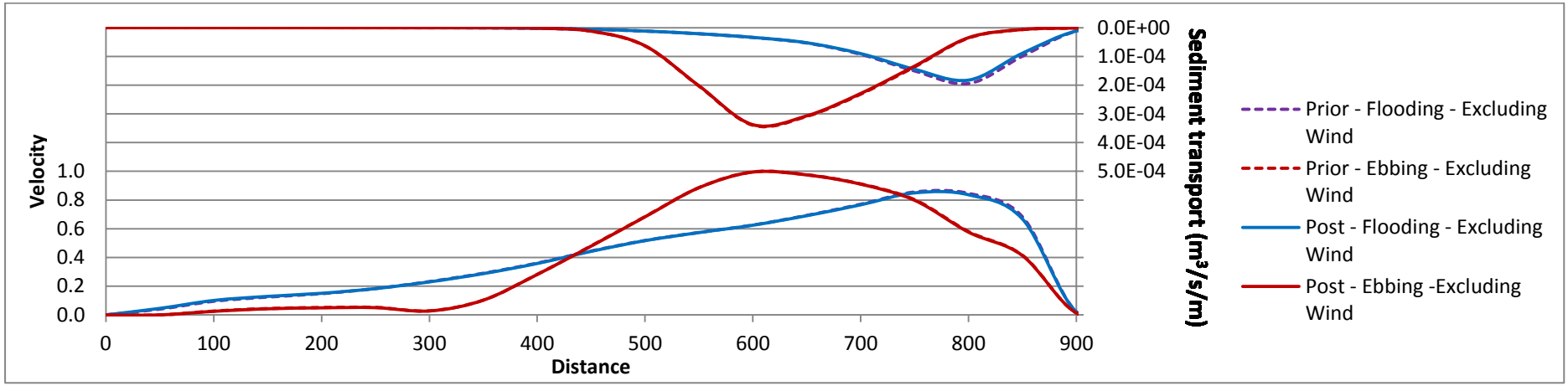

Figure H.1-13: Section L7 during tidal forcing excluding wind

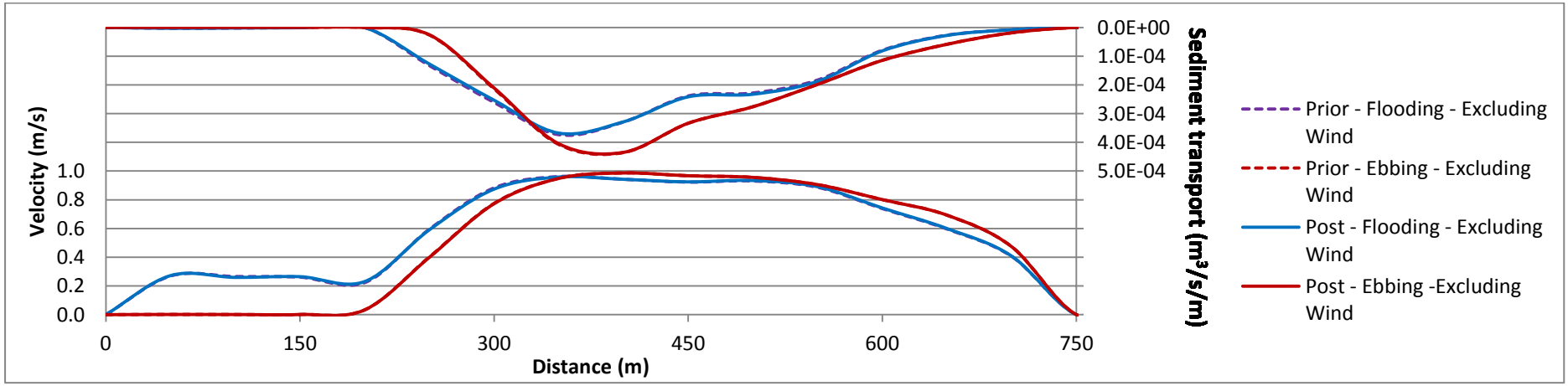

Figure H.1-14: Section L8 during tidal forcing excluding wind

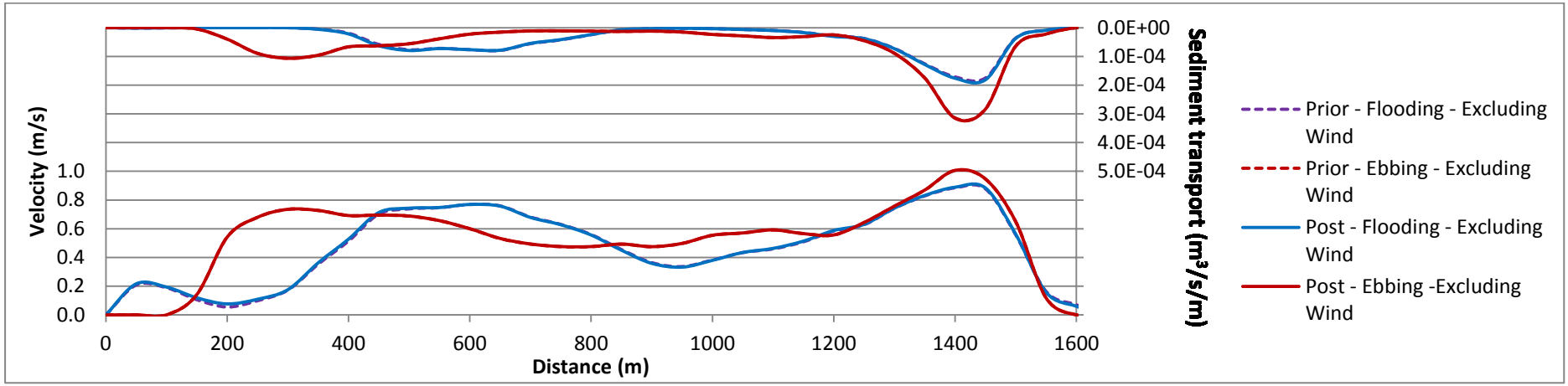

Figure H.1-15: Section L9 during tidal forcing excluding wind

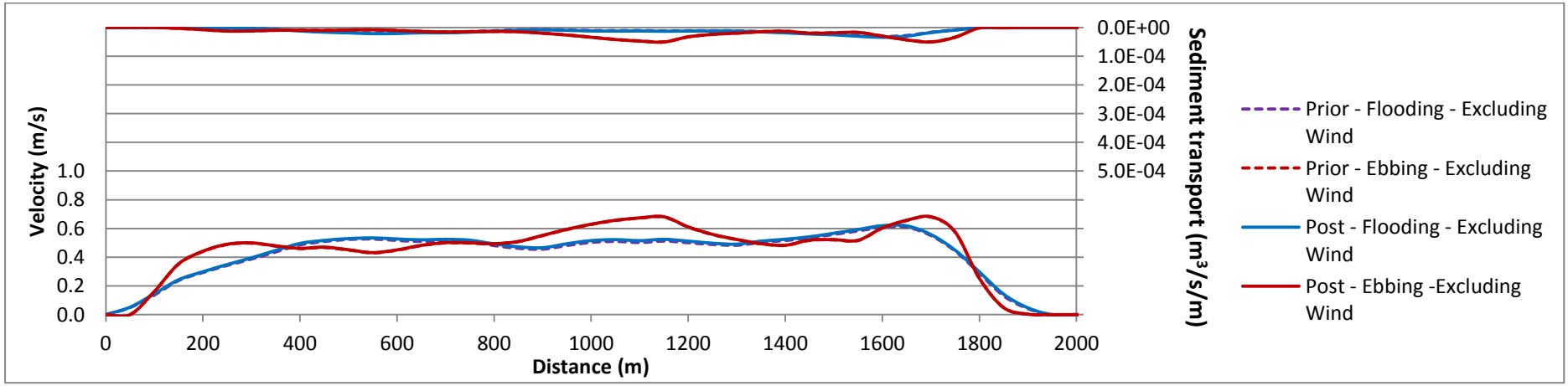

Figure H.1-16: Section L10 during tidal forcing excluding wind

APPENDIX H.2 TIDAL CONDITIONS INCLUDING 1 IN 50 YEAR WIND EVENT FROM THE NORTH

LIST OF FIGURERS

Figure H.2-1: Section S1 after the construction including a 1 in 50 year northern wind
Figure H.2-2: Section S1 prior to construction including 1 in 50 year northern wind
Figure H.2-3: Section S2 after the construction including a 1 in 50 year northern wind
Figure H.2-4: Section S2 prior to construction including a 1 in 50 year northern wind
Figure H.2-5: Section S3 after the construction including a 1 in 50 year northern wind
Figure H.2-6: Section S3 prior to construction including a 1 in 50 year northern wind
Figure H.2-7: Section S4 after the construction including a 1 in 50 year northern wind
Figure H.2-8: Section S4 prior to construction including a 1 in 50 year northern wind
Figure H.2-9: Section S5 after the construction including a 1 in 50 year northern wind
Figure H.2-10: Section S5 prior to construction including a 1 in 50 year northern wind
Figure H.2-11: Section S6 after the construction including a 1 in 50 year northern wind
Figure H.2-12: Section S6 prior to construction including a 1 in 50 year northern wind
Figure H.2-13: Section L1 after the construction including a 1 in 50 year northern wind
Figure H.2-14: Section L1 prior to construction including a 1 in 50 year northern wind
Figure H.2-15: Section L2 after the construction including a 1 in 50 year northern wind
Figure H.2-16: Section L2 prior to construction including a 1 in 50 year northern wind
Figure H.2-17: Section L3 after the construction including a 1 in 50 year northern wind

Figure H.2-18: Section L3 prior to construction including a 1 in 50 year northern wind
Figure H.2-19: Section L4 after the construction including a 1 in 50 year northern wind
Figure H.2-20: Section L4 prior to construction including a 1 in 50 year northern wind
Figure H.2-21: Section L5 after the construction including a 1 in 50 year northern wind
Figure H.2-22: Section L5 prior to construction including a 1 in 50 year northern wind
Figure H.2-23: Section L6 after the construction including a 1 in 50 year northern wind
Figure H.2-24: Section L6 prior to construction including a 1 in 50 year northern wind
Figure H.2-25: Section L7 after the construction including a 1 in 50 year northern wind
Figure H.2-26: Section L7 prior to construction including a 1 in 50 year northern wind
Figure H.2-27: Section L8 after the construction including a 1 in 50 year northern wind
Figure H.2-28: Section L8 prior to construction including a 1 in 50 year northern wind
Figure H.2-29: Section L9 after the construction including a 1 in 50 year northern wind
Figure H.2-30: Section L9 prior to construction including a 1 in 50 year northern wind
Figure H.2-31: Section L10 after the construction including a 1 in 50 year northern wind
Figure H.2-32: Section L9 prior to construction including a 1 in 50 year northern wind

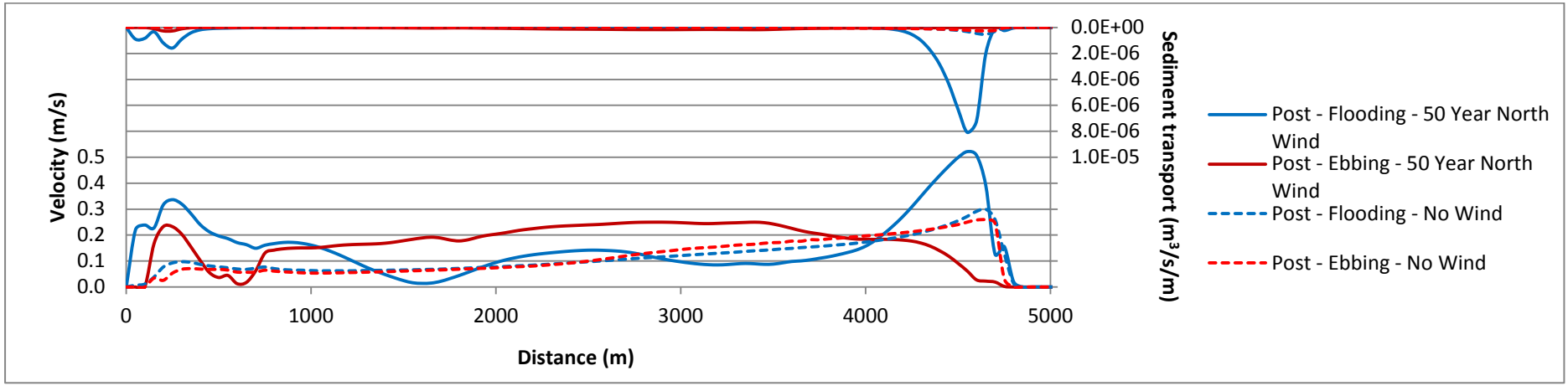

Figure H.2-1: Section S1 after the construction including a 1 in 50 year northern wind

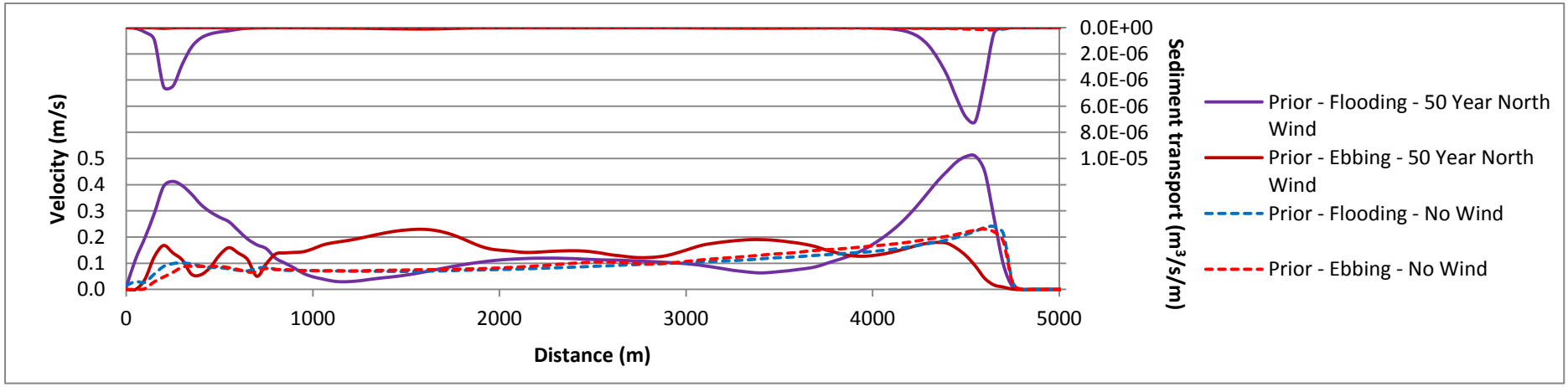

Figure H.2-2: Section S1 prior to construction including 1 in 50 year northern wind

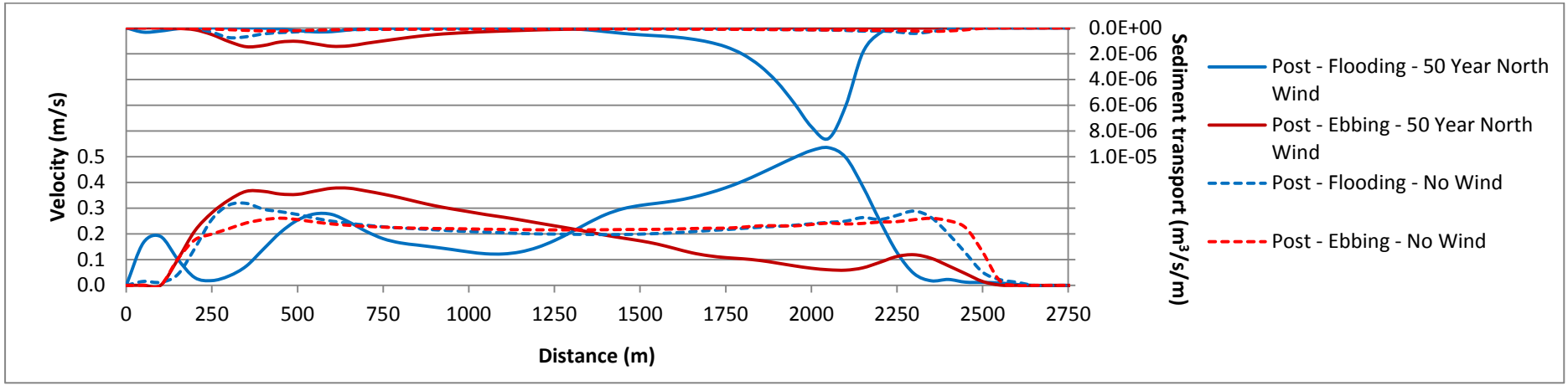

Figure H.2-3: Section S2 after the construction including a 1 in 50 year northern wind

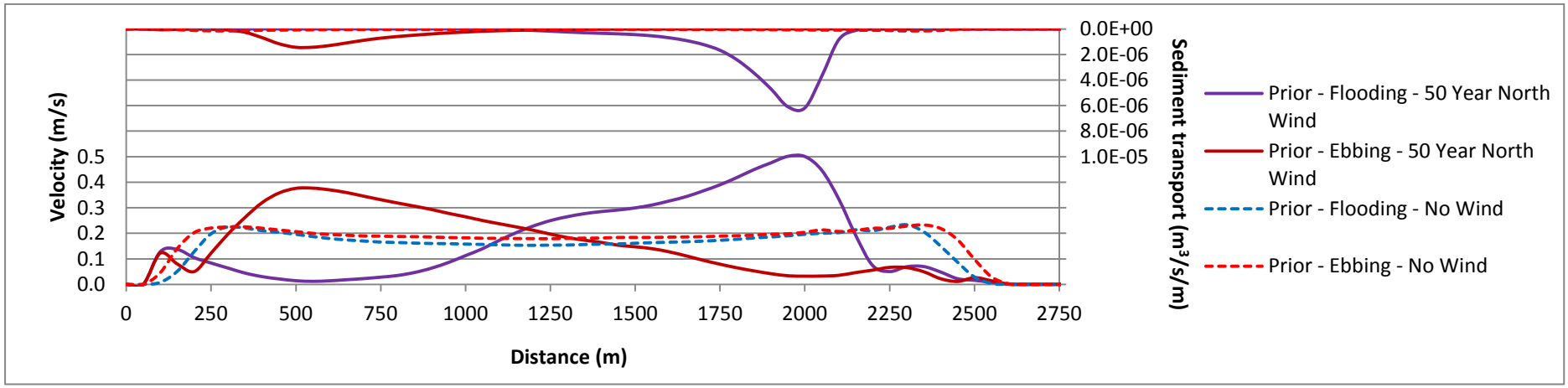

Figure H.2-4: Section S2 prior to construction including a 1 in 50 year northern wind

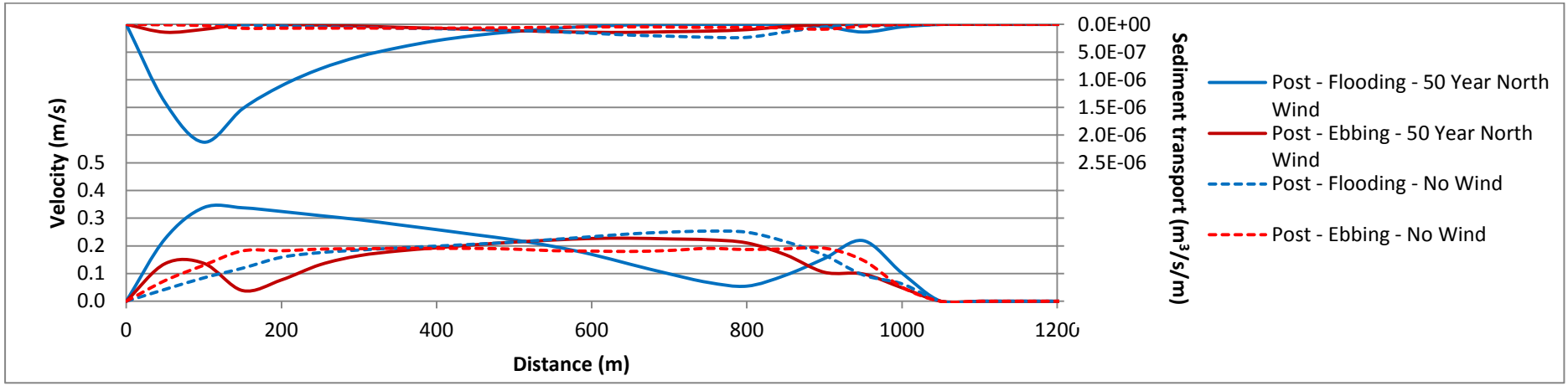

Figure H.2-5: Section S3 after the construction including a 1 in 50 year northern wind

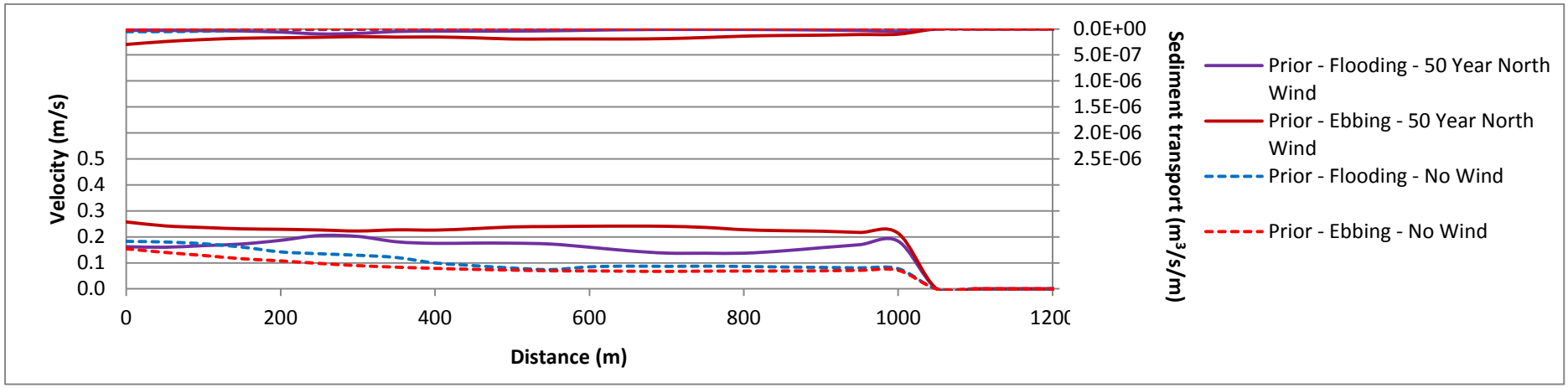

Figure H.2-6: Section S3 prior to construction including a 1 in 50 year northern wind

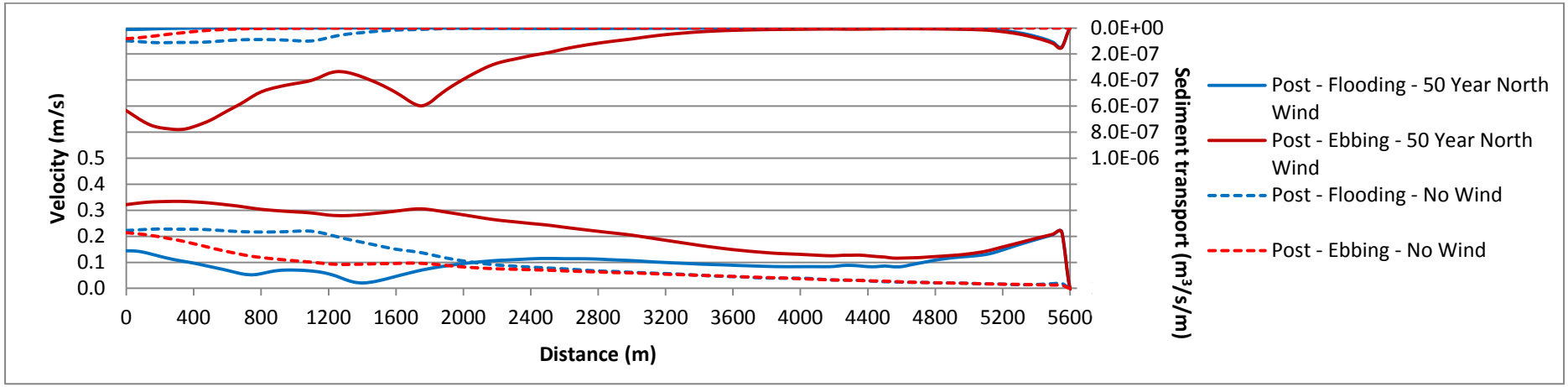

Figure H.2-7: Section S4 after the construction including a 1 in 50 year northern wind

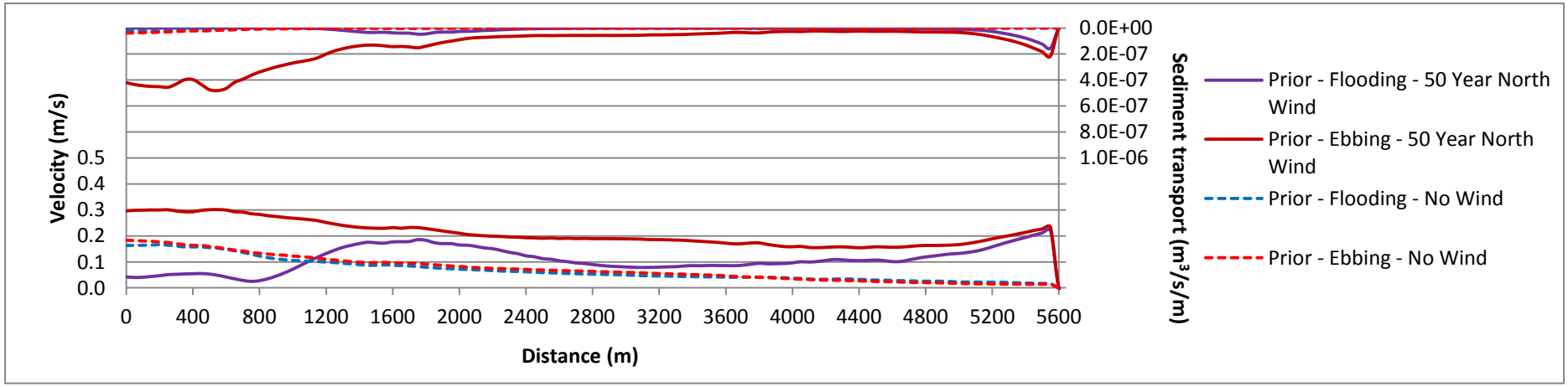

Figure H.2-8: Section S4 prior to construction including a 1 in 50 year northern wind

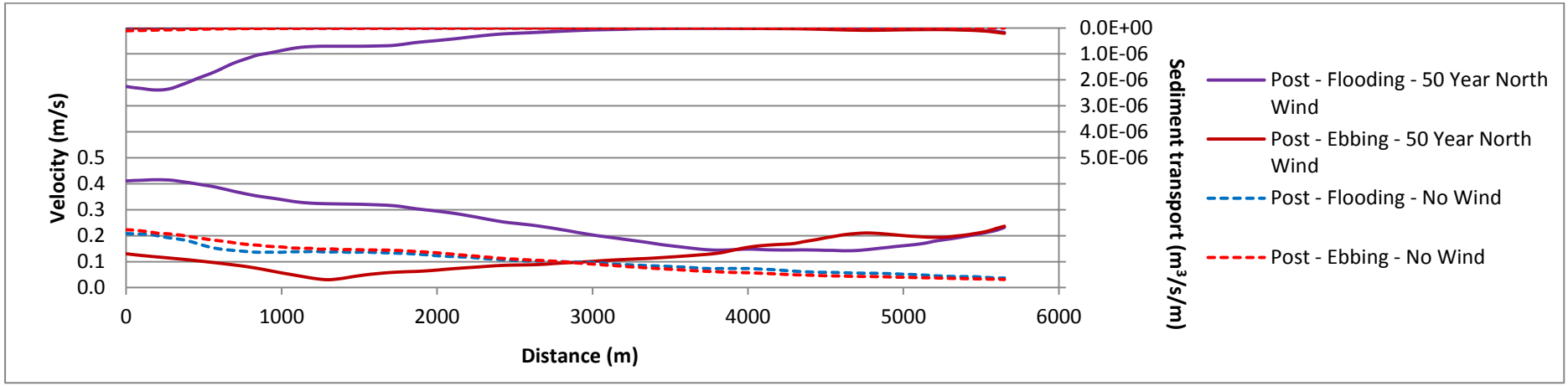

Figure H.2-9: Section S5 after the construction including a 1 in 50 year northern wind

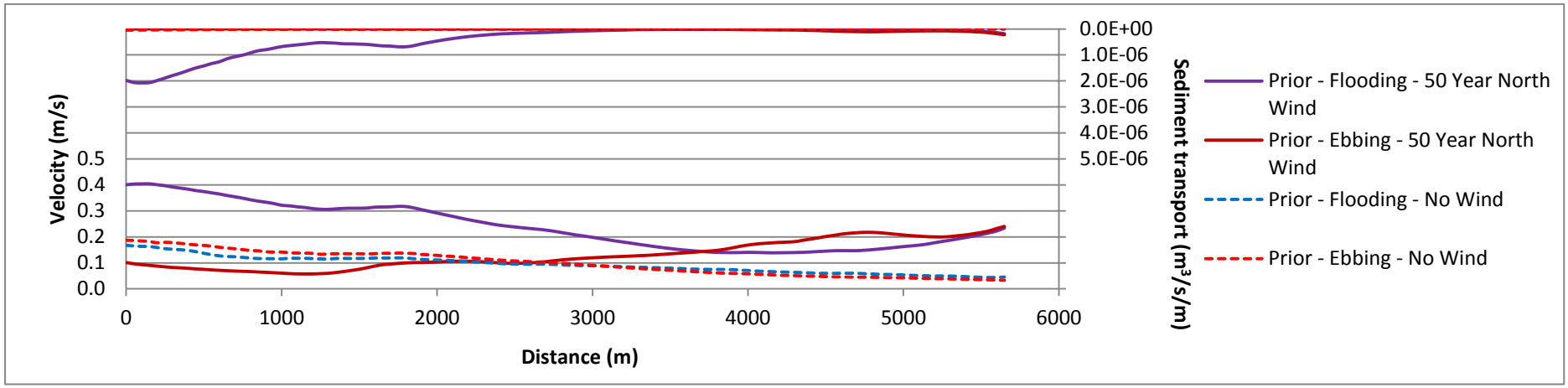

Figure H.2-10: Section S5 prior to construction including a 1 in 50 year northern wind

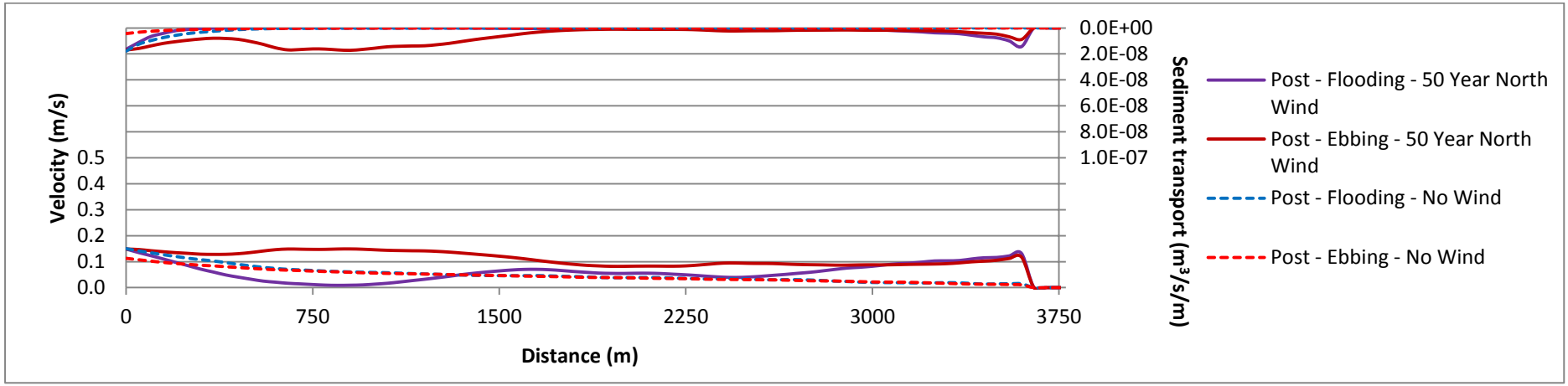

Figure H.2-11: Section S6 after the construction including a 1 in 50 year northern wind

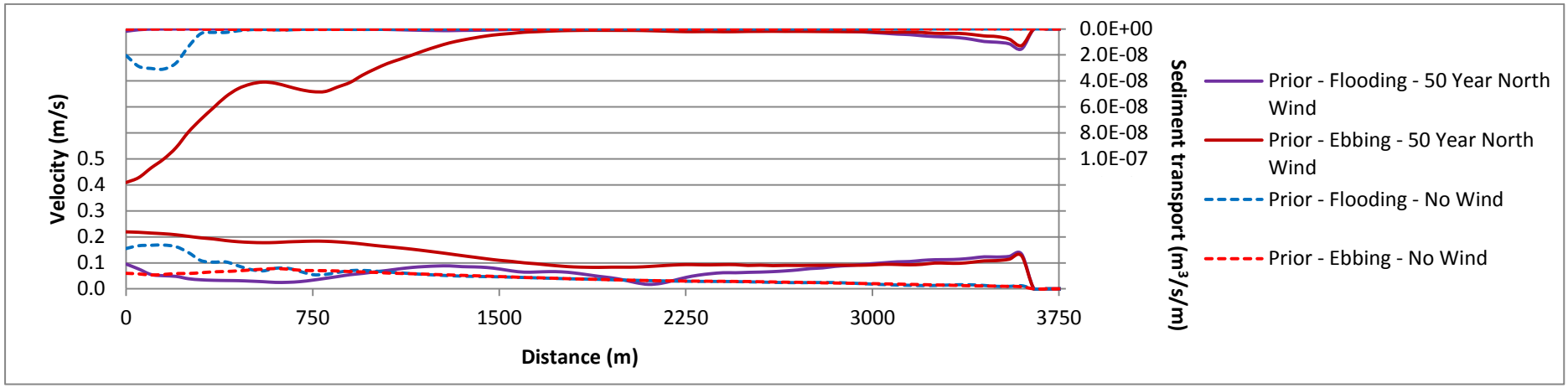

Figure H.2-12: Section S6 prior to construction including a 1 in 50 year northern wind

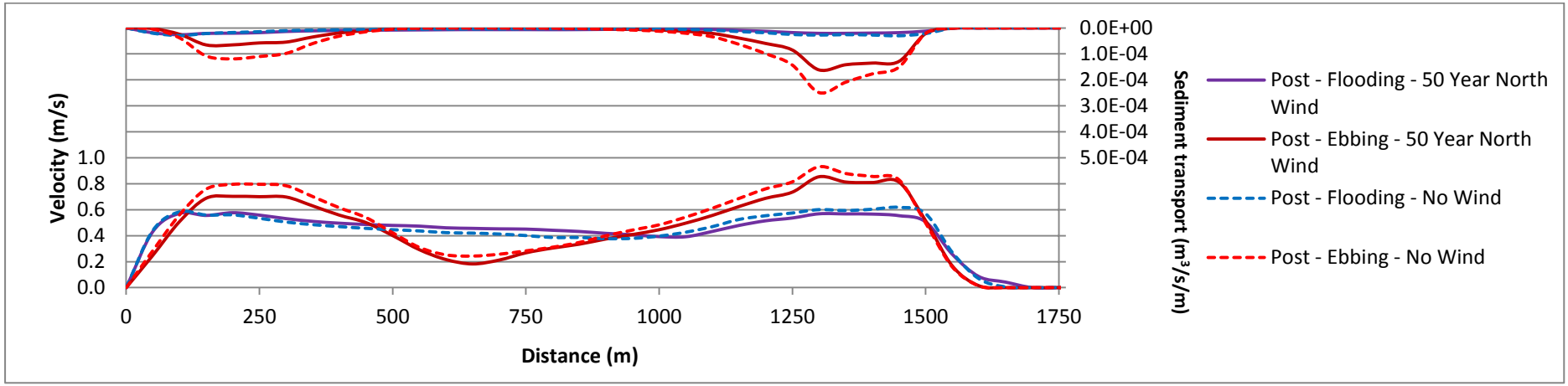

Figure H.2-13: Section L1 after the construction including a 1 in 50 year northern wind

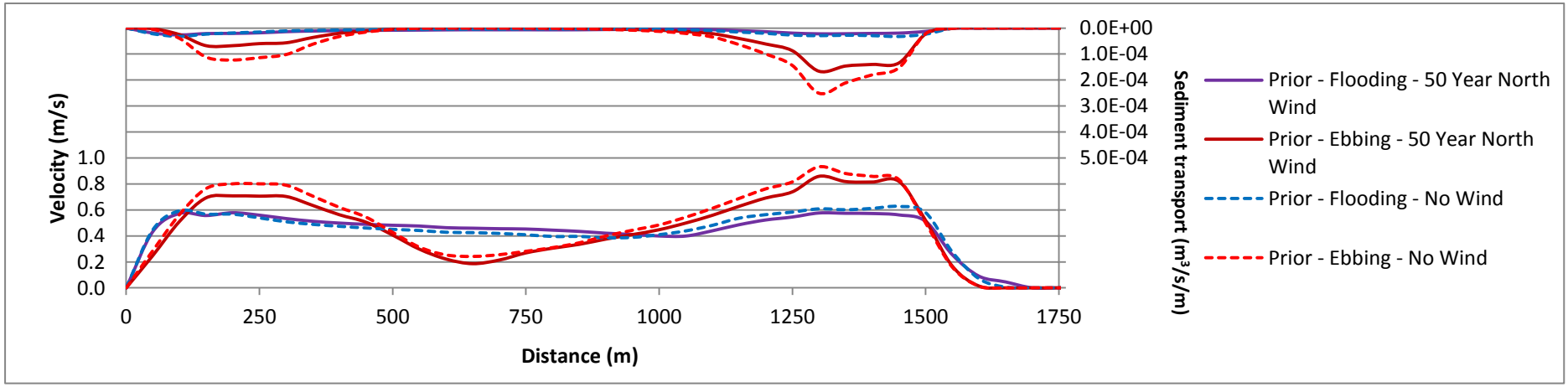

Figure H.2-14: Section L1 prior to construction including a 1 in 50 year northern wind

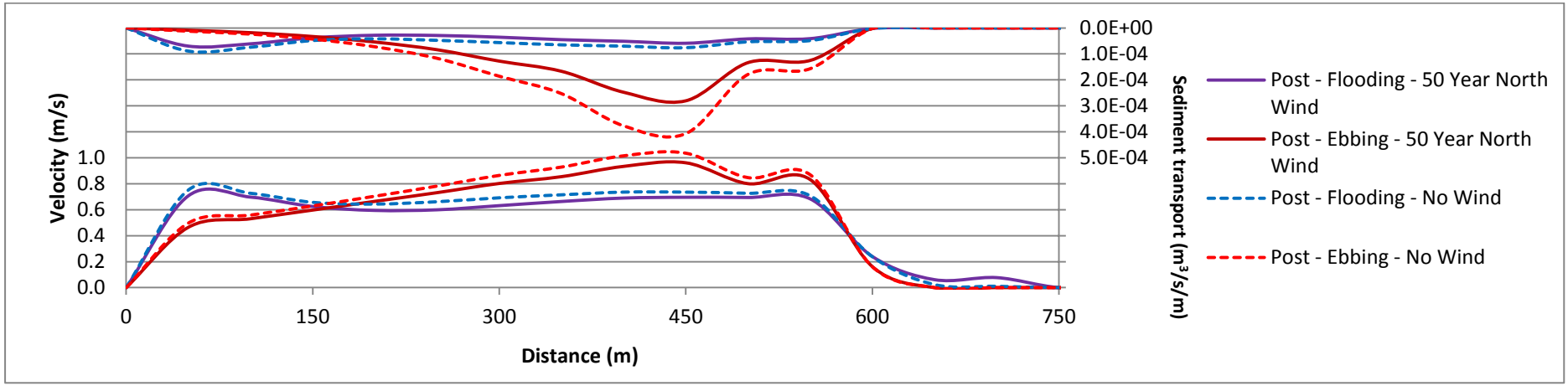

Figure H.2-15: Section L2 after the construction including a 1 in 50 year northern wind

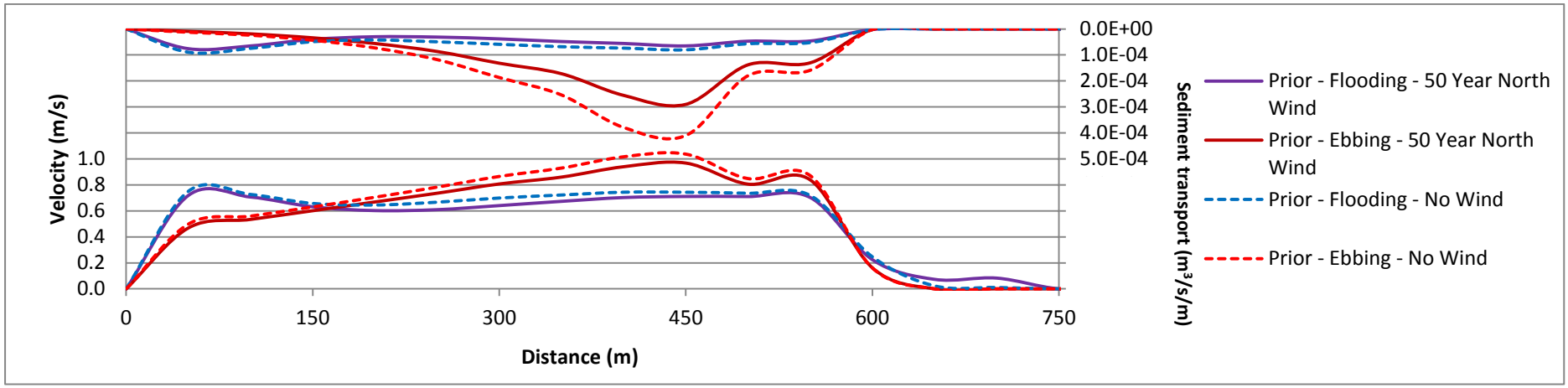

Figure H.2-16: Section L2 prior to construction including a 1 in 50 year northern wind

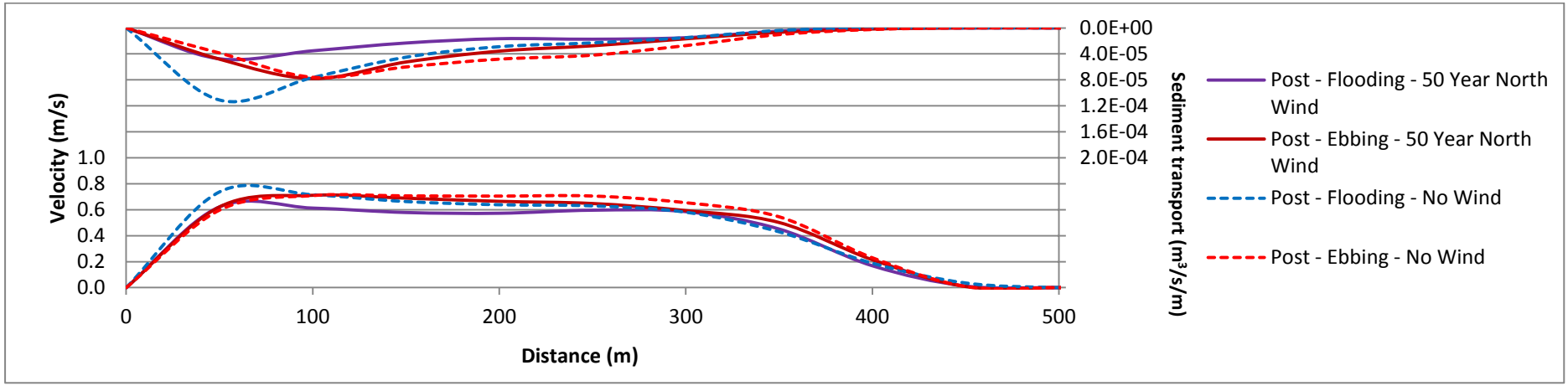

Figure H.2-17: Section L3 after the construction including a 1 in 50 year northern wind

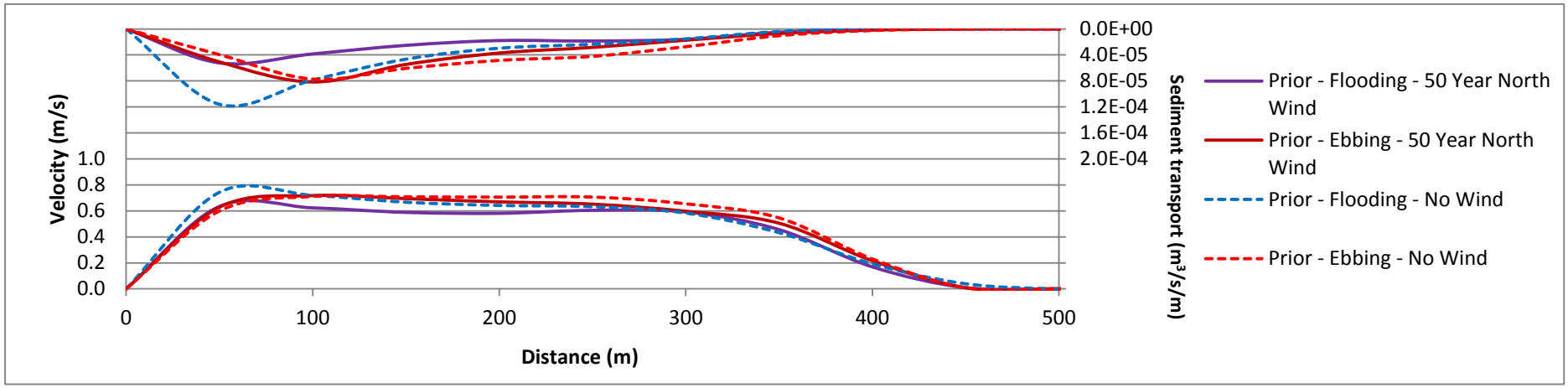

Figure H.2-18: Section L3 prior to construction including a 1 in 50 year northern wind

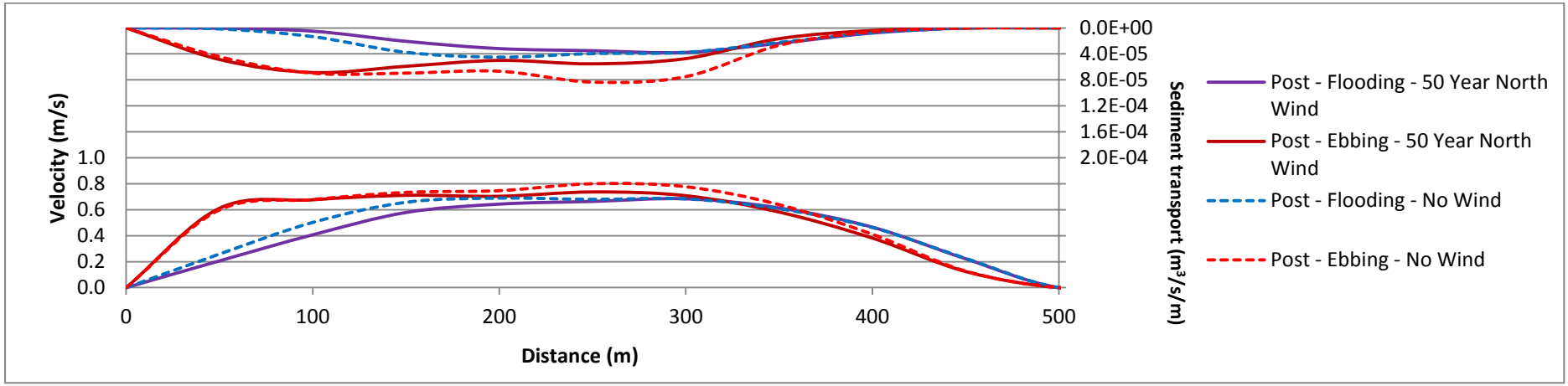

Figure H.2-19: Section L4 after the construction including a 1 in 50 year northern wind

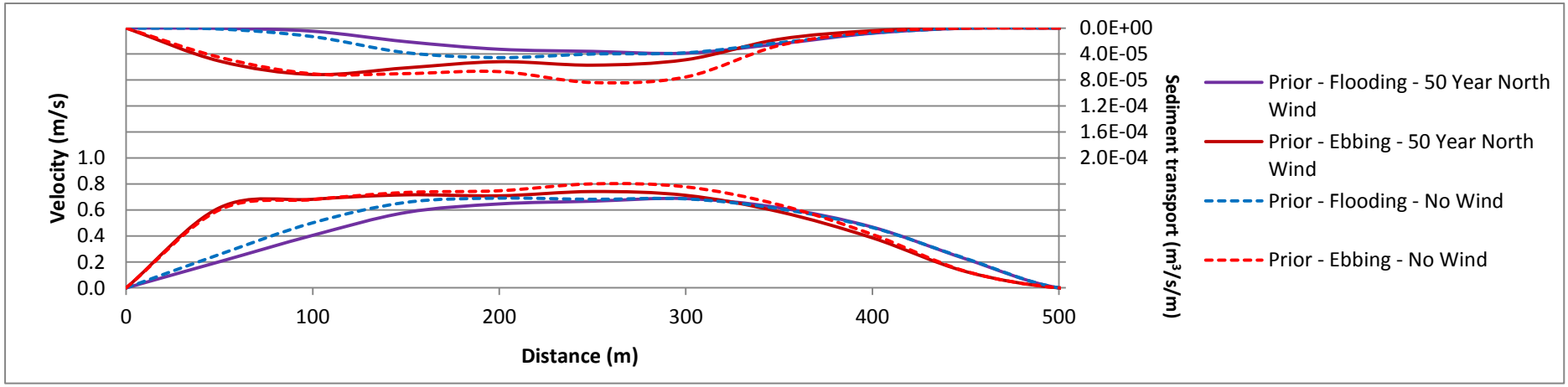

Figure H.2-20: Section L4 prior to construction including a 1 in 50 year northern wind

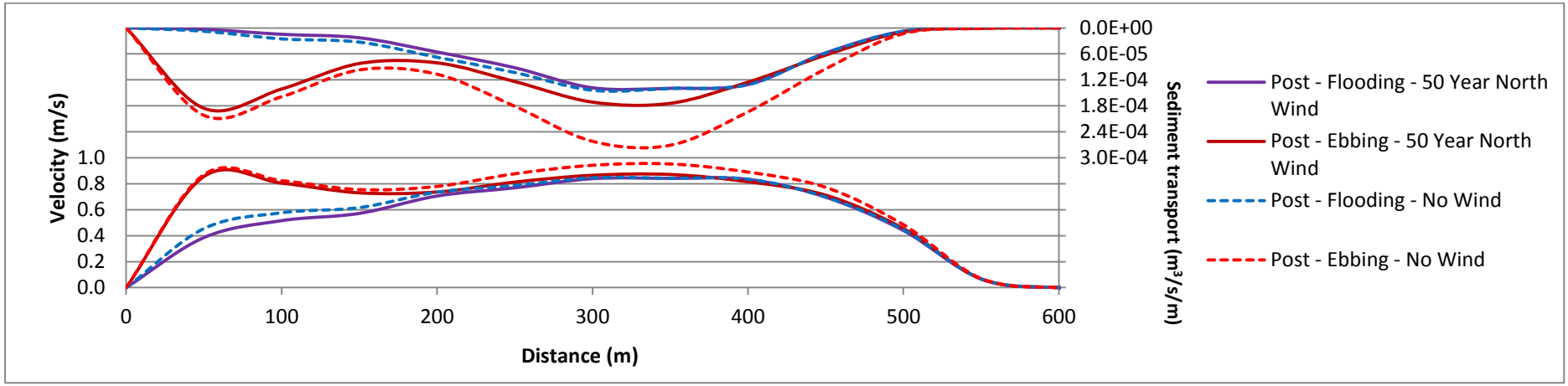

Figure H.2-21: Section L5 after the construction including a 1 in 50 year northern wind

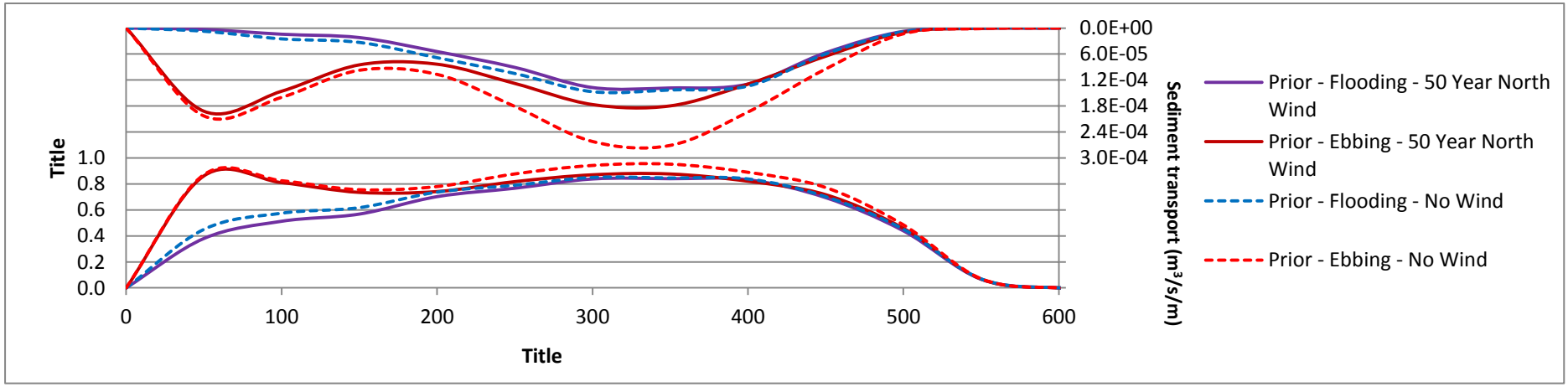

Figure H.2-22: Section L5 prior to construction including a 1 in 50 year northern wind

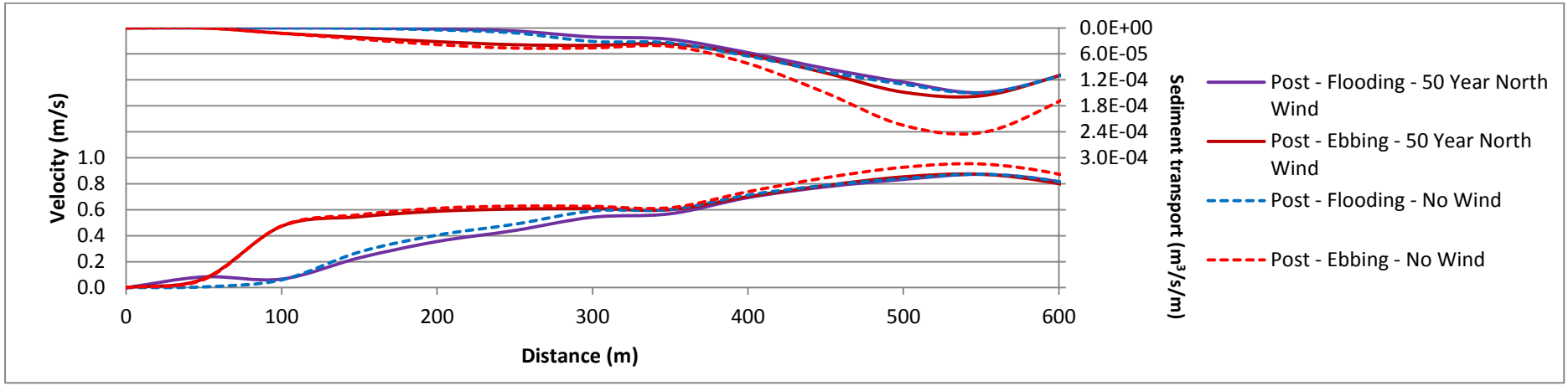

Figure H.2-23: Section L6 after the construction including a 1 in 50 year northern wind

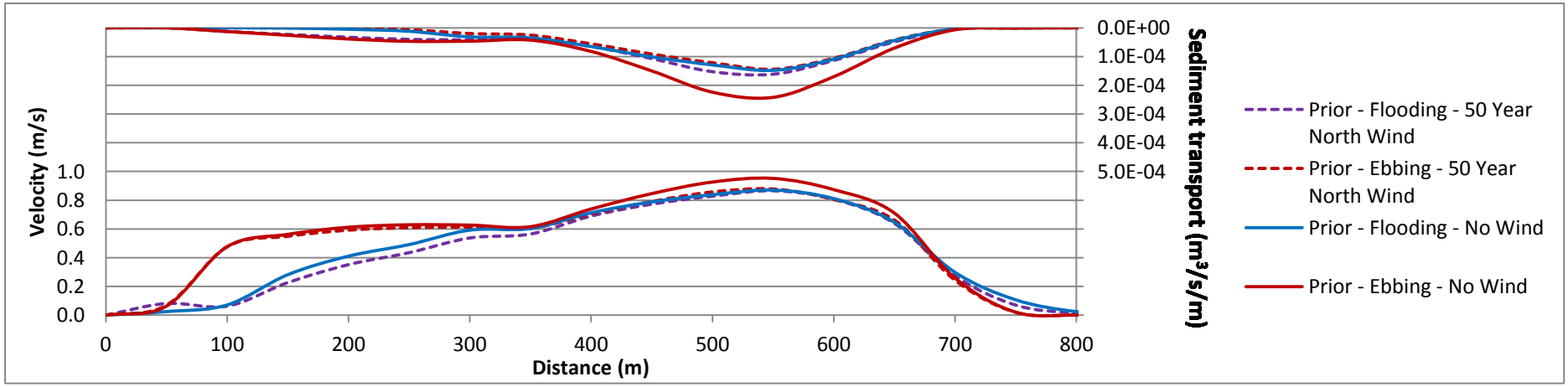

Figure H.2-24: Section L6 prior to construction including a 1 in 50 year northern wind

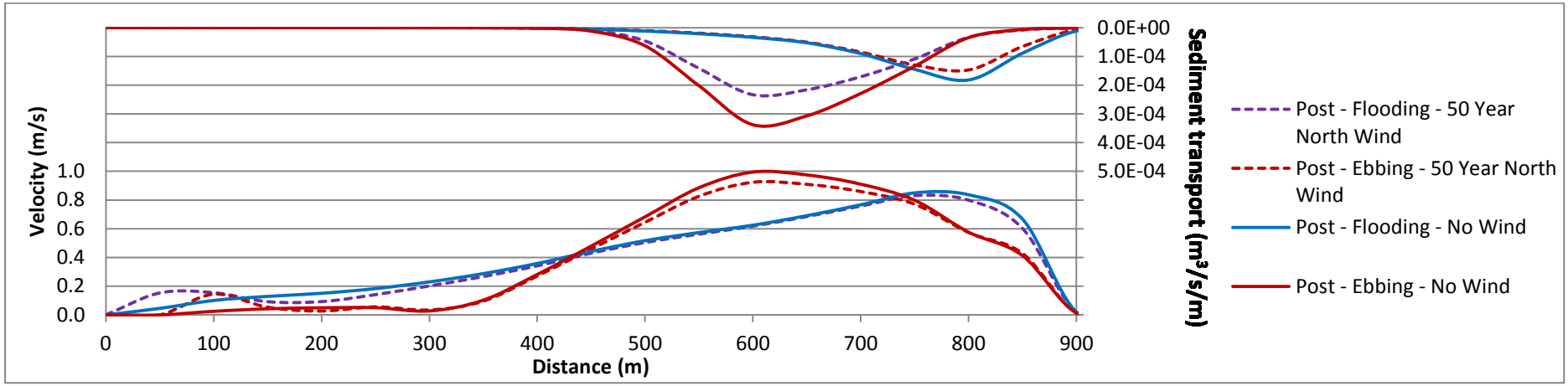

Figure H.2-25: Section L7 after the construction including a 1 in 50 year northern wind

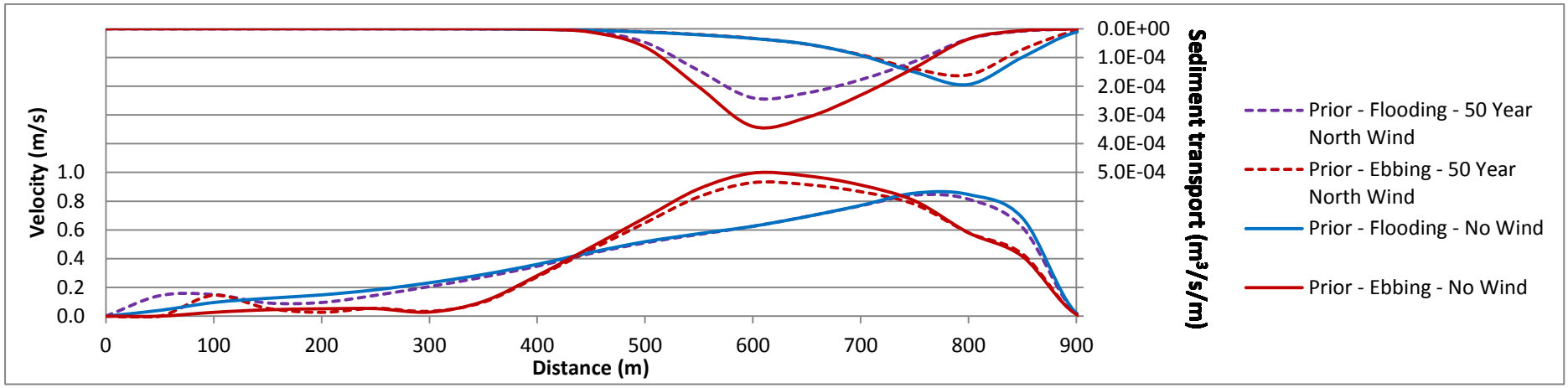

Figure H.2-26: Section L7 prior to construction including a 1 in 50 year northern wind

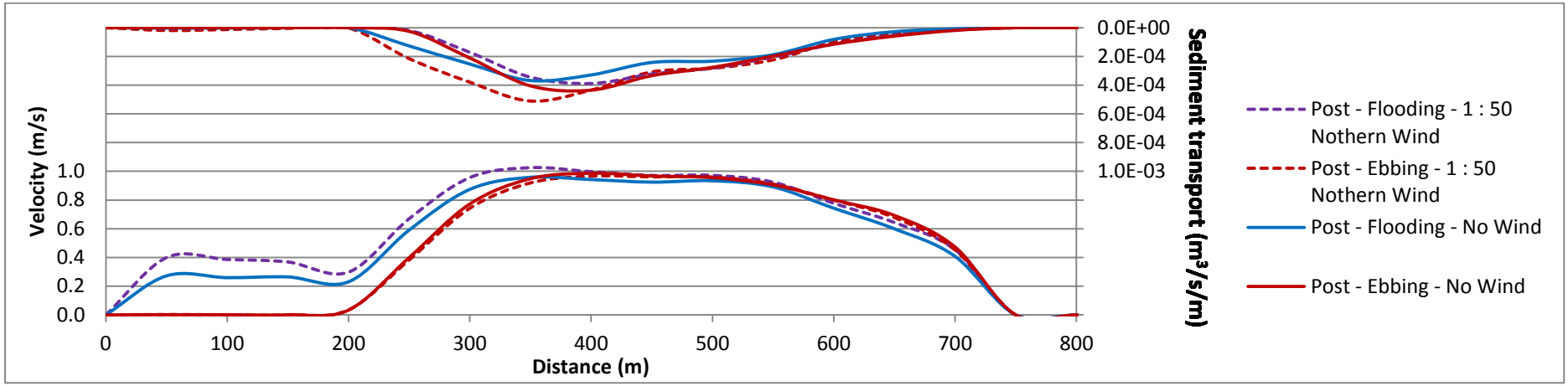

Figure H.2-27: Section L8 after the construction including a 1 in 50 year northern wind

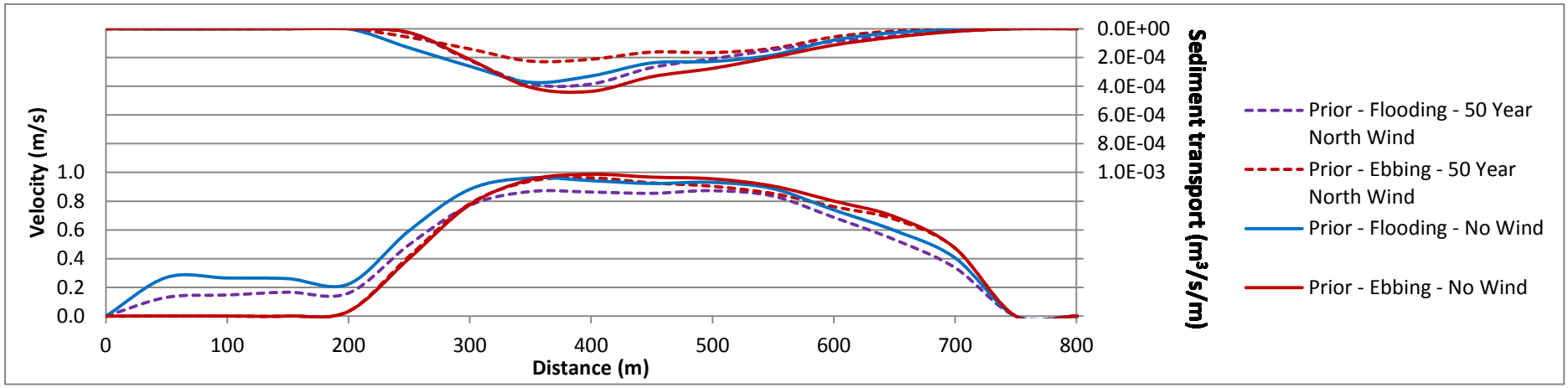

Figure H.2-28: Section L8 prior to construction including a 1 in 50 year northern wind

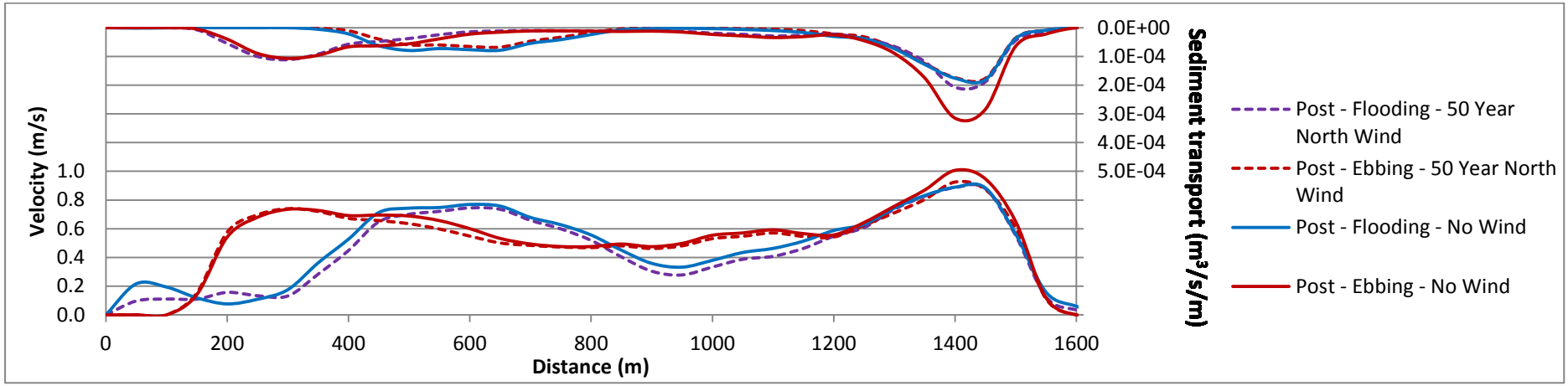

Figure H.2-29: Section L9 after the construction including a 1 in 50 year northern wind

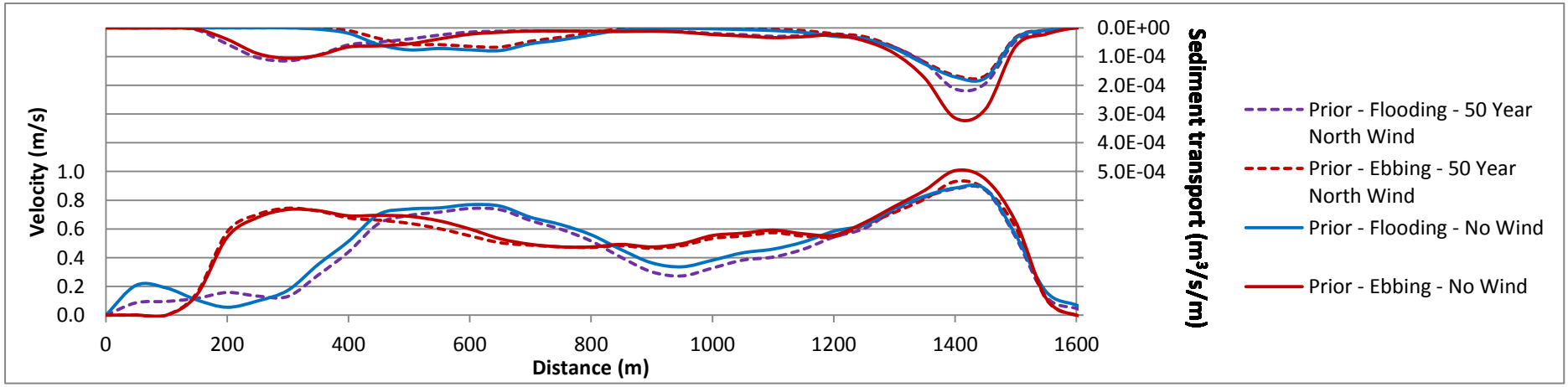

Figure H.2-30: Section L9 prior to construction including a 1 in 50 year northern wind

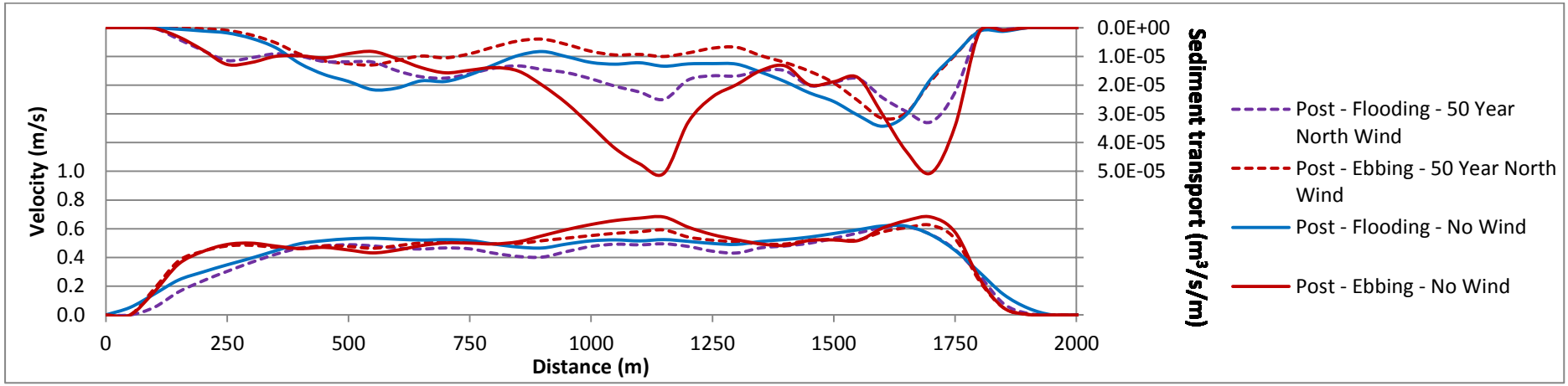

Figure H.2-31: Section L10 after the construction including a 1 in 50 year northern wind

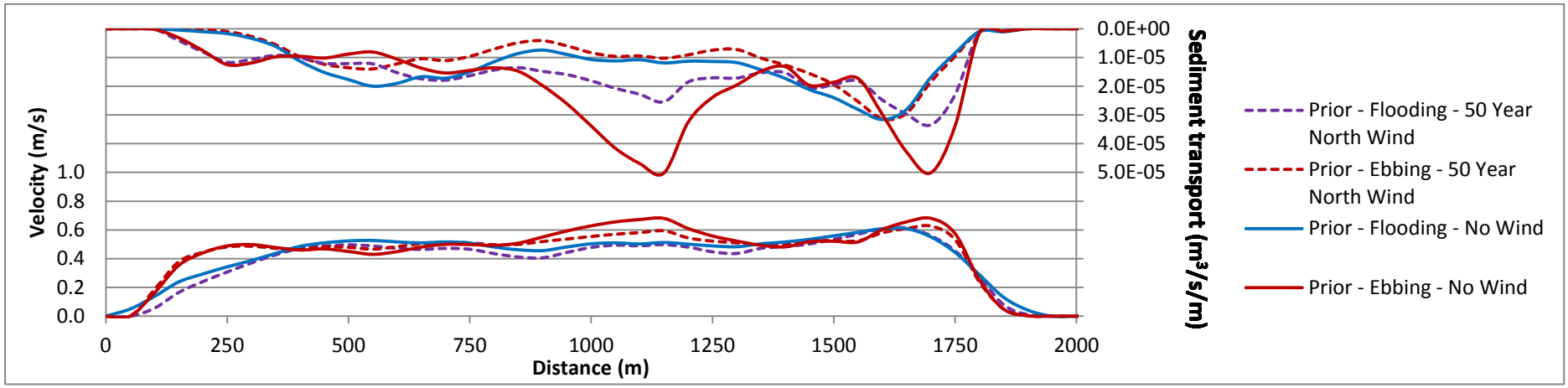

Figure H.2-32: Section L9 prior to construction including a 1 in 50 year northern wind

APPENDIX H.3 TIDAL CONDITIONS INCLUDING 1 IN 50 YEAR SOUTHERN WIND

LIST OF FIGURERS

Figure H.3-1: Section S1 after the construction including a 1 in 50 year southern wind
Figure H.3-2: Section S1 prior to construction including a 1 in 50 year southern wind
Figure H.3-3: Section S2 after the construction including a 1 in 50 year southern wind
Figure H.3-4: Section S2 prior to construction including a 1 in 50 year southern wind
Figure H.3-5: Section S3 after the construction including a 1 in 50 year southern wind
Figure H.3-6: Section S3 prior to construction including a 1 in 50 year southern wind
Figure H.3-7: Section S4 after the construction including a 1 in 50 year southern wind
Figure H.3-8: Section S4 prior to construction including a 1 in 50 year southern wind
Figure H.3-9: Section S5 after the construction including a 1 in 50 year southern wind
Figure H.3-10: Section S5 prior to construction including a 1 in 50 year southern wind
Figure H.3-11: Section S6 after the construction including a 1 in 50 year southern wind
Figure H.3-12: Section S6 prior to construction including a 1 in 50 year southern wind
Figure H.3-13: Section L1 after the construction including a 1 in 50 year southern wind
Figure H.3-14: Section L1 prior to construction including a 1 in 50 year southern wind
Figure H.3-15: Section L2 after the construction including a 1 in 50 year southern wind
Figure H.3-16: Section L2 prior to construction including a 1 in 50 year southern wind
Figure H.3-17: Section L3 after the construction including a 1 in 50 year southern wind

Figure H.3-18: Section L3 prior to construction including a 1 in 50 year southern wind
Figure H.3-19: Section L4 after the construction including a 1 in 50 year southern wind
Figure H.3-20: Section L4 prior to construction including a 1 in 50 year southern wind
Figure H.3-21: Section L5 after the construction including a 1 in 50 year southern wind
Figure H.3-22: Section L5 prior to construction including a 1 in 50 year southern wind
Figure H.3-23: Section L6 after the construction including a 1 in 50 year southern wind
Figure H.3-24: Section L6 prior to construction including a 1 in 50 year southern wind
Figure H.3-25: Section L7 after the construction including a 1 in 50 year southern wind
Figure H.3-26: Section L7 prior to construction including a 1 in 50 year southern wind
Figure H.3-27: Section L8 after the construction including a 1 in 50 year southern wind
Figure H.3-28: Section L8 prior to construction including a 1 in 50 year southern wind
Figure H.3-29: Section L9 after the construction including a 1 in 50 year southern wind
Figure H.3-30: Section L9 prior to construction including a 1 in 50 year southern wind
Figure H.3-31: Section L10 after the construction including a 1 in 50 year southern wind
Figure H.3-32: Section L10 prior to construction including a 1 in 50 year southern wind

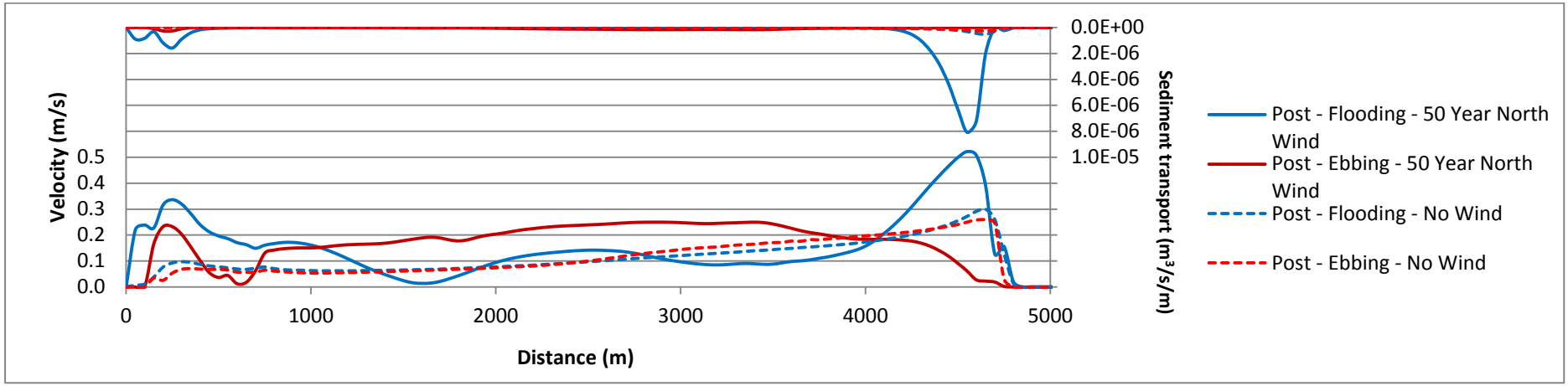

Figure H.3-1: Section S1 after the construction including a 1 in 50 year southern wind

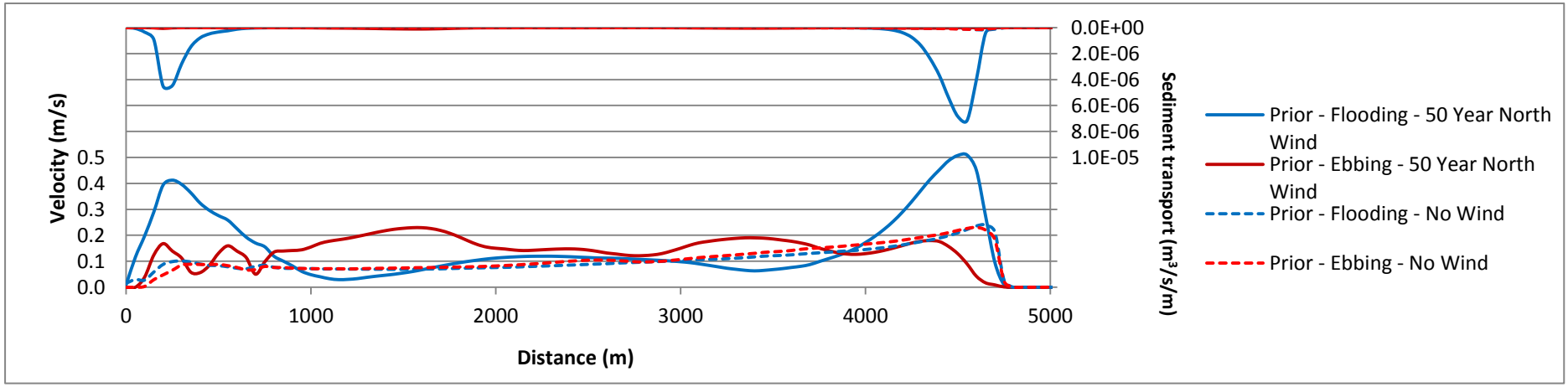

Figure H.3-2: Section S1 prior to construction including a 1 in 50 year southern wind

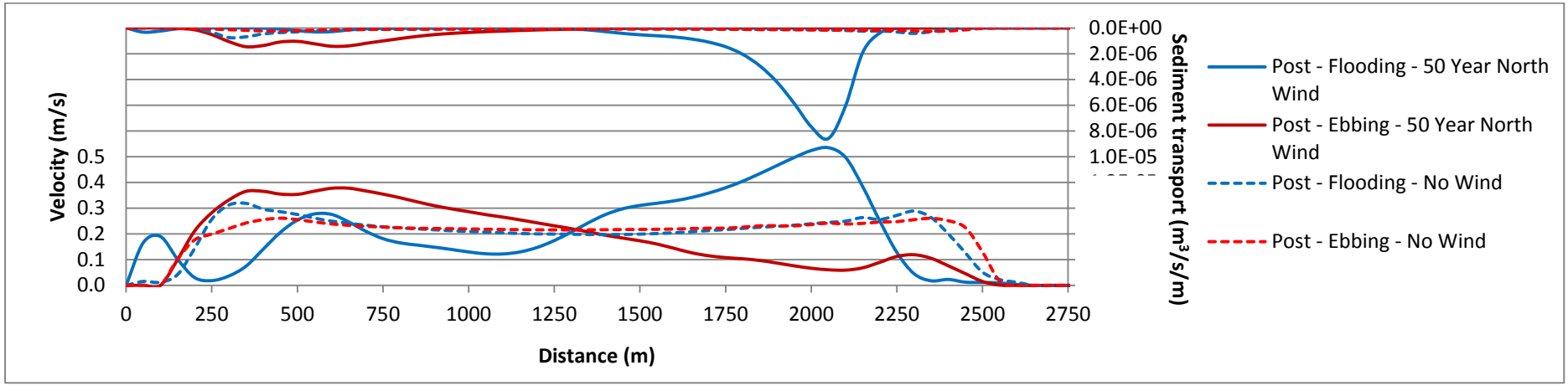

Figure H.3-3: Section S2 after the construction including a 1 in 50 year southern wind

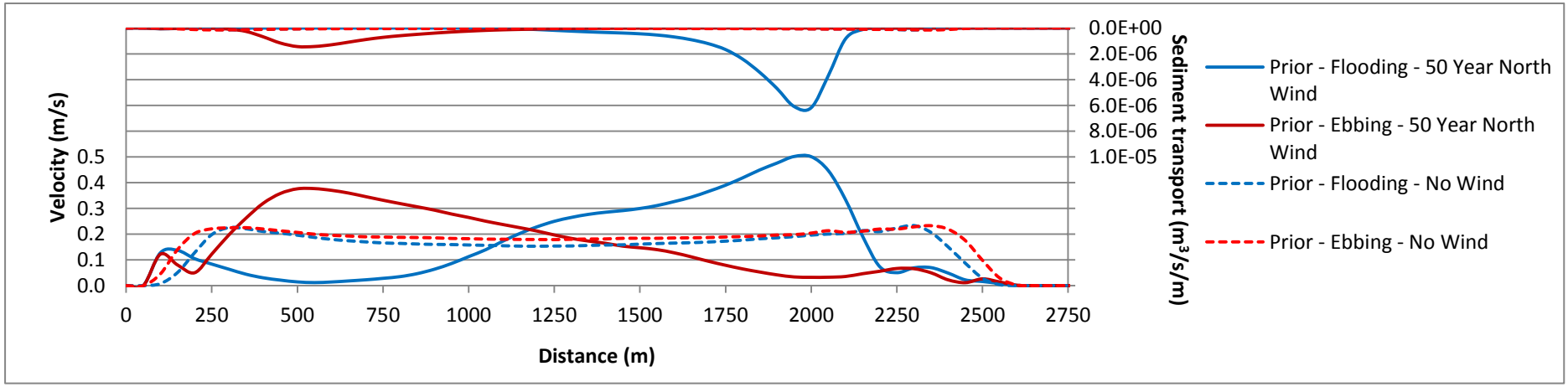

Figure H.3-4: Section S2 prior to construction including a 1 in 50 year southern wind

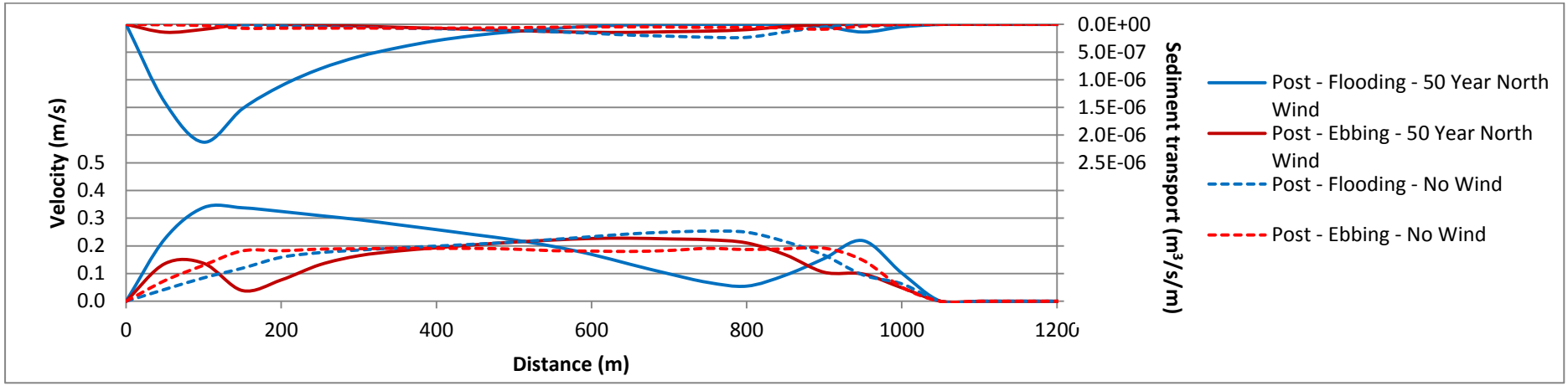

Figure H.3-5: Section S3 after the construction including a 1 in 50 year southern wind

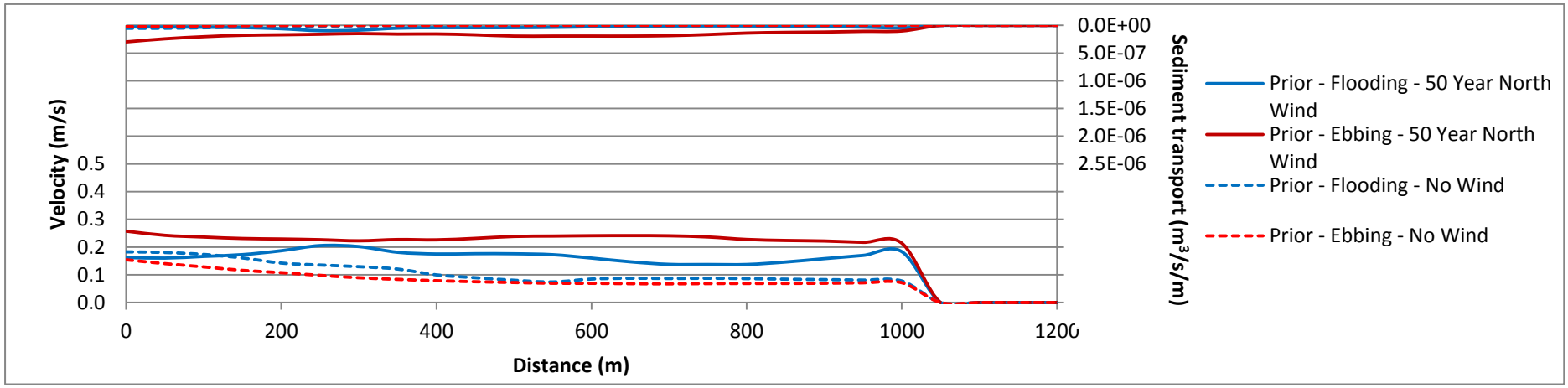

Figure H.3-6: Section S3 prior to construction including a 1 in 50 year southern wind

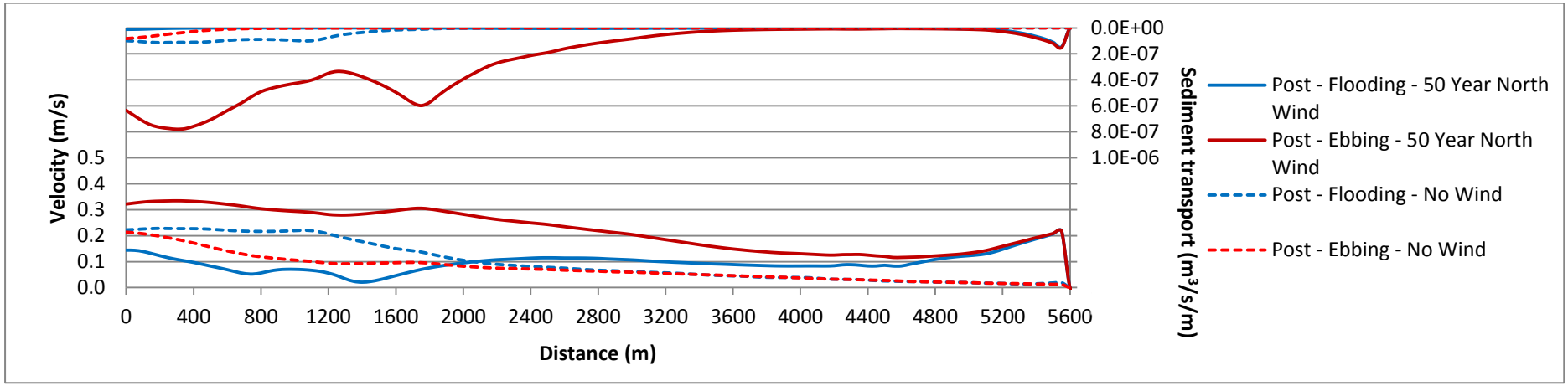

Figure H.3-7: Section S4 after the construction including a 1 in 50 year southern wind

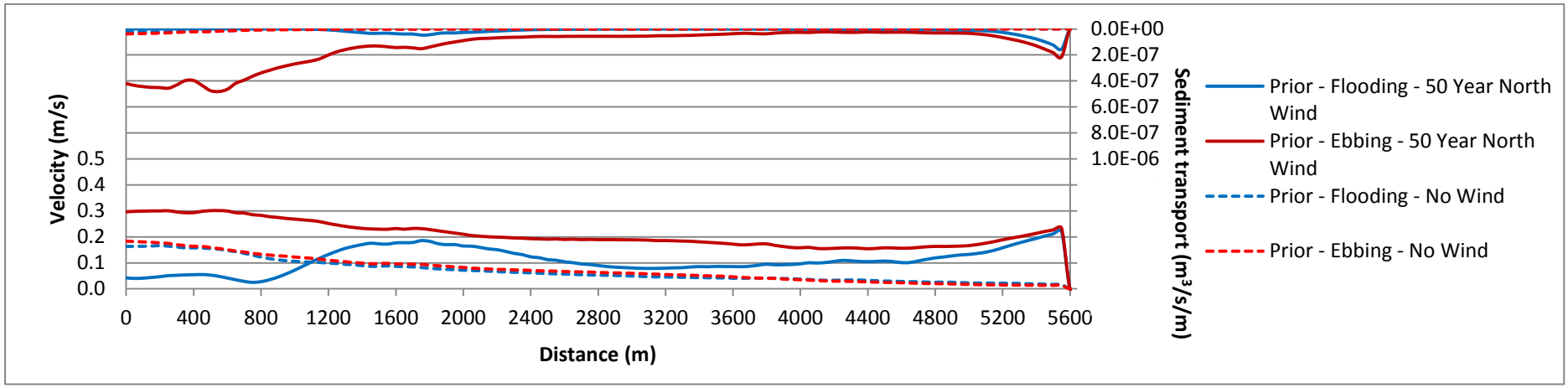

Figure H.3-8: Section S4 prior to construction including a 1 in 50 year southern wind

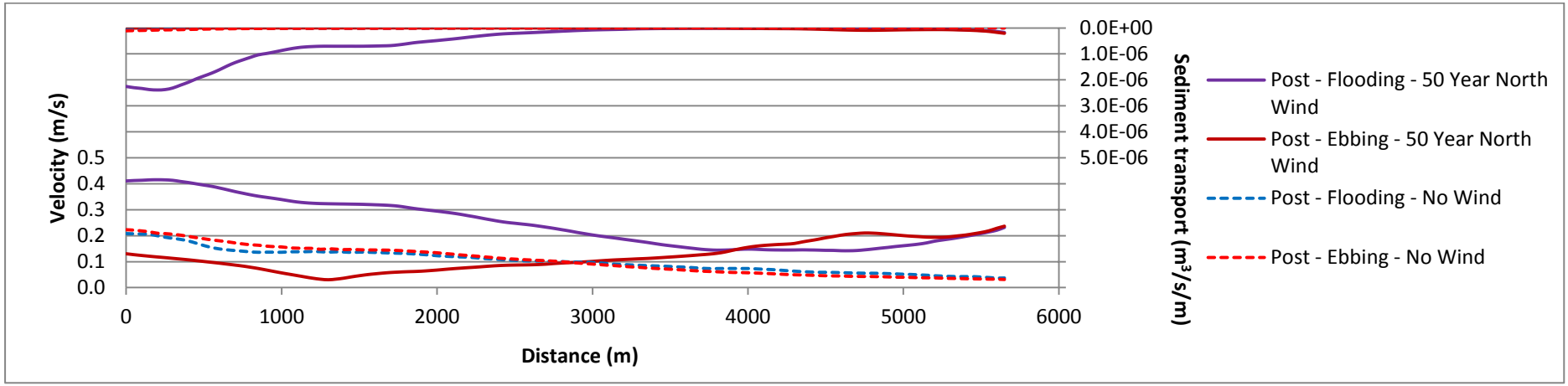

Figure H.3-9: Section S5 after the construction including a 1 in 50 year southern wind

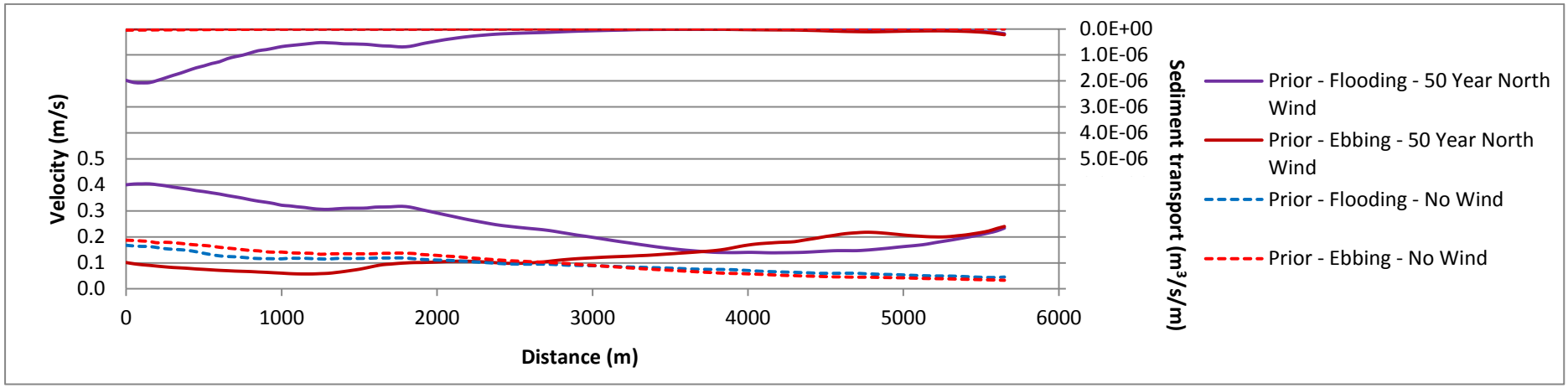

Figure H.3-10: Section S5 prior to construction including a 1 in 50 year southern wind

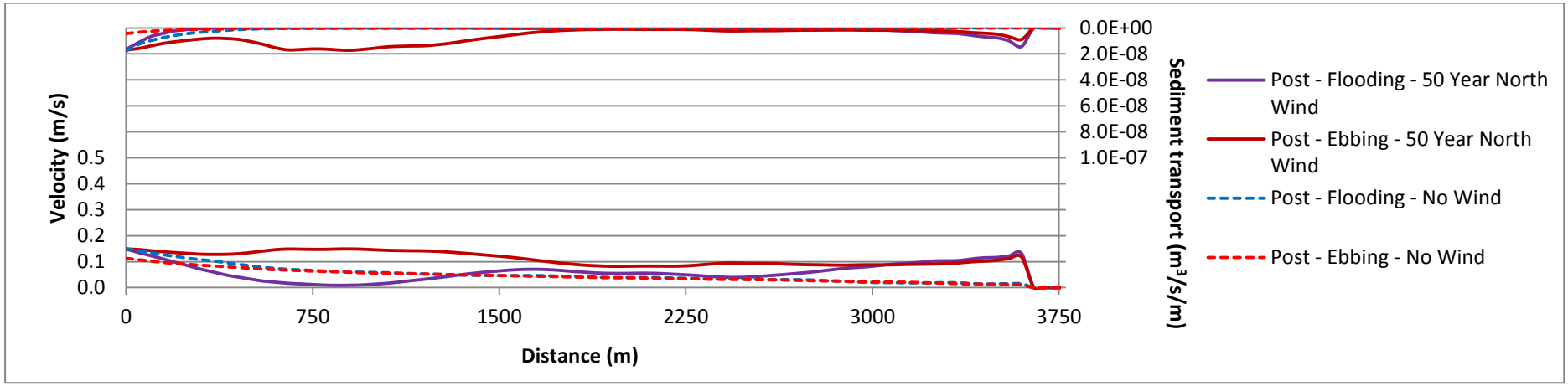

Figure H.3-11: Section S6 after the construction including a 1 in 50 year southern wind

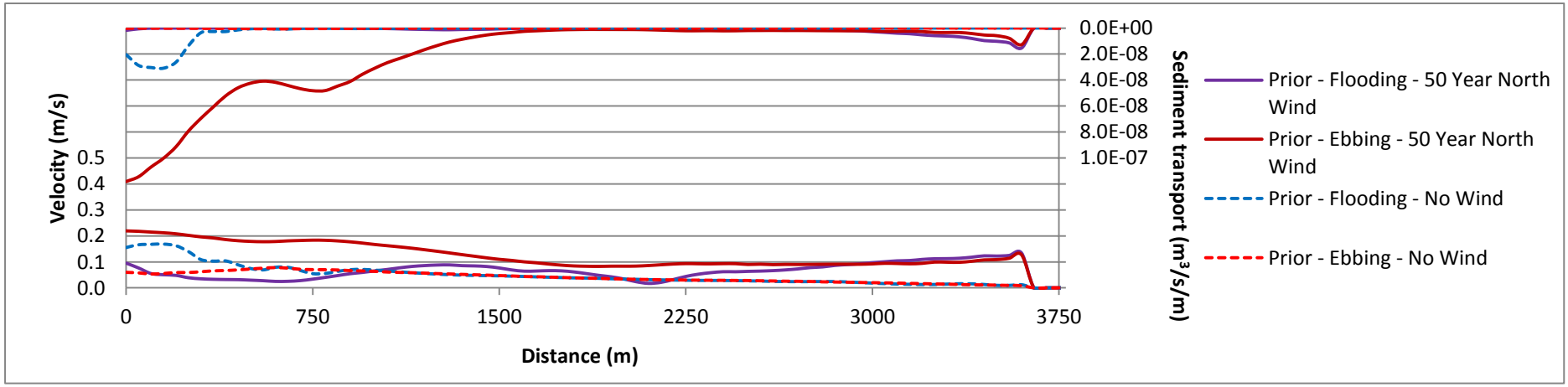

Figure H.3-12: Section S6 prior to construction including a 1 in 50 year southern wind

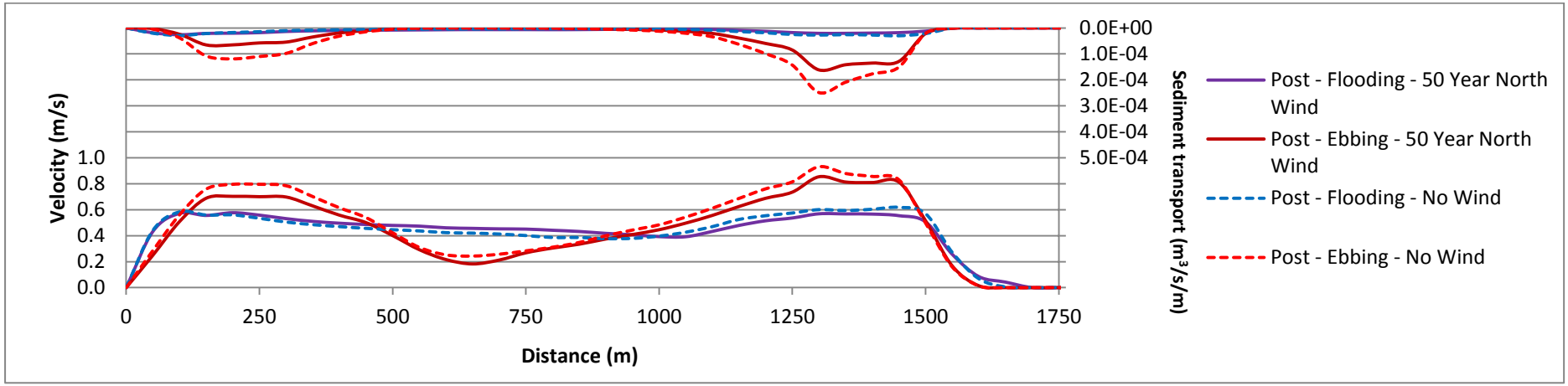

Figure H.3-13: Section L1 after the construction including a 1 in 50 year southern wind

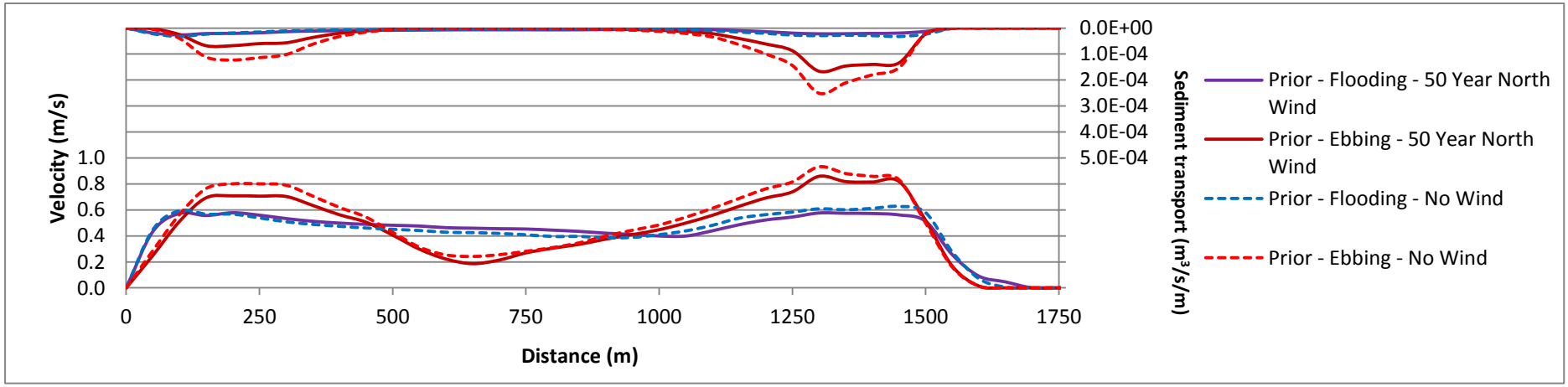

Figure H.3-14: Section L1 prior to construction including a 1 in 50 year southern wind

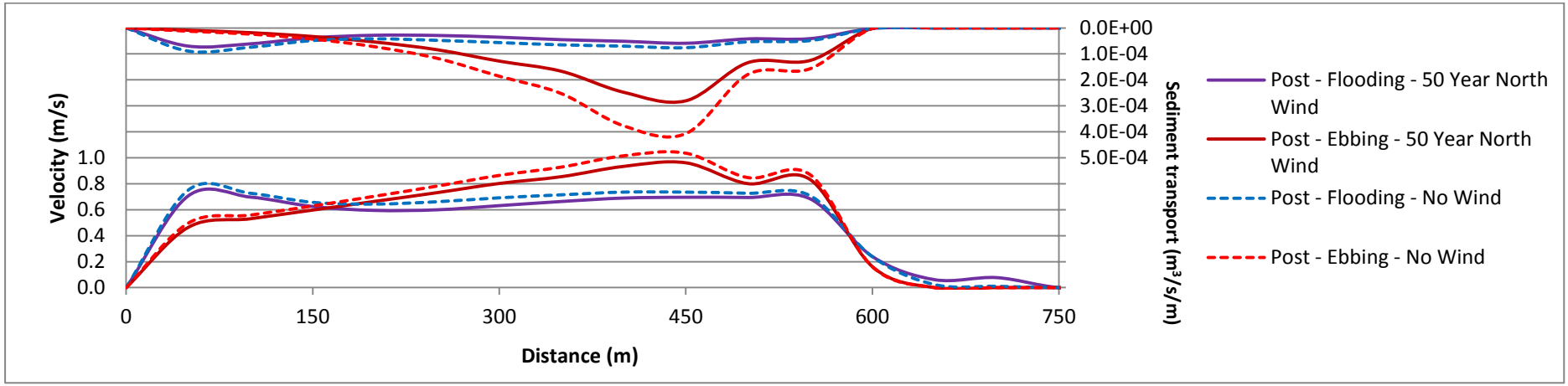

Figure H.3-15: Section L2 after the construction including a 1 in 50 year southern wind

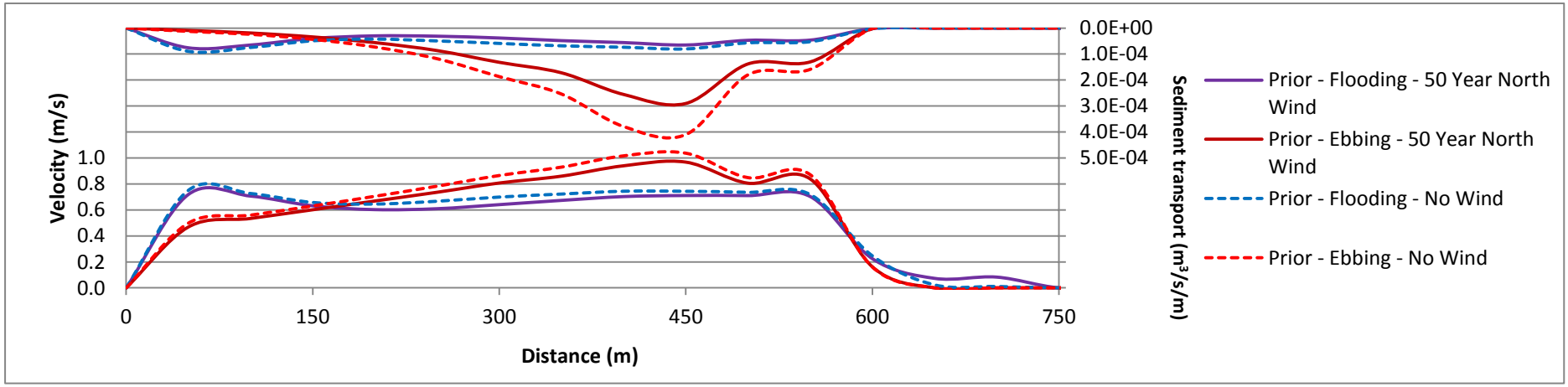

Figure H.3-16: Section L2 prior to construction including a 1 in 50 year southern wind

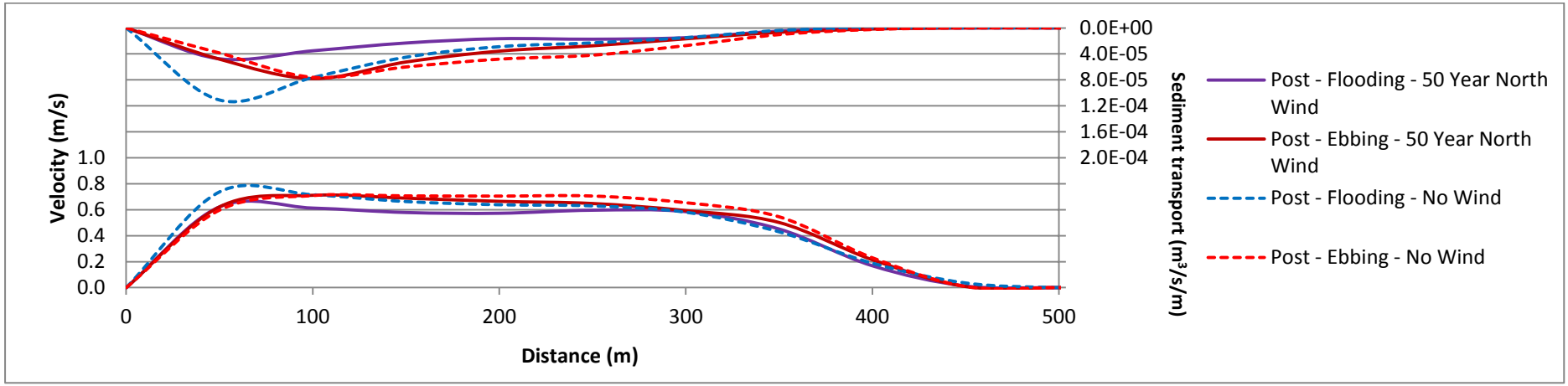

Figure H.3-17: Section L3 after the construction including a 1 in 50 year southern wind

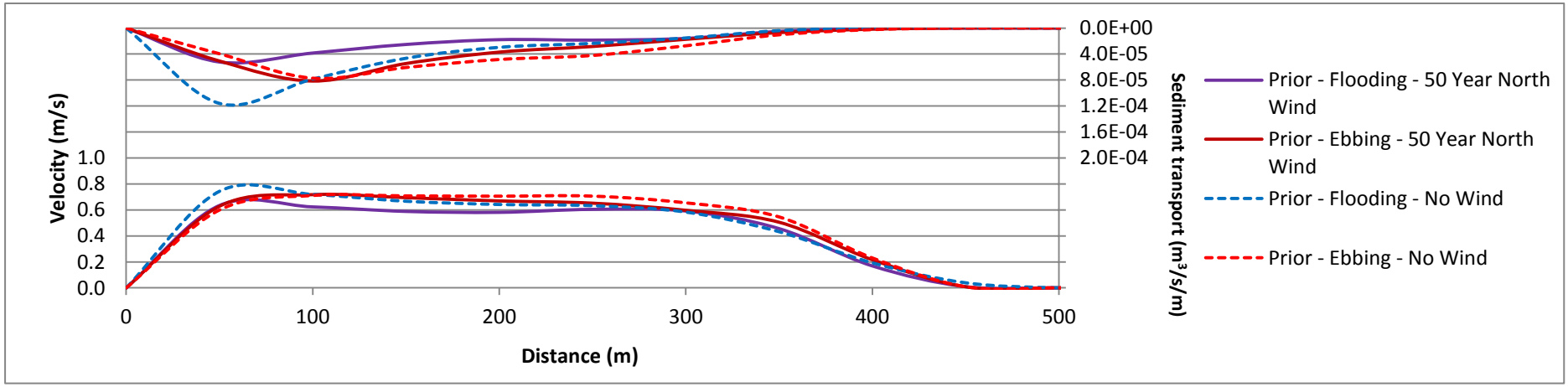

Figure H.3-18: Section L3 prior to construction including a 1 in 50 year southern wind

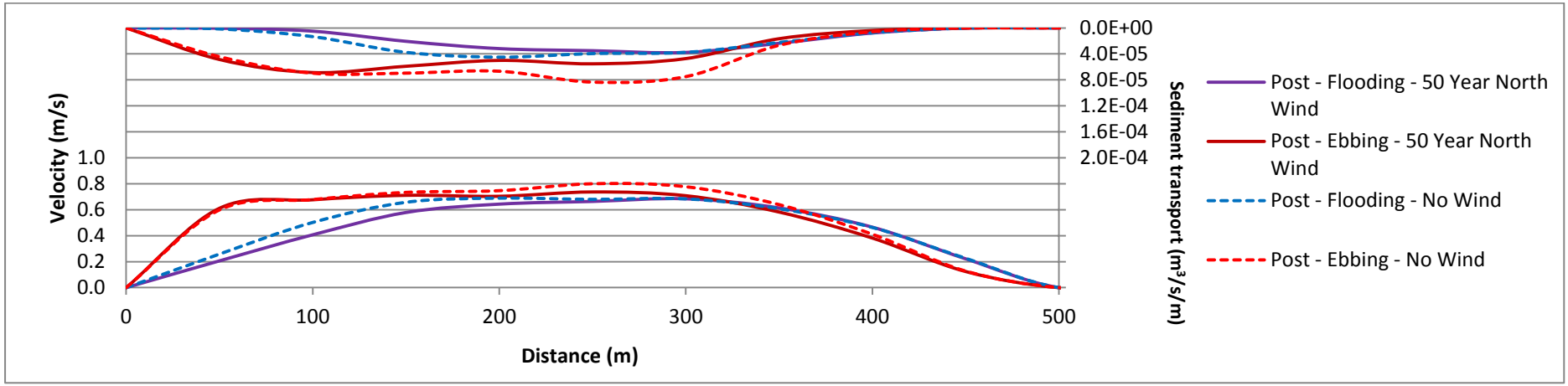

Figure H.3-19: Section L4 after the construction including a 1 in 50 year southern wind

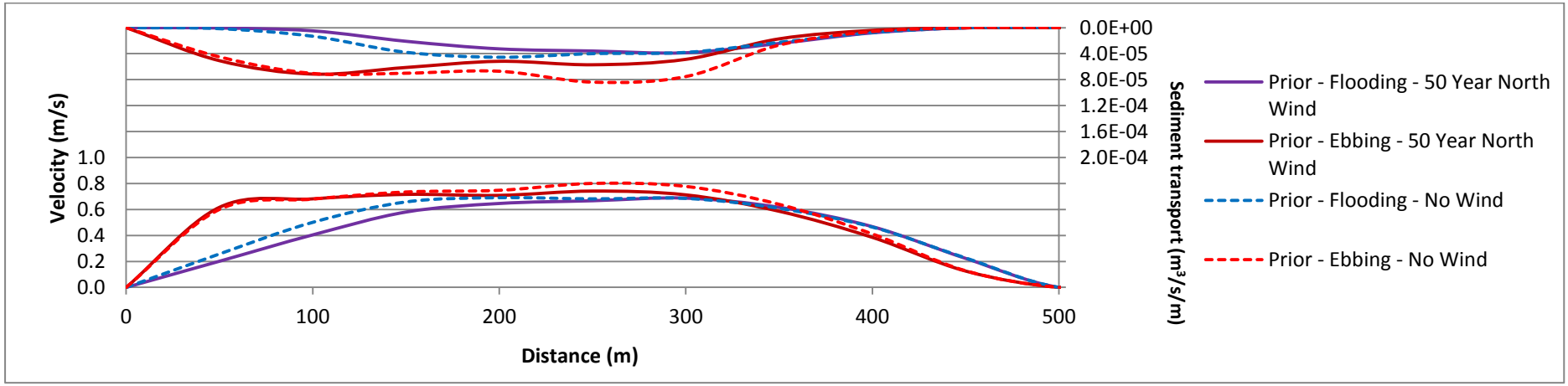

Figure H.3-20: Section L4 prior to construction including a 1 in 50 year southern wind

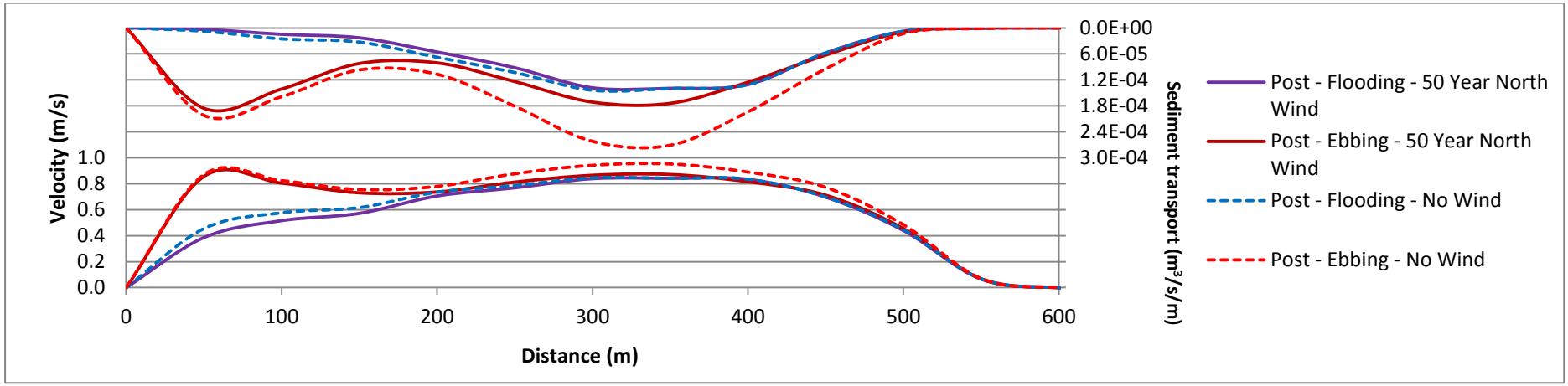

Figure H.3-21: Section L5 after the construction including a 1 in 50 year southern wind

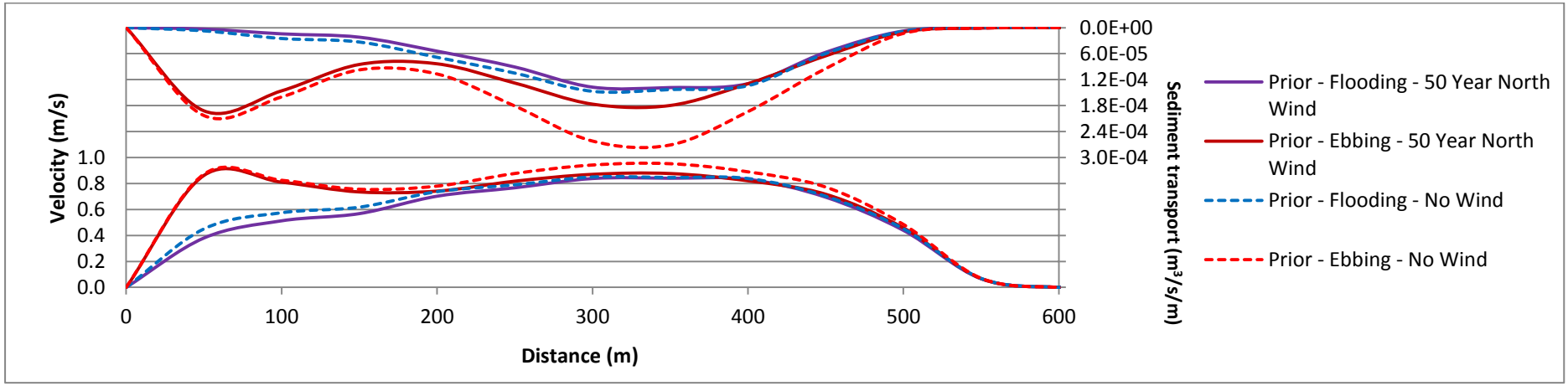

Figure H.3-22: Section L5 prior to construction including a 1 in 50 year southern wind

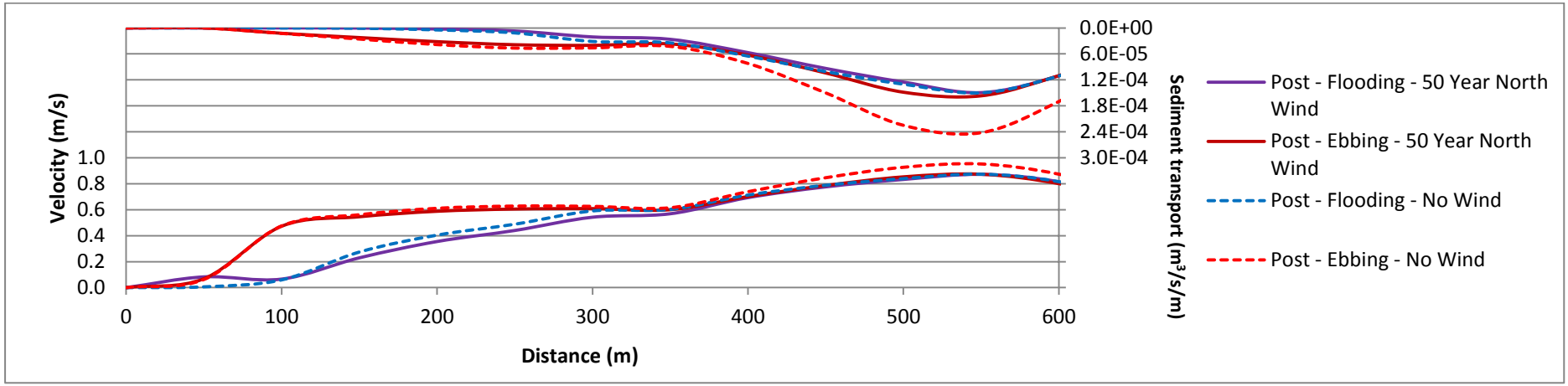

Figure H.3-23: Section L6 after the construction including a 1 in 50 year southern wind

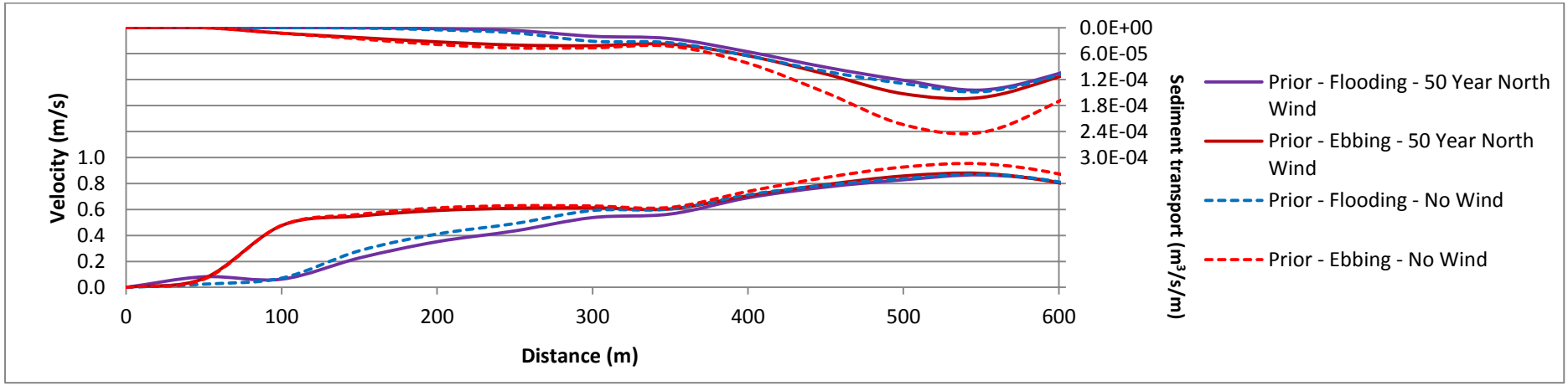

Figure H.3-24: Section L6 prior to construction including a 1 in 50 year southern wind

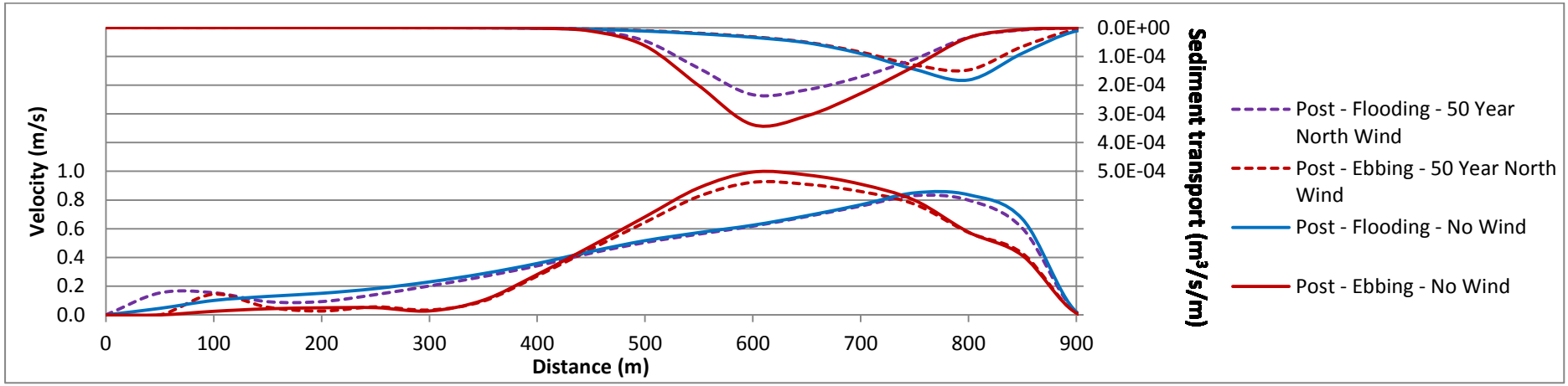

Figure H.3-25: Section L7 after the construction including a 1 in 50 year southern wind

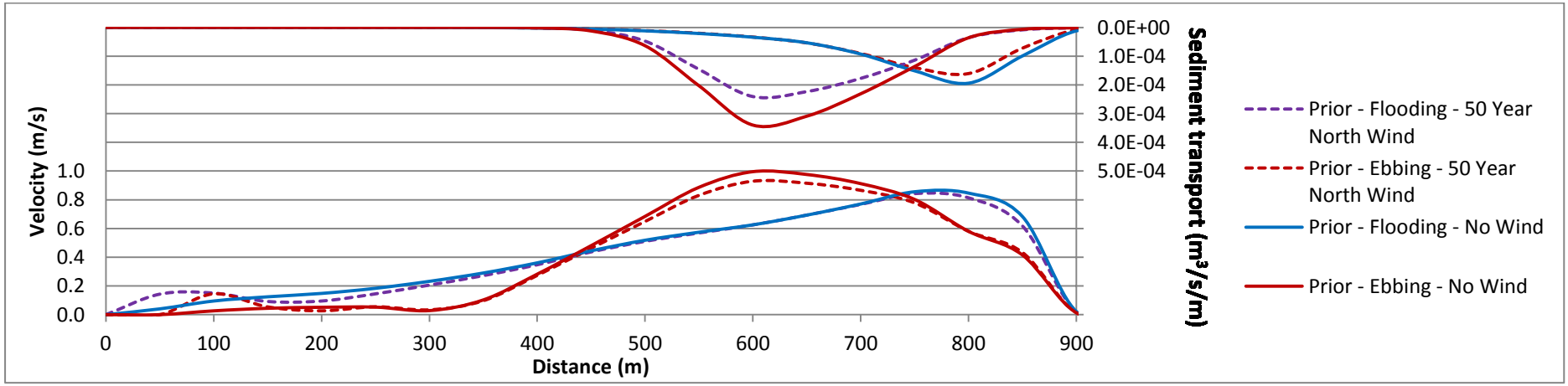

Figure H.3-26: Section L7 prior to construction including a 1 in 50 year southern wind

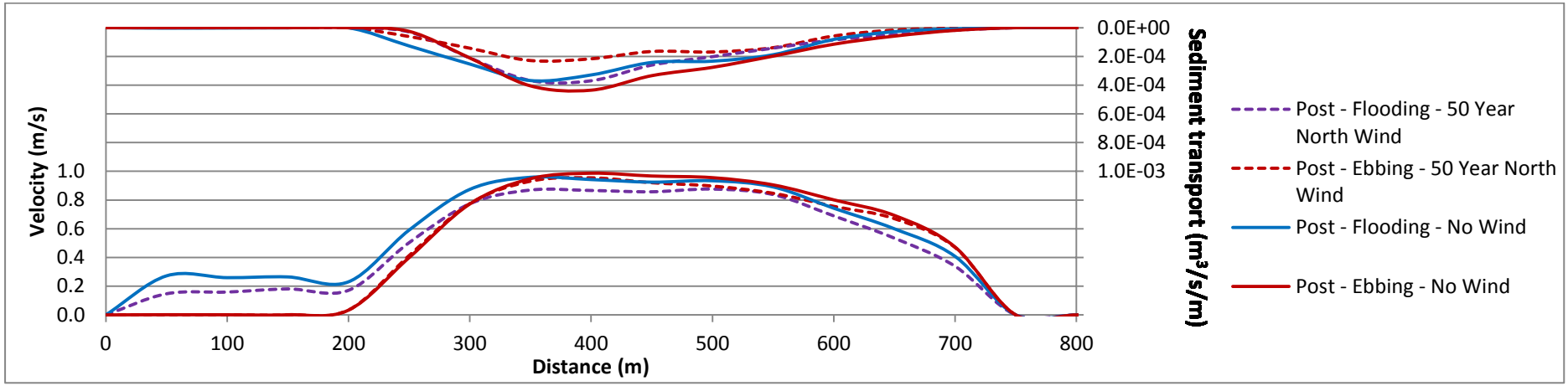

Figure H.3-27: Section L8 after the construction including a 1 in 50 year southern wind

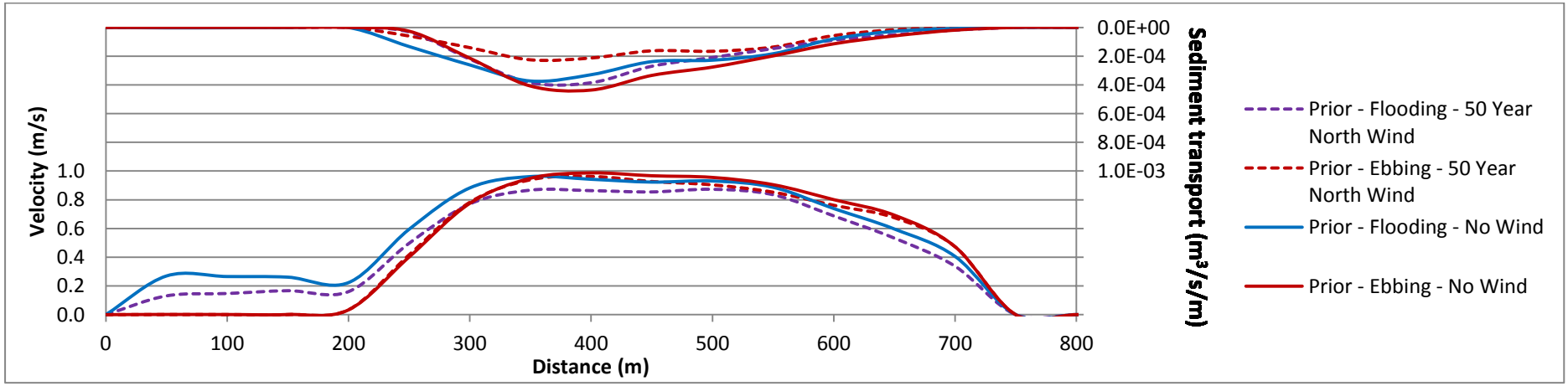

Figure H.3-28: Section L8 prior to construction including a 1 in 50 year southern wind

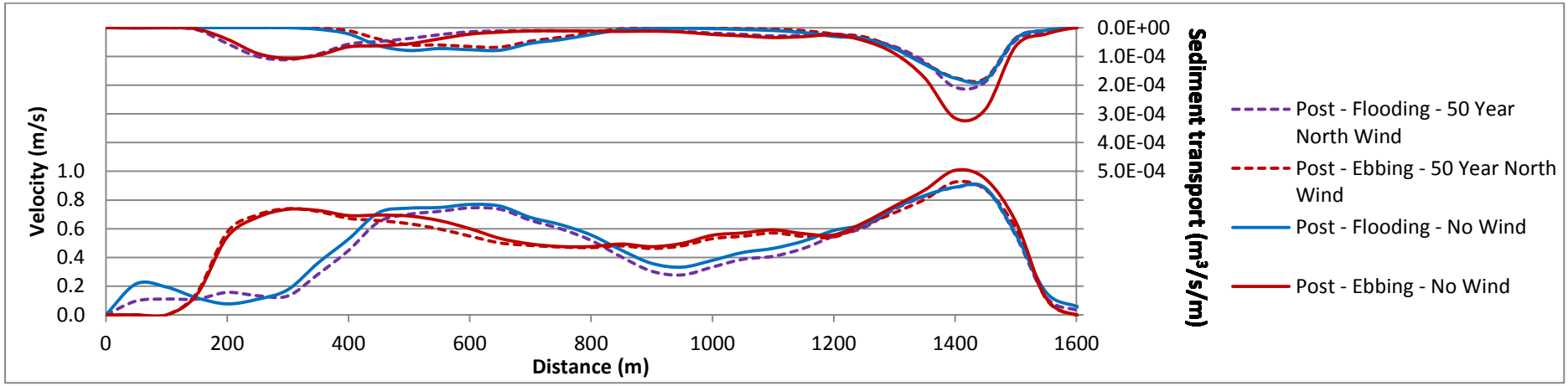

Figure H.3-29: Section L9 after the construction including a 1 in 50 year southern wind

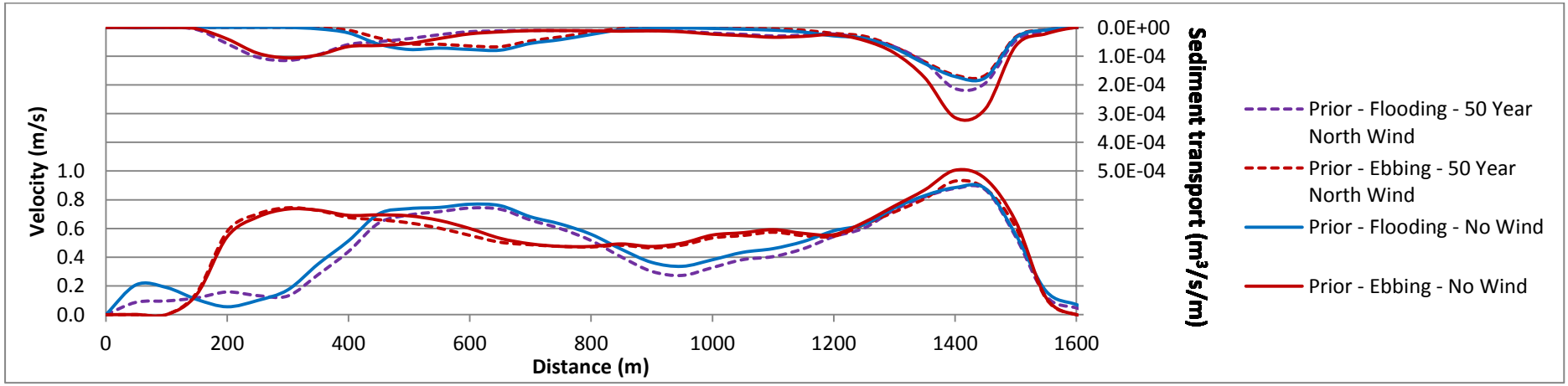

Figure H.3-30: Section L9 prior to construction including a 1 in 50 year southern wind

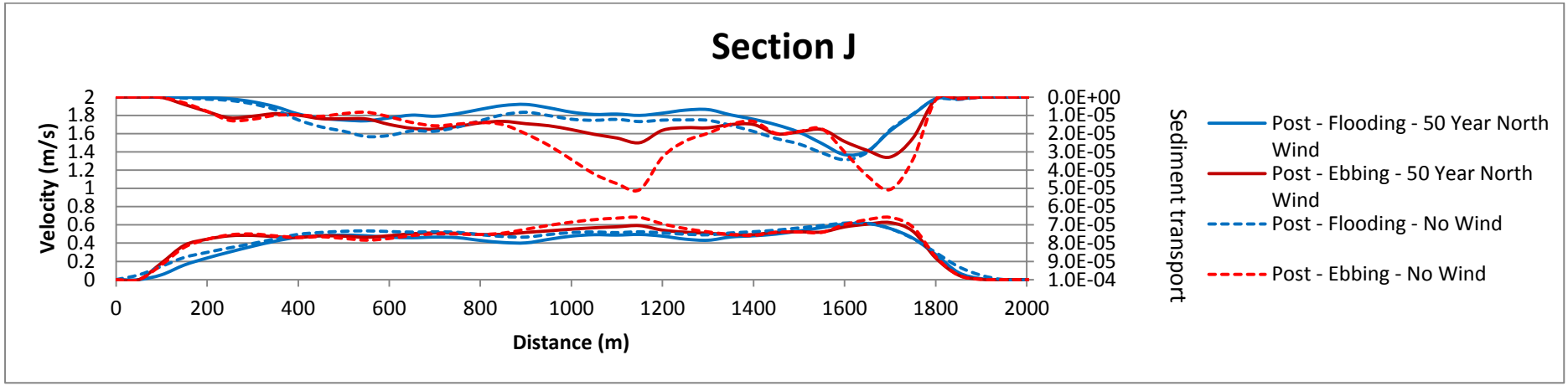

Figure H.3-31: Section L10 after the construction including a 1 in 50 year southern wind

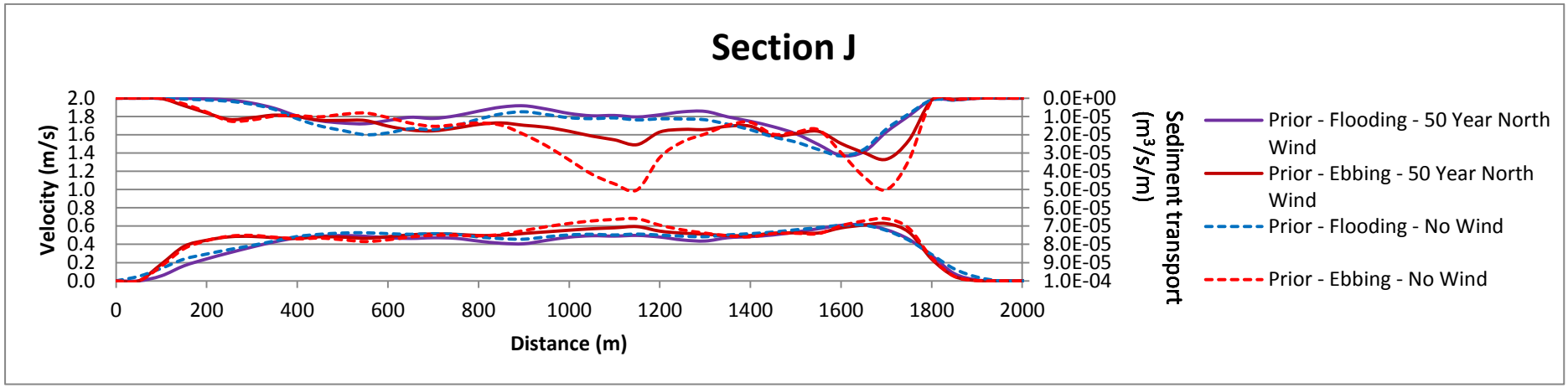

Figure H.3-32: Section L10 prior to construction including a 1 in 50 year southern wind

APPENDIX H.4 TIDAL CONDITIONS INCLUDING 1 IN 50 YEAR WIND EVENT ACROSS THE LONGEST FETCH

LIST OF FIGURERS

Figure H.4-1: Section S1 after the construction including a 1 in 50 year wind across the longest fetch
Figure H.4-2: Section S1 prior to construction including a 1 in 50 year wind across the longest fetch
Figure H.4-3: Section S2 after the construction including a 1 in 50 year wind across the longest fetch
Figure H.4-4: Section S2 prior to construction including a 1 in 50 year wind across the longest fetch
Figure H.4-5: Section S3 after the construction including a 1 in 50 year wind across the longest fetch
Figure H.4-6: Section S3 prior to construction including a 1 in 50 year wind across the longest fetch
Figure H.4-7: Section S4 after the construction including a 1 in 50 year wind across the longest fetch
Figure H.4-8: Section S4 prior to construction including a 1 in 50 year wind across the longest fetch
Figure H.4-9: Section S5 after the construction including a 1 in 50 year wind across the longest fetch
Figure H.4-10: Section S5 prior to construction including a 1 in 50 year wind across the longest fetch
Figure H.4-11: Section S6 after the construction including a 1 in 50 year wind across the longest fetch
Figure H.4-12: Section S6 prior to construction including a 1 in 50 year wind across the longest fetch
Figure H.4-13: Section L1 after the construction including a 1 in 50 year wind across the longest fetch
Figure H.4-14: Section L1 prior to construction including a 1 in 50 year wind across the longest fetch
Figure H.4-15: Section L2 after the construction including a 1 in 50 year wind across the longest fetch
Figure H.4-16: Section L2 prior to construction including a 1 in 50 year wind across the longest fetch
Figure H.4-17: Section L3 after the construction including a 1 in 50 year wind across the longest fetch

Figure H.4-18: Section L3 prior to construction including a 1 in 50 year wind across the longest fetch
Figure H.4-19: Section L4 after the construction including a 1 in 50 year wind across the longest fetch
Figure H.4-20: Section L4 prior to construction including a 1 in 50 year wind across the longest fetch
Figure H.4-21: Section L5 after the construction including a 1 in 50 year wind across the longest fetch
Figure H.4-22: Section L5 prior to construction including a 1 in 50 year wind across the longest fetch
Figure H.4-23: Section L6 after the construction including a 1 in 50 year wind across the longest fetch
Figure H.4-24: Section L6 prior to construction including a 1 in 50 year wind across the longest fetch
Figure H.4-25: Section L7 after the construction including a 1 in 50 year wind across the longest fetch
Figure H.4-26: Section L7 prior to construction including a 1 in 50 year wind across the longest fetch
Figure H.4-27: Section L8 after the construction including a 1 in 50 year wind across the longest fetch
Figure H.4-28: Section L8 prior to construction including a 1 in 50 year wind across the longest fetch
Figure H.4-17: Section L9 after the construction including a 1 in 50 year wind across the longest fetch
Figure H.4-30: Section L9 prior to construction including a 1 in 50 year wind across the longest fetch
Figure H.4-31: Section L10 after the construction including a 1 in 50 year wind across the longest fetch
Figure H.4-32: Section L10 prior to construction including a 1 in 50 year wind across the longest fetch

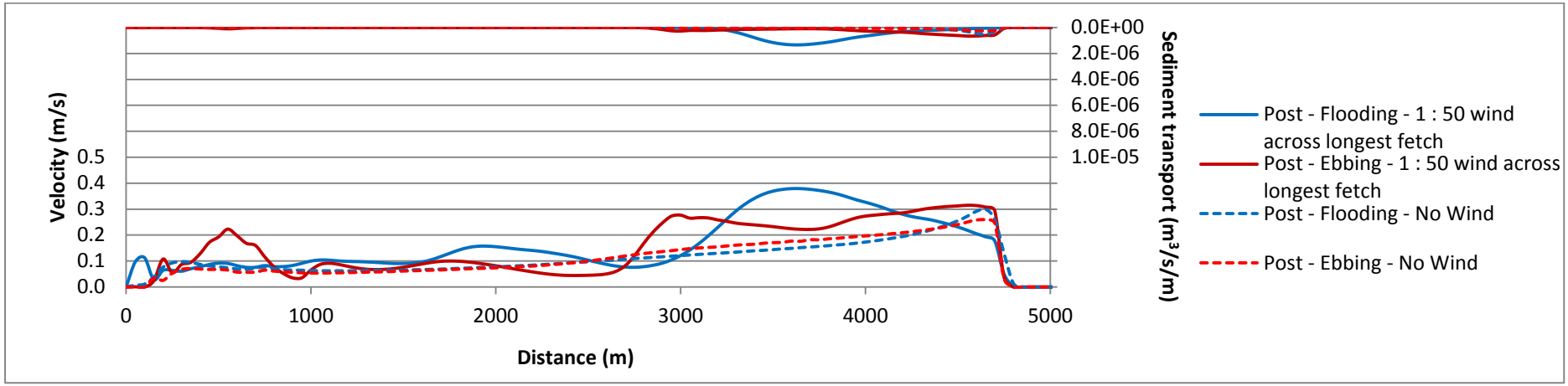

Figure H.4-1: Section S1 after the construction including a 1 in 50 year wind across the longest fetch

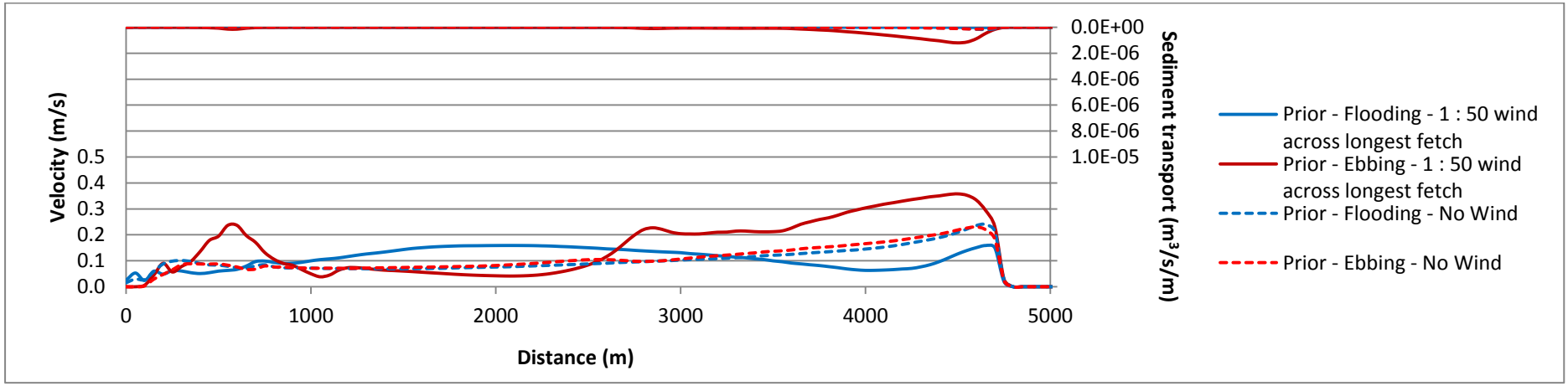

Figure H.4-2: Section S1 prior to construction including a 1 in 50 year wind across the longest fetch

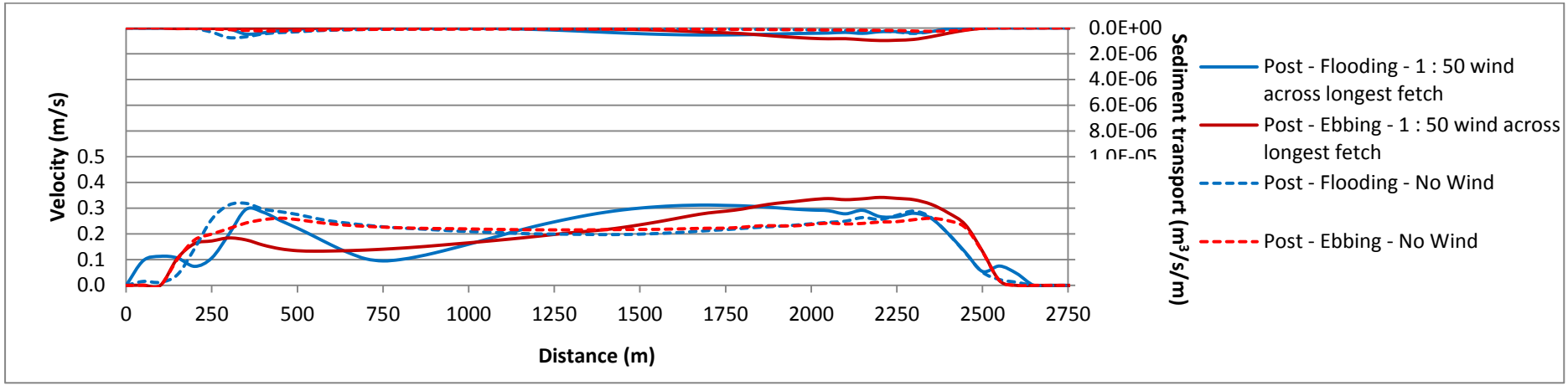

Figure H.4-3: Section S2 after the construction including a 1 in 50 year wind across the longest fetch

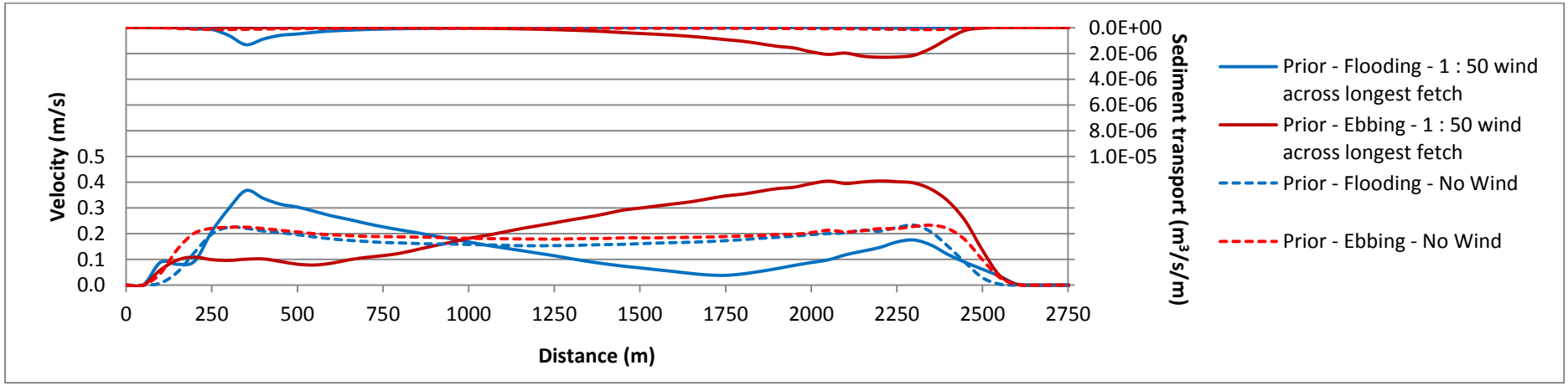

Figure H.4-4: Section S2 prior to construction including a 1 in 50 year wind across the longest fetch

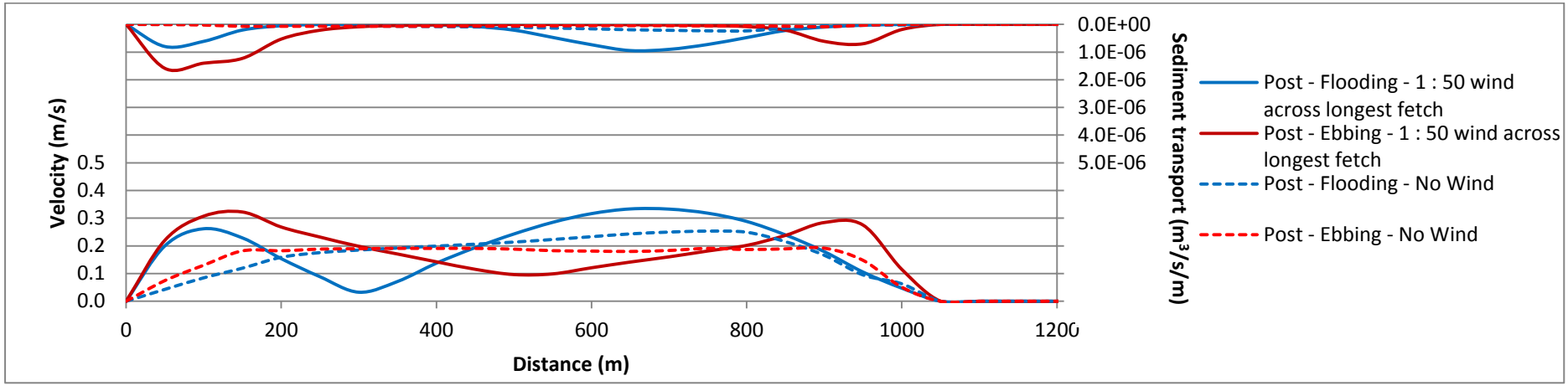

Figure H.4-5: Section S3 after the construction including a 1 in 50 year wind across the longest fetch

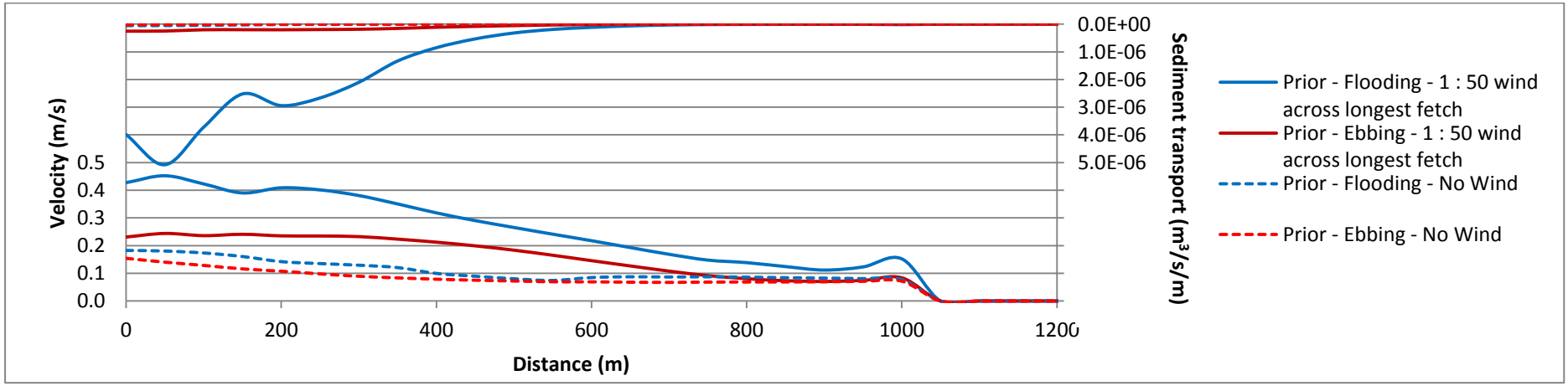

Figure H.4-6: Section S3 prior to construction including a 1 in 50 year wind across the longest fetch

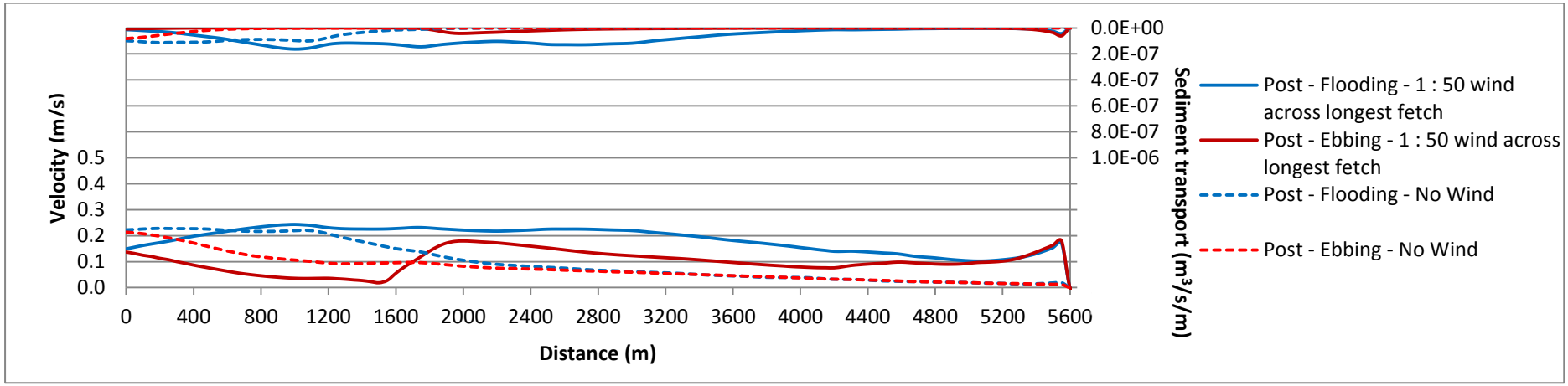

Figure H.4-7: Section S4 after the construction including a 1 in 50 year wind across the longest fetch

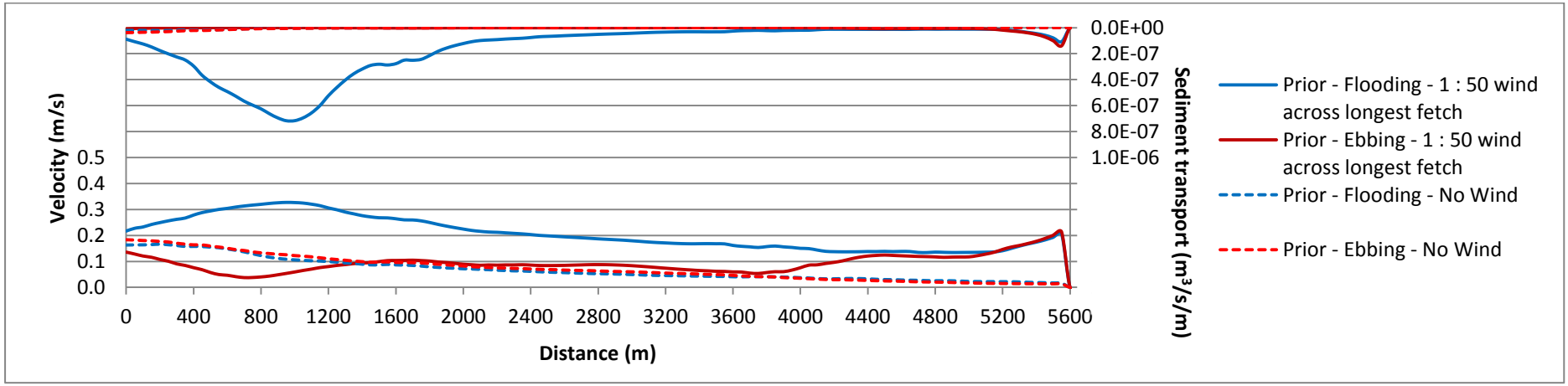

Figure H.4-8: Section S4 prior to construction including a 1 in 50 year wind across the longest fetch

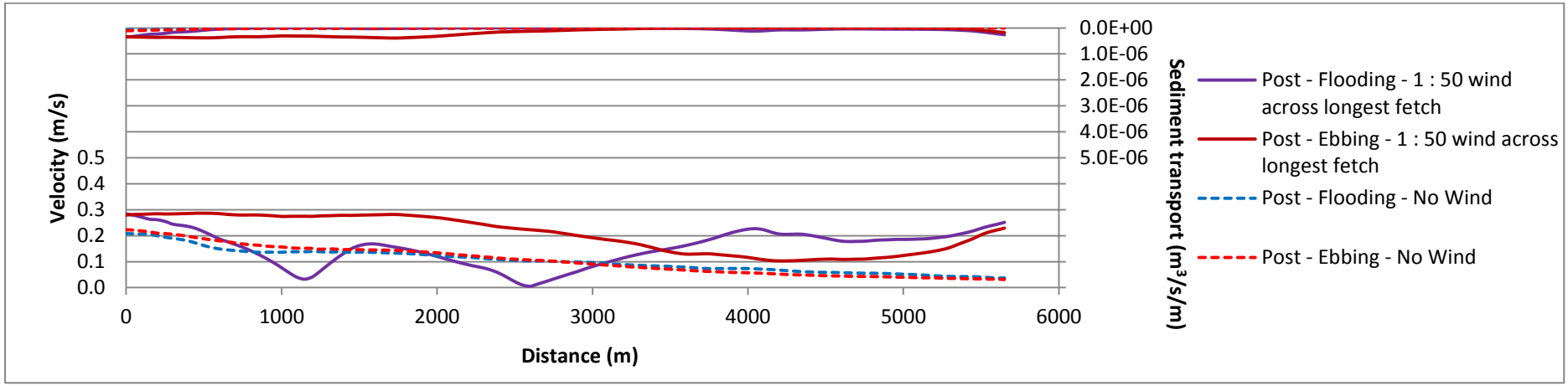

Figure H.4-9: Section S5 after the construction including a 1 in 50 year wind across the longest fetch

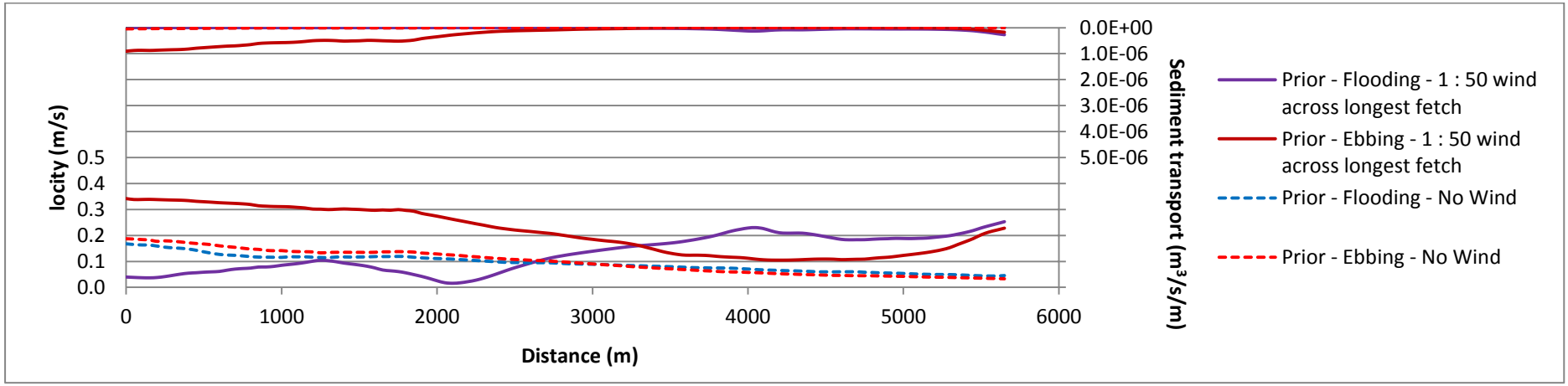

Figure H.4-10: Section S5 prior to construction including a 1 in 50 year wind across the longest fetch

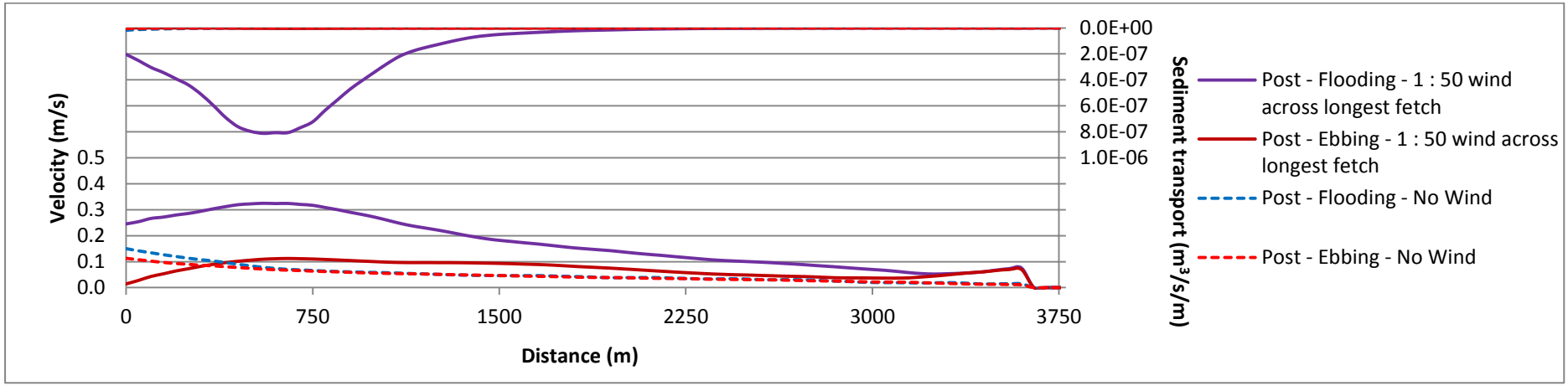

Figure H.4-11: Section S6 after the construction including a 1 in 50 year wind across the longest fetch

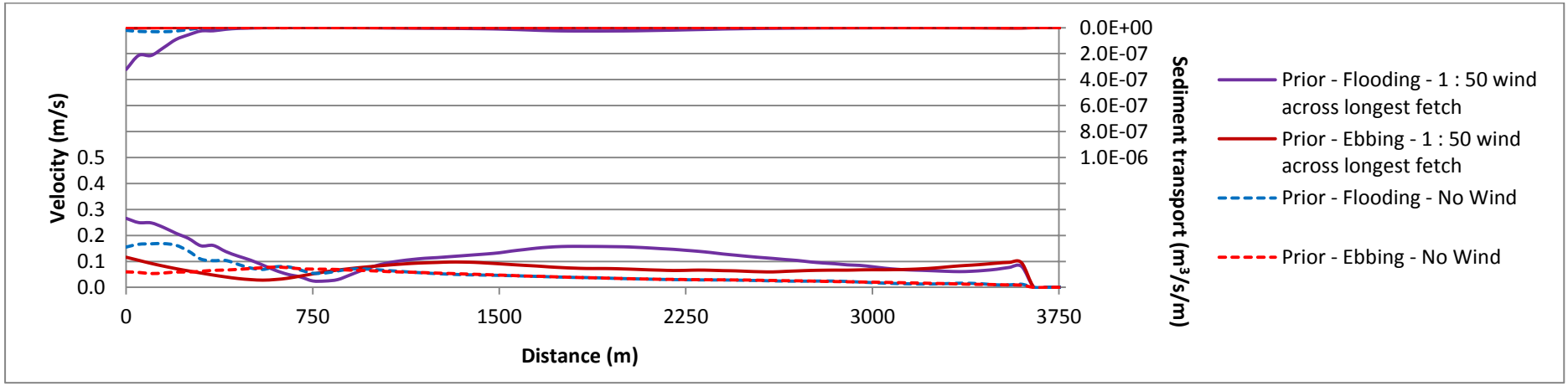

Figure H.4-12: Section S6 prior to construction including a 1 in 50 year wind across the longest fetch

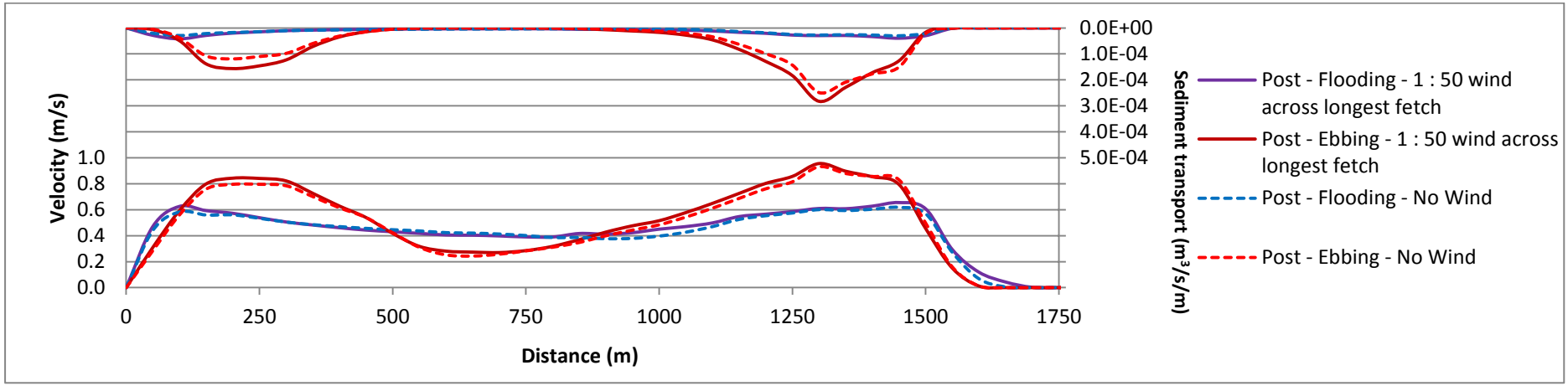

Figure H.4-13: Section L1 after the construction including a 1 in 50 year wind across the longest fetch

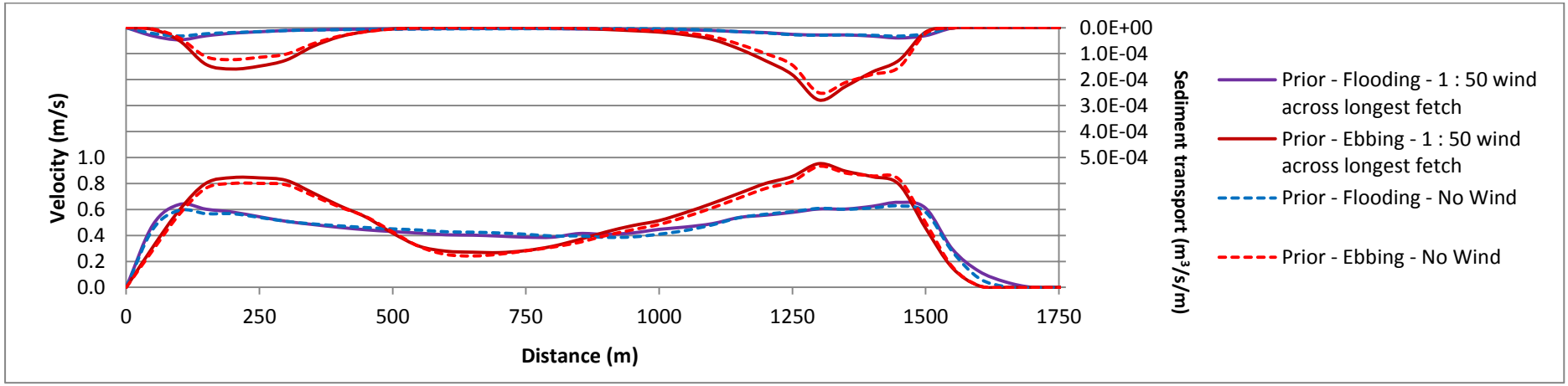

Figure H.4-14: Section L1 prior to construction including a 1 in 50 year wind across the longest fetch

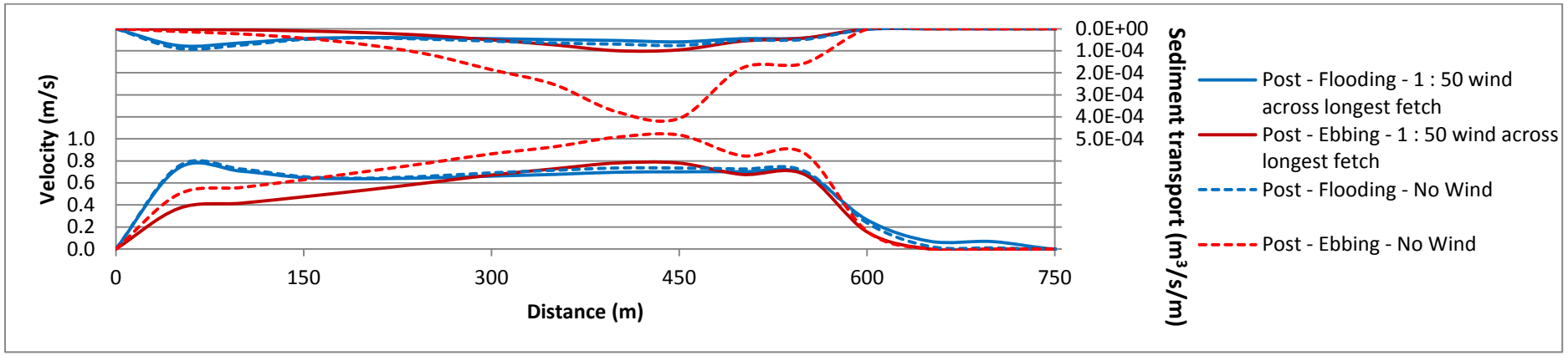

Figure H.4-15: Section L2 after the construction including a 1 in 50 year wind across the longest fetch

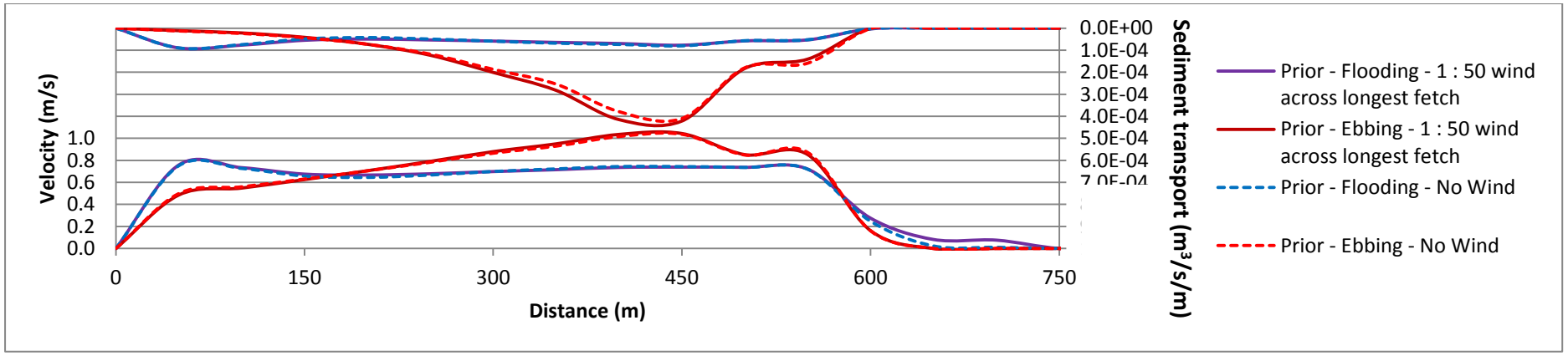

Figure H.4-16: Section L2 prior to construction including a 1 in 50 year wind across the longest fetch

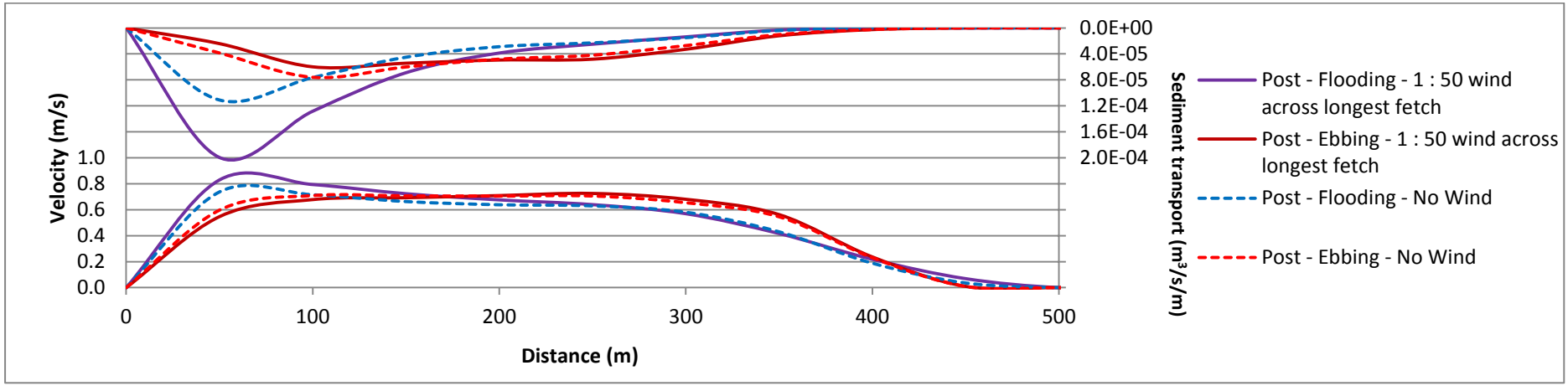

Figure H.4-17: Section L3 after the construction including a 1 in 50 year wind across the longest fetch

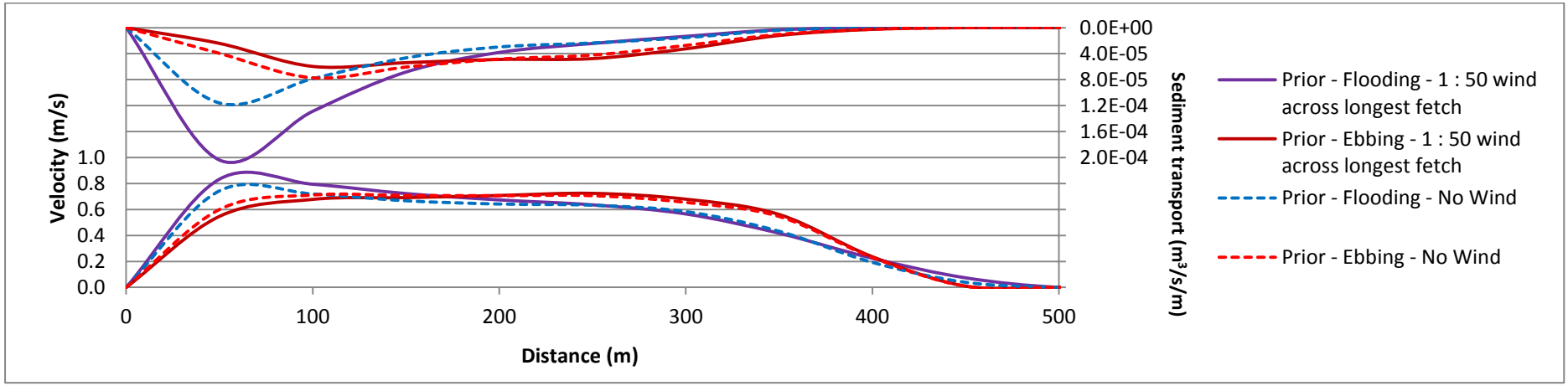

Figure H.4-18: Section L3 prior to construction including a 1 in 50 year wind across the longest fetch

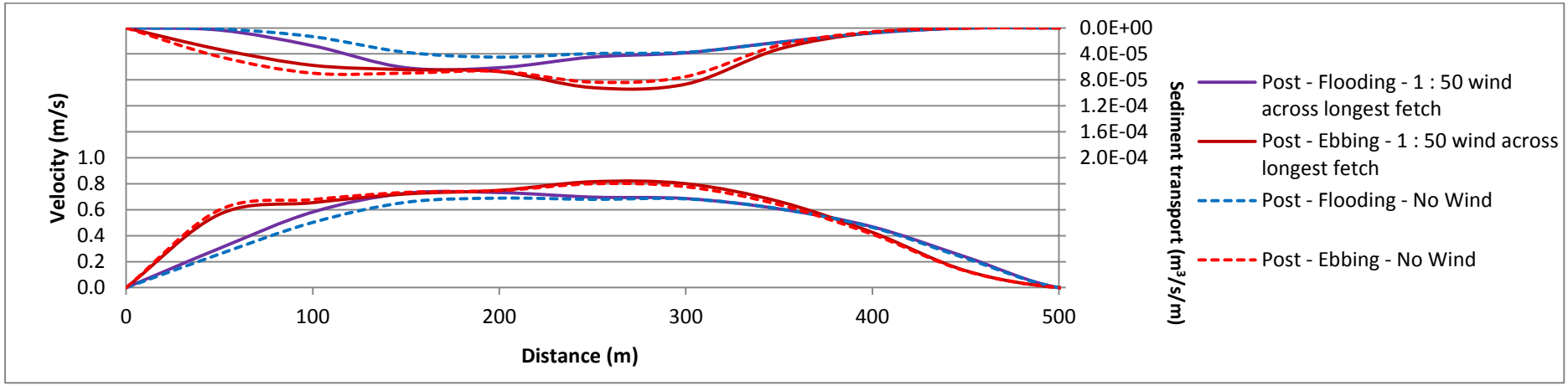

Figure H.4-19: Section L4 after the construction including a 1 in 50 year wind across the longest fetch

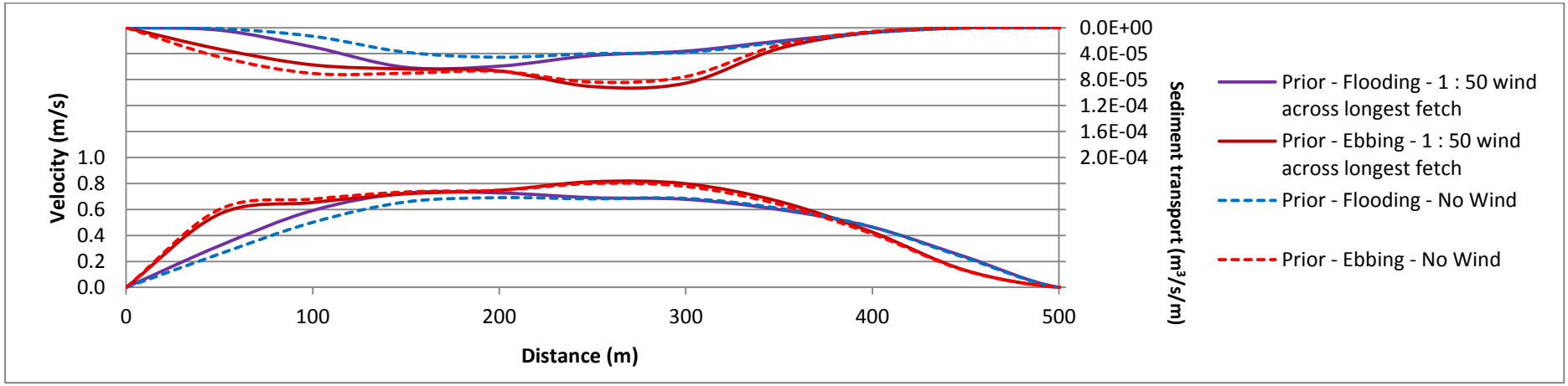

Figure H.4-20: Section L4 prior to construction including a 1 in 50 year wind across the longest fetch

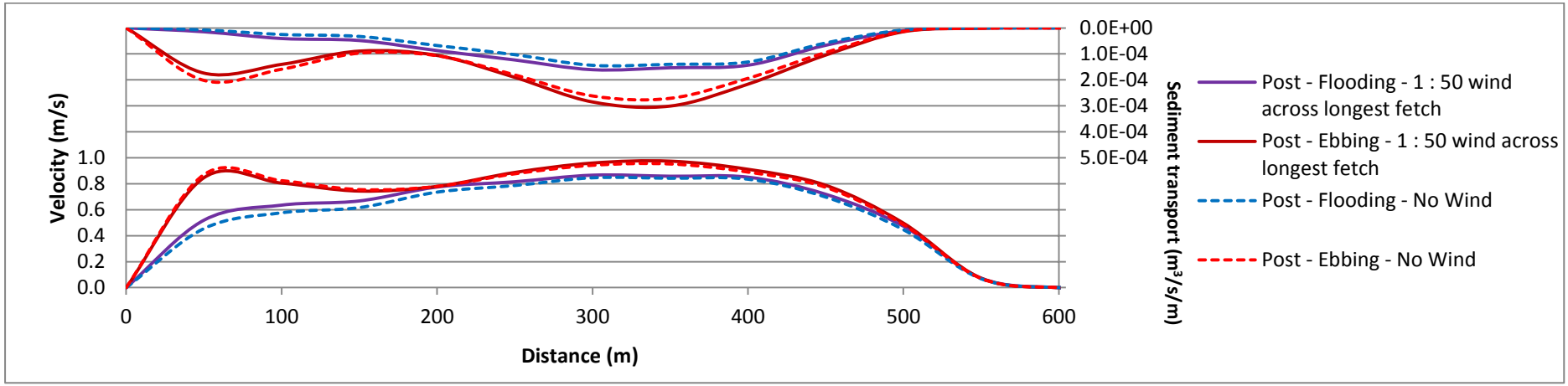

Figure H.4-21: Section L5 after the construction including a 1 in 50 year wind across the longest fetch

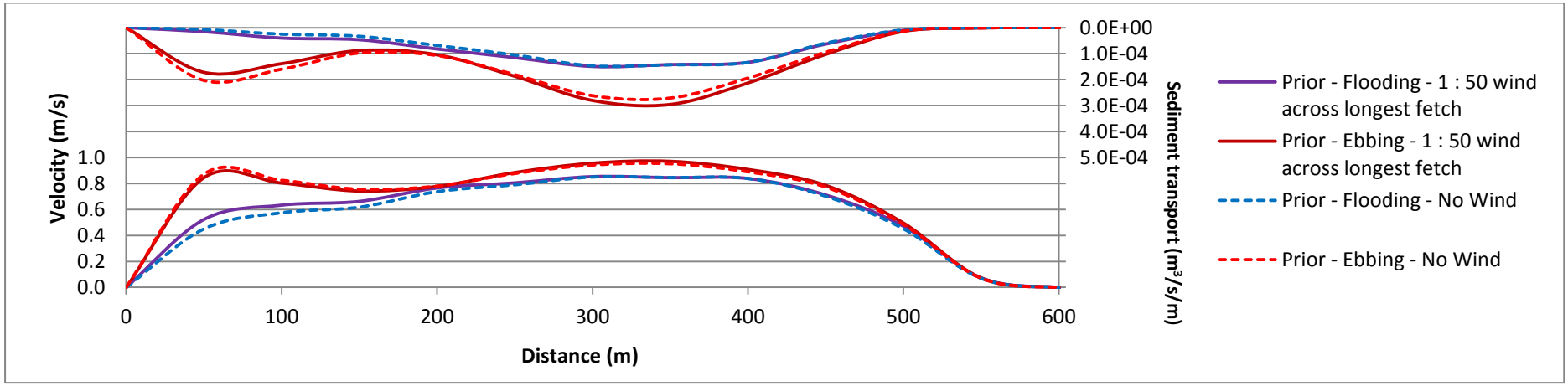

Figure H.4-22: Section L5 prior to construction including a 1 in 50 year wind across the longest fetch

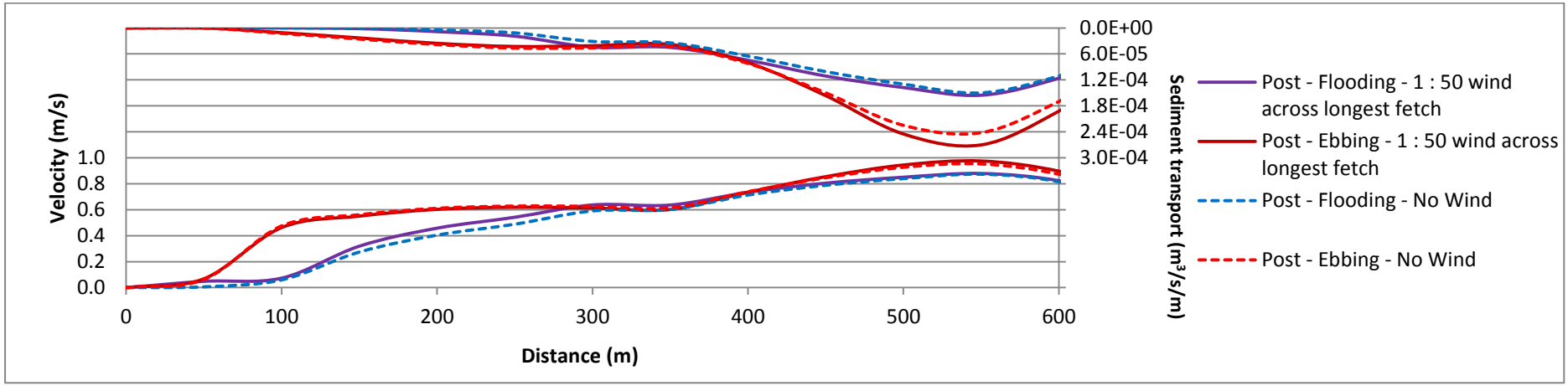

Figure H.4-23: Section L6 after the construction including a 1 in 50 year wind across the longest fetch

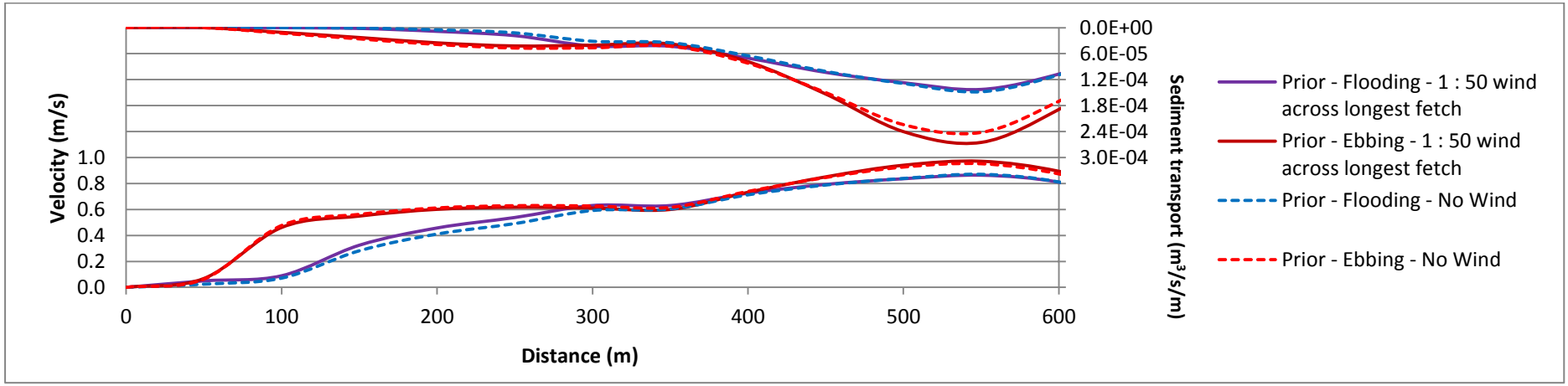

Figure H.4-24: Section L6 prior to construction including a 1 in 50 year wind across the longest fetch

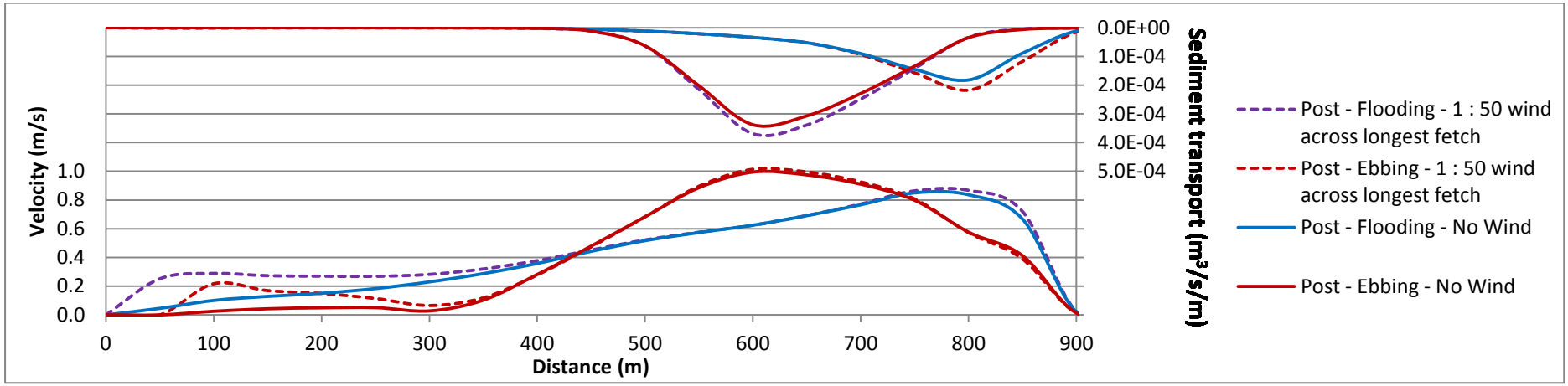

Figure H.4-25: Section L7 after the construction including a 1 in 50 year wind across the longest fetch

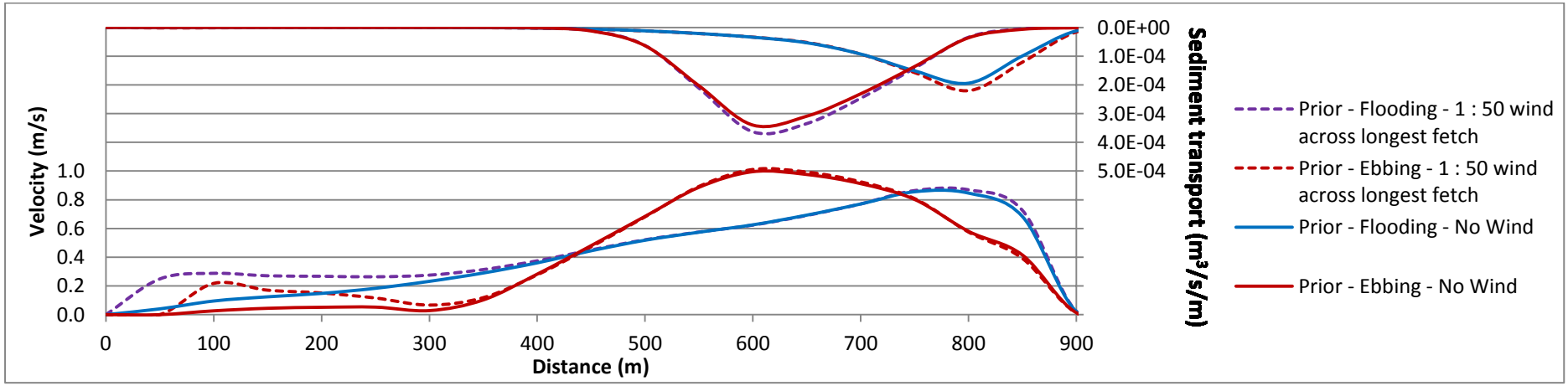

Figure H.4-26: Section L7 prior to construction including a 1 in 50 year wind across the longest fetch

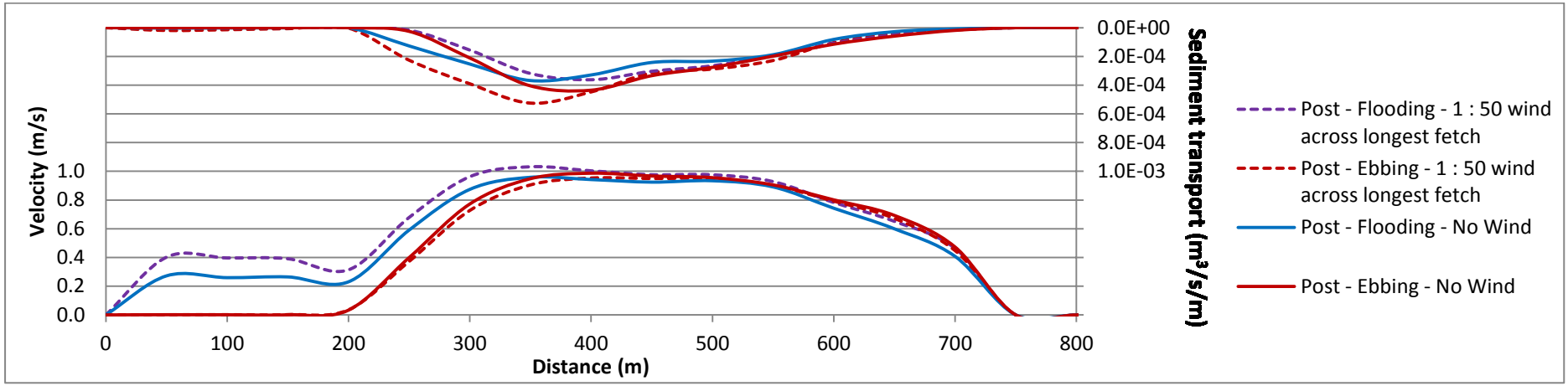

Figure H.4-27: Section L8 after the construction including a 1 in 50 year wind across the longest fetch

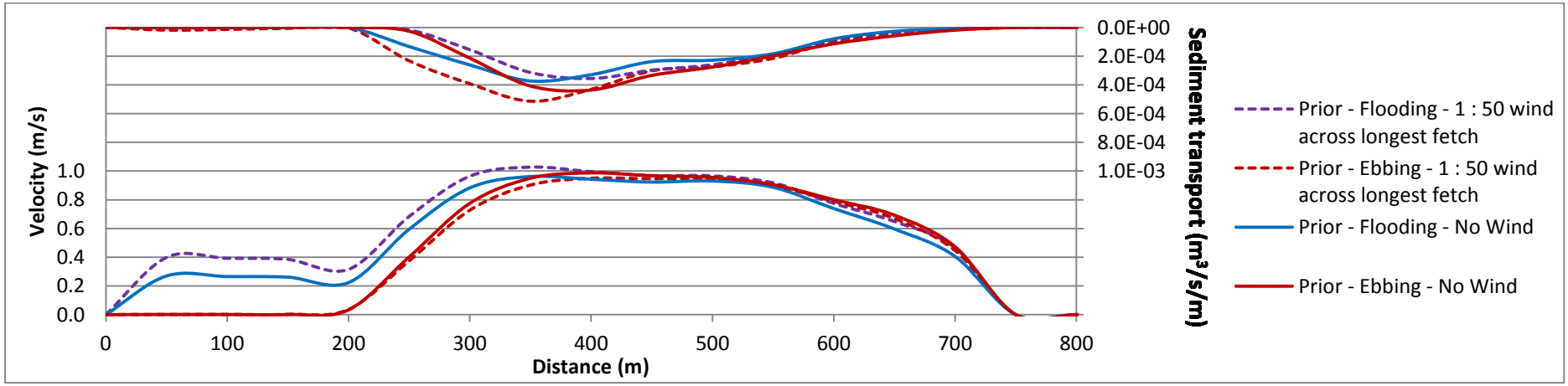

Figure H.4-28: Section L8 prior to construction including a 1 in 50 year wind across the longest fetch

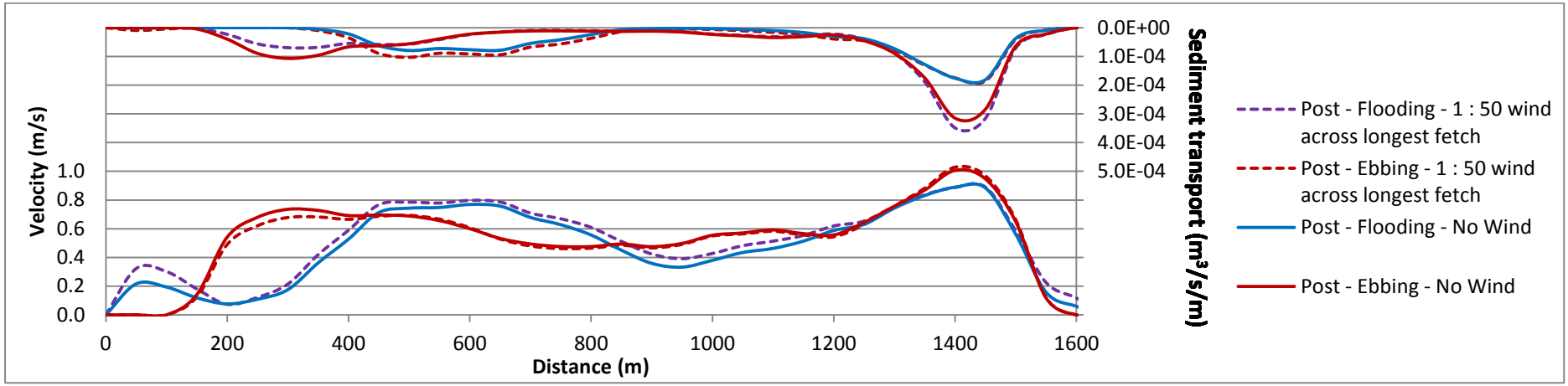

Figure H.4-29: Section L9 after the construction including a 1 in 50 year wind across the longest fetch

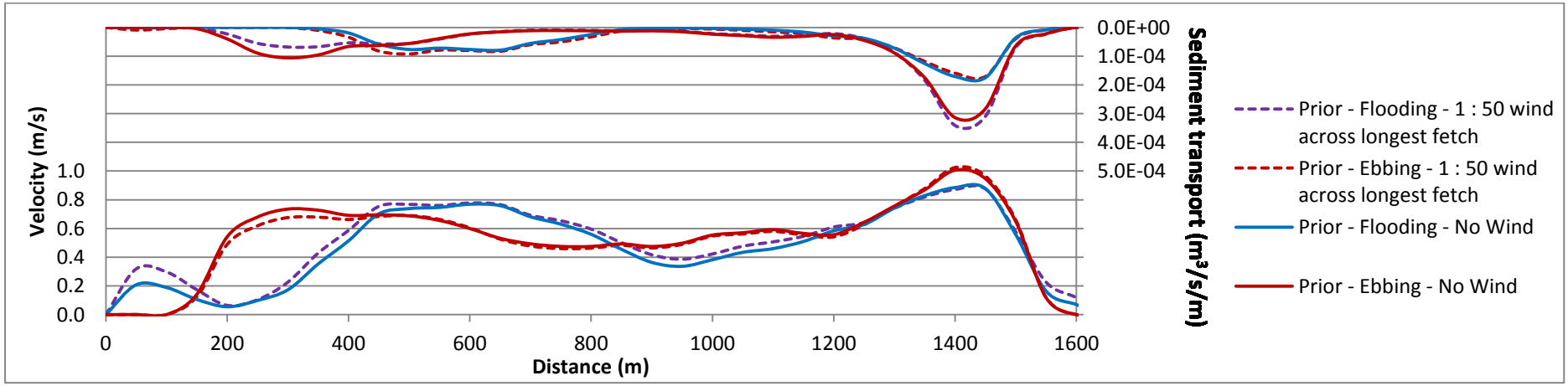

Figure H.4-30: Section L9 prior to construction including a 1 in 50 year wind across the longest fetch

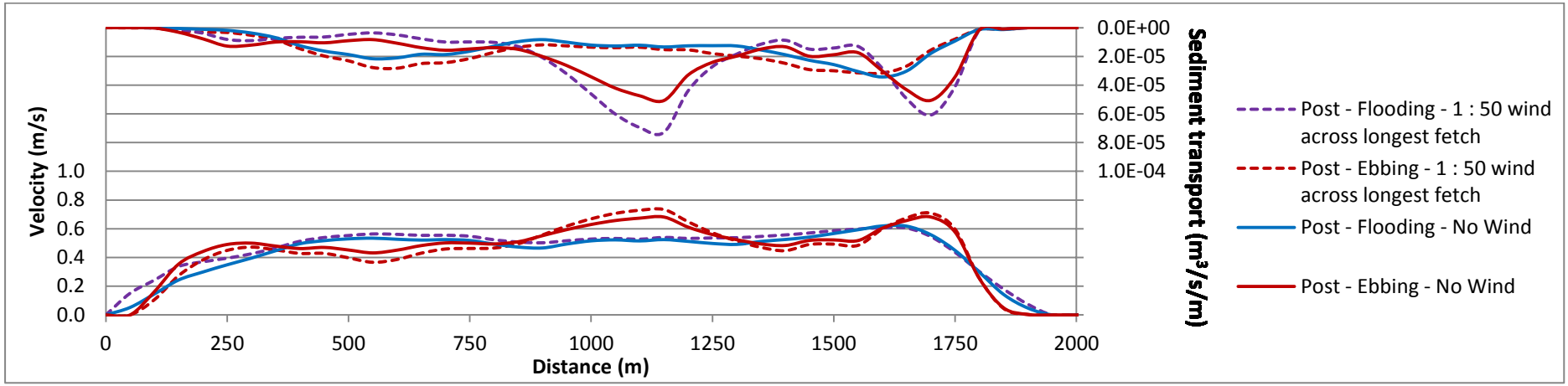

Figure H.4-31: Section L10 after the construction including a 1 in 50 year wind across the longest fetch

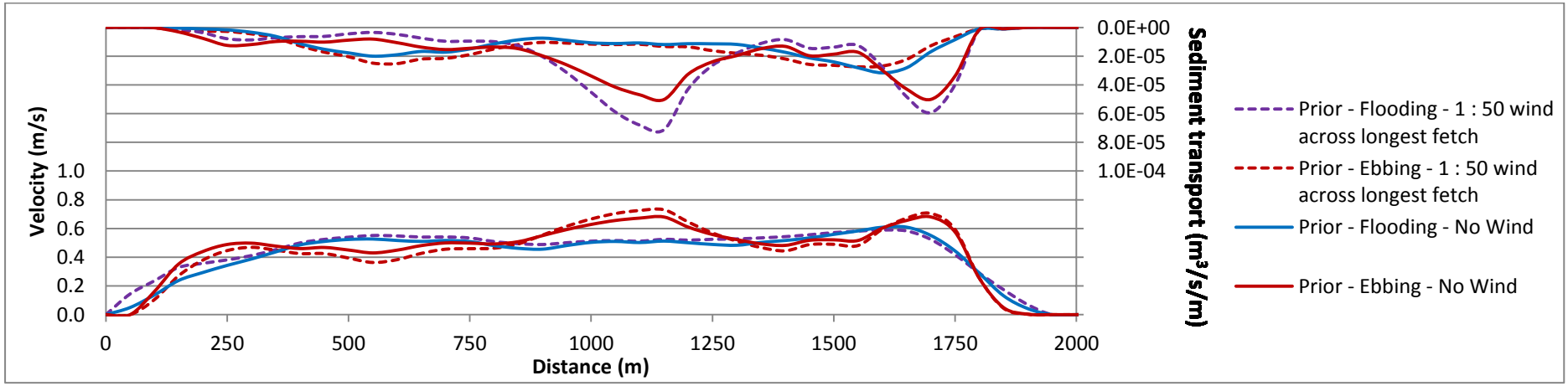

Figure H.4-32: Section L10 prior to construction including a 1 in 50 year wind across the longest fetch

APPENDIX H.5 TIDAL CONDITIONS INCLUDING 1 IN 100 YEAR WIND EVENT ACROSS THE LONGEST FETCH

LIST OF FIGURERS

Figure H.5-1: Section S1 after the construction including a 1 in 100 year wind across the longest fetch
Figure H.5-2: Section S1 prior to construction including a 1 in 100 year wind across the longest fetch
Figure H.5-3: Section S2 after the construction including a 1 in 100 year wind across the longest fetch
Figure H.5-4: Section S2 prior to construction including a 1 in 100 year wind across the longest fetch
Figure H.5-5: Section S3 after the construction including a 1 in 100 year wind across the longest fetch
Figure H.5-6: Section S3 prior to construction including a 1 in 100 year wind across the longest fetch
Figure H.5-7: Section S4 after the construction including a 1 in 100 year wind across the longest fetch
Figure H.5-8: Section S4 prior to construction including a 1 in 100 year wind across the longest fetch
Figure H.5-9: Section S5 after the construction including a 1 in 100 year wind across the longest fetch
Figure H.5-10: Section S5 prior to construction including a 1 in 100 year wind across the longest fetch
Figure H.5-11: Section S6 after the construction including a 1 in 100 year wind across the longest fetch
Figure H.5-12: Section S6 prior to construction including a 1 in 100 year wind across the longest fetch
Figure H.5-13: Section L1 after the construction including a 1 in 100 year wind across the longest fetch
Figure H.5-14: Section L1 prior to construction including a 1 in 100 year wind across the longest fetch
Figure H.5-15: Section L2 after the construction including a 1 in 100 year wind across the longest fetch
Figure H.5-16: Section L2 prior to construction including a 1 in 100 year wind across the longest fetch
Figure H.5-17: Section L3 after the construction including a 1 in 100 year wind across the longest fetch

Figure H.5-18: Section L3 prior to construction including a 1 in 100 year wind across the longest fetch
Figure H.5-19: Section L4 after the construction including a 1 in 100 year wind across the longest fetch
Figure H.5-20: Section L4 prior to construction including a 1 in 100 year wind across the longest fetch
Figure H.5-21: Section L5 after the construction including a 1 in 100 year wind across the longest fetch
Figure H.5-22: Section L5 prior to construction including a 1 in 100 year wind across the longest fetch
Figure H.5-23: Section L6 after the construction including a 1 in 100 year wind across the longest fetch
Figure H.5-24: Section L6 prior to construction including a 1 in 100 year wind across the longest fetch
Figure H.5-25: Section L7 after the construction including a 1 in 100 year wind across the longest fetch
Figure H.5-26: Section L7 prior to construction including a 1 in 100 year wind across the longest fetch
Figure H.5-27: Section L8 after the construction including a 1 in 100 year wind across the longest fetch
Figure H.5-28: Section L8 prior to construction including a 1 in 100 year wind across the longest fetch
Figure H.5-29: Section L9 after the construction including a 1 in 100 year wind across the longest fetch
Figure H.5-30: Section L9 prior to construction including a 1 in 100 year wind across the longest fetch
Figure H.5-31: Section L10 after the construction including a 1 in 100 year wind across the longest fetch
Figure H.5-32: Section L10 prior to construction including a 1 in 100 year wind across the longest fetch

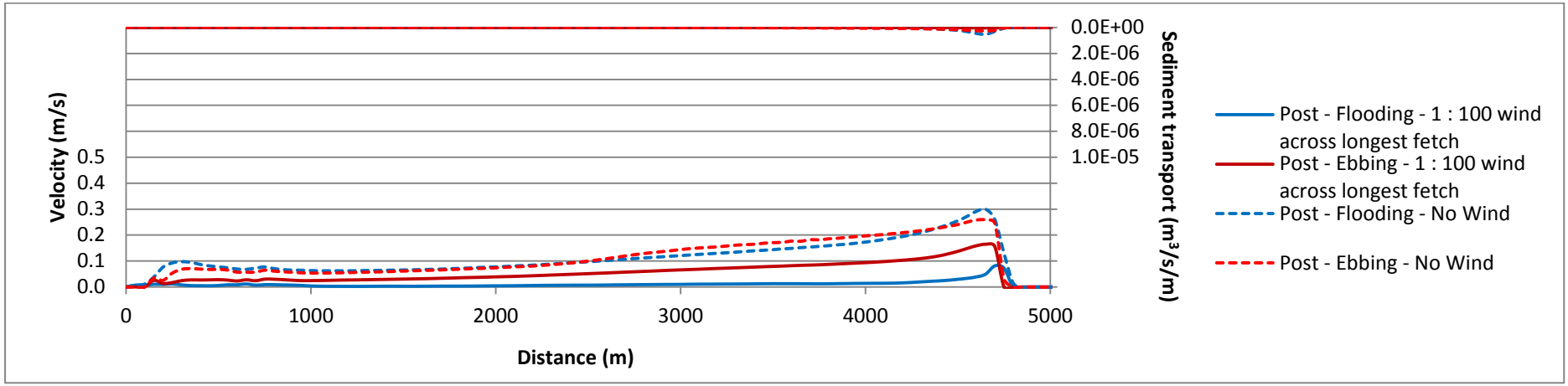

Figure H.5-1: Section S1 after the construction including a 1 in 100 year wind across the longest fetch

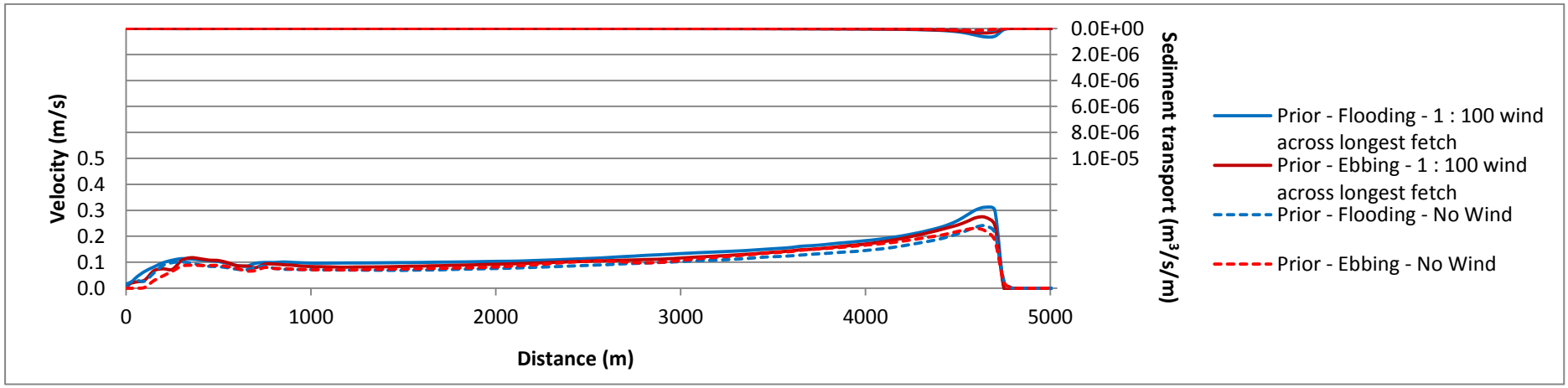

Figure H.5-2: Section S1 prior to construction including a 1 in 100 year wind across the longest fetch

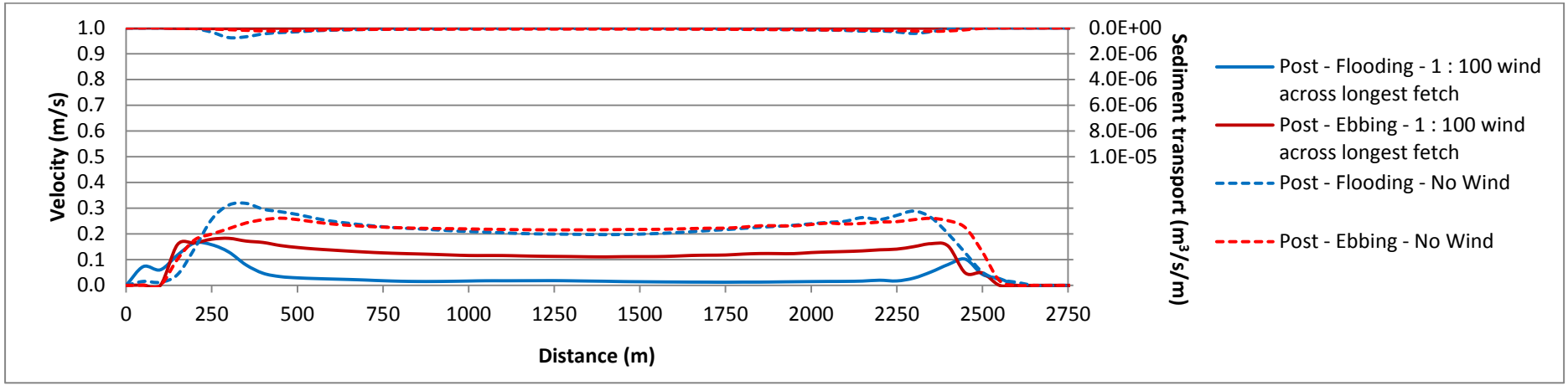

Figure H.5-3: Section S2 after the construction including a 1 in 100 year wind across the longest fetch

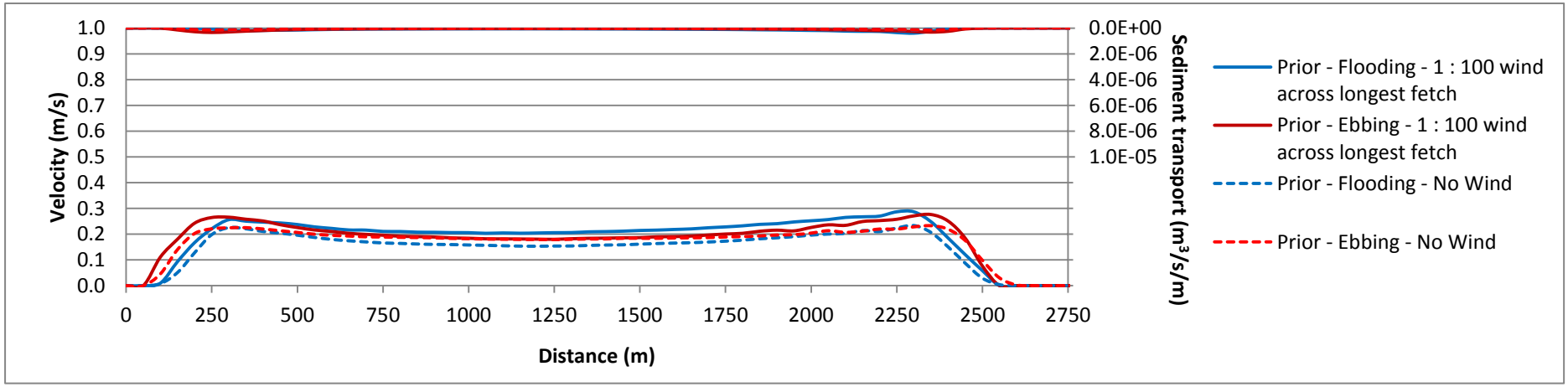

Figure H.5-4: Section S2 prior to construction including a 1 in 100 year wind across the longest fetch

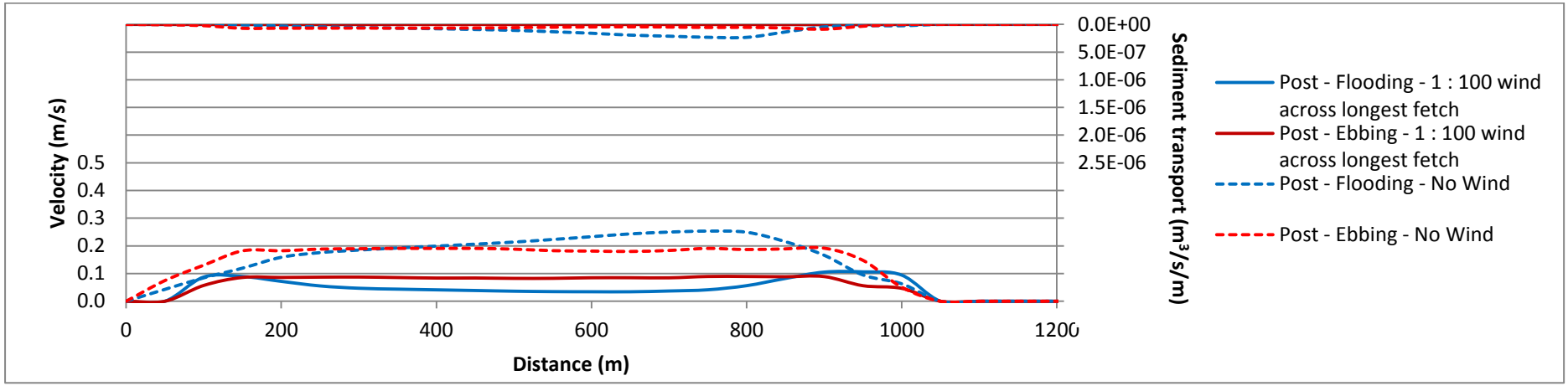

Figure H.5-5: Section S3 after the construction including a 1 in 100 year wind across the longest fetch

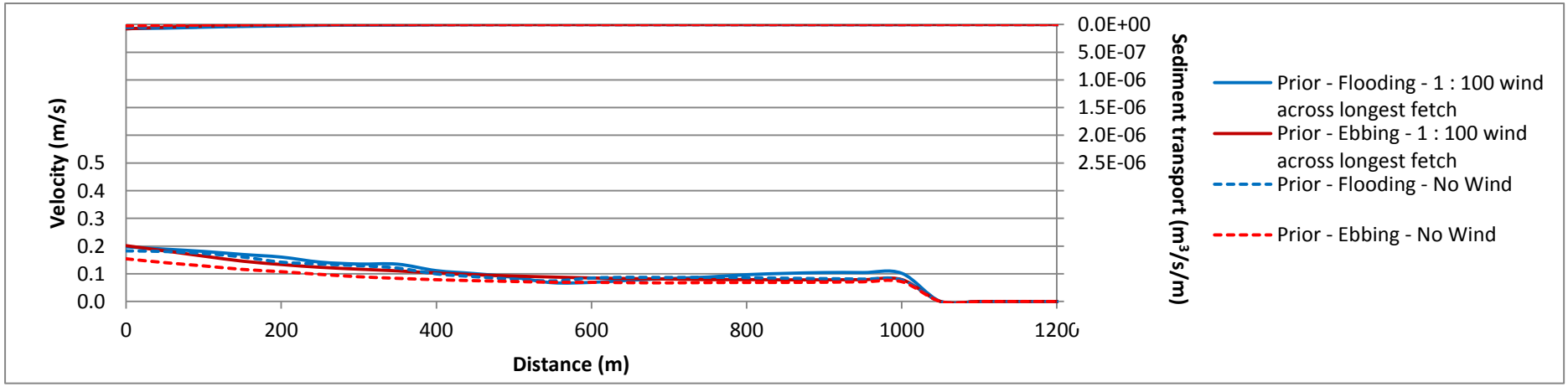

Figure H.5-6: Section S3 prior to construction including a 1 in 100 year wind across the longest fetch

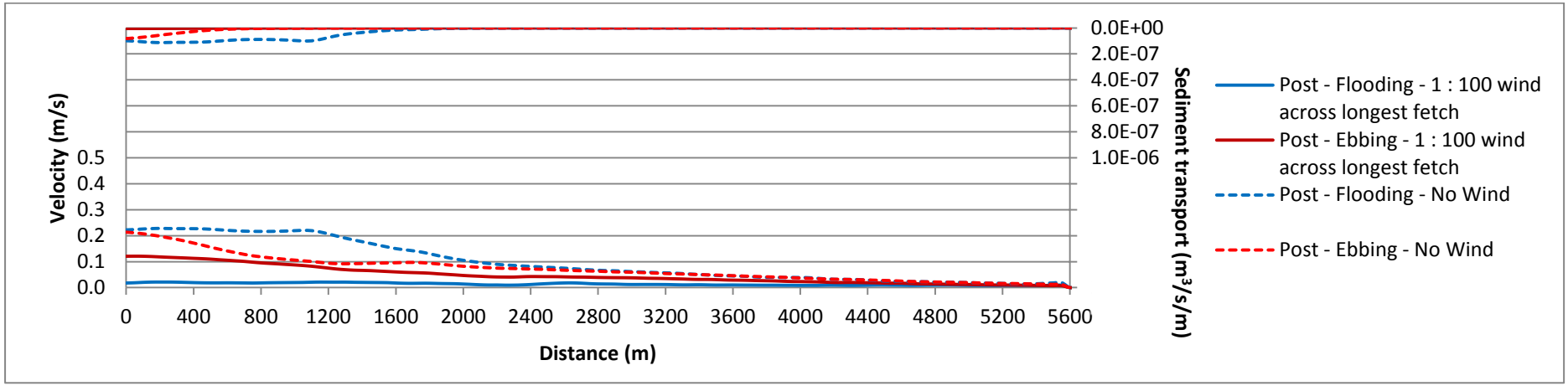

Figure H.5-7: Section S4 after the construction including a 1 in 100 year wind across the longest fetch

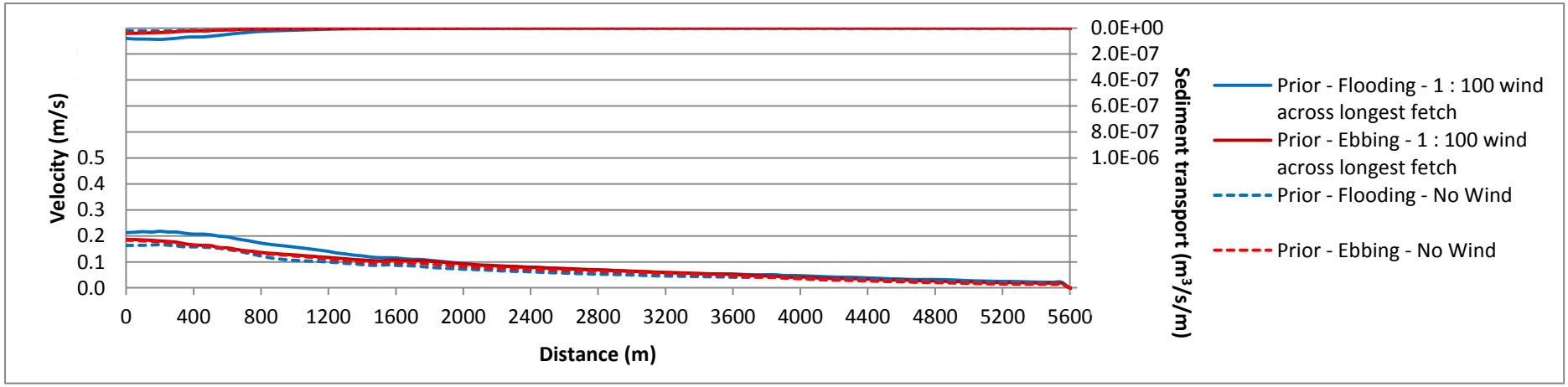

Figure H.5-8: Section S4 prior to construction including a 1 in 100 year wind across the longest fetch

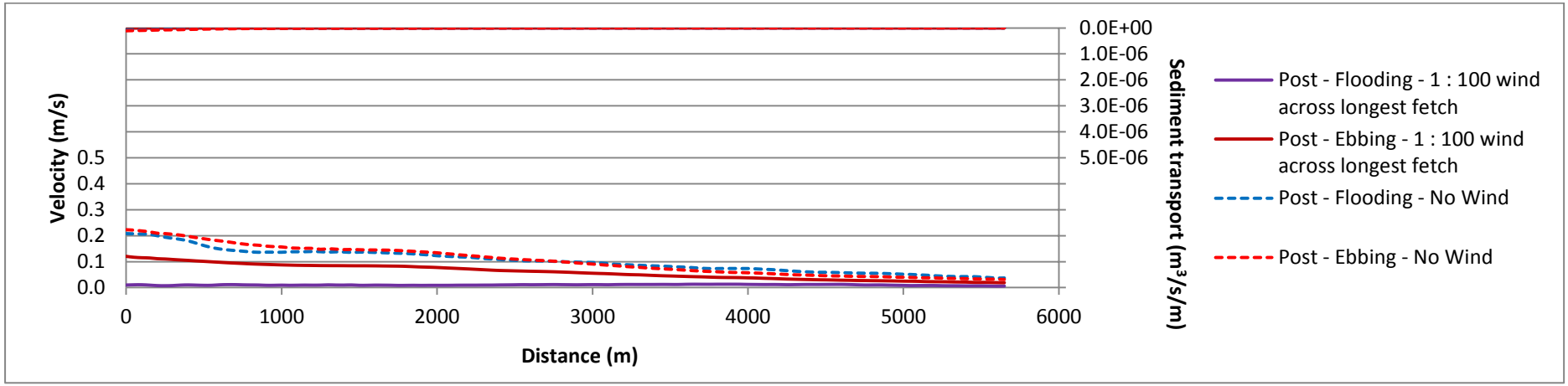

Figure H.5-9: Section S5 after the construction including a 1 in 100 year wind across the longest fetch

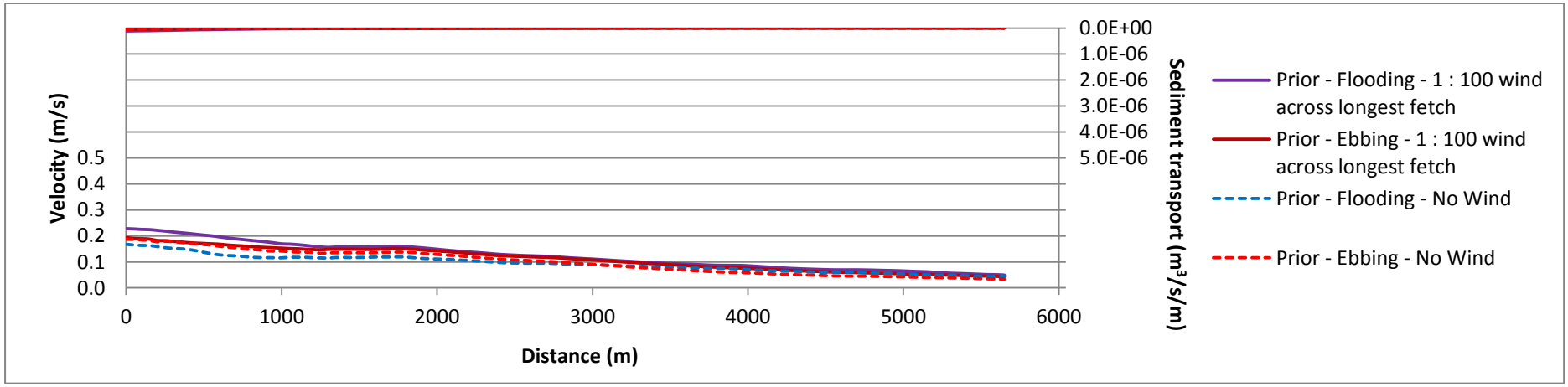

Figure H.5-10: Section S5 prior to construction including a 1 in 100 year wind across the longest fetch

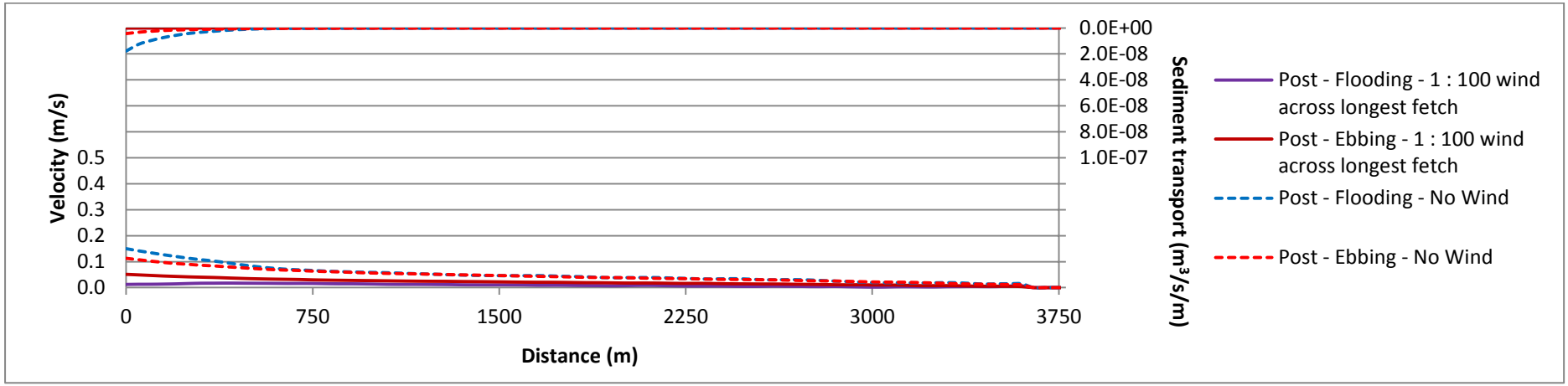

Figure H.5-11: Section S6 after the construction including a 1 in 100 year wind across the longest fetch

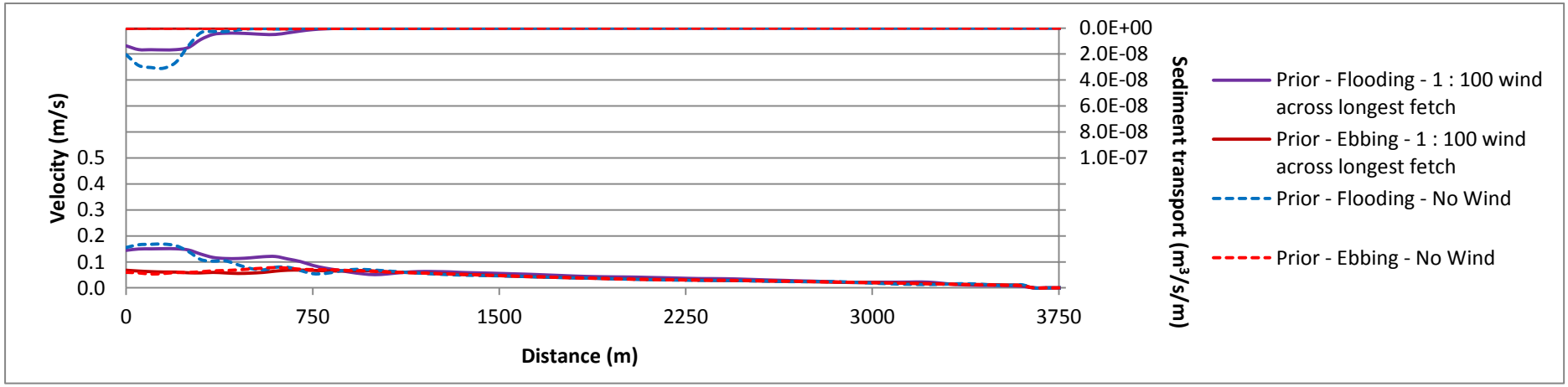

Figure H.5-12: Section S6 prior to construction including a 1 in 100 year wind across the longest fetch

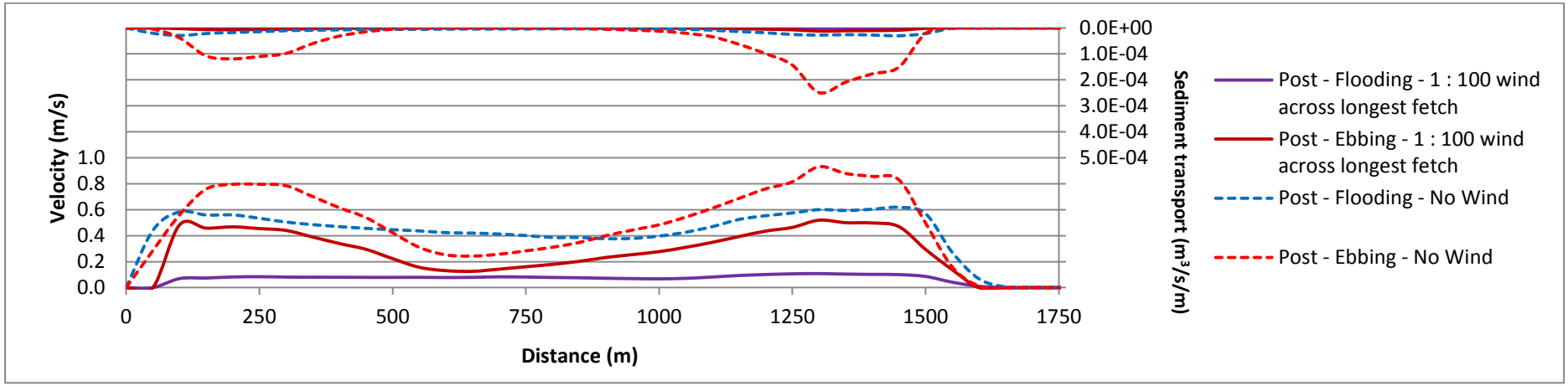

Figure H.5-13: Section L1 after the construction including a 1 in 100 year wind across the longest fetch

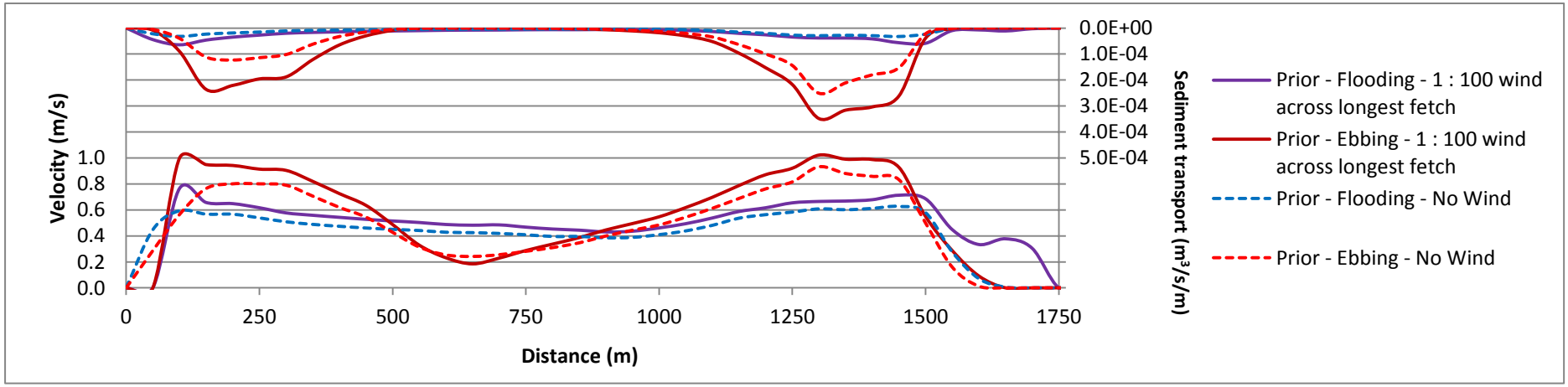

Figure H.5-14: Section L1 prior to construction including a 1 in 100 year wind across the longest fetch

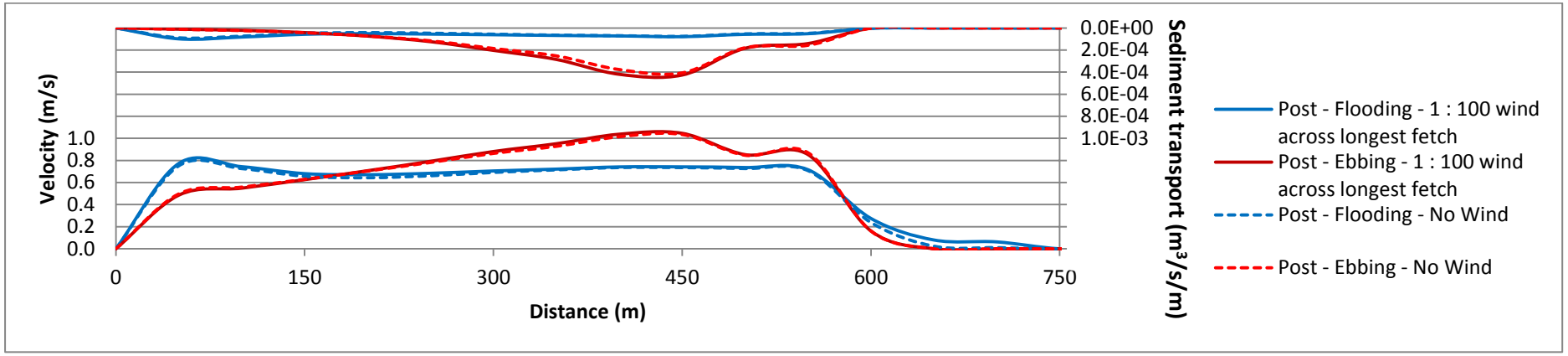

Figure H.5-16: Section L2 after the construction including a 1 in 100 year wind across the longest fetch

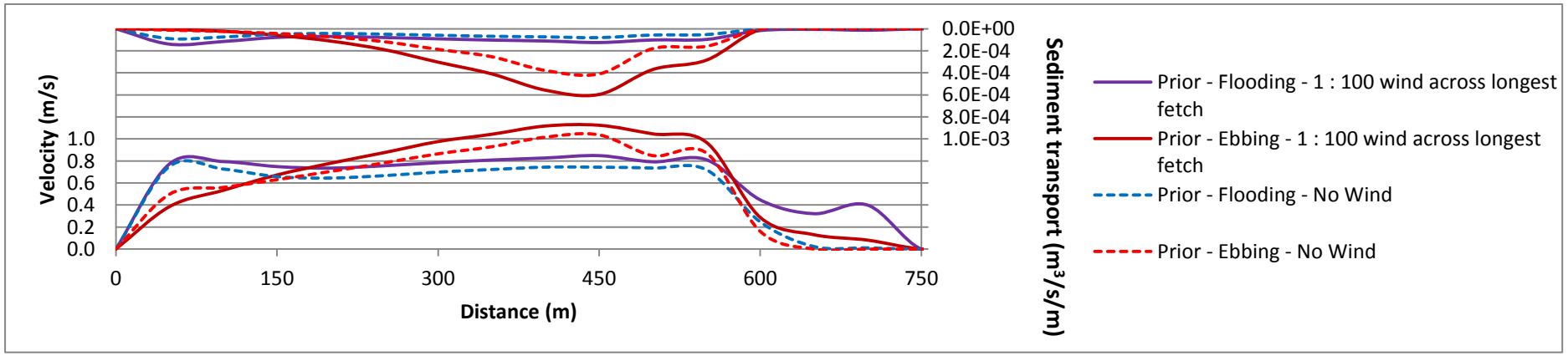

Figure H.5-15: Section L2 prior the construction including a 1 in 100 year wind across the longest fetch

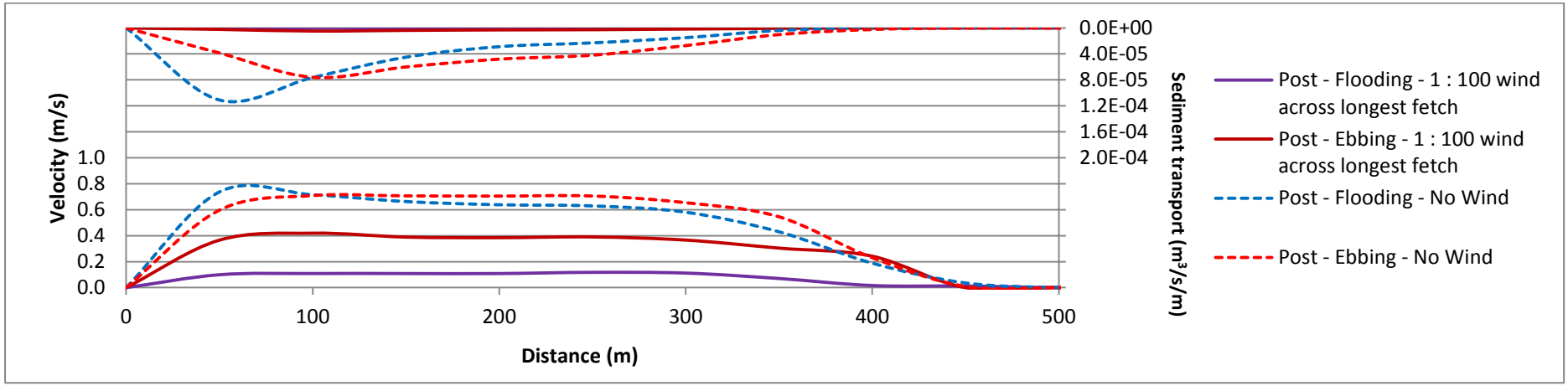

Figure H.5-17: Section L3 after the construction including a 1 in 100 year wind across the longest fetch

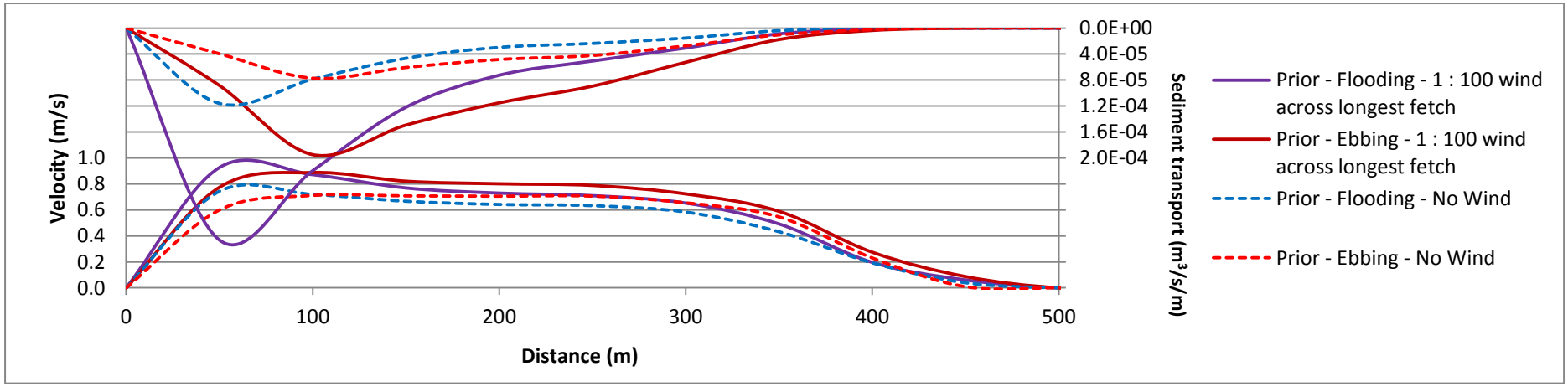

Figure H.5-18: Section L3 prior to construction including a 1 in 100 year wind across the longest fetch

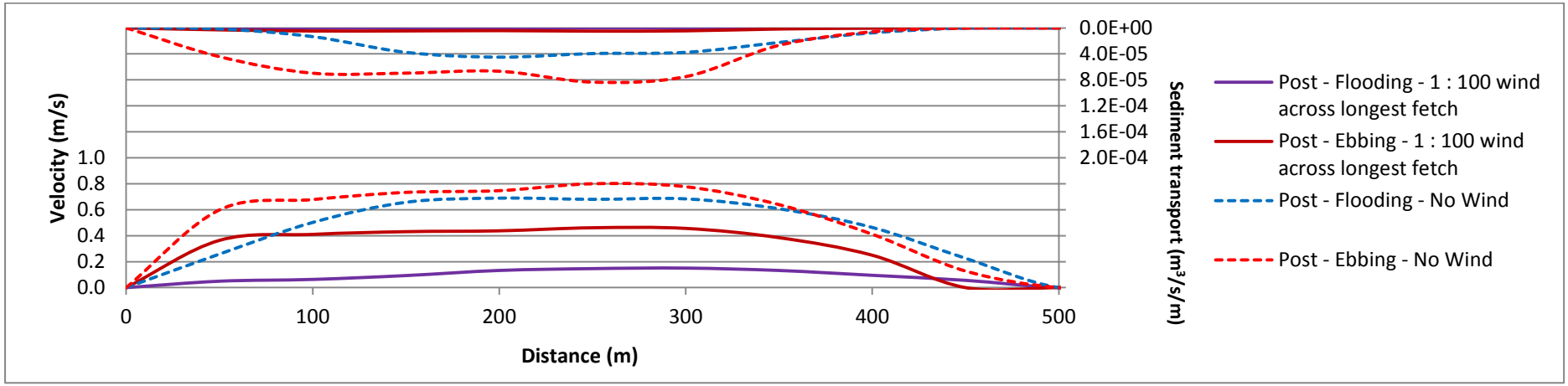

Figure H.5-19: Section L4 after the construction including a 1 in 100 year wind across the longest fetch

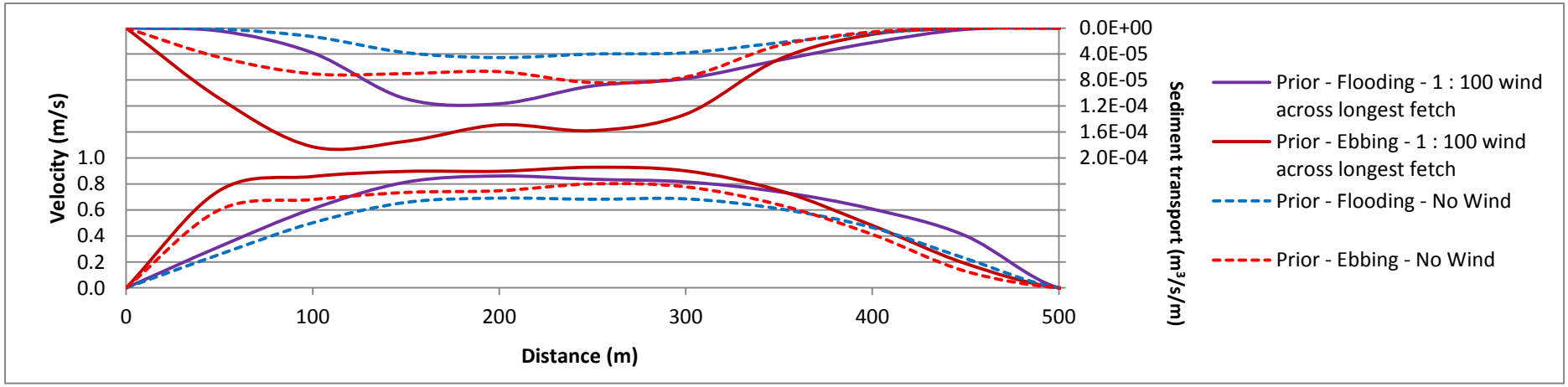

Figure H.5-20: Section L4 prior to construction including a 1 in 100 year wind across the longest fetch

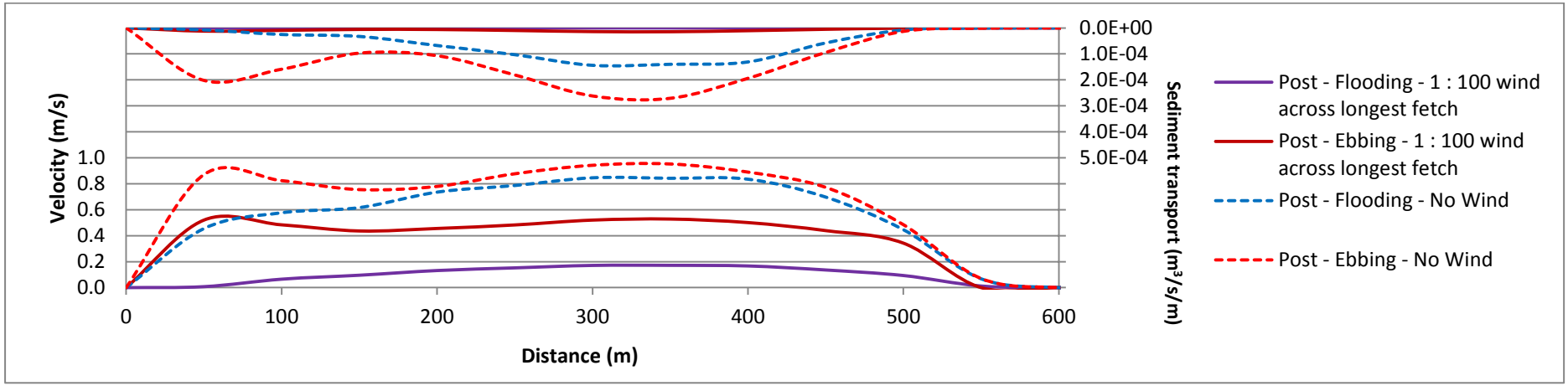

Figure H.5-21: Section L5 after the construction including a 1 in 100 year wind across the longest fetch

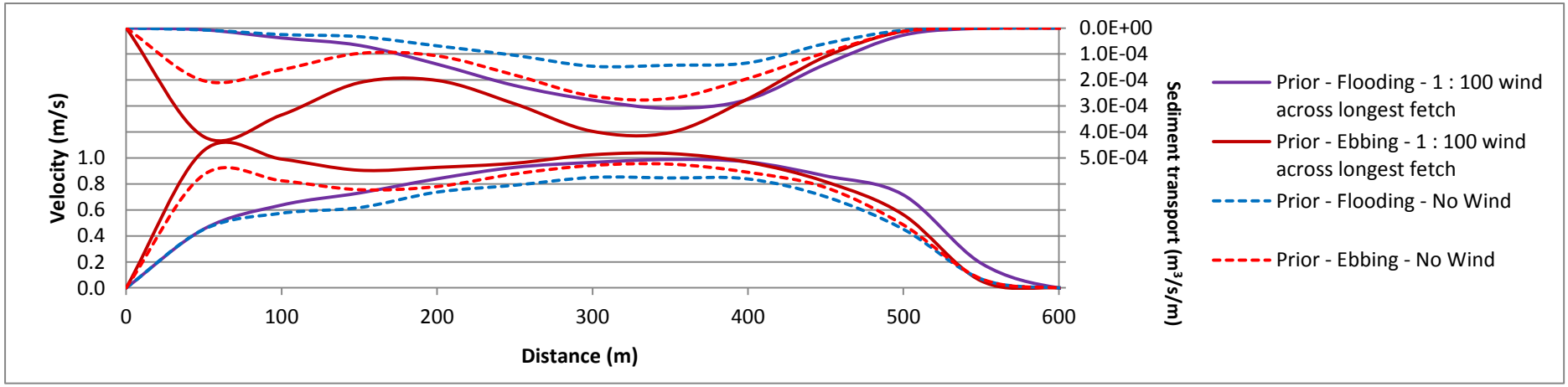

Figure H.5-22: Section L5 prior to construction including a 1 in 100 year wind across the longest fetch

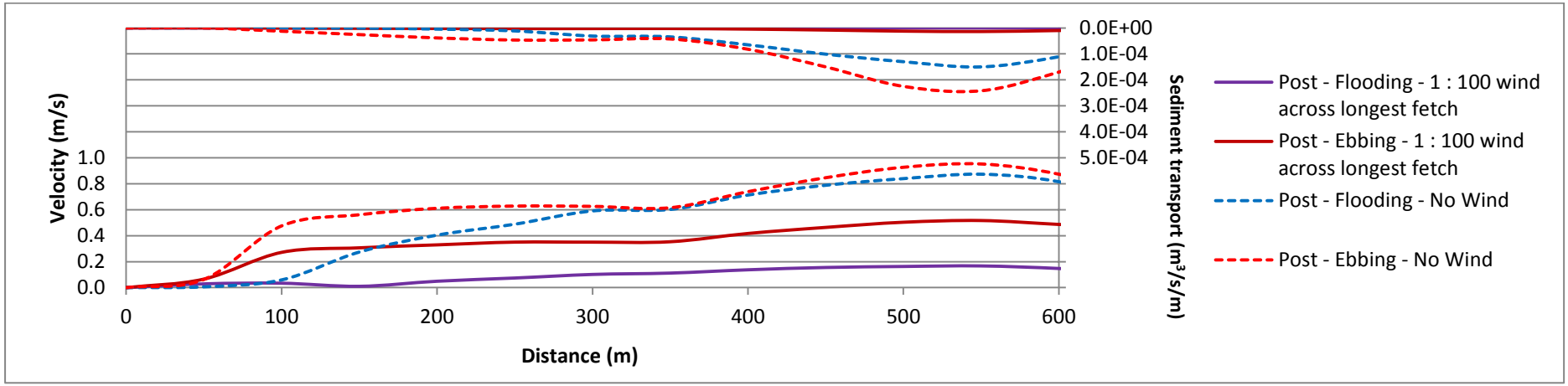

Figure H.5-23: Section L6 after the construction including a 1 in 100 year wind across the longest fetch

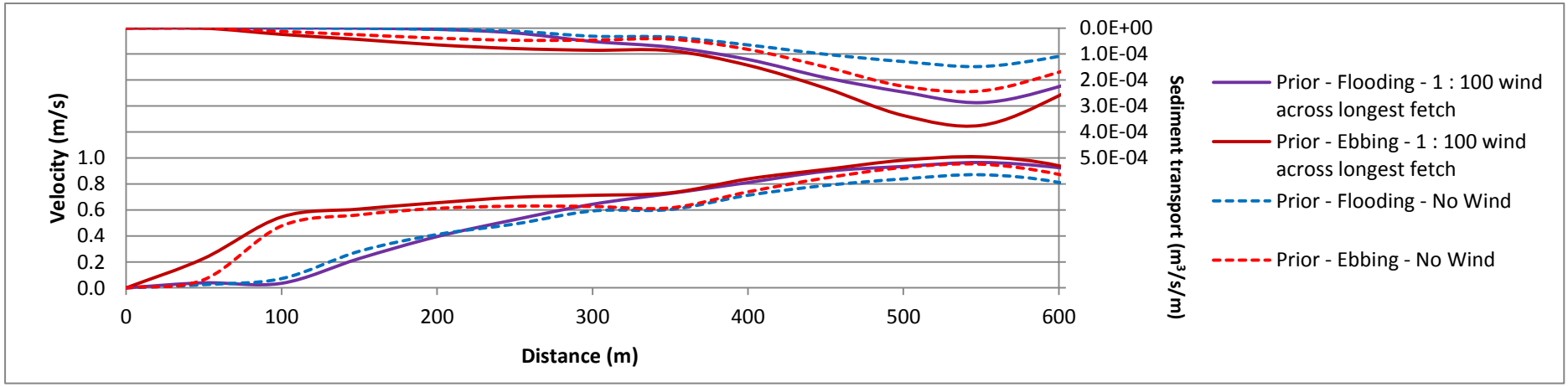

Figure H.5-24: Section L6 prior to construction including a 1 in 100 year wind across the longest fetch

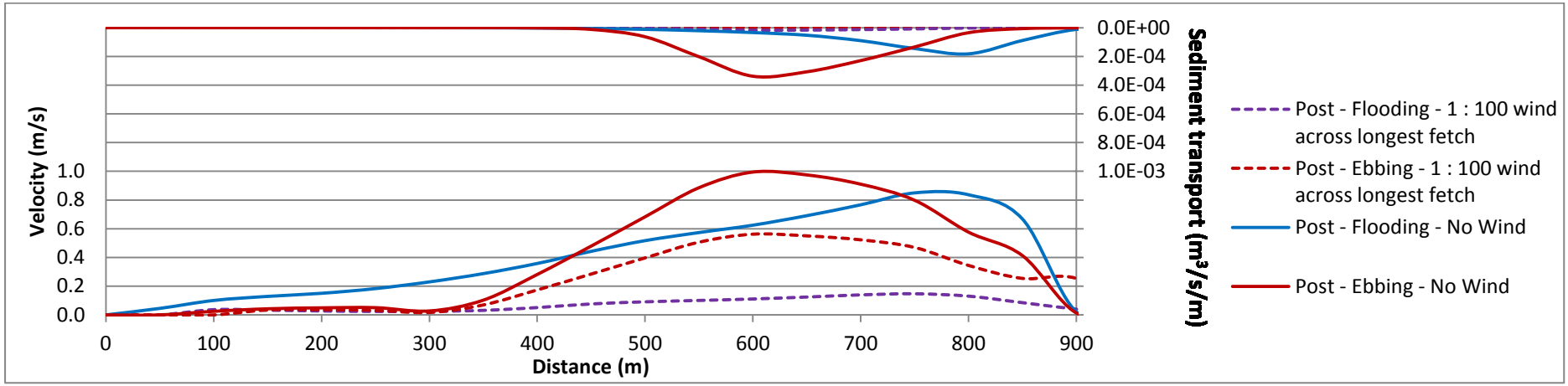

Figure H.5-25: Section L7 after the construction including a 1 in 100 year wind across the longest fetch

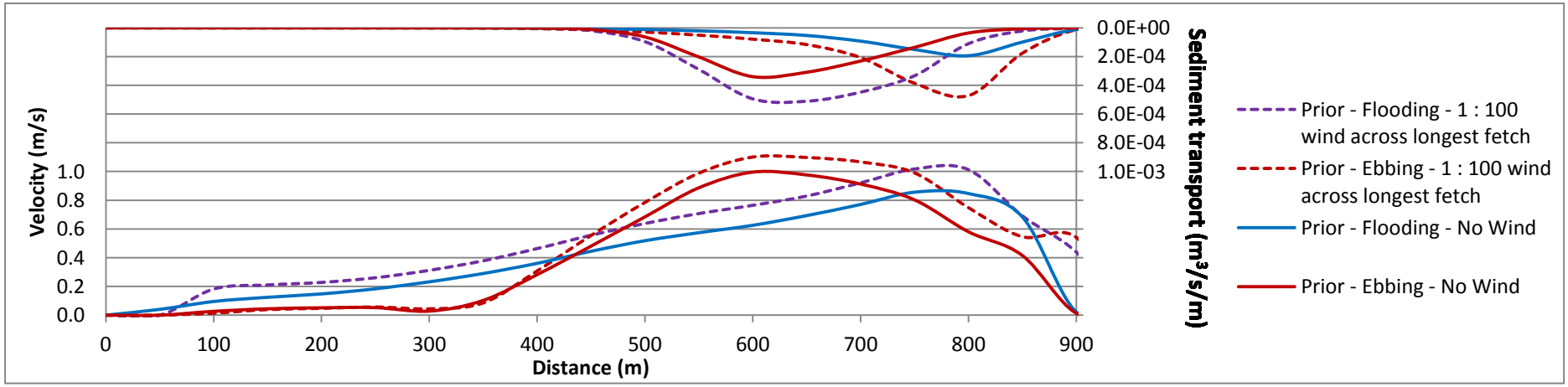

Figure H.5-26: Section L7 prior to construction including a 1 in 100 year wind across the longest fetch

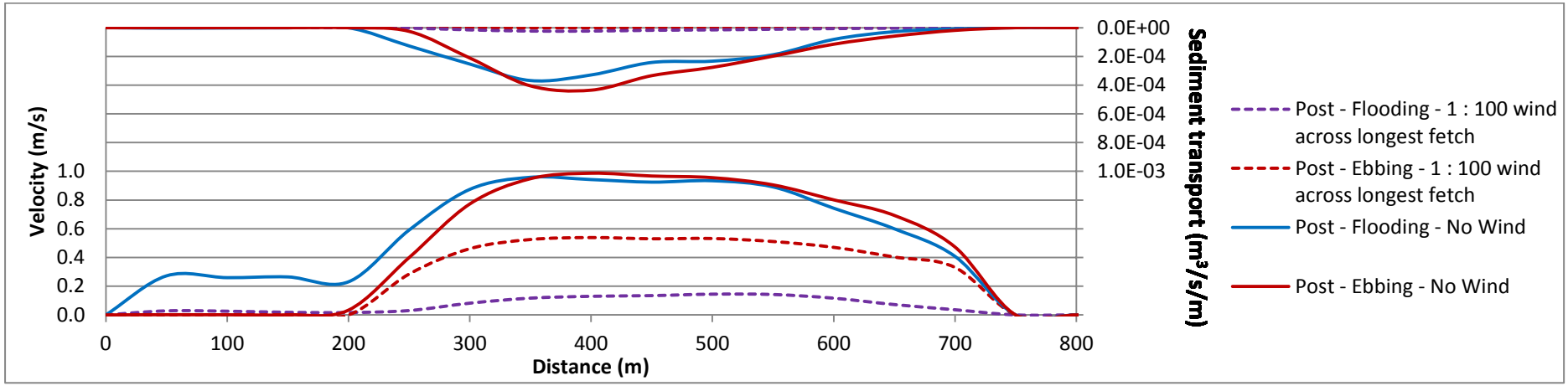

Figure H.5-27: Section L8 after the construction including a 1 in 100 year wind across the longest fetch

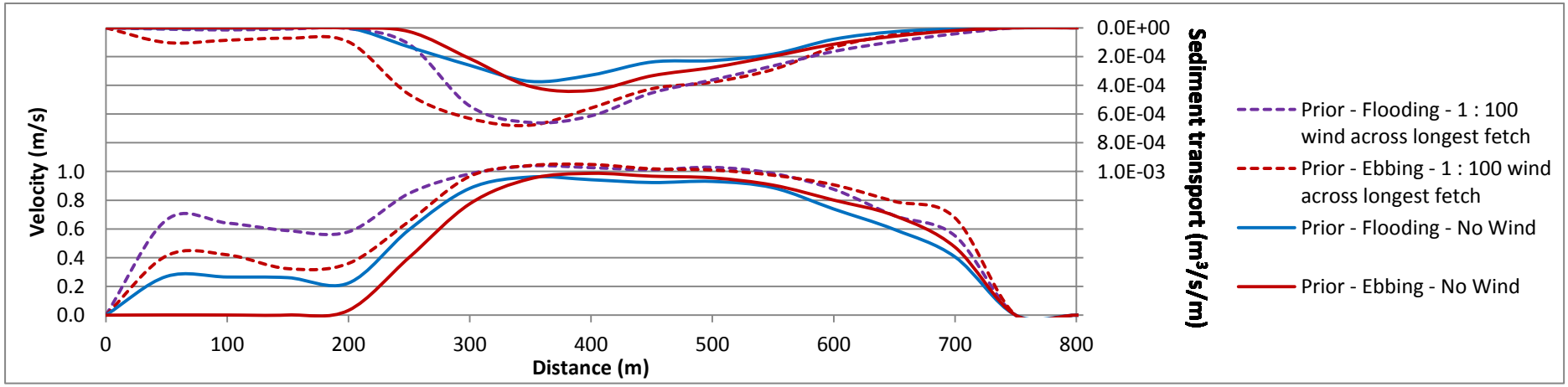

Figure H.5-28: Section L8 prior to construction including a 1 in 100 year wind across the longest fetch

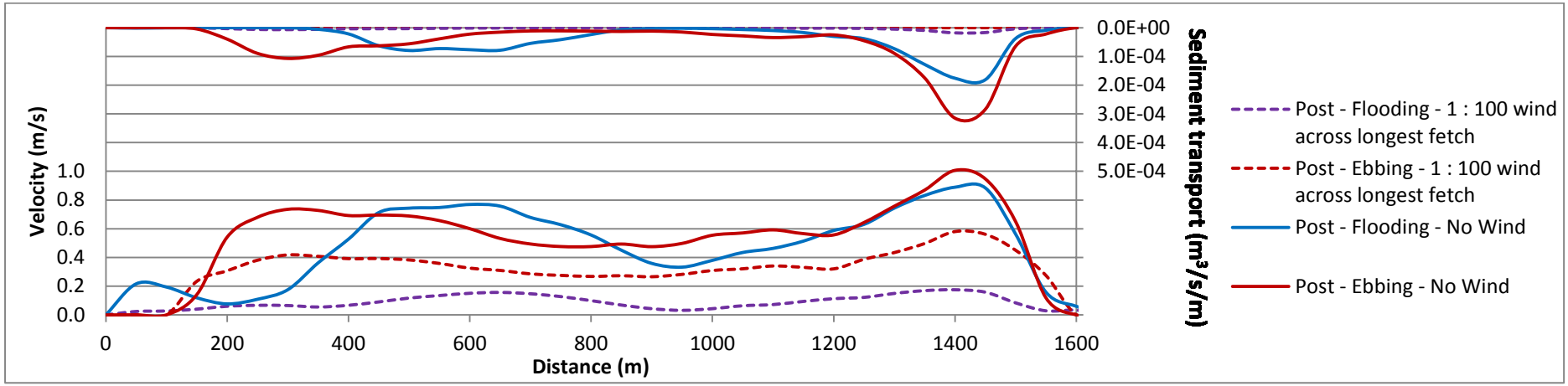

Figure H.5-29: Section L9 after the construction including a 1 in 100 year wind across the longest fetch

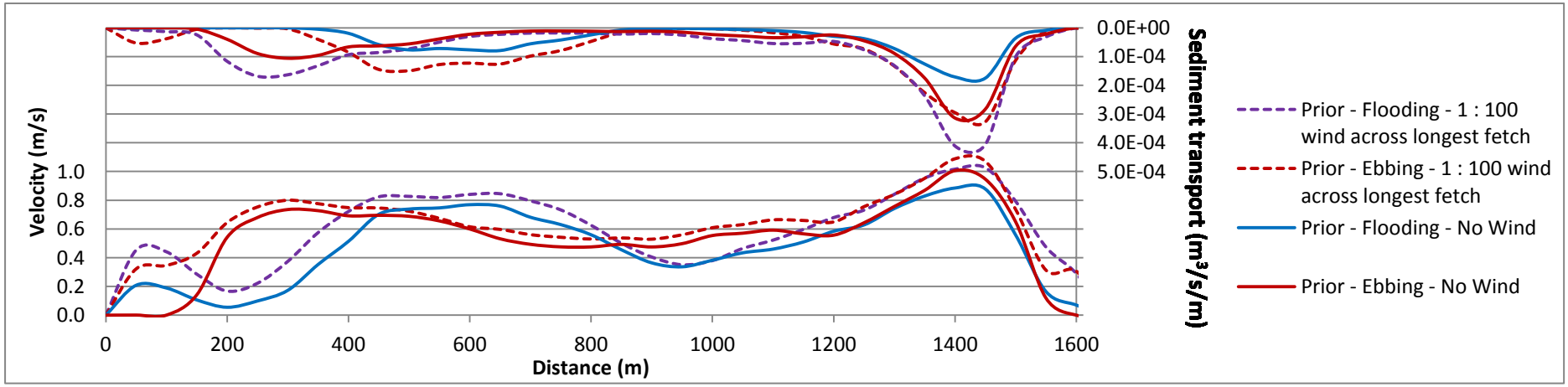

Figure H.5-30: Section L9 prior to construction including a 1 in 100 year wind across the longest fetch

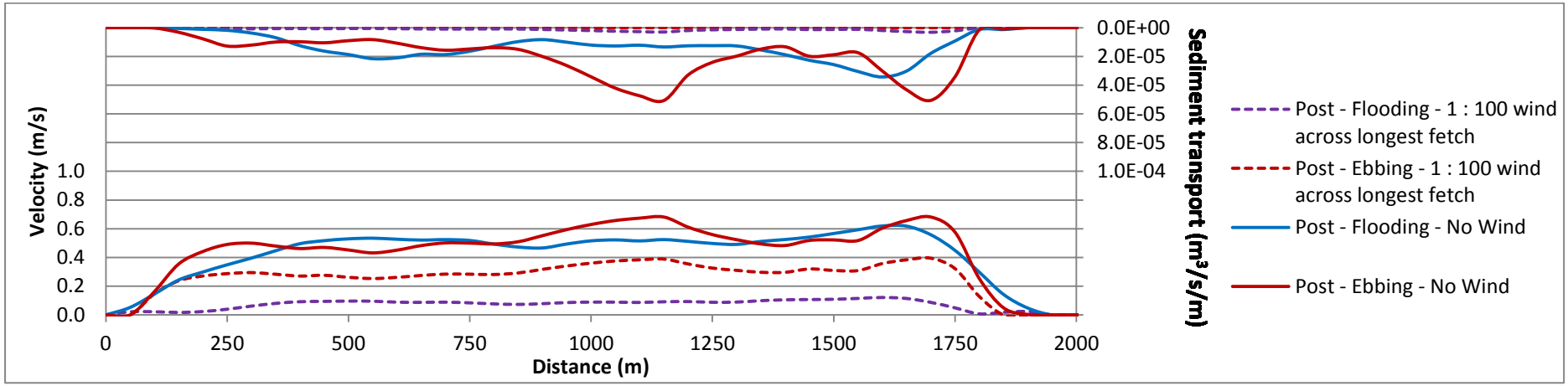

Figure H.5-31: Section L10 after the construction including a 1 in 100 year wind across the longest fetch

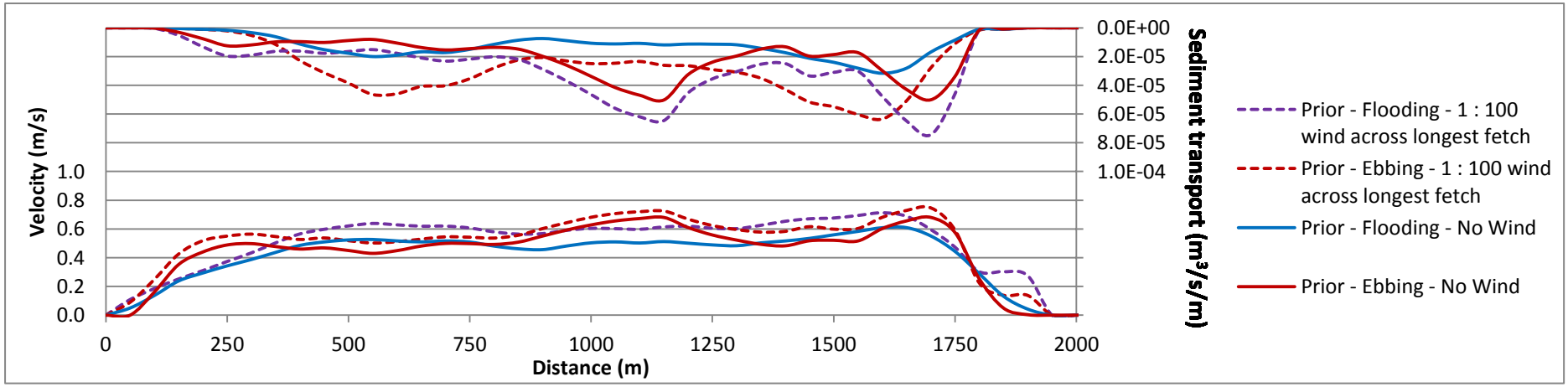

Figure H.5-32: Section L10 prior to construction including a 1 in 100 year wind across the longest fetch

APPENDIX H.6 1 IN 50 YEAR TIDAL STORM

LIST OF FIGURERS

Figure H.6-1: Section S1 after the construction including a 1 in 50 year tidal storm
Figure H.6-2: Section S1 prior to construction including a 1 in 50 year tidal storm
Figure H.6-3: Section S2 after the construction including a 1 in 50 year tidal storm
Figure H.6-4: Section S2 prior to construction including a 1 in 50 year tidal storm
Figure H.6-5: Section S3 after the construction including a 1 in 50 year tidal storm
Figure H.6-6: Section S3 prior to construction including a 1 in 50 year tidal storm
Figure H.6-7: Section S4 after the construction including a 1 in 50 year tidal storm
Figure H.6-8: Section S4 prior to construction including a 1 in 50 year tidal storm
Figure H.6-9: Section S5 after the construction including a 1 in 50 year tidal storm
Figure H.6-10: Section S5 prior to construction including a 1 in 50 year tidal storm
Figure H.6-11: Section S6 after the construction including a 1 in 50 year tidal storm
Figure H.6-12: Section S6 prior to construction including a 1 in 50 year tidal storm
Figure H.6-13: Section L1 after the construction including a 1 in 50 year tidal storm
Figure H.6-14: Section L1 prior to construction including a 1 in 50 year tidal storm
Figure H.6-15: Section L2 after the construction including a 1 in 50 year tidal storm
Figure H.6-16: Section L2 prior to construction including a 1 in 50 year tidal storm
Figure H.6-17: Section L3 after the construction including a 1 in 50 year tidal storm
Figure H.6-18: Section L3 prior to construction including a 1 in 50 year tidal storm
Figure H.6-19: Section L4 after the construction including a 1 in 50 year tidal storm
Figure H.6-20: Section L4 prior to construction including a 1 in 50 year tidal storm
Figure H.6-21: Section L5 after the construction including a 1 in 50 year tidal storm
Figure H.6-22: Section L5 prior to construction including a 1 in 50 year tidal storm
Figure H.6-23: Section L6 after the construction including a 1 in 50 year tidal storm
Figure H.6-24: Section L6 prior to construction including a 1 in 50 year tidal storm
Figure H.6-25: Section L7 after the construction including a 1 in 50 year tidal storm
Figure H.6-26: Section L7 prior to construction including a 1 in 50 year tidal storm
Figure H.6-27: Section L8 after the construction including a 1 in 50 year tidal storm
Figure H.6-28: Section L8 prior to construction including a 1 in 50 year tidal storm
Figure H.6-29: Section L9 after the construction including a 1 in 50 year tidal storm
Figure H.6-30: Section L9 prior to construction including a 1 in 50 year tidal storm
Figure H.6-31: Section L10 after the construction including a 1 in 50 year tidal storm
Figure H.6-32: Section L10 prior to construction including a 1 in 50 year tidal storm

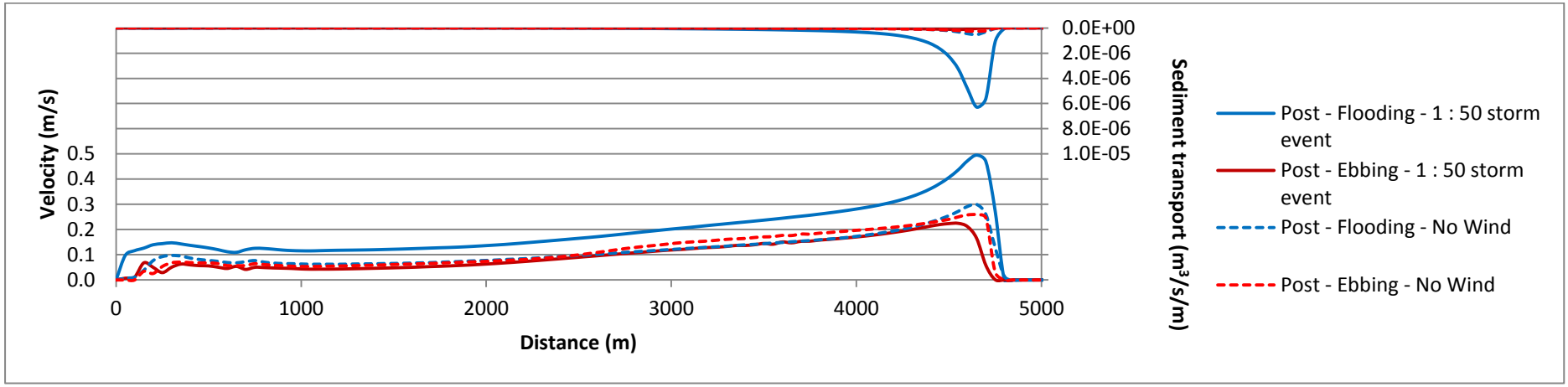

Figure H.6-1: Section S1 after the construction including a 1 in 50 year tidal storm

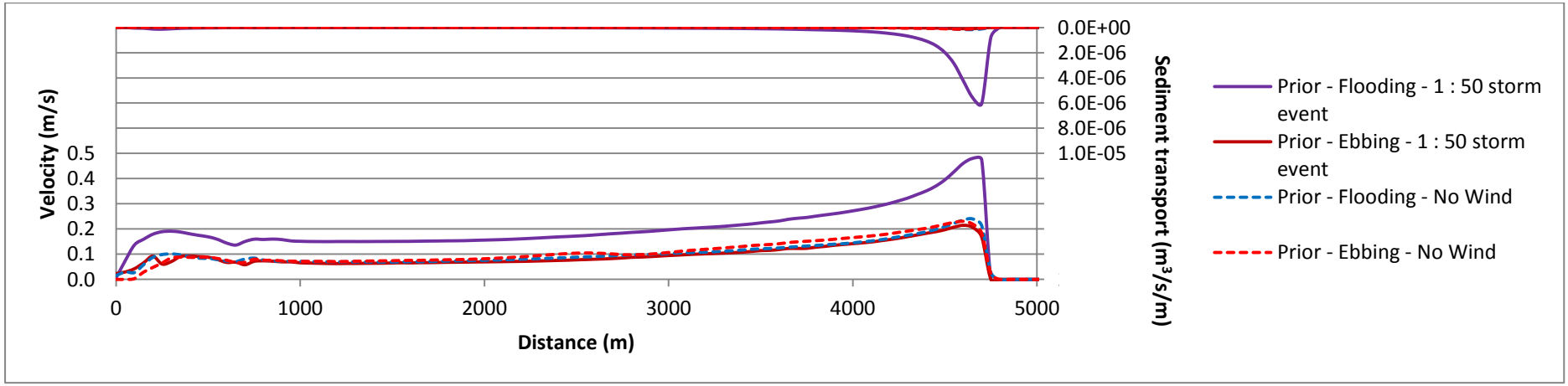

Figure H.6-2: Section S1 prior to construction including a 1 in 50 year tidal storm

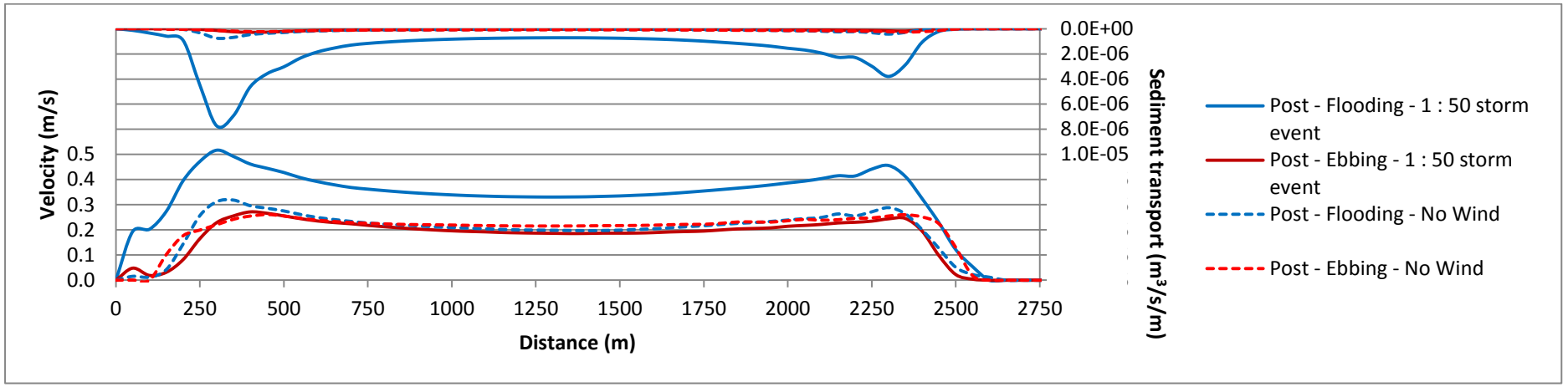

Figure H.6-3: Section S2 after the construction including a 1 in 50 year tidal storm

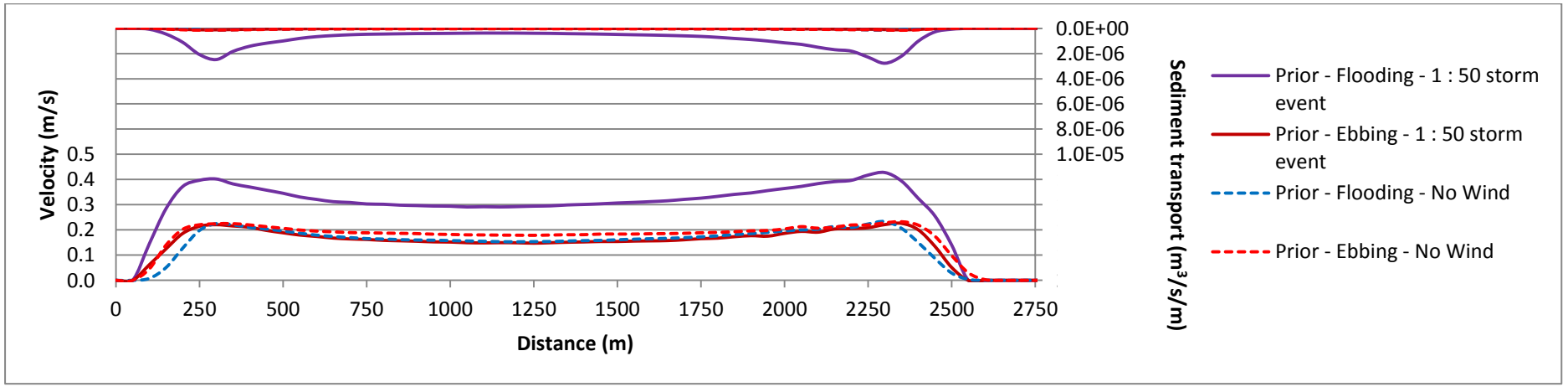

Figure H.6-4: Section S2 prior to construction including a 1 in 50 year tidal storm

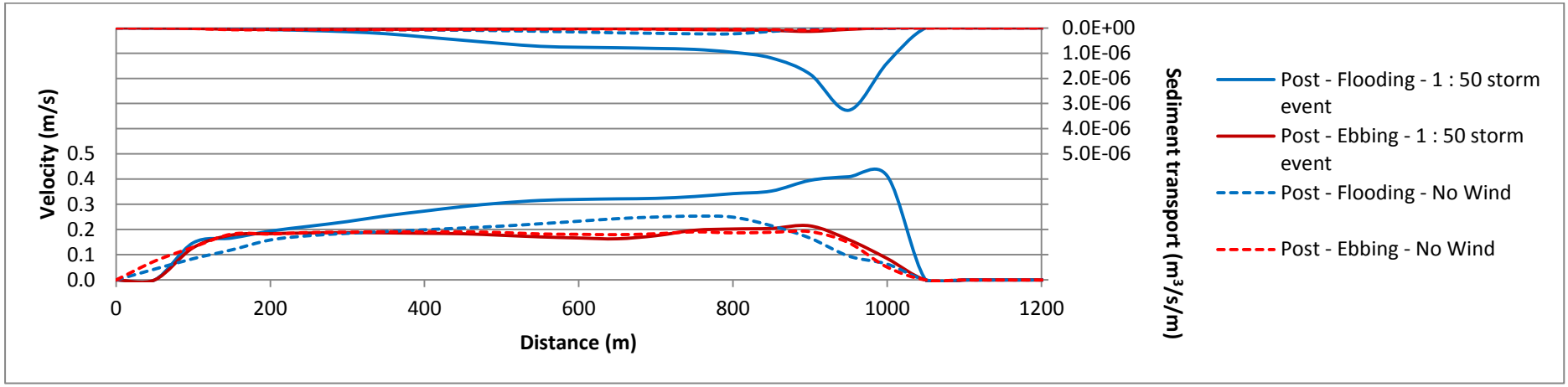

Figure H.6-5: Section S3 after the construction including a 1 in 50 year tidal storm

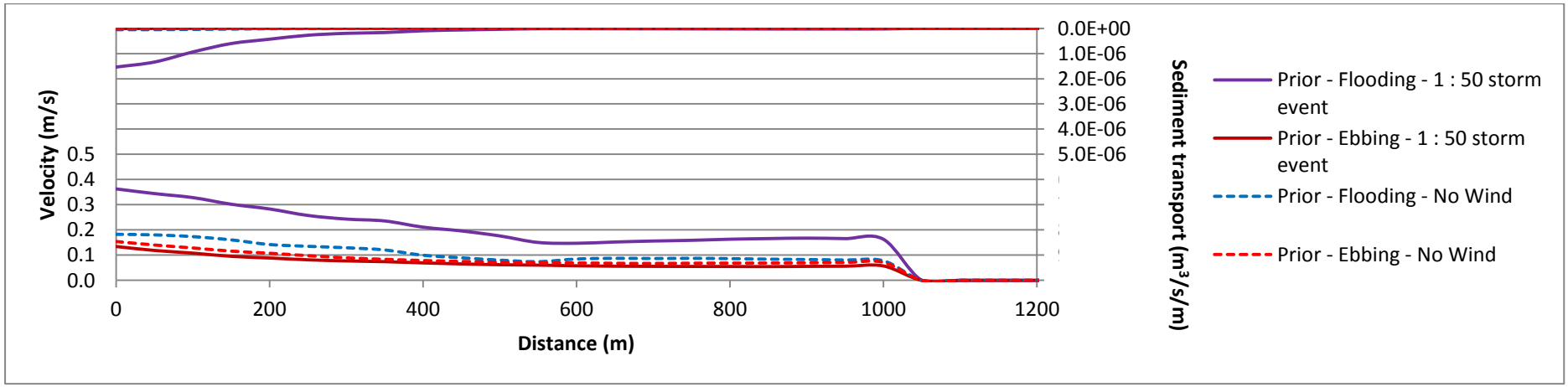

Figure H.6-6: Section S3 prior to construction including a 1 in 50 year tidal storm

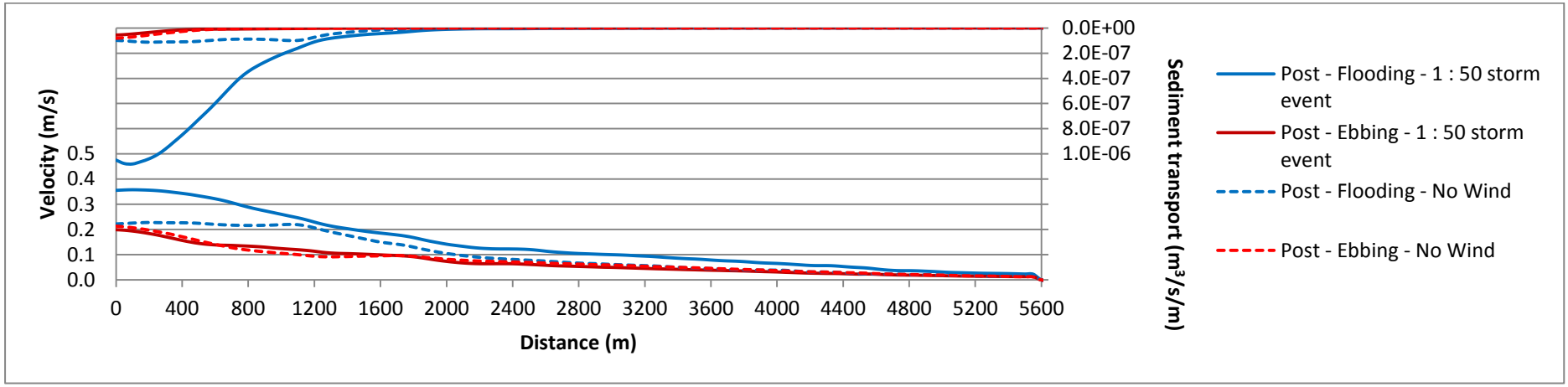

Figure H.6-7: Section S4 after the construction including a 1 in 50 year tidal storm

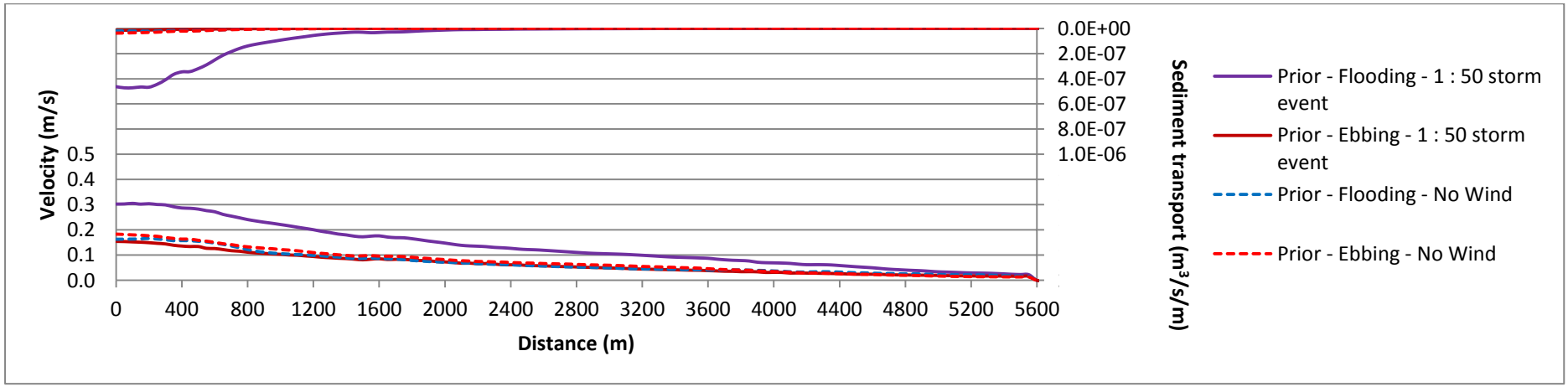

Figure H.6-8: Section S4 prior to construction including a 1 in 50 year tidal storm

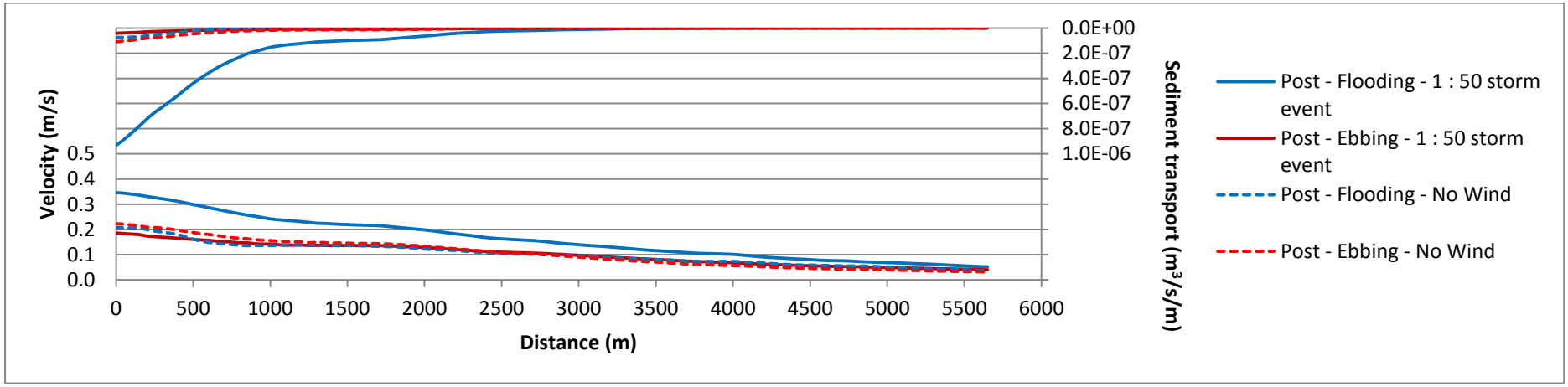

Figure H.6-9: Section S5 after the construction including a 1 in 50 year tidal storm

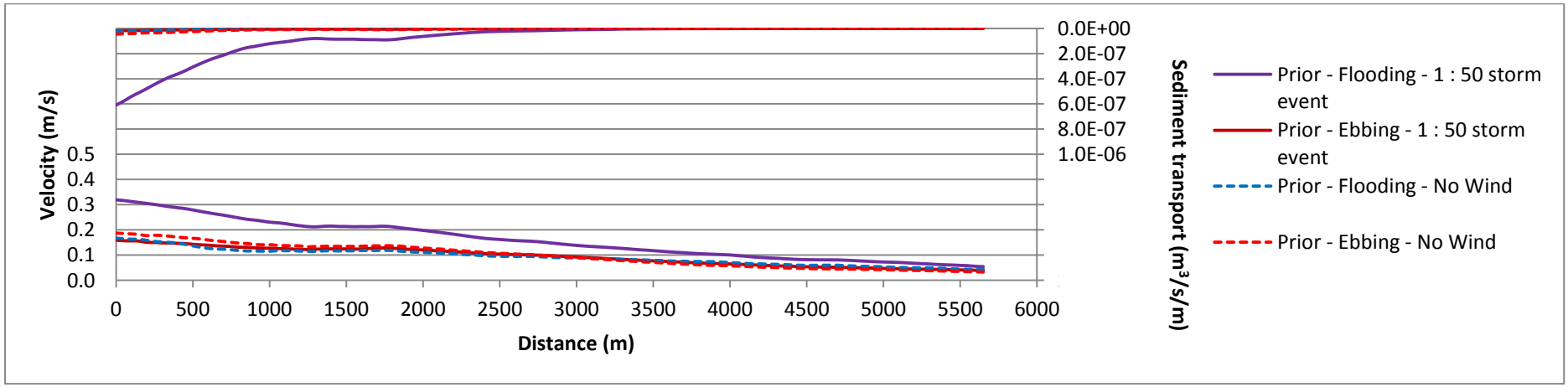

Figure H.6-10: Section S5 prior to construction including a 1 in 50 year tidal storm

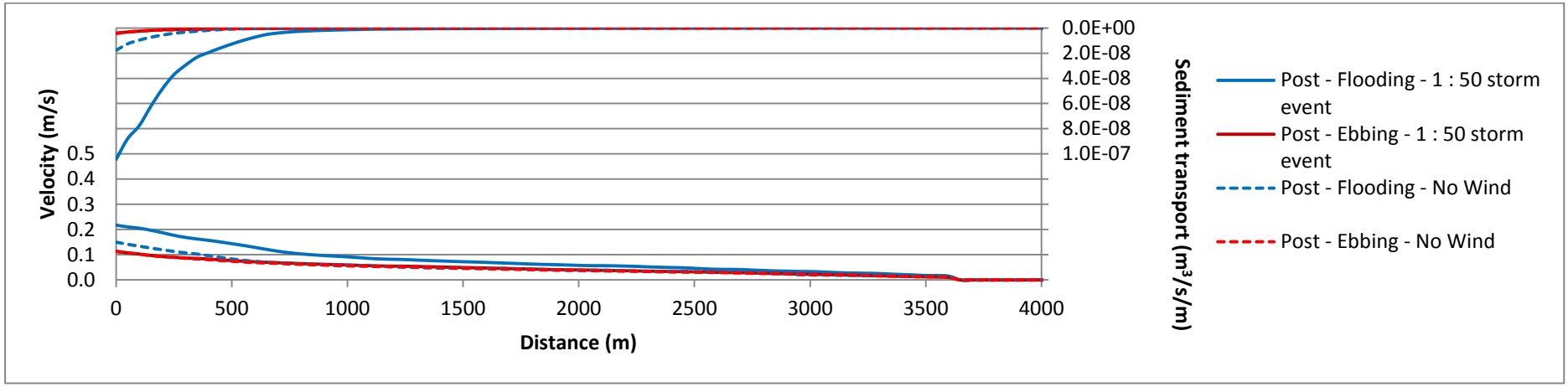

Figure H.6-11: Section S6 after the construction including a 1 in 50 year tidal storm

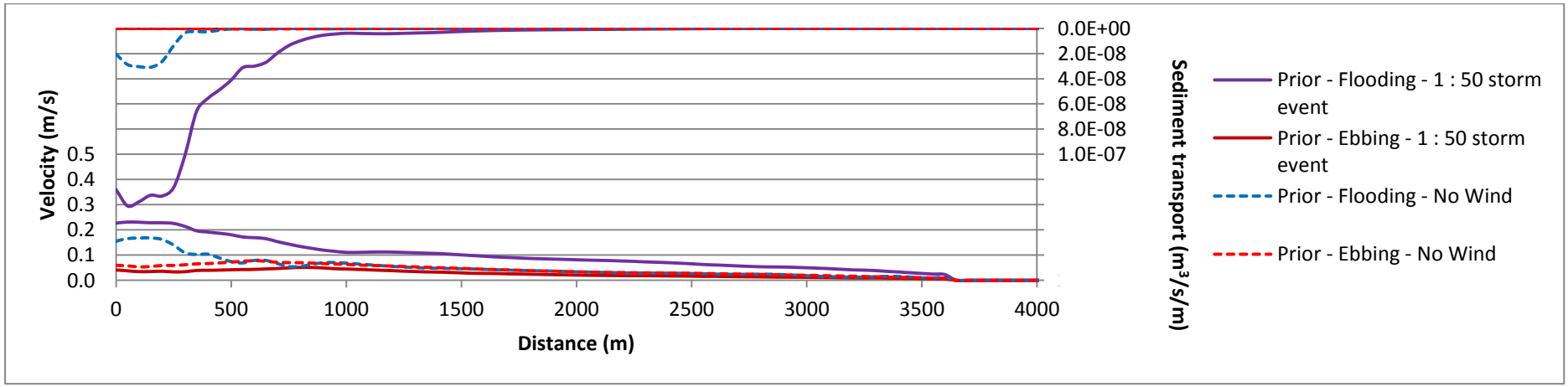

Figure H.6-12: Section S6 prior to construction including a 1 in 50 year tidal storm

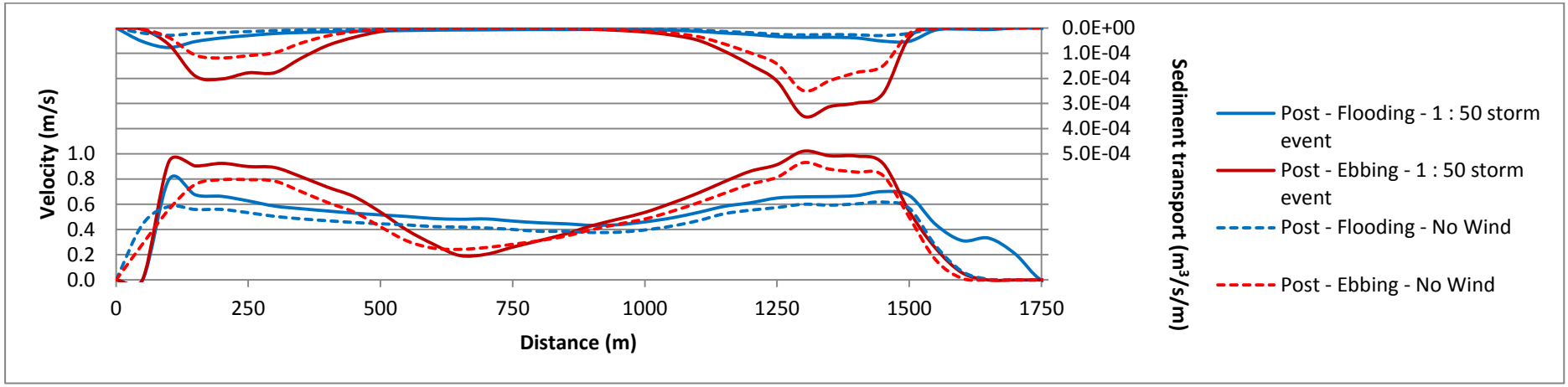

Figure H.6-13: Section L1 after the construction including a 1 in 50 year tidal storm

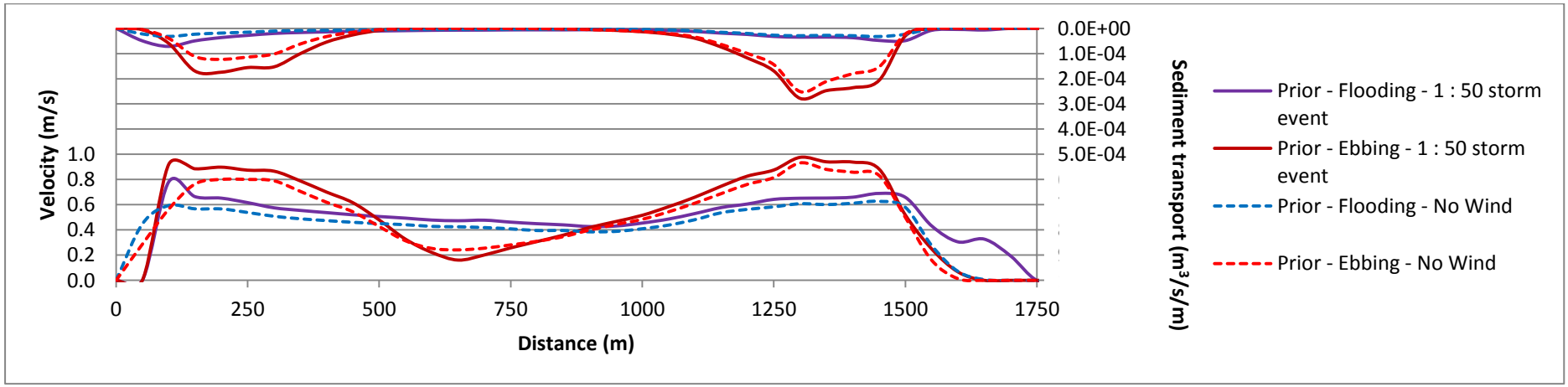

Figure H.6-14: Section L1 prior to construction including a 1 in 50 year tidal storm

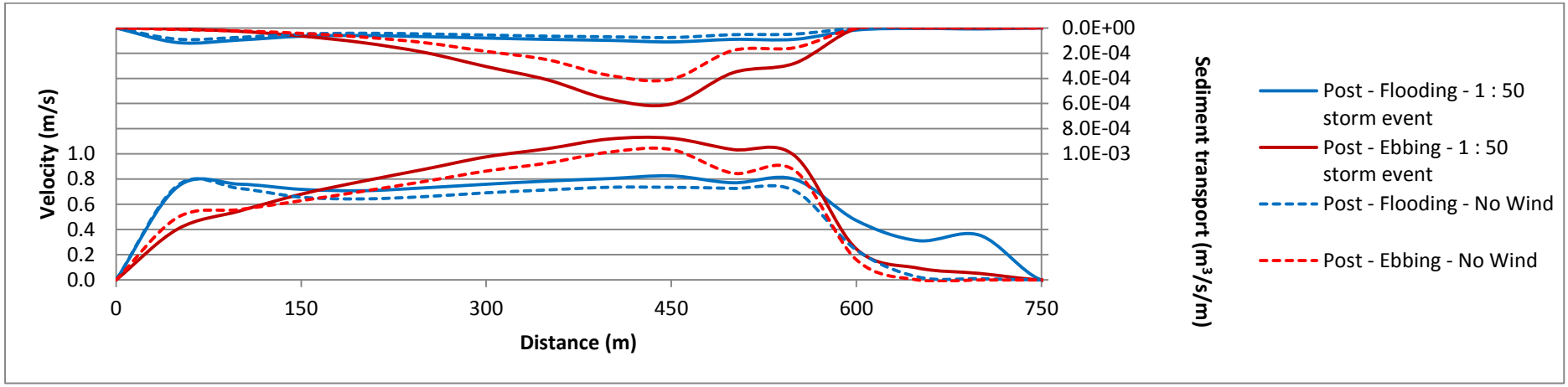

Figure H.6-15: Section L2 after the construction including a 1 in 50 year tidal storm

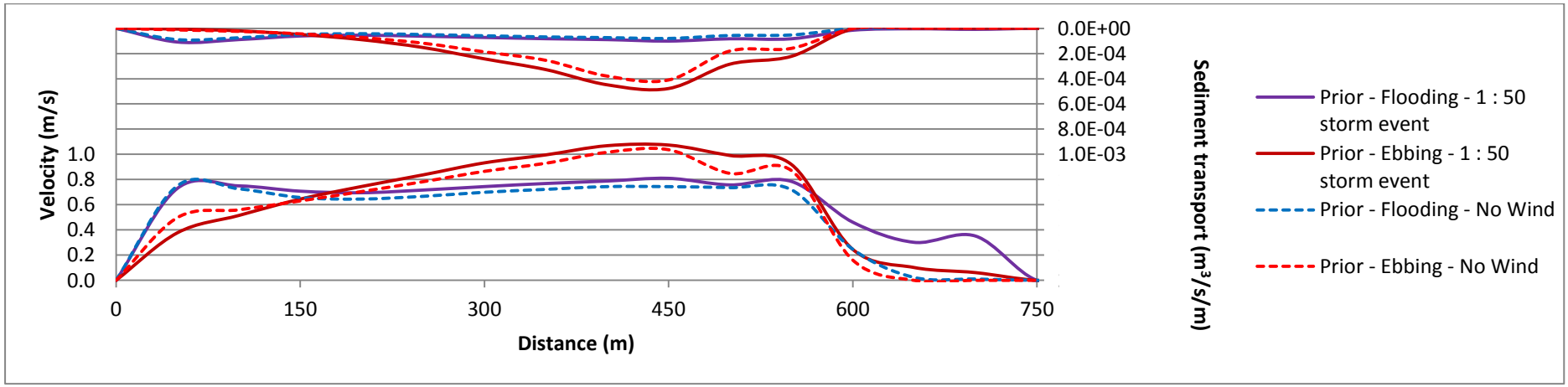

Figure H.6-16: Section L2 prior to construction including a 1 in 50 year tidal storm

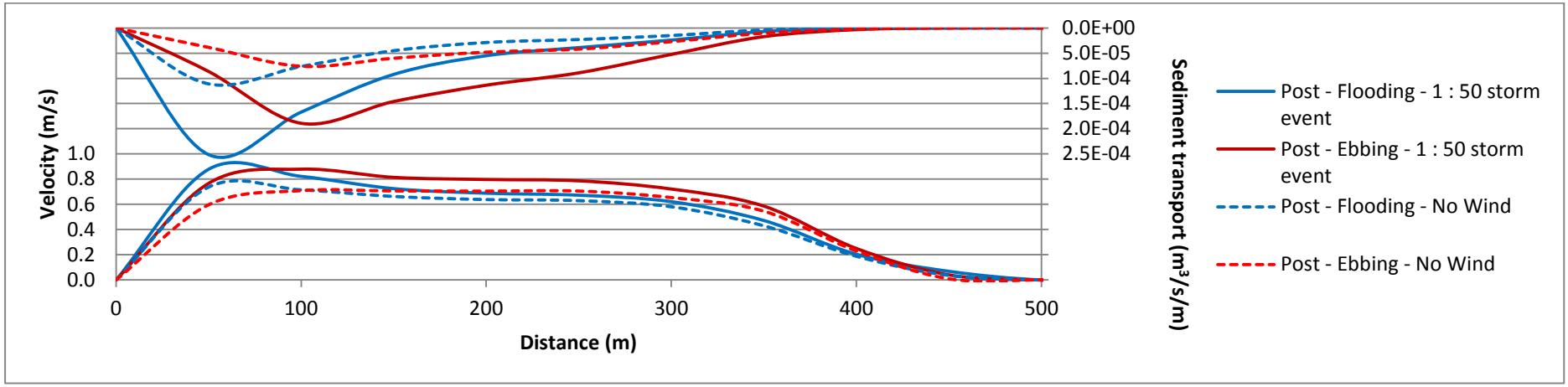

Figure H.6-17: Section L3 after the construction including a 1 in 50 year tidal storm

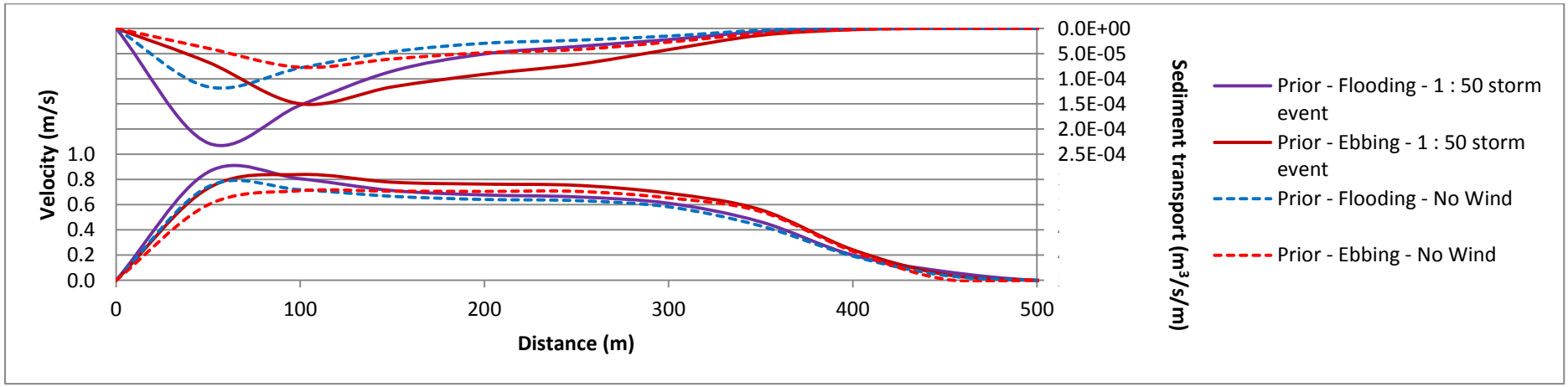

Figure H.6-18: Section L3 prior to construction including a 1 in 50 year tidal storm

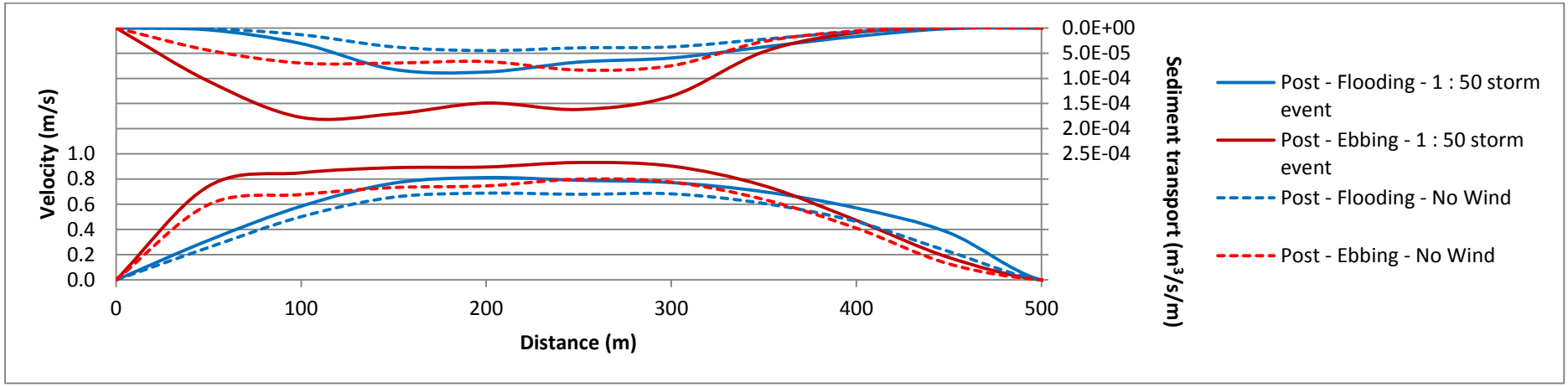

Figure H.6-19: Section L4 after the construction including a 1 in 50 year tidal storm

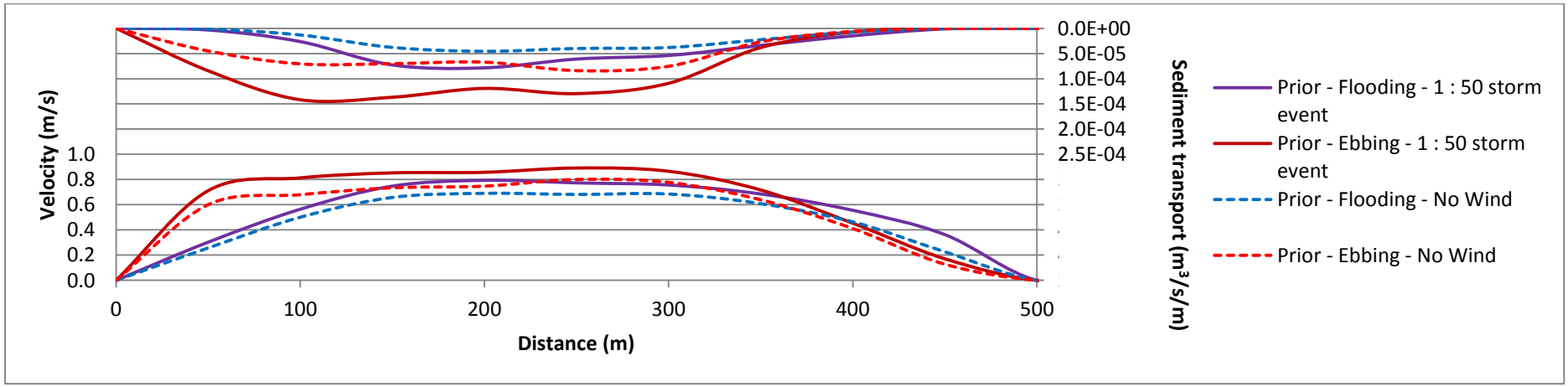

Figure H.6-20: Section L4 prior to construction including a 1 in 50 year tidal storm

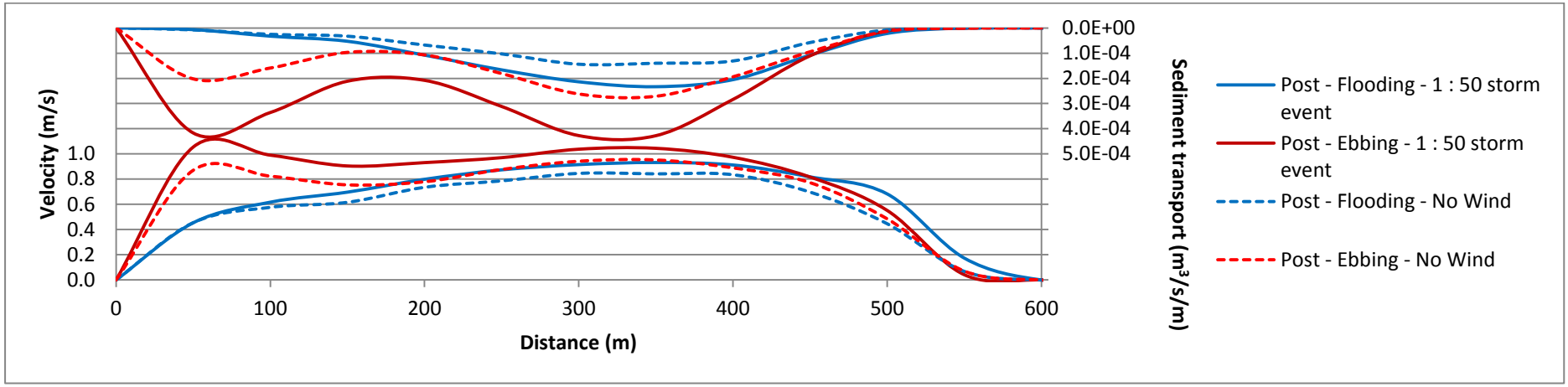

Figure H.6-21: Section L5 after the construction including a 1 in 50 year tidal storm

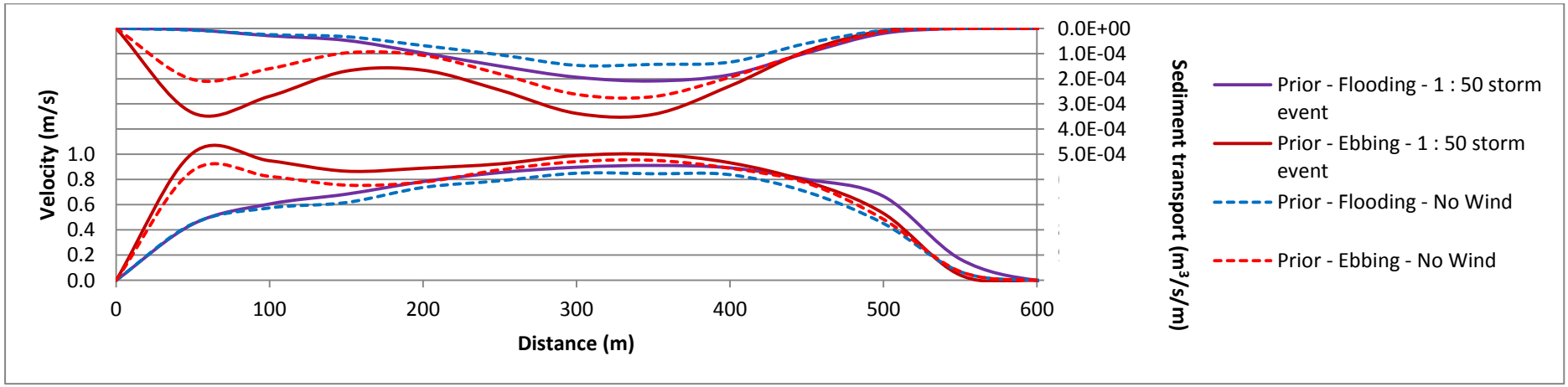

Figure H.6-22: Section L5 prior to construction including a 1 in 50 year tidal storm

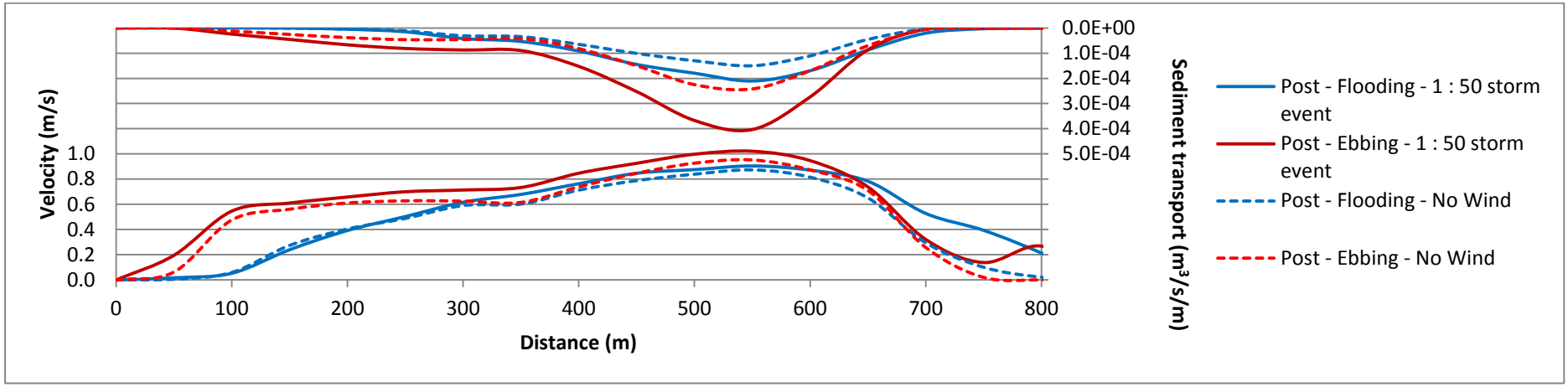

Figure H.6-23: Section L6 after the construction including a 1 in 50 year tidal storm

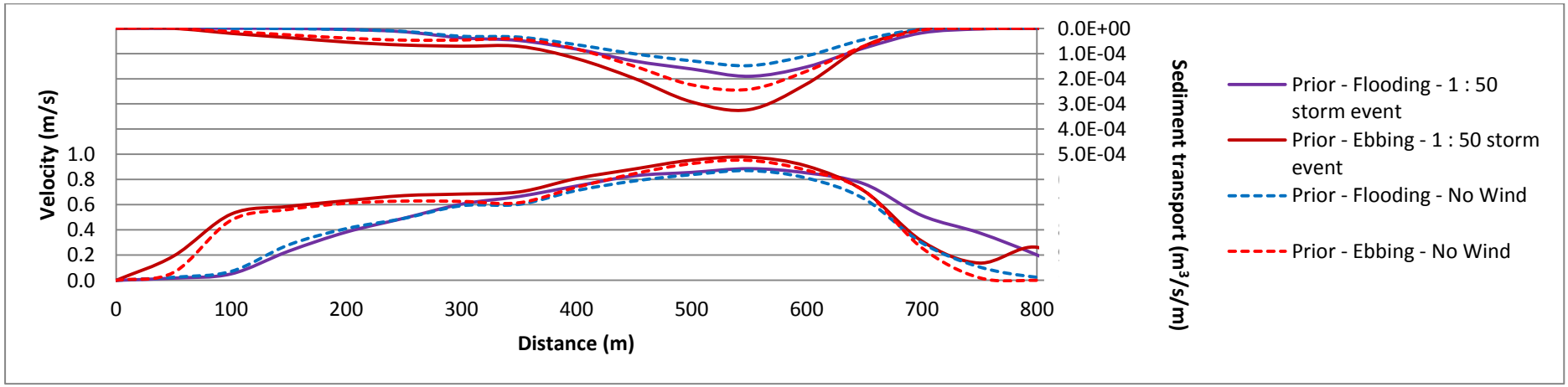

Figure H.6-24: Section L6 prior to construction including a 1 in 50 year tidal storm

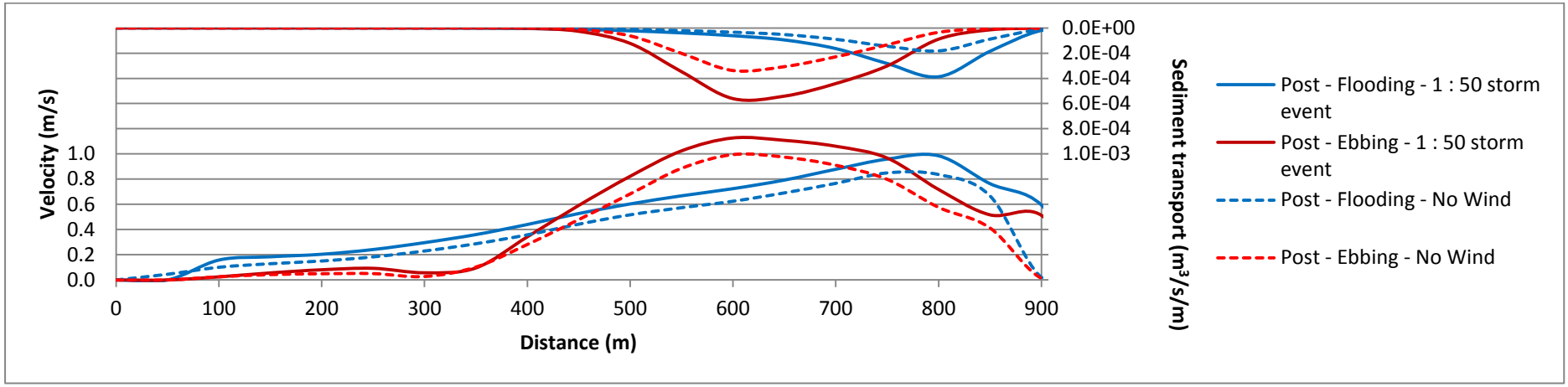

Figure H.6-25: Section L7 after the construction including a 1 in 50 year tidal storm

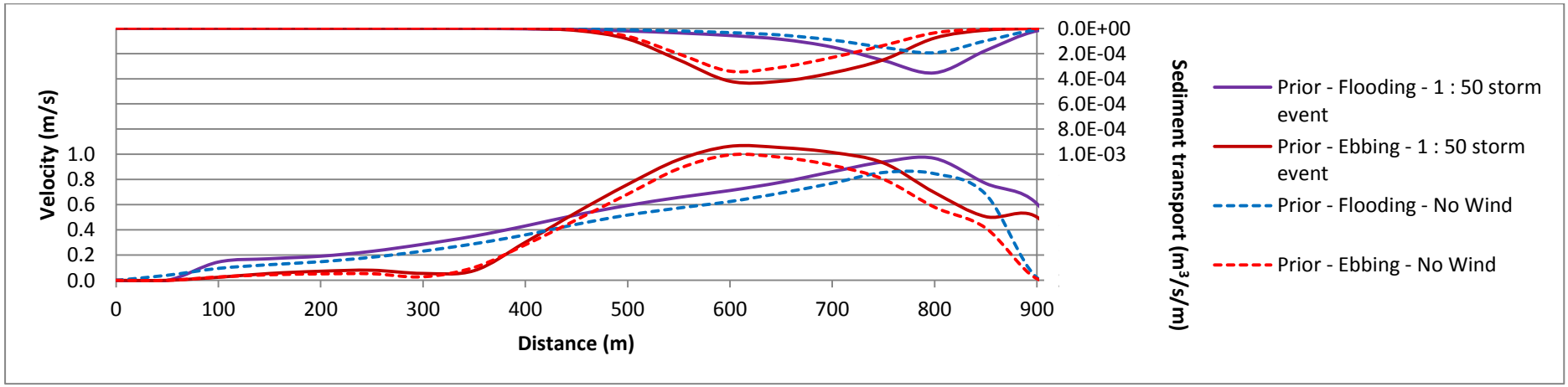

Figure H.6-26: Section L7 prior to construction including a 1 in 50 year tidal storm

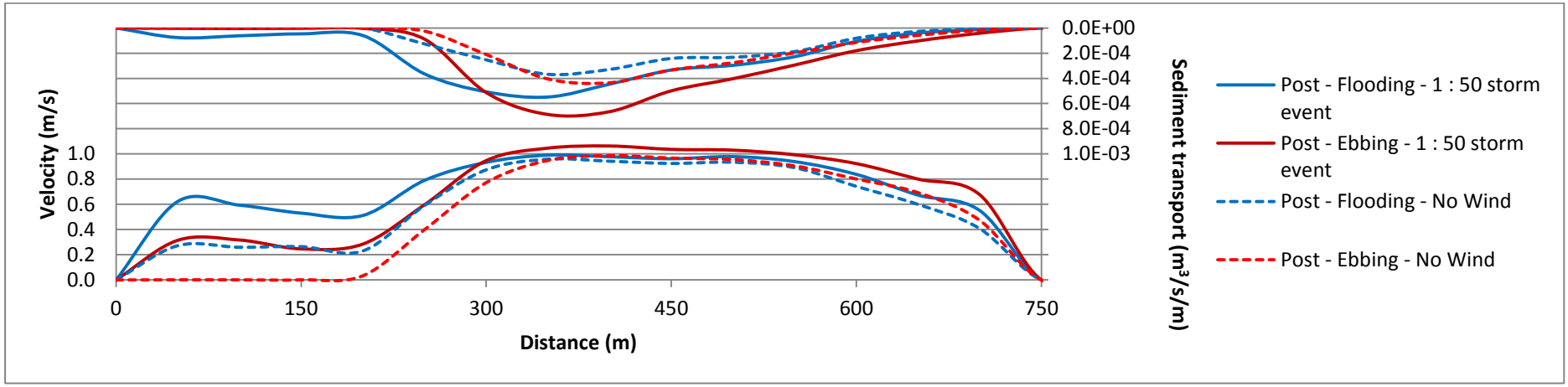

Figure H.6-27: Section L8 after the construction including a 1 in 50 year tidal storm

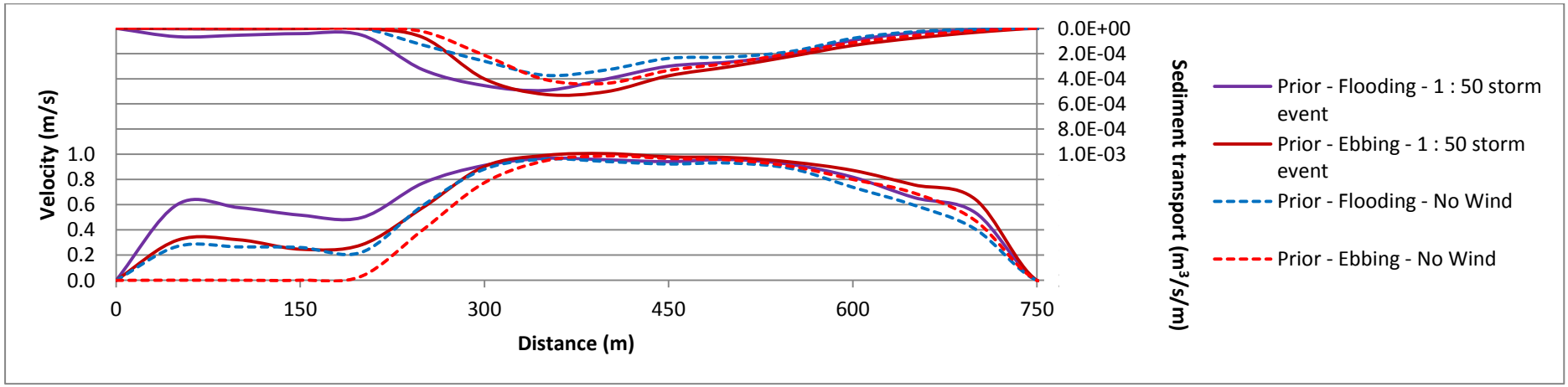

Figure H.6-28: Section L8 prior to construction including a 1 in 50 year tidal storm

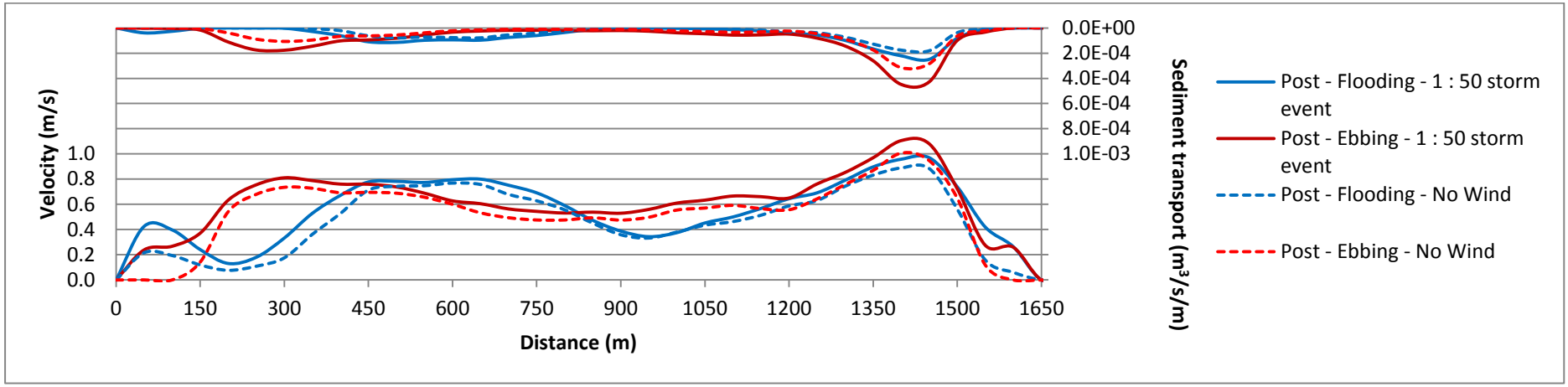

Figure H.6-29: Section L9 after the construction including a 1 in 50 year tidal storm

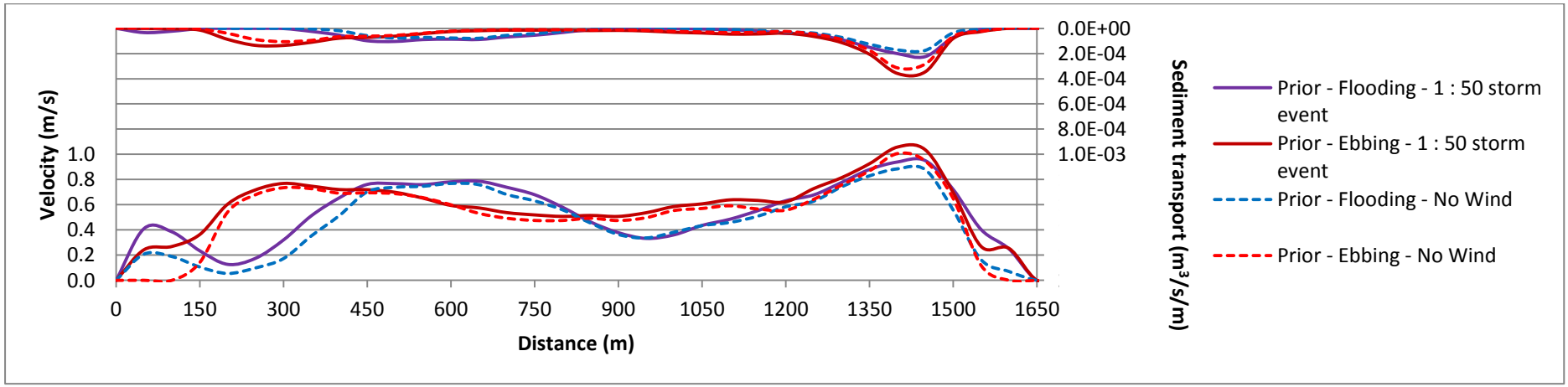

Figure H.6-30: Section L9 prior to construction including a 1 in 50 year tidal storm

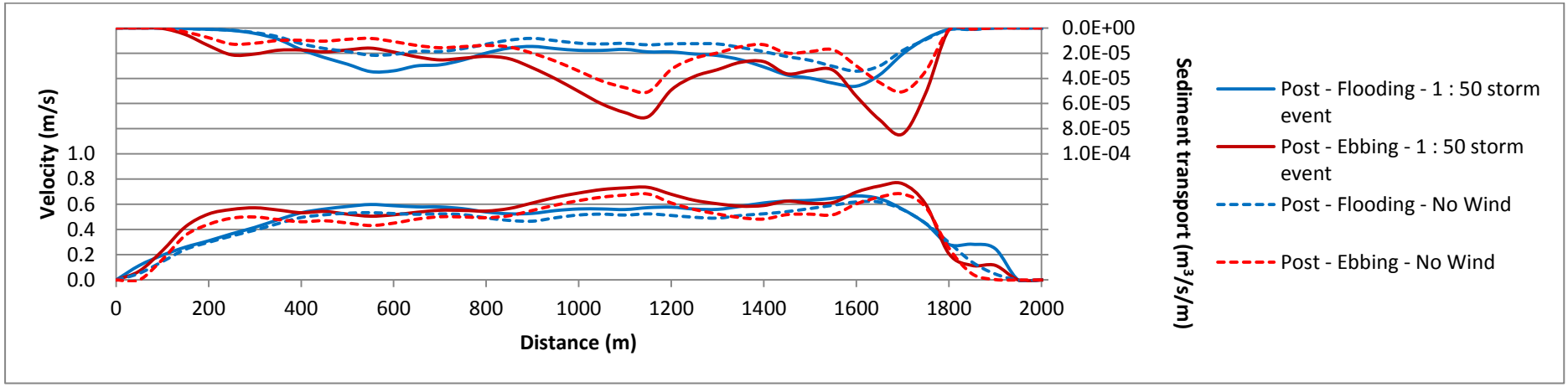

Figure H.6-31: Section L10 after the construction including a 1 in 50 year tidal storm

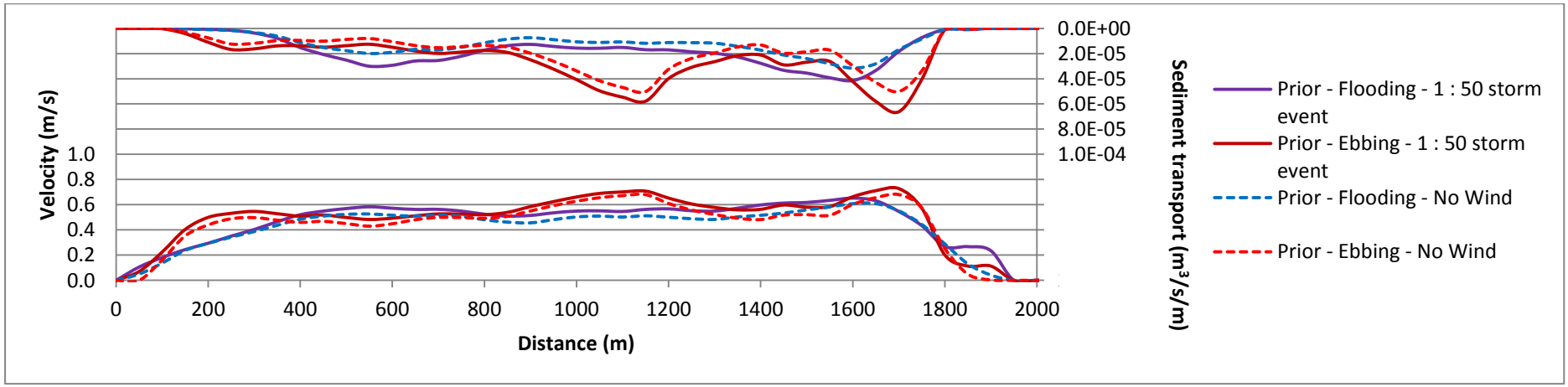

Figure H.6-32: Section L10 prior to construction including a 1 in 50 year tidal storm

APPENDIX H.7 SEA LEVEL RISE

LIST OF FIGURERS

Figure H.7-1: Section S1 after the construction after sea level rise
Figure H.7-2: Section S1 prior to construction after sea level rise
Figure H.7-3: Section S2 after the construction after sea level rise
Figure H.7-4: Section S2 prior to construction after sea level rise
Figure H.7-5: Section S3 after the construction after sea level rise
Figure h.7-6: Section S3 prior to construction after sea level rise
Figure H.7-7: Section S4 after the construction after sea level rise
Figure H.7-8: Section S4 prior to construction after sea level rise
Figure H.7-9: Section S5 after the construction after sea level rise
Figure H.7-10: Section S5 prior to construction after sea level rise
Figure H.7-11: Section S6 after the construction after sea level rise
Figure H.7-12: Section S6 prior to construction after sea level rise
Figure H.7-13: Section L1 after the construction after sea level rise
Figure H.7-14: Section L1 prior to construction after sea level rise
Figure H.7-15: Section L2 after the construction after sea level rise
Figure H.7-16: Section L2 prior to construction after sea level rise
Figure H.6-17: Section L3 after the construction after sea level rise
Figure H.7-18: Section L3 prior to construction after sea level rise
Figure H.7-19: Section L4 after the construction after sea level rise
Figure H.7-20: Section L4 prior to construction after sea level rise
Figure H.7-21: Section L5 after the construction after sea level rise
Figure H.7-22: Section L5 prior to construction after sea level rise
Figure H.7-23: Section L6 after the construction after sea level rise
Figure H.7-24: Section L6 prior to construction after sea level rise
Figure H.7-25: Section L7 after the construction after sea level rise
Figure H.7-26: Section L7 prior to construction after sea level rise
Figure H.7-27: Section L8 after the construction after sea level rise
Figure H.7-28: Section L8 prior to construction after sea level rise
Figure H.7-29: Section L9 after the construction after sea level rise
Figure H.7-30: Section L9 prior to construction after sea level rise
Figure H.7-31: Section L10 after the construction after sea level rise
Figure H.7-32: Section L10 prior to construction after sea level rise

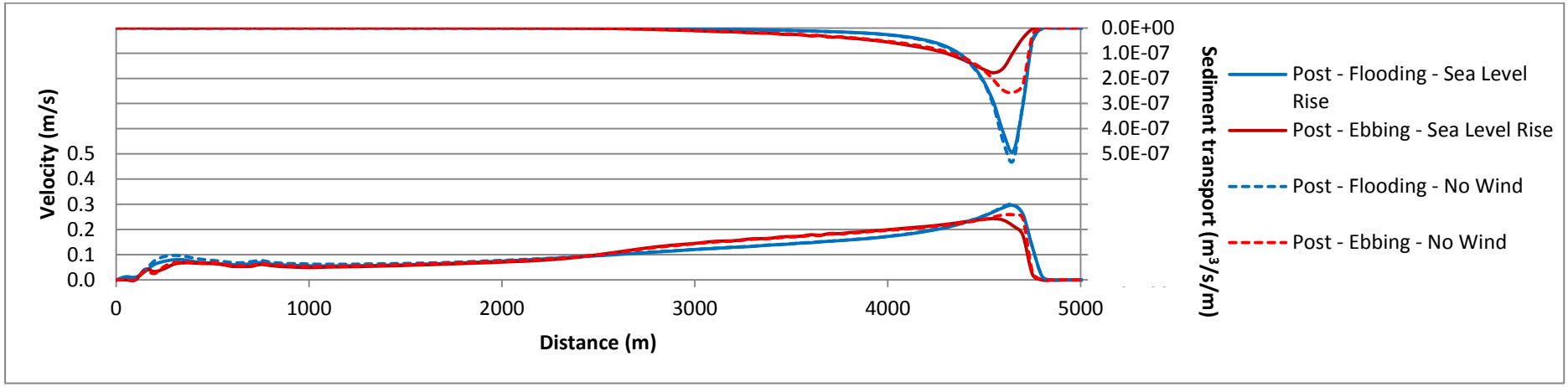

Figure H.7-1: Section S1 after the construction after sea level rise

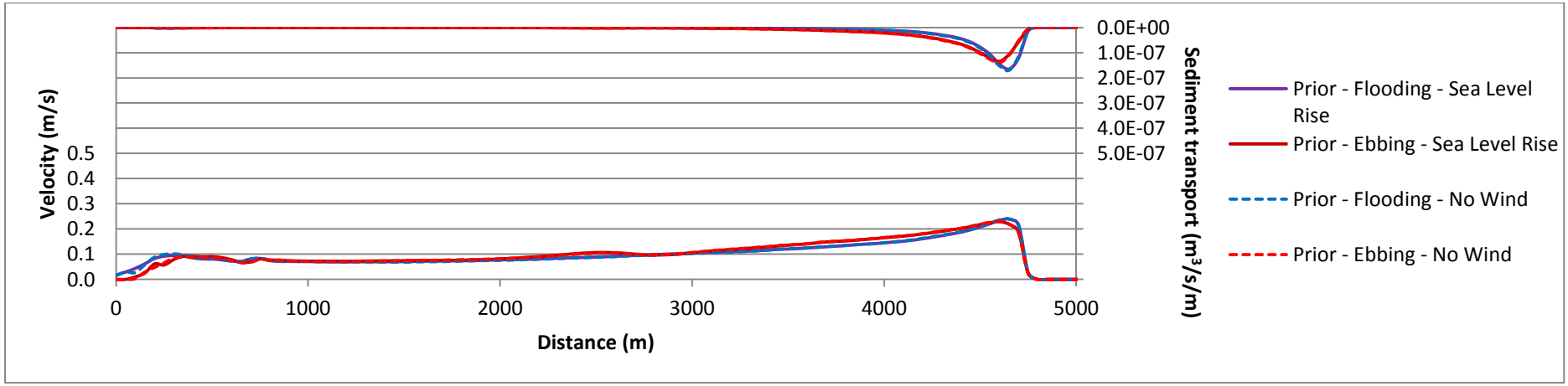

Figure H.7-2: Section S1 prior to construction after sea level rise

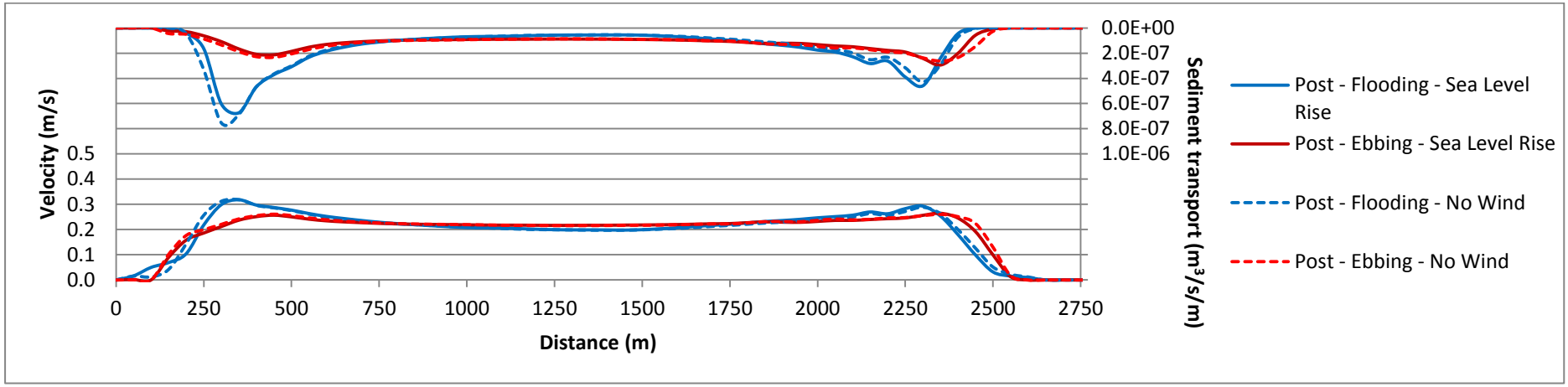

Figure H.7-3: Section S2 after the construction after sea level rise

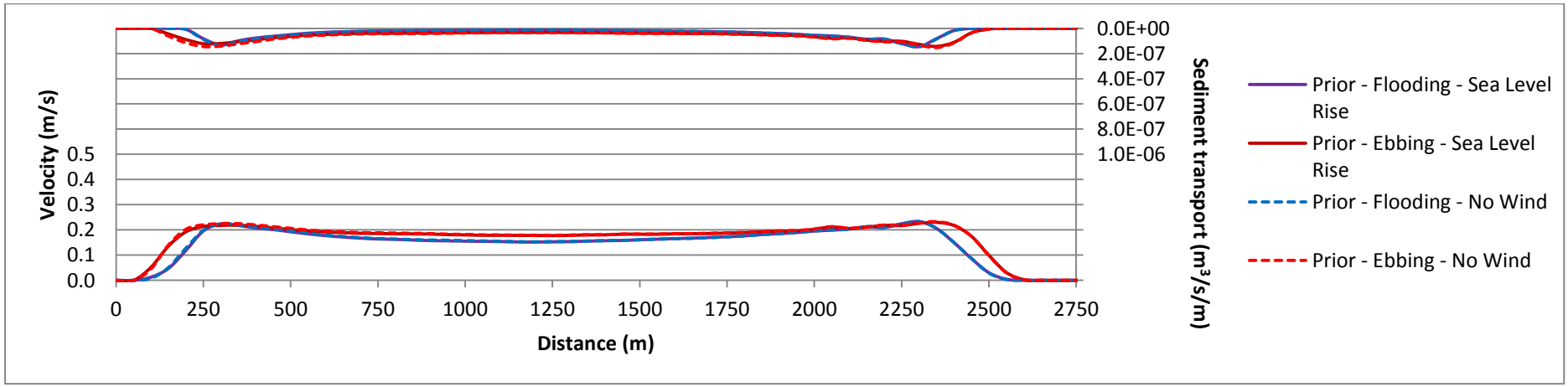

Figure H.7-4: Section S2 prior to construction after sea level rise

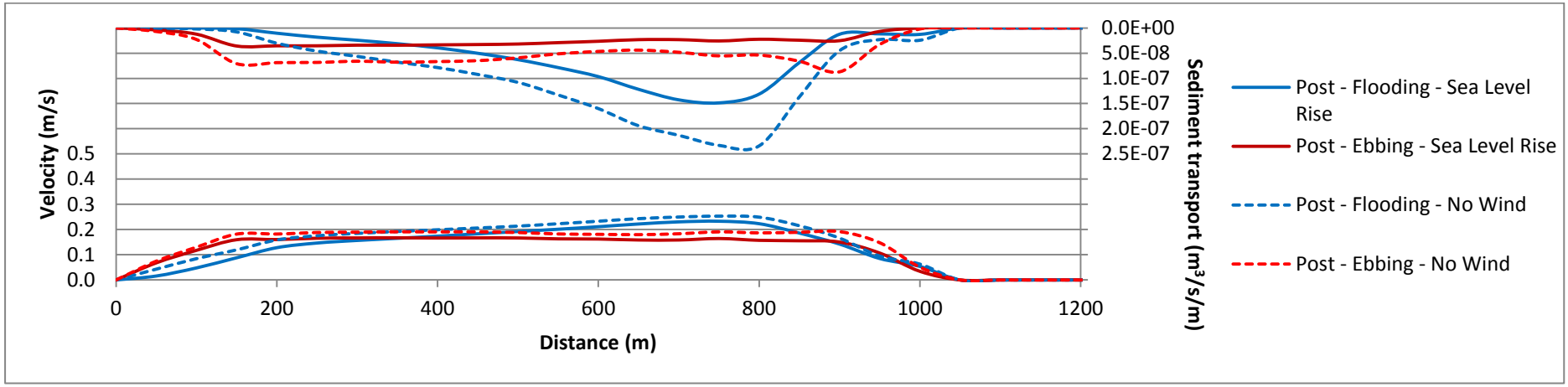

Figure H.7-5: Section S3 after the construction after sea level rise

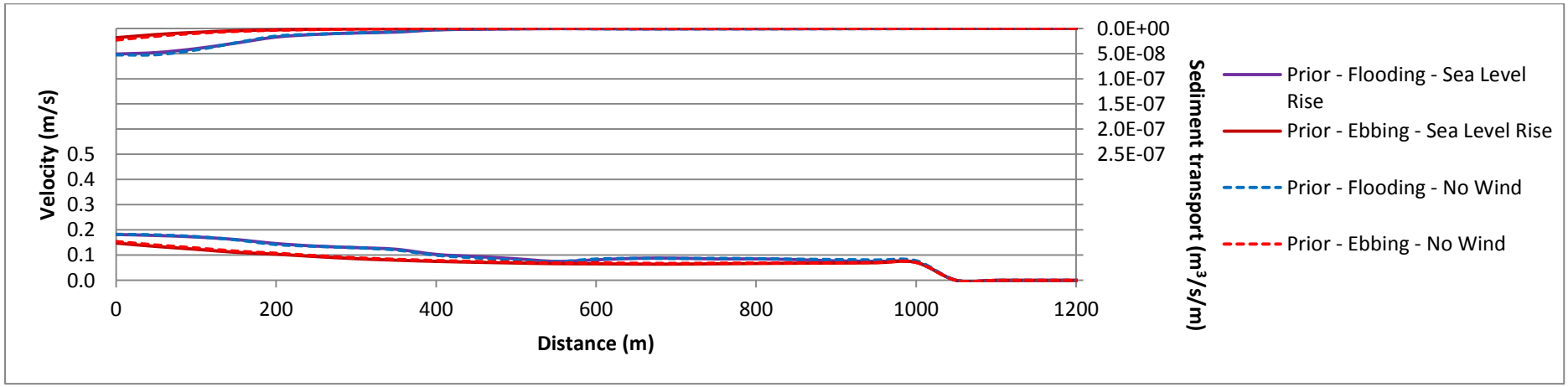

Figure h.7-6: Section S3 prior to construction after sea level rise

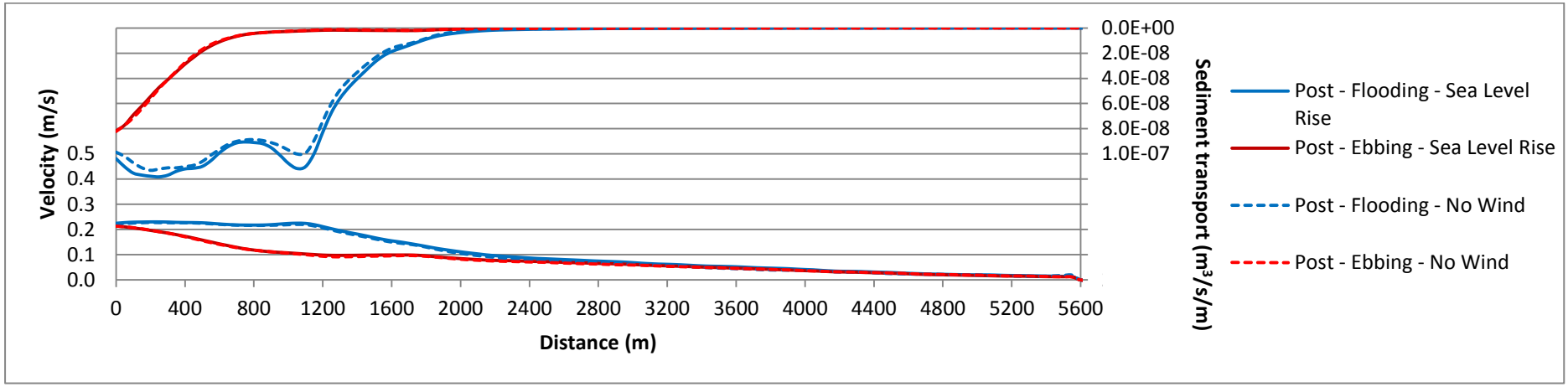

Figure H.7-7: Section S4 after the construction after sea level rise

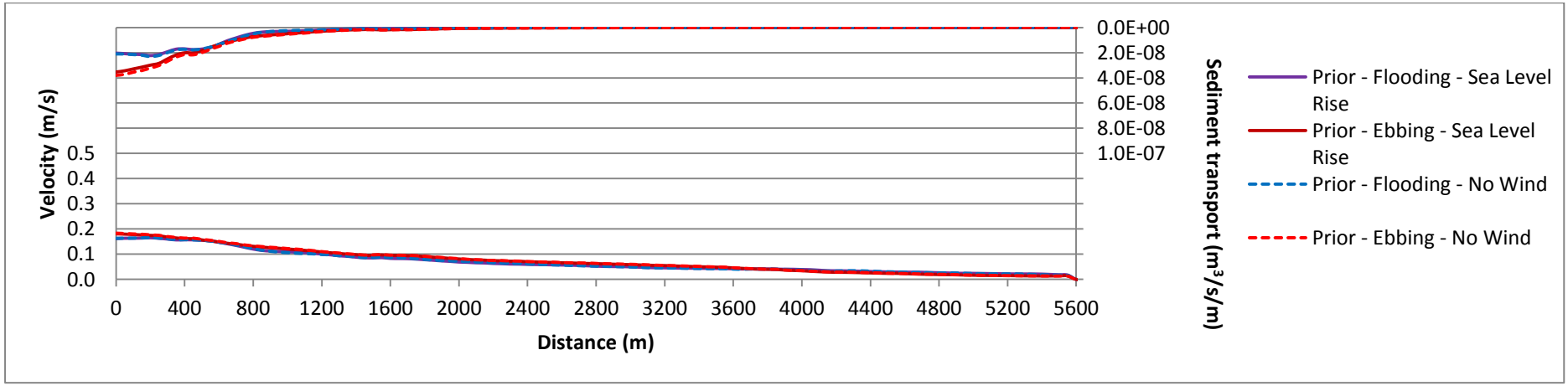

Figure H.7-8: Section S4 prior to construction after sea level rise

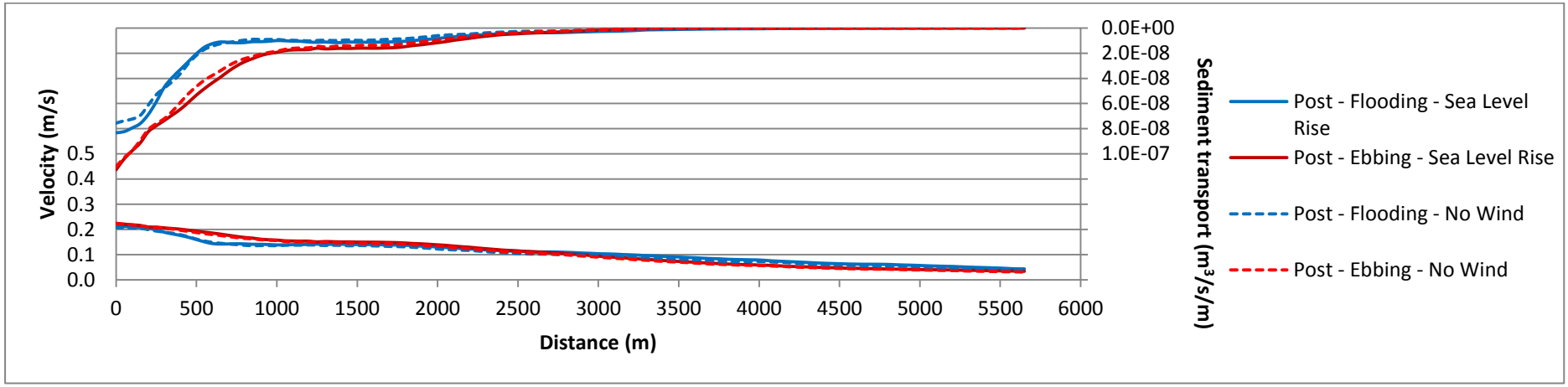

Figure H.7-9: Section S5 after the construction after sea level rise

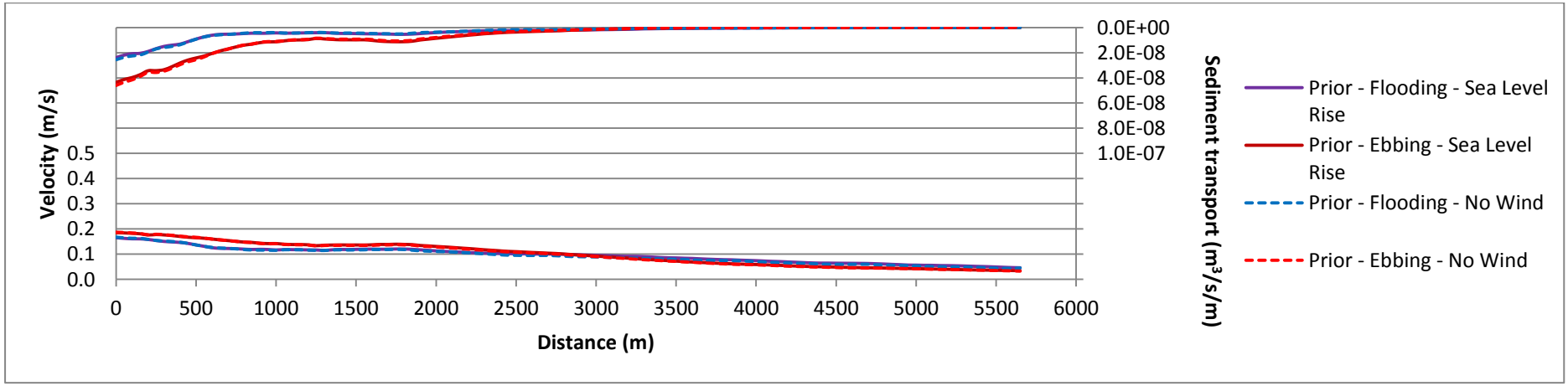

Figure H.7-10: Section S5 prior to construction after sea level rise

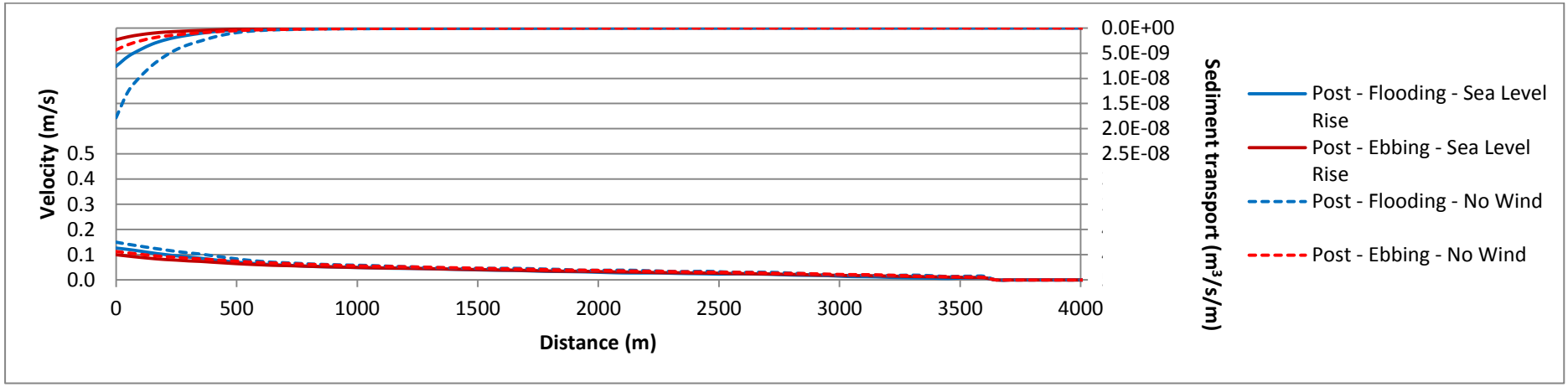

Figure H.7-11: Section S6 after the construction after sea level rise

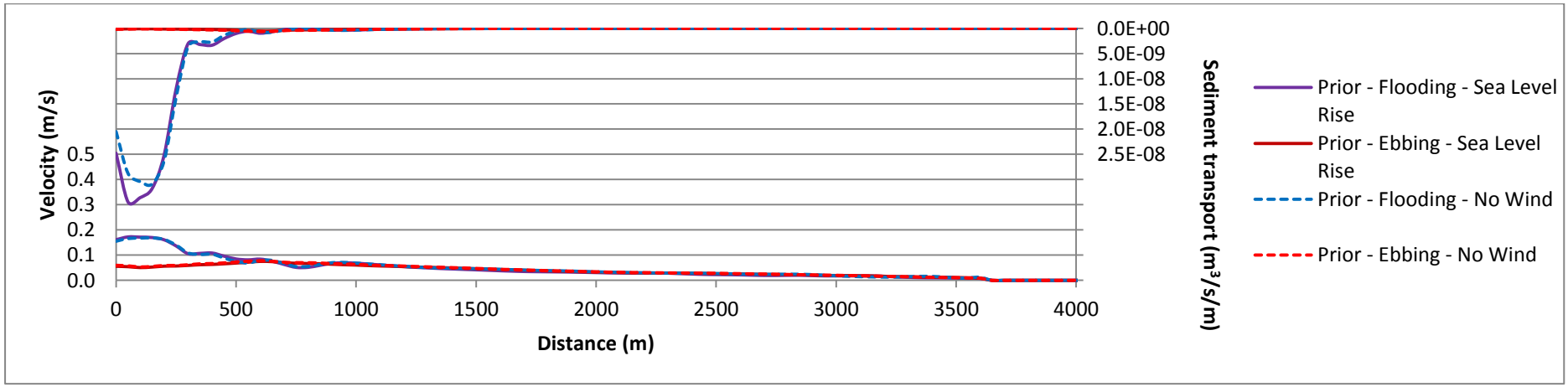

Figure H.7-12: Section S6 prior to construction after sea level rise

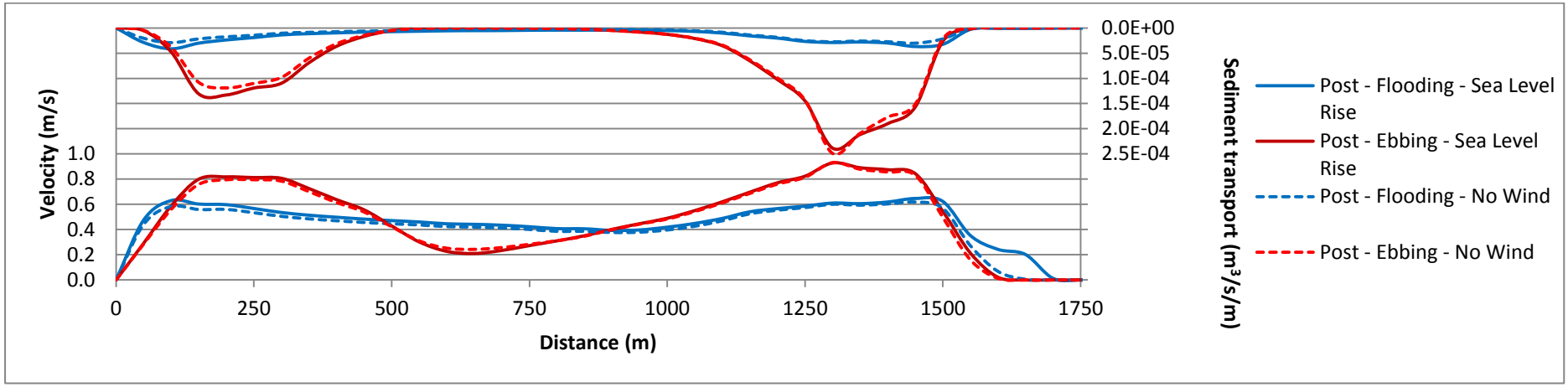

Figure H.7-13: Section L1 after the construction after sea level rise

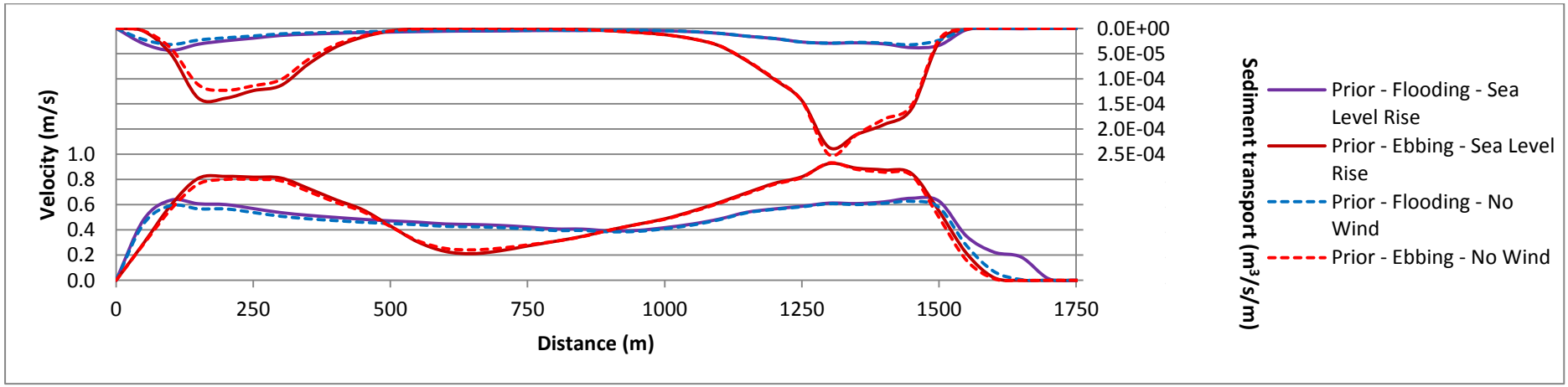

Figure H.7-14: Section L1 prior to construction after sea level rise

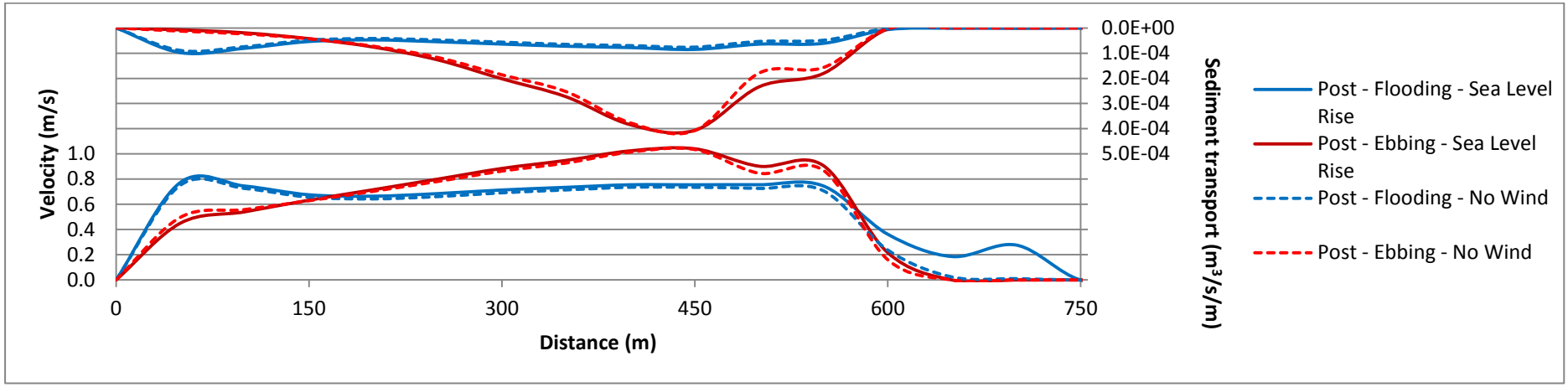

Figure H.7-15: Section L2 after the construction after sea level rise

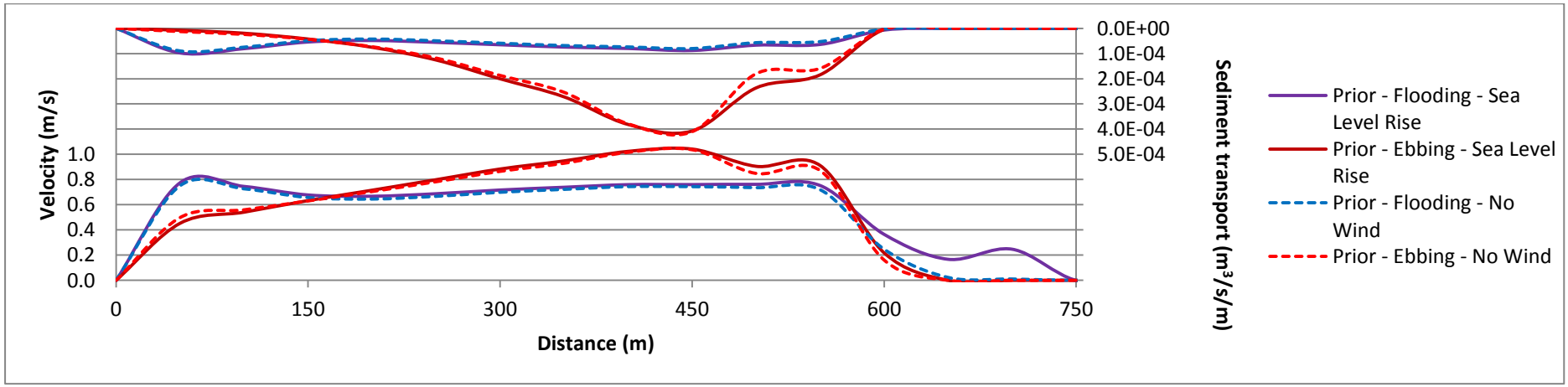

Figure H.7-16: Section L2 prior to construction after sea level rise

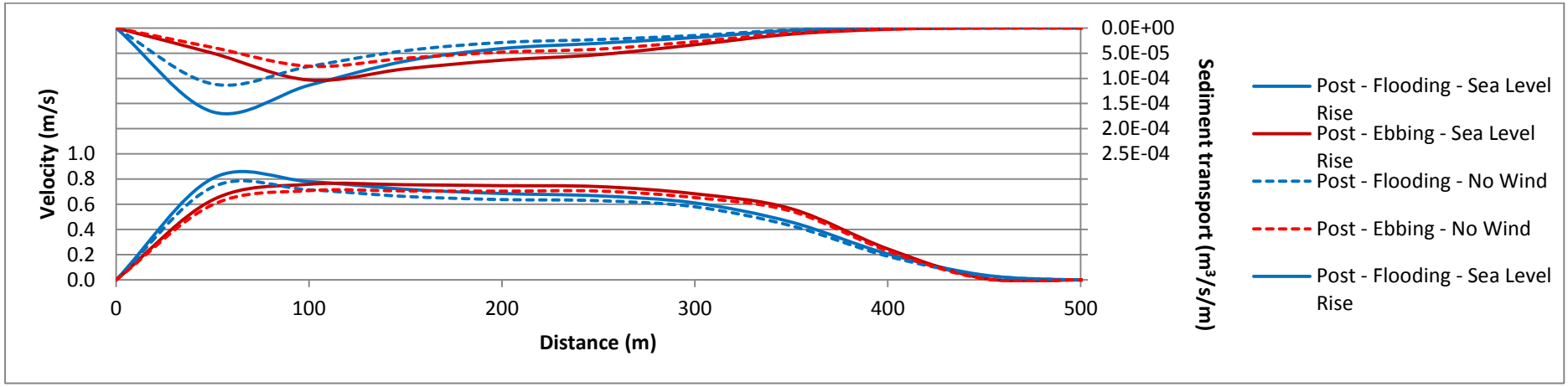

Figure H.6-17: Section L3 after the construction after sea level rise

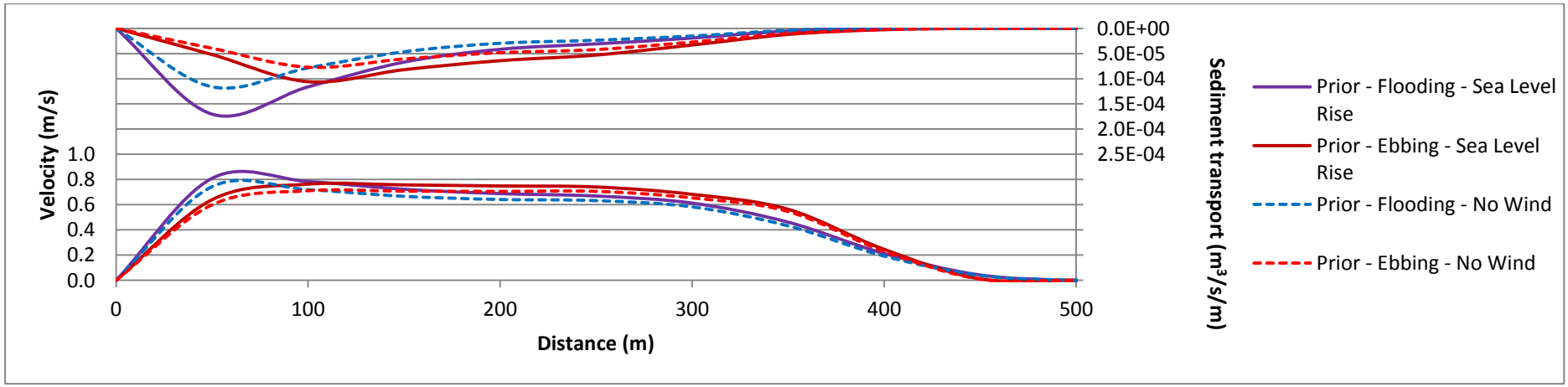

Figure H.7-18: Section L3 prior to construction after sea level rise

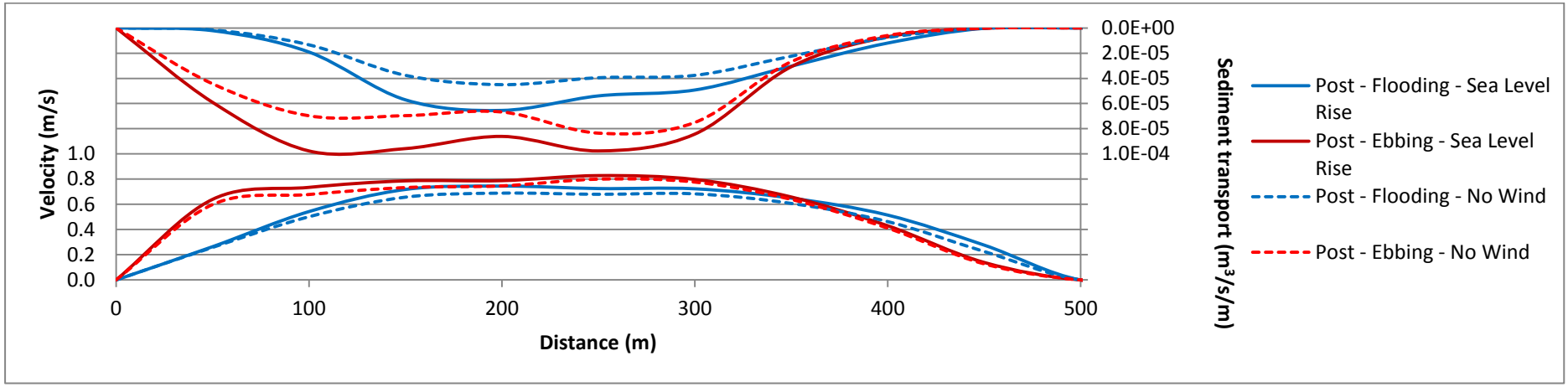

Figure H.7-19: Section L4 after the construction after sea level rise

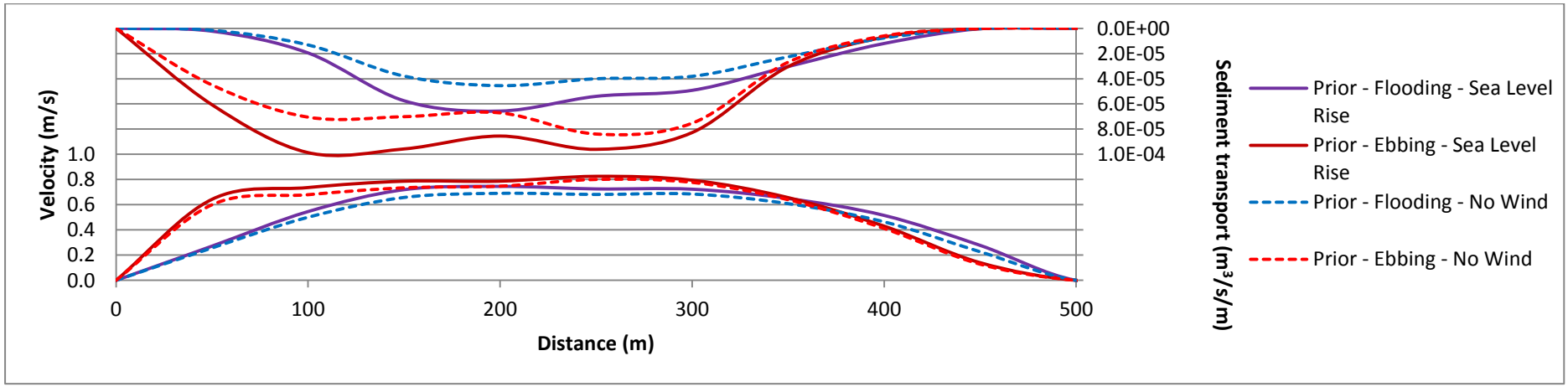

Figure H.7-20: Section L4 prior to construction after sea level rise

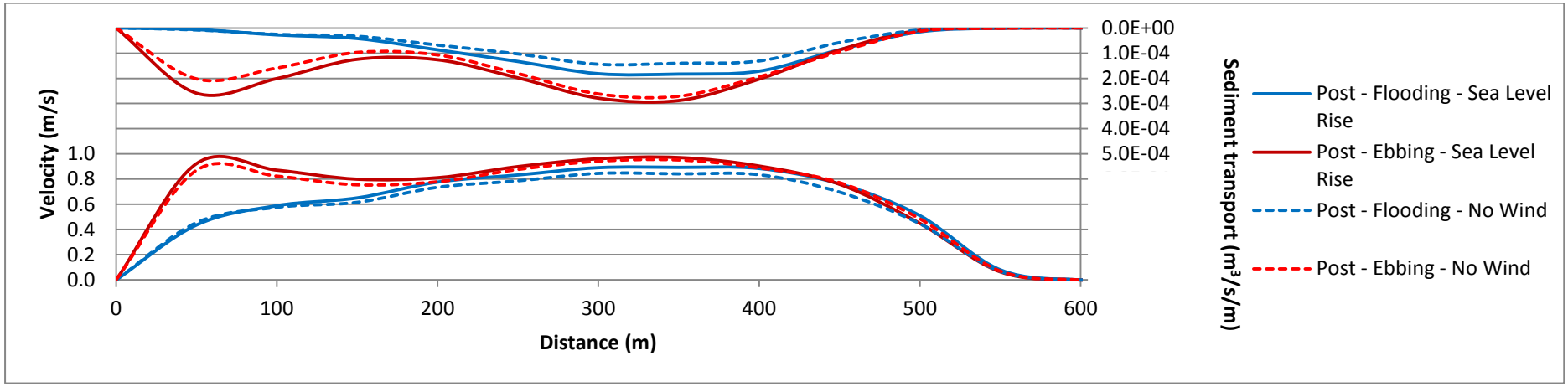

Figure H.7-21: Section L5 after the construction after sea level rise

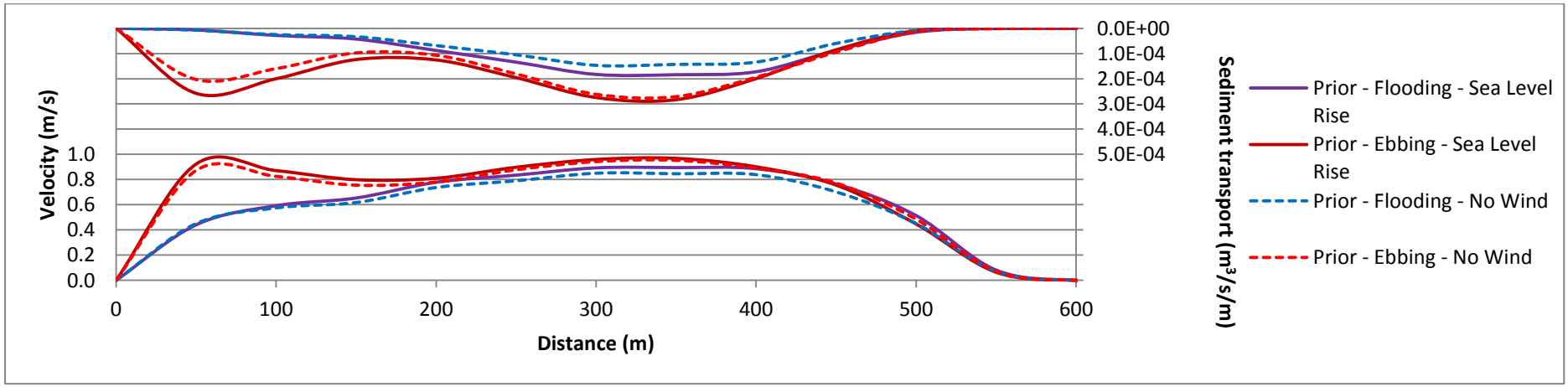

Figure H.7-22: Section L5 prior to construction after sea level rise

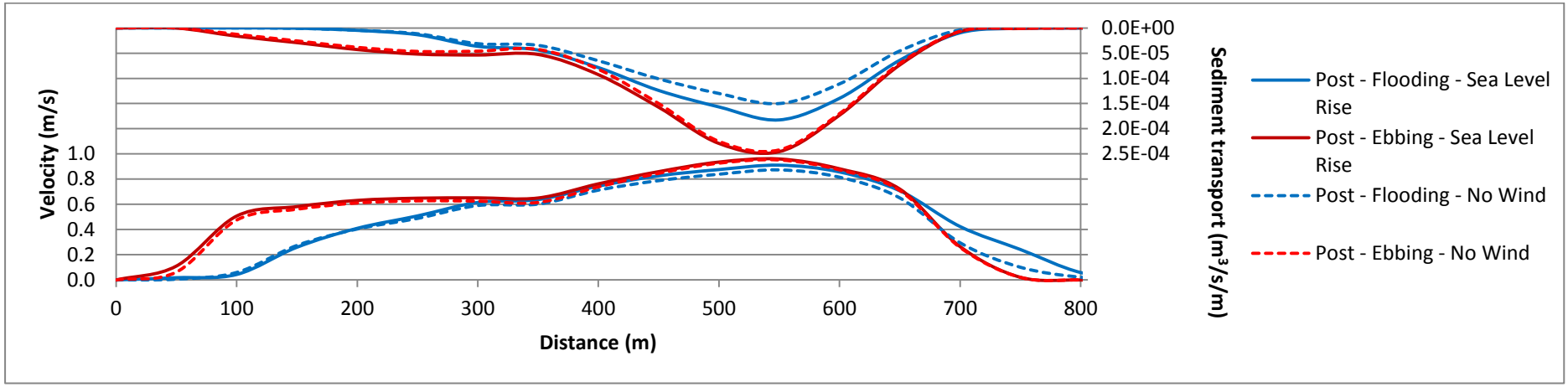

Figure H.7-23: Section L6 after the construction after sea level rise

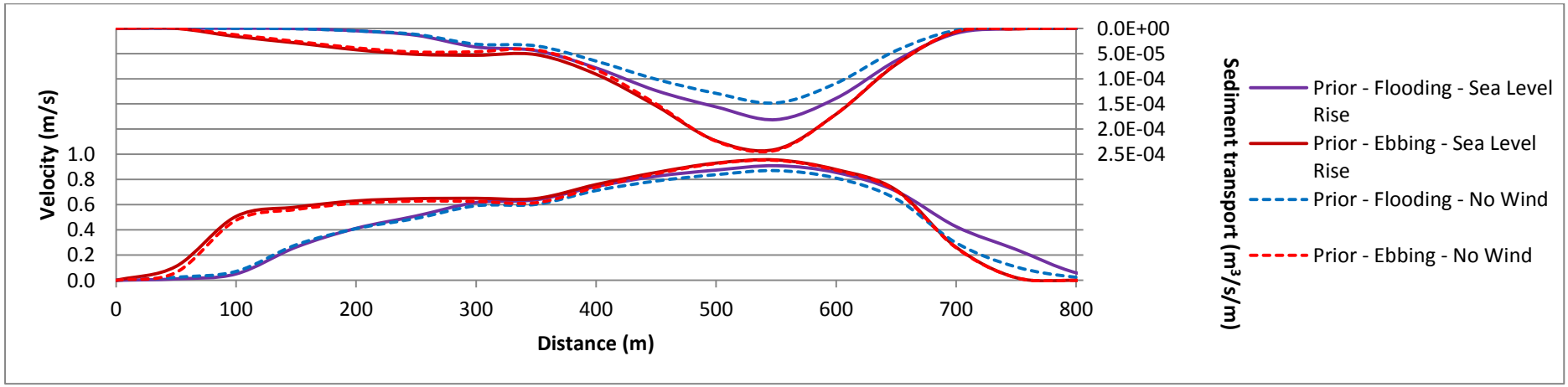

Figure H.7-24: Section L6 prior to construction after sea level rise

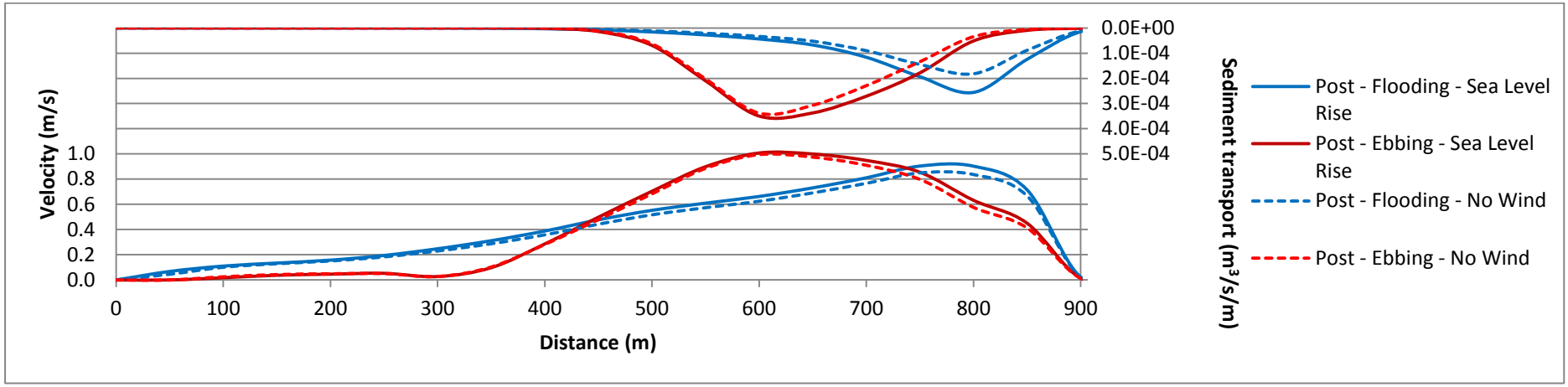

Figure H.7-25: Section L7 after the construction after sea level rise

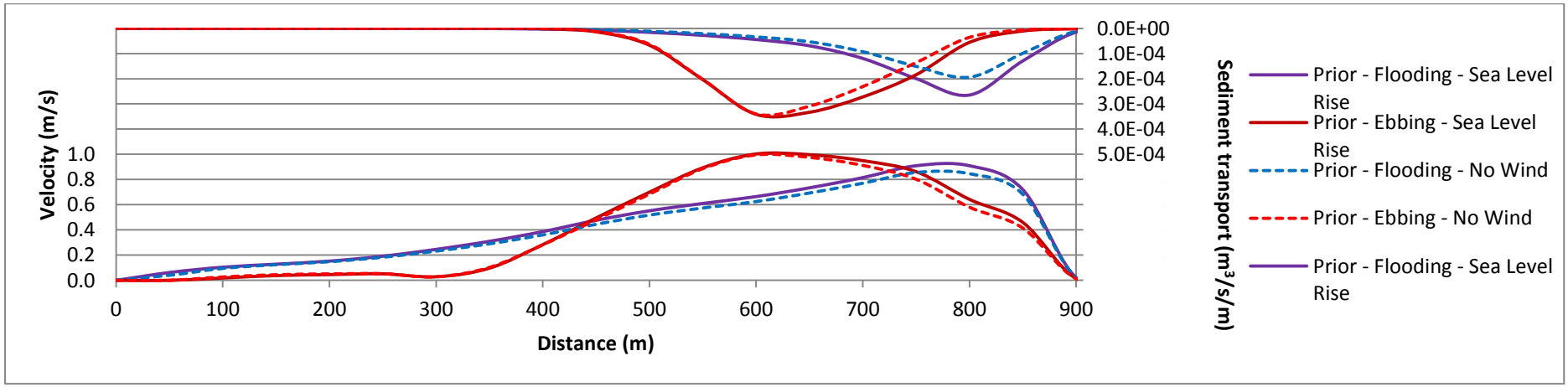

Figure H.7-26: Section L7 prior to construction after sea level rise

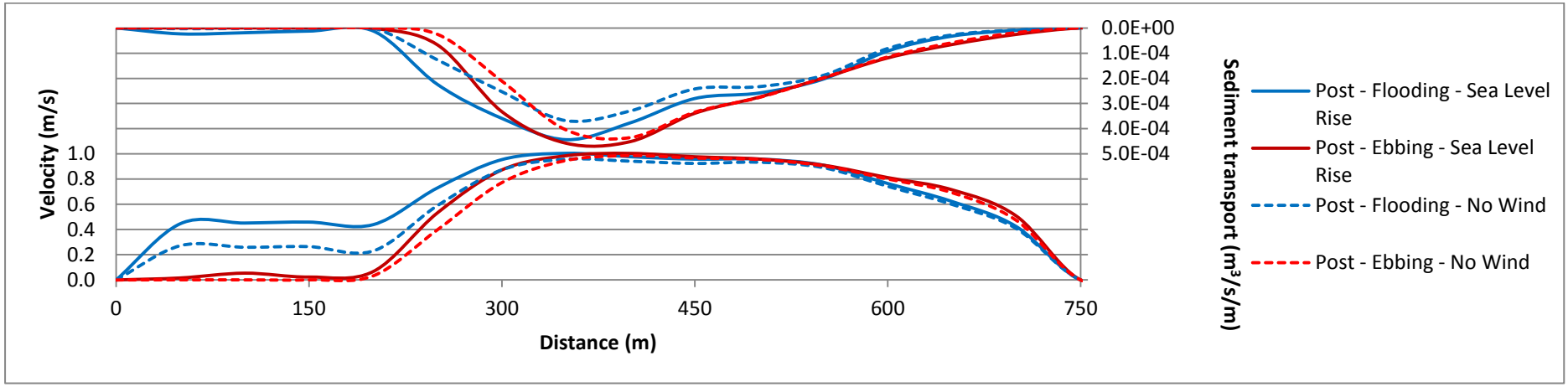

Figure H.7-27: Section L8 after the construction after sea level rise

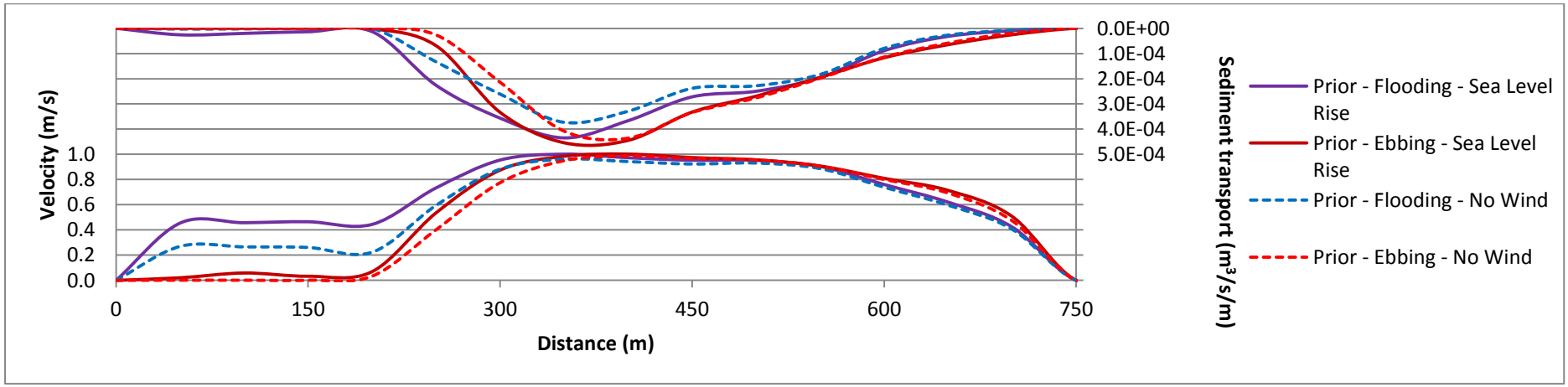

Figure H.7-28: Section L8 prior to construction after sea level rise

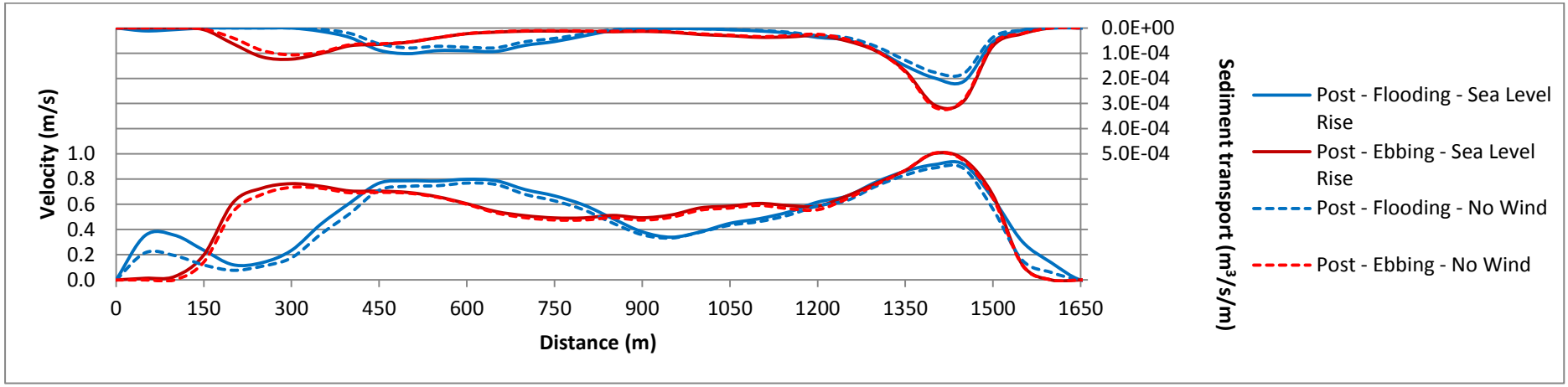

Figure H.7-29: Section L9 after the construction after sea level rise

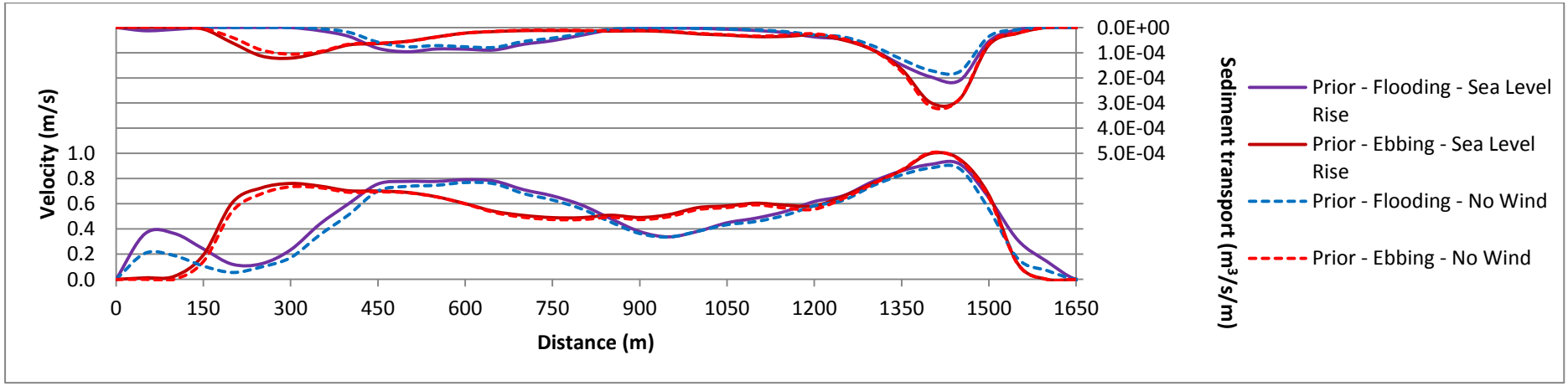

Figure H.7-30: Section L9 prior to construction after sea level rise

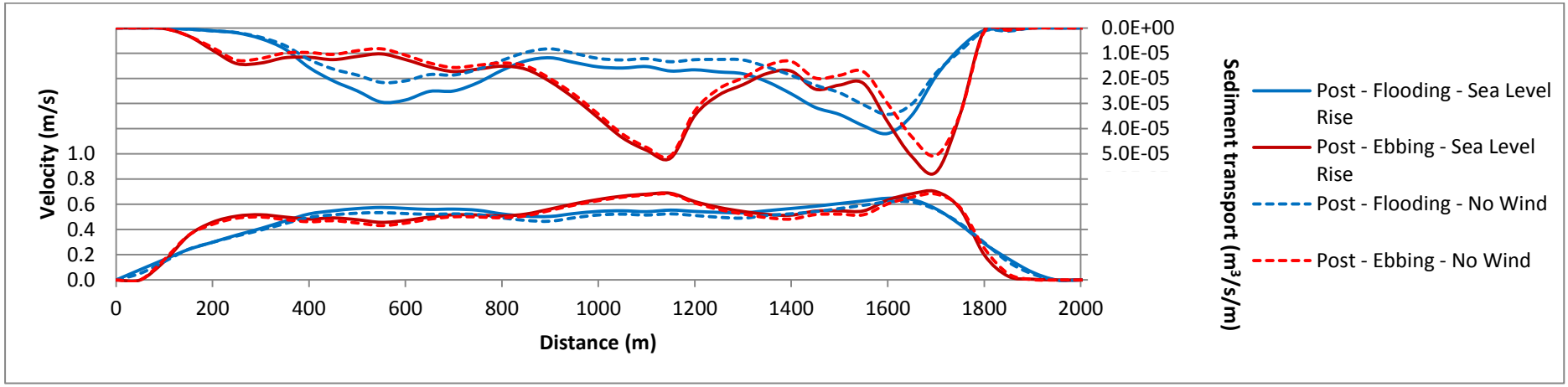

Figure H.7-31: Section L10 after the construction after sea level rise

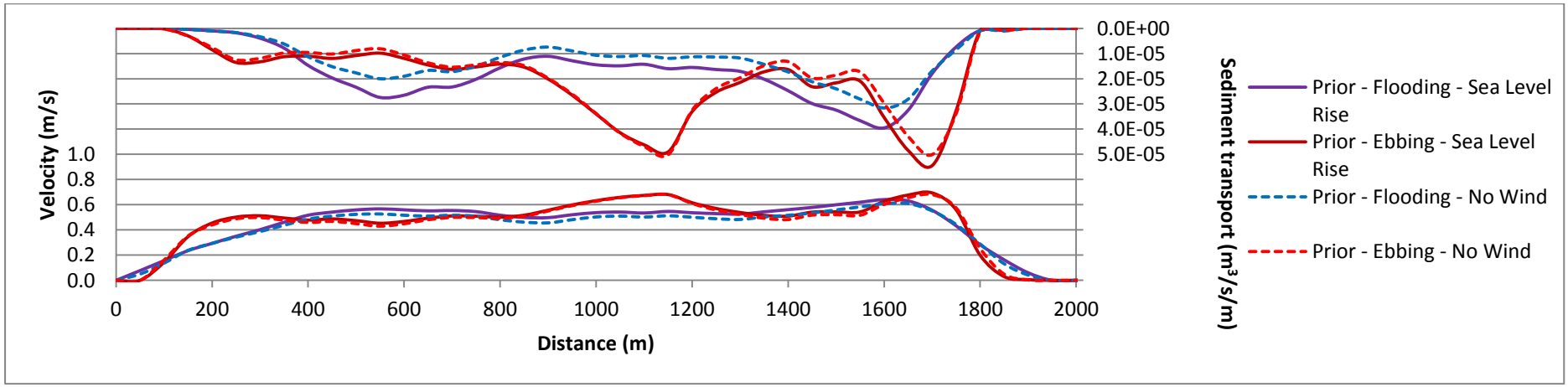

Figure H.7-32: Section L10 prior to construction after sea level rise

APPENDIX I SEDIMENT TRANSPORT FORMULAE

These calculations are as follow, and explained according to the MIKE21 User Manuals (DHI Water and Environment, 2006):

- ***Engelund and Hansen***:

  For the Engelund and Hansen approach, it is assumed that the dimensionless bed shear stress is much larger than the "critical shields parameter" provided by the user. Therefore the dimensionless shear stress is implemented instead of the critical shields parameter.

  The dimensionless rate of total-load transport, as a function of a Chezy number defined for the area and can be determined by means of the following equation:

$$\varphi_t = 0.1\frac{C^2}{2g}\theta^{2.5} \qquad \textbf{(12-1)}$$

  where

φ_t	Dimensionless rate of total-load sediment transport
C	Chezy's roughness coefficient
θ	Dimensionless bed shear stress

  The value for the dimensionless bed shear stress can be determined as follow by:

$$\theta = {U_f^2}\Big/{(s-1)gd} \qquad \textbf{(12-2)}$$

  where

θ	Dimensionless bed shear stress
U_f	Friction velocity
s	Relative density of the sediment

d	Median particle size d_{50}

The total-load sediment transport can be solved by means of the following equation:

$$\varphi_t = {q_t}/{\sqrt{(s-1)gd^3}} \quad \textbf{(12-3)}$$

where

q_t	Total-load sediment transport

Note that the diameter used is the median particle value, d_{50}, with no reference to the gradation of the particles.

- **Engelund and Fredsøe**:

Engelund and Fredsøe subdivided the total sediment transport into two terms, the suspended sediment being transported in the water mass and the bed-load sediments moving along the ocean bed.

$$q_t = q_b + q_s \quad \textbf{(12-4)}$$

where

q_t	Total-load sediment transport
q_b	Bed-load sediment transport
q_s	Suspended sediment transport

This formulation assumes that the base-load sediment only affects a single layer of sediment, thus the depth or layer thickness of the sediment is equal to the particle's diameter. Calculations for the bed-load sediment movement are based on the probability of sediment particles in the single layer being in motion.

$$q_b = 5p\left(\sqrt{\theta'} - 0.07\sqrt{\theta_c}\right)\sqrt{(s-1)gd} \quad \textbf{(12-5)}$$

where

p	Probability of all the particles in a single layer being in motion
θ'	Dimensionless shear stress related to skin friction
θ_c	Shear stress required for the initiation of motion of particles on the bed
s	Relative density of the sediment

Suspended sediment calculations are considered more complicated. Calculations are based on the following equation:

$$q_s = 11.6U'_f\ c_b a\left[I_1 ln\left(\frac{30h}{k_N}\right) + I_2\right] \quad \textbf{(12-6)}$$

where

U'_f	Shear velocity related to the skin friction
c_b	Bed concentration of suspended sediment
a	reference level for the concentration of suspended sediment of $2d_{50}$
h	Water depth
k_N	Nikuradse's equivalent roughness coefficient of $2.5d_{50}$
I_1, I_2	Einstein's integrals

Einstein's integrals mentioned above, is a function of a dimensionless reference level, given by:

$$A = {}^{a}/_{h} \quad \textbf{(12-7)}$$

and Rouse number:

$$z = {w_s}/{\kappa U_{f'}} \tag{12-8}$$

where

z	Shear velocity related to the skin friction
w_s	Settling velocity of the sediment
κ	the Von Karman constant of 0.4

These two integrals are interpolated between the reference level for the concentration of suspended sediment, *y* = *a*, and the water depth, *y* = *h*, where y is the depth measured from the fixed bed level.

However, c_b is developed for a semi-empirical relation at *a* = *2d* and can be calculated with the following equation:

$$c_b = {0.65}\Big/{\left(1 + {1}/{\lambda}\right)^2} \tag{12-9}$$

where

$$\lambda = \sqrt{\frac{\theta' - \varphi_c - \frac{\pi p \beta}{6}}{0.027 s \theta'}} \quad \text{if } \theta' > \theta_c + \frac{\pi p \beta}{6} \tag{12-10}$$

Note that this sediment transport formulation is developed on the basis of experimental data with bed material consisting of sand-fraction sizes, thus more accurate results for particles cohering to these standards are expected.

- ***Zyserman and Fredsøe***:

  This method is very similar to the *Engelund and Fredsøe* approach, with a variation in the calculation of c_b, used in **Equation (12-6)**. This parameter is determined empirically with the following equation and by means of constant parameters:

$$c_b = \frac{A(\theta' - \theta_c)^n}{1 + \frac{A}{c_m}(\theta' - \theta_c)^n} \quad \text{if } \theta' > \theta_c \qquad \textbf{(12-11)}$$

  where

A	= 0.331
n	= 1.75
c_m	= 0.46
θ_c	= 0.045

  Further calculations based on **Equation (12-5)**, **Equation (12-7)**, **Equation (12-8)**, **Equation (12-9)** and **Equation (12-10)** remain similar.

- ***Ackers and White***:

  For the approach followed by Ackers and White, a dimensionless total-load sediment transport rate can be calculated as follow:

$$G_{gr} = C\left[{F_{gr}}/{A} - 1\right]^m \qquad \textbf{(12-12)}$$

where

G_{gr}	Dimensionless total load sediment transport rate
C, m, A	Parameters depending on the dimensionless particle size, D_{gr}
F_{gr}	Sediment mobility number

The dimensionless particle size, D_{gr}, as mentioned above, are defined by the following equation:

$$D_{gr} = d\left[\frac{g(s-1)}{\nu^2}\right]^{1/3} \quad \textbf{(12-13)}$$

where

d	Grain size
g	Gravitational acceleration of 9.81
s	Relative density of bed sediment
ν	Kinematic viscosity of water

A general sediment mobility number, F_{gr}, utilized in **Equation (12-12)** can be defined by **Equation (12-14)**.

$$F_{gr} = \frac{U_f^n}{\sqrt{gd(s-1)}}\left[\frac{V}{\sqrt{32log\left(\frac{10h}{d}\right)}}\right]^{1-n} \quad \textbf{(12-14)}$$

where

U_f^n	Total shear velocity
h	Water depth
V	Depth-averaged current velocity
n	A constant depending on D_{gr} ranging from 0 for coarse materials to 1 for fine materials

The transport parameter G_{gr} is defined in **Equation (12-15)** and can be used to calculate the sediment mass flux per unit mass flow rate by means of the following equation:

$$F_{gr} = \frac{Xh}{sd}\left(\frac{U_f}{V}\right)^n \quad \textbf{(12-15)}$$

where

X	The sediment mass flux per unit mass flow rate

- ***Meyer-Peter and Műller***:

  In the approach followed by Meyer-Peter and Műller, the dimensionless bed-load transport (Φ_b) can be determined with **Equation (12-16)** and **Equation (12-17)** below.

$$\varphi_b = 8(\theta' - \theta_c)^{1.5} \quad \textbf{(12-16)}$$

and

$$\varphi_b = \frac{q_b}{\sqrt{(s-1)gd^3}} \quad \textbf{(12-17)}$$

where

φ_b	Bed-load sediment transport
θ'	Dimensionless bed shear stress
θ_c	Critical shields parameter
q_b	Bed-load sediment movement
s	Relative density
g	Gravitational acceleration of 9.81 m/s^2
d	Particle diameter

Note that for situations where fine sediments and/or great velocities are used in the simulation, the actual transport rate may be underestimated by this approach. This is due to suspended sediment loads being excluded; therefore higher velocities and smaller particles, contributing to suspended sediment loads, are not accounted for.